Safety Analysis Report

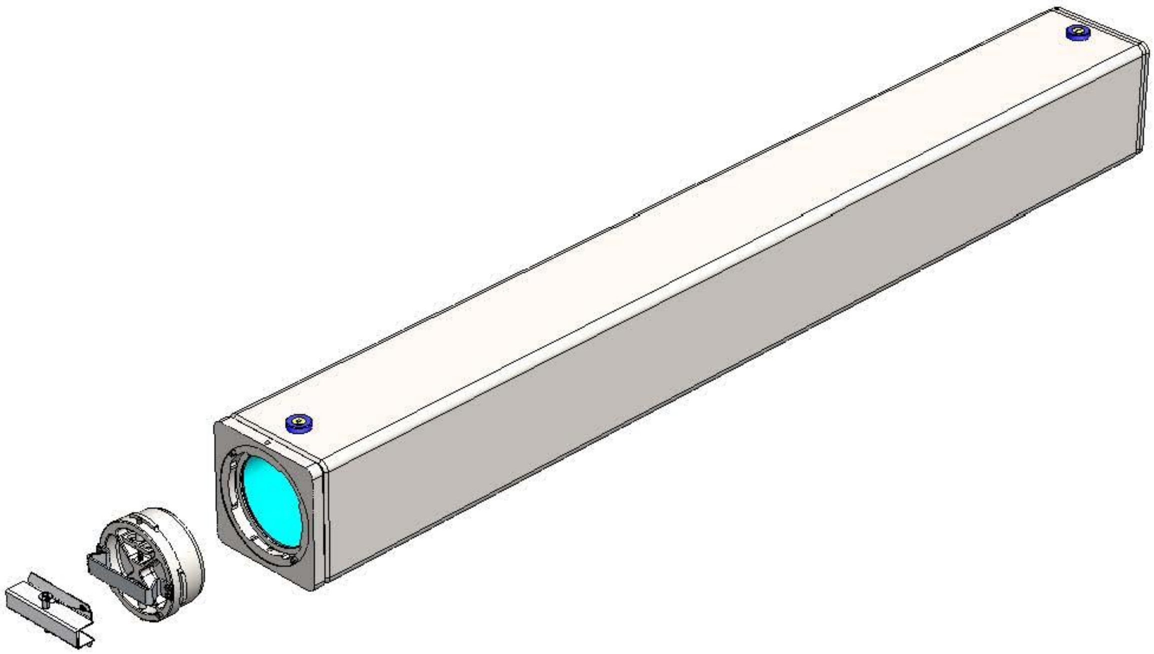

Advanced Test Reactor Fresh Fuel Shipping Container (ATR FFSC)

Revision 11, July 2016

Docket 71-9330

Prepared by:	***Prepared for:***
AREVA **AREVA Federal Services LLC**	Idaho National Laboratory **Battelle Energy Alliance, LLC (BEA)**

TABLE OF CONTENTS

1.0 GENERAL INFORMATION

This chapter of the Safety Analysis Report (SAR) presents a general introduction and description of the Advanced Test Reactor (ATR) Fresh Fuel Shipping Container (FFSC).[1] This application seeks validation of the ATR FFSC as a Type AF fissile materials shipping container in accordance with Title 10, Part 71 of the Code of Federal Regulations (10CFR71).

The major components comprising the package are discussed in Section 1.2.1, *Packaging*, and illustrated in Figure 1.2-1 through Figure 1.2-11 and Figure 1.2-16. Detailed drawings of the package design are presented in Appendix 1.3.2, *Packaging General Arrangement Drawings*. A glossary of terms is presented in Appendix 1.3.1, *Glossary of Terms*.

1.1 Introduction

The ATR FFSC is designated a Type AF-96 packaging per the definition of 10 CFR §71.4[2], and has been designed to transport a single, unirradiated research reactor fuel element or the associated loose plates. The loose plates may either be flat or rolled to the geometry required for assembly into a fuel element. All fuel elements are of the plate-type. All fueled plates consist of a central fuel matrix "meat", clad on both sides and all edges with aluminum alloy cladding. The fuel elements contain various types of fuel matrix containing varying amounts of U-235 ranging between low enrichment (≤ 20% U-235) and high enrichment (≤ 94% U-235). Some fuel matrices include burnable poison. Fuel elements containing up to 2 kg of U-235 may be transported by air.

Since the package transports a Type A quantity of radioactive material (see Section 4.1.1, *Type A Fissile Packages*) and radiation is negligible, the only safety function performed by the package is criticality control. This function is achieved, in the case of a transport accident, by confining the fuel element within the package and by maintaining separation of fuel in multiple packages. The fuel itself is robust and inherently resists unfavorable geometry reconfiguration while contained within the package. For ease of handling and property protection purposes, each fuel element or loose plate group is contained within a lightweight aluminum housing referred to as the fuel handling enclosure (FHE).

For ATR fuel elements, the criticality control function is demonstrated via full-scale testing of a prototypic package followed by a criticality analysis using a model which bounds the test results, ensuring that the calculated $k_{eff} + 2\sigma$ is below the upper subcritical limit (USL) in the most limiting case. Two full-scale prototype models were used to perform a number of performance tests including normal conditions of transport (NCT) free drop and hypothetical accident

[1] In the remainder of this Safety Analysis Report, *Advanced Test Reactor Fresh Fuel Shipping Container* will be abbreviated as *ATR FFSC*. In addition, the term 'packaging' will refer to the assembly of components necessary to ensure compliance with the regulatory requirements, but does not include the payload. The term 'package' includes both the packaging components and the fresh fuel payload.

[2] Title 10, Code of Federal Regulations, Part 71 (10 CFR 71), *Packaging and Transportation of Radioactive Material*, 1-1-06 Edition.

condition (HAC) free drop and puncture tests. Other fuel elements and loose plates are modeled in various ways as described in Chapter 6, *Criticality Evaluation*.

The characteristics and criticality safety index (CSI) of each payload are summarized in Table 1.1-1. Additional fuel information is given in Section 1.2.2, *Contents*. The ATR FFSC packaging is described in Section 1.2.1, *Packaging*.

Table 1.1-1 – Fuel Types in the ATR FFSC Package

Fuel Element	U-235 Mass, max, grams	Enrichment, max, %	Core (Meat) Alloy	FHE Type	CSI
ATR	1,200	94	UAl_x	ATR FHE	4.0
ATR U-Mo Demonstration	1,240	94	UAl_x & U-Mo	ATR FHE	4.0
MIT	515	94	UAl_x	MIT FHE	4.0
MURR	785	94	UAl_x	MURR FHE	4.0
ATR loose plates	600	94	UAl_x	LFPB	4.0
RINSC①	283	20	U_3Si_2	RINSC FHE	25.0
Small Quantity Payload①	400	94	Various②	SQFHE	25.0
Cobra HEU	450	94	UAl_x	Cobra FHE	31.3
Cobra LEU	450	20	U_3Si_2	Cobra FHE	31.3

Notes:

1. The Small Quantity Payload category includes MIT, MURR, or Cobra loose fuel plates, ATR Full-size Plate in Flux Trap Position elements (AFIP), U-Mo foils, and design demonstration elements (DDE). The DDE category includes similar test elements which are bounded by the radiological and physical descriptions of the DDEs. Although it has its own FHE, the RINSC fuel element is included in the Small Quantity Payload category.
2. MIT and MURR loose plates use UAl_x. Cobra loose plates use either UAl_x for HEU or U_3Si_2 for LEU. AFIP, U-Mo foils, and DDEs use U-Mo either as a monolithic alloy or dispersed in a matrix of aluminum and silicon.

1.2 Package Description

This section presents a basic description of the ATR FFSC. General arrangement drawings are presented in Appendix 1.3.2, *Packaging General Arrangement Drawings*.

1.2.1 Packaging

1.2.1.1 Packaging Description

The ATR FFSC is designed as Type AF packaging for transportation of unirradiated research reactor fuel elements and associated loose plates as described in Section 1.2.2, *Contents*. The packaging is rectangular in shape and is designed to be handled singly with slings, or by fork truck when racked. Package components are shown in Figure 1.2-1. Transport of the package is by highway truck or by air. The maximum gross weight of the package in any loaded configuration is 290 lbs.

The ATR FFSC is a two part packaging consisting of the body and the closure. The body is a single weldment that features square tubing as an outer shell and round tubing for the payload cavity. Three 1-inch thick ribs maintain spacing between the inner and outer shells. The components of the packaging are shown in Figures 1.2-2, 1.2-3, 1.2-4, and 1.2-5 and are described in more detail in the sections which follow. With the exception of several minor components, all steel used in the ATR FFSC is ASTM Type 304 stainless steel. Components are joined using full-thickness fillet welds (i.e., fillet welds whose leg size is nominally equal to the lesser thickness of the parts joined) and full and partial penetration groove welds.

1.2.1.1.1 ATR FFSC Body

The ATR FFSC body is a stainless steel weldment 73 inches long and 8 inches square weighing (empty) approximately 230 lbs. It consists of two nested shells; the outer shell a square stainless steel tube with a 3/16 inch wall thickness and the inner shell a 6 inch diameter, 0.120 inch wall, stainless steel round tube. There are three 1 inch thick stiffening plates secured to the round tube by fillet welds at equally spaced intervals. The tube is wrapped with thermal insulation and the insulation is overlaid with 28 gauge stainless steel sheet. The stainless steel sheet maintains the insulation around the inner shell. This insulated weldment is then slid into the outer square tube shell and secured at both ends by groove welds. Thermal insulation is built into the bottom end of the package as shown in Figure 1.2-3, and the closure provides thermal insulation at the closure end of the package as shown in Figure 1.2-4.

1.2.1.1.2 ATR FFSC Closure

The closure is a small component designed to be easily handled by one person. It weighs approximately 10 lbs and is equipped with a handle to facilitate use with gloved hands. The closure engages with the body using a bayonet style design. There are four lugs, uniformly spaced on the closure, that engage with four slots in the mating body feature. The closure is secured by retracting two spring loaded pins, rotating the closure through approximately 45º, and releasing the spring loaded pins such that the pins engage with mating holes in the body. When the pins are properly engaged with the mating holes the closure is locked.

A small post on the closure is drilled to receive a tamper indicating device (TID) wire. An identical post is located on the body and is also drilled for the TID wire. For ease in operation, there are two TID posts on the body. There are only two possible angular orientations for the closure installation and the duplicate TID post on the body enables TID installation in both positions.

A cover is placed over the closure handle during transport to render the handle inoperable for inadvertent lifting or tiedown. Figure 1.2-5 illustrates the placement of the handle cover. The profile of the cover depicted in Appendix 1.3.2, *Packaging General Arrangement Drawings*, is optional and may be modified to fit other handle profiles to ensure lifting and tiedown features are disabled as required by 10 CFR §71.45. As an option, the closure handle may be removed for transport rather than installing the handle cover.

1.2.1.1.3 ATR Fuel Handling Enclosure

The ATR Fuel Handling Enclosure (FHE) is a hinged thin gauge aluminum weldment used with the ATR fuel element or ATR U-Mo demonstration element, as illustrated in Figure 1.2-1. The ATR FHE is a cover used to protect the fuel from handling damage during ATR FFSC loading and unloading operations. It is a thin walled aluminum fabrication featuring a hinged lid and neoprene rub strips to minimize fretting of the fuel element side plates where they are in contact with the container.

During transport the ATR FHE is not relied upon to add strength to the package, or satisfy any safety requirement. For purposes of determining worst case reactivity, the ATR FHE is assumed to be not present.

1.2.1.1.4 MIT Fuel Handling Enclosure

The MIT FHE is comprised of two identical machined segments which surround the MIT fuel element secured by two end spacers and locked together using ball lock pins (see Figure 1.2-6). The primary purpose of end spacers is to secure the two sections of the FHE prior to loading the FHE into the package. The location of the hole in the end plate of the spacer also facilitates easy removal of the FHE from the package. The MIT FHE is a cover used to protect the fuel from handling damage during ATR FFSC loading and unloading operations. It is an aluminum fabrication featuring machined segments and neoprene rub strips to minimize fretting of the fuel element side plates where they are in contact with the container.

During transport the MIT FHE, including the end spacers, is not relied upon to add strength to the package; however the enclosure does maintain the fuel element within a defined dimensional envelope.

1.2.1.1.5 MURR Fuel Handling Enclosure

The MURR FHE is very similar to the MIT FHE and is comprised of two identical machined segments which surround the MURR fuel element secured by two end spacers and locked together using ball lock pins (see Figure 1.2-7). The primary purpose of end spacers is to secure the two sections of the FHE prior to loading the FHE into the package. The location of the hole in the end plate of the spacer also facilitates easy removal of the FHE from the package. The MURR FHE is a cover used to protect the fuel from handling damage during ATR FFSC loading and unloading operations. It is an aluminum fabrication featuring machined segments and neoprene rub strips to minimize fretting of the fuel element side plates where they are in contact with the container.

During transport the MURR FHE, including the end spacers, is not relied upon to add strength to the package; however the enclosure does maintain the fuel element within a defined dimensional envelope.

1.2.1.1.6 RINSC Fuel Handling Enclosure

The RINSC fuel, although classified as a small quantity payload, has its own dedicated FHE. The RINSC FHE is very similar to the MURR and MIT FHEs and is comprised of two identical machined segments which surround the RINSC fuel element and are secured by two end spacers and locked together using ball lock pins (see Figure 1.2-8). The primary purpose of end spacers is to secure the two sections of the FHE prior to loading the FHE into the package. The location of the hole in the end plate of the spacer also facilitates easy removal of the FHE from the package. The RINSC FHE is a cover used to protect the fuel from handling damage during ATR FFSC loading and unloading operations. It is an aluminum fabrication featuring machined segments and neoprene rub strips to minimize fretting of the fuel element side plates where they are in contact with the container.

During transport the RINSC FHE does not add strength to the package nor satisfy any safety requirement. For purposes of determining worst case reactivity, the RINSC FHE is assumed to be not present.

1.2.1.1.7 ATR FFSC Loose Fuel Plate Basket

The Loose Plate Fuel Basket (LFPB) is comprised of four identical machined segments joined by threaded fasteners (reference Figure 1.2-16). The fasteners joining the segments in the lengthwise direction are permanently installed. The basket is opened/closed using the 8 hand tightened fasteners. For criticality control purposes during transport the loose fuel plate basket maintains the fuel plates within a defined dimensional envelope.

Additional aluminum plates may be used as dunnage to fill gaps between the fuel plates and the basket payload cavity. The dunnage is used for property protection purposes only.

1.2.1.1.8 Small Quantity Payload FHE

The small quantity payload FHE (SQFHE) is very similar to the RINSC, MURR, and MIT FHEs. The SQFHE is comprised of two identical machined segments which surround the small quantity payloads and are secured by two end spacers and locked together using ball lock pins (see Figure 1.2-9). The primary purpose of end spacers is to secure the two sections of the FHE prior to loading the FHE into the package. The location of the hole in the end plate of the spacer also facilitates easy removal of the FHE from the package. The SQFHE is a cover used to protect the fuel from handling damage during ATR FFSC loading and unloading operations. It is an aluminum fabrication featuring machined components.

During transport the SQFHE does not add strength to the package nor satisfy any safety requirement. For purposes of determining worst case reactivity, the SQFHE is assumed to be not present.

Dunnage is used to fill gaps between the small quantity payloads and SQFHE. Dunnage may be made from aluminum plates, shapes, and sheets, and may include miscellaneous steel or aluminum fasteners. Dunnage may also be made from cellulosic material such as cardboard. The maximum gap between the fuel plate face and the basket payload cavity is ¼ inches. The SQFHE does not come with neoprene rub strips like the RINSC FHE, however 1/8 inch thick neoprene rub strips may be used in the SQFHE to minimize fretting of the small quantity payloads where there may be contact with the SQFHE or optional aluminum dunnage. Neoprene rub strips may be used between the SQFHE and the small quantity payloads and/or between the dunnage and the small quantity payloads. The 1/8 inch neoprene rub strips shall not be stacked in more than two layers between the small quantity payload and any interior face of the SQFHE.

1.2.1.1.9 Cobra FHE

The Cobra FHE is used for both the HEU and LEU versions of the fuel element, and has a design very similar to the RINSC, MURR, MIT, and Small Quantity Payload FHEs. The Cobra FHE is comprised of two identical machined segments which are secured by two end spacers and locked together using ball lock pins (see Figure 1.2-10). The primary purpose of end spacers is to secure the two sections of the FHE prior to loading the FHE into the package. The location of the hole in the end plate of the spacer also facilitates easy removal of the FHE from the package. The Cobra FHE serves to protect the fuel from handling damage during ATR FFSC loading and unloading operations. It is an aluminum fabrication featuring machined components and neoprene rub strips to minimize fretting of the fuel element where it is in contact with the container.

During transport the Cobra FHE does not add strength to the package nor satisfy any safety requirement. For purposes of determining worst case reactivity, the Cobra FHE is assumed to be not present.

1.2.1.2 Gross Weight

The maximum shipped weight of the ATR FFSC (gross weight) with the specified payload is 290 lbs for all payload configurations. Further discussion of the gross weight is presented in Section 2.1.3, *Weights and Centers of Gravity*.

1.2.1.3 Neutron Moderator/Absorption

There are no moderator or neutron absorption materials in this package.

1.2.1.4 Heat Dissipation

The uranium payload produces a negligible thermal heat load. Therefore, no special devices or features are needed or utilized in the ATR FFSC to dissipate heat. A more detailed discussion of the package thermal characteristics is provided in Chapter 3.0, *Thermal*.

1.2.1.5 Protrusions

The closure handle protrudes 1 3/8-inches from the face of the closure. The handle is secured to the closure by means of four 10-24 UNC screws. The screws will fail prior to presenting any significant loading to either the closure engagement lugs or the locking pins.

On one face of the package body, two index lugs are secured to the package to facilitate stacking of the packages. The opposite face of the package has pockets into which the index lugs nest as illustrated in Figure 1.2-11. Each index lug is secured to the package by means of a 3/8-16 socket flat head cap screw. Under any load condition, the screw will fail prior to degrading the safety function of the package.

1.2.1.6 Lifting and Tiedown Devices

The ATR FFSC may be lifted from beneath utilizing a standard forklift truck when the package is secured to a fork pocket equipped pallet, or in a package rack. Swivel lift eyes may be installed in the package to enable package handling with overhead lifting equipment. The swivel eyes are installed after removing the 3/8-16 socket flat head cap screws and index lugs.

The threaded holes into which the swivel lift eyes are installed for the lifting the package are fitted with a 3/8-16 UNC screw and an index lug (see Figure 1.2-11) during transport. When the packages are stacked and the index lugs are nested in the mating pockets of the stacked packages, the index lugs can serve to carry shear loads between stacked packages.

1.2.1.7 Pressure Relief System

There are no pressure relief systems included in the ATR FFSC design. There are no out-gassing materials in any location of the package that are not directly vented to atmosphere. The package insulation, located in the enclosed volumes of the package, is a ceramic fiber. The insulation does not off-gas under normal or hypothetical accident conditions. The closure is not equipped with either seals or gaskets so that potential out-gassing of the FHE neoprene material and fuel element plastic bag material will readily vent without significant pressure build-up in the payload cavity.

1.2.1.8 Shielding

Due to the nature of the uranium payload, no biological shielding is necessary or specifically provided by the ATR FFSC.

1.2.2 Contents

The ATR FFSC is loaded with contents consisting of unirradiated fuel elements (ATR, ATR U-Mo, MIT, MURR and Cobra), small quantity payloads (RINSC element, AFIP element, U-Mo foils, DDEs, MIT loose fuel element plates, MURR loose fuel element plates, and Cobra loose fuel element plates), and ATR loose fuel element plates. The DDE category includes similar test elements which are bounded by the radiological and physical descriptions of the DDEs. The total mass of polyethylene (including the mass of any plastic material such as adhesive tape) in the packaging shall not exceed 100g. The total mass of neoprene plus any cellulosic material such as paper or cardboard in the packaging shall not exceed 4 kg. The neoprene thickness and arrangement shall be as directed by the drawings in Appendix 1.3.2, *Packaging General Arrangement Drawings*, or as dictated throughout this Chapter.

1.2.2.1 ATR Fuel Element and ATR U-Mo Demonstration Element

Standard ATR Fuel Element: Each standard ATR fuel element contains up to 1,200 g U-235, enriched up to 94% U-235. The weight percents of the remaining uranium isotopes are 1.2 wt.% U-234 (max), 0.7 wt.% U-236 (max), and 5.0-7.0 wt.% U-238. The fuel element (ATR Mark VII) fissile material is uranium aluminide (UAl_x). The fuel element weighs not more than 25 lbs, is bagged, and is enclosed in the ATR FHE weighing 15 lbs.

There are four different ATR Mark VII fuel element types designated 7F, 7NB, 7NBH, and YA. The construction of these fuel elements are identical, varying only in the content of the fuel matrix. In the 7F fuel element, all 19 fuel plates are loaded with enriched uranium in an aluminum matrix with the eight outer plates (1 through 4 and 16 through 19) containing boron as a burnable poison. The fuel element with the greatest reactivity is the 7NB which contains no burnable poison. The 7NBH fuel element is similar to the 7NB fuel element except that it contains one or two borated plates. The YA fuel element is identical to the 7F fuel element except that plate 19 of the YA fuel element is an aluminum alloy plate containing neither uranium fuel nor boron burnable poison. The total U-235 and B-10 content of the YA fuel element is reduced accordingly. A second YA fuel element design (YA-M) has the side plate width reduced by 15 mils.

The ATR fuel elements contain 19 curved fuel plates. A section view of an ATR fuel element is given in Figure 1.2-12. The fuel plates are rolled to shape and swaged into the two fuel element side plates. Fuel plate 1 has the smallest radius, while fuel plate 19 has the largest radius. The fissile material (uranium aluminide) is nominally 0.02-in thick for all 19 plates. Fuel element side plates are fabricated of ASTM B 209, aluminum alloy 6061-T6 or 6061-T651 and are approximately 0.19-in thick. The maximum channel thickness between fuel plates is 0.087 inches.

ATR U-Mo Demonstration Element: The external geometry of the ATR U-Mo demonstration element is essentially identical to the ATR Mark VII YA fuel element and is shown schematically in Figure 1.2-21. The maximum channel thickness between fuel plates is 0.087 inches. The demonstration element contains 18 fueled plates, while plate 19 is an aluminum alloy plate. The demonstration element contains a mixture of UAl_x (HEU) and U-Mo (LEU) fuel plates, with a maximum U-235 mass of 1,240 g. Plates 1 through 4 and 16 through 18 are UAl_x plates identical in construction and composition to a standard HEU ATR fuel element. Boron is included in the UAl_x plates as a burnable poison. Plates 5 through 15 are fueled with an alloy of LEU uranium and molybdenum. The U-Mo fuel meat is nominally 10% molybdenum by weight, and the U-235 is enriched up to 20.0%. For the LEU fuel, the maximum weight percent for U-234 and U-236 are 0.26% and 0.46%, respectively.

The U-Mo fuel meat is nominally 0.013-in thick, and a nominal 0.001-in thick zirconium interlayer is present between the fuel meat and the aluminum cladding (see Figure 1.2-21). The fuel element weighs not more than 32 lbs, is bagged, and is enclosed in the ATR FHE weighing 15 lbs.

1.2.2.2 MIT Fuel Element

Each MIT element contains up to 515 g U-235, enriched up to 94 wt.%. The weight percents of the remaining uranium isotopes are 1.2 wt.% U-234, 0.7 wt.% U-236, and 5.0-7.0 wt.% U-238. Like the ATR fuel element, the MIT fuel element fissile material is uranium aluminide (UAl_x). The fuel element weighs not more than 10 lbs, is bagged, and is enclosed in the MIT FHE weighing 25 lbs.

Each MIT fuel element contains 15 flat fuel plates, as shown in Figure 1.2-13. The fuel plates are fabricated and swaged into the two fuel element side plates. The fuel "meat" is a mixture of uranium metal and aluminum, while the cladding and structural materials are an aluminum alloy. The fissile material (uranium aluminide) is nominally 0.03-in thick and the cladding is nominally 0.025-in thick. Fuel element side plates are fabricated of ASTM B 209, aluminum alloy 6061-T6 and are approximately 0.19-in thick. The maximum channel thickness between fuel plates is 0.090 inches, excluding the thermal grooves. If the 0.012 inch thermal groove is considered, the maximum channel thickness between fuel plates is 0.114 inches.

1.2.2.3 MURR Fuel Element

Each MURR element contains up to 785 g U-235, enriched up to 94 wt.%. The weight percents of the remaining uranium isotopes are 1.2 wt.% U-234, 0.7 wt.% U-236, and 5.0-7.0 wt.% U-238. Like the ATR fuel element, the MURR fuel element fissile material is uranium aluminide (UAl_x). The fuel element weighs not more than 15 lbs, is bagged, and is enclosed in the MURR FHE weighing 30 lbs.

Each MURR fuel element contains 24 curved fuel plates. Fuel plate 1 has the smallest radius, while fuel plate 24 has the largest radius, as shown in Figure 1.2-14. The fuel "meat" is a mixture of uranium metal and aluminum, while the cladding and structural materials are an aluminum alloy. The fuel plates are rolled to shape and swaged into the two fuel element side plates. The fissile material (uranium aluminide) is nominally 0.02-in thick for all 24 plates. Fuel element side plates are fabricated of ASTM B 209, aluminum alloy 6061-T6 or 6061-T651 and are approximately 0.15-in thick. The maximum channel thickness between fuel plates is 0.090 inches.

1.2.2.4 Small Quantity Payload

The small quantity payload consists of a class of research and development plate-type fuels with U-235 as the fissile isotope (i.e., no U-233 or plutonium), with a bounding U-235 loading ≤ 400 g, and U-235 enrichment ≤ 94%. Fuel types that fall into the small quantity payload category include RINSC fuel elements, AFIP elements, U-Mo foils, DDEs, MIT loose fuel element plates, MURR loose fuel element plates, and Cobra loose fuel element plates.

Individual small quantity payloads are discussed below. Although the fissile mass and enrichment is stated for each payload type, the acceptable limits for any small quantity payload are the bounding quantity of 400 g fissile mass and 94% enrichment. The maximum weight of any small quantity payload, including the SQFHE, is 50 lbs. As stated above, the RINSC fuel element is shipped in the dedicated RINSC FHE.

With the exception of RINSC fuel, which utilizes the RINSC FHE, all small quantity payload items fall within the maximum dimensional bounds of the SQFHE, or approximately 55-in x

3.4-in x 3.4-in. The minimum dimensions for a small quantity payload item are approximately 10-in x 1.5-in x 0.008-in.

1.2.2.4.1 RINSC Fuel Element

Each RINSC element contains up to 283 g U-235, enriched up to 20 wt.%. The weight percents of the remaining uranium isotopes are 0.5 wt.% U-234 (max), 1.0 wt.% U-236 (max), with the balance U-238. The RINSC fuel element fissile material is uranium silicide (U_3Si_2) dispersed in aluminum powder. The fuel element weighs not more than 17 lbs, and is enclosed in the RINSC FHE weighing 28 lbs.

Each RINSC fuel element contains 22 flat fuel plates, as shown in Figure 1.2-15. The fuel plates are fabricated and swaged into the two fuel element side plates. The fuel "meat" is a mixture of uranium silicide and aluminum powder, while the cladding and structural materials are an aluminum alloy. The fissile material (uranium silicide) is nominally 0.02-in thick and the cladding is nominally 0.015-in thick. Fuel element side plates are fabricated of ASTM B 209, aluminum alloy 6061-T6 and 6061-T651 and are approximately 0.187-in thick. The maximum channel thickness between fuel plates is 0.096 inches.

1.2.2.4.2 AFIP Fuel Element

Each AFIP element contains up to 365 g U-235, enriched up to approximately 20 wt.%. Each AFIP element typically contains 4 curved fuel plates, as shown in Figure 1.2-17. The fuel plates are fabricated and swaged into the two fuel element side plates. The fuel "meat" may be either dispersion or monolithic. Dispersion fuel meat consists of uranium 7 wt.% molybdenum alloy (U-7Mo) particles dispersed in an aluminum-silicon matrix. Monolithic fuel meat consists of uranium 10 wt.% molybdenum alloy (U-10Mo) coated with a thin zirconium interlayer. Both fuel types are clad in 6061 aluminum. Fuel side plates are fabricated from 6061 aluminum. Loose plates from an AFIP fuel element are also an allowed content.

1.2.2.4.3 U-Mo Foils

Uranium-Molybdenum (U-Mo) foils are used in the fabrication of test fuels, such as AFIPs and DDEs. A U-Mo foil contains up to 160 g U-235, enriched up to 94%. The foils are thin and may contain a zirconium coating, although cladding would not typically be present. The fuel meat description provided for the AFIP elements also applies to U-Mo foils. More than one U-Mo foil type may be transported per ATR FFSC.

1.2.2.4.4 Design Demonstration Elements (DDEs)

Each DDE contains up to 365 g U-235, enriched up to 94 wt.%. DDEs are available for the National Bureau of Standard Reactor (NBSR), the Massachusetts Institute of Technology Reactor (MITR), and the University of Missouri Reactor (MURR), and are abbreviated as DDE-NBSR, DDE-MITR, and DDE-MURR. Sketches of the three DDEs are provided in Figures 1.2-18, -19, and -20. Loose plates from a DDE are also an allowed content.

DDEs may contain either flat or curved fuel plates. Fuel meat consists of U-Mo, so the fuel meat description provided for the AFIP elements also applies to DDEs.

1.2.2.4.5 MIT and MURR Loose Fuel Element Plates

MIT and MURR loose plates transported as a small quantity payload are limited to 400 grams U-235. MIT fuel plates have approximately 34.3 g U-235 per plate, and MURR fuel plates have approximately 19 to 46 g U-235 per fuel plate. The plates may either be flat or rolled to the geometry required for assembly into the fuel element. The plates may be packaged using kraft paper, and taped or wire tied together. A mixture of MIT and MURR fuel plates may be shipped together.

1.2.2.4.6 Cobra Loose Fuel Element Plates

Cobra loose plates transported as a small quantity payload are limited to 400 grams U-235. The U-235 content per plate is variable, and may be HEU or LEU. The composition of the plates is presented in Section 1.2.2.6, *Cobra Fuel Element*. The plates may either be flat or rolled to the geometry required for assembly into the fuel element. The plates may be packaged using kraft paper, and taped or wire tied together.

1.2.2.5 ATR Loose Fuel Plates

The maximum weight of the ATR loose plate payload (Figure 1.2-16) is 50 lbs. This weight is made up of the maximum basket contents weight of 20 lbs and the loose fuel plate basket weight of 30 lbs.

The loose plate payload is limited to 600 grams U-235. The plates are limited to those used in ATR fuel elements. The plates may either be flat or rolled to the geometry required for assembly into the fuel element. For handling convenience, the loose plate basket will be loaded with either flat or rolled plates. Additionally, the plates may be banded or wire tied in a bundle.

1.2.2.6 Cobra Fuel Element

The Cobra fuel element (shown in Figure 1.2-22) is used at the BR2 reactor in Belgium. This category includes HEU (enriched to ≤ 94% U-235 as UAl_x dispersed in aluminum powder), and LEU (enriched to ≤ 20% U-235 as U_3Si_2 dispersed in aluminum powder). The bounding loading is 450g of U-235 in either HEU or LEU. The bounding fuel element weight is 20 lb, is bagged, and is enclosed in a Cobra FHE weighing 28 lb.

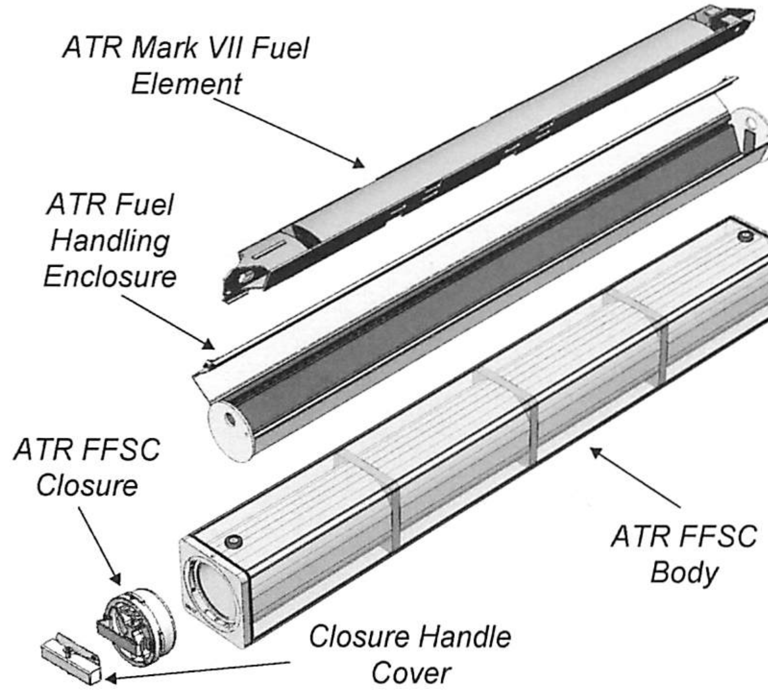

Figure 1.2-1 - Overview of the ATR FFSC (Outer Body Shell Shown Transparent)

Security-Related Information Figure Withheld Under 10 CFR 2.390.

Figure 1.2-2 - Top End Body Sectional View

Security-Related Information Figure Withheld Under 10 CFR 2.390.

Figure 1.2-3 - Bottom End Body Sectional View

Security-Related Information Figure Withheld Under 10 CFR 2.390.

Figure 1.2-4 - Closure Sectional View

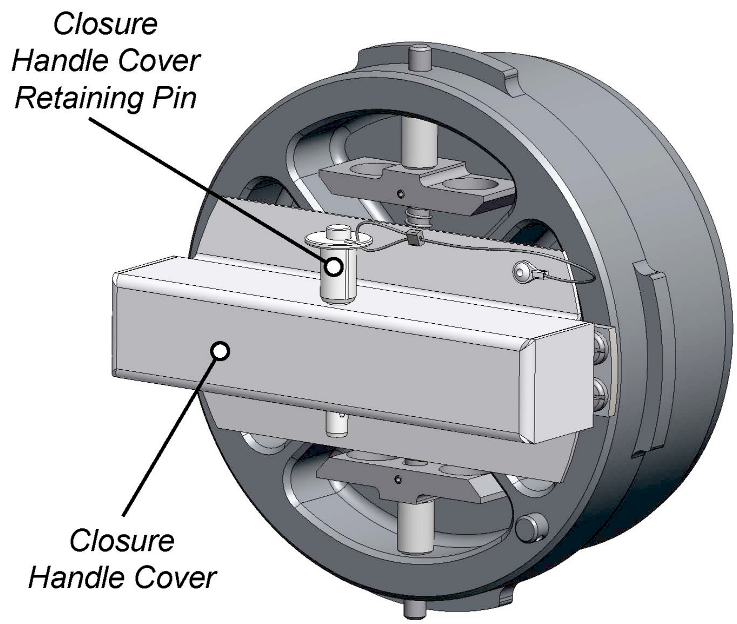

Figure 1.2-5 – Closure Handle Cover

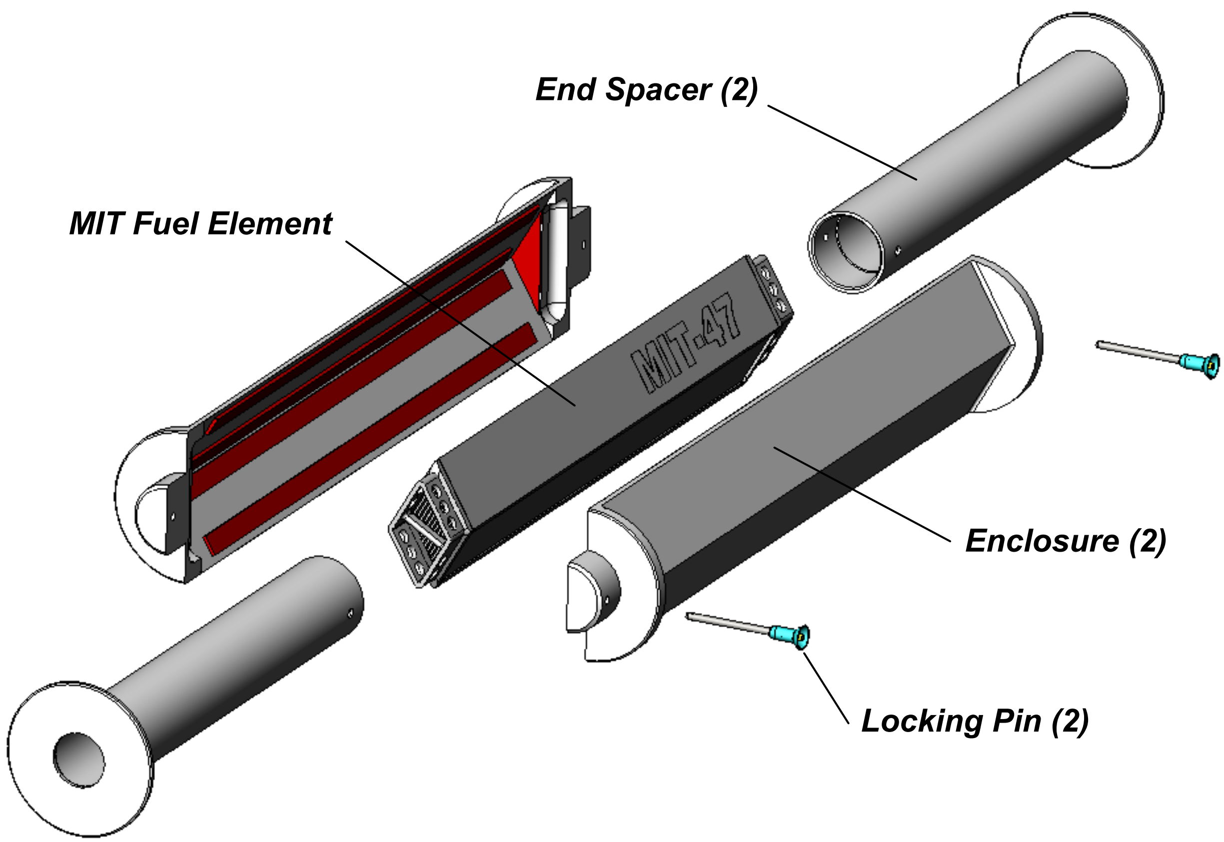

Figure 1.2-6 – MIT Fuel Handling Enclosure

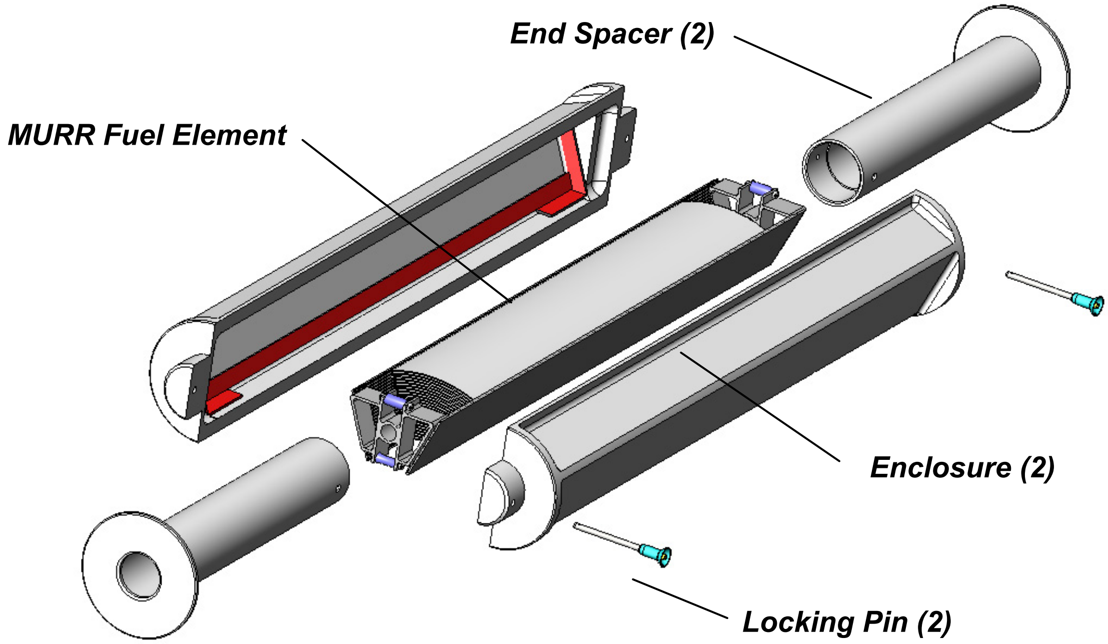

Figure 1.2-7 – MURR Fuel Handling Enclosure

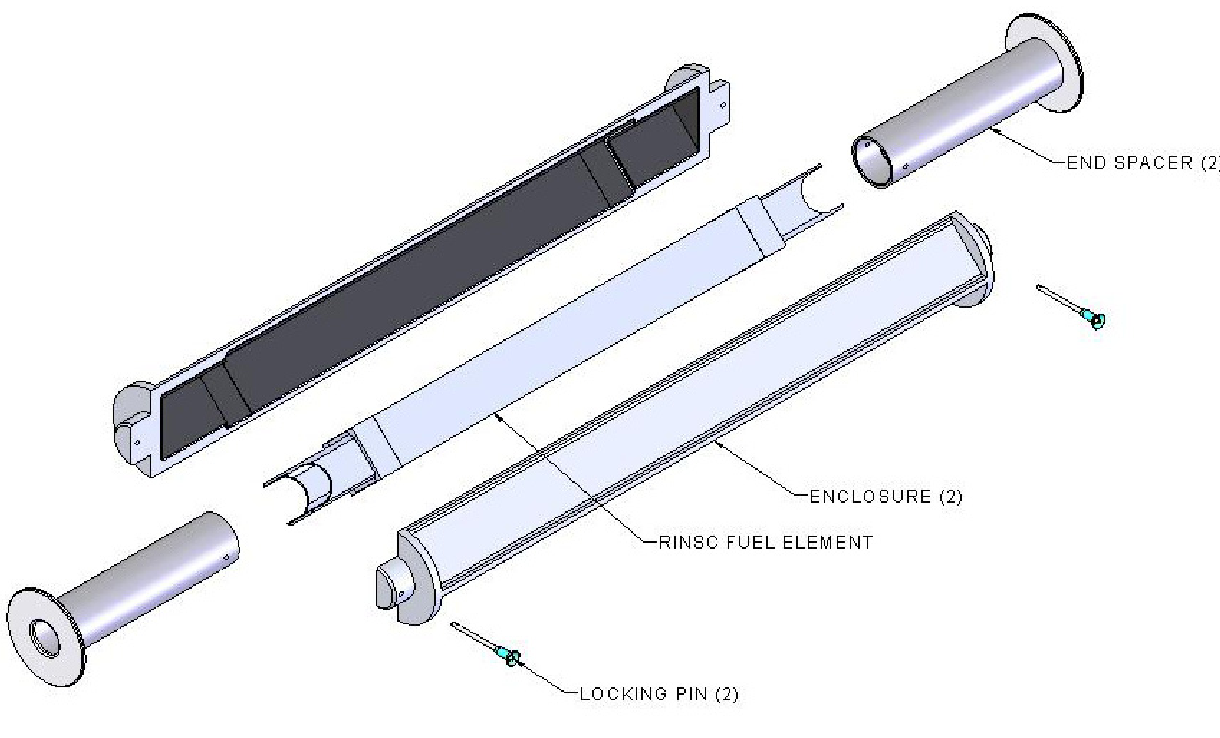

Figure 1.2-8 – RINSC Fuel Handling Enclosure

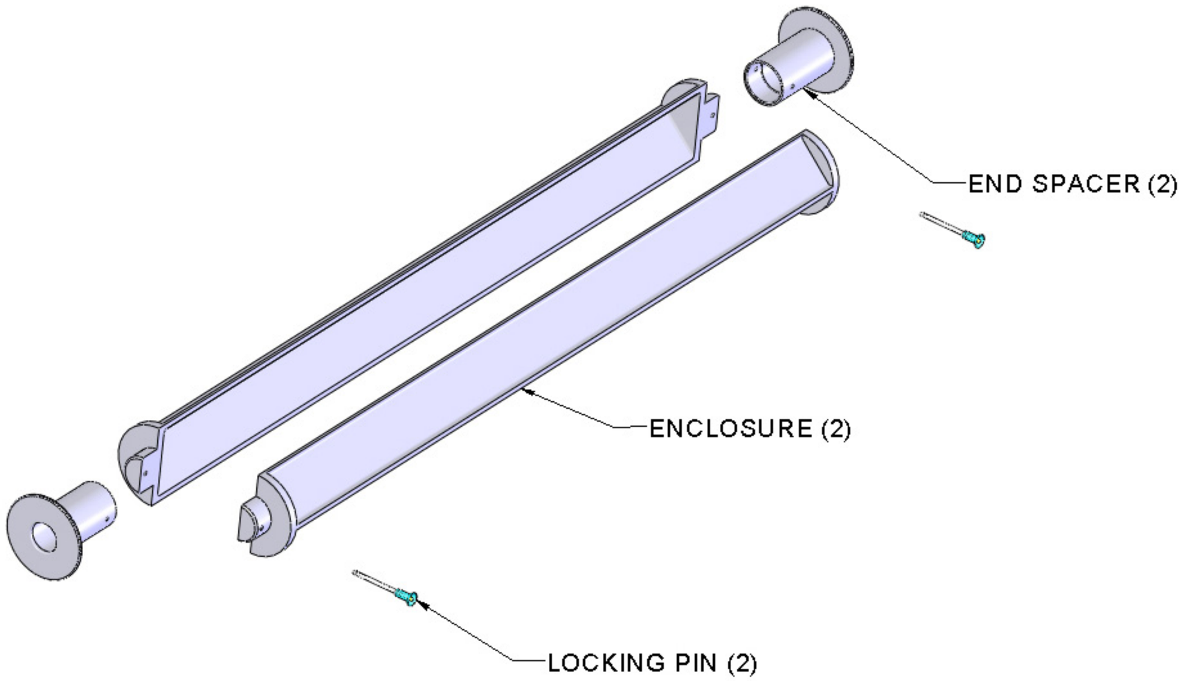

Figure 1.2-9 – Small Quantity Fuel Handling Enclosure

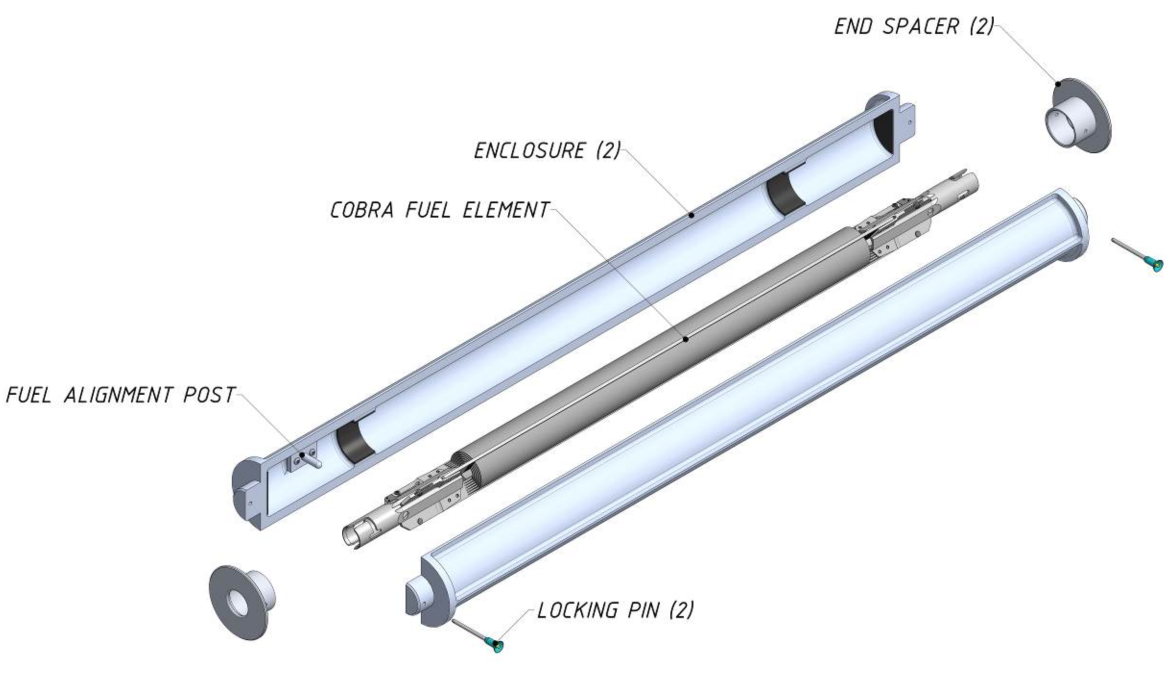

Figure 1.2-10 – Cobra Element Fuel Handling Enclosure

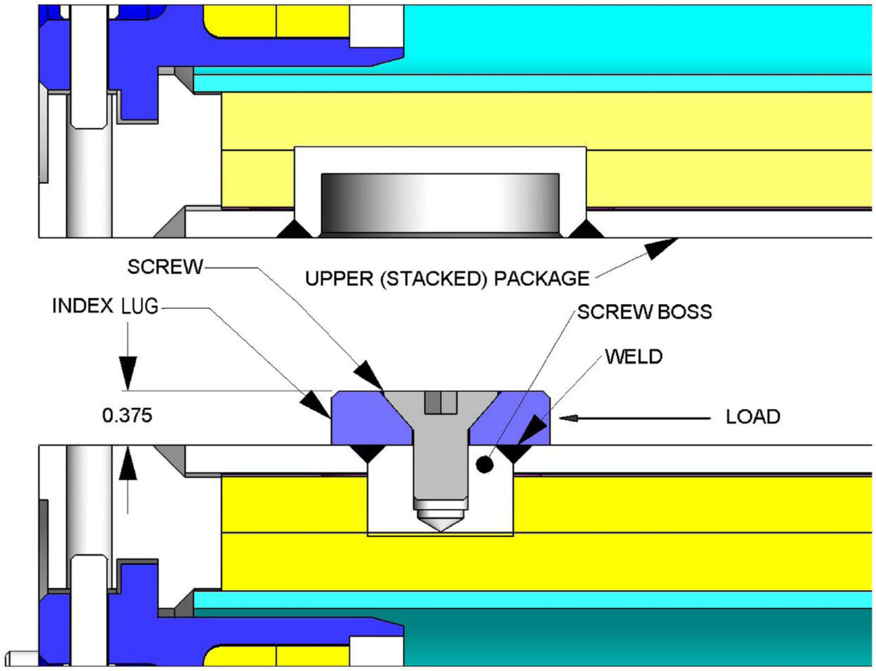

Figure 1.2-11 - Index Lug and Mating Pocket of Stacked Packages

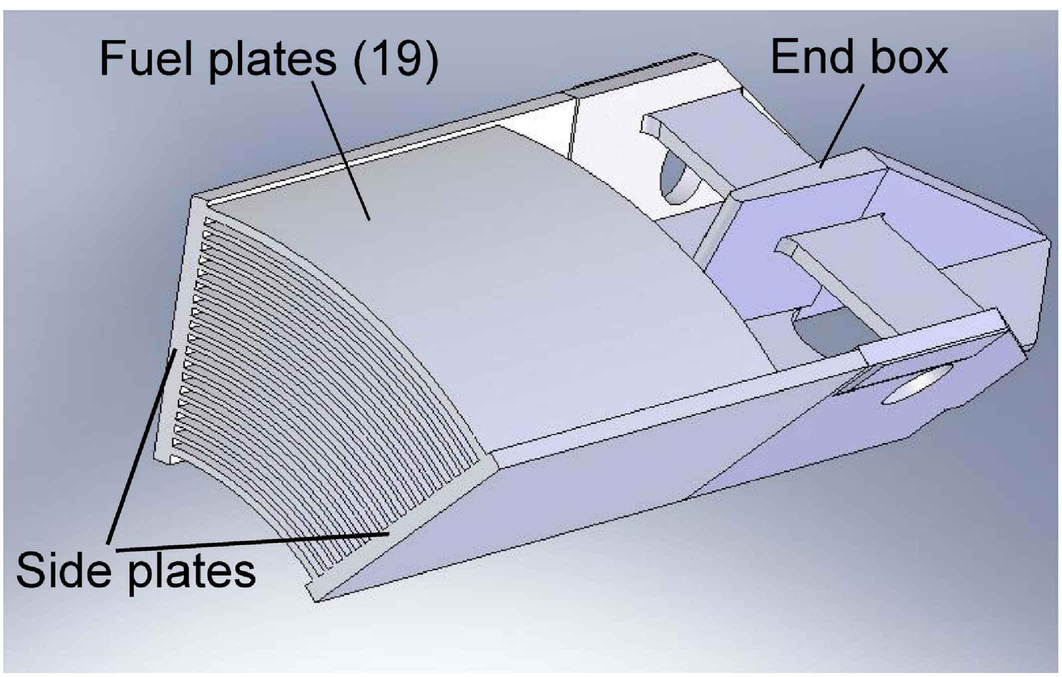

Figure 1.2-12 - ATR Fuel Element – Section View

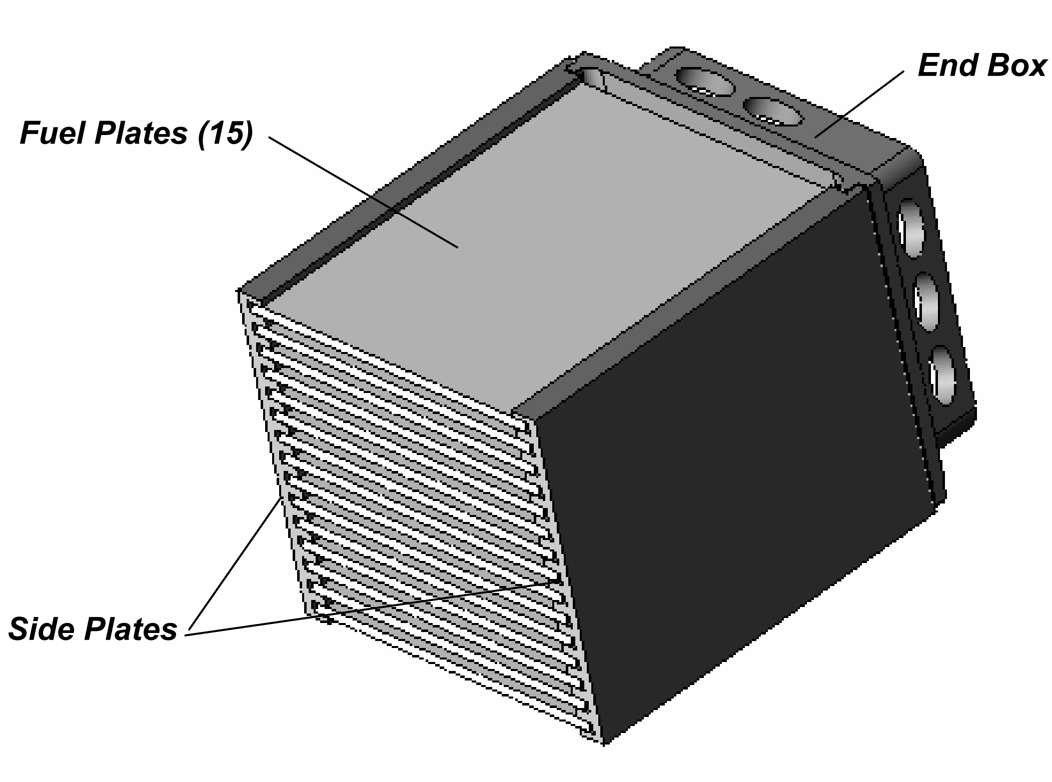

Figure 1.2-13 - MIT Fuel Element – Section View

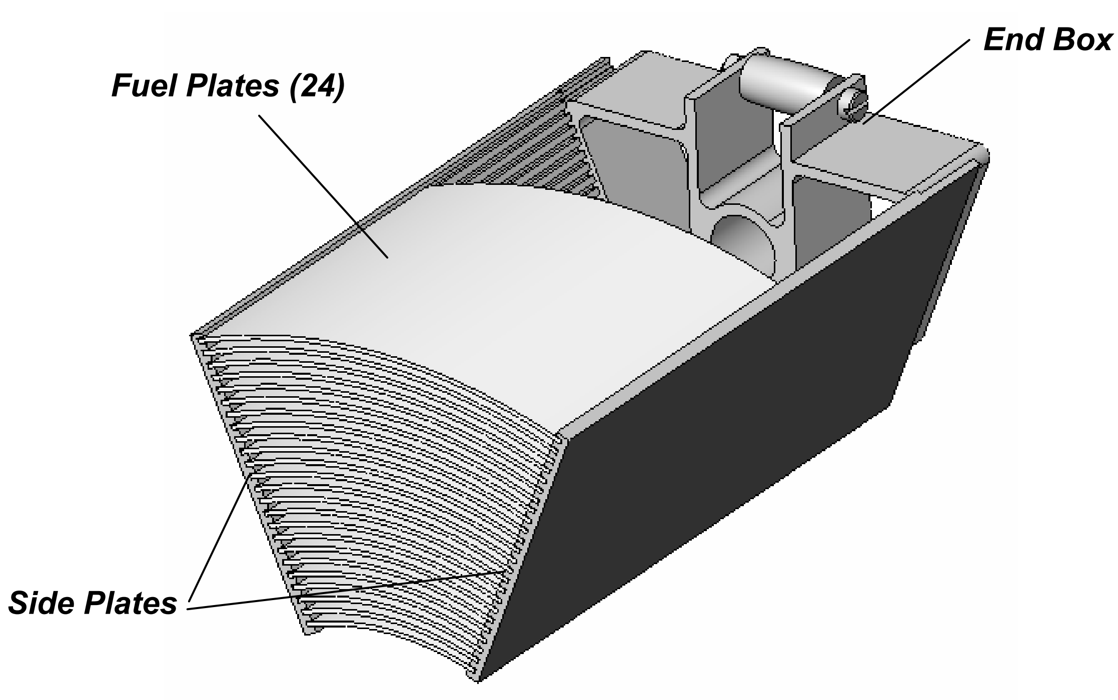

Figure 1.2-14 - MURR Fuel Element – Section View

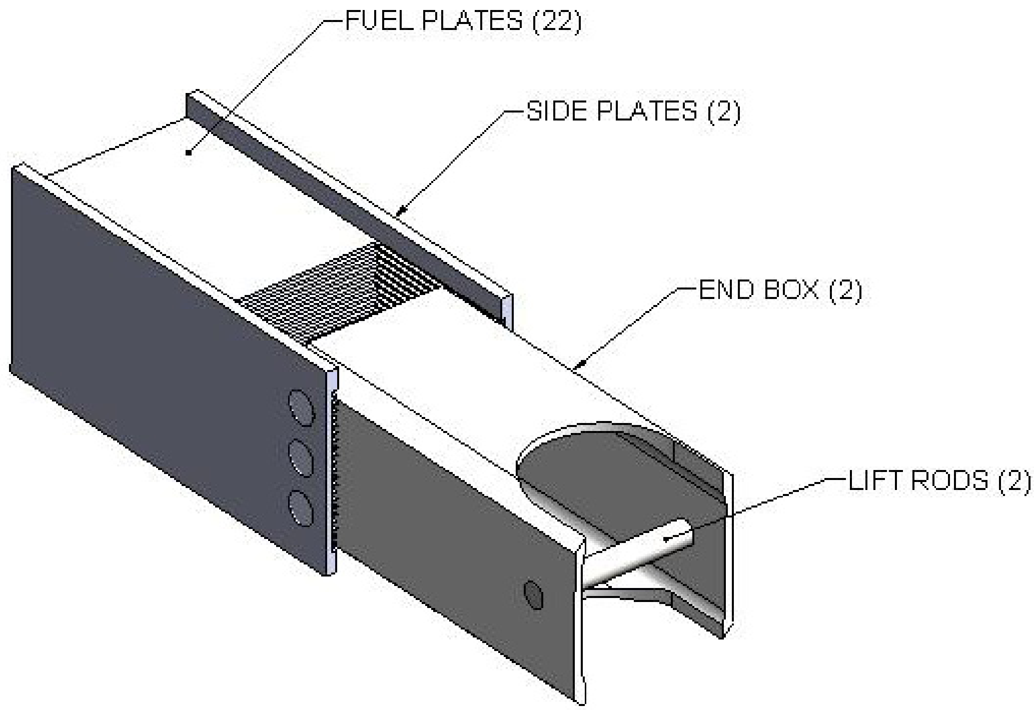

Figure 1.2-15 - RINSC Fuel Element – Section View

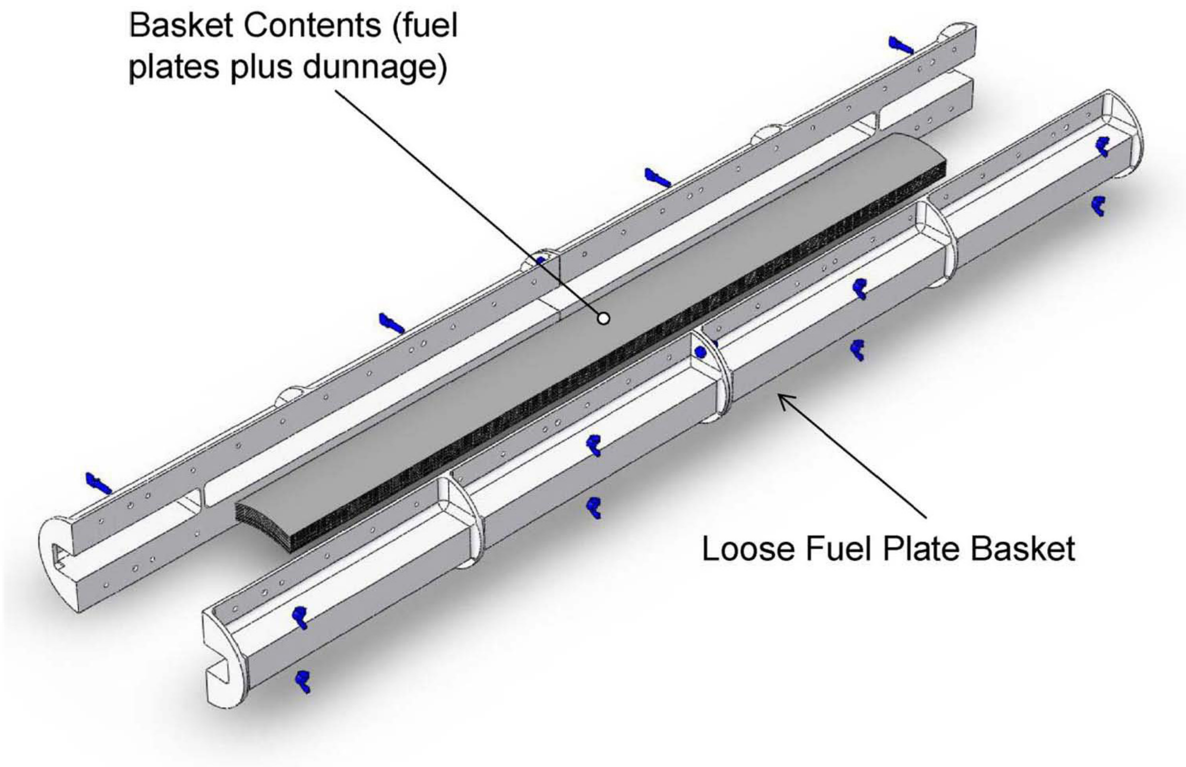

Figure 1.2-16 - Loose Fuel Plate Basket – Exploded View

Security-Related Information Figure Withheld Under 10 CFR 2.390.

Figure 1.2-17 – AFIP Element

Security-Related Information Figure Withheld Under 10 CFR 2.390.

Figure 1.2-19 – DDE-MITR Element

Security-Related Information Figure Withheld Under 10 CFR 2.390.

Figure 1.2-20 – DDE-MURR Element

Security-Related Information Figure Withheld Under 10 CFR 2.390.

Figure 1.2-21 – ATR U-Mo Demonstration Element

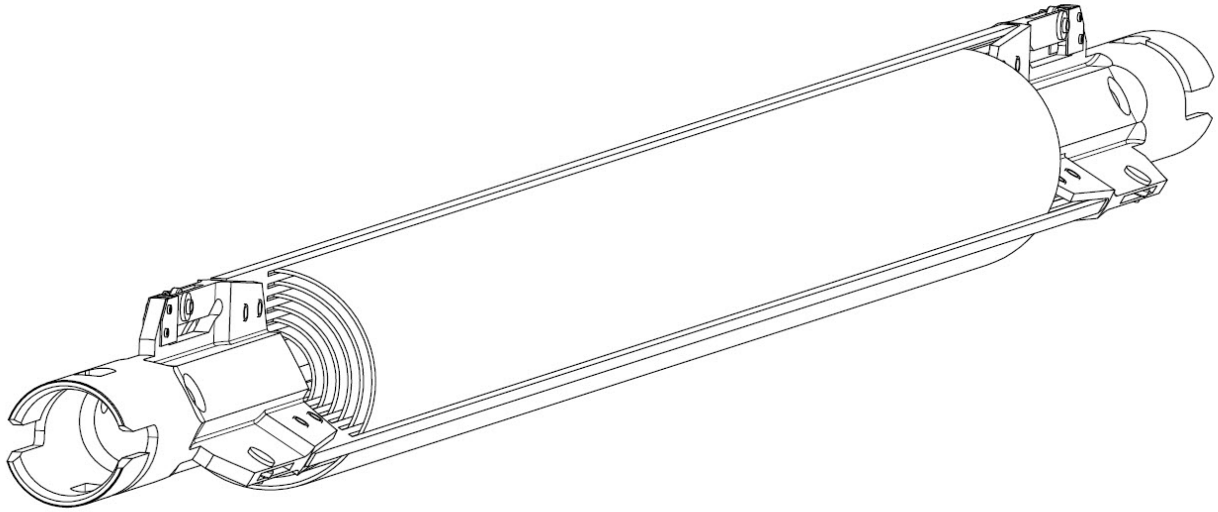

Figure 1.2-22 – Cobra Fuel Element

1.2.3 Special Requirements for Plutonium

Because the ATR FFSC does not contain any plutonium, this section does not apply.

1.2.4 Operational Features

There are no operationally complex features in the ATR FFSC. All operational features are readily apparent from an inspection of the drawings provided in Appendix 1.3.2, *Packaging General Arrangement Drawings*. Operation procedures and instructions for loading, unloading, and preparing an empty ATR FFSC for transport are provided in Chapter 7.0, *Operating Procedures*.

1.3 Appendix

1.3.1 Glossary of Terms

AFIP –	ATR Full-size plate In Flux trap Position
ANSI –	American National Standards Institute.
ASME B&PV Code –	American Society of Mechanical Engineers Boiler and Pressure Vessel Code.
ASTM –	American Society for Testing and Materials.
ATR FFSC –	Advanced Test Reactor Fresh Fuel Shipping Container
AWS –	American Welding Society.
DDE –	Design Demonstration Element
HAC –	Hypothetical Accident Conditions.
NCT –	Normal Conditions of Transport.
Closure –	The ATR FFSC package component used to close the package.
Body –	The ATR FFSC package component which houses the payload.
Fuel element	Fuel element and fuel assembly are used interchangeably throughout this document to be the ATR, MIT, MURR, RINSC, AFIP, Cobra, or DDE fuel element as described in Section 1.2.2, *Contents*.
Index lug –	A thick washer like component secured to the package body at the lift point locations. The index lug provides shear transfer capability between stacked packages.
Pocket –	A recessed feature on the package body that accepts the index lug when packages are stacked.
Fuel Handling Enclosure (FHE)–	Aluminum fabrications used to protect the ATR, MIT, MURR, RINSC, and Cobra fuel elements from handling damage. The enclosures are faced with neoprene at locations where the fuel element contacts the FHE to minimize fretting of the fuel element at the contact points.
Loose fuel plate basket (LFPB) –	A machined aluminum container in which the unassembled fuel element plates are secured during transport in the ATR FFSC. The loose plate basket is a geometry based criticality control component.

Small Quantity Payload FHE (SQFHE) – see Fuel Handling Enclosure (FHE).

1.3.2 Packaging General Arrangement Drawings

The packaging general arrangement drawings consist of:

- 60501-10, *ATR Fresh Fuel Shipping Container SAR Drawing,* 5 sheets
- 60501-20, *Loose Plate Basket Assembly ATR Fresh Fuel Shipping Container SAR Drawing,* 1 sheet
- 60501-30, *Fuel Handling Enclosure, ATR Fresh Fuel Shipping Container SAR Drawing,* 1 sheet
- 60501-40, *MIT Fuel Handling Enclosure, ATR Fresh Fuel Shipping Container SAR Drawing,* 1 sheet
- 60501-50, *MURR Fuel Handling Enclosure, ATR Fresh Fuel Shipping Container SAR Drawing,* 1 sheet.
- 60501-60, *RINSC Fuel Handling Enclosure, ATR Fresh Fuel Shipping Container SAR Drawing,* 1 sheet.
- 60501-70, *Small Quantity Payload Fuel Handling Enclosure*, *ATR Fresh Fuel Shipping Container SAR Drawing,* 1 sheet.
- 60501-90, *Cobra Fuel Handling Enclosure, ATR Fresh Fuel Shipping Container SAR Drawing,* 1 sheet.

60501-10 | 1 | 3

Security-Related Information Figure Withheld Under 10 CFR 2.390.

REL	B. HARGIS		12/6/11
APPD	D. Hillstrom		12/5/11
APPD	C. TEMUS		12/6/11
ENGR	S. KLEIN		12/5/11
QA	K. KING		12/5/11
CHECK	A. ROSS		5 Dec 11
DRAWN	R. LE		12/01/11

AREVA

AREVA Federal Services LLC
Packaging Projects
Tacoma, WA

ATR FRESH FUEL SHIPPING CONTAINER
SAR DRAWING

MACHINE TOLERANCES:
FRACTIONS ± 1/4 2 PLACE DECIMALS ± .06
ANGLES ± 2° 1 PLACE DECIMALS ± .2

WELD & FORMED TOLERANCES:
FRACTIONS ± 1/4 2 PLACE DECIMALS ± .1
ANGLES ± 2° 1 PLACE DECIMALS ± .2

SCALE: 1:4 | WT. ~240 LBS
REV: 3 | SHEET 1 OF 5
DWG SIZE D | DWG NO. 60501-10
CADFILE: 6050110SAR3.SLDDRW
DWG-3000401-001

Security-Related Information Figure
Withheld Under 10 CFR 2.390.

Security-Related Information Figure
Withheld Under 10 CFR 2.390.

60501-10 | 4 | 3

Security-Related Information Figure Withheld Under 10 CFR 2.390.

REV: 3 SHEET 4 OF 5
DWG NO. 60501-10

60501-10 5 3

Security-Related Information Figure
Withheld Under 10 CFR 2.390.

REV: 3 SHEET 5 OF 5
DWG NO.
60501-10

60501-20 | 1 | 1

Security-Related Information Figure Withheld Under 10 CFR 2.390.

REL	B. HARGIS	B Hargis	3/27/08
APPD			
APPD	AT KEE		3/26/08
ENGR	B FLANAGAN		3/26/08
QA	B. COUNTERMAN		3/24/08
CHECK	DL STEVENSON		3-24-08
DRAWN	R. LE		3/24/08

AREVA

PACKAGING TECHNOLOGY, INC.
TACOMA, WA

LOOSE PLATE BASKET ASSEMBLY
ATR FRESH FUEL SHIPPING CONTAINER
SAR DRAWING

MACHINE TOLERANCES:
FRACTIONS ± 1/4 2 PLACE DECIMALS ± .06
ANGLES ± 2° 1 PLACE DECIMALS ± .2

WELD & FORMED TOLERANCES:
FRACTIONS ± 1/4 2 PLACE DECIMALS ± .1
ANGLES ± 2° 1 PLACE DECIMALS ± .2

SCALE: 1/4 | WT. ~84 LBS
REV: 1 | SHEET 1 OF 1
DWG SIZE D | DWG NO. 60501-20
CADFILE: 6050120SAR1.SLDDRW
DWG 3000249

60501-30 | 1 | 1

Security-Related Information Figure Withheld Under 10 CFR 2.390.

REL	B. HARGIS	BHargis	3/27/08
APPD			
APPD	AT KEE		3/26/08
ENGR	B FLANAGAN		3/26/08
QA	B. COUNTERMAN		3/24/08
CHECK	DL STEVENSON		3-24-08
DRAWN	R. LE		3/24/08

AREVA

PACKAGING TECHNOLOGY, INC.
TACOMA, WA

FUEL HANDLING ENCLOSURE
ATR FRESH FUEL SHIPPING CONTAINER
SAR DRAWING

MACHINE TOLERANCES:
FRACTIONS ± 1/4 2 PLACE DECIMALS ± .06
ANGLES ± 2° 1 PLACE DECIMALS ± .2

WELD & FORMED TOLERANCES:
FRACTIONS ± 1/4 2 PLACE DECIMALS ± .1
ANGLES ± 2° 1 PLACE DECIMALS ± .2

SCALE: 1/4
WT. ~15 LBS
REV: 1
SHEET 1 OF 1
DWG SIZE D
DWG NO. 60501-30
CADFILE: 6050130SAR1.SLDDRW
DWG-3000250

DWG NO 60501-40 | SH 1 | REV 0

Security-Related Information Figure
Withheld Under 10 CFR 2.390.

REL	[illegible]	8-14-08
APPD	[illegible]	8/14/08
APPD	[illegible]	8/14/08
ENGR	[illegible]	8/14/08
QA	[illegible]	8/14/08
CHECK	[illegible]	8-14-08
DRAWN	DC SHELDON	8/14/2008

AREVA

AREVA Federal Services LLC
Packaging Projects
Tacoma, WA 98402

DWG TITLE
MIT FUEL HANDLING ENCLOSURE
ATR FRESH FUEL SHIPPING CONTAINER
SAR DRAWING

MACHINE TOLERANCES:
FRACTIONS ± 1/4 | 2 PLACE DECIMALS ± .06
ANGLES ± 2° | 1 PLACE DECIMALS ± .2

WELD & FORMED TOLERANCES:
FRACTIONS ± 1/4 | 2 PLACE DECIMALS ± .1
ANGLES ± 2° | 1 PLACE DECIMALS ± .2

SCALE: SHOWN	WT. ~ 25 LBS
REV: 0	SHEET 1 OF 1
DWG SIZE D	DWG NO. 60501-40
	CADFILE: 6050140A.SI DDRW

DWG-3000784-000

DWG NO 60501-50 SH 1 REV 0

Security-Related Information Figure Withheld Under 10 CFR 2.390.

REL	[signature]	8-14-08
APPD	[signature]	8/14/08
APPD	[signature]	8/14/08
ENGR	[signature]	8/14/08
QA	[signature]	8/14/08
CHECK	[signature]	8-14-08
DRAWN	DC SHELDON	8/14/2008

AREVA

AREVA Federal Services LLC
Packaging Projects
Tacoma, WA 98402

DWG TITLE MURR FUEL HANDLING ENCLOSURE
ATR FRESH FUEL SHIPPING CONTAINER
SAR DRAWING

MACHINE TOLERANCES:
FRACTIONS ± 1/4 ANGLES ± 3° 2 PLACE DECIMALS ± .06 1 PLACE DECIMALS ± .3

WELD & FORMED TOLERANCES:
FRACTIONS ± 1/4 ANGLES ± 2° 2 PLACE DECIMALS ± .1 1 PLACE DECIMALS ± .2

SCALE: SHOWN | WT. ~ 30 LBS
REV: 0 | SHEET 1 OF 1
DWG SIZE D | DWG NO. 60501-50
CADFILE: [illegible]
DWG-3000785-000

DWG NO 60501-60 REV 0 SH 1

Security-Related Information Figure Withheld Under 10 CFR 2.390.

AREVA
JUL 20 2010
Records Management
Released By Bterqis

REV	DESCRIPTION	DRAWN	CHECKER	VERIFIED

REVISION HISTORY

	NAME/SIGNATURE	DATE
APPD		
APPD	P NOSS	7/15/10
ENGR	M KAMALIAN	7/15/10
QA	B COUNTERMAN	7/15/10
CHECK	DL STEVENSON	7-15-10
DRAWN	P PIKULIN	7-6-10

AREVA
AREVA Federal Services LLC
Packaging Projects
Tacoma, WA 98402

DWG TITLE RINSC FUEL HANDLING ENCLOSURE
ATR FRESH FUEL SHIPPING CONTAINER
SAR DRAWING

MACHINE TOLERANCES
FRACTIONS ± 1/4 2 PLACE DECIMALS ± .06
ANGLES ± 2° 1 PLACE DECIMALS ± .2

WELD & FORMED TOLERANCES
FRACTIONS ± 1/4 2 PLACE DECIMALS ± .1
ANGLES ± 2° 1 PLACE DECIMALS ± .2

SCALE 1:6 | WT. ~30LBS
REV 0 | SHEET 1 OF 1
DWG SIZE D | DWG NO 60501-60
CADFILE 60501600.SLDDRW
DWG-3003601-000

DWG NO	REV	SH
60501-70	0	1

Security-Related Information Figure Withheld Under 10 CFR 2.390.

Released By BHargis

AREVA

MAR 1 2011

Records Management

REV	DESCRIPTION	DRAWN	CHECKER	VERIFIED

REVISION HISTORY

	NAME/SIGNATURE	DATE
APPD	D.H. Wetrom	3-29-11
APPD	C. Temus	3-29-11
ENGR	Tom Castelli	3-25-11
QA	Kevin King	3-25-11
CHECK	DL STEVENSON	3-25-11
DRAWN	P PIKULIN	3-25-11

AREVA

AREVA Federal Services LLC
Packaging Projects
Tacoma, WA 98402

DWG TITLE
SMALL QUANTITY PAYLOAD FUEL HANDLING ENCLOSURE
ATR FRESH FUEL SHIPPING CONTAINER
SAR DRAWING

MACHINE TOLERANCES:
FRACTIONS ± 1/4 | 2 PLACE DECIMALS ± .06
ANGLES ± 2° | 1 PLACE DECIMALS ± .2

WELD & FORMED TOLERANCES:
FRACTIONS ± 1/4 | 2 PLACE DECIMALS ± .1
ANGLES ± 2° | 1 PLACE DECIMALS ± .2

SCALE: 1:4 | WT. -
REV: 0 | SHEET 1 OF 1

DWG SIZE D | DWG NO. 60501-70

CADFILE: 60501700.SLDDRW

DWG-3004623-000

DWG NO 60501-90 REV 0 SH 1

Security-Related Information Figure Withheld Under 10 CFR 2.390.

REV	DESCRIPTION	DRAWN	CHECKER	VERIFIED
REVISION HISTORY				

	NAME/SIGNATURE	DATE
EM	[illegible]	5/31/16
RE	P. Noss [illegible]	5/27/16
TECH CHK	S. Klein [illegible]	5/27/16
DFTG CHK	S. [illegible]	5-27-16
DRAWN	P. PIKULIN	5/27/16

NEXT ASSY	FINAL ASSY
NA	NA

THIRD ANGLE PROJECTION

UNLESS OTHERWISE SPECIFIED:
INTERPRET DRAWINGS & TOLERANCES PER ASME Y14.5-2009 (REVISION OF ASME Y14.5M-1994)
INTERPRET WELD CALLOUTS PER ANSI/AWS A2.4
DIMENSIONS ARE IN INCHES

AREVA
AREVA Federal Services LLC
Packaging Projects
Federal Way, WA 98003

DWG TITLE
COBRA FUEL HANDLING ENCLOSURE
ATR FRESH FUEL SHIPPING CONTAINER
SAR DRAWING

TOLERANCE BLOCK
FRACTIONS ± 1/4 2 PLACE DECIMALS ± .06
ANGLES ± 2° 1 PLACE DECIMALS ± .2

SCALE: 1:4 | WT. -
REV: 0 | SHEET 1 OF 1
DWG SIZE D | DWG NO. 60501-90
CADFILE: 60501-000.SLDDRW
DWG-3019051-000

2.0 STRUCTURAL EVALUATION

This section presents evaluations demonstrating that the ATR FFSC package meets all applicable structural criteria. The ATR FFSC packaging, consisting of the body and closure, is evaluated and shown to provide adequate protection for each payload listed in Section 1.2.2, *Contents*. Each payload fuel element is transported in a fuel handling enclosure (FHE) within the ATR FFSC package. The loose fuel plate basket (LFPB) is evaluated to contain only loose fuel plates associated with the ATR fuel element. The small quantity payload loose fuel plates, fuel elements, or foils are contained within a small quantity fuel handling enclosure.

Normal conditions of transport (NCT) and hypothetical accident condition (HAC) evaluations are performed to address 10 CFR §71[1] performance requirements primarily through physical testing. Physical demonstration by testing, including the free drop and puncture events, consists of certification testing utilizing two full-scale certification test units (CTU-1 and CTU-2). CTU-1 included the ATR fuel element payload and CTU-2 included the ATR LFPB and loose plates payload. Certification testing has demonstrated that the key performance objective of criticality control will be met by the ATR FFSC package. Details of the certification test program are provided in Appendix 2.12.1, *Certification Tests on CTU-1*, and Appendix 2.12.2, *Certification Tests on CTU-2*. The evaluation for the MIT and MURR fuel elements is provided in Appendix 2.12.3, *Structural Evaluation for MIT and MURR Fuel*.

2.1 Structural Design

2.1.1 Discussion

The ATR FFSC is a two part packaging consisting of the body and the closure. The body is a single weldment that features square tubing as an outer shell and round tubing for the payload cavity. The closure engages with the body using a bayonet style design. There are four lugs, uniformly spaced on the closure that engages with four slots in the mating body feature. The closure is secured by retracting two spring loaded pins, rotating the closure through approximately 45º, and releasing the spring loaded pins such that the pins engage with mating holes in the body. When the pins are properly engaged with the mating holes the closure is locked.

With the exception of several minor components, all steel used in the ATR FFSC packaging is of a Type 304 stainless steel. Components are joined using full-thickness fillet welds (i.e., fillet welds whose leg size is nominally equal to the lesser thickness of the parts joined) and full and partial penetration groove welds. The fuel containers for the package, the FHEs and the LFPB, are principally of aluminum construction and secured with stainless steel fasteners. The FHEs are a fabrication and the LFPB consists of four machined aluminum components.

A comprehensive discussion of the ATR FFSC packaging design and configuration is provided in Section 1.2, *Package Description*.

[1] Title 10, Code of Federal Regulations, Part 71 (10 CFR §71), *Packaging and Transportation of Radioactive Material*, 01-01-06 Edition.

2.1.2 Design Criteria

The ATR FFSC package has been designed to meet the majority of applicable structural requirements of 10 CFR §71 through physical testing. The design objectives for the package are threefold:

1. For NCT, demonstrate that the ATR FFSC package contains the payload without dispersal and that it does not experience a significant reduction in its effectiveness to withstand HAC; and
2. For HAC, demonstrate that the ATR FFSC package contains the payload without dispersal, consistent with conservative bounding assumptions utilized in the criticality analysis.
3. For HAC, demonstrate that the insulation used in the ATR FFSC package remains in place, to protect the payload from excessive heat from the thermal test, within the assumptions utilized in the thermal analysis.

Consequently, the design criteria for NCT are that the ATR FFSC package exhibit only minor damage subsequent to the NCT conditions and tests, including no damage that would materially affect the outcome of the subsequent HAC tests.

For HAC, the design criteria is that the payload will be retained within the packaging subsequent to the HAC test series of free drop, puncture, thermal, and the immersion test of 10 CFR §71.73(c)(5), or subsequent to immersion of an undamaged specimen per 10 CFR §71.73(c)(6).

Material properties are controlled by the acquisition of critical components to ASTM standards, testing, and process control, as described in Section 2.2, *Materials*. Lifting devices that are a structural part of the package are designed with a minimum safety factor of three against yielding. The index lugs located at the top of the package are considered a tiedown devices and are designed to withstand the loading requirements per 10 CFR §71.45(b)(1).

2.1.2.1 Miscellaneous Structural Failure Modes

2.1.2.1.1 Brittle Fracture Assessment

The steel materials utilized in the ATR FFSC package provide adequate fracture toughness. All critical structural components of the packaging are made of Type 304 stainless steel and have a nil ductility transition temperature less than -40ºF (-40ºC). Therefore, brittle fracture is not a concern for the ATR FFSC packaging.

To confirm the performance of the uranium aluminide (UAl_x) fuel types at reduced temperatures, the ATR fuel element in CTU-1, was subjected to two HAC drops with the payload at approximately -20ºF (-29ºC). Following all CTU-1 testing, as discussed in Appendix 2.12.1, *Certification Tests on CTU-1*, the package was disassembled and the payload inspected. Upon inspection, the performance of both the payload and packaging, including the reduced temperature tests, was satisfactory. Following all testing, the payload remained within the assumptions presented in Section 6.0, *Criticality Evaluation*.

2.1.2.1.2 Fatigue Assessment

Normal operating cycles do not present a fatigue concern for the ATR FFSC. The packaging does not retain pressure, and consequently fatigue due to pressure cycling cannot occur. Since all structural components of the packaging are made of the same alloy, and since thermal gradients are small, thermally-induced fatigue is not of concern. Since the packaging is normally handled on a pallet, the lifting features of the packaging are infrequently used, and fatigue of the lifting load path is not of concern.

The only components which are routinely handled are the closure and the fuel handling enclosures and loose plate basket. The closure is designed as a bayonet-type attachment with two spring-loaded locking pins which prevent rotation during transport. Neither the bayonet lugs nor the locking pins experience any significant loading (such as preload or other repeating mechanical loads) in routine usage. If damage to these components were to occur, it will be identified during the inspections discussed in Section 7.1.1, *Preparation for Loading*. Consequently, fatigue of the closure components is not of concern.

The fuel handling structures (fuel handling enclosures and loose plate basket) are simple structures that do not have significant handling loads. These structures are fully exposed to view during loading and unloading, and can be inspected to ensure integrity.

For these reasons, normal operating cycles are not a failure mode of concern for the ATR FFSC packaging. Fatigue associated with normal vibration over the road is discussed in Section 2.6.5, *Vibration*.

2.1.2.1.3 Buckling Assessment

Certification testing has demonstrated that buckling of the ATR FFSC package does not occur as a result of any normal conditions of transport or as a result of the HAC primary test sequence (e.g., the free drop and puncture tests). Buckling of the ATR FFSC body is also shown to not be a concern during the 50 ft immersion test specified under 10 CFR §71.73(c)(6). A discussion of the response to the 50 ft immersion test is provided in Section 2.7.6, *Immersion – All Packages*.

2.1.3 Weights and Centers of Gravity

The maximum gross weight of the ATR FFSC package is 290 lb. The packaging component weights and maximum payload weights are summarized in Table 2.1-1. The U-Mo demonstration element is the same as ATR element payload except plates 5 through 15 are replaced with reduced enrichment plates of the same size, and plate 19 is solid aluminum. The Cobra HEU fuel element is bounded by a weight of 16 lb and the Cobra LEU fuel element is bounded by a weight of 20 lb. The greater of these is shown in Table 2.1-1. Due to symmetry of design, the center of gravity (CG) of the package is located essentially at the geometric center of the package. Regardless of payload, the center of gravity remains 35 inches from the face of the closure end and 4 inches from the bottom and sides of the package. The packaging components are illustrated in Figure 2.1-1 through Figure 2.1-7.

Table 2.1-1 – ATR FFSC Component Weights

Item	Weight, lb	
	Component	Assembly
ATR FFSC Packaging	- -	240
Body Assembly	230	- -
Closure Assembly	10	- -
Payload – ATR Fuel Assembly	- -	40
ATR Fuel Assembly	25	- -
ATR Fuel Handling Enclosure	15	- -
Payload – MIT Fuel Assembly	- -	35
MIT Fuel Assembly	10	- -
MIT Fuel Handling Enclosure	25	- -
Payload – MURR Fuel Assembly	- -	45
MURR Fuel Assembly	15	- -
MURR Fuel Handling Enclosure	30	- -
Payload – RINSC Fuel Assembly	- -	45
RINSC Fuel Assembly	17	- -
RINSC Fuel Handling Enclosure	28	- -
Payload – Fuel Plates	- -	50
ATR Loose Fuel Plates (including optional dunnage)	20	- -
Loose Fuel Plate Basket	30	- -
Payload – Small Quantities (except RINSC)	- -	50
MIT, MURR, or Cobra Loose Plates, AFIP Elements, U-Mo Foils, or DDEs	20	- -
Small Quantity Fuel Handling Enclosure	30	- -
Payload – ATR U-Mo Demo Element		47
ATR U-Mo Demo Element	32	--
ATR Fuel Handling Enclosure	15	--
Payload – Cobra Fuel Assembly	- -	48
Cobra Fuel Element (bounding)	20	--
Cobra Fuel Handling Enclosure	28	--
Total LFPB Loaded Package (maximum)	- -	290
Total MURR Loaded Package	- -	285
Total ATR Loaded Package	- -	280
Total MIT Loaded Package	- -	275
Total RINSC Loaded Package	- -	285
Total Small Quantity Loaded Package	- -	290
Total ATR U-Mo Demo Package	- -	287
Total Cobra Loaded Package	- -	288

2.1.4 Identification of Codes and Standards for Package Design

As a Type AF package, the ATR FFSC is designed to meet the performance requirements of 10 CFR 71, Subpart E. Compliance with these requirements is demonstrated via full scale testing of the package under both NCT and HAC, as documented in Section 2.12, *Appendices*. In addition, structural materials which are important to safety are specified using American Society for Testing and Materials (ASTM) standards as shown on the drawings in Appendix 1.3.2, *Packaging General Arrangement Drawings*. Welding procedures and personnel are qualified in accordance with the ASME Code, Section IX. All welds are visually examined on each pass per the requirements of AWS D1.6:1999[2] for stainless steel and AWS D1.2:2003[3] for aluminum. All welds which are important to safety are examined by liquid penetrant test on the final pass using procedures compliant with ASTM E165-02[4].

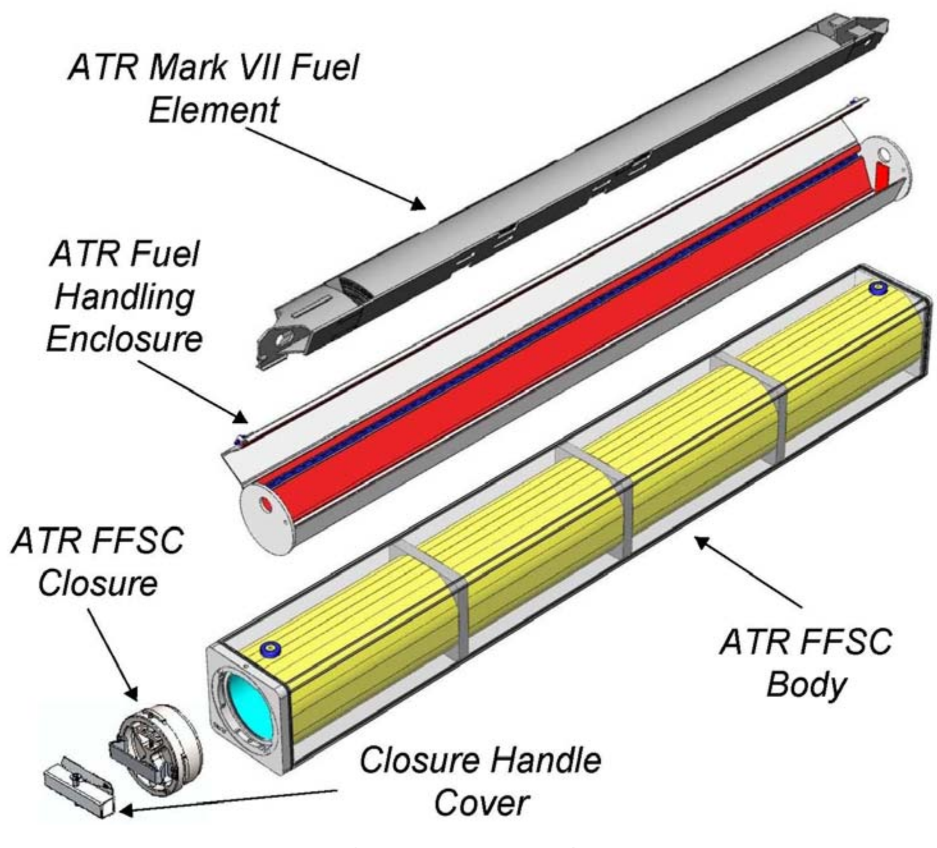

Figure 2.1-1 –Package Components (With ATR Fuel Element)

[2] ANSI/AWS D1.6:1999, *Structural Welding Code – Stainless Steel*, American Welding Society (AWS).

[3] ANSI/AWS D1.2:2003, *Structural Welding Code – Aluminum*, American Welding Society (AWS)

[4] American Society for Testing and Materials (ASTM International), ASTM E165-02, *Standard Test Method for Liquid Penetrant Examination*, Feb 2002.

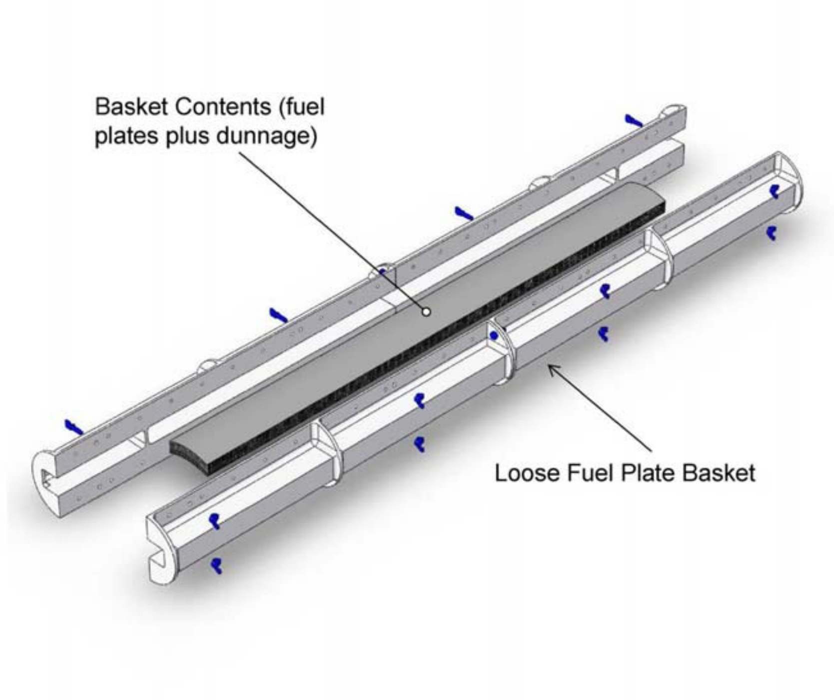

Figure 2.1-2 –Loose Fuel Plate Basket Components

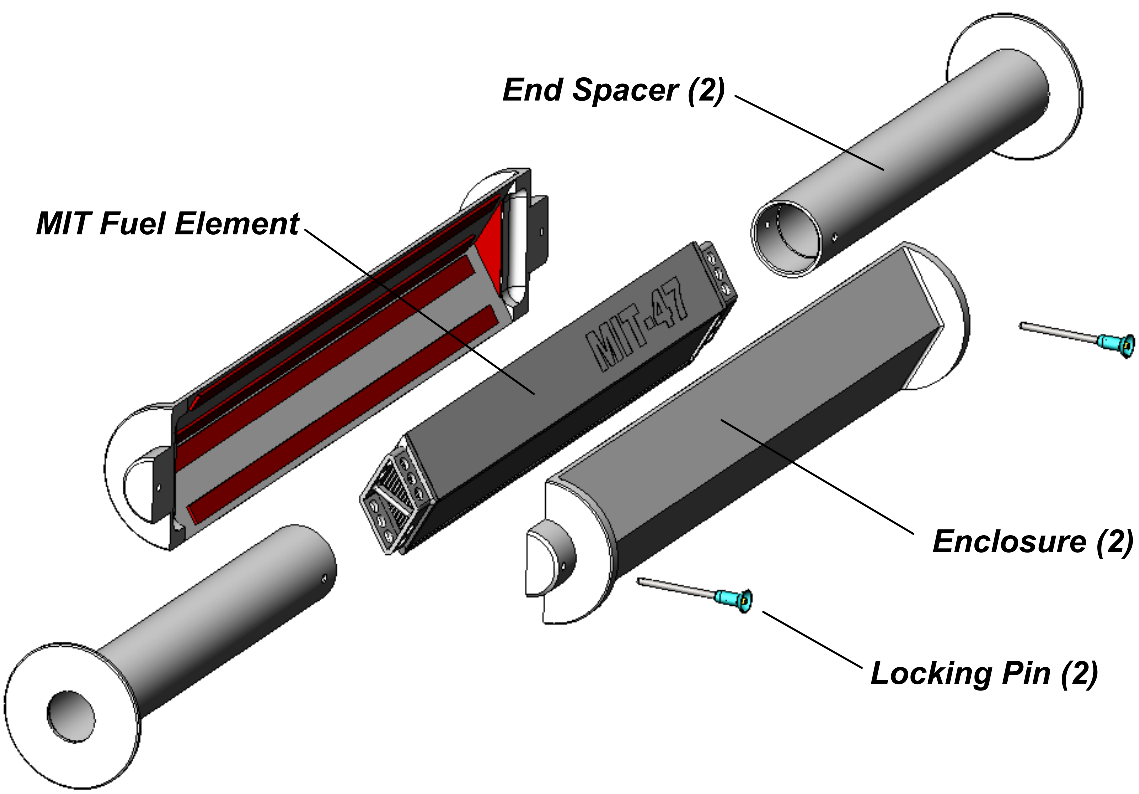

Figure 2.1-3 – MIT Fuel Handling Enclosure

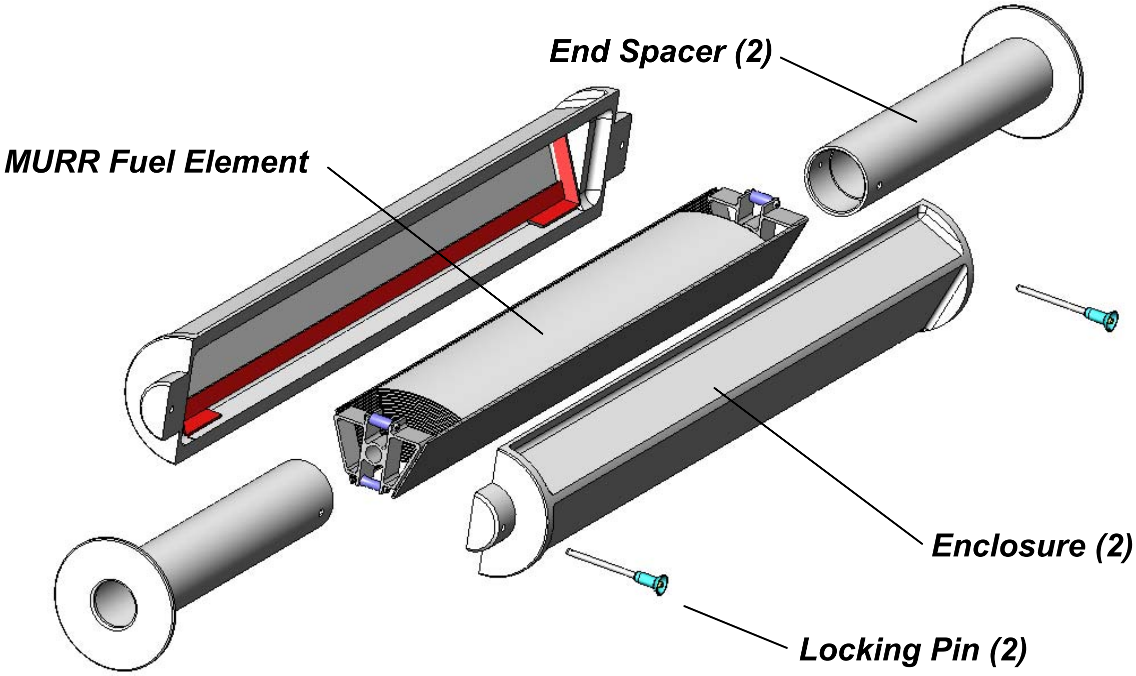

Figure 2.1-4 – MURR Fuel Handling Enclosure

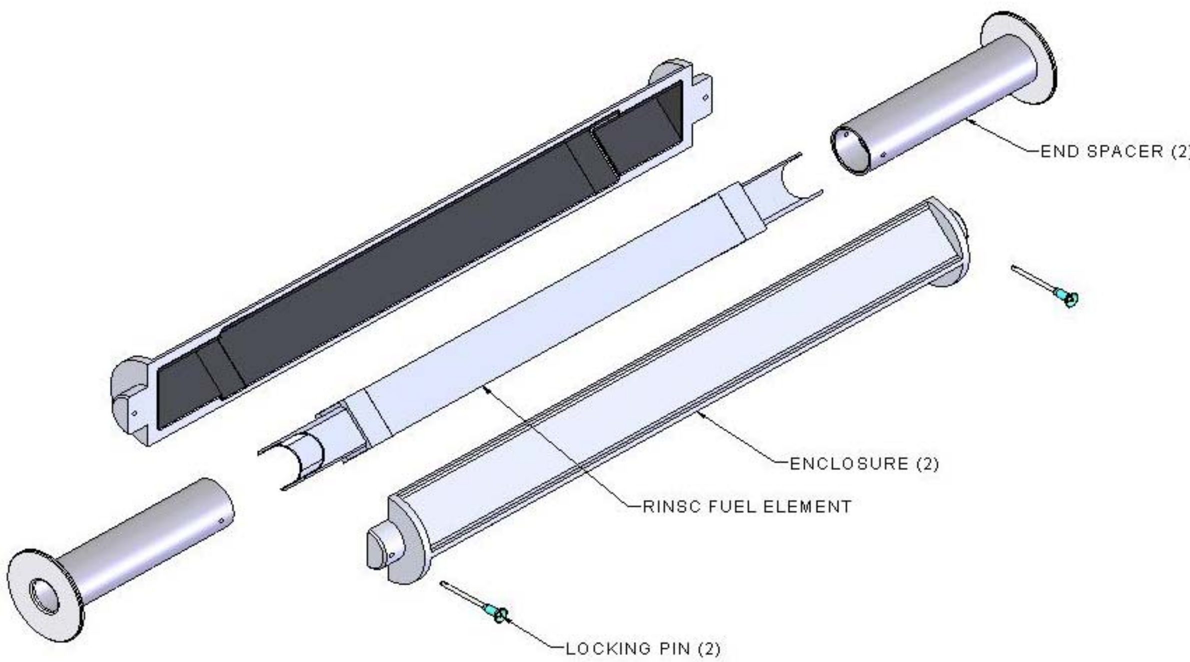

Figure 2.1-5 – RINSC Fuel Handling Enclosure

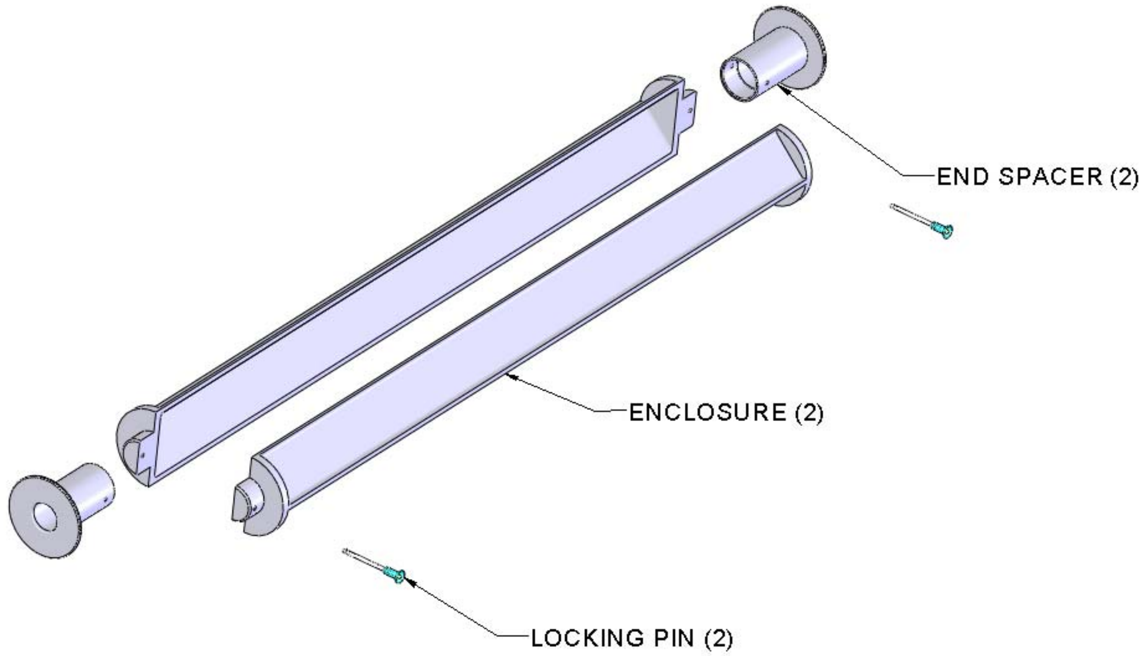

Figure 2.1-6 – Small Quantity Fuel Handling Enclosure

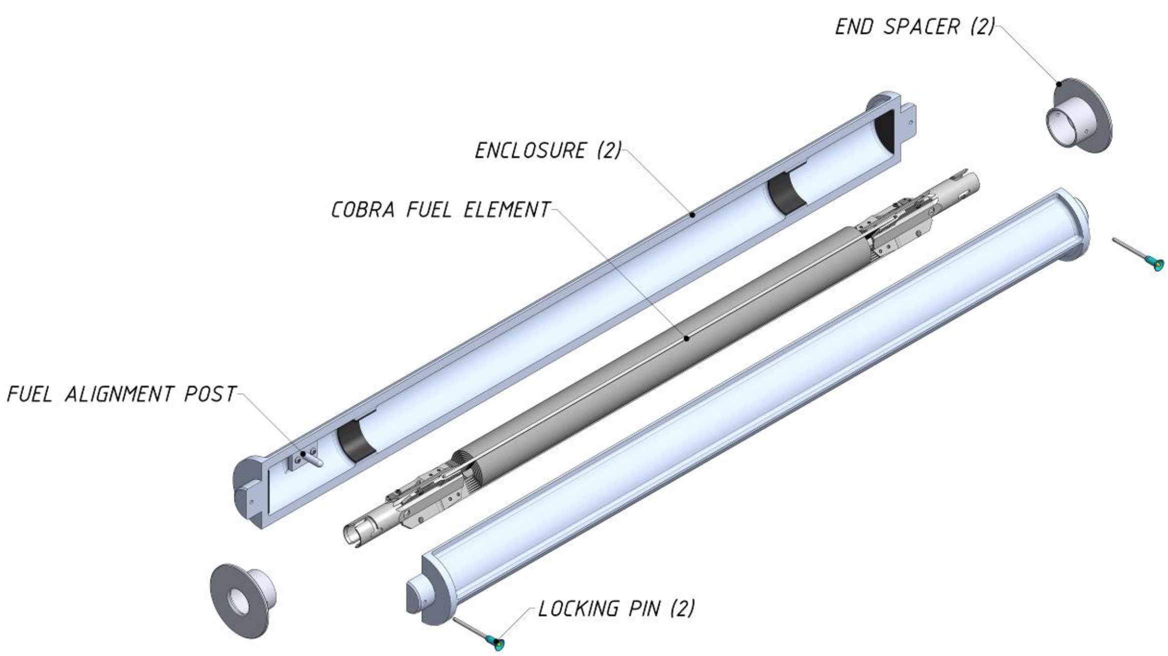

Figure 2.1-7 – Cobra Fuel Handling Enclosure

2.2 Materials

The ATR FFSC package is constructed primarily from Type 304 stainless steel structural materials. The drawings presented in Appendix 1.3.1, *Packaging General Arrangement Drawings*, delineate the specific materials used for each ATR FFSC packaging components.

2.2.1 Mechanical Properties and Specifications

Since the demonstration of compliance with the regulations is primarily via performance testing of full-scale prototypes, analytical structural evaluations are in general not performed. Properties of structural materials are controlled either by purchase to an ASTM or other standard or via a written specification.

2.2.1.1 Stainless Steel

All of the structural steel used in the ATR FFSC packaging is an ASTM grade stainless steel. The weld consumable material is ASTM Type 308-308L, which results in weld metal deposits which have properties at least as great as the base metal. The minimum properties of the stainless steel items are given in Table 2.2-1.

Table 2.2-1 –Material Properties of Stainless Steel

Material	Yield Strength, minimum, psi	Ultimate Strength, minimum, psi
ASTM A240 Type 304	30,000	75,000
ASTM A269 Type 304	30,000	75,000
ASTM A276 Type S21800	50,000	95,000
ASTM A479 Type 304	30,000	75,000
ASTM A554 Grade MT-304	30,000	75,000

2.2.1.2 Aluminum

The internal FHEs and LFPB are fabricated from aluminum alloy. Minimum material properties are given in Table 2.2-2.

Table 2.2-2 –Material Properties of Aluminum

Material	Yield Strength, minimum, psi	Ultimate Strength, minimum, psi
ASTM B209, Alloy 5052 – H32	23,000	31,000
ASTM B209, Alloy 6061 – T651, 4” Plate	35,000	40,000
ASTM B210, Alloy 6061 – T6 ¼" Thick	35,000	42,000
ASTM B211, Alloy 6061 – T6 or 6061 – T651	35,000	42,000
ASTM B221 or B241, Alloy 6061 – T6, T6510, or T6511	35,000	38,000

2.2.2 Chemical, Galvanic, or Other Reactions

The materials of construction of the ATR FFSC packaging are primarily Type 304 stainless steel and refractory insulation. Since these materials are relatively unreactive, no excessive corrosion or other reactions will occur during normal use. The package is normally transported in a closed van, and is not subject to immersion or exposure to water or chemicals other than occasional precipitation or mild cleaning agents. In addition, all of these materials have been used in Type A and Type B packagings for many years without incident. If unusual corrosion of the stainless steel components occurs, it can be readily detected during preparation of the packaging for use. The refractory insulation is sealed within the body and is not subject to chemical degradation or corrosion during normal use.

The payloads, consisting of either the FHE and corresponding fuel element or the LFPB and fuel plates, are constructed primarily of aluminum alloy. There is no galvanic or other reactions between the stainless steel package and aluminum alloy payload. Furthermore, the FHEs and LFPB are inspected prior to placement within the packaging.

2.2.3 Effects of Radiation on Materials

Since the payload of the ATR FFSC consists of contact handled un-irradiated fuel elements (or loose fuel plates), enriched to a maximum of 94% U-235, the radiation from the payload is insignificant. Consequently, there will be no radiation effects on the materials of construction and the requirements of 10 CFR §71.43(d) are met.

2.3 Fabrication and Examination

2.3.1 Fabrication

The metallic components of the ATR FFSC packaging are fabricated using conventional metal forming and welding techniques. Structural materials which are important to safety are specified using American Society for Testing and Materials (ASTM) standards as shown on the drawings in Appendix 1.3.2, *Packaging General Arrangement Drawings*. All materials and components are procured and assembled under a 10 CFR 71, Subpart H quality assurance program. Welding procedures and personnel are qualified in accordance with the ASME Code, Section IX. Each packaging and its components are fabricated in accordance with the requirements delineated on the drawings in Appendix 1.3.2, *Packaging General Arrangement Drawings*.

2.3.2 Examination

Each packaging and its components are examined per the requirements delineated on the drawings in Appendix 1.3.2, *Packaging General Arrangement Drawings*. All welds are visually examined on each pass per the requirements of AWS D1.6:1999 for stainless steel and AWS D1.2:2003 for aluminum. All welds which are important to safety are examined by liquid penetrant test on the final pass using procedures compliant with ASTM E165-02. Personnel performing NDE shall be qualified in accordance with ASNT SNT-TC-1A[5]. Any deviations from SAR drawing requirements will be dispositioned and corrected under a 10 CFR 71, Subpart H quality assurance program prior to the application of the model number, per 10 CFR §71.85(c).

2.4 General Requirements for All Packages

This section defines the general standards for all packages. The ATR FFSC package meets all requirements of this section.

2.4.1 Minimum Package Size

The minimum dimension of the ATR FFSC package is 8 inches square. Thus, the 4 inch minimum requirement of 10 CFR §71.43(a) is satisfied.

2.4.2 Tamper-Indicating Feature

A tamper-indicating device (TID) lock wire and seal is installed through a small post on the closure provided to receive the wire. An identical post is located on the body for the TID wire. For ease in operation, there are two TID posts on the body. There are only two possible angular orientations for the closure installation and the duplicate TID post on the body enables TID installation in both positions. Thus, the requirement of 10 CFR §71.43(b) is satisfied.

---

[5] American Society for Nondestructive Testing (ASNT), Recommended Practice No. ASNT SNT-TC-1A, 2001 Edition.

2.4.3 Positive Closure

The ATR FFSC package cannot be opened unintentionally. The closure engages with the body using a bayonet style design. There are four lugs, uniformly spaced on the closure, that engage with four slots in the mating body feature. The closure is secured by retracting two spring loaded pins, rotating the closure through approximately 45º, and releasing the spring loaded pins such that the pins engage with mating holes in the body. When the pins are properly engaged with the mating holes the closure is locked. Thus, the requirements of 10 CFR §71.43(c) are satisfied.

2.4.4 Valves

The ATR FFSC does not contain any valves.

2.4.5 External Temperatures

As discussed in Section 3.3.1.1, *Maximum Temperatures*, the maximum accessible surface temperature with no insolation is 100ºF (38ºC). Since the maximum external temperature does not exceed 122ºF (50ºC), the requirements of 10 CFR §71.43(g) are satisfied.

2.5 Lifting and Tiedown Standards for All Packages

2.5.1 Lifting Devices

The ATR FFSC package may be lifted from beneath utilizing a standard forklift truck when the package is secured to a fork pocket equipped pallet, or in a package rack. Swivel lift eyes can be installed in the package to enable package handling with overhead lifting equipment. The swivel eyes are installed after removing the 3/8-16 socket flat head cap screws and index lugs used for stacking.

Assuming both lift eyes carry half the load, the weight at each lug is:

$$P = \left(\frac{290}{2}\right) = 145\ lbf$$

Applying a minimum horizontal sling angle of 30º, the maximum load on each sling is:

$$T = \frac{145}{\sin(30)} = 290\ lbf$$

Therefore, all lifting devices shall have a minimum working load limit of 300 lb.

2.5.1.1 Attachment Capacity

Per 10 CFR §71.45(a) any lifting attachment that is a structural part of the package must be designed with a minimum safety factor of three against yielding. This evaluation verifies the adequacy of the groove weld securing the threaded bar to the wall of the 8 inch square tube. By inspection, the groove weld is the weakest point of the lifting point and all other items will have a greater margin of safety. The lift eye is required to have a minimum working load limit of 300 lb. The lift eye components are therefore assumed to meet the lifting requirements.

The allowable force on the groove weld is equal to the shear strength of the base material, $0.6*\sigma_{yield}$.

Allowable weld stresses:

$$\sigma_{yield} = 30{,}000 \ psi$$

$$w_{allow} = 0.6 \cdot 30{,}000 = 18{,}000 \ psi$$

Maximum tension in each of the two lift slings is 290 lbf at an angle of 30º.

$$T_y = P = 145\,lbf$$

$$T_x = 290 \cdot \cos(30) = 251\,lbf$$

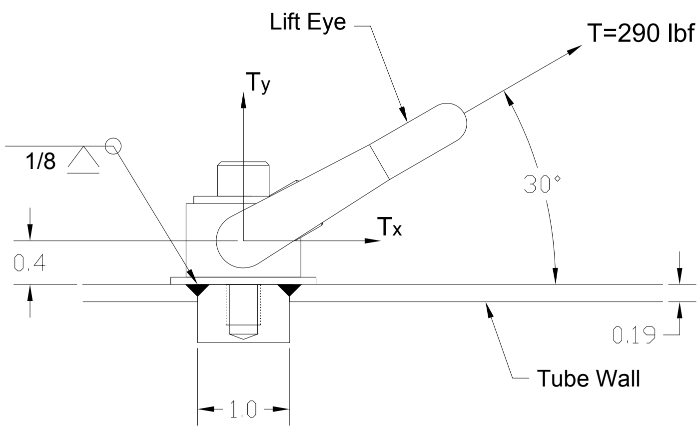

Figure 2.5-1 – Lift Attachment Diagram

Including the safety factor of three, the maximum horizontal and vertical forces are:

$$P_h = 3 \cdot T_x = 753\,lbf$$

$$P_v = 3 \cdot T_y = 435\,lbf$$

Using Blodgett[6], the given load is divided by the length of the weld to arrive at the applied unit force, lb per linear inch of weld. From this force, the proper throat of the grove weld is determined.

The properties of the weld, treated as a line, are:

$$A_w = \pi \cdot d$$

$$S_w = \frac{\pi \cdot d^2}{4}$$

[6] Omer Blodgett, *Design of Welded Structures*, 1982, The James F. Lincoln Arc Welding Foundation, Cleveland, Ohio.

Where,

d = diameter of weld = 1.0 inch

$$A_w = \pi \cdot (1) = 3.14\, in$$

$$S_w = \frac{\pi \cdot (1)^2}{4} = 0.785\, in^2$$

Vertical tension on the weld is:

$$f_v = \frac{P_v}{A_w} = \frac{435}{3.14} = 139\ \frac{lbf}{in}$$

Horizontal shear on the weld is:

$$f_h = \frac{P_h}{A_w} = \frac{753}{3.14} = 240\ \frac{lbf}{in}$$

The bending force on the weld is

h = height of applied load from lift eye = 0.4 in, plus half of the weld thickness of 0.125/2

$$h = 0.4 + (.125/2) = 0.463\ in$$

$$M = P_h \cdot h = 753 \cdot 0.463 = 349\, in \cdot lb$$

$$f_b = \frac{M}{S_w} = \frac{349}{0.785} = 445\ \frac{lbf}{in}$$

The vertical tension and bending forces are in the same direction and additive:

$$f_{v+b} = f_v + f_b = 139 + 445 = 584\ \frac{lbf}{in}$$

The vertical and horizontal loads are perpendicular, therefore the combined load is:

$$f_r = \sqrt{(f_{v+b})^2 + {f_h}^2} = \sqrt{(584)^2 + (240)^2} = 631\ \frac{lbf}{in}$$

The required grove weld is:

$$w = \frac{f_r}{w_{allow}} = \frac{631}{18{,}000} = 0.035\ in$$

Thus the weld margin of safety is:

$$MS_{weld} = \frac{.125}{.035} - 1 = +2.6$$

2.5.1.2 Conclusion

From the above analyses, the lifting attachment points adequately lift the fully loaded package with a margin of safety of 2.6. The conservative minimum lifting angle of the slings is 30º above horizontal. Failure of this lifting component under excessive load would not impair the ability of this package to meet other requirements of 10 CFR §71, per the requirements of 10 CFR §71.45(a).

2.5.2 Tiedown Devices

For transport, the package will be strapped or otherwise restrained inside or on the transport vehicle. Any features used to lift the ATR FFSC will be removed or rendered unusable for tiedown. The index lugs used to align the package during stacking are evaluated for the tiedown loads. Per 10 CFR §71.45(b)(1) the tiedown system must withstand a vertical loading of 2g, horizontal for/aft loading of 10g, and horizontal lateral loading of 5g. Because there is no vertical restraint capability of the index lug, the 2g vertical load is neglected. Combining the loads, the maximum horizontal g loading is $\sqrt{10^2 + 5^2} = 11.18g$. The loaded ATR FFSC package weighs 290 lb.

2.5.2.1 Tiedown Method

The ATR FFSC may be stacked in a 4 wide by 3 high array during transport. The packages are secured by means which resist the vertical loading. However, any axial/lateral restraint is conservatively neglected.

The index lugs at each end of the packages are used to align and secure the packages within the array and are subjected to g-loads from neighboring packages. The index lugs are attached to the package by a single flat head, socket cap screw such that horizontal loading causes shearing in the threaded area of the screw as shown in Figure 2.5-2.

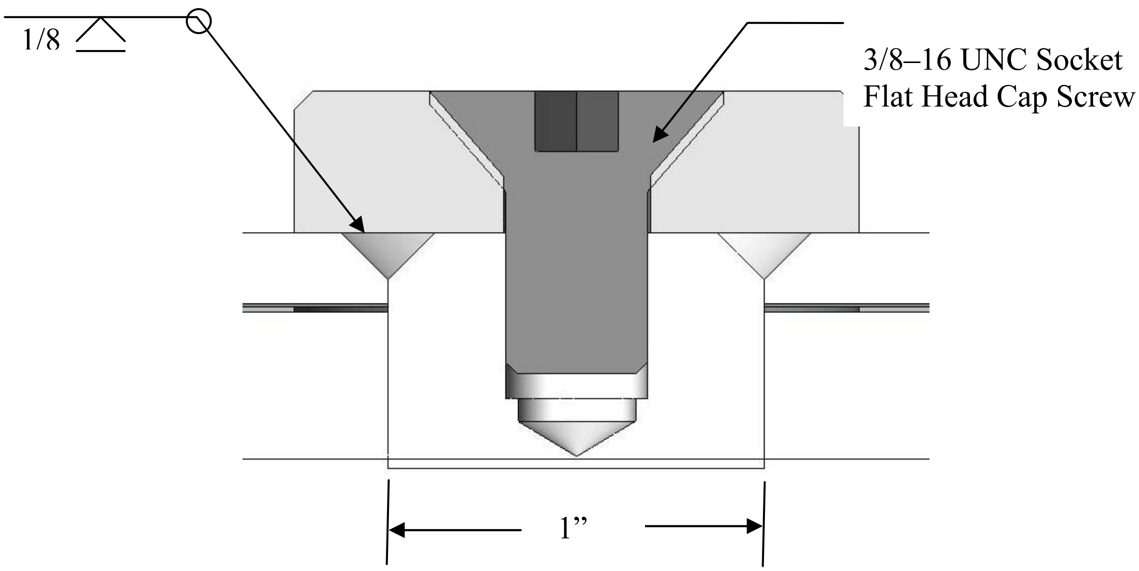

Figure 2.5-2 – Index Lug

2.5.2.2 Tiedown Capacity

By assuming the package is not restrained horizontally, the index lugs of the first tier must resist the horizontal loading of the middle and top tiers. The maximum load on each button is 2W times the g loading.

$$P_h = \frac{(2)(290)(11.18)}{2} = 3{,}242 \ \ lbf$$

2.5.2.3 Fasteners

The screw thread shear area is 0.0775 in^2 and the screw material is ASTM F835 which has minimum tensile strength of 145 ksi. The yield strength is 116 ksi; conservatively assuming yield to be 80% of tensile strength for alloy steel. The shear force allowable is $0.6\sigma_{\text{yield}}$.

Fastener shear stress = $\dfrac{3{,}242}{0.0775} = 41{,}832 \ \ psi$

$$MS = \frac{(116{,}000)(.6)}{41{,}832} - 1 = +0.66$$

The load required to fail the screw is:

$$P_{h-failure} = 0.6 \cdot \sigma_{ult} \cdot A = (0.6 \cdot 145{,}000) \cdot (0.0775) = 6{,}743 \ lbf$$

2.5.2.4 Weld Structure

The allowable force on the groove weld is equal to the shear strength of the base material, $0.6\sigma_{\text{yield}}$.

Allowable weld stresses:

$$\sigma_{yield} = 30{,}000 \ \ psi$$

$$w_{allow} = 0.6 \cdot 30{,}000 = 18{,}000 \ \ psi$$

Using Blodgett, the given load is divided by the length of the weld to arrive at the applied unit force, lb per linear inch of weld. From this force, the proper throat of the grove weld is determined.

The properties of the weld, treated as a line, are:

$$A_w = \pi \cdot d$$

$$S_w = \frac{\pi \cdot d^2}{4}$$

Where,

d = diameter of weld = 1.0 inch

$$A_w = \pi \cdot (1) = 3.14 \, in$$

$$S_w = \frac{\pi \cdot (1)^2}{4} = 0.785 \, in^2$$

Horizontal shear on the weld is:

$$f_h = \frac{P_h}{A_w} = \frac{3{,}242}{3.14} = 1{,}033\ lbf / in$$

Assume for simplicity that the index lug diameter matches that of the weld (conservative). The moment on the weld is equal to the applied load times the distance from the weld c.g. to the mid-height of the 3/8 inch high index lug, or:

$$\frac{0.125}{2} + \frac{0.375}{2} = 0.25\ in$$

The bending force on the weld, as a vertical component, is

h = height of applied load to index lug = 0.25 in

$$M = P_h \cdot h = 3{,}242 \cdot 0.25 = 811 in \cdot lb$$

$$f_b = \frac{M}{S_w} = \frac{811}{0.785} = 1{,}033\ lbf / in$$

The vertical and horizontal loads are perpendicular, therefore the combined load is:

$$f_r = \sqrt{{f_b}^2 + {f_h}^2} = \sqrt{(1{,}033)^2 + (1{,}033)^2} = 1{,}461\ lbf / in$$

The required grove weld is:

$$w = \frac{f_r}{w_{allow}} = \frac{1{,}461}{18{,}000} = .081\ in$$

Thus the weld margin of safety is:

$$MS_{weld} = \frac{.125}{.081} - 1 = +0.54$$

The load required to fail the weld is:

$$f_r = w \cdot (0.6 \cdot w_{ult}) = (0.125) \cdot (0.6 \cdot 75{,}000) = 5{,}625\ lbf / in$$

Since $f_b = f_h$: $f_h = \sqrt{{f_r}^2 / 2} = \sqrt{(5{,}625)^2 / 2} = 3{,}977\ lbf / in$

The load required to fail the weld is:

$$P_{h-failure} = f_h \cdot A_w = (3{,}977) \cdot (3.14) = 12{,}488\ lbf$$

2.5.2.5 Conclusion

From the above analysis, the index lugs adequately withstand the combined horizontal tiedown g-loads for the fully loaded package. Furthermore, it is shown that the index lug screw will fail prior to the weld. This satisfies the requirements of 10 CFR §71.45(b)(1).

2.5.3 Closure Handle

The closure handle, deemed a structural part of the package, must be rendered inoperable for lifting and tiedown during transport in compliance with 10 CFR §71.45. To satisfy this requirement, a cover will be secured over the closure handle during transport to prevent any straps or hooks from being attached to the handle or to prevent any hardware from being placed between the handle and closure as illustrated in Figure 1.2-5. As an option, the handle may also be removed during transport.

The attachment of the closure handle to the closure assembly is evaluated here to show that its failure will not impair the ability of the package to meet other requirements. A lifting or tiedown load applied to the closure handle is expected to deform the handle and fail the closure screws causing the handle to become detached from the closure assembly. The closure handle is used only for operator convenience in handling the 10 lb closure assembly by hand. The four small fasteners securing the handle to the closure are designed to fail under light loads and well before impairment of any safety related packaging feature.

This evaluation conservatively neglects any tension (pulling) on the handle and handle screws since a load in this direction would pull on the closure locking tabs and not the locking pins. A simple comparison between the area of the closure tabs and the area of the handle screws shows that the closure tabs consist of significantly more material and the screws will fail well before any significant loads are applied to the closure tabs.

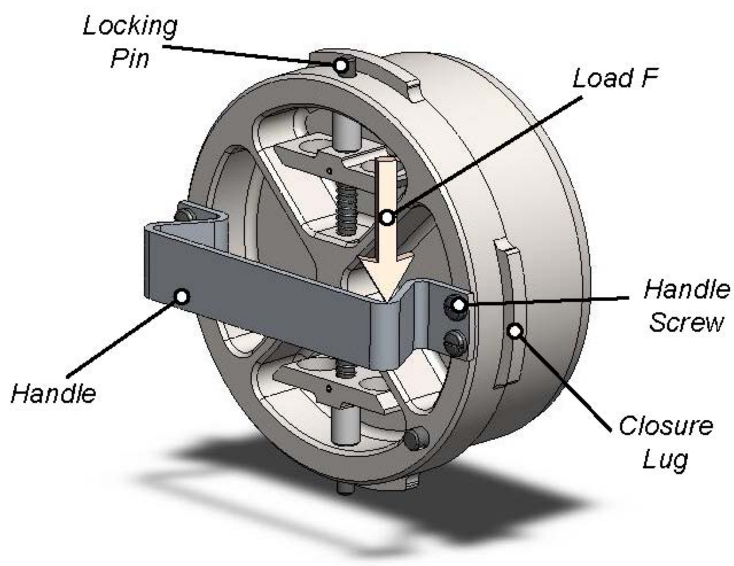

Figure 2.5-3 – Closure Assembly Handle

2.5.3.1 Handle Fasteners

The closure handle is secured by four #10-24 UNC screws (two per side). For this evaluation the load F is applied at the outside edge of the handle: 0.5 inches radially out from the screws and 0.5 inches above the face of the closure assembly.

This evaluation is based on the load *F* necessary to fail the handle screws. The load will be a function of the ultimate strength of the handle screws, which are given as a minimum of 72,000 psi for 18-8 material. To account for possible strain hardening due to the manufacturing process, that value will be conservatively multiplied by a factor of 2. Therefore:

$$\sigma_{\text{ultimate}} = 144{,}000 \text{ psi}$$

For the handle screws, the area across the threads is equal to the area of the minor diameter. For a #10-24UNC screw the minor diameter is 0.1389 inches.

$$A_s = \frac{\pi {d_m}^2}{4} = \frac{\pi (0.1389)^2}{4} = 0.0152 \text{ in}^2$$

The shear force in each screw is now determined. The largest forces will be at the two screws closest to the applied force. See Figure 2.5-4.

$$M = F \cdot r = 3.25\ F\ \ in \cdot lb$$

$$r = 3.25\ in\ \ (dist.to\, centroid)$$

Where *r* is taken as the maximum distance possible for any handle configuration.

The primary shear is:

$$\text{n} = 4 \text{ (number of screws)}$$

$$S' = \frac{F}{n} = \frac{F}{4} = 0.25F \text{ lb}$$

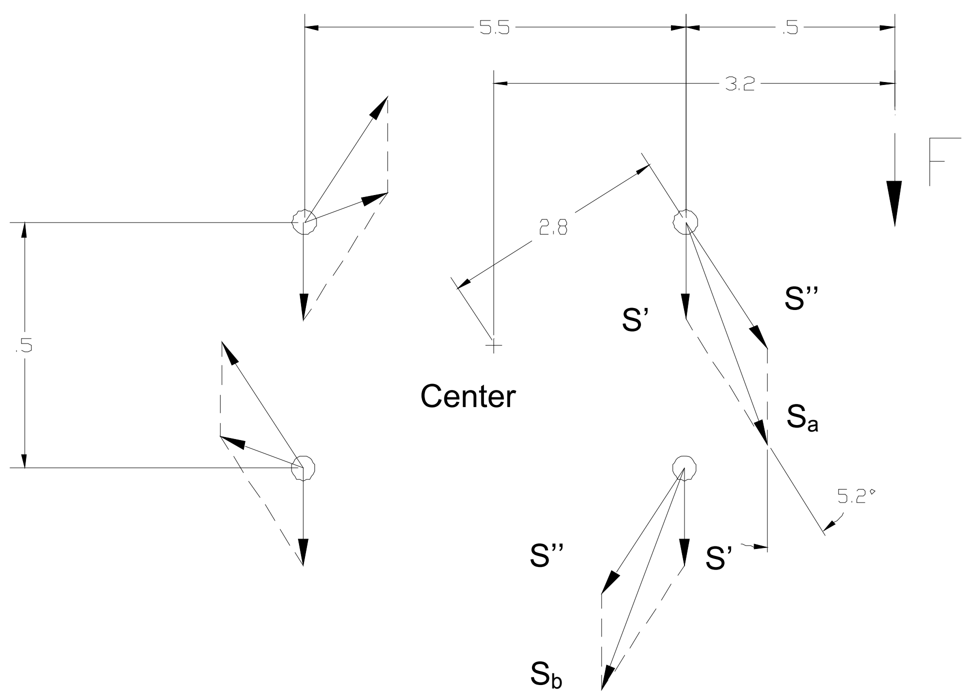

Figure 2.5-4 – Screw Pattern Diagram

The secondary shear is:

$$S'' = \frac{M}{4 \cdot R} = \frac{3.25F}{4 \cdot 2.8} = 0.29F \text{ lb}$$
$$R = 2.8 \text{ in. (dist. to centroid)}$$

The combined shear force is:

$$S_a = S_b = 0.29F + 0.25F(\cos 5.2) = 0.29F + 0.249F = 0.539F$$

The shear stress is:

$$\tau = \frac{S_a}{A_s} = \frac{0.539F}{0.0152} = 35.46F \text{ psi}$$

The tensile load on the screws due to the load *F* is applied to only two of the four screws, since the handle, due to its flexibility, cannot effectively transfer the load to the screws on the opposite side of the handle. The tensile load on the two screws closest to the load is:

$$\sum M_A = F \cdot (0.5) - R_1 \cdot (0.25) - R_2 \cdot (0.75) = 0$$
$$F = 0.5R_1 + 1.5R_2$$

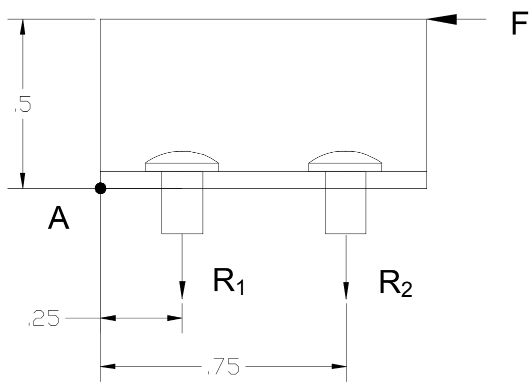

Figure 2.5-5 – Screw Prying Diagram

The relation between the screws is:

$$\frac{R_1}{R_2} = \frac{0.25}{0.75}$$
$$R_1 = \frac{1}{3} R_2$$

Substitute into the sum of moments equation:

$$F = 0.5R_1 + 1.5R_2$$

$$F = (\frac{1}{3}0.5R_2) + 1.5R_2$$

$$R_2 = 0.6F\ lb$$

$$R_1 = 0.2F\ lb$$

The peak tension appears in R_2. The maximum tensile stress is:

$$\sigma = \frac{R_2}{A_s} = \frac{0.6F}{0.0152} = 39.47F \text{ psi}$$

Combine the shear and tensile stresses to find the force necessary to fail the screws:

$$\sigma_{ultimate} = \sqrt{\sigma^2 + 4\tau^2} = \sqrt{(39.47F)^2 + 4(35.46F)^2}$$

$$144{,}000 = \sqrt{6{,}588F^2} = 81.17F$$

$$F = 1{,}774 \text{ lb}$$

2.5.3.2 Locking Pin Loading

To show that the handle attachment fails prior to the closure components of the package, the force necessary to fail the screws is applied to the two locking pins. The yield strength of the locking pins is conservatively used in the comparison.

The locking pins are 0.25 inch in diameter and made of ASTM A276, Type S21800 material, having a yield strength of σ_{yield} = 50,000 psi. The pin area is:

$$A_p = \frac{\pi d^2}{4} = \frac{\pi(.25)^2}{4} = 0.049 in^2$$

The load *P* must be calculated from the screw failure load *F*. The distance from the center of the closure assembly to the point of shear in the locking pin is half of the diameter of the closure at the location of the pin, or r_p = 5.97/2 = 2.99 inches. The distance from the center of the closure assembly to the load *F* is 3.25 inches.

$$P = \frac{3.25F}{2.99} = 1{,}928 \text{ lb}$$

The shear stress for each pin is:

$$\tau = \frac{1}{2} \cdot \frac{P}{A} = \frac{1{,}928}{2(.049)} = 19{,}673 \text{ psi}$$

The margin of safety on the locking pins (against pin yield) at the point of handle screw failure is:

$$MS = \frac{0.6\sigma_{yield}}{\tau} - 1 = \frac{0.6 \times 50{,}000}{19{,}673} - 1 = +0.52$$

where the factor of 0.6 converts the tensile yield of the pin material to shear yield. Thus, should the closure handle be incorrectly used as a tiedown device, the handle screws will break off before the pins yield.

2.5.3.3 Conclusion

From the above analysis, should a force be applied to the closure handle, the handle screws will fail before the closure locking pins yield. Therefore, adverse loading of the closure handle does not impair the ability of the package to meet other requirements.

2.6 Normal Conditions of Transport

2.6.1 Heat

2.6.1.1 Summary of Pressures and Temperatures

As presented in Table 3.1-1 of Section 3.1.3, *Summary Tables of Temperatures*, the maximum ATR FFSC package temperature under conditions of 100ºF ambient temperature and full insolation is 186°F on the outer shell. As presented in Table 3.1-2 of Section 3.1.4, *Summary Table of Maximum Pressures*, the maximum normal operating pressure (MNOP) of the ATR FFSC package is zero. This is assured because there are no seals provided between the body and closure to retain pressure.

The ATR FFSC body cavity is also discussed in Section 3.1.4, *Summary Table of Maximum Pressures*. The maximum pressure that may develop between the inner and outer shells will be limited to that achieved due to ideal gas expansion. The maximum pressure rise within the sealed cavity under NCT will be less than 4 psi gauge.

2.6.1.2 Differential Thermal Expansion

Because of the simple design of the ATR FFSC package, there are no features, such as rigid lids and containment seals, which could be affected by the differential thermal expansion of the package components. In addition, since the package has a negligible internal decay heat, any temperature differences will arise only from the solar loading, and consequently be modest in nature.

The nominal end gap between the package cavity and the FHEs or the LFPB is 0.63 inches and 0.38 inches respectively. These gaps are large enough to prevent the payload from expanding enough to load the closure. Therefore, differential thermal expansion is not of concern.

2.6.1.3 Stress Calculations

Since the MNOP is zero and the maximum sealed cavity pressure is 4 psi gauge, stresses due to NCT pressures and temperatures are negligible.

2.6.1.4 Comparison with Allowable Stresses

Since NCT stresses are negligible, this section does not apply.

2.6.2 Cold

With an internal decay heat load of zero, no insolation, and an ambient temperature of -40ºF, the average package temperature will be -40ºF. None of the materials of construction (i.e., stainless steel) undergo a ductile-to-brittle transition at temperatures of -40 ºF or higher. Therefore, the minimum NCT temperature is of negligible consequence.

2.6.3 Reduced External Pressure

As discussed in Section 2.6.1.1, *Summary of Pressures and Temperatures*, the ATR FFSC packaging is not capable of retaining pressure. Therefore, there is no effect of a reduced external pressure on the package of 3.5 lbf/in^2 (25 kPa) absolute, per 10 CFR §71.71(c)(3).

2.6.4 Increased External Pressure

10 CFR §71.71(c)(4) requires exposure of the ATR FFSC package to an increased external pressure of 20 psi (140 kPa) absolute. Since there are no sealing surfaces, there is no effect of an increased external pressure to the ATR FFSC package.

Section 2.7.6.1, *Cavity Evaluation*, evaluates the effect of pressure on the sealed cavity between the outer 8 inch tube and inner 6 inch diameter pipe. This cavity is welded closed during fabrication and has no relation to the payload. The cavity evaluation conservatively considers the satisfactory performance of a 22 psi gauge external pressure to the packaging.

2.6.5 Vibration

The effects of vibration normally incident to transport are not significant for the ATR FFSC packaging. Table 2 of ANSI N14.23[7] shows peak vibration accelerations of a trailer bed as a function of package and tie-down system natural frequency. For the frequency range 0 to 5 Hz, assuming a light package, Table 2 of ANSI N14.23 gives peak accelerations (99% level) of 2g in the vertical direction, and 0.1g in both the lateral and longitudinal directions. All other frequency ranges give significantly lower acceleration levels.

The ATR FFSC is very resistant to damage from transportation vibration. The closure is subject to the ± 0.1g longitudinal (axial) loading, but since friction between the closure and its opening will exceed 0.1, the closure is not expected to apply any vibrational loadings to the bayonet lugs. The insulating material located between the inner, round tube and the outer, square tube is retained in place by a jacket of 28 gauge stainless steel. The resistance to displacement of the insulation was demonstrated in the testing program (see Section 2.12.2.5.1, *CTU Inspection*). When exposed to axial impacts which were many times larger than the vibration load of 0.1g, the insulation displaced an insignificant distance which was bounded by the assumptions made in the thermal analysis. Therefore, vibration will have no effect on the placement or condition of the insulation.

When supported on the shipping rack, the package is supported near index lugs which interface with the two pockets on the lower face of the package. Conservatively, an analysis of the package as a simply supported beam, supported at the extreme ends, is performed. The overall length of the package is L = 72.5 inches, and the maximum weight, from Table 2.1-1, is 290 lb. The distributed load is therefore 290/72.5 = 4 lb/in. The outer square tube has a square dimension of 8 inches and a wall thickness of 0.188 inches. AISC[8] gives the moment of inertia of the tube as 58.2 in^4. The c-distance is 4 inches. The bending moment is:

[7] ANSI N14.23, *Design Basis for Resistance to Shock and Vibration of Radioactive Material Packages Greater Than One Ton in Truck Transport*, 1980, American National Standards Institute, Inc. (ANSI).

[8] American Institute of Steel Construction, *Manual of Steel Construction, Allowable Stress Design*, Ninth Edition, 1989.

$$M = \frac{wL^2}{8}(2) = 5{,}256\ in \cdot lb$$

where the factor of 2 accounts for the inertia loading of ± 2g. The reversing bending stress in the outer square tube is:

$$\sigma = \frac{Mc}{I} = 361\ \text{psi}$$

This value is well below the fatigue limit for stainless steel. Since the inner round tube is supported at three places along its length, the unsupported length is much shorter than for the outer square tube. In addition, the distributed weight, which consists of only the self-weight and payload weight, is significantly less than for the outer square tube. For these reasons, the stress in the inner round tube will be bounded by the stress in the outer square tube.

The FHEs and loose fuel plate basket are designed to be form fitting and supported by the inner stainless steel round tube. Furthermore, the FHEs and loose fuel plate basket are completely removed and in view at both the shipping and receiving sites, and consequently, a complete fatigue failure of either basket due to transportation vibration is not to be expected.

For these reasons, the effect of vibration normally incident to transport is not of concern for the ATR FFSC package.

2.6.6 Water Spray

The external surfaces of the ATR FFSC package are made from stainless steel, whose properties are not affected by water spray. For this reason, the effect of water spray, per 10 CFR §71.71(c)(6), is not of concern for the ATR FFSC package.

2.6.7 Free Drop

10 CFR §71.71(c)(7) requires a free drop for the ATR FFSC package. Since the package gross weight is less than 11,000 lb, the applicable free drop distance is 4 ft. As discussed in Appendix 2.12.1, *Certification Tests on CTU-1,* one NCT free drop preceded the HAC drop tests performed on CTU-1. The damage from the NTC drop case was minor as illustrated in Figure 2.12.1-5 through Figure 2.12.1-7. There was no loss or dispersal of package contents, and no substantial reduction in the effectiveness of the packaging. The latter result was confirmed by the successful completion of the subsequent HAC testing.

From the test results, the amount of deformation in the top corner was approximately 1/8 inch. Because there are no crushable materials of construction, the deformation of the package in any other NCT drop orientation is assumed to be the same or less than this CG over top corner orientation. This assumption is verified by the degree of damage recorded during the HAC drop orientations discussed in Section 2.7, *Hypothetical Accident Conditions*.

By observation, the NCT damage is much less than 5% of the total effective volume of the package, approximately 230 in^3, based on 5% of the volume of the 72.5-inch long, by 8-inch square tube. Therefore, the requirement of 10 CFR §71.55(d)(4)(i) is met. Further, the effective spacing between fissile contents is 8 inches, based on a center-to-center distance between packages which are in side to side and top to bottom contact. Five percent of this distance is 0.4 inches, and therefore the requirement of 10 CFR §71.55(d)(4)(ii) is met. Finally, no opening capable of admitting a 4-inch cube was created, and the requirement of 10 CFR §71.55(d)(4)(iii) is also met. Thus, the effect of the free drop test, per 10 CFR §71.71(c)(7), is not of concern.

2.6.8 Corner Drop

This test does not apply, since the ATR FFSC package is a rectangular fissile material package weighing more than 110 lb, as specified in 10 CFR §71.71(c)(8).

2.6.9 Compression

As specified in 10 CFR §71.71(c)(9), the ATR FFSC must be subjected, for a period of 24 hours, to a compressive load applied uniformly to the top and bottom of the package in the normal transport position. The greater of the following uniformly distributed loads is to be used: (a) the equivalent of 5 times the weight of the package, or (b) the equivalent of 2 lbf/in^2 multiplied by the vertically projected area of the package. For these two cases, the loads are:

$$P_{(a)} = 5 \cdot W = 5 \cdot 290\,lbf = 1{,}450\ lbf$$

$$P_{(b)} = 2\ psi \cdot L \cdot w = 2\ psi \cdot (72.5\,in) \cdot (8\,in) = 1{,}160\ lbf$$

Where,

W is the maximum weight of one package

w is the overall width of the package

L is the overall length of the package.

Thus, it is seen that case (a) governs with a compressive load of 1,450 lbf.

The exterior side of the ATR FFSC packaging is a reinforced 8 inch by 8 inch square stainless steel tube with a 0.188 inch wall thickness. The closure end includes a 1.5 inch thick stainless steel plate and the bottom end includes a 0.88 inch thick stainless steel plate. By observation, buckling of the outer tube is not a concern due to its reinforcement, short height, wall thickness, and the relatively small load applied. A conservative evaluation is performed in the following section to demonstrate the adequacy of the design under the compression load.

2.6.9.1 Compression Evaluation

To conservatively evaluate the compressive load, buckling of the square tube under a uniform load is evaluated neglecting the reinforcing end plates and interior ribs. The applied load, as determined in Section 2.6.9, *Compression*, is 1,450 lbf. The average stress in the 8 inch tube is:

$$\sigma_{tube} = \frac{P}{A_{tube}}$$

Where,

P = applied load = 1,450 lbf

A_{tube} = area of vertical legs of the tube = 2 x t x L $= 2 \cdot (0.19) \cdot 72.5 = 27.6\,in^2$

t = thickness = 0.19 in

L = length of tube = 72.5 in

Therefore:

$$\sigma_{tube} = \frac{P}{A_{tube}} = \frac{1450}{27.6} = 52.5\ psi$$

Using Roark[9], Table 35 Case 1a, a rectangular plate under equal uniform compression, all edges simply supported, the critical unit compressive stress σ' is:

$$\sigma' = K \cdot \frac{E}{1-v^2} \cdot \left(\frac{t}{L}\right)^2$$

Where,

E = modulus of elasticity for stainless steel = 27.6 Mpsi

v = Poisson's ratio = 0.3

K = conservatively chosen as equal to 10.9

$$\sigma' = 10.9 \cdot \frac{27600000}{1-(.3)^2} \cdot \left(\frac{0.19}{72.5}\right)^2 = 2{,}271\ psi$$

By comparison:

$$\sigma_{tube} << \sigma'$$

Therefore, buckling of the outer tube due to the compression load is not a concern.

2.6.10 Penetration

10 CFR §71.71(c)(10) requires that a bar of hemispherical end, weighing at least 13 lb be dropped from a height of 40 inches onto the most vulnerable part of the packaging. As documented in Appendix 2.12.1, *Certification Tests on CTU-1*, the ATR FFSC package, weighing approximately 290 lb, was subjected to the much more demanding test of being dropped from 40 inches onto the puncture bar described in §71.73(c)(3) without experiencing any damage which could compromise confinement or criticality control. Therefore, this test does not need to be performed, and the penetration test requirement is satisfied.

2.7 Hypothetical Accident Conditions

When subjected to the hypothetical accident conditions of 10 CFR §71.73, the ATR FFSC prevents loss or dispersal of the enriched uranium payload. The analysis given in Chapter 6, *Criticality*, which includes conservative assumptions regarding damaged geometry and moderation, demonstrates the criticality safety of the ATR FFSC under hypothetical accident conditions.

10 CFR §71.55 requires that packages containing fissile material be evaluated for criticality with the inclusion of any damage resulting from the NCT tests specified in §71.71 plus the damage from the HAC tests specified in §71.73. The ATR FFSC was subjected to accident condition

[9] Young, Warren C., *Roark's Formulas for Stress and Strain*, Sixth Edition, 1989, McGraw Hill, New York, New York.

loadings by means of full scale certification testing. Each test specified by §71.73 was applied sequentially, as specified in Regulatory Guide 7.8[10]. One full scale certification test unit (CTU-1) using the ATR fuel element as the payload was subjected to the full series of free drop and puncture testing. A second full scale certification test unit (CTU-2) using the loose fuel plates as the payload was subjected to a series of worst case free drops. Puncture drops were not performed on CTU-2 because the testing focused on the performance of the insulation and payload, which would not be affected by any puncture damage. The puncture testing performed on CTU-1 demonstrated that the effects of the puncture test on the insulation and on the payload are negligible. Utilizing the results of drop testing, the fire test was evaluated analytically. The immersion tests are also evaluated analytically.

The payload for CTU-1 used during testing was an un-irradiated ATR fuel element, enriched to a maximum of 94% U-235. The ATR fuel element used was a rejected production fuel element. The defects were considered cosmetic only and had no structural significance for purposes of the certification tests. Further discussion of the CTU-1 payload is provided in Appendix 2.12.1, *Certification Tests on CTU-1*.

The simulated loose fuel plate payload for CTU-2 was a combination of 2- and 4-inch wide, 0.06-inch thick, 5052H32 aluminum flat plates. All plates were 49.5 inches long. There were 15, 2-inch wide plates and 10, 4-inch wide plates. The weight of the aluminum plates totaled 20.7 lb. Further discussion of the CTU-2 payload is provided in Appendix 2.12.2, *Certification Tests on CTU-2*.

Rationale for the selection of the test series is given below. The tests actually performed, and their sequence, are summarized in Table 2.7-1. Test results are summarized in the sections which follow and in Section 2.7.8, *Summary of Damage*, with details given in Appendix 2.12.1, *Certification Tests on CTU-1* and Appendix 2.12.2, *Certification Tests on CTU-2*.

The performance of the MIT and MURR fuel elements is bounded by the test results using the ATR fuel element. A full discussion and comparison of the three fuel elements is given in Appendix 2.12.3, *Structural Evaluation for MIT and MURR Fuel*. As with the ATR fuel element, the criticality evaluation performed in Section 6.10, *Appendix B: Criticality Analysis for MIT and MURR Fuel*, makes conservative assumptions designed to encompass a wide range of damage exceeding the actual damage observed during testing of the ATR fuel element. Since Section 6.11, *Appendix C: Criticality Analysis for Small Quantity Payloads* conservatively models the fuel as a homogeneous mixture of uranium and water, a structural evaluation of the RINSC and other small quantity payloads, and the corresponding FHE is not required. The same is true for Cobra fuel. Section 6.13, *Appendix E: Criticality Analysis for the Cobra Fuel Element* conservatively models the Cobra fuel as a homogeneous mixture of uranium and water. Therefore, a structural evaluation of the Cobra fuel and the Cobra FHE is not required.

2.7.1 Free Drop

10 CFR §71.73(c)(1) requires a free drop of the specimen through a distance of 30 ft onto a flat, essentially unyielding surface in the orientation for which maximum damage is expected. The primary mode of failure of the ATR FFSC would be loss of the ability of the closure to retain the

[10] U. S. Nuclear Regulatory Commission, Regulatory Guide 7.8, *Load Combinations for the Structural Analysis of Shipping Casks for Radioactive Material*, Revision 1, March 1989.

payload. This could occur through loss of the bayonet style lugs, or through failure of the retracting pins allowing the lid to rotate, or through excessive deformation of the closure area which could cause separation of the body from the closure. If a sufficient gap is formed between the body and closure, the payload may no longer be retained, consequently possibly affecting criticality safety.

The object of the free drop tests in the current instance is to create the maximum amount of damage in critical locations and components. Therefore, free drop orientations are selected which would result in the greatest amount of critical damage and which would render the package most vulnerable to damage from the puncture drop test.

The ability of the payload to remain in a critically safe geometry is also confirmed through the free drop tests. Following all drop tests, the fuel assembly in CTU-1 and the simulated loose fuel plates in CTU-2, are inspected to confirm the geometries remain within the assumptions used in Section 6.0, *Criticality Evaluation*.

To confirm the performance of the payload at reduced temperatures CTU-1 was subjected to two HAC drops with the payload temperature at approximately -20ºF (-29ºC). Following all CTU-1 testing, as discussed in Appendix 2.12.1, *Certification Tests on CTU-1*, the package was destructively disassembled and the payload inspected.

Upon inspection of both CTU-1 and CTU-2, the performance of both the payload and packaging, including the reduced temperature tests, was satisfactory.

2.7.1.1 Side Drop

The horizontal side drops for CTU-1 include CD1-1, CD2-1, and CD3-1. The first three HAC drops primarily address the packaging closure and shell response to the free drops. Also, the side drop orientations represent large impact loads to the ATR fuel element for geometry control. CD1-1 presents the highest acceleration to the locking pins when the pins are oriented vertically with respect to the target surface. CD2-1 is directed at challenging the outer shell in the vicinity of the index lugs. The intent is to demonstrate that the outer shell is not penetrated by the impacted index lugs which could represent a thermal concern. In CD3-1, the locking pins are oriented horizontally with respect to the target surface presenting the worst case bending load to the locking feature.

The horizontal side drops for CTU-2 include CD1-2 and CD3-2. These two HAC drops address the performance of the LFPB in maintaining the geometry of the loose plates. Furthermore, the intent is to demonstrate the similar performance of the outer packaging in response to the LFPB as the payload.

2.7.1.2 CG Over Bottom Drop

The CG over bottom drop for CTU-1 includes CD4-1. This vertical orientation is expected to have the greatest potential for deformation to the insulation cavity at the bottom end. CD4-1 is considered to present the worst case loading to the 3/8 inch thick plate located at the bottom of the payload cavity. The intent of the drop is to demonstrate the insulation cavity at the bottom end of the package is not breached or significantly reduced. Additionally, the CD4-1 drop presents the worst case buckling load to the ATR fuel element.

For CTU-2, the CG over bottom drop includes CD4-2. As with CD4-1, this orientation is expected to have the greatest local deformation to the bottom end plate and insulation cavity and present the worst case buckling load to the LFPB and loose plates.

2.7.1.3 CG Over Corner Drop

The CG over corner drop was only performed on CTU-1. CD5-1, the CG over top corner drop, produces the greatest deformation in the closure region and also presents the greatest challenge for the closure locking tabs. The intent of the drop is to demonstrate the effectiveness of the closure in retaining the payload.

2.7.1.4 Oblique Drops

An oblique free drop orientation, also known as a slap-down drop, was not performed for this package. Consequences from the slap-down event are considered bounded by the CG over bottom (CD4-1/CD4-2) and CG over corner (CD5-1) drop tests performed. The slap-down drop challenges the closure and the fuel by producing high angular velocities and accelerations to the packaging and contents. However, in the case of the ATR FFSC, the end drops present a greater challenge to the closure and the fuel than the slap-down condition. In bolted closure designs, the slap-down side loads have the tendency to shear the closure bolts. Since the ATR FFSC closure is secured by a bayonet type design rather than bolts, this is not a concern. The axial load imparted to the closure in a slap-down drop will be lower than the axial loading developed in an end drop. And the greater the axial load, the greater the challenge to the locking tabs on the closure. The CD5-1 drop therefore presents the greatest challenge to closure retention, and the CD4-1/CD4-2 drop presents the greatest potential for fuel buckling.

2.7.1.5 Results of the Free Drop Tests

CD1-1 Flat Side Drop (CTU-1). See Figure 2.12.1-8 through Figure 2.12.1-13. The visible damage resulting from the 30 ft flat side drop, pocket side down, was negligible. There were minor visible exterior scratches resulting from the drop. The areas showing the greatest impact marks are at each end plate and near the three internal stiffening ribs. There was no significant bowing or other visible deformation. There was no visible deformation or rotation of the closure and the locking pins remained in the locked position.

Following the CD1-1 drop, CTU-1 was opened and the FHE and fuel element payload were visually inspected for damage. As illustrated in Figure 2.12.1-11 in Section 2.12.1, there were no major deformations and no cracked welds noticed. As illustrated in Figure 2.12.1-12, there was no visible damage to the fuel element.

With the closure assembly removed from the body of the CTU, one locking pin was noticeably bent approximately 1/32 inch as illustrated in Figure 2.12.1-13. It was noticed that the bent locking pin tended to bind when compressed to the open position. The other locking pin was not deformed and there was no other visible deformation of the closure assembly.

CD2-1 Flat Side Drop (CTU-1). Due to CTU-1 not impacting square on the index lugs, this orientation was tested three different times. The three tests in this orientation are identified as CD2.A-1, CD2.B-1, and CD2.C-1 throughout this section. For CD2.A-1, CTU-1 rotated during its descent and impacted at a slight angle causing the package to bounce and spin somewhat on the longitudinal axis after impact. The visible damage resulting from the CD2.A-1 drop was minor with the index lugs at each end pressed into the body approximately 1/8 inch. See Figure 2.12.1-14 through Figure 2.12.1-17.

For CD2.B-1 the package again rotated during its decent and impacted at an angle causing the package to bounce and spin on the longitudinal axis after impact. Also, a gust of wind blew the rigging straps into the adjacent stadia board during the drop. The visible damage resulting from the CD2.B-1 drop was minor with the index lugs at each end now pressed into the body approximately 3/16 inch. See Figure 2.12.1-18 through Figure 2.12.1-20.

CD2.C-1, which was performed after CD5-1, impacted in the correct orientation directly on the index lugs; see Figure 2.12.1-37 through Figure 2.12.1-40. The index lug near the closure end was flush with the original surface, pressed in approximately 3/8 inch (the height of the lug) as seen in Figure 2.12.1-39. The index lug at the bottom end was pushed in to approximately 1/8 inch from the original surface. A cracked weld was found under the index lug near the closure end as shown in Figure 2.12.1-40. The length of the cracked weld was approximately ½ inch.

CD3-1 Flat Side Drop – Reduced Temperature (CTU-1). See Figure 2.12.1-22 through Figure 2.12.1-25. The visible damage resulting from the 30 ft flat side drop performed with the payload at reduced temperature (-20ºF) was negligible. Similar to CD1-1, the impact side exhibited scratches and impact marks near the locations of the internal ribs. Upon inspection of the closure assembly, one of the two locking pins was found sheared off from the outside edge of the closure as it interfaces with the package body. There was no other visible damage or any signs of rotation to the closure assembly as the second locking pin remained in the locked position.

CD4-1 CG Over Bottom End – Reduced Temperature (CTU-1). See Figure 2.12.1-26 through Figure 2.12.1-28. The visible damage resulting from the 30 ft CG over bottom end drop performed with the payload at reduced temperature (-20ºF) was minor. The outer shell of CTU-1 exhibited minor bowing near the impact end with the greatest deformation measuring approximately 1/8 inch on one side. The overall length of the package body was compared with the initial measurements at eight locations and found to have compressed a maximum of approximately 1/8 inch. There was no visible deformation or rotation of the closure following the drop and the remaining locking pin remained in the locked position.

CD5-1 CG Over Top Corner Drop (CTU-1). See Figure 2.12.1-32 through Figure 2.12.1-36. The visible damage resulting from the 30 ft CG over top corner drop was prominent in the closure area. The impact corner was deformed in approximately 5/8 inch. There was modest deformation on the sides of the package near the impact location bulging in approximately 1/2 inch near the index lug pocket and bulged out approximately 5/8 inches on the adjoining side.

Following the drop, the closure assembly exhibited deformation with the end of the package and was unable to be rotated more than 1/8 inch in either direction. The locking pins showed no visible signs of deformation and the remaining locking pin remained in the locked position.

CD1-2 Flat Side Drop (CTU-2). See Figure 2.12.2-5 through Figure 2.12.2-7. This drop is a repeat of CD1-1 using the loose fuel plate payload rather than the ATR fuel element. The orientation of the LFPB parting lines is shown in Figure 2.12.2-3 through Figure 2.12.2-4. There was minor visible exterior damage, principally scuff marks, resulting from the drop. There was no bowing or other significant visible deformation. There was no visible deformation or rotation of the closure assembly, and the locking pins were unaffected by the drop.

Following the CD1-2 drop, CTU-2 was opened and the LFPB and payload were inspected. The basket was not affected by the drop, however the finger operated screws securing the two basket halves were loosened slightly. One tie wrap was broken but the simulated loose fuel plates were not damaged. The broken tie wrap was not replaced for the subsequent drops.

CD3-2 Flat Side Drop (CTU-2). See Figure 2.12.2-8 through Figure 2.12.2-10. This drop is a repeat of CD3-1 but at ambient temperature and using the loose fuel plate payload rather than the ATR fuel element. As with the other side drop events, the outer shell exhibited minor impact marks at the stiffening rib locations. There was no visible deformation or rotation of the closure assembly, and the locking pins were undamaged and in good working order.

The closure was opened and the payload inspected following the CD3-2 drop. The basket exhibited no signs of deformation and again the basket screws were loosened slightly. The second plastic tie wrap was broken and the simulated fuel plates exhibited no significant damage as seen in Figure 2.12.2-10. The broken tie wrap was not replaced for the subsequent drop.

CD4-2 CG Over Bottom End (CTU-2). See Figure 2.12.2-11 through Figure 2.12.2-16. This drop orientation is a repeat of CD4-1 but at ambient temperature and using the loose fuel plate payload rather than the ATR fuel element. CTU-2 appeared to impact slightly off of true vertical and impacted near one corner of the package. The impact caused one side to dent inward approximately ½ inch and the adjacent side to bulge out approximately ½ inch. There was no overall bowing of the package or other significant visible deformation. There was no visible damage to the closure or the locking pins.

The closure was removed and the basket extracted following the CD4-2 drop. The basket damage was minor and limited to a small dent at the end of the basket that was situated closest to the package bottom and a small deformation to the basket end plate from the package inner shell. As illustrated in Figure 2.12.2-15 and Figure 2.12.2-16, the simulated fuel plates experienced localized deformation at the end of the basket closest to the package bottom. The remaining area above the localized deformation was not deformed.

The gap between the thermal shield and the stiffening rib, where the shield pulls away from the rib was found to be less than 1/16-inch during the disassembly of CTU-2 discussed in Section 2.7.8.2, *CTU-2 Package Disassembly – Results*. With the thermal shields removed the maximum compaction for all insulation sections ranged from 1 inch to 1¾ inches.

2.7.2 Crush

10 CFR §71.73(c)(2) requires that the crush test be performed on fissile material packages which have a mass not greater than 1,100 lb and a density not greater than 62.4 lb/ft^3. The ATR FFSC package has a maximum weight of 290 lb and a volume of 2.69 ft^3 (based on outside dimensions of 8 in x 8 in x 72.5 in), leading to a maximum density of 290/2.69 = 108 lb/ft^3. Therefore, the crush test is not applicable.

2.7.3 Puncture

10 CFR §71.73(c)(3) requires the drop of the package onto a 6-inch diameter steel bar from a height of 40 inches. The primary modes of failure of the ATR FFSC would be closure damage, closure rotation, and penetration of the outer shell. The object of the puncture drop tests in the current instance is to create the maximum amount of damage in critical locations and

components. Therefore, drop orientations are selected which would result in the greatest amount of critical damage and which would render the package most vulnerable to the thermal event. For the ATR FFSC, these are the CG over center of closure, 30º oblique CG over side, and an oblique drop onto the closure.

The CG over center of closure position was chosen to confirm the performance of the closure assembly and verify at least one locking pin remained locked to prevent rotation. The 30º oblique CG over side was chosen to confirm the resistance of the outer shell to penetration from the puncture bar. The oblique drop onto the closure assembly confirms that the puncture bar can not cause rotation of the closure and was added after the CD3-1 drop sheared one of the locking pins.

CTU-2 was not subjected to puncture, since the purpose of the CTU-2 test unit was to demonstrate the effectiveness of the LFPB and the performance of the thermal insulation. The puncture test would have no impact on these features.

2.7.3.1 Results of the Puncture Tests

CG Over Center of Closure, Vertical (CP1-1). See Figure 2.12.1-44 through Figure 2.12.1-46. The puncture bar impacted directly on the closure assembly (the handle was removed during previous free drop tests). The drop resulted in only minor damage with the TID post deformed into the closure and the closure assembly exhibiting minor scratches from the puncture bar. The locking pins showed no visible signs of deformation and the remaining functional locking pin remained in the locked position.

CG Over Side, 30º Oblique (CP2-1). See Figure 2.12.1-41 through Figure 2.12.1-43. The initial impact caused a deformation of approximately 1/2 inch deep by 5 inches across with a radius the same as the puncture bar. There were no tears or fissures in the ATR FFSC outer skin and there was no change to the closure assembly.

Oblique Drop onto Closure (CP3-1). See Figure 2.12.1-29 through Figure 2.12.1-31. CP3-1 was an unscheduled puncture drop with the purpose of causing rotation to the closure assembly. This extra drop was chosen due to the failure of one of two locking pins during CD3-1. The puncture bar squarely impacted the closure rib and the CTU bounced away from the puncture bar onto the drop pad. Following the drop, the closure assembly rib exhibited minor deformations at the impact point made by the puncture bar. There was no rotation of the closure, and the remaining functional locking pin remained in the locked position and showed no visible signs of deformation.

2.7.4 Thermal

10 CFR §71.73(c)(4) requires the exposure of the ATR FFSC packaging to a hypothetical fire event. Performance of the package under the thermal event is addressed analytically in Chapter 3, *Thermal Evaluation*. Disassembly of the package following the structural tests confirmed that the compaction to the insulation features, as assumed in the thermal analyses, was shown to still perform in a satisfactory manner.

2.7.4.1 Summary of Pressures and Temperatures

As shown in Section 3.4.3, *Maximum Temperatures and Pressures*, the maximum peak temperature of the outer shell was evaluated to be 1,471ºF. The annular space between the outer shell and inner shell pressurized to a maximum 39 psi gauge during the HAC thermal event. The payload cavity of the ATR FFSC is vented to the atmosphere and therefore the inner shell (6 inch diameter pipe) experiences an external pressure of 39 psi gauge. Since the ATR FFSC does not provide leaktight containment, this pressure is not significant to the package.

2.7.4.2 Differential Thermal Expansion

The thermal analysis presented in Section 3.4.4, *Thermal Evaluation under Hypothetical Accident Conditions,* identifies that the peak temperature difference between the inner and outer shells occurs approximately six minutes into the thermal event and results in a free differential thermal expansion of approximately 0.9-inches between the two shells. This places the outer shell in compression and the inner shell in tension. The packaging could respond structurally to the forces developed by this differential expansion by:

- failure of one of the two inner shell to end plate welds (allowing free expansion of the outer shell relative to the inner shell), or
- no weld failure, but buckling of the outer shell, or
- a combination of the above two scenarios.

In any case, none of theses scenarios results in a geometry change to the packaging that leads to an increase in reactivity. The only concern is a condition that could allow an increase in heat transfer to the fuel such that the fuel approaches the melting point.

As identified in Section 3.4.4, *Thermal Evaluation under Hypothetical Accident Conditions,* the thermal consequences of the above events results in insignificant changes to the fuel temperature. The fuel does not approach the melting point and therefore there will be no impact to reactivity. The effect of differential thermal expansion on the various packaging components is therefore considered negligible.

At 72ºF, the nominal length of the packaging cavity is 67.88 inches, the nominal length of the FHE is 67.25 inches and the nominal length of the LFPB is 67.5 inches. Both the LFPB and the FHE are fabricated from aluminum so the worst case for potential interference due to thermal expansion is with the LFPB. From Figure 3.4-5 it can be seen that above 700ºF the inner shell temperature is much greater than the LFPB temperature and so the inner shell thermal expansion rate exceeds that of the LFPB. During the cooling period below 700ºF, the temperatures of the two components track within about 50 ºF with the inner shell temperature always less than the LFPB. The worst condition for potential thermal expansion interference is near the peak temperature of the LFPB. For this evaluation, conservatively assume the LFPB temperature is 750ºF and the inner shell is at 700ºF. The length of the two components at these temperatures is calculated as follows:

$$L = \alpha \cdot L_{Original} \cdot (\Delta T) + L_{Original}$$

Where,

$L_{Original}$ = the original length of the component at 72ºF

α = the coefficient of thermal expansion[11]

[11] Coefficients of thermal expansion are taken from ASME B&PV Code, Section II, Part D, coefficient B. For aluminum, Table TE-2, and for stainless steel, Table TE-1, Group 3.

For aluminum: $\alpha_{Al} = 14.7\left(10^{-6}\right) \text{ in/in/}^{o}\text{ F}$ at 750 ºF
For stainless steel: $\alpha_{SST} = 10.0\left(10^{-6}\right) \text{ in/in/}^{o}\text{ F}$ at 700 ºF

ΔT = the change in temperature from 72ºF

L = the length of the component at the elevated temperature

Loose fuel plate basket length at 750ºF is:

$$L_{LFPB} = 14.7\left(10^{-6}\right)(67.5)(750 - 72) + 67.5 = 68.17 \text{ inches}$$

Inner shell length at 700ºF is:

$$L_{IS} = 10.0\left(10^{-6}\right)(67.88)(700 - 72) + 67.88 = 68.31 \text{ inches}$$

$L_{IS} > L_{LFPB}$, therefore there is no interference under worst case conditions.

2.7.4.3 Stress Calculations

Since there is no differential thermal expansion interference between FHE or LFPB and the packaging, and since the packaging internal pressure is zero, there are no stresses to report.

2.7.4.4 Comparison with Allowable Stresses

Since there are no stresses to report, this section does not apply.

2.7.5 Immersion – Fissile Material

10 CFR §71.73(c)(5) requires performance of the immersion test for packages containing fissile material. The criticality evaluation presented in Chapter 6.0, *Criticality Evaluation*, assumes optimum hydrogenous moderation of single ATR FFSC packages and arrays of packages. Since the criticality consequences of water in-leakage are accounted for, and leakage of the payload from the packaging did not occur, the immersion test of 10 CFR §71.73(c)(5) is not of concern.

2.7.6 Immersion – All Packages

10 CFR §71.73(c)(6) requires performance of an immersion test on an undamaged specimen under a head of water of at least 50 ft or 21.7 psig. The package payload cavity does not provide a leak tight containment. Since the criticality consequences of water in-leakage are accounted for, and leakage of the payload from the packaging did not occur, the immersion test of 10 CFR §71.73(c)(6) is not of concern.

The ATR FFSC does contain a sealed annular space between the outer square tube and the inner pipe where the insulation is located. The possible consequence of a 21.7 psig pressure applied to the outside surface of the square tube and the inside surface of the 6 inch diameter tube are considered insignificant to both the packaging and the payload.

2.7.7 Deep Water Immersion Test

The ATR FFSC package is a Type A Fissile package; hence, this requirement does not apply.

2.7.8 Summary of Damage

The discussions of sections 2.7.1, *Free Drop*, through 2.7.7, *Deep Water Immersion Test*, demonstrate that the ATR FFSC package prevents loss or dispersal of the payload when subjected to all applicable hypothetical accident tests. In addition, the ATR fuel element and loose fuel plates retain a geometry consistent with the analysis presented in Section 6.0, *Criticality Evaluation*. The physical test series consisted of multiple 30 ft free drop and puncture drop tests conservatively applied to two CTUs. Following the drop tests, each CTU was destructively disassembled to inspect various aspects of the packaging. Table 2.7-1 presents the certification drop test series in the sequential order performed for both CTU-1 and CTU-2.

Table 2.7-1 – ATR FFSC Certification Drop Test Series

Test No.	Test Description	Purpose of Test
CN1-1 (CTU-1)	CG over top corner	Confirm: • Fuel element does not penetrate the closure insulation pocket. • Fuel retains geometry necessary to maintain sub-criticality. • Closure is retained on the body and has not rotated relative to the package body.
CD1-1 (CTU-1)	Flat side drop, pocket side down.	Confirm: • Closure is retained and has not rotated relative to the package body. • Fuel retains geometry necessary to maintain sub-criticality.
CD2.A-1 (CTU-1)	Flat side drop, index lugs down	Confirm: • Impact on index lugs does not cause a fracture in the outer shell. • Closure is retained and has not rotated relative to the package body.
CD2.B-1 (CTU-1)	Flat side drop, index lugs down	Same purpose as CD2.A-1. This test was repeated due to the impact during CD2.A-1 being slightly rotated on the longitudinal axis and not fully impacting the index lugs.
CD3-1 (CTU-1)	Flat side drop, pocket and index lugs on side (-20ºF)	Confirm: • Closure is retained and does not rotate relative to the package body. • Fuel element performance at cold temperature. • Fuel retains geometry necessary to maintain sub-criticality.
CD4-1 (CTU-1)	CG over bottom end (-20ºF)	Confirm: • Fuel element does not penetrate into the packaging bottom end insulation pocket. This is a thermal performance requirement. • Fuel element performance at cold temperature. • Fuel retains geometry necessary to maintain sub-criticality.
CP3-1 (CTU-1)	Oblique drop onto closure assembly	Confirm: • Closure is retained on the body and does not rotate relative to the package body. This was an unscheduled test to confirm the performance of the remaining locking pin after the failure of the other pin during CD3-1.

Table 2.7-1 – ATR FFSC Certification Drop Test Series (continued)

Test No.	Test Description	Purpose of Test
CD5-1 (CTU-1)	CG over top corner (same orientation as CN1)	Confirm: • Fuel element does not penetrate the closure insulation pocket. • Fuel retains geometry necessary to maintain sub-criticality. • Closure is retained and does not rotate relative to the package body.
CD2.C-1 (CTU-1)	Flat side drop, index lugs down	Same purpose as CD2.A-1. This test was repeated for a third time due to the impact during CD2.B-1 being slightly rotated on the longitudinal axis and not fully impacting the index lugs.
CP2-1 (CTU-1)	CG over side, 30° oblique	Confirm: • Resistance of outer shell to puncture bar penetration.
CP1-1 (CTU-1)	CG over center of closure (Vertical)	Confirm: • Closure is retained and does not rotate relative to the package body.
CD1-2 (CTU-2)	Flat side drop, pocket side down.	Confirm: • Closure is retained and has not rotated relative to the package body. • Simulated fuel plates and basket retain geometry necessary to maintain sub-criticality.
CD3-2 (CTU-2)	Flat side drop, pocket and index lugs on side	Confirm: • Closure is retained and does not rotate relative to the package body. • Simulated fuel plates and basket retain geometry necessary to maintain sub-criticality.
CD4-2 (CTU-2)	CG over bottom end	Confirm: • Simulated fuel plates or basket do not penetrate into the packaging bottom end insulation pocket. This is a thermal performance requirement. • The insulation is not excessively compacted along the axial length of the package at the inner tube. • Simulated fuel plates and basket retain geometry necessary to maintain sub-criticality.

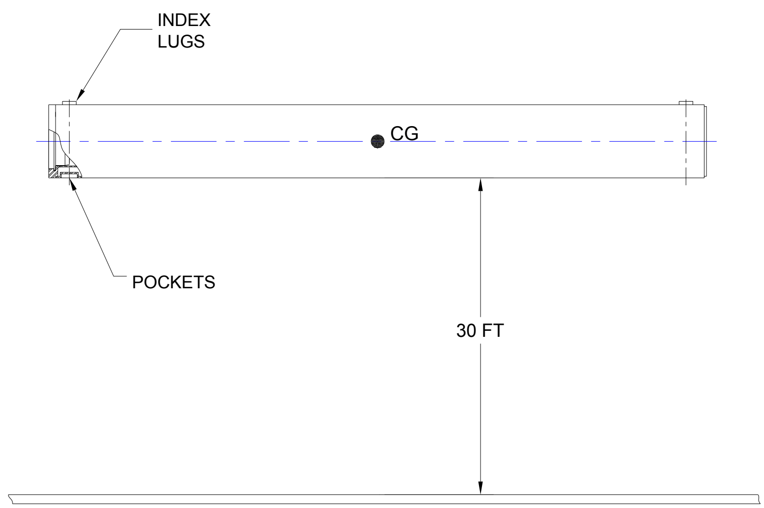

Index lugs and pockets rotated depending on drop series.

Figure 2.7-1 – ATR FFSC Certification Tests CD1-1, CD2-1, CD3-1, CD1-2, & CD3-2 (Test CD1-1 Shown)

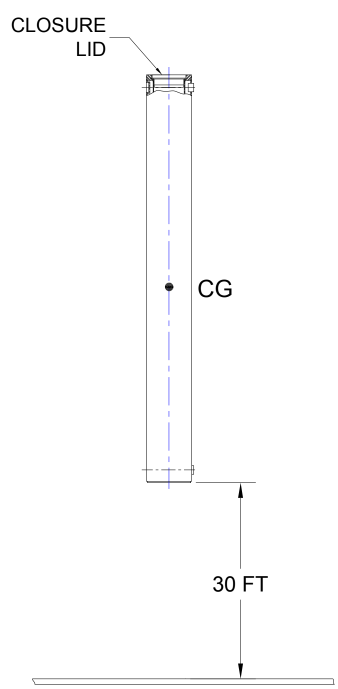

Figure 2.7-2– ATR FFSC Certification Tests CD4-1 & CD4-2

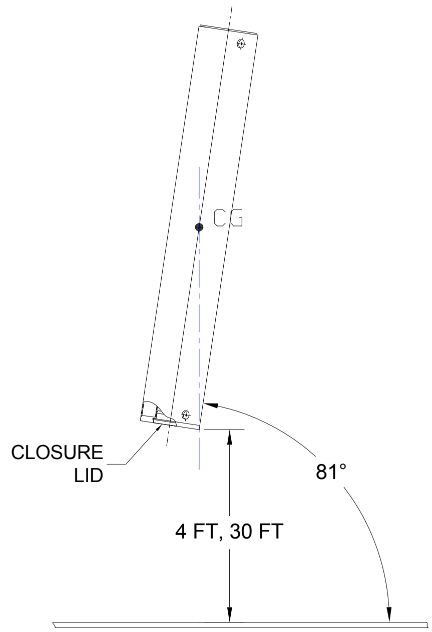

Figure 2.7-3 – ATR FFSC Certification Tests CN1-1 & CD5-1

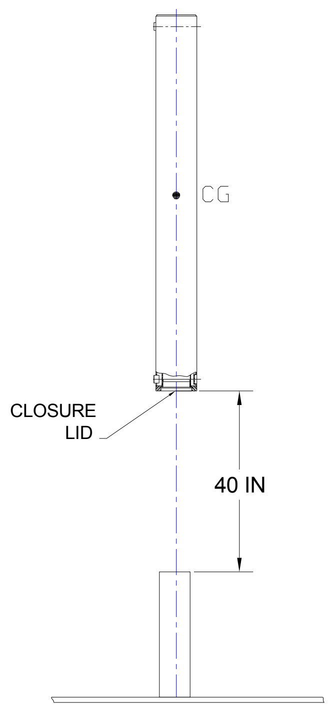

Figure 2.7-4– ATR FFSC Certification Test CP1-1

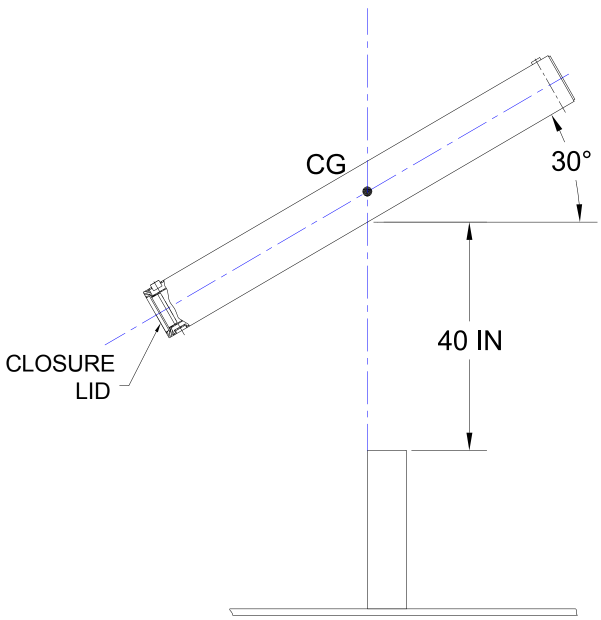

Figure 2.7-5– ATR FFSC Certification Test CP2-1

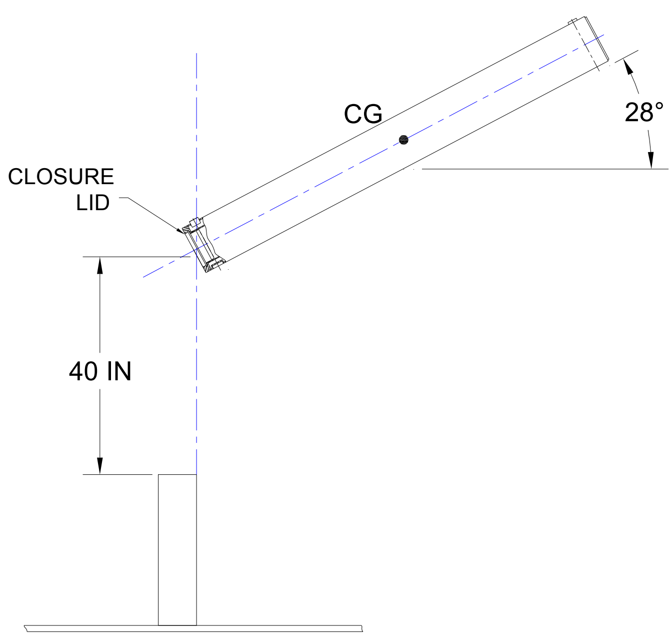

Figure 2.7-6– ATR FFSC Certification Test CP3-1

2.7.8.1 CTU-1 Package Disassembly - Results

Following the nine free drop tests and three punctures, CTU-1 was disassembled to examine the internal features. The items of critical importance focused on during the disassembly included:

- Loss or dispersal of any radioactive/fissile material
- Movement or compaction of the insulation material wrapped around the inner shell and condition of each end plate as related to the thermal evaluation.
- Deformations associated with the position and geometry of the ATR fuel element as related to the criticality evaluation.

To confirm the thermal performance features of the package the inner shell insulation and the insulation pockets at each end were visually inspected. The inner thermal shields remained in place and the maximum compaction for all insulation sections ranged from 1-1/8 inches to 1-½ inches. The closure end and bottom end insulation pockets were not penetrated and exhibited only minor deformation. For photographs of the disassembly see Figure 2.12.1-47 through Figure 2.12.1-51.

The inner tube was inspected as shown in Figure 2.12.1-52 and Figure 2.12.1-53. Due to the CG over corner drop deformation, CD5-1, the inner tube bowed out approximately ¼ inch in one localized area near the closure end. In the same area the inner tube also bowed inward approximately 3/16 inch slightly deforming the FHE aluminum end plate. There were no visible signs of any weld failures associated with the inner tube.

The FHE was removed from the inner shell and visually inspected as shown in Figure 2.12.1-56. The welds joining the endplates to the FHE body had failed at both ends. There was minor bowing and deformation located near the closure end of the package and some of the neoprene padding on the inside had become detached.

The ATR fuel element end boxes were shattered as expected. The geometry of the fissile material within the fuel element was not significantly altered and clearly was within the assumptions used in the criticality analysis as illustrated in Figure 2.12.1-57 through Figure 2.12.1-62. The post test inspection of the fuel element revealed large impact marks in the fuel plates as shown in Figure 2.12.1-58 through Figure 2.12.1-59 from fragments of the fuel element end boxes deforming the ends of the fuel plates. However, the uranium aluminide fissile material within each fuel plate was not exposed and the deformations at each end did not extend to the fissile material within each fuel plate. A comparison between the pre-test and post-test inspections of the fuel element is provided in Table 2.7-2. The measurements were generally taken at five locations along the length of the fuel plates. Note that, due to the numerous free drops and punctures applied to CTU-1, the damage experienced by the ATR fuel element was much greater than is to be expected for a single, 30 ft free drop and 40-inch puncture drop. Further detail is provided in Appendix 2.12.1, *Certification Tests on CTU-1*.

Table 2.7-2 – ATR Fuel Element Measurements

Measurement Area	Pre-Test Range (in)	Post-Test Range (in)
Side Plate Flatness	±0.010	±0.075
In-Plane Bending of Side Plates	±0.011	±0.025
Side Plate Spacing - Top	4.113 – 4.130	4.015 – 4.131
Side Plate Spacing - Bottom	1.840 – 1.845	1.837 – 1.845
Height of Top Fuel Plate from Table (top side up)	2.675 – 2.691	2.655 – 2.785
Height of Bottom Fuel Plate from Table (bottom side up)	2.500 – 2.540	2.415 – 2.508
Fuel Plate to Fuel Plate Spacing	0.075 to 0.080	0.023 to 0.098①

① The minimum and maximum fuel plate spacing measurements were in localized areas near the side vents and not representative of the general spacing.

2.7.8.2 CTU-2 Package Disassembly - Results

Following the three free drop tests, CTU-2 was disassembled to examine the internal features. The items of critical importance focused on during the disassembly included:

- Loss or dispersal of any parts of the simulated loose fuel plate payload.
- Movement or compaction of the insulation material wrapped around the inner shell and condition of each end plate as related to the thermal evaluation.
- Deformations associated with the position and geometry of the simulated loose fuel plates as related to the criticality evaluation.

To confirm the thermal performance features of the package the inner shell insulation and the insulation pockets at each end were visually inspected. The gap between the thermal shield and the stiffening rib, where the shield pulls away from the rib, is less than 1/16-inch. With the thermal shields removed the maximum compaction for all insulation sections ranged from 1 inch to 1 ¾ inches. The closure end and bottom end insulation pockets were not penetrated and exhibited only minor deformation. The bottom end plate was cut open and there was no indication of compression of the insulation in that region. For photographs of the disassembly see Figure 2.12.2-18 through Figure 2.12.2-27.

The inner tube was inspected and a minor deformation occurred near the bottom end of the package as shown in Figure 2.12.2-28 and Figure 2.12.2-29. The tube was bulged out approximately 1/16-inch and, closer to the end, an inward deformation of approximately ¼ inch.

These deformations were localized and did not impair free movement of the basket in the payload cavity. There were no visible signs of any weld failures associated with the inner tube.

Following each of the three drop tests the package was opened and both the LFPB and simulated fuel plates visually inspected. The damage to the LFPB was limited to a small dent at the end of the basket that was situated closest to the package bottom and the impact point as shown in Figure 2.12.2-14. The damage was minor and did not impair the ability of the LFPB to retain the simulated fuel plates.

The simulated fuel plates within the LFPB experienced visible deformation only during the CD4-2 drop. The plates experienced localized deformation at the end of the basket closest to the package bottom as seen in Figure 2.12.2-15 and Figure 2.12.2-16. Above this area the simulated fuel plates were not deformed. Further details can be found in Appendix 2.12.2, *Certification Tests on CTU-2*.

By meeting all of the structural approval standards of Subpart E of 10 CFR §71, the ATR FFSC ensures criticality safety of the package under normal conditions of transport and hypothetical accident conditions.

2.8 Accident Conditions for Air Transport of Plutonium

The ATR FFSC package does not transport plutonium; hence, this section does not apply.

2.9 Accident Conditions for Fissile Material Packages for Air Transport

10 CFR §71.55(f) requires that a package be subcritical subsequent to the application of a series of accident condition tests applicable to the transport of fissile materials by air. The effects of these tests on the ATR FFSC have not been specifically evaluated. Instead, for purposes of the criticality evaluation, a worst-case reconfiguration of the package and contents materials is assumed. Under the bounding assumption, all of the materials of the package and of the contents are assumed to reconfigure into a spherical shape. Materials which moderate or reflect neutrons are placed in positions which lead to the greatest reactivity of the system. Materials whose presence would reduce system reactivity are not credited. The sphere is surrounded by 20 cm of water. The ATR FFSC package meets the requirements of 10 CFR §71.55(f) for the air transport of up to 2 kg of U-235. Details of the criticality analysis are given in Section 6.7, *Fissile Material Packages for Air Transport*.

2.10 Special Form

The ATR FFSC payload is not in special form; hence, this section does not apply.

2.11 Fuel Rods

The ATR FFSC package does not carry irradiated fuel rods; hence, this section does not apply.

2.12 Appendices

2.12.1 Certification Tests on CTU-1

2.12.2 Certification Tests on CTU-2

2.12.3 Structural Evaluation for MIT and MURR Fuel

2.12.1 Certification Tests on CTU-1

This report describes the methods and results of a series of tests performed on the Advanced Test Reactor (ATR) Fresh Fuel Shipping Container (FFSC) transportation package shown in Figure 2.12.1-1. The objective of testing was to conduct drop tests in accordance with the requirements of 10 CFR 71, §71.71 Normal Conditions of Transport (NCT), and §71.73 Hypothetical Accident Conditions (HAC). The verification of the loose fuel plate basket structural integrity and the performance of the package insulation are supported by the tests described in Section 2.12.1, *Certification Tests on CTU-2*.

Testing was performed at Sandia National Laboratories (SNL) in Albuquerque, New Mexico between May 21 and May 23, 2007. Data logs were maintained to track the testing that was performed. In addition, color photographs and videos were taken to document relevant events.

2.12.1.1 Overview

There are three primary objectives for the certification test program:

1. To demonstrate that, after a worst-case series of NCT and HAC free drop and puncture events, the package maintains containment of radioactive contents.
2. To demonstrate that, after a worst-case series of NCT and HAC free drop and puncture events, geometry of both the fuel and package are controlled as necessary to maintain subcriticality.
3. To demonstrate that, after the free drop and puncture bar events, the package retains the thermal protection necessary to maintain the fuel below its melting point during the thermal evaluation.

Several orientations were tested to ensure that the worst-case series of free and puncture drop events had been considered. Post-impact examination demonstrated that the package sufficiently met the design objectives. The design objectives include:

- The package closure remained attached to the body and did not become unlocked as evidenced by no rotation of the closure, thus maintaining containment.
- The package dimensions remained essentially the same providing adequate geometry control.
- Punctures and tears in the outer shell were prevented and thermal insulation was retained for protection during the fire event.
- Reconfiguration of the ATR fuel element and/or Fuel Handling Enclosure (FHE) is bounded by the criticality analysis.

2.12.1.2 Pretest Measurements and Inspections

The ATR FFSC packaging, the FHE, and ATR fuel element were received at SNL and identified as the ATR Fuel Element Certification Test Unit (CTU). The components arrived fully constructed, although not assembled, and ready for testing. The fabrication serial number of the ATR FFSC test unit is CTU3. The serial number for the FHE is FHA 2. The packaging and payload are identified as ATR FFSC Certification Test Unit CTU-1.

The ATR fuel element is an ATR Mark VII high enriched uranium (HEU) fuel element. The ATR fuel element, serial number XA-877R, is a rejected production fuel element based on minor dimensional discrepancies. Prior to assembly of the CTU, some basic dimensions from the fuel element were recorded for post-test comparison. Figure 2.12.1-2 is a photograph of the ATR fuel element prior to testing.

The CTU was dimensionally inspected to the drawings at the fabricator and the fabrication records forwarded to PacTec. A Certificate of Compliance was issued by the fabricator of the CTUs documenting compliance with the fabrication drawings. Minor discrepancies between the drawings and the CTUs were identified and independently evaluated. The evaluations concluded that the discrepancies were minor and would not significantly affect the CTU during testing.

There were four fabrication deviations associated with the serial number CTU3 package fabrication:

- The 3/8-16 UNC index lug screws were obtained without specified ASTM F-879 certifications.
- The #10-24 UNC closure handle screws were obtained without specified ASTM F-879 certifications.
- Chemical over testing of the package body closure plate material identified manganese content 0.02% above the ASTM A479 maximum allowable.
- The handle width is specified to be 7.5 ±.3-inches. When measured in the free state (not secured to the closure), the handle width was undersized by approximately 0.1-inches.

Other deviations relative to the CTU are the absence of the stainless nameplate and the use of temporary rigging attachments. These items are also insignificant relative to the weight of the CTU and their impact upon the drop tests.

2.12.1.2.1 Component Weights

Component weights were measured and recorded as shown in Table 2.12.1-1.

2.12.1.2.2 Drop Test Pad and Puncture Bar Measurement and Description

The drop pad consists of a 10.2 x 28-ft x 4 to 8-in. steel plate firmly anchored to a 300 inch reinforced concrete slab embedded in the ground. The estimated weight of the pad is greater than 2 million lbs. Thus the test pad was qualified as an essentially unyielding surface for the approximately 300 lb CTU. The puncture bar measured 6 in. (150 mm) in diameter and was 36 inches above the drop pad for the puncture drops CP1 and CP2. The puncture bar was securely mounted to the drop pad by welding.

2.12.1.2.3 Equipment and Instruments

Instrumentation used for the component weights and drop tests is given in Table 2.12.1-2. All applicable test and measurement equipment were calibrated in accordance with SNL procedures. The instrumentation used was associated with physical measurements, drop height, angle of the package, and temperature. It is noted that the SNL calibration procedures require National Institute of Standards and Technology (NIST) traceability and that SNL records adequately demonstrated that the calibrations were NIST traceable.

A few different methods were used to confirm the drop height of the package including:

- A plumb bob with a stretch resistant string.
- A tape measure.
- A surveyor theodolite.

SNL project personnel under the supervision of PacTec personnel verified the correct height prior to each drop. The angle of the CTU prior to each drop was measured using a digital level.

Photographic backdrops were fabricated and erected 54 ¼ inches away to the North and 103 ½ inches to the West from the center of the drop pad. The squares on the backdrop are approximately 10.5 inches horizontal and 14.4 inches vertical on the North stadia and 12 inches square on the West stadia.

Two high speed digital video cameras were used to record the drop events. The video views were from the front and side of the drop pad, 90 degrees apart. In addition, color photographs were taken to document the testing.

2.12.1.3 Summary of Tests and Results

2.12.1.3.1 Initial Conditions

The initial conditions for the two HAC drops CD3-1 and CD4-1 were performed at reduced temperature. All other NCT drops, HAC drops, and puncture drops were performed at ambient temperature. Figure 2.12.1-3 shows the chilling unit used to chill the CTU. The chilling unit internal temperature cycled between approximately -25 to -75ºF as it circulated cold air. The CTU was in the chiller for 15 hours and 17 minutes. Just prior to removing the CTU from the chiller, the surface temperature was approximately -60ºF. The target temperature for the ATR fuel element at the time of drop was -20ºF. The surface temperature was recorded before CD3-1 and CD4-1 and varied due to the length of time between removal from the chilling unit to the drop. It is estimated that although the surface temperature raised quickly, the internal temperature of the fuel element was close to the target temperature.

2.12.1.3.2 Summary of Testing

Table 2.12.1-3 identifies the sequential order and testing performed on the ATR FFSC CTU.

2.12.1.4 Certification Tests

2.12.1.4.1 Drop Tests

Only one NCT drop was performed followed by seven HAC drops and three drops onto a puncture bar. The testing conditions are considered conservative due to the large number of HAC drops in various orientations on the single CTU. Relatively minor deformations were recorded due to impact attenuating devices (impact limiters) not being used in the design.

Two 30 ft HAC drops performed on the ATR fuel element CTU were at reduced temperature. These two drops were considered the worst case for the ATR fuel element payload with a targeted temperature of -20ºF. The other orientations confirmed the performance of the packaging.

Figure 2.12.1-4 illustrates the orientation markings on the CTU to aid in the descriptions provided throughout this report. The test identification numbering reflects the same drop orientation as performed in CTU-2. For example, CD3-1 is the same orientation as the third HAC drop in CTU-2, test CD3-2. The "-1" identifies this drop as a CTU-1 test.

2.12.1.4.1.1 CN1-1 – CG Over Top Corner NCT Drop

A rigging attachment was welded to the bottom end of the CTU to attain the proper orientation. The drop configuration for CN1-1 was with the CG over the top corner of the closure end. Figure 2.12.1-5 illustrates the drop orientation. Initial conditions were as follows:

- Ambient temperature: 71ºF
- Avg. surface temperature: 71ºF
- Time: 11:21 a.m. 5/21/2007
- Drop height: 4 ft

The impact location was at corner number 5 identified in Figure 2.12.1-4. Following impact, the CTU bounced slightly and tipped over onto its side. There was minor visible exterior damage at the impact corner. The maximum deformation at the corner was approximately 1/8 inch. The closure handle was also deformed as a result of the drop. The overall length of the package did not change other than the 1/8 inch at the impact corner and compression of the closure handle of approximately 1/2 inch on one side. There was also a 1/8 inch deformation on the side corner approximately 1 ¼ inch from the impact corner. There was no visible deformation or rotation of the closure, other than the handle. Figure 2.12.1-6 and Figure 2.12.1-7 show the CTU following the NCT drop.

2.12.1.4.1.2 CD1-1 – Flat Side, Pockets Down, HAC Drop

Following CN1-1, the temporary rigging attachments were removed. To rig CD1-1 the index lugs on the CTU were removed and lifting eyes installed in their place. The drop configuration for CD1-1 was with the CTU in the typical lifting orientation, horizontal position, with the alignment pockets facing down. Figure 2.12.1-8 illustrates the drop orientation. Initial conditions were as follows:

- Ambient temperature: 76ºF

- Avg. surface temperature: 78ºF
- Time: 12:20 p.m. 5/21/2007
- Drop height: 30 ft

Following impact, the CTU bounced and rotated slightly in the air. The high speed video was reviewed and the impact was determined to be sufficiently flat. The justification for the determination was the large number of drops planned for the CTU, and that there were two more similar flat side drops. Also, data gathered during engineering test were consistent with the deformation exhibited from the CD1-1 drop.

There were minor visible exterior scratches resulting from the drop. The areas showing the greatest impact marks are at each end plate and near the three internal stiffening ribs. There was no significant bowing or other visible deformation. There was no visible deformation or rotation of the closure and the locking pins remained in the locked position. Figure 2.12.1-9 shows the CTU following the drop.

Upon inspection of the CTU the closure assembly was fully functional and able to be opened as illustrated in Figure 2.12.1-10. The FHE was removed and visually inspected as illustrated in Figure 2.12.1-11. There were no major deformations or cracked welds noticed. One of the spring plungers on the FHE lid was bent slightly but still functional.

As illustrated in Figure 2.12.1-12, there was no visible damage to the fuel element. The fuel element was not removed from the FHE but both end boxes were clearly visible and fully intact.

With the closure assembly removed from the body of the CTU, the locking pin was noticeably bent approximately 1/32 inch as illustrated in Figure 2.12.1-13. This locking pin was located near position number 8 identified in Figure 2.12.1-4. The other locking pin was not deformed and there was no other visible deformation of the closure assembly. It was noticed that the bent locking pin tended to bind when compressed to the open position.

2.12.1.4.1.3 CD2.A-1 – Flat Side, Index Lugs Down, HAC Drop

Following CD1-1, the FHE was reinserted with the hinged lid facing up towards the index lugs and then temporary rigging attachments were welded to the CTU to orient the package in the horizontal position with the index lugs facing down. The lifting eyes used in CD1-1 were removed and the index lugs re-installed with a 22 ft-lb torque applied to the screws. The drop configuration for CD2-1 was with the CTU in the horizontal position, with the index lugs facing down. Figure 2.12.1-14 illustrates the drop orientation. Initial conditions were as follows:

- Ambient temperature: 80ºF
- Avg. surface temperature: 82ºF
- Time: 2:59 p.m. 5/21/2007
- Drop height: 30 ft

Following impact, the CTU bounced and spun in the air about its longitudinal axis. After viewing the high speed video it was confirmed that the CTU impacted the drop pad at a slight angle on the longitudinal axis which caused the CTU to spin during the rebound. The index lugs did receive much of the impact but due to the angle it may not have been the worst case impact to the index lugs. There was visible exterior damage resulting from the drop at the index lugs. The index lugs were both pressed inward approximately 1/8 inch. There were no visible signs of broken welds.

The center of the package had an inward bow of about 1/16 inch. There was no other significant visible deformation. There was no visible rotation of the closure. Figure 2.12.1-15 and Figure 2.12.1-16 show the CTU following the drop. Following CD2.A-1 the closure could no longer be opened due to the body opening becoming slightly out-of-round. As illustrated in Figure 2.12.1-17, the body and closure assembly pinched in two locations.

The locking pin on the left side (near #8) of Figure 2.12.1-17 is shown stuck in the open – unlocked position. This happened during the inspection and not as a result of the drop. As the locking pins and closure assembly were inspected functionally by the test engineer, the one locking pin would bind in the open position and require a light tap from a hammer to become unstuck. The photo however, was taken before the locking pin was returned to the locked position.

2.12.1.4.2 CD2.B-1 – Flat Side, Index Lugs Down, HAC Drop

Following CD2.A-1, a second drop in the same orientation, package in the horizontal position with the index lugs facing down, was performed. The purpose of the re-test was to confirm the performance of the package in this orientation. It was felt that due to the slight incline of the package at impact, the maximum load on the index lugs was not experienced. Figure 2.12.1-18 illustrates the drop orientation which was rotated slightly to account for rotation during the drop. Initial conditions were as follows:

- Ambient temperature: 77ºF
- Avg. surface temperature: 80ºF
- Time: 4:07 p.m. 5/21/2007
- Drop height: 30 ft

During the drop the high speed video showed that the CTU rotated past the horizontal position in the air and impacted at an incline again. Furthermore, the rigging caught a gust of wind and blew to the side and caught the North stadia board. Following impact, the CTU bounced and spun in the air about the longitudinal axis indicating a non-flat impact. The index lugs were both pressed inward approximately 3/16 inch, at the greatest point, from the original surface of the tube. There were no visible signs of broken welds. The handle of the closure assembly broke loose at point #6 shown in Figure 2.12.1-4. The two screws both sheared off and the opposite side remained attached. There was no other significant visible deformation. There was no visible deformation or rotation of the closure and the locking pins remained in the locked position following the drop. During a functional test of the closure assembly the locking pins functioned well (with the locking pin near #8 binding in the open position) and the closure could rotate approximately ¼ inch. Figure 2.12.1-19 and Figure 2.12.1-20 show the CTU following the drop.

2.12.1.4.3 CD3-1 –Flat Side HAC Drop

The CTU was fitted with temporary rigging attachments for both CD3-1 and CD4-1 prior to chilling to minimize warming of the CTU prior to the drops. The CTU was removed from the chilling unit after 15 hours and 17 minutes with the average surface temperature reading -57ºF, 14 minutes prior to CD3-1. Figure 2.12.1-21 shows the CTU in the chiller prior to removal. The CTU was oriented for a drop onto the long side with the pockets and index lugs oriented at 90º to the drop pad. The drop configuration was with the CTU's side parallel to the horizontal. Figure 2.12.1-22 illustrates the drop orientation. Initial conditions were as follows:

- Ambient temperature: 67ºF
- Avg. surface temperature: +13ºF
- Time: 9:31 a.m. 5/22/2007
- Drop height: 30 ft

Following impact, the CTU bounced slightly and came to rest in its standard position with the index lugs facing up. The impact side showed just minor scratches and impact marks from the drop. Figure 2.12.1-23 and Figure 2.12.1-24 show the CTU following the drop. The impact side showed a slight bowing of the ends. Using a straight edge, the maximum gap at each end was approximately 1/8 inch. There was no visible rotation of the closure and the locking pins remained in the locked position following the CD3-1 drop.

As illustrated in Figure 2.12.1-25, the closure assembly was functionally tested and upon close inspection it was found that the locking pin near point #4 (bottom of picture) had sheared off between the closure assembly and body preventing the locking pin from engaging in the body. The locking pin near point #8 was engaged following the drop but continued to bind in the open - unlocked position when depressed by hand. Figure 2.12.1-25 shows this locking pin in the open position following the attempt to open the closure. The closure assembly could partially rotate approximately ¼ inch but was unable to fully rotate to the open position. The locking pin near point #8 was returned to the locked position following the inspection. The dull gray color seen on the photographs is frost.

2.12.1.4.4 CD4-1 –CG Over Bottom End HAC Drop

Immediately after CD3-1, rigging was attached to the pre-welded lugs near the closure and the CTU prepared for the CD4-1 drop. The time between CD3-1 and CD4-1 was 33 minutes. During that time the CTU was kept elevated above the drop pad. The drop configuration was with the CTU in the vertical position, with the bottom end down (closure end up). Figure 2.12.1-26 illustrates the drop orientation. Initial conditions were as follows:

- Ambient temperature: 64ºF
- Avg. surface temperature: 42ºF
- Time: 10:04 a.m. 5/22/2007
- Drop height: 30 ft

Following impact the outer shell of the CTU exhibited minor bowing near the impact end with the greatest deformation measuring approximately 1/8 inch on the 90º side per Figure 2.12.1-4. The overall length of the package body was compared with the initial measurements at the eight locations and found to have compressed a maximum of approximately 1/8 inch. There was no visible deformation or rotation of the closure following the drop and the functionality of the closure assembly did not change. Figure 2.12.1-27 and Figure 2.12.1-28 show the CTU following the drop.

2.12.1.4.5 CP3-1 – Oblique, CTU Closure Over Puncture Bar

Following CD4-1 the CTU was positioned for an unscheduled puncture bar drop onto the closure. The purpose for this drop was to attempt to rotate the closure assembly prior to the CD5-1 drop which would severely deform the closure area of the body preventing any chance of rotation. The temporary rigging attachments from CD3-1 and CD4-1 were removed and new attachments welded for this drop. The puncture bar, 36 inches in height, was welded to the drop pad. For CP3-1, the CTU was hoisted at a 28.3º orientation from horizontal and a 225º twist on the longitudinal axis so the puncture bar would impact one of the ribs in the closure assembly. The closure handle, which had broke off from one side during CD2.B-1, was bend outward to keep from interfering with the targeted impact location. Figure 2.12.1-29 and Figure 2.12.1-30 illustrate the drop orientation. Initial conditions were as follows:

- Ambient temperature: 72ºF
- Avg. surface temperature: 73ºF
- Time: 11:50 a.m. 5/22/2007
- Drop height: 40 inches

The puncture bar squarely impacted the closure rib and the CTU bounced away from the puncture bar onto the drop pad. Following the drop, the closure assembly rib exhibited minor deformations at the impact point made by the puncture bar. There was no rotation of the closure assembly and the locking pins showed no visible signs of deformation. The locking pin by #8 remained in the locked position. Both locking pins were functioning and able to be moved and compressed against the spring when tested by hand. Note that the locking pin by #4 was previously sheared during the CD3-1 drop. Figure 2.12.1-31 shows the CTU closure following CP3-1.

2.12.1.4.6 CD5-1 – CG Over Top Corner HAC Drop

For CD5-1, the CTU was hoisted in the same orientation as CN1 with the CG over the top corner; point #5 in Figure 2.12.1-4. The closure handle was removed for convenience since it was loose and obstructing the drops. Figure 2.12.1-32 illustrates the drop orientation. Initial conditions were as follows:

- Ambient temperature: 76ºF
- Avg. surface temperature: 81ºF
- Time: 1:54 p.m. 5/22/2007
- Drop height: 30 ft

Following impact, the CTU bounced slightly and tipped over onto its side. The impact corner was deformed in approximately 5/8 inch. There was modest deformation on the sides of the package near the impact location bulging in approximately 1/2 inch near the index lug pocket and bulged out approximately 5/8 inches on the adjoining side. The impacted corner deformed in approximately 5/8 inch and the opposite corner, #1, had no change in length. Figure 2.12.1-33 through Figure 2.12.1-36 show the CTU following CD5-1.

Following the drop, the closure assembly exhibited deformation with the end of the package and was unable to be rotated more than 1/8 inch in either direction. The locking pins showed no visible signs of deformation and the pin by #8 remained in the locked position. Both locking pins were functioning and able to be moved and compressed against the spring when tested by hand.

2.12.1.4.7 CD2.C-1 – Flat Side, Index Lugs Down, HAC Drop

Following CD5-1 a third drop in the same CD2 orientation, package in the horizontal position with the index lugs facing down, was performed. The purpose of third re-test was to confirm the performance of the package in this orientation. It was felt that due to the incline of the package at impact during the previous drops, the maximum load on the index lugs was not experienced. Both the release mechanism and rigging cables were changed to aid the drop. Figure 2.12.1-37 illustrates the drop orientation. Initial conditions were as follows:

- Ambient temperature: 79ºF
- Avg. surface temperature: 79ºF
- Time: 2:37 p.m. 5/22/2007
- Drop height: 30 ft

The third try produced a satisfactory drop orientation. Following impact, the CTU bounced and spun just slightly indicating the impact was directly on the index lugs. The index lugs were both pressed inward. The index lug at the closure end was flush with the general surface. The index lug at the bottom end was pushed in to approximately 1/8 inch from the general surface. Figure 2.12.1-38 and Figure 2.12.1-39 show the index lugs following the drop. The index lugs were removed and a cracked weld was revealed under the index lug near the closure end as shown in Figure 2.12.1-40. The length of the cracked weld was approximately ½ inch. There was no other significant visible deformation. There was no visible deformation or rotation of the closure as a result of the drop.

2.12.1.4.8 CP2-1 – CG Over Side, 30º Oblique, HAC Puncture Drop

For CP2-1, the CTU was hoisted at a 30º oblique angle with the CG over the edge of the puncture bar. Figure 2.12.1-41 illustrates the drop orientation. Initial conditions were as follows:

- Ambient temperature: 76ºF
- Avg. surface temperature: 77ºF
- Time: 3:19 p.m. 5/22/2007
- Drop height: 40 inches

As the CTU impacted the puncture bar, there was no tearing of severe deformation. The initial impact caused a deformation of approximately 1/2 inch deep by 5 inches across with a radius the same as the puncture bar. There was no fracture of the outer shell. Figure 2.12.1-42 and Figure 2.12.1-43 show the CTU following the CP2-1 drop.

2.12.1.4.9 CP1-1 – CG Over Center of Closure HAC Puncture Drop

For CP1-1, the CTU was hoisted in the vertical orientation with the closure directly over the puncture bar. Figure 2.12.1-44 illustrates the drop orientation. Initial conditions were as follows:

- Ambient temperature: 79ºF
- Avg. surface temperature: 81ºF
- Time: 4:06 p.m. 5/22/2007

- Drop height: 40 inches

Following impact, the CTU bounced slightly on the puncture bar, as verified by high speed video, and came to rest in the vertical position on top of the puncture bar as seen in Figure 2.12.1-45. Following the drop, the tamper indicating device (TID) post was deformed into the closure. The closure assembly exhibited minor scratches from the puncture bar. The locking pins showed no visible signs of deformation and the remaining locking pin by #8 remained in the locked position. Both locking pins were functioning and able to be moved and compressed against the spring when tested by hand. Figure 2.12.1-46 shows the CTU in the up-side-down position following CP1-1. Note that both locking pins were binding somewhat following testing and shown in the photographs in the open – unlocked position following the functional tests.

2.12.1.5 Post-test Disassembly and Inspection

The final acceptance criteria for the ATR FFSC package lies with the criticality and thermal evaluations. Any increase in reactivity of the contents resulting from the certification tests must not exceed the allowable as defined in the criticality evaluation. The inspections required to support determination of compliance with the acceptance criteria are identified as follows:

- Inspect the outer shell to verify the thermal performance of the package is unimpaired by the free drop and puncture events. The thermal analysis assumes that the outer shell is intact such that there is no significant communication between the environment and the outer/inner shell annular space during the thermal event.
- Inspect the insulation to verify compliance with the assumptions of the thermal analysis.
- Inspect the overall package to verify that the package geometry remains within the criticality analyses assumptions.
- Inspect the Mark VII fuel element to verify that the fuel geometry remains within the assumptions of the criticality analyses.

Any deviation of the test results from these acceptance criteria must be reconciled with the criticality or thermal evaluations.

2.12.1.5.1 CTU Inspection

Radiological surveys were performed after each drop test and during the disassembly of the package. The radiological survey reports confirm that there was no loss or dispersal of radioactive material from the package or from the ATR fuel element.

The ATR fuel element CTU was disassembled and inspected on May 23, 2007. Prior to disassembly the exterior dimensions were recorded for comparison to the pre-test condition. Table 2.12.1-4 lists the measured dimensions and Figure 2.12.1-4 identifies the location of the identified measurements.

The closure handle was flattened, loosened, and finally removed during testing for convenience. Due to the relatively weak nature of the handle, its presence or absence had no significant effect on any test outcome. The height of the handle changed from 1 3/8 inches to ½ inch on one side before being removed. There was very little bowing or change in shape of the package. The maximum bowing of the package over its length is estimated at approximately ¼ inch. During the CD5-1, CG over corner HAC drop, deformation of the outer wall caused the width of the package to increase from 8 inches to approximately 8 5/8 inches. The same CD5-1 impact caused the outer wall to deform inward approximately ½ inch.

The CTU was disassembled systematically by cutting away the outer layers of the packaging using an abrasive saw. The destructive examination was necessary due to the deformation of the closure and the need to inspect the interior insulation. Figure 2.12.1-47 illustrates the unsuccessful attempt to rotate the closure assembly and open the package with a steel bar and 5 lb hammer. The closure could not be rotated more than approximately 3/8 inch using the bar and hammer.

The package was cut with an abrasive saw lengthwise along two opposite corners and at the ends to expose the thermal shield. Figure 2.12.1-48 through Figure 2.12.1-50 show the condition of the thermal shields and insulation. The thermal shields were in relatively good shape with dents from both the index lug bosses and pockets on the shields. There was also some minor deformation at each end of the shields by the stiffening rib plates.

The insulation tended to compact towards the closure end except for the bottom end which compacted towards the bottom. The compaction was not uniform but varied around the circumference of the internal pipe. The maximum compaction for all section ranged from 1-1/8 inches to 1-½ inches.

Two thermal shield designs were used; one with a simple overlapping design and the other secured by rivets. There was no appreciable difference between the performance of either design. Both experienced minor deformation at the pockets and index lugs, and at the ends due to impacting the adjoining plates. Furthermore, the compaction of the insulation under each shield was very similar. On the riveted design, there was no failure of any rivet.

The thermal shields and insulation were removed and using an abrasive saw the bottom end plate was removed by cutting the inner tube. Figure 2.12.1-51 illustrates the condition of the bottom end plate. There were no large deformations or punctures of the stainless steel plate. There were no visual indications of broken welds or other damage near the end plate.

As shown in Figure 2.12.1-52 and Figure 2.12.1-53, the inner tube was inspected and the photographs show the areas of greatest deformation. Due to the CG over corner drop deformation, CD5-1, the inner tube bowed out approximately ¼ inch. The inner tube also bowed inward approximately 3/16 inch slightly deforming the FHE aluminum end plate. There were no visible signs of any weld failures associated with the inner tube.

Figure 2.12.1-54 illustrates the relatively unchanged position of the FHE and fuel element within the CTU. Also seen in this figure are pieces of the broken end box at the bottom end and also pieces of neoprene padding from the FHE during removal. The FHE was somewhat difficult to remove and the aluminum end plate had broken off so the ATR fuel element was carefully pulled from the bottom end of the package as illustrated in Figure 2.12.1-55. Both end boxes of the fuel element had shattered into several pieces. These pieces were collected and kept with the fuel element. There were no pieces of the fuel element end boxes found outside the FHE. Once the fuel element was removed, the FHE was pulled from the inner tube. The welds securing each FHE end plate to the body were completely broken and both the end plates were loose. Figure 2.12.1-56 illustrates the area of greatest deformation to the FHE which was at the closure end.

2.12.1.5.2 ATR Fuel Element Inspection

The ATR fuel element was placed on an inspection table and compared against the same pre-test measurements for the fuel plates. Because the fuel element end boxes had shattered and bent the ends of the side plates, some of the fuel plate measurements taken from the side plates could be slightly exaggerated. The measurements included side plate flatness, in plane bending of the side plates, side plate spacing, overall fuel plate spacing, and fuel plate to fuel plate spacing. Table 2.12.1-5 provides the general change in dimensions to the fuel plates. Measurements were generally taken at five locations along the length of the fuel element. The five locations include 1 inch from the end of the fuel plate (neglecting the end boxes), 12 inches from each end of the fuel plate, and at the center of the fuel plate.

Figure 2.12.1-57 through Figure 2.12.1-62 illustrate the condition of the ATR fuel element. As shown in Figure 2.12.1-58 and Figure 2.12.1-59, fragments from the fuel element end boxes deformed and cut into the ends of the fuel plates during testing. At no point did the fuel meat, the embedded uranium within the aluminum cladding, become exposed.

In conclusion, the CTU satisfied the acceptance criteria of preventing loss or dispersal of the contents, the outer shell remained intact, the insulation remained within the assumptions of the thermal analysis, and the package and fuel geometry remained greatly unchanged. The deformations of the package and condition of the ATR fuel element were evaluated against the criticality and thermal evaluations and determined to be within the bounds of the assumptions and conditions used to ensure safety.

Table 2.12.1-1 - Component Weights

Component	Weight (lbs)
Body Assembly	225.0
Closure Assembly	9.0
Fuel Handling Enclosure	14.3
ATR Fuel Element	22.1
Package (fully loaded)	270.4

Table 2.12.1-2 - Instrumentation for Drop Tests

Item Description	Model	Serial Number	Calibration Due Date	Comments
Drop Height Indicators	N/A	N/A	N/A	String plumb bobs made specifically for this testing. The length was established using a metal tape measure.
Tape Measure	Stanley	N/A	N/A	35-ft. steel tape
Digital Level 2’	M-D Building Products	SNL 3665	1/23/09	Used to identify CTU orientation
Digital Level 4’	M-D Building Products	SNL 3666	1/23/09	Used to identify CTU orientation
Scale	NCI	D798311	2/12/08	Used to measure weights of CTU components
Hook Scale	Dively	60418/46180	Aug 2007	Used to measure the weight of the ATR FFSC body
Multilogger Thermometer	Omega Engineering	06000855	10/19/07	Handheld temperature reader for measuring ambient temperature and CTU surface temperature
Temperature Probe	N/A	56194	10/19/07	Probe which attaches to multimeter
Torque Wrench 0-25 ft-lbs	N/A	SNL 1933	2/26/09	Used to apply measured torque to index lug screws

Table 2.12.1.3 - Summary of Testing

Test No.	Test Description	Comments
CN1-1	CG over top corner	CG over top corner drop from 4 ft. Minor deformation at impact corner. Maximum change in length approximately 1/8 inch at impact point only. Closure handle deformed. Closure functions properly.
CD1-1	Flat side drop, pocket side down	Flat side drop from 30 ft. Minor visible scratches and impact marks. Closure functions properly. Package opened and inspected. One locking pin on closure bent slightly but still operable. No visible damage to fuel element.
CD2.A-1	Flat side drop, index lugs facing down	Flat side drop from 30 ft. Impact pushed index lugs into package approximately 1/8 inch. CTU impact was not level on the longitudinal axis causing the package to bounce and spin after impact. A second drop in the same orientation was chosen.
CD2.B-1	Flat side drop, index lugs facing down	Flat side drop from 30 ft. Impact pushed index lugs into package approximately 3/16 inch. CTU impact again was not level due to a gust of wind blowing the rigging straps into the stadia board.
CD3-1	Flat side drop, pockets and index lugs on side, reduced temperature	Flat side drop from 30 ft. Minor visible scratches and impact marks. One locking pin sheared during impact. No rotation of closure. Surface temperature approximately 13ºF.
CD4-1	CG over bottom end (vertical), reduced temperature	Flat bottom drop from 30 ft. No appreciable deformation on impact side but minor bowing outward on side near impact end. Maximum change in length approximately 1/8 inch. Surface temperature approximately 41ºF.
CP3-1	Closure assembly over puncture bar	Unscheduled drop chosen to ensure performance of closure assembly due to broken locking pin from CD3. Impact caused small deformation to closure assembly rib. There was no rotation of the closure and no other visible damage.
CD5-1	CG over top corner (same orientation as CN1)	CG over top corner drop from 30 ft. Deformation of the corner, including adjoining sides, and minor bending of the closure assembly. Maximum change in length at impact point approximately 5/8 inches.
CD2.C-1	Flat side drop, index lugs facing down	Flat side drop from 30 ft. This third drop on the index lugs was chosen to ensure performance of the outer skin and index lugs in this orientation. The previous two drops did not impact flat on the lugs. Index lug at closure end pushed in flush with general package surface, approximately ½ inch. A small crack in the weld between the index lug boss and square tube was recorded.
CP2-1	CG over side, 30° oblique	CG over side puncture drop from 40 in. Minor deformation from impact. Depth of impact approximately ½ inch. Width of impact approximately 5” across.

Table 2.12.1.3 - Summary of Testing

Test No.	Test Description	Comments
CP1-1	CG over center of closure (Vertical)	Vertical puncture drop on closure from 40 in.. The tamper indicating device stud pushed into closure assembly. No other visible damage. No rotation of closure assembly.

Table 2.12.1-4 – Package Length Measurements

Test ID	1	2	3	4	5	6	7	8
Pre-Test (in.)	72 ½	72 ½	72 ½	72 ½	72 ½	72 ½	72 ½	72 ½
Post-Test (in.)	72 5/16*	72 ½	72 7/16	72 ¼	71 11/16*	72 ¼	72 ½	72 7/16

*These locations were modified slightly due to the welding and removal of temporary rigging attachments. The change to position #5 was approximately -1/16 inch. There was approximately no change to position #1.

Table 2.12.1-5 - ATR Fuel Element Measurements

Measurement Area	Pre-Test Range (in)	Post-Test Range (in)
Side Plate Flatness	±0.010	±0.075
In-Plane Bending of Side Plates	±0.011	±0.025
Side Plate Spacing - Top	4.113 – 4.130	4.015 – 4.131
Side Plate Spacing - Bottom	1.840 – 1.845	1.837 – 1.845
Height of Top Fuel Plate from Table (top side up)	2.675 – 2.691	2.655 – 2.785
Height of Bottom Fuel Plate from Table (bottom side up)	2.500 – 2.540	2.415 – 2.508
Fuel Plate to Fuel Plate Spacing	0.075 to 0.080	0.023 to 0.098*

* The minimum and maximum fuel plate spacing were in localized areas near the side vents and not representative of the general spacing.

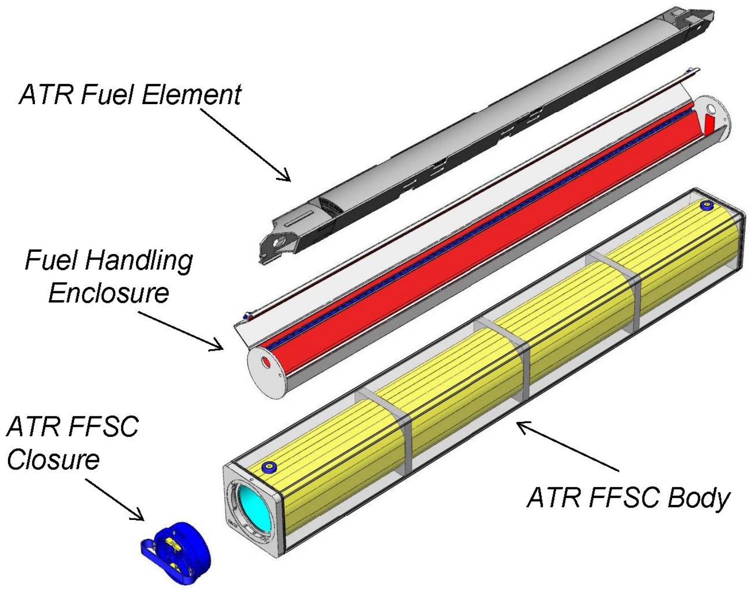

Figure 2.12.1-1 - ATR FFSC

Figure 2.12.1-2 – ATR Fuel Element

Figure 2.12.1-3 – Chilling Unit

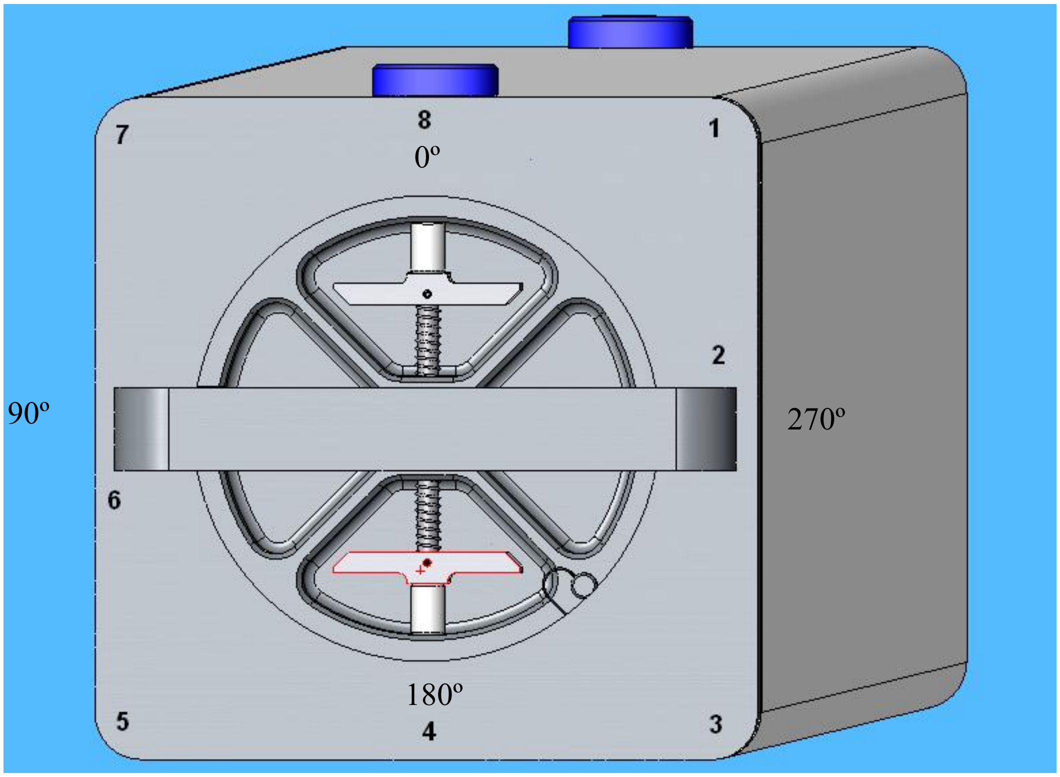

Figure 2.12.1-4 – ATR Package Orientation Markings

Figure 2.12.1-5 - CN1-1 Drop Orientation

Impact
corner

Figure 2.12.1-6 - CN1-1 Impact Damage

Figure 2.12.1-7 - CN1-1 Impact on Closure Handle

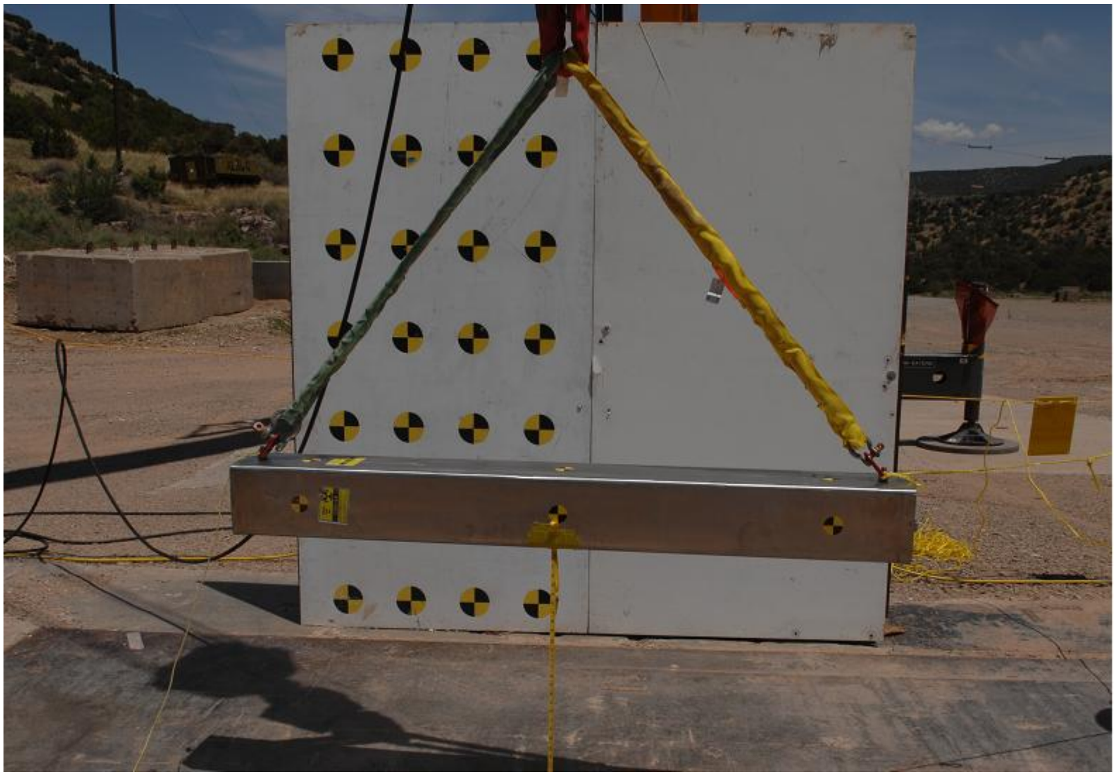

Figure 2.12.1-8 – CD1-1 Drop Orientation

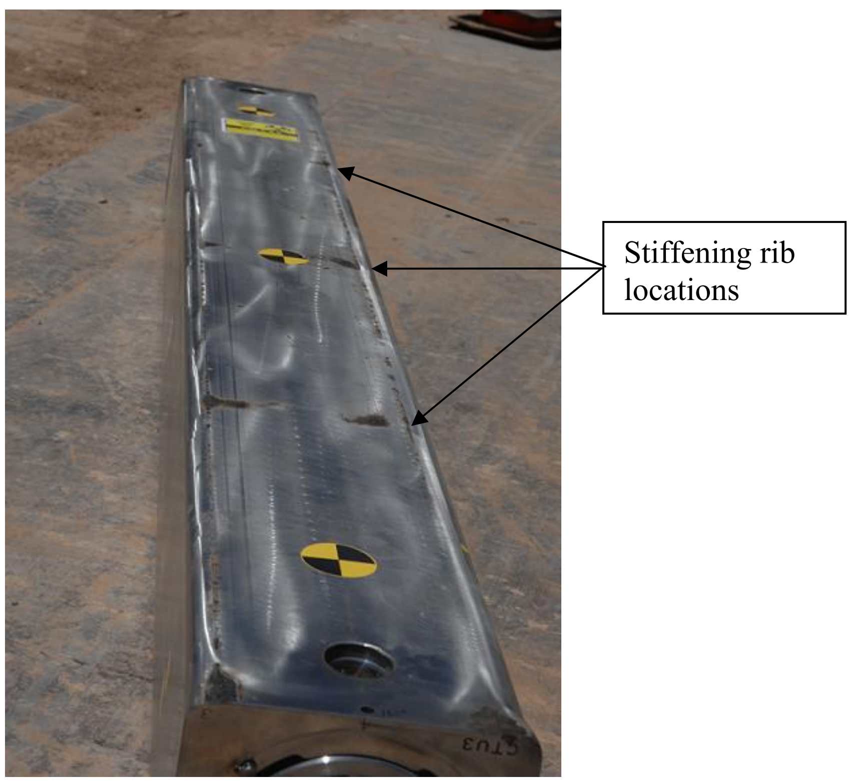

Figure 2.12.1-9 – CD1-1 Impact Side

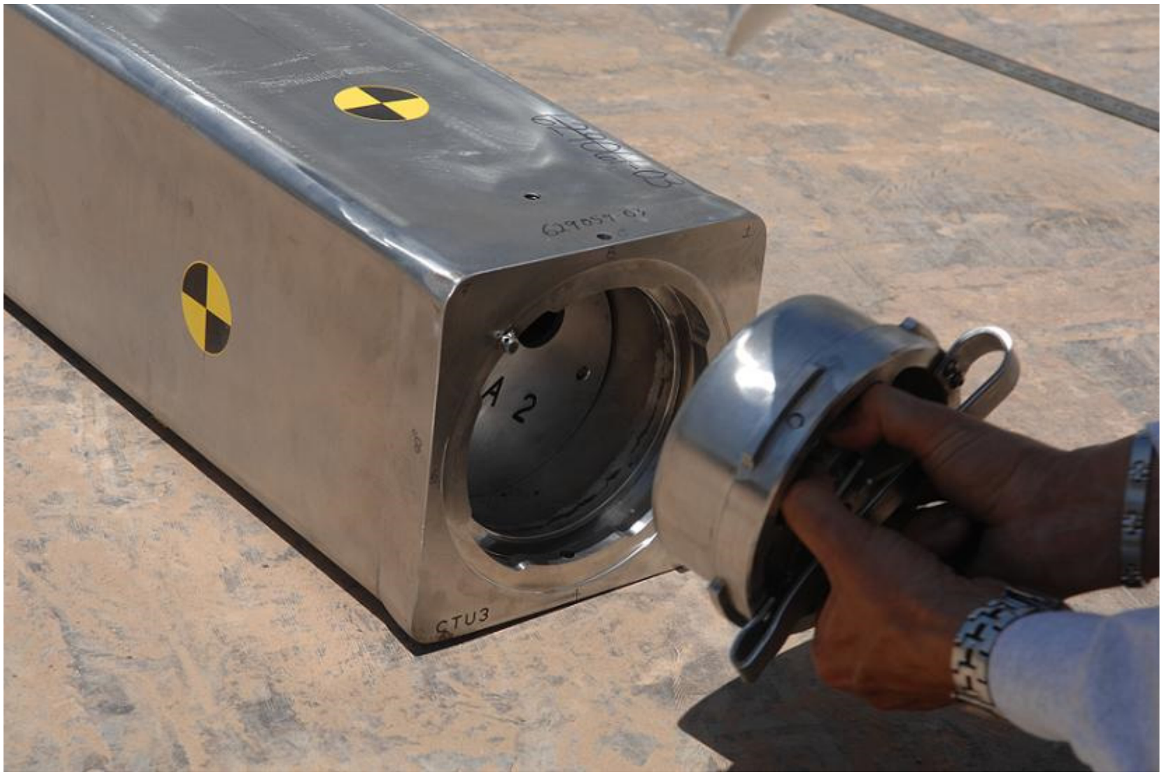

Figure 2.12.1-10 - Opening of CTU Following CD1-1

Figure 2.12.1-11 - Inspection of Payload Following CD1-1

Figure 2.12.1-12 - Inspection of Fuel Element Following CD1-1

Figure 2.12.1-13 - Inspection of Closure Assembly Following CD1-1

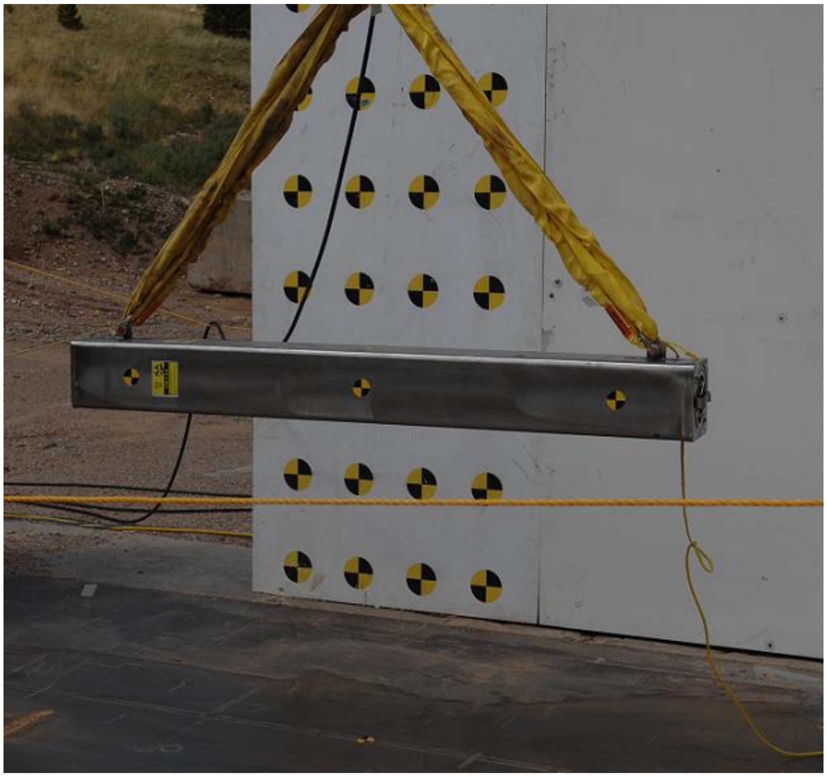

Figure 2.12.1-14 – CD2.A-1

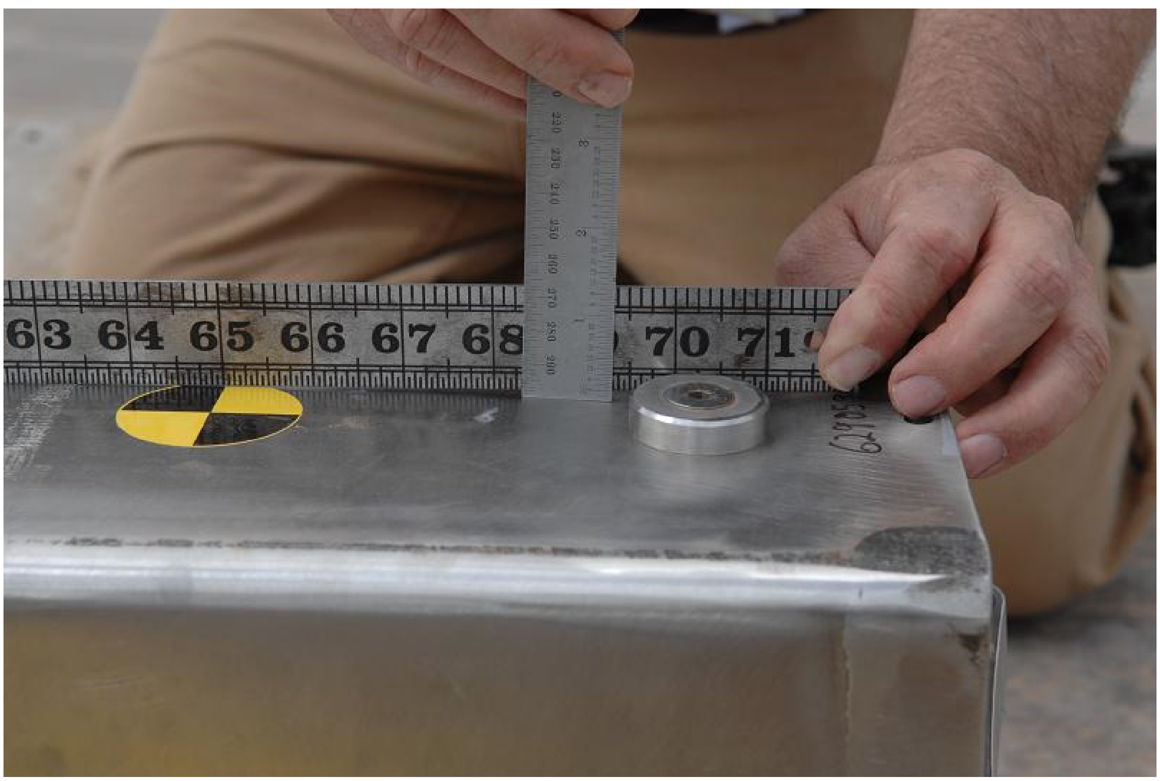

Figure 2.12.1-15 - Index Lug Near Closure End, CD2.A-1

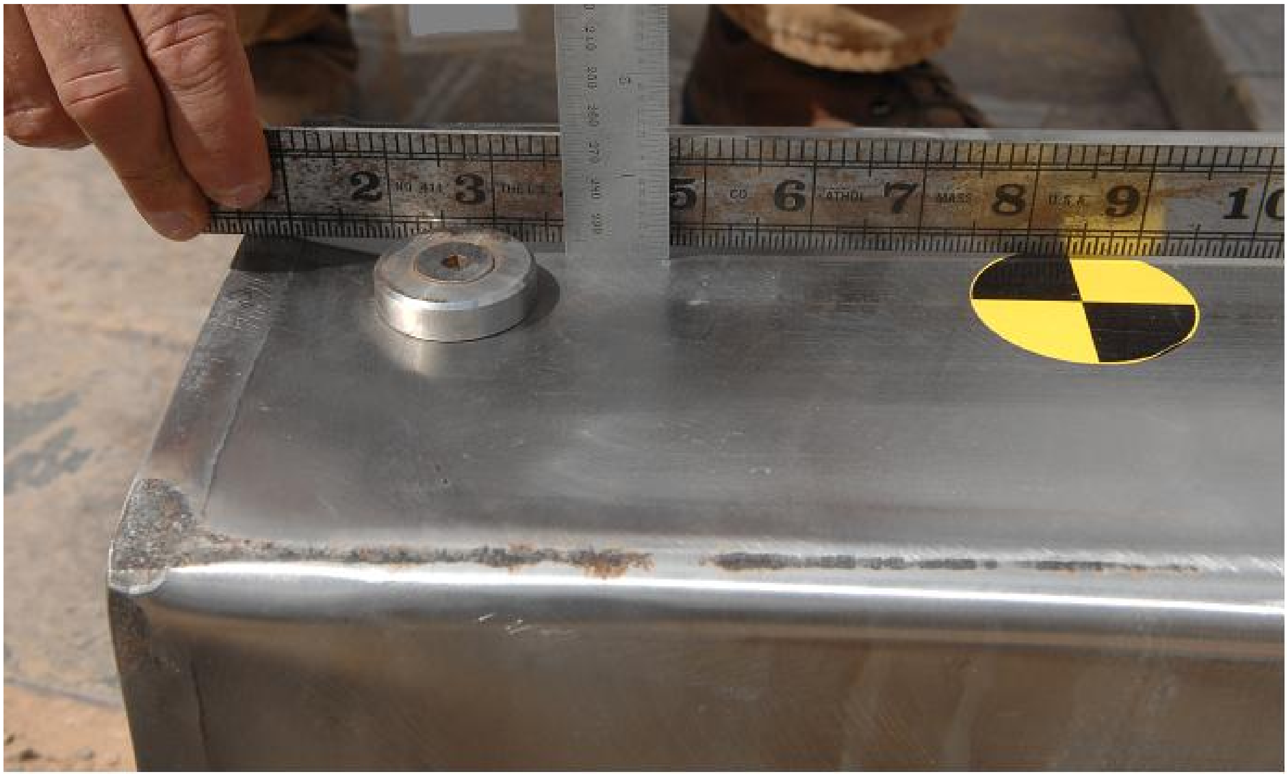

Figure 2.12.1-16 - Index Lug Near Bottom End, CD2.A-1

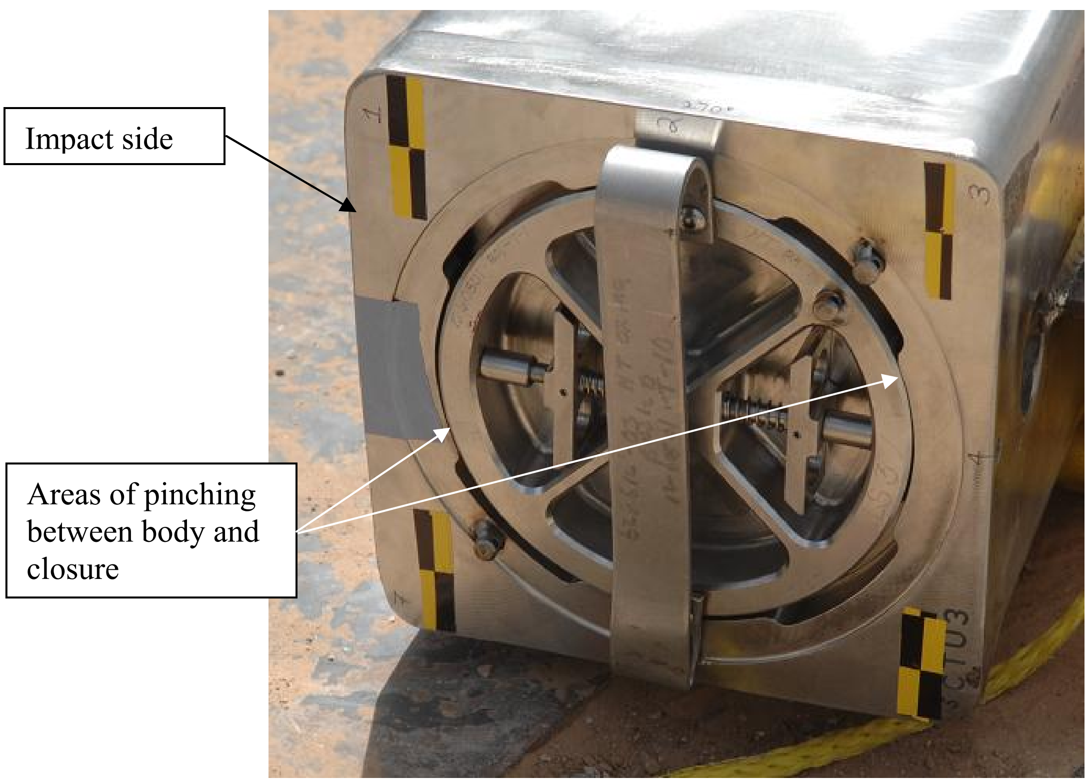

Figure 2.12.1-17 - View of Closure Following CD2.A-1

Figure 2.12.1-18 - CD2.B-1 Drop Orientation

Figure 2.12.1-19 - CTU Position Following CD2.B-1 Drop

Figure 2.12.1-20 - Index Lug Near Bottom End, CD2.B-1

Figure 2.12.1-21 - CTU in Chiller Unit

Figure 2.12.1-22 - CD3-1 Drop Orientation

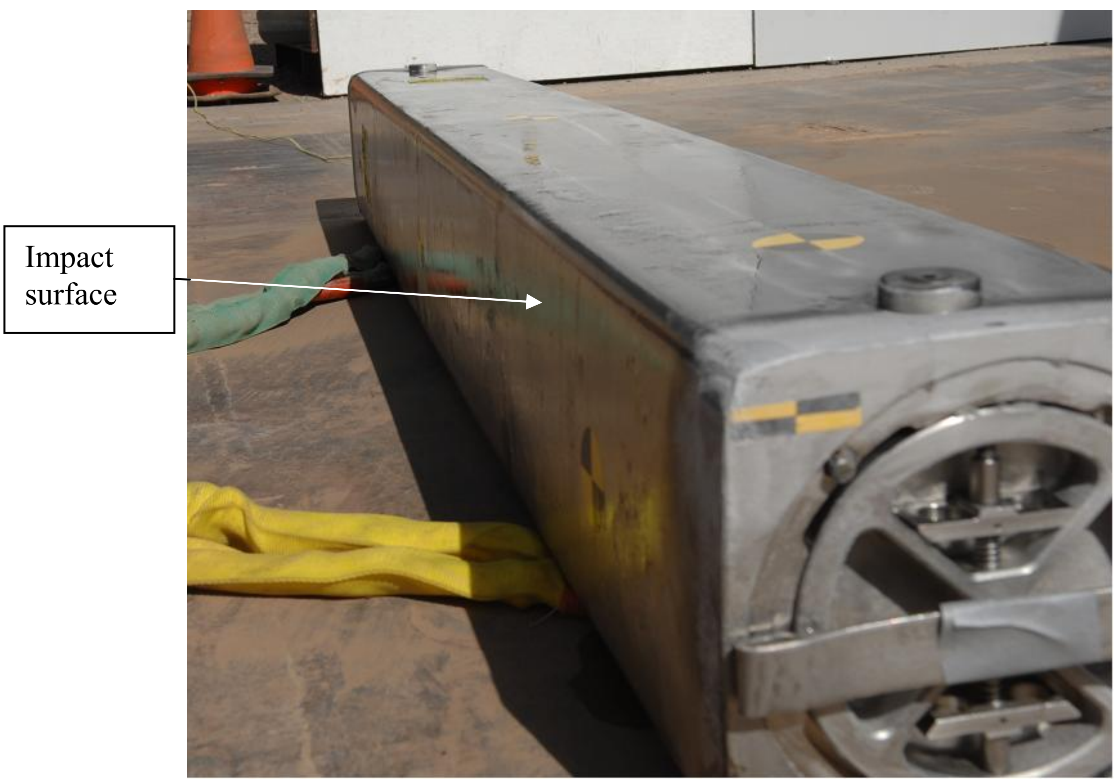

Figure 2.12.1-23 - CTU Following CD3-1 Impact

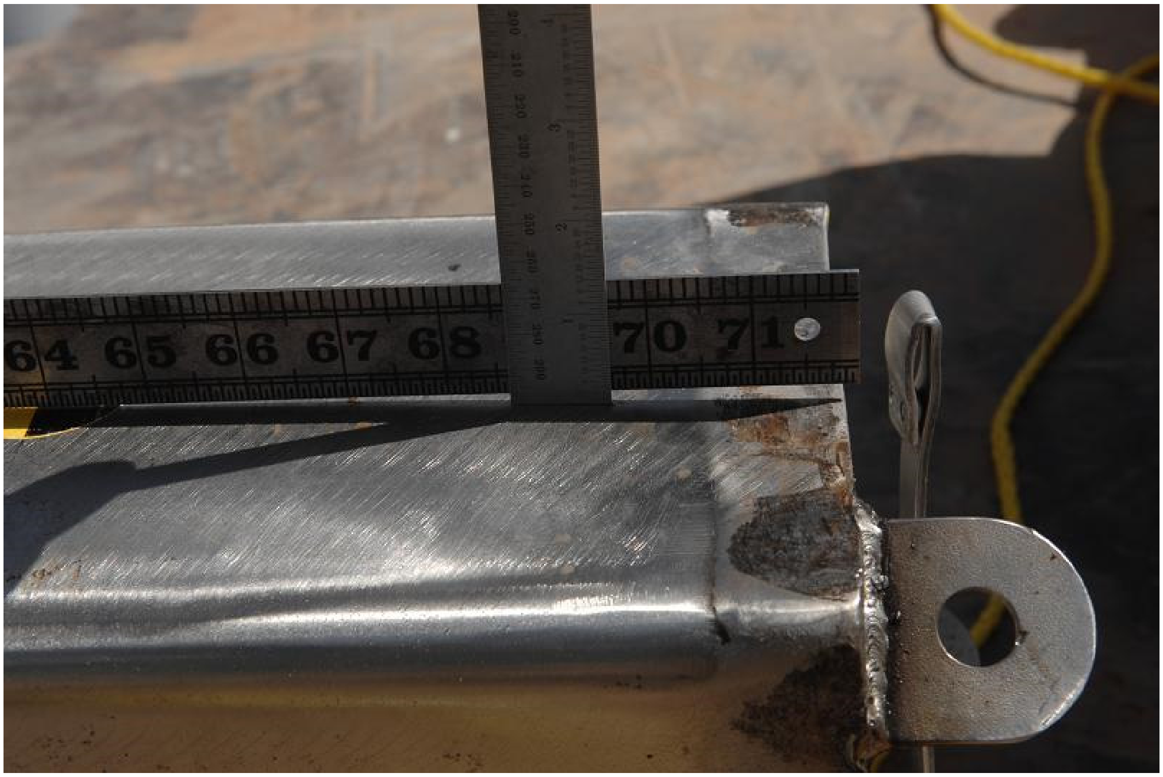

Figure 2.12.1-24 - Deformation Near Closure End Following CD3-1

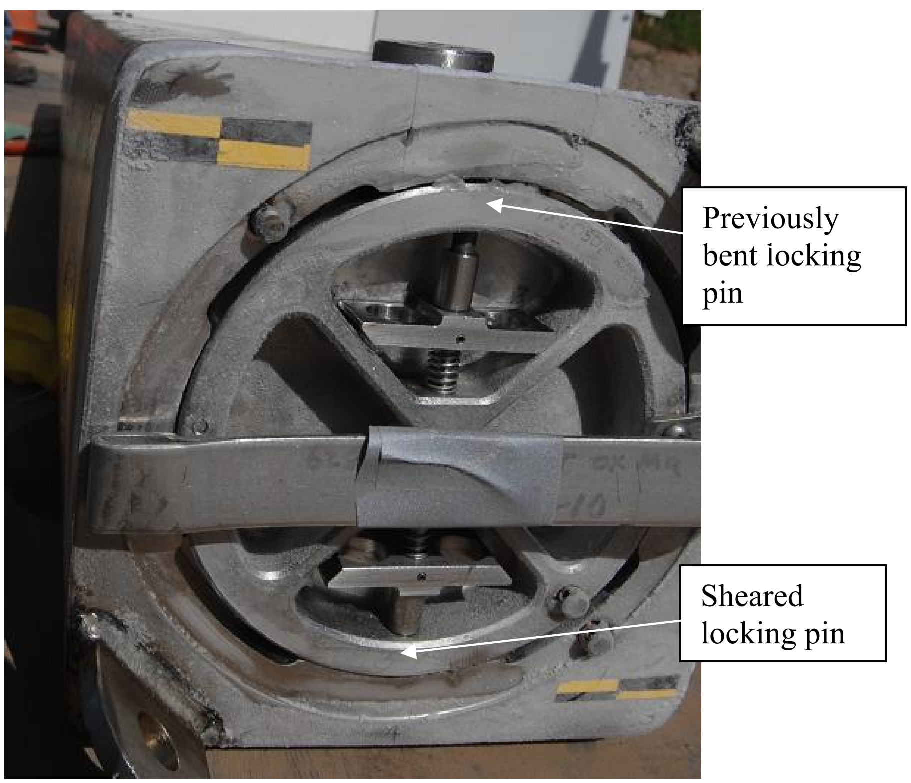

Figure 2.12.1-25 - View of Closure Following CD3-1

Figure 2.12.1-26 - CD4-1 Drop Orientation

Figure 2.12.1-27 - View of Impact End Following CD4-1

Figure 2.12.1-28 - View of Side Bowing Following CD4-1

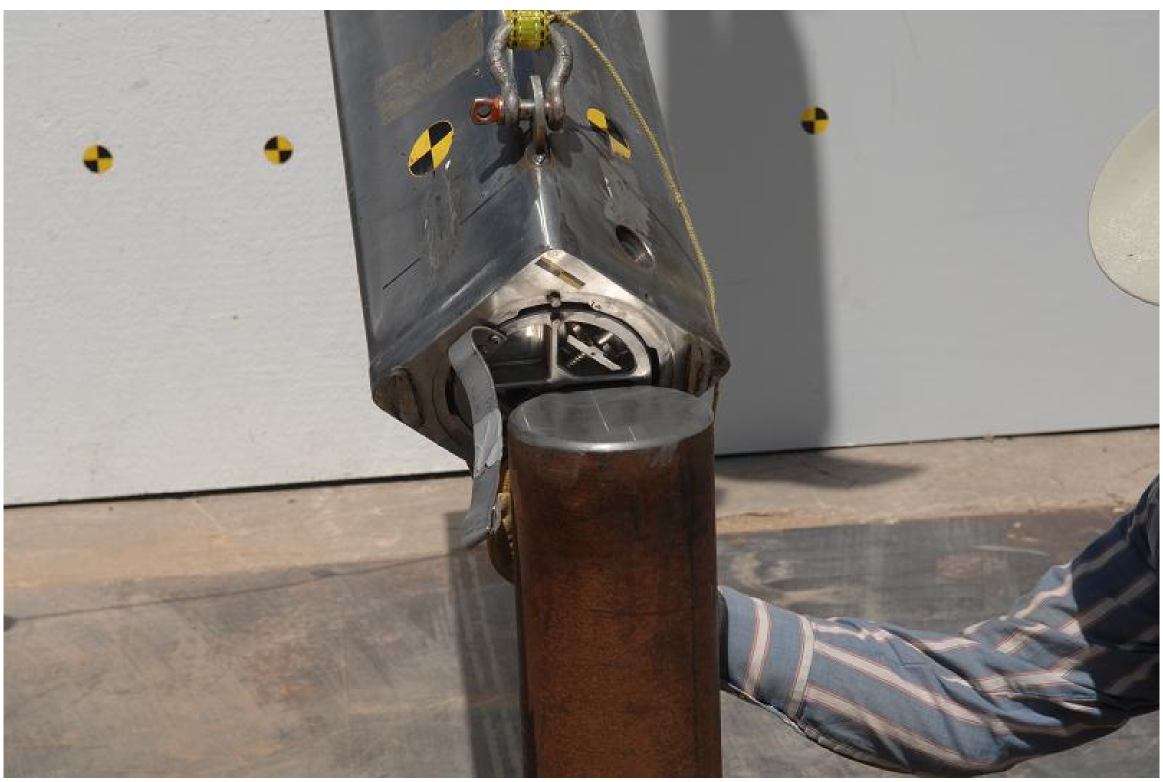

Figure 2.12.1-29 - CP3-1 Drop Orientation – Front

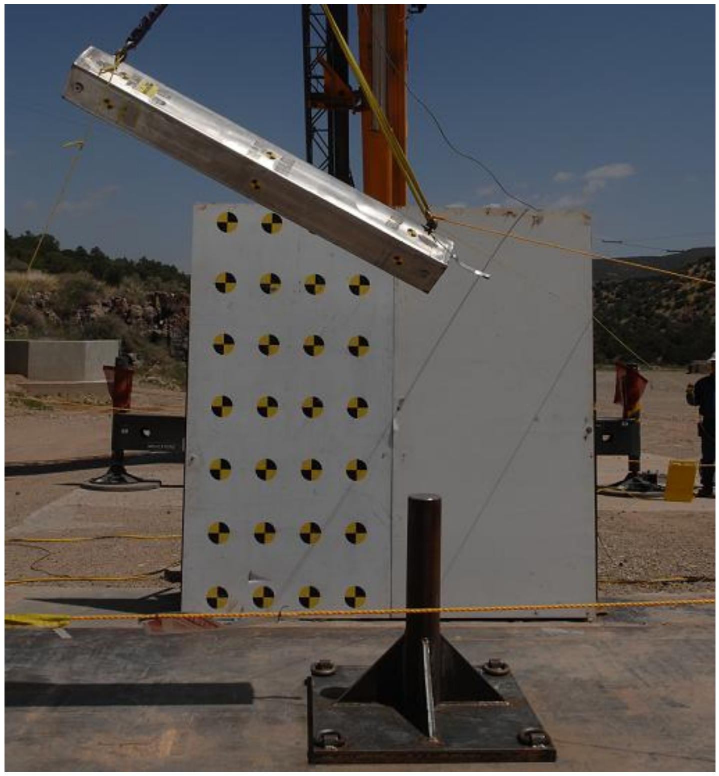

Figure 2.12.1-30 - CP3-1 Drop Orientation – Front

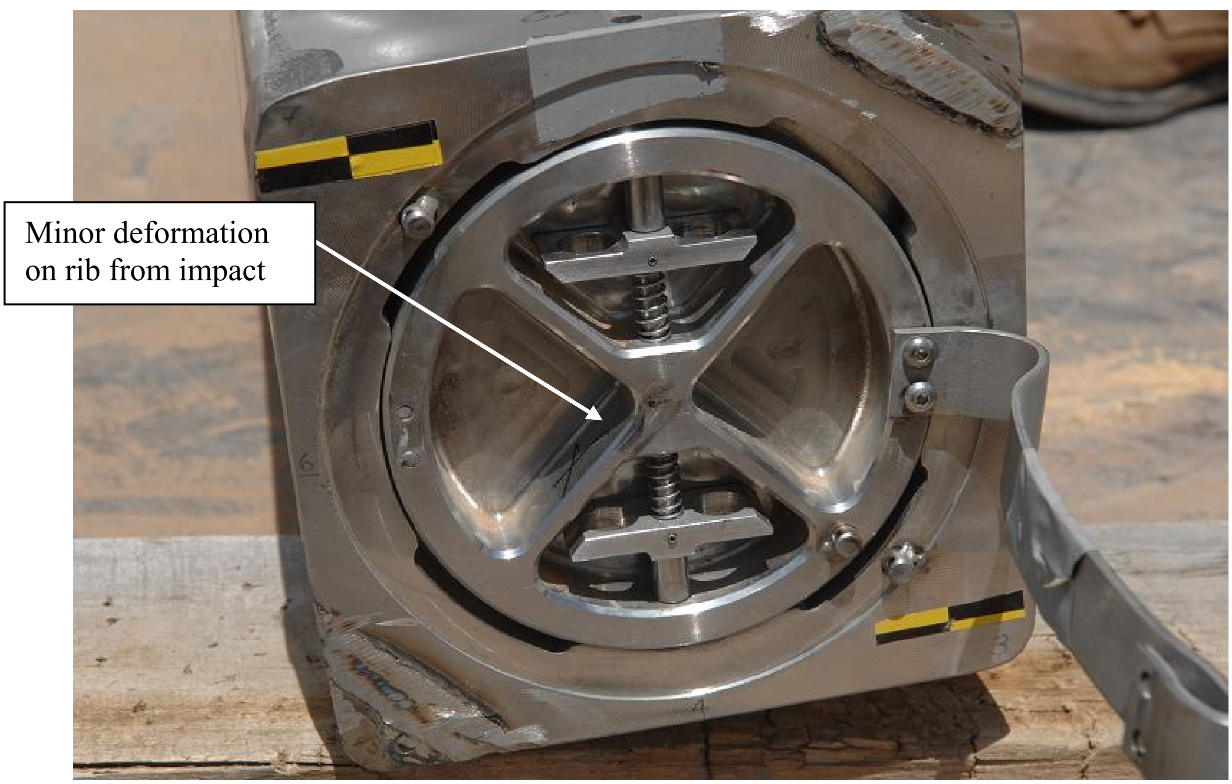

Figure 2.12.1-31 - CTU Following CP3-1 Impact

Figure 2.12.1-32 - CD5-1 Drop Orientation

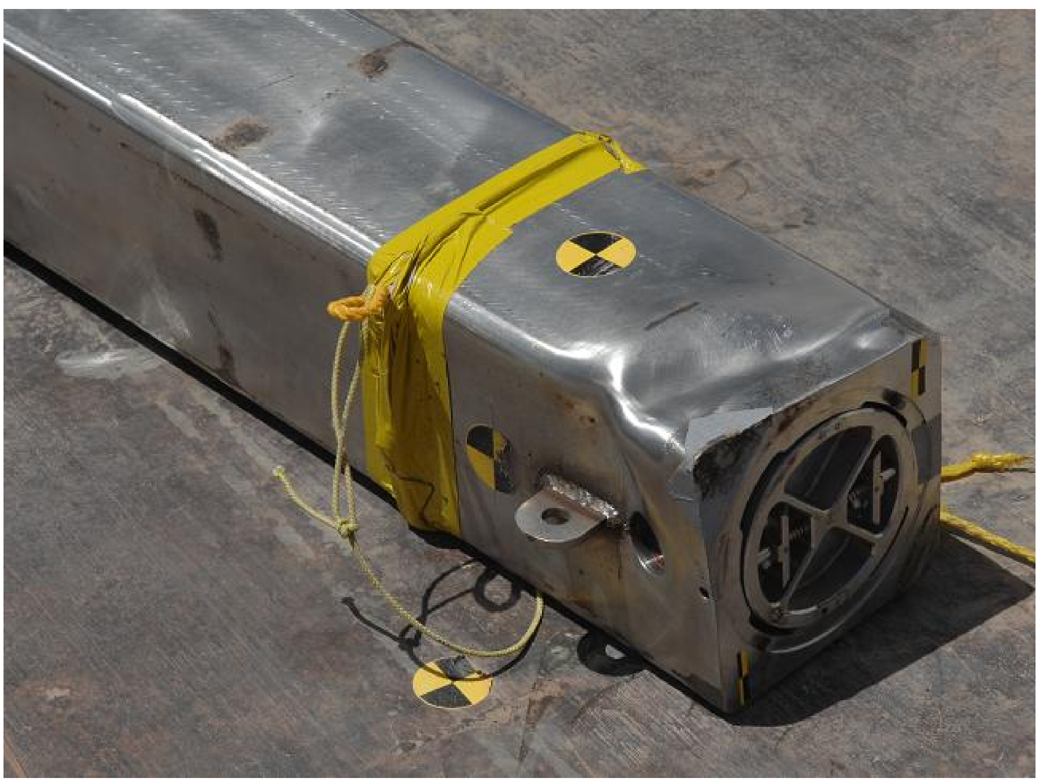

Figure 2.12.1-33 - CTU Following CD5-1 Impact

Figure 2.12.1-34 - CD5-1 Impact Damage on Bottom 180º Side

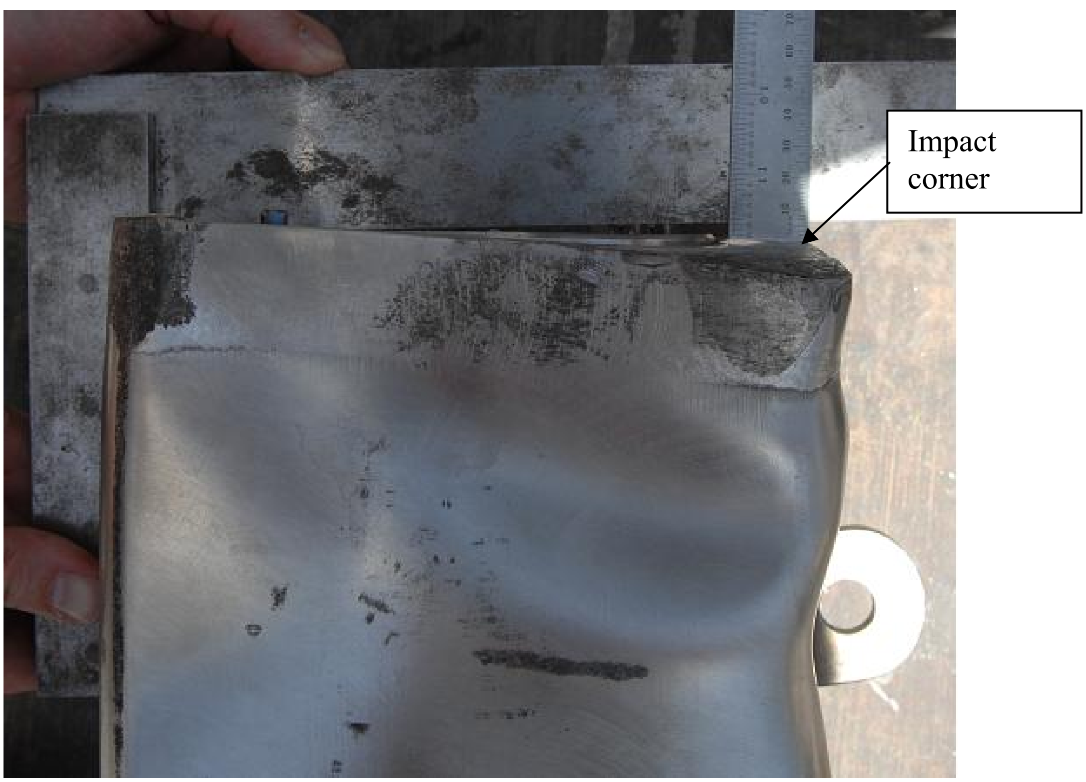

Figure 2.12.1-35 - CD5-1 Impact Damage on Closure End

Figure 2.12.1-36 - CD5-1 Impact Damage on Closure Area

Figure 2.12.1-37 - CD2.C-1 Drop Orientation

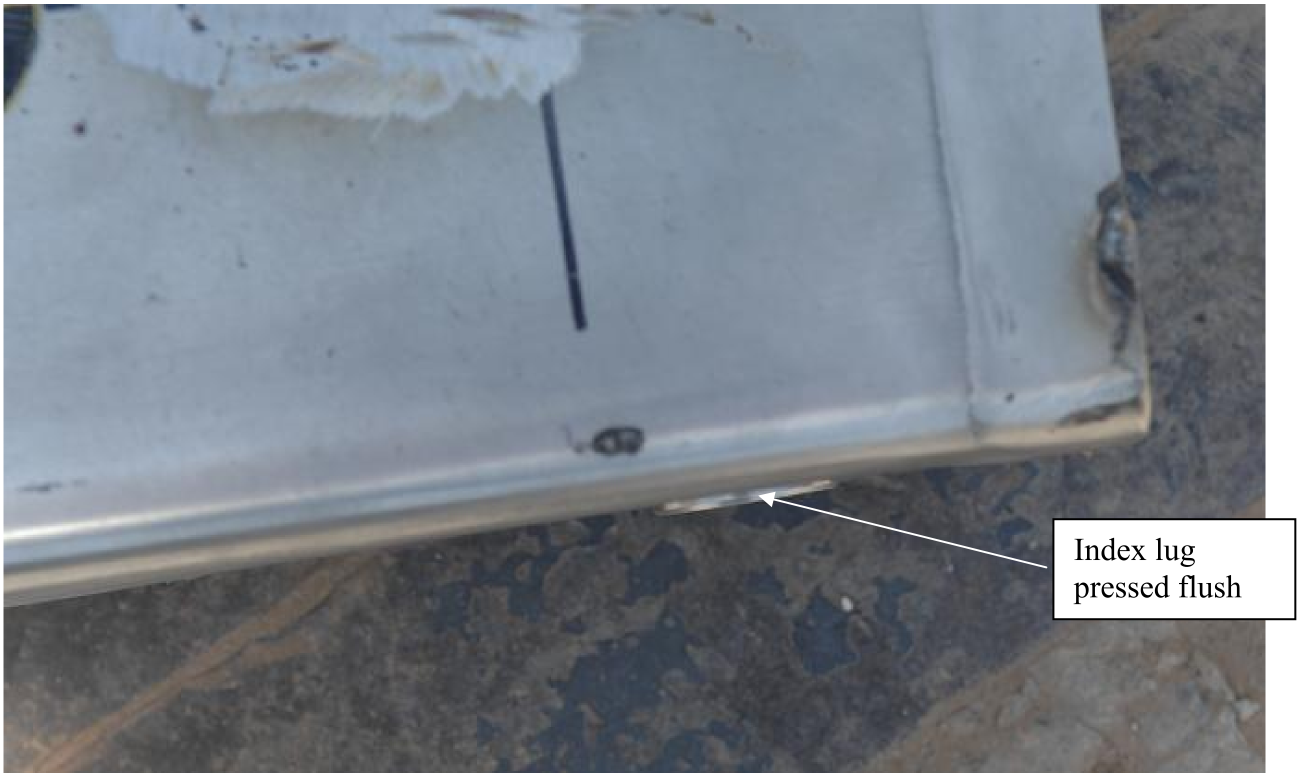

Figure 2.12.1-38 - Side View of CTU Following CD2.C-1 Drop

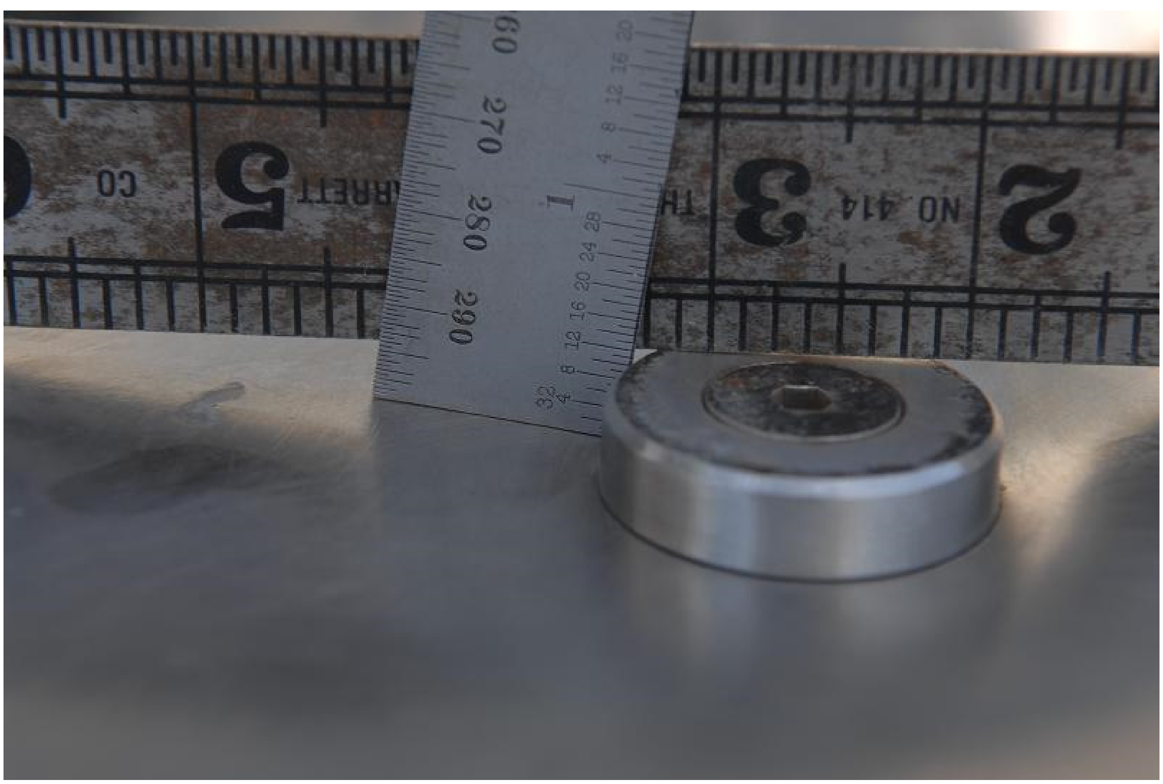

Figure 2.12.1-39 - Index Lug Near Closure End, CD2.C-1

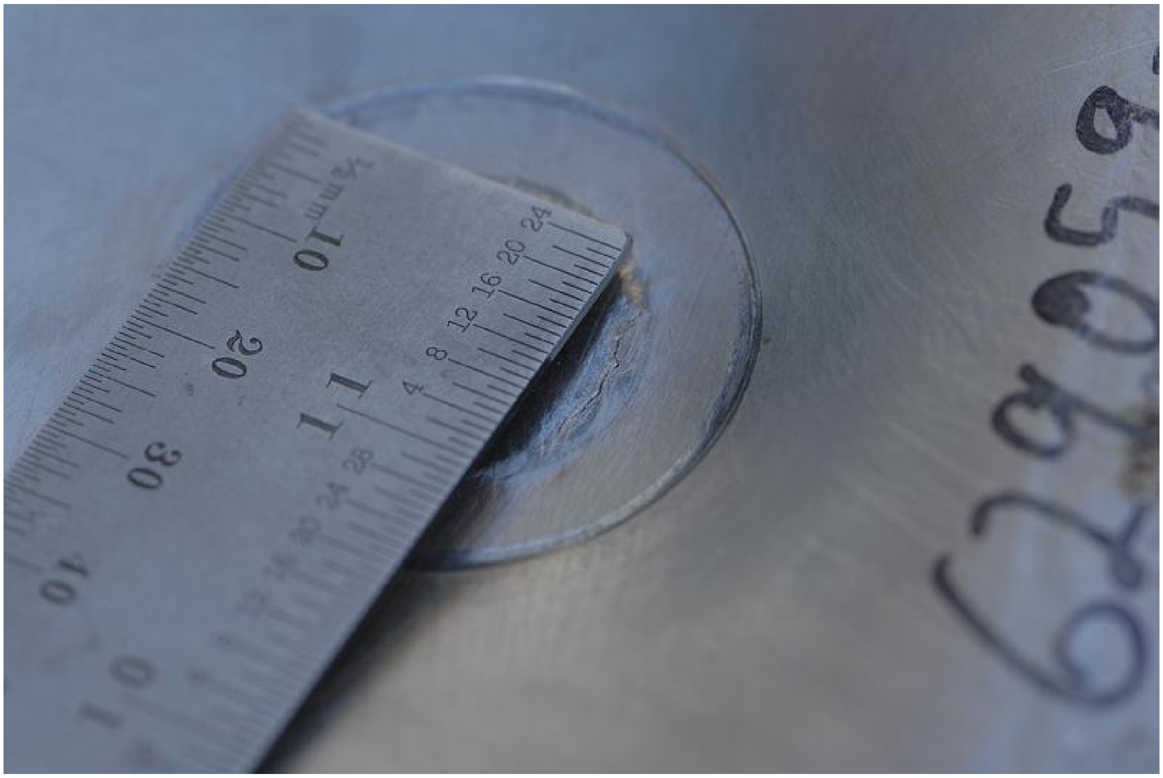

Figure 2.12.1-40 - Cracked Weld Under Index Lug, CD2.C-1

Figure 2.12.1-41 - CP2-1 Drop Orientation

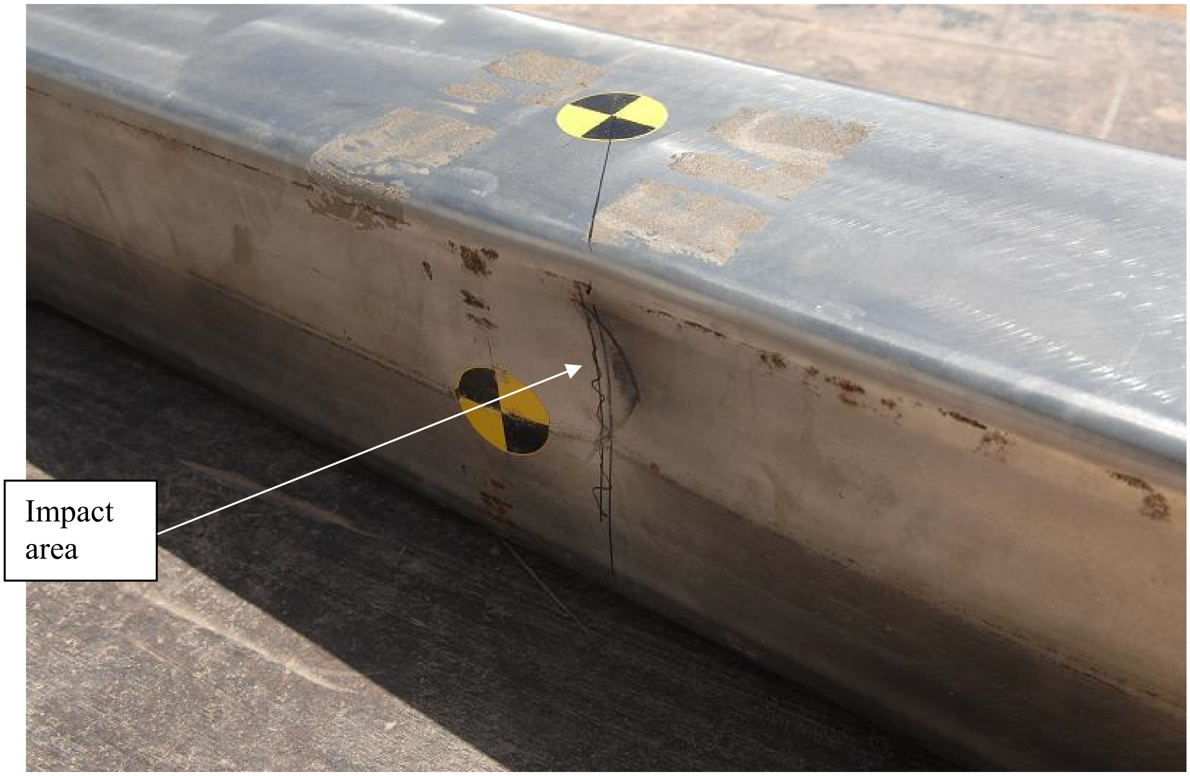

Figure 2.12.1-42 - CTU Following CP2-1 Impact

Figure 2.12.1-43 - CP2-1 Impact Damage

Figure 2.12.1-44 - CP1-1 Drop Orientation

Figure 2.12.1-45 - CTU Following CP1-1 Impact

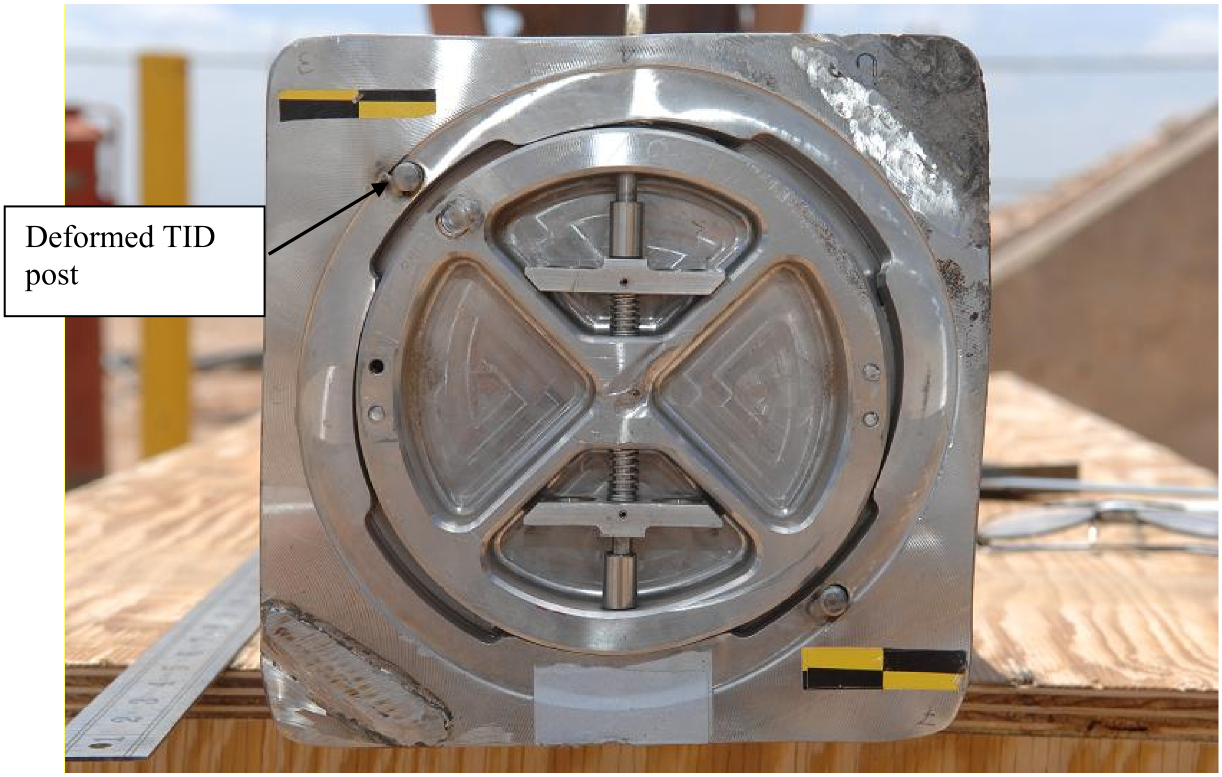

Figure 2.12.1-46 - CP1-1 Impact Damage (Shown Index Lugs Down)

Figure 2.12.1-47 - Attempted Closure Removal

Figure 2.12.1-48 - Exposure of Thermal Shield

Figure 2.12.1-49 - Insulation After Removal of Thermal Shield

Figure 2.12.1-50 - Middle Insulation After Removal of Thermal Shield

Figure 2.12.1-51 - Bottom End Plate Condition

Figure 2.12.1-52 - View of Inner Tube at Closure End

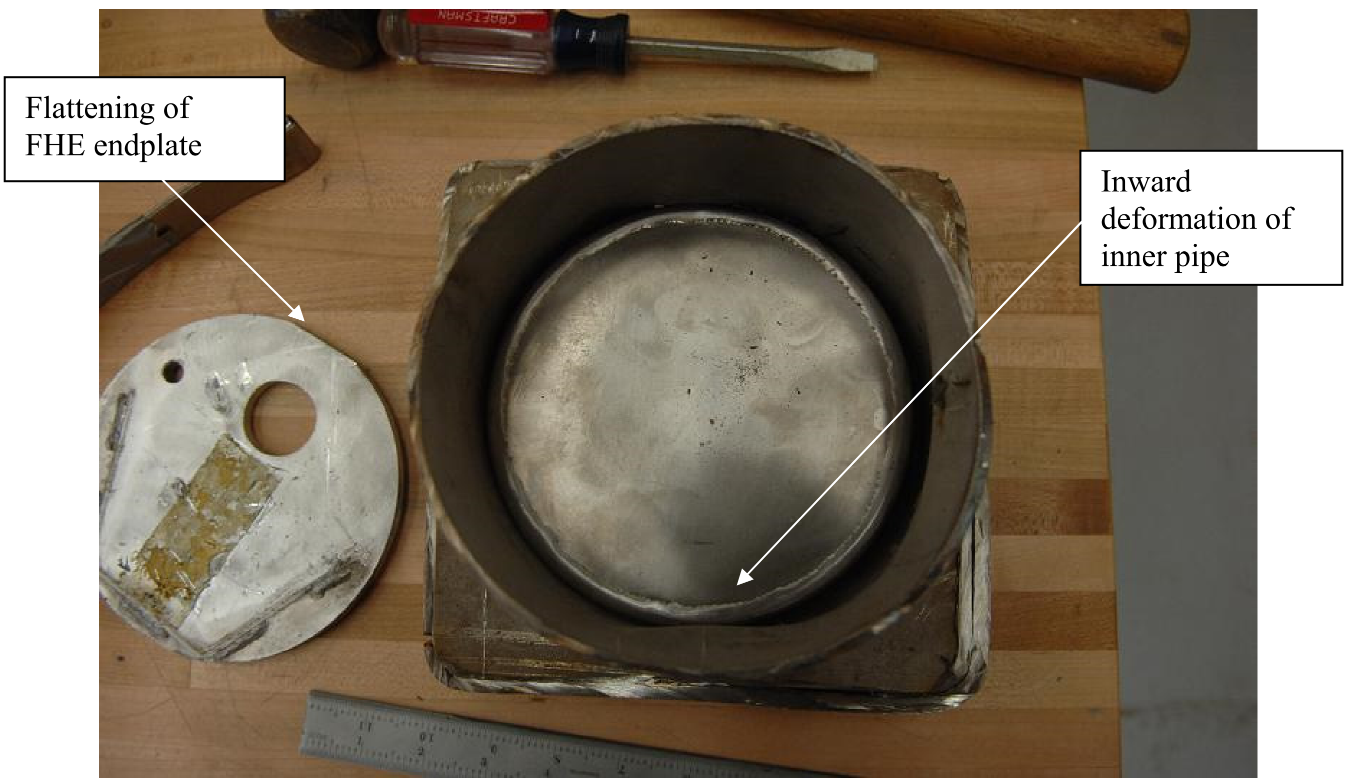

Figure 2.12.1-53 - Inner Tube Deformation at Closure End

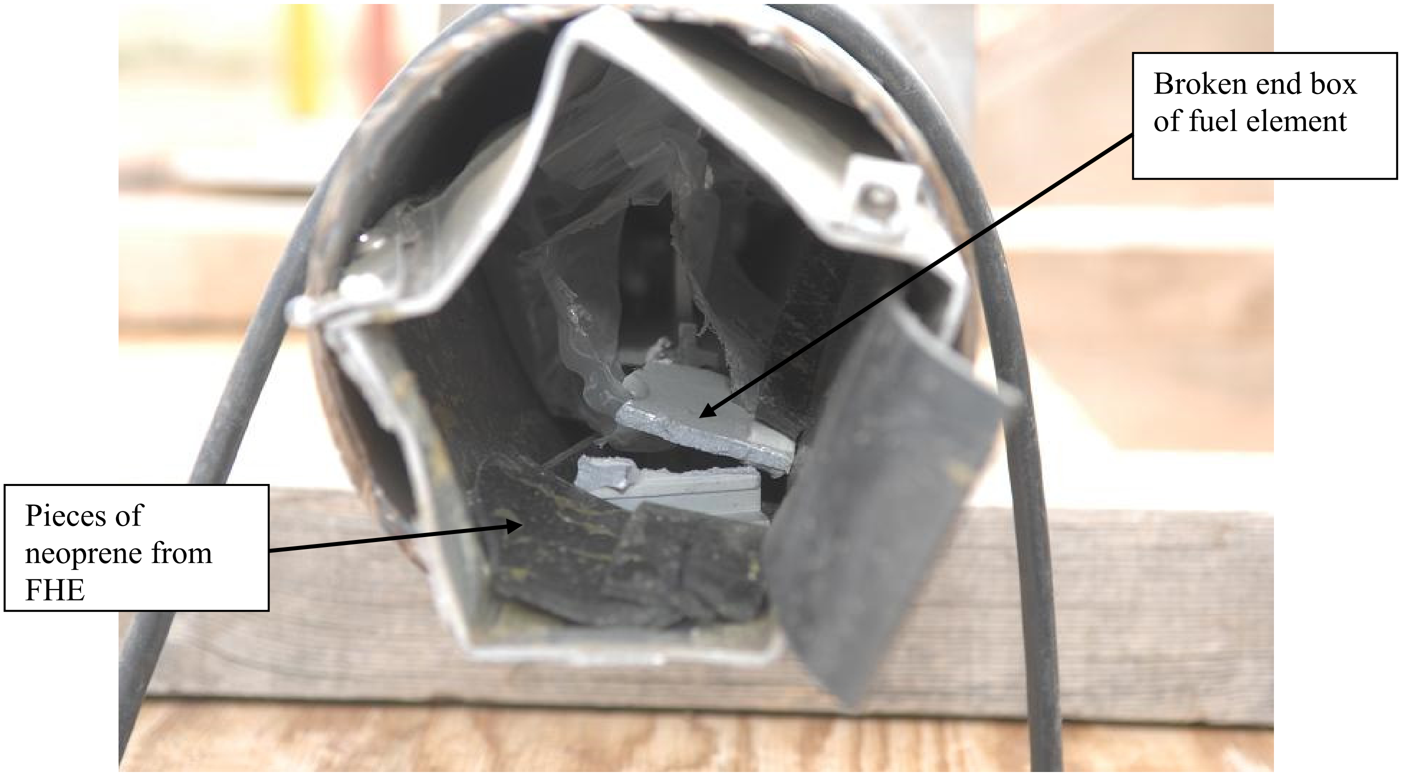

Figure 2.12.1-54 - End View (Bottom) of Opened CTU

Figure 2.12.1-55 - Removal of ATR Fuel Element

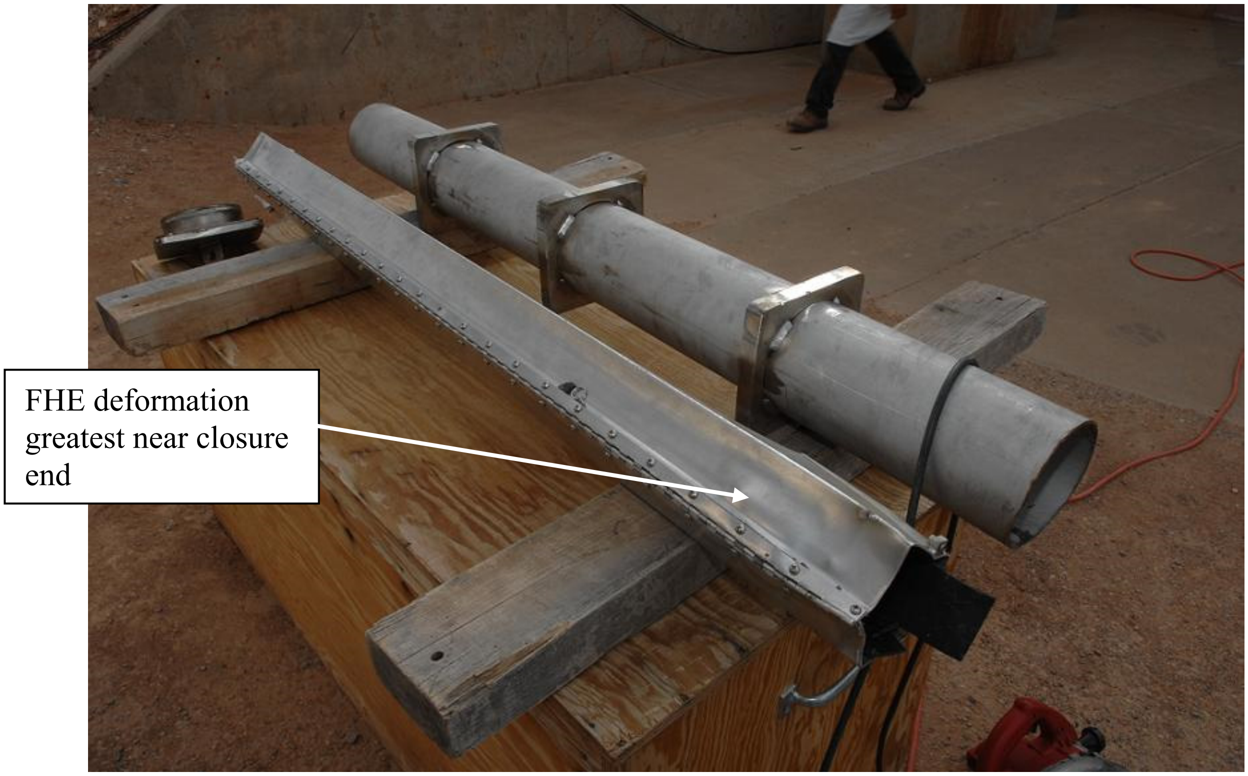

Figure 2.12.1-56 - Fuel Handling Enclosure Deformation

Figure 2.12.1-57 - ATR Fuel Element Inspection

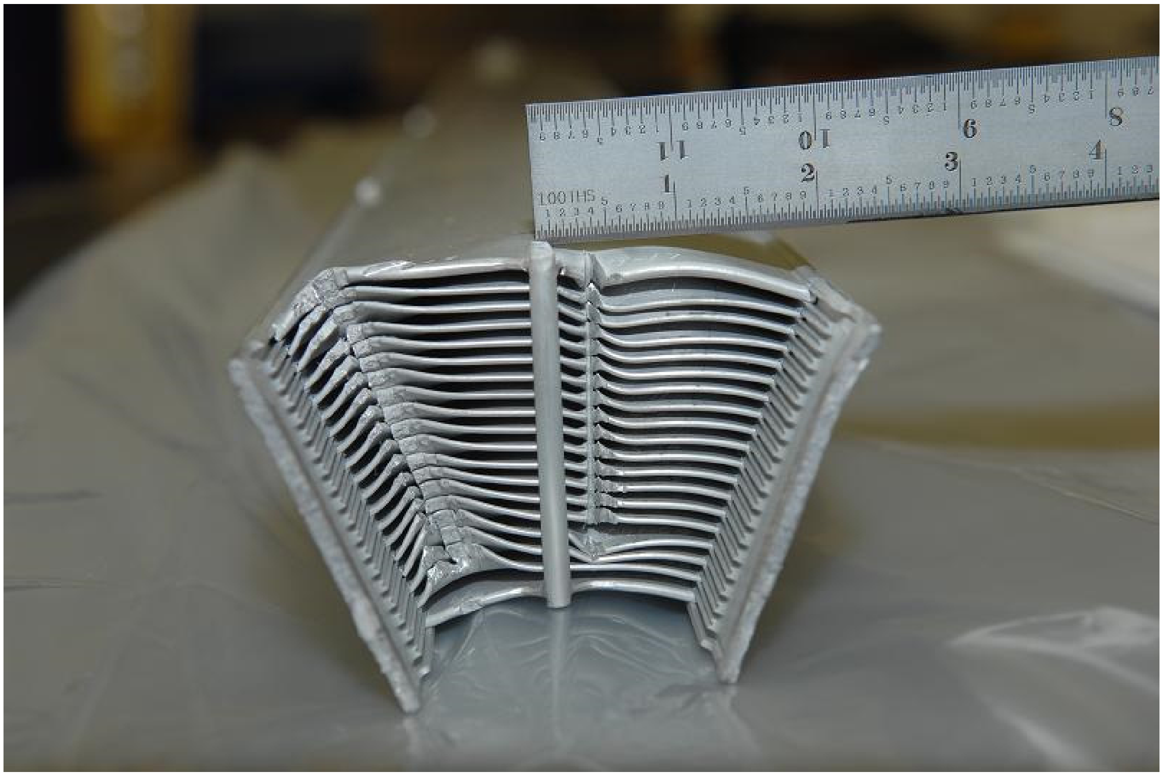

Figure 2.12.1-58 - ATR Fuel Element at Head End

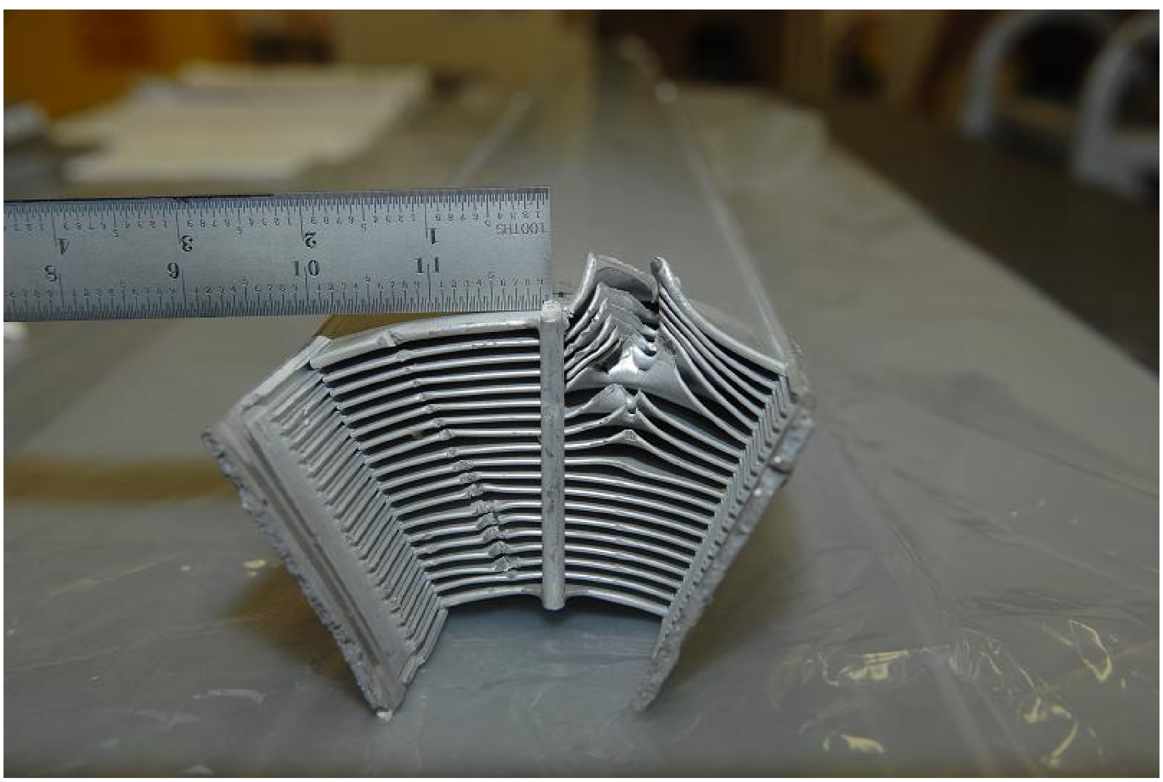

Figure 2.12.1-59 - ATR Fuel Element Damage at Bottom End

Figure 2.12.1-60 - Top View ATR Fuel Element at Bottom End

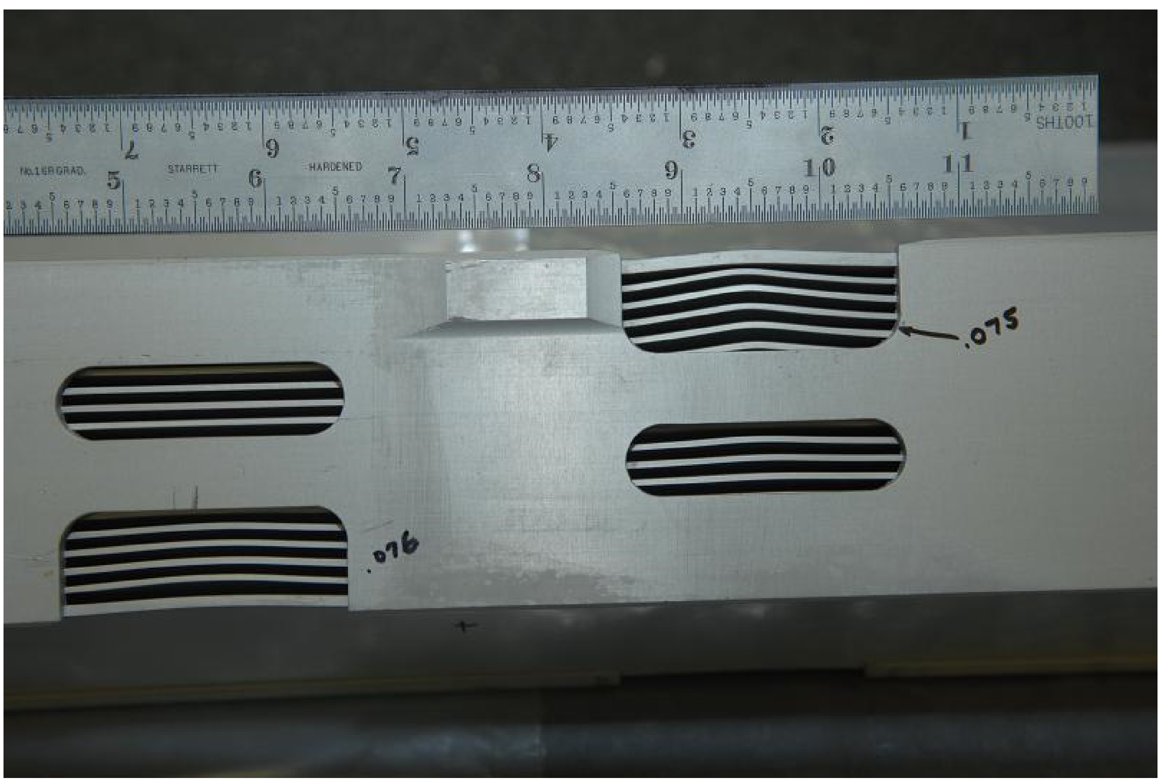

Figure 2.12.1-61 - ATR Fuel Element Fuel Plates Left Side

Figure 2.12.1-62 - ATR Fuel Element Fuel Plates Right Side

This page intentionally left blank.

2.12.2 Certification Tests on CTU-2

This report describes the methods and results of a series of tests performed on the Advanced Test Reactor (ATR) Fresh Fuel Shipping Container (FFSC) transportation package, shown in Figure 2.12.2-1. The objective of testing was to conduct drop tests in accordance with the requirements of 10 CFR 71, §71.71 Normal Conditions of Transport (NCT), and §71.73 Hypothetical Accident Conditions (HAC). This test was primarily directed at verification of the loose fuel plate basket structural integrity and the performance of the package insulation. The package and ATR fuel element payload performance are supported by the tests described in Section 2.12.1, *Certification Tests on CTU-1*.

Testing was performed at HiLine Engineering in Richland, Washington on May 17, 2007. Color photographs and videos were taken to document the test events and results.

2.12.2.1 Overview

There are three primary objectives for the certification test program:

1. To demonstrate that, after a worst-case series of HAC free drops, the package maintains containment of radioactive contents.
2. To demonstrate that, after a worst-case series of HAC free drops, geometry of both the fuel and package are controlled as necessary to maintain subcriticality.
3. To demonstrate that, after the free drops, the package retains the thermal protection necessary to maintain the fuel below its melting point during the thermal evaluation.

Several orientations were tested to ensure that the worst-case series of free and puncture drop events had been considered. Post-impact examination demonstrated that the package sufficiently met the design objectives. The specific objectives of this test were to demonstrate:

- Any displacement of package insulation and/or thermal shields are bounded in the thermal analysis,
- Reconfiguration of the loose fuel plate basket and/or loose fuel plate payload is bounded in the criticality analysis.

2.12.2.2 Pretest Measurements and Inspections

The ATR FFSC packaging (serial number CTU1), loose fuel plate basket (serial number 1), and simulated ATR loose fuel plates were received at HiLine. The packaging and payload are identified as ATR FFSC Certification Test Unit CTU-2. The components arrived fully constructed and ready for testing.

The ATR loose fuel plates were simulated. The payload was comprised of a combination of 2- and 4-inch wide, .06-inch thick, 5052H32 aluminum flat plates. All plates were 49.5-inches long. There were 15, 2-inch wide plates and 10, 4-inch wide plates making up a total payload weight of 20.7 lbs.

The CTU was dimensionally inspected to the drawings at the fabricator and the fabrication records forwarded to PacTec. A Certificate of Compliance was issued by the fabricator of the CTUs documenting compliance with the fabrication drawings. Minor discrepancies between the drawings and CTUs were identified and independently evaluated. The evaluations concluded that the discrepancies were minor and would not significantly affect the CTU during testing.

There were five fabrication deviations associated with the S/N CTU1 package fabrication:

- The 3/8-16 UNC index lug screws were obtained without specified ASTM F-879 certifications.
- The #10-24 UNC closure handle screws were obtained without specified ASTM F-879 certifications.
- Chemical overtesting of the package body closure plate material identified a manganese content 0.02% above the ASTM A479 maximum allowable.
- The tap failed when tapping one of the four #10-24 tapped holes for the closure handle screws. As a result, one of the four tapped holes had full threads to a depth of .44-inches rather than the specified .5-inches.
- The handle width is specified to be 7.5 ± .3-inches. When measured in the free state (not secured to the closure), the handle width was undersized by approximately 0.1-inches.

Other deviations relative to the CTU are the absence of the stainless nameplate and the use of temporary rigging attachments. These items are also insignificant relative to the weight of the CTU and their impact upon the drop tests.

2.12.2.2.1 Component Weights

Component weights were measured and recorded as shown in Table 2.12.2-1.

2.12.2.2.2 Drop Test Pad Measurement and Description

The drop pad consists of a 7-foot square x 5-foot thick concrete block covered with a 6-foot square x 2.5-inch thick steel plate. The estimated weight of the pad is greater than 44,000 lbs. Thus the test pad was qualified as an essentially unyielding surface for the approximately 300 lb CTU.

2.12.2.2.3 Equipment and Instruments

Instrumentation used for the component weights and drop tests is given in Table 2.12.2-2. Calibrated test and measurement equipment used were the weight scale and temperature meter. Those two instruments were calibrated in accordance with HiLine procedures. It is noted that the HiLine calibration procedures require National Institute of Standards and Technology (NIST) traceability and that the HiLine records adequately demonstrated that the calibrations were NIST traceable.

A plumb bob with a stretch resistant string was used to determine the appropriate drop height. HiLine project personnel under the supervision of PacTec personnel measured the plumb bob and string using steel tape measures. The angle of the CTU prior to each drop was measured using a mechanical inclinometer.

One low speed digital video camera was used to record the drop events. In addition, color photographs were taken to document the testing.

2.12.2.3 Summary of Tests and Results

2.12.2.3.1 Initial Conditions

All three HAC drops, CD1-2, CD3-2, and CD4-2, were performed at ambient temperature. Ambient temperature and the package surface temperature was recorded before and after each drop. After each drop the closure was removed and the basket inspected. The basket was reassembled (the basket screws tightened to the “finger tight” condition) and the package re-closed for the following test. One tie wrap (securing the loose fuel plate payload) failed in the CD1-2 test and the second tie wrap failed in the CD3-2 test. Neither of the two tie wraps were replaced between tests.

2.12.2.3.2 Summary of Testing

Table 2.12.2-3 identifies the testing performed on the ATR FFSC CTU.

2.12.2.4 Certification Tests

2.12.2.4.1 Drop Tests

The three CTU-2 HAC drop tests were performed to augment the CTU-1 tests for the package, and to demonstrate acceptable performance of the loose fuel plate basket payload. In CTU-1, the package was subjected to end drops on both the closure and the bottom ends of the package. CTU-2 restricted the end drop test to just the bottom end to properly assess axial insulation displacement.

There were no NCT or puncture bar tests performed on the package, since CTU-1 adequately demonstrates acceptable package performance under those conditions. The two side drops subjected the loose fuel plate basket and simulated fuel to worst case impact conditions with the basket oriented perpendicular and parallel to the target surface.

The test identification numbering reflects the same drop orientation as performed in CTU-1. For example, CD3-2 is the same orientation as the third HAC drop in CTU-1, test CD3-1. The “-2” identifies this drop as a CTU-2 test.

2.12.2.4.1.1 CD1-2 –Flat (pocket side down) Side HAC Drop

The CTU was fitted with swivel lift eyes, and the lift eyes were threaded into the package lift points. This configuration oriented the package such that the package pocket side impacted the target surface. Slings were used to rig the CTU from the swivel lift eyes to the crane remote release hook. Figure 2.12.2-5 illustrates the drop orientation. Initial conditions were as follows:

- Ambient temperature: 73 ºF
- Avg. surface temperature: 78 ºF
- Time: 10:04 a.m. 5/17/2007
- Drop height: 30 ft

Following impact, the CTU bounced slightly and landed on the impact side. There was minor visible exterior damage, principally scuff marks, resulting from the drop. Close examination of the package, on the impacted surface side, reveals minor distortion of the outer shell localized at the stiffening ribs. Figures 2.12.2-6 and 2.12.2-7 show the CTU prior to and following the drop. There was no bowing or other significant visible deformation. There was no visible deformation or rotation of the closure, and the locking pins condition and function were unaffected by the drop.

The basket was not affected by the drop, however the finger operated screws securing the two basket halves were loosened approximately one turn. One fuel tie wrap was broken but the simulated loose fuel plates were not damaged. The simulated fuel plates were replaced in the basket without installing new tie wraps, and the basket closure screws again tightened to the finger tight condition.

2.12.2.4.1.2 CD3-2 – Flat Side HAC Drop (90º from CD1-2)

Following the CD1-2 drop, lift points were welded to the package to enable a side drop rotated 90º from CD1-2 (Figure 2.12.2-8):

- Ambient temperature: 78 ºF
- Avg. surface temperature: 85 ºF
- Time: 10:50 a.m. 5/17/2007
- Drop height: 30 ft

The CTU rebounded from the drop pad approximately 1 ft following the 30 ft drop and came to rest on its side (rotated 90º from the drop orientation). As with the CD1-2 event, the outer shell exhibited minor deformation at the stiffening rib locations (reference Figure 2.12.2-9). There was no visible deformation or rotation of the closure, and the locking pins were undamaged and in good working order.

The closure was opened and the basket removed following the drop. The basket exhibited no signs of any deformation but the finger tightened basket screws were loosened approximately 1 turn by the drop.

The basket was opened and it was discovered that the second plastic tie wrap was broken (Figure 2.12.2-10). The simulated fuel plates were found to exhibit no significant damage. The simulated fuel plates were replaced in the basket without installing new tie wraps, and the basket closure screws again tightened to the finger tight condition.

2.12.2.4.1.3 CD4-2 – CG over Bottom End (Vertical)

Following CD3-2, the temporary rigging attachments were removed and the CTU rigged for CD4-2 by lifting the package from the closure handle (Figure 2.12.2-11). Initial conditions were recorded as follows:

- Ambient temperature: 88 ºF
- Avg. surface temperature: 90 ºF
- Time: 11:20 a.m. 5/17/2007
- Drop height: 30 ft

The CTU appeared to impact slightly off of true vertical; impacting near one corner of the package. This impact dented the lift point feature inward approximately ½-inch, and on one adjacent side, bulged out the square outer tube surface by approximately ½-inch. Following impact, the CTU rebounded vertically approximately 2-feet, tipped over, and landed on the CD3-2 impact side. There was no overall bowing or of the package or other significant visible deformation. There was no visible deformation or rotation of the closure. Figure 2.12.2-12 shows the bottom end of the CTU following the drop.

There was no visible damage to the closure or the locking pins. The closure was removed and the basket extracted following CD4-2. Damaged to the basket was limited to a small dent at the end of the basket that was situated closest to the package bottom. Upon destructive examination of the package, it was discovered that the weld between the package inner shell and the component at the bottom of the payload cavity had intruded into the payload cavity in a localized area (Figure 2.12.2-13). When the package impacted in CD4-2, the basket was partially supported by that weld bead. The end plate of the basket was slightly deformed (Figure 2.12.2-14) as the basket seated on the bottom of the package payload cavity. The damage was minor and did not impair the ability of the basket to retain the fuel plates.

The simulated fuel plates experienced localized deformation at the end of the basket closest to the package bottom (Figure 2.12.2-15 and Figure 2.12.2-16). Above this area the simulated fuel plates were not deformed.

2.12.2.5 Post-test Disassembly and Inspection

The final acceptance criteria for the ATR FFSC package lies with the criticality evaluation. Any increase in reactivity of the contents resulting from the certification tests must not exceed the allowable as defined in the criticality evaluation. The inspections required to support determination of compliance with the acceptance criteria are identified as follows:

- Inspect the outer shell to verify the thermal performance of the package is unimpaired by the free drop events. The thermal analysis assumes that the outer shell is intact such that there is no significant communication between the environment and the outer/inner shell annular space during the thermal event.
- Inspect the insulation to verify compliance with the assumptions of the thermal analysis.

- Inspect the overall package to verify that the package geometry remains within the criticality analyses assumptions.
- Inspect the simulated fuel plate payload to verify that the fuel geometry remains within the assumptions of the criticality analyses.

Any deviation of the test results from these acceptance criteria must be reconciled with the criticality evaluation.

2.12.2.5.1 CTU Inspection

The CTU-2 was disassembled and inspected on May 17, 2007. Prior to disassembly the exterior dimensions were recorded for comparison to the pre-test condition. Table 2.12.2-4 lists the measured dimensions and Figure 2.12.2-17 identifies the location of the identified measurements.

The closure handle was unaffected by the first two drops. In the CD4-2 drop, the handle was dented when it was struck by the rigging shackle. During the CD4-2 CG over bottom (vertical) HAC drop, the outer wall bulged out at the bottom end of the package and caused the width of the package to increase from 8 inches to approximately 8 5/8 inches in that area.

The CTU was disassembled systematically by cutting away the outer layers of the packaging using an abrasive saw. The destructive examination was necessary due to the required inspection of the interior insulation. The package was cut lengthwise along two opposite corners and at the ends to expose the thermal shield.

The stainless steel thermal shields were all intact (Figure 2.12.2-18 through Figure 2.12.2-20). There was minor deformation of the thermal shields at the interface to the stiffening rib. This deformation resulted from the CD4-2 drop and caused the thermal shields to buckle one end and pull away from the stiffening rib at the other end. Figure 2.12.2-21 is typical of this condition. The gap between the thermal shield and the stiffening rib, where the shield pulls away from the rib, is less than 1/16-inch.

Following documentation of the thermal shields the shields were removed to enable examination of the insulation. For reference purposes the ribs are labeled 1 through 3 (Figure 2.12.2-22). The number 1 rib is closest to the bottom end of the package.

As can be seen in Figure 2.12.2-23 through Figure 2.12.2-26 the largest gap occurred at the closure end of the package. The gap ranges from 1-inch to 1 ¾ inches at that location. At the rib 3 and rib 2 locations the gap ranged from 1- to 1 ½-inches. At the rib 3 location the gap ranged from ½- to 1-inch. All gaps are within the 1.85-inch gap assumed in the thermal analysis.

Following thermal shield and insulation removal an abrasive saw was used to separate the bottom end plate from the inner tube. Figure 2.12.2-13 illustrates the condition of the end plate. The endplate showed no drop related deformation and there were no visual indications of broken welds or other damage near the end plate. Using a lathe, the bottom end plate was cut from the insulation pocket to determine the extent of possible insulation compression in the insulation pocket (Figure 2.12.2-27). There was no indication of compression in that region and it was determined that there was no need to open the closure insulation pocket.

The inner tube was inspected and, in general, showed no signs of buckling or large deformations. A minor deformation occurred near the bottom end of the package (Figure 2.12.2-28 and Figure 2.12.2-29) corresponding to the same area of deformation as the outer shell. The tube was bent in that area yielding a slight outward bulge of about 1/16-inch and, closer to the weld between the inner shell and the package bottom, an inward deformation of approximately ¼-inch. These deformations were localized and did not impair free movement of the basket in the payload cavity. There were no weld failures.

The closure assembly remained fully functional throughout the test series. The only damage to the closure was the handle deformation caused by the rigging shackle. The locking pins and the engagement lugs showed no signs of any deformation. The closure could be freely removed and installed through the tests.

In conclusion, CTU-2 satisfied the acceptance criteria of preventing loss or dispersal of the contents, the outer shell remained intact, the insulation remained within the assumptions of the thermal analysis, and the package and fuel geometry remained greatly unchanged. The deformations of the package and condition of the ATR loose fuel plates were evaluated, against both the criticality evaluation and thermal analysis, and determined to be within the bounds of the assumptions and conditions used to ensure safety.

Table 2.12.2-1 - Component Weights

Component	Weight (lbs)
Body Assembly	224.1
Closure Assembly	8.9
Loose Plate Fuel Basket	29.9
Simulated Fuel Plate Weight	20.7
Package (fully loaded)	283.6

Table 2.12.2-2 - Instrumentation for Drop Tests

Item Description	Model	Serial Number	Calibration Due Date	Comments
Drop Height Indicators	N/A	N/A	N/A	String plumb bobs made specifically for this testing. The length was established using a metal tape measure.
Tape Measure	N/A	N/A	N/A	35-ft. steel tape
Mechanical inclinometer	N/A	N/A	N/A	Used to identify CTU orientation
Weight Scale	Ohaus, Model CD11	0042508-6BD	7/19/2007	Used to measure weights of CTU components. The scale calibration documents included NIST traceable records.
Temperature meter	Carson, Model 4085	41372269	3/1/2008	Handheld temperature reader for measuring ambient temperature and CTU surface temperature. Meter calibration documents included NIST traceable records.

Table 2.12.2.3 - Summary of Testing

Test No.	Test Description	Comments
CD1-2	Flat side drop, pocket side down. Fuel plates oriented perpendicular to target (see Figure 2.12.2-3).	Flat side drop from 30-feet. No visible damage to package. Both closure locking pins remained in the locked position. Closure could be freely opened and payload extracted. The eight hand tightened screws securing the basket halves together were loose (approximately one turn). No visible damage to basket or simulated fuel plates.
CD3-2	Flat side drop, pockets and index lugs on side. Fuel plates oriented parallel to target (see Figure 2.12.2-4).	Flat side drop from 30-feet. No visible damage to package. Both closure locking pins remained in the locked position. Closure could be freely opened and payload extracted. The eight hand tightened screws securing the basket were loose (approximately one turn). The plastic wire ties securing the fuel bundle failed as shown in Figure 2.12.2-10. No significant deformation was observed in the fuel plates.
CD4-2	CG over bottom end (vertical)	Vertical end drop from 30-feet; bottom end of package impacting the target. Both closure locking pins remained in the locked position. Closure could be freely opened and payload extracted. The eight hand tightened screws securing the basket were loose (approximately one turn). The bottom end of the package was deformed on two surfaces (Figure 2.12.2-12). The surface with the threaded hole was dented inward and the adjacent surface 90º apart was bulged outward. The surface of the basket end plate contacting the bottom of the package was slightly dented. The simulated fuel plates were deformed at the bottom end of the basket (Figure 2.12.2-15 and Figure 2.12.2-16).

Table 2.12.2-4 - Package Length Measurements

Test ID	1	2	3	4	5	6	7	8
Pre-Test (in.)	72 7/16	72 1/2	72 7/16	72 1/2	72 7/16	72 7/16	72 7/16	72 1/2
CD1-2 (in.)	72 7/16	72 1/2	72 7/16	72 1/2	72 7/16	72 7/16	72 7/16	72 7/16
CD3-2 (in.)	72 7/16	72 1/2	72 7/16	72 1/2	72 7/16	72 7/16	72 7/16	72 7/16
CD4-2 (in.)	72 7/16	72 1/2	72 3/8	72 7/16	72 5/16	72 5/16	72 3/16	72 3/8

Figure 2.12.2-1 - ATR FFSC CTU-2
(CTU-2 uses package S/N CTU1)

Figure 2.12.2-2 - Loose Fuel Plate Basket and Simulated Fuel Plates

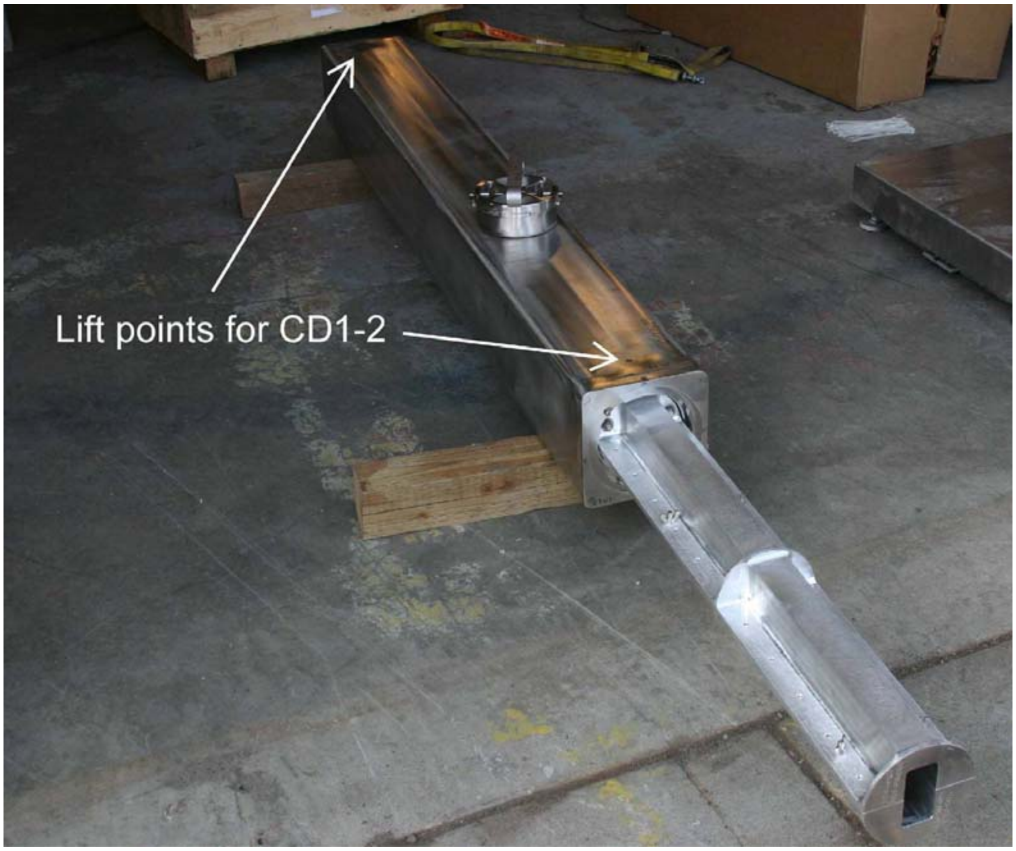

Figure 2.12.2-3 - Basket Orientation in CD1-2

Figure 2.12.2-4 - Basket Orientation in CD3-2

Figure 2.12.2-5 - CD1-2 Drop Orientation

Figure 2.12.2-6 - CTU Following CD1-2 Impact
(impact side facing up)

Figure 2.12.2-7 - CD1-2, Extracting Basket Following Drop

Figure 2.12.2-8 - CD3-2 Drop Orientation

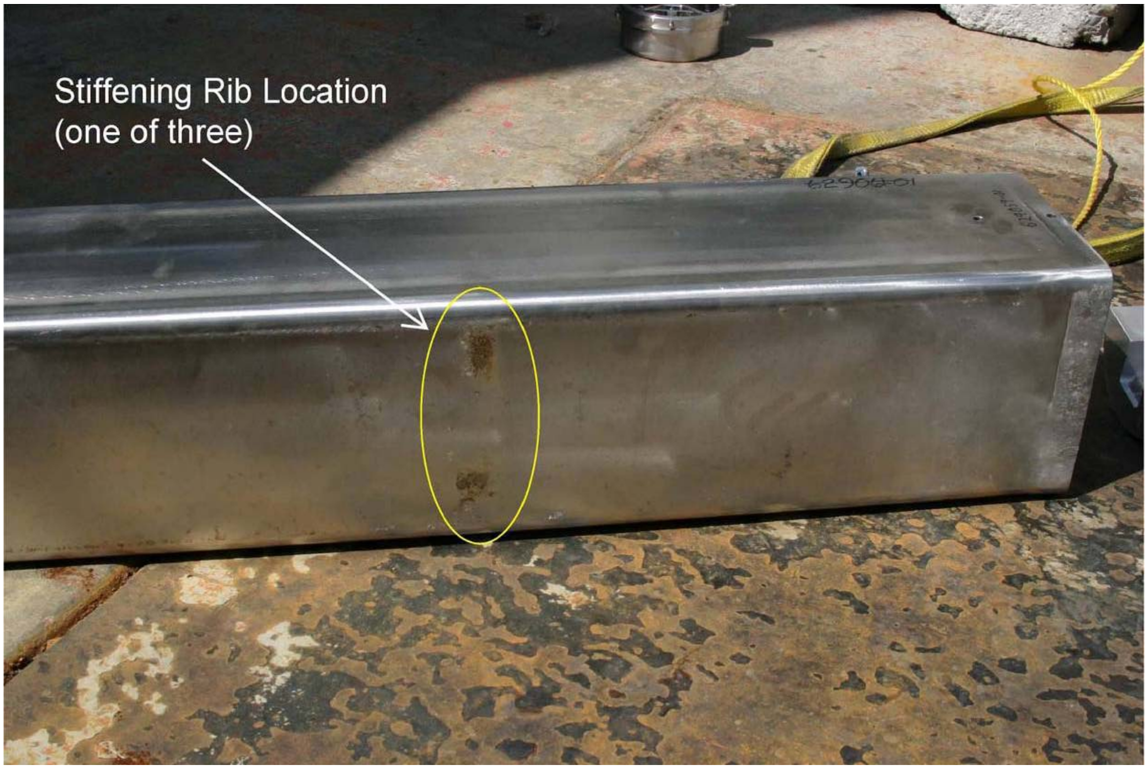

Figure 2.12.2-9 - CD3-2 Deformation at Stiffening Rib Location

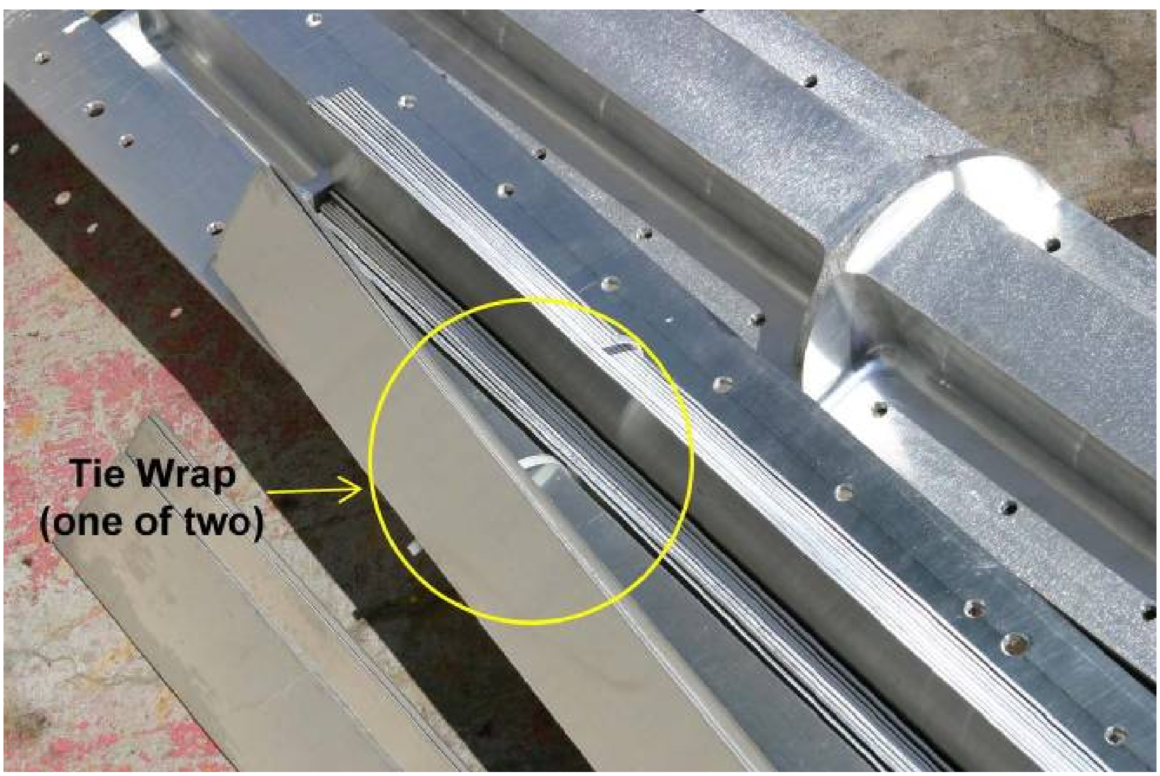

Figure 2.12.2-10 - CD3-2 – Failed tie wraps

Figure 2.12.2-11 - CD4-2 – Drop Orientation

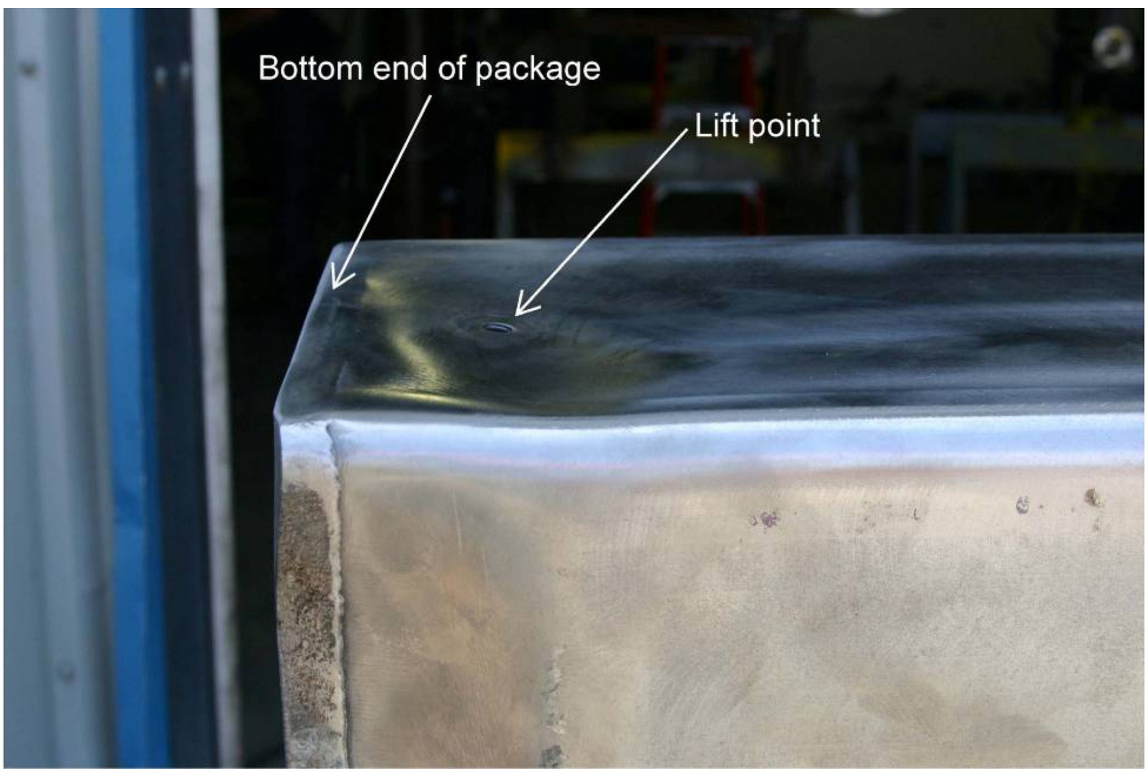

Figure 2.12.2-12 - CD4-2 Impact Damage to Package

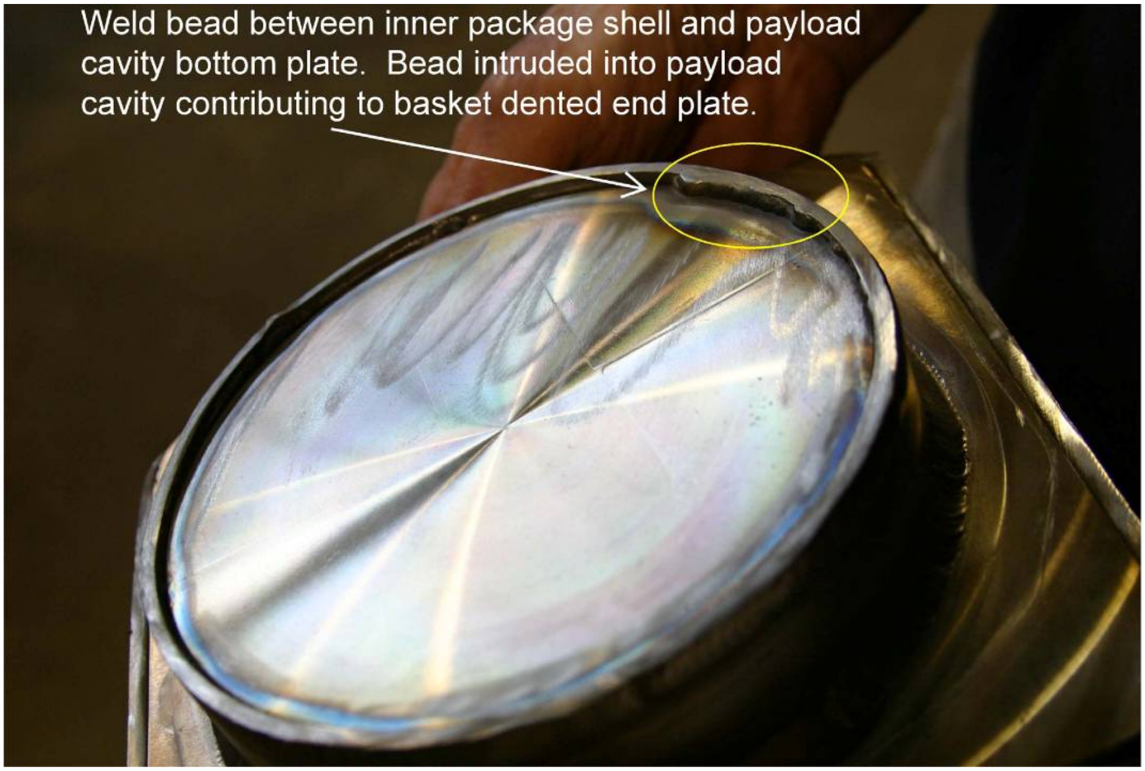

Figure 2.12.2-13 - Weld bead protruding into package payload cavity (inner shell has been removed in this photo)

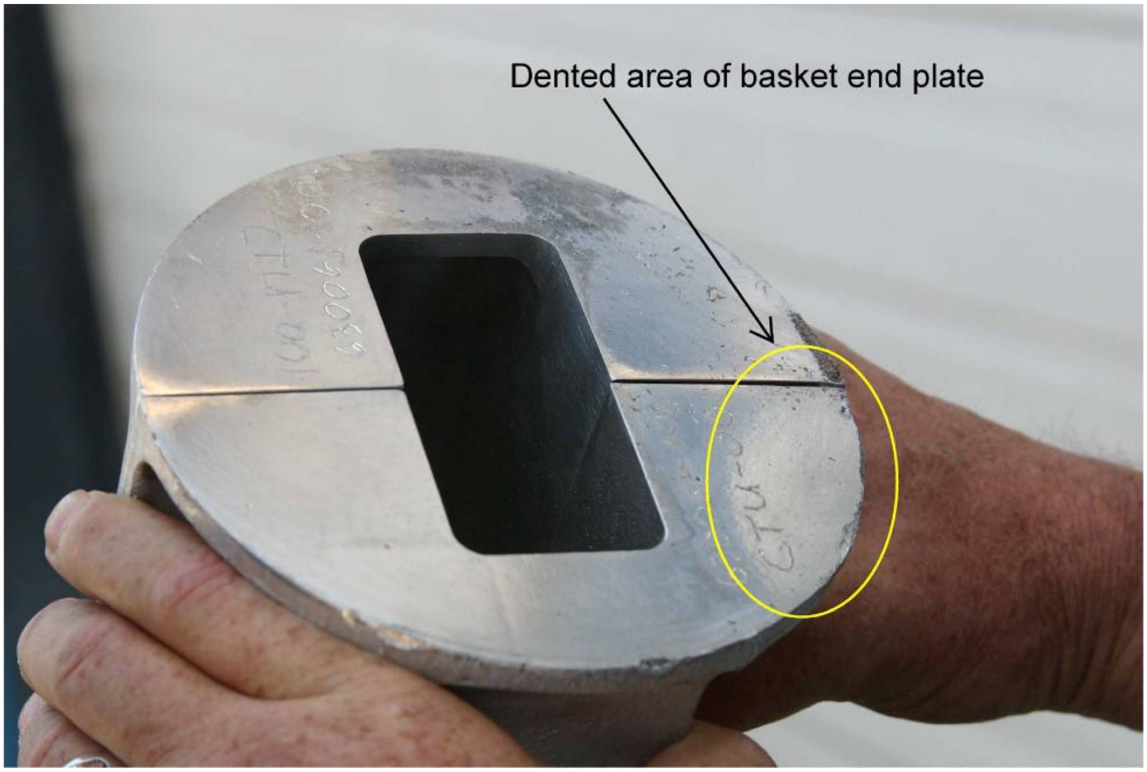

Figure 2.12.2-14 - Dented area – basket end plate

Figure 2.12.2-15 - CD4-2 Impact Damage to Simulated Fuel Plates

Figure 2.12.2-16 - CD4-2 Impact Damage to Simulated Fuel Plates (close up view)

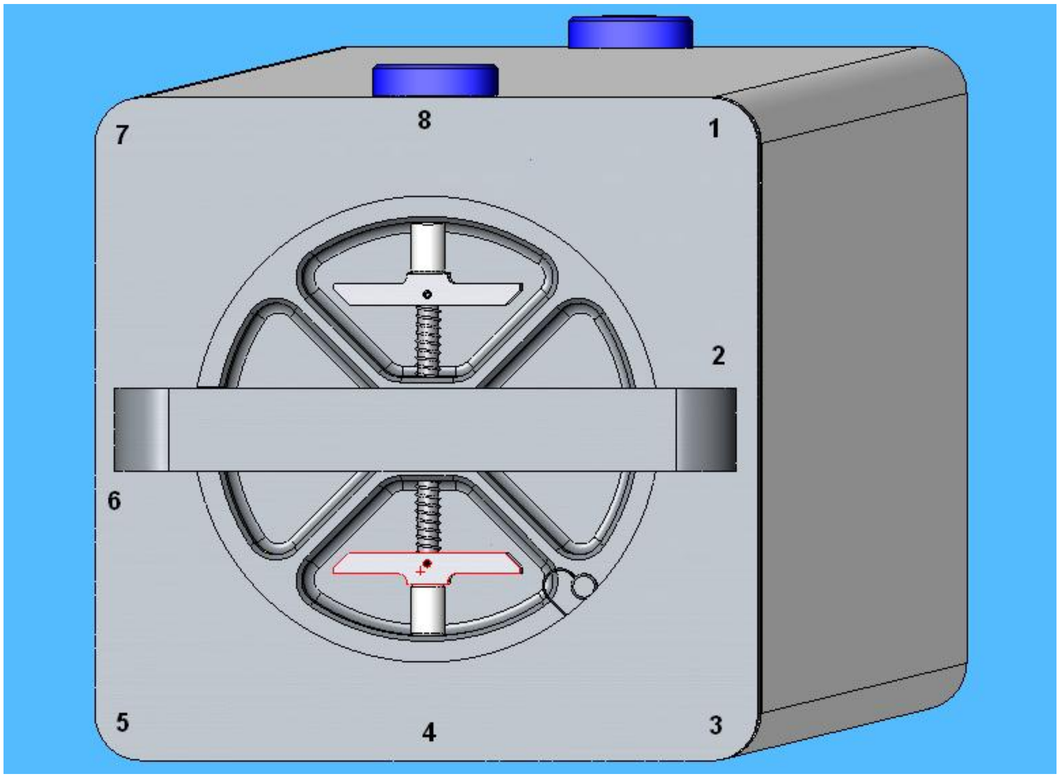

Figure 2.12.2-17 - CTU Measurement Locations

Figure 2.12.2-18 - Thermal Shield Condition, View 1

Figure 2.12.2-19 - Thermal Shield Condition, View 2

Figure 2.12.2-20 - Thermal Shield Condition, View 3

Figure 2.12.2-21 - Thermal Shields at Interface to Stiffening Rib

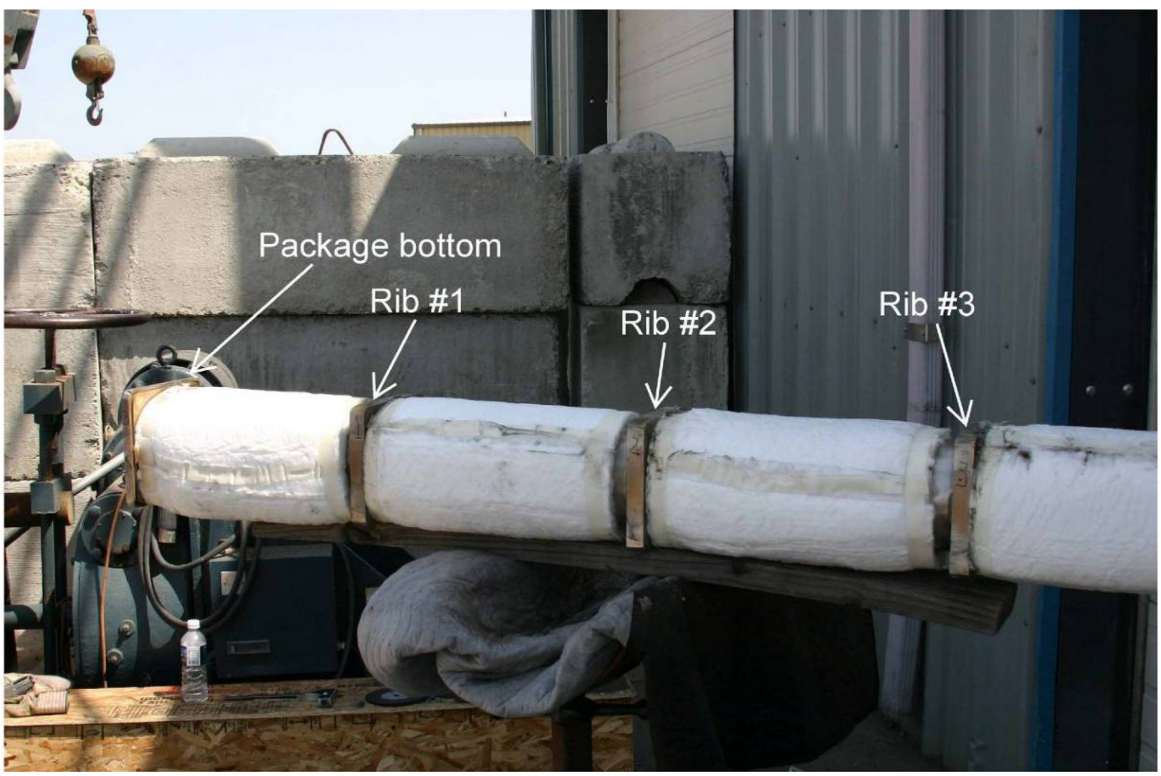

Figure 2.12.2-22 - Exposed Insulation - Overview

Figure 2.12.2-23 - Insulation Gap at Package Closure End

Figure 2.12.2-24 - Insulation Gap at Rib #3

Figure 2.12.2-25 - Insulation Gap at Rib #2

Figure 2.12.2-26 - Insulation Gap at Rib #1 (nearest impact)

Figure 2.12.2-27 - End Plate Insulation Condition

Figure 2.12.2-28 - Tube to Bottom End Plate – View 1

Figure2.12.2-29 - Tube to Bottom End Plate – View 2

2.12.3 Structural Evaluation for MIT and MURR Fuel

The ATR FFSC may be utilized to transport a MIT fuel assembly or a MURR fuel assembly. Both of these fuels are high-enriched aluminum-clad uranium aluminide plate type fuel elements similar to the ATR fuel evaluated in this chapter. Since no MIT or MURR fuel elements were included in the drop tests, the following evaluation conservatively estimates a degree of failure and movement of the MIT and MURR Fuel Handling Enclosures (FHE) to develop a worst case pitch expansion of the corresponding fuel elements for evaluation in Section 6.10, *Appendix B: Criticality Analysis for MIT and MURR Fuel*. By conservatively bounding potential damage and evaluating the exceptional worst case pitch expansion of the MIT and MURR fuel elements the ATR FFSC complies with the performance requirements of 10 CFR §71.

2.12.3.1 Structural Design Discussion

A comparison is provided to highlight the similarities and differences between the MIT and MURR designs and the physically tested ATR design. Through this comparison, it is expected that both NCT and HAC testing would result in similar results for the MIT and MURR fuel elements. Similar to the ATR LFPB, the MIT and MURR FHEs are designed to restrict postulated fuel element pitch expansion under the HAC conditions.

The results of NCT conditions on the MIT and MURR payload are assumed to be equivalent to the ATR payload; i.e. there is no damage to the FHE or fuel element under NCT.

For conservatism in evaluating the HAC conditions, the MIT and MURR FHE damage postulated exceeds the results obtained during testing of the ATR payloads. The MIT and MURR FHEs are assumed to separate (fail) and spread apart to permit a worst case reactivity configuration of the fuel elements. The individual fuel plates of the fuel elements are assumed to spread apart uniformly to fill the resulting space.

2.12.3.1.1 Fuel Elements

The ATR FFSC packaging is not modified for the use of the MIT and MURR fuel elements. The MIT and MURR FHE are used in place of the ATR FHE or the LFPB within the ATR FFSC packaging. Similar to the ATR FHE and LFPB, the MIT and MURR FHEs are principally fabricated of aluminum construction and secured with stainless steel locking pins.

The MIT and MURR fuel elements are very similar to the ATR fuel element in design, materials, and fabrication. The weight of the fuel elements are 10 lb, 15 lb, and 25 lb, for the MIT, MURR, and ATR fuel elements respectively. All three fuel elements are fabricated of the same fuel type, aluminum-clad uranium aluminide fuel plates, with all fuel plates swaged into the side plates, and include cast or wrought aluminum end boxes. As such, the structural performance of the MIT and MURR fuel types are anticipated to behave very similarly to the ATR fuel element. Table 2.12.3-1 compares the three fuel element design dimensions. Figure 2.12.3-1 compares the three fuel elements in their overall length and fuel plate length in inches. In this figure, the inside dimension identifies the fuel plate length.

For comparative purposes, an approximate moment of inertia is calculated for all three fuel elements using AutoCAD®. The results are presented in Figure 2.12.3-2. The values were determined by taking a cross section of the fuel plate region and selecting the solid boundaries to compute the moments of inertia about the identified axes.

The comparison of the moments of inertia demonstrates that the three fuel elements are similar in stiffness and expected to perform in a similar fashion during NCT and HAC drop events. The length and weight of the fuel elements is clearly bounded by the ATR fuel element. The materials of construction and fabrication techniques are the same for each fuel type. The relatively minor dimensional changes of the ATR fuel element plates as a consequence of the testing identified in Section 2.6, *Normal Conditions of Transport*, and Section 2.7, *Hypothetical Accident Conditions*, further justifies the similar performance of the MIT and MURR fuel elements.

Table 2.12.3-1 –Fuel Element Design

Component	MIT	MURR	ATR
Approximate Weight, lbs	10	15	25
Number of Fuel Plates	15	24	19
Nominal Plate Spacing, in.	.08	.08	.08
Fuel Plate Length, in.	23.00	25.50	49.50
Fuel Plate Thickness, in.	.08	.05	.05, .08, .10
Approximate Fuel Plate Width, in.	2.5	2.0 - 4.3	2.0 – 3.9

Security-Related Information Figure Withheld Under 10 CFR 2.390.

Figure 2.12.3-1 – MIT, MURR, and ATR Fuel Elements

This page left intentionally blank.

$I_{X\text{-}X} = 5.4\ in^4$
$I_{Y\text{-}Y} = 10.5\ in^4$

$I_{X\text{-}X} = 11.0\ in^4$
$I_{Y\text{-}Y} = 15.1\ in^4$

$I_{X\text{-}X} = 6.4\ in^4$
$I_{Y\text{-}Y} = 3.8\ in^4$
$I_{A\text{-}A} = 7.7\ in^4$
$I_{B\text{-}B} = 2.6\ in^4$

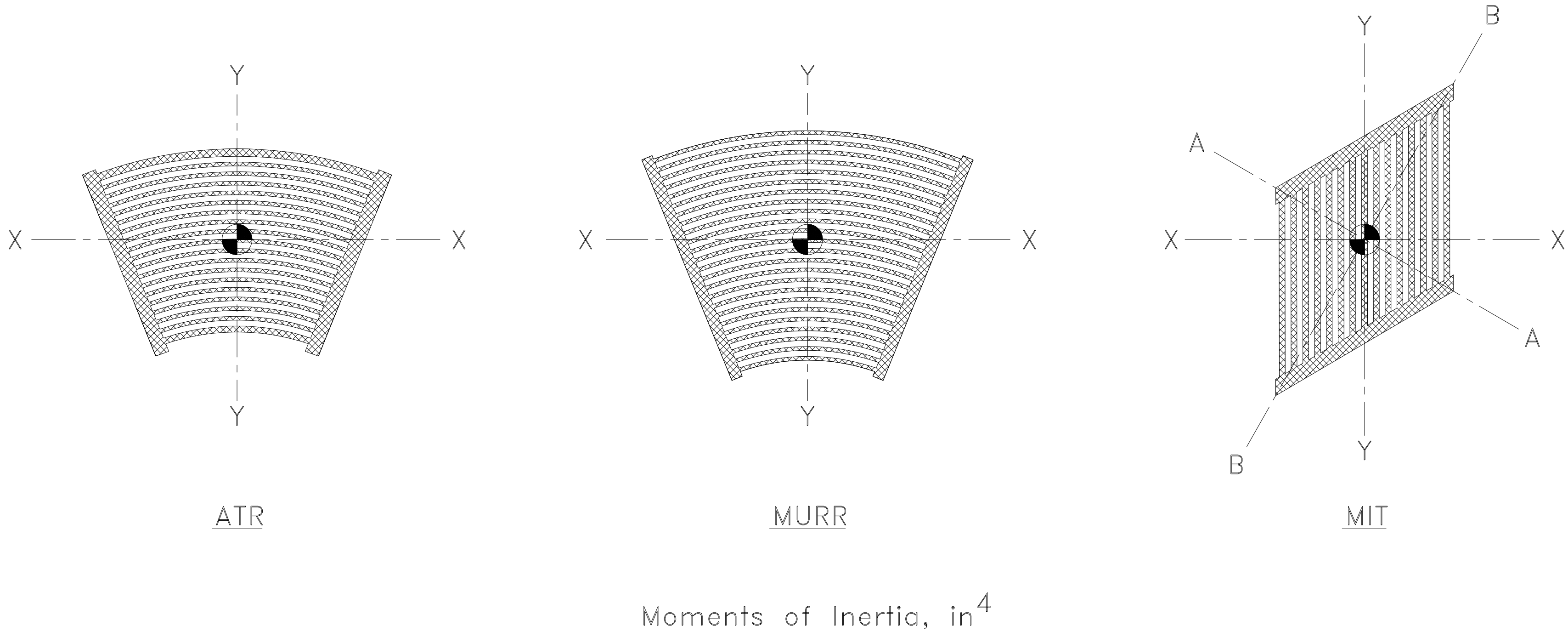

Figure 2.12.3-2 – Fuel Element Moments of Inertia

This page left intentionally blank.

2.12.3.1.2 Fuel Handling Enclosures

The MIT FHE incorporates two end spacers and a two-piece machined aluminum enclosure to protect the MIT fuel element from damage during loading and unloading operations. The enclosure halves are identical segments machined from 6061 aluminum plate. Neoprene rub strips are used to cushion the contact points between the fuel element and enclosure. The end spacers are also fabricated of 6061 aluminum. The end spacers lock the enclosure halves together and are secured using stainless steel ball lock pins. The end spacers also prevent axial movement since the MIT fuel element is much shorter than the package cavity. The weight of the MIT FHE is 25 lb. Figure 2.1-3 illustrates the assembly view of the MIT FHE.

The MURR FHE is designed in the same manner as the MIT FHE. The weight of the MURR FHE is 30 lb. Figure 2.1-4 illustrates the assembly view of the MIT FHE.

The MIT and MURR FHE design is similar to the 30-lb LFPB in that it utilizes machined enclosure halve segments to encase the payload. The use of the enclosure halves makes the MIT and MURR FHEs more robust than the ATR FHE, which weighs 15 lb. The wall thickness of the enclosure halves is 0.19 in compared to the 0.09 in thick sheet used in the ATR FHE. For comparison, the typical machined wall thickness of the LFPB is also 0.19 in thick. The weight of the enclosures and fuel elements are 35 lb, 45 lb, 40 lb, and 50 lb for the MIT payload, MURR payload, ATR payload, and LFPB payload respectively.

Based on the similarity in design and function, the structural and thermal performance of the MIT and MURR FHEs is anticipated to be similar to the physical testing performed using the ATR FHE and LFPB.

2.12.3.1.3 Loose Fuel Plates

MIT and MURR loose fuel plates are not evaluated for use within the LFPB.

2.12.3.2 Allowable Damage

For HAC tests the MIT and MURR fuel elements are anticipated to perform in a similar manner to the ATR fuel element based on the comparable designs and assembly techniques. To conservatively encompass potential damage, the FHE halves are considered to separate while each half is sized at the extreme tolerances to encourage the maximum space around each fuel element. Based on the maximum space developed by the separated FHE, the fuel element plates separate to create a more reactive configuration for the fuel. The proposed pitch expansion greatly exceeds the results of the physical testing performed on the ATR fuel element.

Axial movement of the fuel element within the package inner tube, which occurs by hypothetical neglect of the FHE end spacers, has no adverse effect on the performance of the ATR FFSC. Energy dissipated by failure of the spacers would result in lowering the HAC loads to the MIT and MURR elements. However, the structural tests identified that the ATR fuel element survives the impact loads with damage that has no impact on reactivity. The MURR and MIT fuel elements are of similar materials and of similar construction to the ATR fuel elements. Assuming the spacers to fail with no energy absorption, the impact velocities of the MURR and MIT FHEs on the end fitting of the package would be nearly identical. It is therefore concluded that the damage to MURR and MIT fuel elements is bounded by the damage sustained by the ATR fuel element in the structural tests. However, for conservatism, the fuel plate pitch of the

MURR and MIT elements is set to the condition that results in the worst case reactivity under the volumetric constraints presented by the FHEs.

The HAC criticality array model is a 5x5x1 array of packages and all fuel elements are positioned at the same axial location. The FHE end spacers are conservatively neglected and modeled as water. Axial shifting of fuel elements from the modeled configuration would result in a less reactive condition; therefore, failure of the FHE end spacers is not a criticality concern. For the thermal evaluation, the position of the MIT or MURR fuel element is naturally bounded by the ATR fuel element since its length extends to each end of the package.

The modeled separation of the FHE halves inside the inner tube of the package is determined by using the maximum inner diameter of the package's inner tube and the minimum outer radius of each FHE half as illustrated in Figures 2.12.3-3 and 2.12.3-4. The FHE cavity dimensions are expanded using the maximum tolerance of the parts. Note that this is only hypothetically possible, since this causes the corners of the FHE for both the MIT and MURR to exceed the point of interference with the inner tube wall.

The dimensions for the criticality model of the MIT FHE are determined in the following manner:

- Package inner tube maximum inside diameter: Diameter is specified as 6.0 in. OD X 0.12 in. wall thickness ± 0.030 in. OD and ± 10% thickness (per drawing 60501-10 and ASTM A269). Resulting maximum ID is 5.814 in.
- Minimum outside radius of the FHE half: Radius is specified as 2.8 in ± 0.2 (per drawing 60501-40). Resulting minimum radius is 2.6 in.
- Minimum wall thickness of the FHE half: Wall is specified as 0.19 in ± 0.06 (per drawing 60501-40). Resulting minimum thickness is 0.13 in.
- Maximum cavity height of the FHE half: Wall height specified as 2.82 in ± 0.06 (per drawing 60501-40). Resulting maximum height is 2.88 in. (which is greater than the 2.6 maximum radius).
- Maximum cavity width of the FHE half: Wall width specified as 1.62 in ± 0.06 (per drawing 60501-40). Resulting maximum width is 1.68 in.

The dimensions for the criticality model of the MURR FHE are determined in the following manner:

- Package inner tube maximum inside diameter: Diameter is specified as 6.0 in. OD X 0.12 in. wall thickness ± 0.030 in. OD and ± 10% thickness (per drawing 60501-10 and ASTM A269). Resulting maximum ID is 5.814 in.
- Minimum outside radius of the FHE half: Radius is specified as 2.8 in ± 0.2 (per drawing 60501-50). Resulting minimum radius is 2.6 in.
- Minimum wall thickness of the FHE half: Wall is specified as 0.19 in ± 0.06 (per drawing 60501-50). Resulting minimum thickness is 0.13 in.
- Maximum cavity height of the FHE half: Wall height specified as 2.00 in ± 0.06 (per drawing 60501-50). Resulting maximum height is 2.06 in.
- Maximum cavity width of the FHE half: Wall width specified as 1.85 in ± .06 (per drawing 60501-50). Resulting maximum width is 1.91 in.

The thermal evaluation in Section 3.6, *Thermal Evaluation for MIT, MURR, and Small Quantity Payloads*, makes the following conservative assumptions to bound damage to the fuel elements and FHEs as a result of NCT and HAC events.

- Idealized contact between the FHE and the package inner tube. The majority of the heat input to the fuel element comes from the radial direction rather than the axial direction. By maximizing the contact, the greatest heat is transferred. Deformation of the payload would have the effect of reducing the contact area, and therefore reducing the conductive heat input.
- Axial movement of the fuel element, as a result of deformation of the FHE end spacers has a negligible effect. The majority of the heat input to the fuel element comes from the radial direction rather than the axial direction (ends). As the fuel element moves closer to the ends of the package the heat input rises. However, the heat input from either end of the package is negligible compared to the heat input received axially from the sides. Furthermore, any credible axial distance of the MIT and MURR fuel elements to the end of the package is bounded by the ATR fuel element.

The criticality evaluation in Section 6.10, *Appendix B: Criticality Analysis for MIT and MURR Fuel*, makes the following conservative assumptions to bound damage to the fuel element as a result of HAC events.

- Neglecting the function of the end spacers, the two halves are pushed apart to the maximum extent to maximize the available space for pitch expansion.
- Although it is not feasible in actual practice to push the FHEs to the center of the array if the two FHE halves are already pushed apart, both the MIT and MURR models are shifted by 0.307-in towards the center of the array.
- Fuel element end boxes are not modeled. For criticality purposes, any amount of damage to the end boxes is acceptable.
- Note that the MIT and MURR FHEs are “sliced off” in the corners because such a translation is not possible without interference.

Due to the conservative assumptions utilized for the thermal and criticality evaluations, the allowable damage to the FHEs is considered severe and therefore far exceeding the physical testing results performed using the ATR fuel element and LFPB payloads covered in Section 2.12.1, *Certification Tests on CTU-1*, and Section 2.12.2, *Certification Tests on CTU-2*.

For containment purposes, the MIT and MURR fuel element plates must remain intact to prevent the fuel meat from within the fuel plate from exiting the package. The MIT and MURR fuel elements are fully supported over the length of the fuel plates by the FHE enclosure halves. The enclosure halves are specifically designed to fully support each fuel element and minimize any deformation or change in the fuel plate geometry. By design the MIT and MURR FHEs are more robust (thicker side walls) than the ATR FHE and therefore provide better support compared to the testing performed using the ATR fuel element and ATR FHE.

Security-Related Information Figure Withheld Under 10 CFR 2.390.

Figure 2.12.3-3 – MIT FHE Damage

Security-Related Information Figure Withheld Under 10 CFR 2.390.

Figure 2.12.3-4 – MURR FHE Damage

This page left intentionally blank.

3.0 THERMAL EVALUATION

This chapter identifies and describes the principal thermal design aspects of the ATR FFSC. Further, this chapter presents the evaluations that demonstrate the thermal safety of the ATR FFSC package[1] and compliance with the thermal requirements of 10 CFR 71[2] when transporting a payload consisting of an assembled, unirradiated fuel element or a payload of loose, unirradiated fuel plates. The payloads are summarized in Table 1.1-1 and described in Section 1.2.2, *Contents*.

Specifically, all package components are shown to remain within their respective temperature limits under the normal conditions of transport (NCT). Further, per 10 CFR §71.43(g), the maximum temperature of the accessible package surfaces is demonstrated to be less than 122 °F for the maximum decay heat loading, an ambient temperature of 100 °F, and no insolation. Finally, the ATR FFSC package is shown to retain sufficient thermal protection following the HAC free and puncture drop scenarios to maintain all package component temperatures within their respective short term limits during the regulatory fire event and subsequent package cool-down.

The analysis in the main body of Chapter 3 pertains only to the ATR fuel element, ATR U-Mo demonstration element, and ATR loose plate basket. The analysis for MIT, MURR, RINSC, Cobra, and small quantity payloads is contained in Section 3.6, *Thermal Evaluation for MIT, MURR, Cobra, and Small Quantity Payloads*.

3.1 Description of Thermal Design

The ATR FFSC package, illustrated in Figure 1.2-1 through Figure 1.2-5 from Section 1.0, *General Information*, consists of three basic components: 1) a Body assembly, 2) a Closure assembly, and 3) either a Fuel Handling Enclosure (FHE) or a Loose Fuel Plate Basket (LFPB). The FHE is configured to house an assembled ATR fuel element or ATR U-Mo demonstration element, while the LFPB is configured to house loose ATR fuel element plates. The maximum gross weight of the package loaded with an FHE and ATR fuel element or ATR U-Mo demonstration element is approximately 290 pounds. The maximum gross weight of the package loaded with a LFPB containing its maximum payload is approximately 290 pounds.

The ATR FFSC is designed as a Type AF packaging for transportation of an ATR fuel element or a bundle of loose ATR fuel element plates. The packaging is rectangular in shape and is intended to be transported in racks of multiple packages by highway truck. Since the payload generates essentially no decay heat, the worst case thermal conditions will occur with an individual package fully exposed to ambient conditions. The package performance when

[1] In the remainder of this chapter, the term ‘packaging’ refers to the assembly of components necessary to ensure compliance with the regulatory requirements, but does not include the payload. The term ‘package’ includes both the packaging components and the payload of ATR fuel.

[2] Title 10, Code of Federal Regulations, Part 71 (10 CFR 71), *Packaging and Transportation of Radioactive Material*, 01-01-03 Edition.

configured in a rack of multiple packages will be bounded by that seen for an individual package.

The principal components of the packaging are shown in Figure 1.2-1 and described in more detail below. With the exception of minor components, all steel used in the ATR FFSC packaging is Type 304 stainless steel. Components are joined using full-thickness fillet welds and full and partial penetration groove welds.

3.1.1 Design Features

The primary heat transfer mechanisms within the ATR FFSC are conduction and radiation, while the principal heat transfer from the exterior of the packaging is via convection and radiation to the ambient environment. The Body and Closure assemblies serve as the primary impact and thermal protection for the FHE or the LFPB and their enclosed payloads of an ATR fuel element, ATR U-Mo demonstration element, or loose fuel plates. The FHE and LFPB provide additional thermal shielding of their enclosed payloads during the transient HAC event.

There is no pressure relief system included in the ATR FFSC packaging design. The portions of the packaging that are not directly vented to atmosphere do not contain out-gassing materials. The package insulation is the only non-metallic component located in the enclosed volumes of the package and it is fabricated of a ceramic fiber. The Closure assembly is not equipped with either seals or gaskets so that potential out-gassing of the neoprene material used in ATR fuel tray and the plastic bag material used as a protective sleeve for the fuel element will readily vent without significant pressure build-up in the payload cavity.

The principal thermal design features of each package component are described in the following paragraphs.

3.1.1.1 ATR FFSC Body

The ATR FFSC body is a stainless steel weldment that is approximately 73 inches long and 8 inches square and weighs about 230 lbs (empty). It consists of two nested shells; the outer shell is fabricated of a square stainless steel tube with a 3/16 inch wall thickness, while the inner shell is fabricated from a 6 inch diameter, 0.120 inch wall, stainless steel tube. Three, 1-inch thick stiffening plates (i.e., ribs) are secured to the inner shell by fillet welds at four equally spaced intervals. The ribs are not mechanically attached to the outer shell. Instead, a nominal 0.06 inch air gap exists between the ribs and the outer shell, with a larger nominal gap existing at the corners of the ribs. These design features help to thermally isolate the inner shell from the outer shell during the HAC event.

Further thermal isolation of the inner shell is provided by ceramic fiber thermal insulation which is wrapped around the inner shell between the ribs and by the 28 gauge stainless steel sheet used as a jacket material over the insulation. The insulation is applied in two 0.5-inch thick layers in order to permit over-lapping joints between the layers and prevents direct line-of-sight between the inner shell and the jacket should the insulation shift under normal or accident conditions. The stainless steel jacket maintains the insulation around the inner shell and provides a relatively low emissivity barrier to radiative heat exchange between the insulation and the outer sleeve. The insulation jacket is pre-formed to the design shape and dimensions prior to installation. As such, the potential for inadvertent compression of the insulation during installation is minimized.

Once assembled, the inner shell, ribs, and the jacketed insulation wrap are slid as a single unit into the outer shell and secured to closure plates at both ends by welding. Thermal insulation is built into the bottom end closure plate of the packaging, while the ATR FFSC closure (see below) provides thermal insulation at the top end closure.

Cross-sectional views showing key elements of the ATR FFSC body are provided in Figure 1.2-2 and Figure 1.2-3. Figure 1.2-2 illustrates a cross sectional view at the top end closure of the package and 1.2-3 presents a similar cross sectional view of the package at the bottom end closure.

3.1.1.2 ATR FFSC Closure

The ATR FFSC closure engages with the body using a bayonet style engagement via four uniformly spaced lugs on the closure that engage with four slots in the mating body feature. The closure incorporates 1 inch of ceramic fiber thermal insulation to provide thermal protection and is designed to permit gas to easily vent through the interface between the closure and the body. The closure weighs approximately 10 pounds and is equipped with a handle to facilitate use with gloved hands.

A cross sectional view of the ATR FFSC closure is illustrated in Figure 1.2-4.

3.1.1.3 Fuel Handling Enclosure (FHE)

The Fuel Handling Enclosure (FHE) is a hinged, aluminum weldment used to protect either an ATR fuel element or ATR U-Mo demonstration element from damage during loading and unloading operations. It is fabricated of thin wall (i.e., 0.09 inch thick) 5052-H32 aluminum sheet and features a hinged lid and neoprene rub strips to minimize fretting of the fuel element side plates where they contact the FHE. The surface of the FHE is neither anodized nor coated, but is left as an 'unfinished' aluminum sheet. Figure 1.2-1 presents an illustration of the FHE. A polyethylene bag is used as a protective sleeve over the ATR fuel and ATR U-Mo demonstration elements.

3.1.1.4 ATR FFSC Loose Fuel Plate Basket (LFPB)

The Loose Fuel Plate Basket (LFPB) serves to maintain the fuel plates within a defined dimensional envelope during transport. The four identical machined segments are machined from a billet of 6061-T651 aluminum and are joined by threaded fasteners (see Figure 1.2-15). A variable number of ATR fuel plates may be housed in the basket, with the maximum payload weight being limited to 20 lbs. or less. The empty weight of the loose fuel plate basket is approximately 30 lbs. Like the FHE, the surface of the LFPB is neither anodized nor coated, but is left with its 'as machined' finish.

3.1.2 Content's Decay Heat

The ATR FFSC is designed as a Type AF packaging for transportation of an unirradiated ATR fuel element, an ATR U-Mo demonstration element, or a bundle of loose, unirradiated ATR fuel plates. The decay heat associated with unirradiated ATR fuel is negligible. Therefore, no special devices or features are needed or utilized in the ATR FFSC packaging to dissipate the decay heat. Section 1.2.2, *Contents*, provides additional details.

3.1.3 Summary Tables of Temperatures

Table 3.1-1 provides a summary of the package component temperatures under normal and accident conditions. The temperatures for normal conditions are based on an analytical model of the ATR FFSC package for extended operation with an ambient temperature of 100°F and a diurnal cycle for the insolation loading. The temperatures for accident conditions are based on an analytical model of the ATR FFSC package with the worst-case, hypothetical pre-fire damage as predicted based on drop tests using full-scale certification test units (CTUs).

The results for NCT conditions demonstrate that significant thermal margin exists for all package components. This is to be expected since the only significant thermal loads on the package arise from insolation and ambient temperature changes. The payload dissipates essentially zero decay heat. Further, the evaluations for NCT demonstrate that the package skin temperature will be below the maximum temperature of 122°F permitted by 10 CFR §71.43(g) for accessible surface temperature in a nonexclusive use shipment when transported in a 100°F environment with no insolation.

The results for HAC conditions also demonstrate that the design of the ATR FFSC package provides sufficient thermal protection to yield component temperatures that are significantly below the acceptable limits defined for each component. While the neoprene rubber and polyethylene plastic material used to protect the ATR fuel and U-Mo demonstration elements from damage are expected to reach a sufficient temperature level during the HAC fire event to induce some level of thermal degradation (i.e., melting, charring, the chemical breakdown of the materials into 2 or more substances, etc.), the loss of these components is not critical to the safety of the package. Further, the potential combustion of these materials will be restricted due to the lack of available oxygen to the point that any potential temperature rise will be insignificant. See Sections 3.2.2, *Technical Specifications of Components*, 3.4.3.1, *Maximum HAC Temperatures*, and 3.5.3, *Thermal Decomposition/Combustion of Package Organics*, for more discussion.

3.1.4 Summary Tables of Maximum Pressures

Table 3.1-2 presents a summary of the maximum pressures achieved under NCT and HAC conditions. Since the ATR FFSC package is a vented package, both the maximum normal operating pressure (MNOP) and the maximum pressure developed within the payload compartment under the HAC condition are 0 psig.

Although the volume between the outer and inner shells is sealed, it does not contain organic or other materials that may outgas or thermally degrade. Therefore, the maximum pressure that may develop within the space will be limited to that achieved due to ideal gas expansion. The maximum pressure rise under NCT will be less than 4 psig, while the pressure rise under HAC conditions will be 39 psig.

Table 3.1-1 – Maximum Temperatures for NCT and HAC Conditions

Location / Component	NCT Hot Conditions	Accident Conditions	Maximum Allowable ①	
			Normal	Accident
ATR Fuel Element Fuel Plate	147°F	730°F	400°F	1,100°F
ATR Fuel Element Side Plate	148°F	827°F	400°F	1,100°F
Neoprene Rub Strips/Polyethylene Bag	151°F ②	1,017°F ②	225°F	N/A
Fuel Handling Enclosure (FHE)	151°F	1,017°F	400°F	1,100°F
Loose Fuel Plate Basket (LFPB)	151°F ②	746°F	400°F	1,100°F
Inner Shell	157°F	1,422°F	800°F	2,700°F
Ceramic Fiber Insulation, Body				
- Maximum	185°F	1,460°F	2,300°F	2,300°F
- Average	151°F	1,220°F	2,300°F	2,300°F
Ceramic Fiber Insulation, Closure				
- Maximum	145°F	1,418°F	2,300°F	2,300°F
- Average	144°F	1,297°F	2,300°F	2,300°F
Closure	145°F	1,445°F	800°F	2,700°F
Outer Shell	186°F	1,471°F	800°F	2,700°F

Table Notes:

① Maximum allowable temperatures are defined in Section 3.2.2, *Technical Specifications of Components*.

② Component temperature assumed to be equal to that of the FHE.

Table 3.1-2 – Summary of Maximum Pressures

Condition	Fuel Cavity Pressure	Outer/Inner Shell Cavity Pressure
NCT Hot	0 psi gauge	4 psi gauge
HAC Hot	0 psi gauge	39 psi gauge

3.2 Material Properties and Component Specifications

The ATR FFSC is fabricated primarily of Type 304 stainless steel, 5052-H32 and 6061-T651 aluminum, ceramic fiber insulation, and neoprene rubber. The payload materials include 6061-T6 and/or 6061-0 aluminum, uranium aluminide (UAl_x), and uranium-molybdenum (i.e., U-10Mo in a foil coated with thin zirconium interlayers). A polyethylene plastic bag is used as a protective sleeve over the fuel element.

3.2.1 Material Properties

Table 3.2-1 presents the thermal properties for Type 304 stainless steel and 5052-H32 aluminum from Table TCD of the ASME Boiler and Pressure Vessel Code[3]. Since the HAC analysis requires thermal properties in excess of the maximum temperature point of 400°F provided in Table TCD for 5052-H32 aluminum, the property values for 1100°F (i.e., the approximate melting point for aluminum) are assumed to be the same as those at 400°F. This approach is appropriate for estimating the temperature rise within the fuel basket during the HAC event since the thermal conductivity of aluminum alloys tends to decrease with temperature while the specific heat tends to increase. The density values listed in the table are taken from an on-line database[4]. Properties between the tabulated values are calculated via linear interpolation within the heat transfer code.

Table 3.2-2 presents the thermal properties for the ATR fuel element. For analysis purposes, the material used for the side plates, covers, and fuel cladding are assumed to be 6061-0 aluminum. The thermal properties for the fuel plates are determined as a composite of the cladding and the fuel core materials based on the geometry data for the ATR fuel element[5] and the thermal properties for the ATR fuel element materials[6]. The details of the computed values are presented in Section 3.5.2.4, *Determination of Composite Thermal Properties for ATR Fuel Plates*. For simplicity and given the low sensitivity to temperature, a conservatively high, fixed thermal conductivity value is used for the fuel plates in order to maximize the heat transfer into the fuel components during the HAC event. The specific heat values are computed as a function of temperature to more accurately capture the change in thermal mass for the fuel plates during the HAC event.

The ATR U-Mo demonstration fuel elements are not specifically modeled for this evaluation. Instead, the thermal response of these elements is bounded by the results predicted for other elements. See Section 3.5.2.5, *Thermal Properties for ATR U-Mo Demonstration Element,* for details.

The thermal properties for the non-metallic materials used in the ATR FFSC are presented in Table 3.2-3. The thermal properties for neoprene rubber are based on the *Polymer Data*

[3] American Society of Mechanical Engineers (ASME) Boiler and Pressure Vessel Code, Section II, *Materials*, *Part D – Properties*, Table TCD, Material Group J, 2001 Edition, 2002 and 2003 Addenda, New York

[4] Matweb, Online Material Data Sheets, www.matweb.com.

[5] *ATR Mark VII Fuel Element Assembly*, INEEL Drawing No. DWG-405400.

[6] *Thermophysical And Mechanical Properties Of ATR Core Materials*, Report No. PG-T-91-031, August 1991, EG&G Idaho, Inc.

Handbook[7], while the thermal properties for the ceramic fiber insulation are based on the Unifrax Durablanket® S insulation product[8] with a nominal density of 6 lb/ft^3. The thermal properties are for the uncompressed material in both cases. Although the package design requires that the insulation blanket be compressed by up to 20% at the quadrant points, ignoring the compression for the purposes of the thermal modeling and using the thermal properties for the uncompressed material at all locations provides a conservative estimate of the package's performance under the HAC condition. This conclusion arises from the fact that the insulation's thermal conductivity decreases with density for temperatures above approximately 500°F (see Table 3.2-3). For example, the thermal conductivity of 8 pcf insulation at 1000°F and 1400°F is 0.0814 and 0.1340 Btu/hr-ft-°F, respectively, versus the 0.0958 and 0.1614 Btu/hr-ft-°F values for 6 pcf insulation at the same temperatures. While compression will increase conductivity below 500°F, ignoring the effects of compression for NCT conditions has an insignificant effect since the peak package temperatures occur in the vicinity of the ribs and are therefore unaffected by a local increase in the thermal conductivity of the insulation. Further, large thermal margins exist for the NCT conditions.

The thermal properties for air presented in Table 3.2-4 are derived from curve fits[9]. Because the thermal conductivity of air varies significantly with temperature, the computer model calculates the thermal conductivity across thin air filled gaps as a function of the mean gap temperature. All void spaces within the ATR FFSC package are assumed to be filled with air at atmospheric pressure.

Table 3.2-5 and Table 3.2-6 present the assumed emissivity (ε) for each radiating surface and the solar absorptivity (α) value for the exterior surface. The emissivity of 'as-received' Type 304 stainless steel has been measured[10] as 0.25 to 0.28, while the emissivity of weathered Type 304 stainless steel has been measured[11] from 0.46 to 0.50. For the purpose of this analysis, an emissivity of 0.30 is assumed for the emittance from all interior radiating stainless steel surfaces, while the emissivity for the exterior surfaces of the package is assumed to be 0.45. The solar absorptivity of Type 304 stainless steel is approximately 0.52[12]. Under HAC conditions, the outside of the package is assumed to attain an emissivity of 0.8 in compliance with 10 CFR §71.73(c)(4) and to have a solar absorptivity of 0.9 to account for the possible accumulation of soot.

The 5052-H32 aluminum sheet used to fabricate the FHE will be left with a plain finish while the 6061-T651 billets used to fabricate the Loose Fuel Plate Basket will have a machined surface. The emissivity for either type of finish can be expected to be low (i.e., 0.10 or lower)[12] however, for conservatism, an emissivity of 0.25[12] representative of a heavily oxidized surface is assumed for

---

[7] *Polymer Data Handbook*, Oxford University Press, Inc., 1999.

[8] Unifrax DuraBlanket S ceramic fiber insulation, Unifrax Corporation, Niagara Falls, NY.

[9] Rohsenow, Hartnett, and Cho, *Handbook of Heat Transfer*, 3rd edition, McGraw-Hill Publishers, 1998.

[10] Frank, R. C., and W. L. Plagemann, *Emissivity Testing of Metal Specimens.* Boeing Analytical Engineering coordination sheet No. 2-3623-2-RF-C86-349, August 21, 1986. Testing accomplished in support of the TRUPACT-II design program.

[11] *"Emissivity Measurements of 304 Stainless Steel"*, Azzazy, M., prepared for Southern California Edison, September 6, 2000, Transnuclear File No. SCE-01.0100.

[12] G. G. Gubareff, J. E. Janssen, and R. H. Torborg, *Thermal Radiation Properties Survey*, 2nd Edition, Honeywell Research Center, 1960.

this evaluation. The 6061-0 aluminum used for the ATR fuel components are assumed to have a surface coating of boehmite ($Al_2O_3H_2O$). A 25 µm boehmite film will exhibit a surface emissivity of approximately 0.92[13]. While a fresh fuel element may have a lower surface emissivity, the use of the higher value will provide a conservative estimate of the temperatures achieved during the HAC event.

The ceramic fiber insulation has a surface emissivity of approximately 0.90[12] based on a combination of the material type and surface roughness. The same emissivity is assumed for the neoprene rubber.

3.2.2 Technical Specifications of Components

The materials used in the ATR FFSC that are considered temperature sensitive are the aluminum used for the FHE, the LFPB, the ATR fuel, and the ATR U-Mo demonstration element, the neoprene rubber, and the polyethylene wrap used as a protective sleeve around the ATR fuel element and ATR U-Mo demonstration element. Of these materials, only the aluminum used for the ATR fuel and ATR U-Mo demonstration element is considered critical to the safety of the package. The other materials either have temperature limits above the maximum expected temperatures or are not considered essential to the function of the package.

Type 304 stainless steel has a melting point above 2,700°F[4], but in compliance with the ASME B&PV Code[14], its allowable temperature is limited to 800°F if used for structural purposes. However, the ASME temperature limit generally applies only to conditions where the material's structural properties are relied on for loads postulated to occur in the respective operating mode or load combination (such as the NCT and HAC free drops). Since the package is vented to atmosphere, no critical structural condition exists following the HAC free drop events and, as such, the appropriate upper temperature limit is 800°F for normal conditions and 2,700°F for accident conditions

Aluminum (5052-H32, 6061-0/6061-T6) has a melting point of approximately 1,100°F[4] however for strength purposes the normal operational temperature should be limited to 400°F[3].

The ceramic fiber insulation has a manufacturer's recommended continuous use temperature limit of 2,300°F[8]. There is no lower temperature limit.

The polyethylene plastic wrap used as a protective sleeve around the ATR fuel element and ATR U-Mo demonstration element has a melting temperature of approximately 225 to 250°F[4]. For the purposes of this analysis, the lower limit of 225°F is used. As a thermoplastic, the polyethylene wrap will melt and sag onto the fuel element when exposed to temperatures in excess of 250°F. Further heating could lead to charring (i.e., oxidation in the absence of open combustion) and then thermal decomposition into its volatile components. Thermal decomposition will begin at approximately 750°F. Unpiloted, spontaneous ignition could occur at temperatures of

[13] *Heat Transfer in Window Frames with Internal Cavities*, PhD Thesis for Arild Gustavsen, Norwegian University of Science and Technology, Trondheim, Norway, September 2001.

[14] American Society of Mechanical Engineers (ASME) Boiler & Pressure Vessel Code, Section III, *Rules for Construction of Nuclear Facility Components*, Division 1, Subsection NB, *Class 1 Components*, & Subsection NG, *Core Support Structures*, 2001 Edition, 2002 Addendum.

approximately 650°F[15] or higher. The plastic wrap is approximately 7 inches wide (when pressed flat), 67.5 inches long, and weights approximately 3 oz. As demonstrated in Section 3.5.3, *Thermal Decomposition/Combustion of Package Organics*, the available oxygen in the package is sufficient for consumption of less than 1% of the polyethylene. Loss of the plastic wrap is of no consequence to the thermal safety of the ATR FFSC since its effect on conductive and radiative heat transfer is negligible.

The neoprene rub strips used to minimize fretting of the fuel element side plates have a continuous temperature rating of 200 to 250°F and a short term (i.e., 0.5 hour or less) temperature limit of approximately 525°F [16]. For the purposes of this analysis, a limit of 225°F is used for NCT conditions, while a peak temperature of 525°F is assumed for HAC conditions before thermal degradation begins. Since neoprene is a thermoset polymer, it will not melt, but decompose into volatiles as it degrades. The same limitation on oxygen affecting the combustion of polyethylene also affects neoprene. As discussed in Section 3.5.3, *Thermal Decomposition/Combustion of Package Organics*, the thermal damage expected for the neoprene material is expected to be limited to potential de-bonding from the FHE surfaces and a very limited thermal decomposition. Loss of the neoprene rub strips is of no consequence to the thermal safety of the ATR FFSC.

The minimum allowable service temperature for all ATR FFSC components is below -40 °F.

[15] Troitzsch, J., *Plastics Flammability Handbook*, 2nd Edition, Oxford University Press, New York, 1990.

[16] Parker O-Ring Handbook, ORD 5700/USA, 2001, www.parker.com.

Table 3.2-1 – Thermal Properties of Package Metallic Materials

Material	Temperature (°F)	Thermal Conductivity (Btu/hr-ft-°F)	Specific Heat (Btu/lb_m-°F)	Density (lb_m/in^3)
Stainless Steel Type 304	70	8.6	0.114	0.289
	100	8.7	0.115	
	200	9.3	0.119	
	300	9.8	0.123	
	400	10.4	0.126	
	500	10.9	0.128	
	600	11.3	0.130	
	700	11.8	0.132	
	800	12.2	0.133	
	1000	13.2	0.136	
	1200	14.0	0.138	
	1400	14.9	0.141	
	1500	15.3	0.142	
Aluminum Type 5052-H32	70	79.6	0.214	0.097
	100	80.8	0.216	
	150	82.7	0.219	
	200	84.4	0.222	
	250	85.9	0.225	
	300	87.2	0.227	
	350	88.4	0.229	
	400	89.6	0.232	
	1100 ①	89.6	0.232	

Notes:

① Values for 1100°F are assumed equal to values at 400°F.

Table 3.2-2 – Thermal Properties of ATR Fuel Materials

Material	Temperature (ºF)	Thermal Conductivity (Btu/hr-ft-ºF)	Specific Heat (Btu/lb_m-ºF)	Density (lb_m/in^3)
Aluminum Type 6061-0	32	102.3	-	0.0976
	62	-	0.214	
	80	104.0	-	
	170	107.5	-	
	260	109.2	0.225	
	350	109.8	-	
	440	110.4	0.236	
	530	110.4	-	
	620	109.8	0.247	
	710	108.6	-	
	800	106.9	0.258	
	890	105.2	-	
	980	103.4	0.269	
	1080	101.1	0.275	
ATR Fuel Plate 1①	80	60.5	0.177	0.114
	800		0.213	
ATR Fuel Plates 2 and 18①	80	78.5	0.189	0.108
	800		0.228	
ATR Fuel Plates 3,4,16 & 17①	80	76.2	0.182	0.112
	800		0.220	
ATR Fuel Plates 5 to 15①	80	74.6	0.176	0.115
	800		0.212	
ATR Fuel Plate 19①	80	54.5	0.173	0.115
	800		0.209	

Notes:

① Values determined based on composite value of aluminum cladding and fuel core material (see Appendix 3.5.2.4). Thermal conductivity value is valid for axial and circumferential heat transfer within fuel plate.

Table 3.2-3 – Thermal Properties of Non-Metallic Materials

Material	Temperature (ºF)	Thermal Conductivity (Btu/hr-ft-ºF)	Specific Heat (Btu/lb_m-ºF)	Density (lb_m/ft^3)	Comments
Neoprene①	---	0.11	0.52	76.8	
Ceramic Fiber Insulation②	70	0.0196	0.28	6	
	200	0.0238			
	400	0.0343			
	600	0.0499			
	800	0.0703			
	1000	0.0958			
	1200	0.1262			
	1400	0.1614			
	1600	0.2017			
Ceramic Fiber Insulation② ③	70	0.0300	0.28	8	
	200	0.0313			
	400	0.0369			
	600	0.0463			
	800	0.0620			
	1000	0.0814			
	1200	0.1053			
	1400	0.1340			
	1600	0.1669			

Notes:

① Conductivity value represents uncompressed neoprene.

② Conductivity values are for uncompressed insulation. Compression of the material will increase the thermal conductivity for temperatures below approximately 500°F where conduction dominates and decrease the thermal conductivity for temperatures above 500°F where heat transfer via radiation dominates.

③ 8 pcf ceramic fiber insulation is not used in the ATR FFSC Package. Data is provided for comparison purposes to demonstrate the effect of insulation compression on thermal conductivity.

Table 3.2-4 – Thermal Properties of Air

Temperature (ºF)	Density lb_m/in^3) [1]	Specific Heat (Btu/lb_m-ºF)	Dynamic Viscosity (lb_m /ft-hr)	Thermal Conductivity (Btu/hr-ft-ºF)	Prandtl Number [2]	Coef. Of Thermal Exp. ($ºR^{-1}$) [3]
-40	Use Ideal Gas Law w/ Molecular wt = 28.966	0.240	0.03673	0.0121	Compute as $Pr = c_p\mu / k$	Compute as $\beta = 1/(ºF+459.67)$
0		0.240	0.03953	0.0131		
50		0.240	0.04288	0.0143		
100		0.241	0.04607	0.0155		
200		0.242	0.05207	0.0178		
300		0.243	0.05764	0.0199		
400		0.245	0.06286	0.0220		
500		0.248	0.06778	0.0240		
600		0.251	0.07242	0.0259		
700		0.253	0.07680	0.0278		
800		0.256	0.08098	0.0297		
900		0.259	0.08500	0.0315		
1000		0.262	0.08887	0.0333		
1200		0.269	0.09620	0.0366		
1400		0.274	0.10306	0.0398		
1500		0.277	0.10633	0.0412		

Table Notes:

1) Density computed from ideal gas law as $\rho = PM/RT$, where R= 1545.35 ft-lbf/lb-mole-R, T= temperature in °R, P= pressure in lbf/ft^2, and M= molecular weight of air. For example, at 100°F and atmospheric pressure of $14.69 lbf/in^2$, $\rho = (14.69*144\ in^2/ft^2*28.966\ lbm/lb\text{-}mole)/1545.35*(100+459.67) = 0.071\ lbm/ft^3 = 4.099x10^{-5}\ lbm/in^3$.
2) Prandtl number computed as $Pr = c_p\mu / k$, where c_p = specific heat, μ = dynamic viscosity, and k = thermal conductivity. For example, at 100°F, Pr = 0.241*0.04607/0.0155 = 0.72.
3) Coefficient of thermal expansion is computed as the inverse of the absolute temperature. For example, at 100°F, $\beta = 1/(100+459.67) = 0.00179$.

Table 3.2-5 – NCT Thermal Radiative Properties

Material	Assumed Conditions	Assumed Emissivity (ε)	Absorptivity (α)
Outer Shell, Exterior Surfaces (Type 304 Stainless Steel)	Weathered	0.45	0.52
Outer Shell, Interior Surface and Inner Shell (Type 304 Stainless Steel)	'As- Received'	0.3	---
Ceramic Fiber Insulation & Neoprene	---	0.90	---
Fuel Handling Enclosure and Loose Fuel Plate Basket (6061-T651 &5052-H32 Aluminum)	Oxidized	0.25	---
ATR Fuel Side Plates and Fuel Cladding (6061-0 Aluminum)	Boehmite film	0.92	---
Ambient Environment	---	1.00	N/A

Table 3.2-6 – HAC Thermal Radiative Properties

Material	Assumed Conditions	Assumed Emissivity (ε)	Absorptivity (α)
Outer Shell, Exterior Surfaces (Type 304 Stainless Steel)	Sooted/Oxidized	0.80	0.90
Outer Shell, Interior Surface and Inner Shell (Type 304 Stainless Steel)	Slightly Oxidized	0.45	---
Ceramic Fiber Insulation & Neoprene	---	0.90	---
Fuel Handling Enclosure and Loose Fuel Plate Basket (6061-T651 &5052-H32 Aluminum)	Oxidized	0.25	---
ATR Fuel Side Plates and Fuel Cladding (6061-0 Aluminum)	Boehmite film	0.92	---
Ambient Environment	---	1.00	N/A

3.3 Thermal Evaluation for Normal Conditions of Transport

This section presents the thermal evaluation of the ATR FFSC for normal conditions of transport (NCT). Under NCT, the package will be transported horizontally. This establishes the orientation of the exterior surfaces of the package for determining the free convection heat transfer coefficients and insolation loading. While the package would normally be transported in tiered stacks of multiple packages, the evaluation for NCT is conservatively based on a single, isolated package since this approach will yield the bounding maximum and minimum temperatures achieved by any of the packages. Further, the surface of the transport trailer is conservatively assumed to prevent heat exchange between the package and the ambient. Thus, the bottom of the ATR FFSC is conservatively treated as an adiabatic surface.

The details of the thermal modeling used to simulate the ATR FFSC package under NCT conditions are provided in Appendix 3.5.2, *Analytical Thermal Model*.

3.3.1 Heat and Cold

3.3.1.1 Maximum Temperatures

The maximum temperature distribution for the ATR FFSC occurs with a diurnal cycle for insolation loading and an ambient air temperature of 100°F, per 10 CFR §71.71(c)(1). The evaluation of this condition is conducted as a transient using the thermal model of an undamaged ATR FFSC described in Appendix 3.5.2.1, *Description of Thermal Model for NCT Conditions*. Figure 3.3-1 and Figure 3.3-2 illustrate the expected heat-up transient for an ATR FFSC loaded with an ATR fuel element. The transient analysis assumes a uniform temperature condition of 70ºF for all components prior to loading and exposure to the specified NCT condition at time = 0. The figures demonstrate that the ATR FFSC package will respond rapidly to changes in the level of insolation and will reach it peak temperatures within the first day or two after loading. Table 3.3-1 presents the maximum temperatures reached for various components of the package. As seen from the table, all components are within in their respective temperature limits. Figure 3.3-3 illustrates the predicted temperature distribution within the ATR FFSC package at the time of peak temperature.

The maximum temperature distribution for the ATR FFSC without insolation loads occurs with an ambient air temperature of 100°F. Since the package payload dissipates essentially zero watts of decay heat, the thermal analysis of this condition represents a trivial case and no thermal calculations are performed. Instead, it is assumed that all package components achieve the 100°F temperature under steady-state conditions. The resulting 100°F package skin temperature is below the maximum temperature of 122°F permitted by 10 CFR §71.43(g) for accessible surface temperature in a nonexclusive use shipment.

The ATR FFSC with the ATR U-Mo demonstration element payload is not specifically modeled as part of this evaluation. Instead, its thermal performance is estimated using a qualitative approach based on the thermal characteristics of the other payloads and their associated thermal performance (see Section 3.5.2.5, *Thermal Properties for ATR U-Mo Demonstration Element* for details). Using this approach, it is estimated that the maximum temperatures attained for the transportation of the ATR U-Mo demonstration element are considered bounded by the analysis of the ATR fuel element and no additional analysis is required.

3.3.1.2 Minimum Temperatures

The minimum temperature distribution for the ATR FFSC occurs with a zero decay heat load and an ambient air temperature of -40°F per 10 CFR §71.71(c)(2). The thermal analysis of this condition also represents a trivial case and no thermal calculations are performed. Instead, it is assumed that all package components achieve the -40°F temperature under steady-state conditions. As discussed in Section 3.2.2, *Technical Specifications of Components*, the -40°F temperature is within the allowable operating temperature range for all ATR FFSC package components.

3.3.2 Maximum Normal Operating Pressure

The payload cavity of the ATR FFSC is vented to the atmosphere. As such, the maximum normal operating pressure (MNOP) for the package is 0 psig.

While the volume between the outer and inner shells is sealed, it does not contain organic or other materials that may outgas or thermally degrade. Therefore, the maximum pressure that may develop within the space will be limited to that achieved due to ideal gas expansion. Assuming a temperature of 70°F at the time of assembly and a maximum operating temperature of 190°F (based on the outer shell temperature, see Table 3.3-1, conservatively rounded up), the maximum pressure rise within the sealed volume will be less than 4 psi.

Table 3.3-1 - Maximum Package NCT Temperatures

Location / Component	NCT Hot Conditions	Maximum Allowable ①
ATR Fuel Element Fuel Plate	147°F	400°F
ATR Fuel Element Side Plate	148°F	400°F
Neoprene Rub Strips/Polyethylene Bag	151°F ②	225°F
Fuel Handling Enclosure (FHE)	151°F	400°F
Loose Fuel Plate Basket (LFPB)	151°F ②	400°F
Inner Shell	157°F	800°F
Ceramic Fiber Insulation, Body - Maximum - Average	 185°F 151°F	 2,300°F 2,300°F
Ceramic Fiber Insulation, Closure - Maximum - Average	 145°F 144°F	 2,300°F 2,300°F
Closure	145°F	800°F
Outer Shell	186°F	800°F

Table Notes:
① The maximum allowable temperatures under NCT conditions are provided in Section 3.2.2, Technical Specifications of Components.
② Component temperature assumed to be equal to that of the FHE.

.

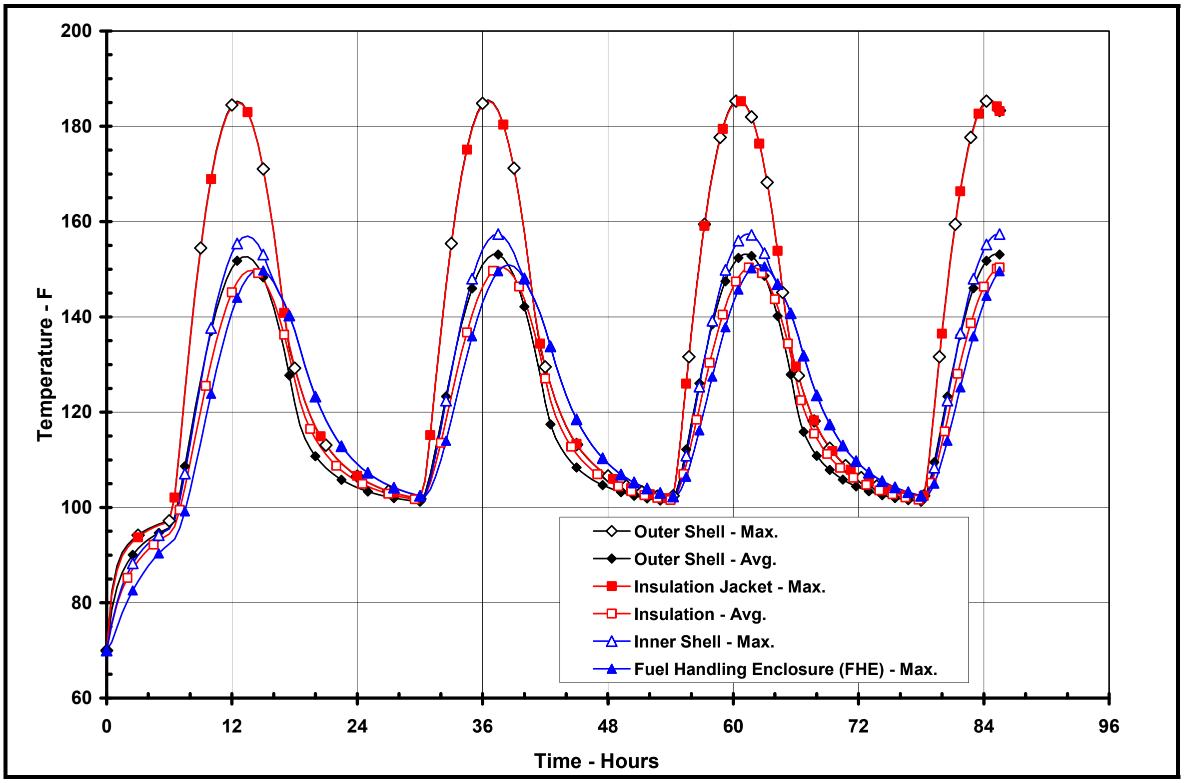

Figure 3.3-1 – ATR FFSC Package Heat-up, NCT Hot Conditions

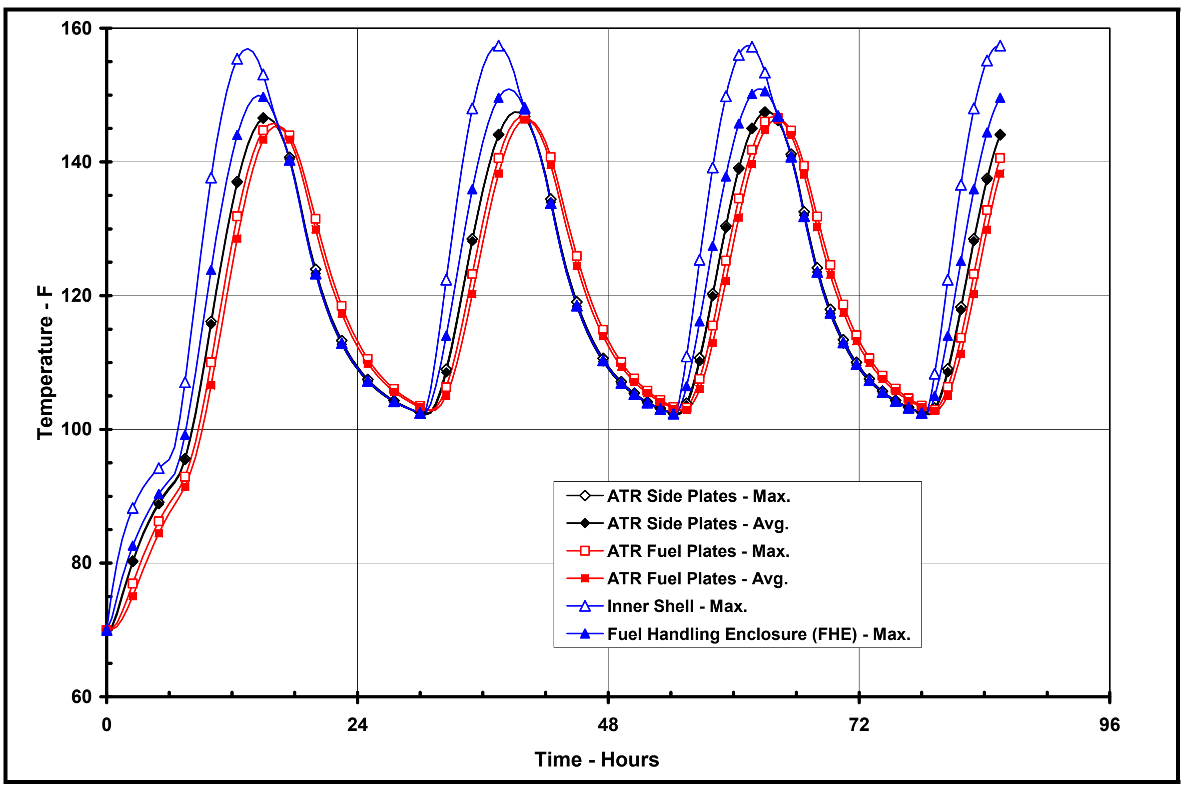

Figure 3.3-2 – ATR Fuel Element Heat-up, NCT Hot Conditions

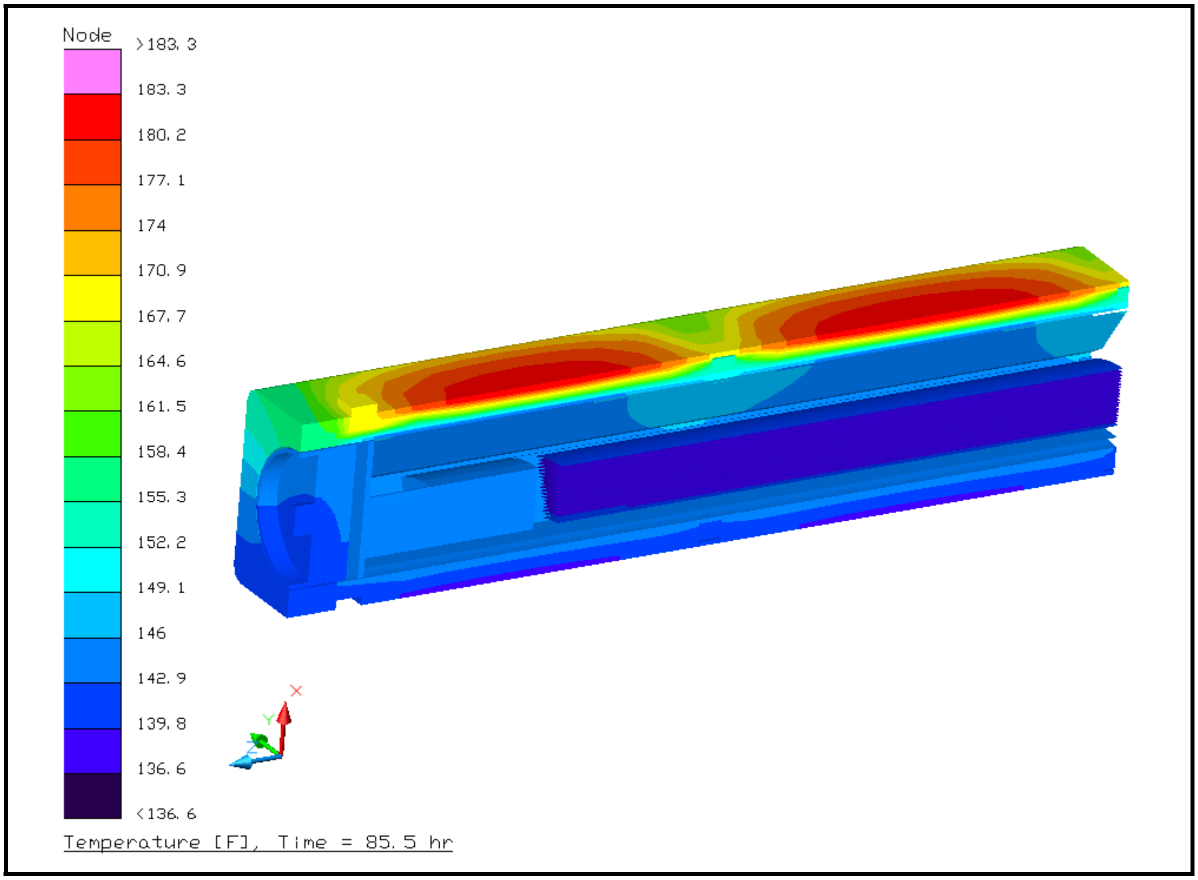

Figure 3.3-3 – Package NCT Temperature Distribution

3.4 Thermal Evaluation for Hypothetical Accident Conditions

This section presents the thermal evaluation of the ATR FFSC package under the hypothetical accident condition (HAC) specified in 10 CFR §71.73(c)(4) based on an analytical thermal model of the ATR FFSC. The analytical model for HAC is a modified version of the quarter symmetry NCT model described in Section 3.5.2.1, *Description of Thermal Model for NCT Conditions*, with the principal model modifications consisting of simulating the expected package damage resulting from the drop events that are assumed to precede the HAC fire and changing the package surface emissivities to reflect the assumed presence of soot and/or surface oxidization.

Physical testing using full scale certified test units (CTUs) is used to establish the expected level of damage sustained by the ATR FFSC package from the 10 CFR 71.73 prescribed free and puncture drops that are assumed to precede the HAC fire event. Appendix 2.12.1, *Certification Tests on CTU-1* and Appendix 2.12.2, *Certification Tests on CTU-2* provide the configuration and initial conditions of the test articles, the test facilities and instrumentation used, and the test results. Section 3.5.2.2, *Description of Thermal Model for HAC Conditions*, provides an overview of the test results, the rationale for selecting the worst-case damage scenario, and the details of the thermal modeling used to simulate the package conditions during the HAC fire event.

3.4.1 Initial Conditions

The initial conditions assumed for the package prior to the HAC event are described below in terms of the modifications made to the NCT thermal model to simulate the assumed package conditions prior to and during the HAC event. These modifications are:

- Simulated the worst-case damage arising from the postulated HAC free and puncture drops as described in Section 3.5.2.2, *Description of Thermal Model for HAC Conditions*,
- Assume an initial, uniform temperature distribution of 100ºF based on a zero decay heat package at steady-state conditions with a 100ºF ambient with no insolation. This assumption complies with the requirement of 10 CFR §71.73(b)[2] and NUREG-1609[17],
- Increased the emissivity of the external surfaces from 0.45 to 0.8 to account for possible soot accumulation on the surfaces, per 10 CFR §71.73(c)(4),
- Increased the emissivity of the interior surfaces of the outer shell from 0.30 to 0.45 to account for possible oxidization of the surfaces during the HAC event,

Following the free and puncture bar drops, the ATR FFSC package is assumed come to rest in a horizontal position prior to the initiation of the fire event. Since the package geometry is essentially symmetrical about its axial axis, there are no significant thermal differences whether the

[17] NUREG-1609, *Standard Review Plan for Transportation Packages for Radioactive Material*, §3.5.5.1, U.S. Regulatory Commission, Office of Nuclear Materials Safety and Standards, March 1999.

package is right-side up, up-side down, or even on its end. The potential for the ATR fuel element payload being re-positioned depending upon the package orientation is not significant to the peak temperatures developed under HAC conditions given the modeling approach used to compute the heat transfer from the inner shell to the ATR fuel element. Therefore, the peak package temperatures predicted under this evaluation are representative of those achieved for any package orientation.

3.4.2 Fire Test Conditions

The fire test conditions analyzed to address the 10 CFR §71.73(c) requirements are as follows:

- The initial ambient conditions are assumed to be 100ºF ambient with no insolation,
- At time = 0, a fully engulfing fire environment consisting of a 1,475ºF ambient with an emissivity of 1.0 is used to simulate the hydrocarbon fuel/air fire event. The assumption of a flame emissivity of 1.0 bounds the minimum average flame emissivity coefficient of 0.9 specified by 10 CFR §71.73(c)(4),
- The convection heat transfer coefficients between the package and the ambient during the 30-minute fire event are based on an average gas velocity[18] of 10 m/sec. Following the 30-minute fire event the convection coefficients are based on still air,
- The ambient condition of 100ºF with insolation is assumed following the 30-minute fire event. Since a diurnal cycle is used for insolation, the evaluation assumes that the 30-minute fire begins at noon so as to maximize the insolation heating during the post-fire cool down period. A solar absorptivity of 0.9 is assumed for the exterior surfaces to account for potential soot accumulation on the package surfaces.

The transient analysis is continued for 11.5 hours after the end of the 30-minute fire to ensure that the peak package temperatures are captured.

3.4.3 Maximum Temperatures and Pressure

3.4.3.1 Maximum HAC Temperatures

The outer shell and the ceramic fiber insulation provide thermal protection to the ATR FFSC package during the HAC fire event. The level of thermal protection can be seen via the thermal response curves presented in Figure 3.4-1 and Figure 3.4-2. As illustrated in the figures, while the exterior of the package quickly rises to nearly the temperature of the fire, the heat flow to the FHE and its enclosed ATR fuel element payload is sufficiently restricted that the maximum temperatures of both the FHE and the ATR fuel element are well below the melting point of aluminum. This result occurs despite the conservative assumption of direct contact between the FHE and the inner shell at 3 locations (e.g., the equivalent of four locations for a full model).

---

[18] Schneider, M.E and Kent, L.A., *Measurements Of Gas Velocities And Temperatures In A Large Open Pool Fire, Heat and Mass Transfer in Fire* - HTD Vol. 73, 1987, ASME, New York, NY.

This level of thermal protections is further illustrated by the perspective views presented in Figure 3.4-3 and Figure 3.4-4 of the temperature distribution in the ATR FFSC package after 30 minutes of exposure to the HAC fire and at the point when the peak ATR fuel element temperature is attained (approximately 22 minutes after the end of the fire). The figures show that the ceramic fiber insulation limits the elevated temperatures resulting from the fire event to regions adjacent to the outer shell. The assumed absence of the ceramic fiber insulation adjacent to the ribs as a result of the pre-fire free drop event can be seen in each figure.

A similar thermal performance is seen for the package when loaded with the Loose Fuel Plate Basket (LFPB). Figure 3.4-5 presents the thermal response curve, while Figure 3.4-6 and Figure 3.4-7 present perspective views of the temperature distribution in the ATR FFSC package after 30 minutes of exposure to the HAC fire and at the point when the peak LFPB temperature is attained (approximately 22 minutes after the end of the fire). A lower maximum temperature is achieved in the LFPB vs. that seen for the FHE because of the higher thermal mass associated with the LFPB. Further, since the LFPB is modeled without its payload of loose fuel plates, these results will bound those seen for a LFPB with a payload.

Table 3.4-1 presents the component temperatures seen prior to the fire, at the end of the 30-minute fire event, and the peak temperature achieved during the entire simulated HAC thermal event. As seen, all temperatures are within their allowable limit. It is expected that the neoprene rub strips and the polyethylene bag used as a protective sleeve for the ATR fuel element will thermally degrade due to the level of temperature achieved. In the case of the polyethylene bag, the bag is expected to melt and sag onto the fuel element when exposed to temperatures in excess of 250°F. Further heating will lead to charring and then thermal decomposition into its volatile components. While spontaneous ignition is unexpected under the unpiloted conditions, the effect would be minimal since, per Section 3.5.3, *Thermal Decomposition/Combustion of Package Organics*, the available oxygen in the package is sufficient for consumption of less than 1% of the polyethylene. As a thermoset polymer, the neoprene is expected to simply decompose into volatiles as it thermally degrades. These components are not critical to the safety of the package and any out-gassing associated with their thermal degradation will not contribute to package pressurization since package is vented.

The results presented above also demonstrate that inclusion of insolation effects prior to the fire would not have affected the safety basis of the design. The low thermal mass of the package effectively mitigates the HAC impact of higher initial component temperatures due to insolation. As seen from Table 3.3-1, consideration of the maximum insolation loading raises the package component temperatures by approximately 50°F above the initial 100°F level assumed by the HAC evaluation. The thermal response curves presented in Figures 3.4-1 and 3.4-2 demonstrate that the fire condition recovers this 50°F temperature difference for the outer components within the first few seconds of fire exposure. Further, since all package components exhibit thermal margins greater than 50°F as shown in Table 3.4-1, the inclusion of insolation effects prior to the fire event would not have impacted the safety basis for the design.

As with the evaluation for NCT, the thermal performance of the ATR FFSC with the ATR U-Mo demonstration element payload under HAC conditions is not specifically modeled as part of this evaluation. Instead, its thermal performance is estimated using a qualitative approach based on the thermal characteristics of the other payloads and their associated thermal performance (see Section 3.5.2.5, *Thermal Properties for ATR U-Mo Demonstration Element,* for details). Using this approach, it is estimated that the maximum temperatures attained for the transportation of the ATR U-Mo demonstration element are considered bounded by the analysis of the ATR fuel element and no additional analysis is required.

3.4.3.2 Maximum HAC Pressures

The payload cavity of the ATR FFSC is vented to the atmosphere. As such, the maximum pressure achieved under the HAC event will be 0 psig. Section 3.5.3, *Thermal Decomposition/Combustion of Package Organics*, provides the justification for assuming a 0 psig package pressure for the HAC event.

Although the volume between the outer and inner shells is sealed, it does not contain organic or other materials that may outgas or thermally degrade. Assuming a temperature of 70°F at the time of assembly and a maximum temperature of 1,475°F (based on the outer shell temperature, see Table 3.4-1), the maximum pressure rise within the sealed volume due to ideal gas expansion will be less than 39 psig. This level of pressurization will occur for only a few minutes and then quickly reduce as the package cools.

3.4.4 Maximum Thermal Stresses

The temperature difference between the inner and outer shells during the HAC event (see the average inner and outer shell temperatures presented in Figure 3.4-1) will result in differential thermal expansion between the shells. This differential thermal expansion is expected to peak at approximately 6 minutes after the initiation of fire exposure when the average outer shell temperature is 1,344°F and the average inner shell temperature is 196°F. Based on the differential thermal expansion for Type 304 stainless steel[19] the change in length is computed as:

$$DTE = \Delta L_{OuterShell} - \Delta L_{InnerShell} = \left[\alpha_{OS}\left(T_{OS} - 70\right) - \alpha_{IS}\left(T_{IS} - 70\right)\right]L = 0.9\ inches$$

where:

$\alpha_{OS} = 10.7(10^{-6})$ in/in/ºF at 1,300 ºF
$\alpha_{IS} = 8.9(10^{-6})$ in/in/ºF at 200 ºF
$T_{OS} = 1{,}344$ ºF
$T_{IS} = 196$ ºF
L = 73 inches (conservatively for both shells)

After 6 minutes of exposure to the fire the difference in shell lengths will decrease as the inner shell heats up. The differential expansion will reach 0-inches approximately 6 minutes after the end of the fire event when the inner and outer shells reach thermal equilibrium and then go negative as the outer shell continues to cool faster than the inner shell. The largest negative thermal differential expansion achieved is approximately 0.22-inches.

The result of this variation in differential thermal expansion may take one of three forms:

1) the outer shell buckles outward,

[19] American Society of Mechanical Engineers (ASME) Boiler and Pressure Vessel Code, Section II, *Materials*, *Part D – Properties*, 2001 Edition, 2002 and 2003 Addenda, New York ,Table TE-1, Group 3. Coefficient B = 8.9×10^{-6} inches/inch/°F at 200°F and 10.7×10^{-6} inches/inch/°F at 1,300°F.

2) the outer shell buckles inward, or
3) the weld attaching the inner shell to either the closure plate or the bottom end plate will fail and permit the outer shell and the affected plate to move freely.

While in reality, a square tube is likely to buckle inward on two of the four faces and outward on the remaining two faces simultaneously, the two buckling modes are treated independently for the purposes of this evaluation. The possibility of the outer shell buckling outwards is the assumption upon which the thermal modeling presented in Section 3.5.2.2, *Description of Thermal Model for HAC Conditions* is based. This mode is seen as likely given the level of metal softening that will occur with the outer shell quickly reaching over 1,200°F and the expected pressurization of the void space between the inner and outer shells. Buckling the outer shell in this fashion will act to lower the rate of inward heat transfer. As such, ignoring the outer shell's displacement due to differential thermal expansion, as assumed by the HAC thermal modeling, yields conservatively high package temperatures.

The second possibility is that the outer shell buckles inward under the differential thermal expansion. Should this occur, the maximum deflection would be 0.9-inches/2 = 0.45-inches assuming a zero length deflection and only one buckle along the length of the outer shell. In reality, the actual deflection would measure perhaps 0.33-inches after properly accounting for the curvature in the buckled section. Since this level of deflection would still leave 0.5-inches or more of insulation separating the inner shell from the outer shell, no significant impact on the predicted peak HAC temperatures will occur.

The final possibility which the differential thermal expansion may manifest itself is in the failure of the one of the welds attaching the inner shell to the closure and bottom end plates. If this occurs, besides releasing any potential pressure buildup in the void between the inner and outer shells, the outer shell and the associated end plate will extend away from the inner shell at the point of the weld failure. The size of the gap will maximize at about 0.9-inches and then decrease. Since the insulation jacket is cut out to fit around the hardware used to index the packages to one another, the insulation jacket and the underlying insulation will be pulled in the same direction as the outer shell, thus preventing the creation of a gap between the interface of the insulation wrap and the end plate. Even if such a gap would occur, no direct exposure of cavity within the inner shell to the outer shell surfaces will result since the closure plugs at each end of the package are longer than the predicted movement under differential thermal expansion. Instead, the likely and worst case scenario is that the movement of the outer shell, the insulation jacket, and the insulation will create a gap of approximately 0.9-inches at the interface between the first support rib and the insulation. Combining this gap with an insulation shift of up to 1.75-inches at this same locations due to a pre-fire, 30-foot end drop (see Section 3.5.2.2, *Description of Thermal Model for HAC Conditions*) could result in a scenario where there is a 0.9-inch gap between the support rib and the insulation jacket and up to a 0.9 + 1.75 = 2.65-inch gap between the support rib and the end of the insulation wrap. A sensitivity thermal analysis of this geometry showed that the peak inner shell temperature reported in Table 3.4-1 remained bounding, while the maximum temperature of the ATR fuel element increased by less than 25ºF. This modest change in temperature occurs because there is little difference in temperature between the outer shell and the stainless steel insulation wrap. Since this level of temperature increase is well within the thermal margins apparent from Table 3.4-1, the potential thermal impact due to the package geometry displacement under differential thermal expansion is seen as being not significant to the safety of the package.

3.4.5 Accident Conditions for Air Transport of Fissile Material

10 CFR §71.55(f) requires that the package be subcritical subsequent to the application of a series of accident condition tests, including a thermal test. A criticality analysis of the worst-case geometric configuration of the packaging and contents materials is performed in Section 6.7, *Fissile Material Packages for Air Transport*, which considers the presence of all of the moderating and reflecting material in the package. The tendency of the fire event to decrease the availability of moderating material due to combustion is conservatively neglected. Thus, the effects of the fire test of 10 CFR §71.55(f)(1)(iv) do not need to be specifically evaluated.

Table 3.4-1 – HAC Temperatures

Location / Component	Pre-fire	End of Fire	Peak	Maximum Allowable ①
ATR Fuel Element Fuel Plate	100°F	586°F	730°F	1,100°F
ATR Fuel Element Side Plate	100°F	676°F	827°F	1,100°F
Neoprene Rub Strips/ Polyethylene Bag	100°F	1,016°F	1,017°F	N/A
Fuel Handling Enclosure (FHE)	100°F	1,016°F	1,017°F	1,100°F
Loose Fuel Plate Basket (LFPB)	100°F	584°F	746°F	1,100°F
Inner Shell	100°F	1,422°F	1,422°F	2,700°F
Ceramic Fiber Insulation, Body				
- Maximum	100°F	1,460°F	1,460°F	2,300°F
- Average	100°F	1,220°F	1,220°F	2,300°F
Ceramic Fiber Insulation, Closure				
- Maximum	100°F	1,418°F	1,418°F	2,300°F
- Average	100°F	1,297°F	1,297°F	2,300°F
Closure	100°F	1,445°F	1,445°F	2,700°F
Outer Shell	100°F	1,471°F	1,471°F	2,700°F

Table Notes:

① The maximum allowable temperatures under HAC conditions are provided in Section 3.2.2, Technical Specifications of Components.

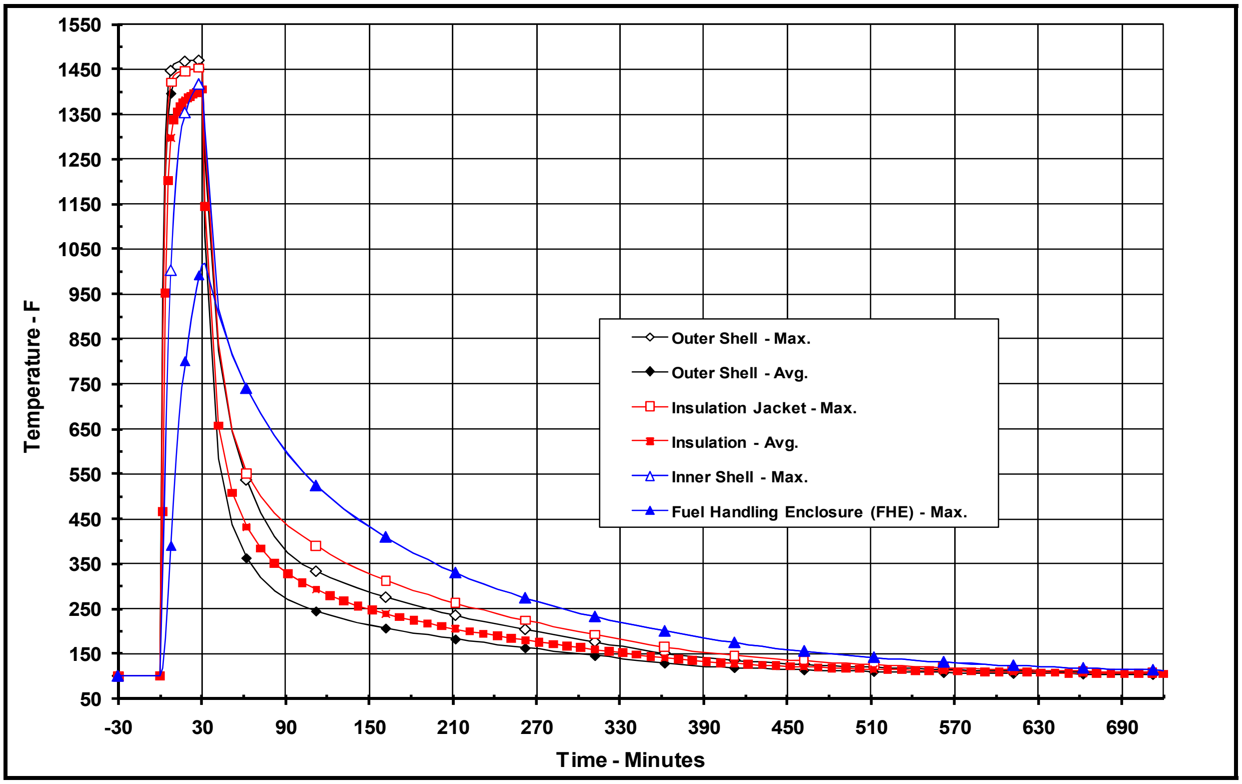

Figure 3.4-1 – ATR FFSC Package Thermal Response to HAC Event

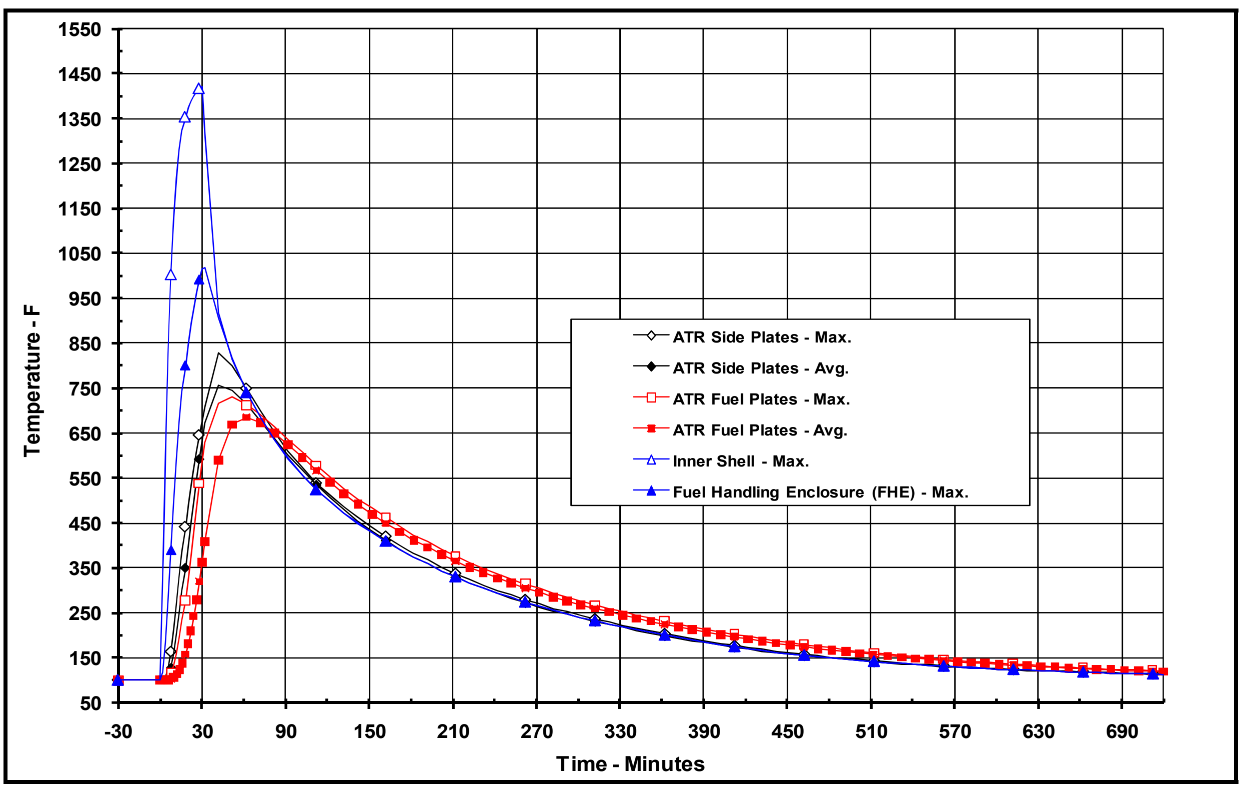

Figure 3.4-2 – ATR Fuel Element Thermal Response to HAC Event

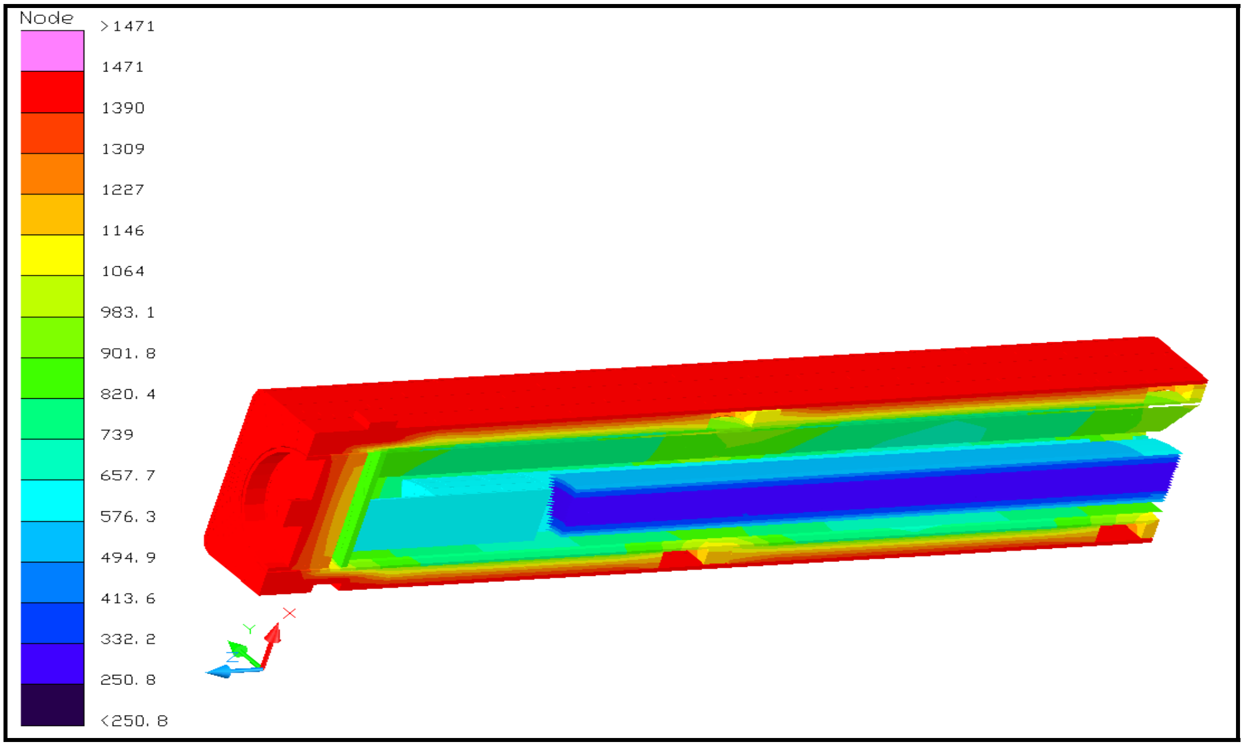

(Note: the positive x-axis is oriented towards the top of the package and the positive z-axis towards the package closure end)

Figure 3.4-3 –Temperature Distribution at End of HAC 30-Minute Fire

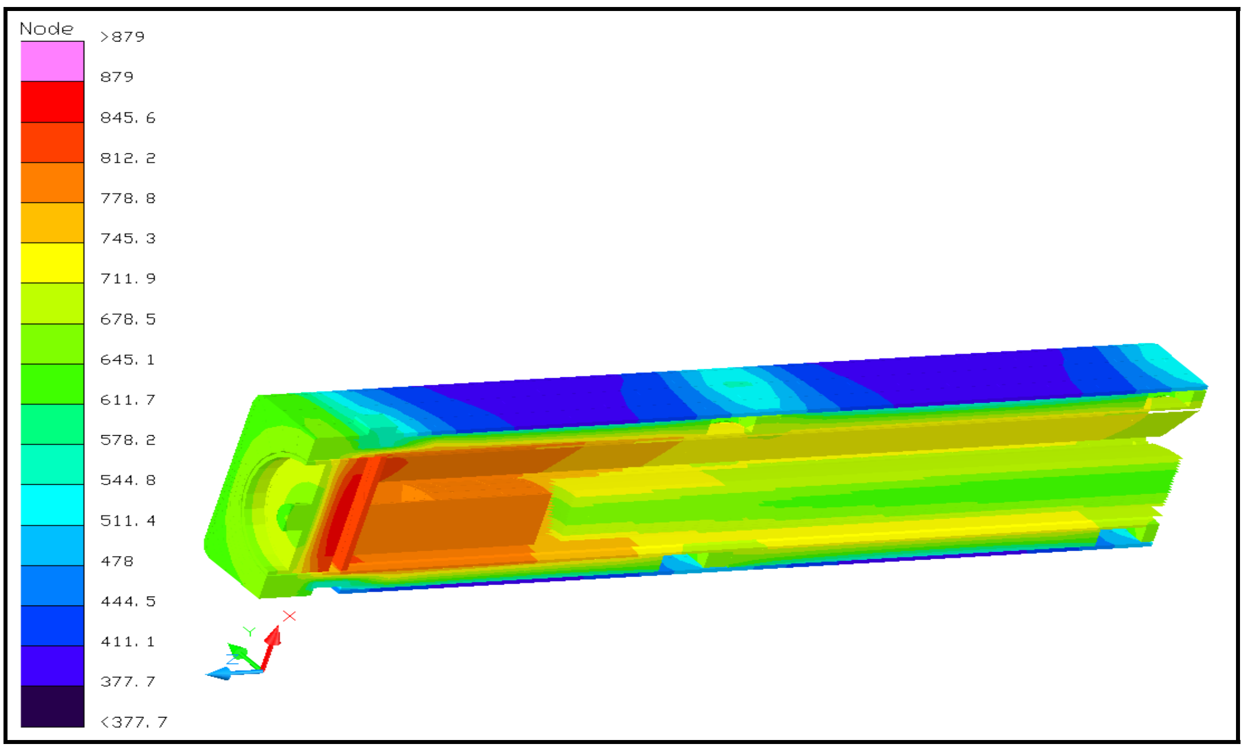

(Note: the positive x-axis is oriented towards the top of the package and the positive z-axis towards the package closure end)

Figure 3.4-4 –Temperature Distribution at Peak ATR Fuel Element Temperature

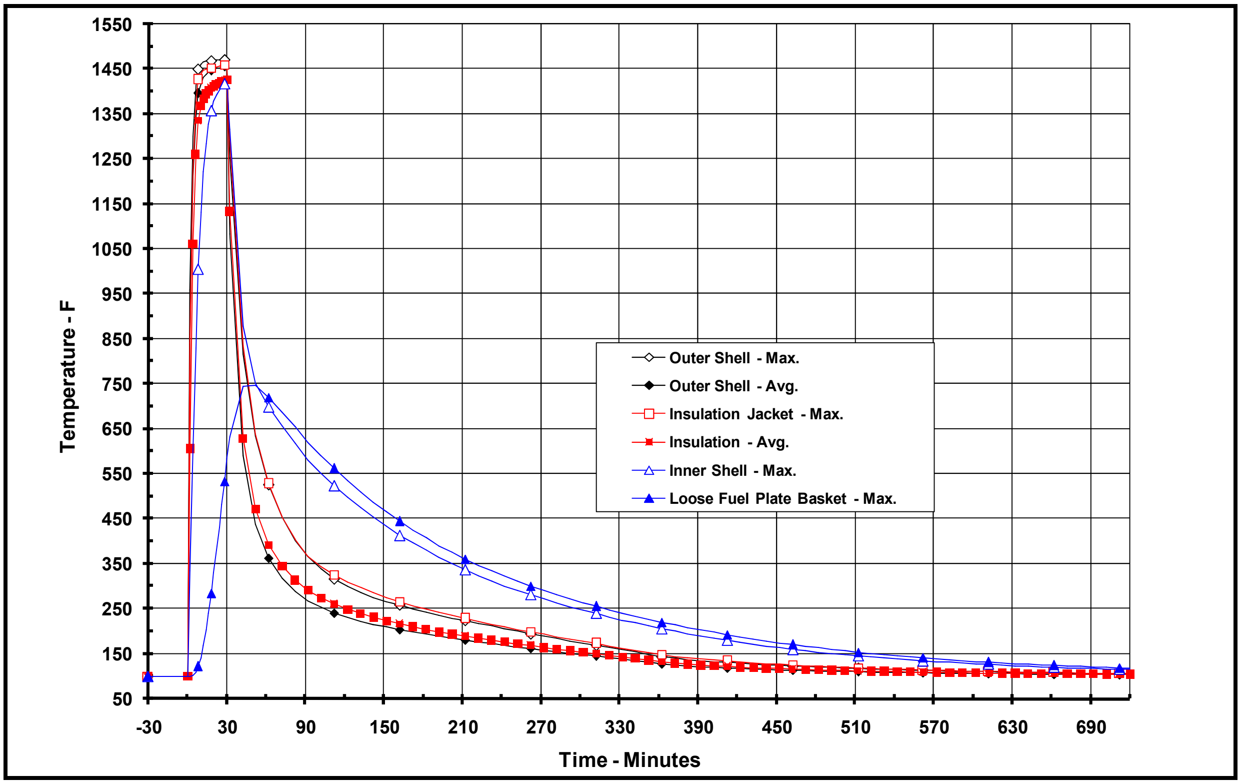

Figure 3.4-5 – ATR FFSC Package with LFPB Thermal Response to HAC Event

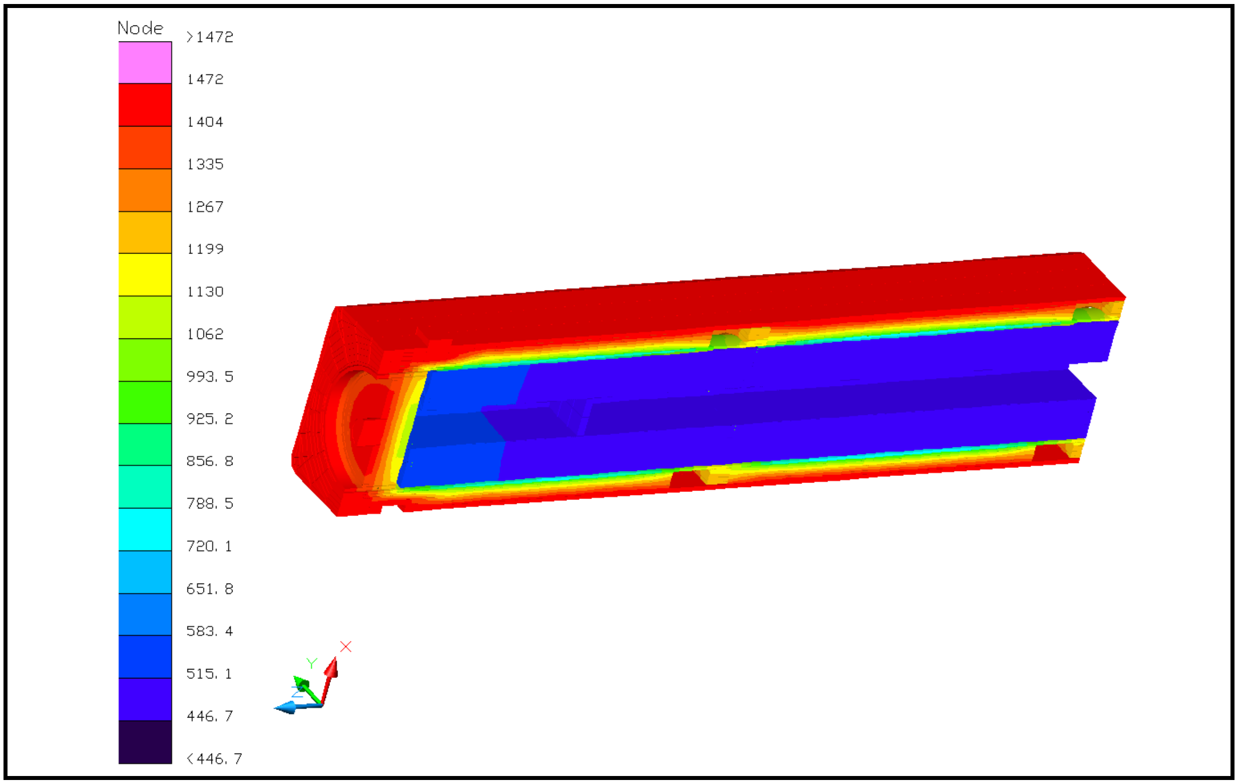

(Note: the positive x-axis is oriented towards the top of the package and the positive z-axis towards the package closure end)

Figure 3.4-6 – FFSC-LFPB Temperature Distribution at End of HAC Fire

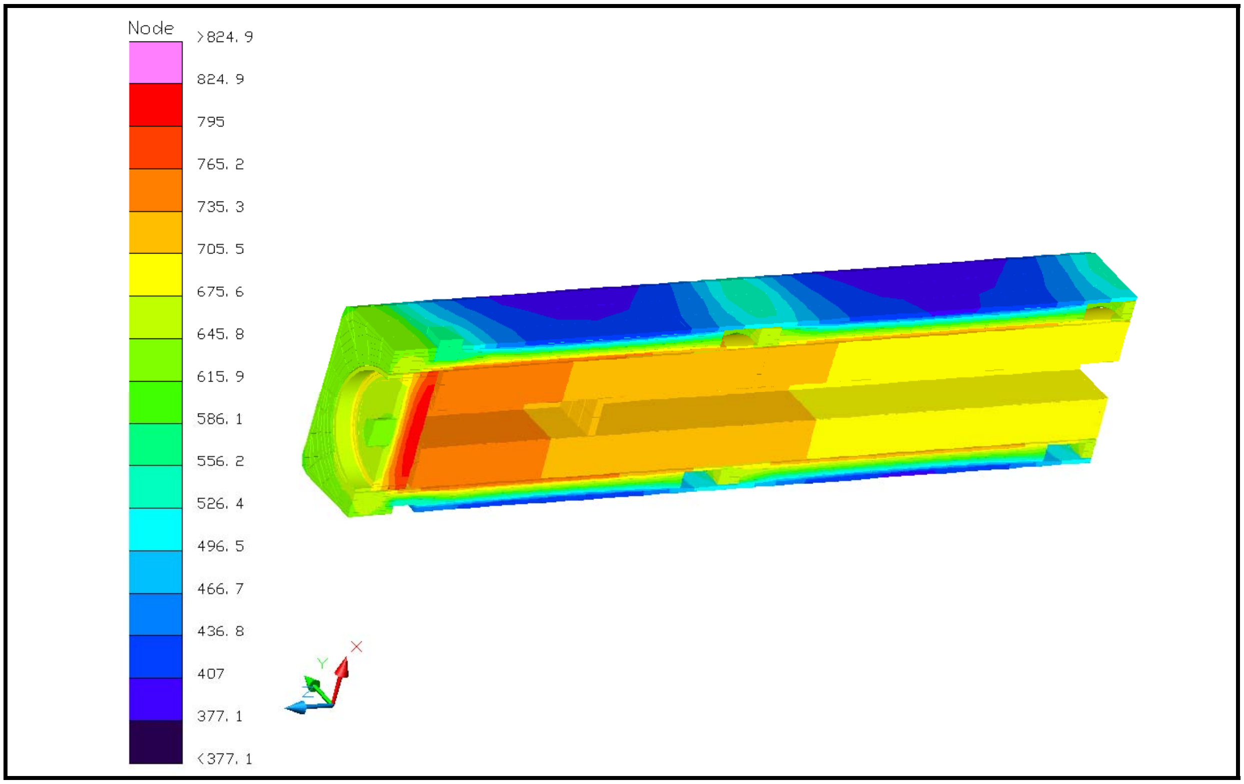

(Note: the positive x-axis is oriented towards the top of the package and the positive z-axis towards the package closure end)

Figure 3.4-7 – FFSC-LFPB Temperature Distribution at Peak LFPB Temperature

3.5 Appendices

3.5.1 Computer Analysis Results

Due to the size and number of the output files associated with each analyzed condition, results from the computer analysis are provided on a CD-ROM.

3.5.2 Analytical Thermal Model

The analytical thermal model of the ATR FFSC package was developed for use with the Thermal Desktop® [20] and SINDA/FLUINT[21] computer programs. These programs are designed to function together to build, exercise, and post-process a thermal model. The Thermal Desktop® computer program is used to provide graphical input and output display function, as well as computing the radiation exchange conductors for the defined geometry and optical properties. Thermal Desktop® is designed to run as an AutoCAD® application. As such, all of the CAD tools available for generating geometry within AutoCAD® can be used for generating a thermal model. In addition, the use of the AutoCAD® layers tool presents a convenient means of segregating the thermal model into its various elements.

The SINDA/FLUINT computer program is a general purpose code that handles problems defined in finite difference (i.e., lumped parameter) and/or finite element terms and can be used to compute the steady-state and transient behavior of the modeled system. Although the code can be used to solve any physical problem governed by diffusion-type equations, specialized functions used to address the physics of heat transfer and fluid flow make the code primarily a thermal code.

The SINDA/FLUINT and Thermal Desktop® computer programs have been validated for safety basis calculations for nuclear related projects[22,23].

Together, the Thermal Desktop® and SINDA/FLUINT codes provide the capability to simulate steady-state and transient temperatures using temperature dependent material properties and heat transfer via conduction, convection, and radiation. Complex algorithms may be programmed into the solution process for the purposes of computing heat transfer coefficients as a function of the local geometry, gas thermal properties as a function of species content, temperature, and pressure, or, for example, to estimate the effects of buoyancy driven heat transfer as a function of density differences and flow geometry.

3.5.2.1 Description of Thermal Model for NCT Conditions

A 3-dimensional, one-quarter symmetry thermal model of the ATR FFSC is used for the NCT evaluation. The model simulates one-quarter of the package, extending from the closure to the

---

[20] Thermal Desktop®, Versions 4.8 and 5.1, Cullimore & Ring Technologies, Inc., Littleton, CO, 2005/2007.

[21] SINDA/FLUINT, *Systems Improved Numerical Differencing Analyzer and Fluid Integrator*, Versions 4.8 and 5.1, Cullimore & Ring Technologies, Inc., Littleton, CO, 2005/2007.

[22] *Software Validation Test Report for Thermal Desktop® and SINDA/FLUINT*, Versions 4.8 and 5.1, Packaging Technology, Inc., File No. TR-VV-05-001, Rev. 1 and Rev. 2.

[23] *Thermal Desktop® and SINDA/FLUINT Testing and Acceptance Report*, Version 5.1, AREVA Federal Services, LLC, File No. AFS-TR-VV-006, Rev. 0.

axial centerline of the package. Symmetry conditions are assumed about the package's vertical axis and at the axial centerline. This modeling choice captures the full height of the package components and allows the incorporation of the varying insolation loads that will occur at the top and sides of the package. Program features within the Thermal Desktop® computer program automatically compute the various areas, lengths, thermal conductors, and view factors involved in determining the individual elements that make up the thermal model of the complete assembly.

Figure 3.5-1 and Figure 3.5-2 illustrate the 'solid' and 'hidden line' views of the package thermal model. The model simulates one-half of the closure end half of the package (i.e., symmetry is assumed about the package's vertical plane) and extends approximately 36.5 inches in the axial direction (e.g., from closure to the mid-point of the center support rib). As seen from the figure, the modeling captures the various components of the packaging, including the index lug and mating pocket used to align the stacked packages, the recessed exterior surface area of the package closure, the FHE, and the ATR fuel element. Also captured, but not easily seen in the figure due to the scale of the figures, are the nineteen (19) individual fuel plates that comprise the ATR fuel element.

The model is composed of solid and plate type elements representing the various package components. Thermal communication between the various components is via conduction, radiation, and surface-to-surface contact. Since the ATR FFSC Package dissipates essentially no decay heat, the peak temperatures internal to the package are driven by the external heating occurring during NCT and HAC conditions. While the potential for developing convective flows within the air filled cavity between the outer shell and the insulation jacket is small due to the cavity dimensions, if convective heat transfer was to develop it could raise the peak temperatures developed under either NCT or HAC conditions since it would reduce the thermal resistance to heat flowing inward from the outer shell. To address this possibility, the thermal conductivity associated with the air overpack nodes in the lower quadrant of the package are increased by a factor of 2 from that for conduction as a means of simulating the type of enhanced heat transfer that convection would cause. The affected nodes are limited to those in the lower quadrant of the package since, in the assumed horizontal orientation of the package under both NCT and HAC conditions, the buoyancy forces associated with convection will tend to drive the flow in this portion of the package in a circular motion, but would only produce a stratified temperature layer in the upper quadrant. However, since subsequent examination of the temperature distribution at the end of the fire event showed no discernible difference in the insulation jacket temperature between the upper and lower quadrants, it is concluded that the heat transfer within these cavities is dominated by radiation and conduction and the potential for convective heat transfer can be ignored. Despite this conclusion, the factor of 2 has been retained in the models as a conservatism.

A total of approximately 8,050 nodes, 2,800 planar elements, and 3,700 solid elements are used to simulate the modeled components. In addition, one boundary node is used to represent the ambient environment for convection purposes and a second boundary node is used to represent the ambient temperature for the purpose of radiation heat transfer.

Figure 3.5-3 and Figure 3.5-4 illustrate the quarter symmetry thermal models of the FHE and the ATR fuel element. The FHE thermal model uses planar elements to represent the 0.09 inch thick sides of the enclosure, while solid elements are used to represent the 0.25 inch thick end cap.

Heat transfer between the FHE and the inner shell of the package is modeled as a combination of radiation and conduction across the air-filled void space, as well as via direct contact along 3 edges of the FHE. The contact conductance simulates the physical contact between an impact deformed FHE and the inner shell. Figure 3.5-5 illustrates a cross-section through the combined modeling for the inner shell, the FHE, and the ATR fuel element. The left side of the figure illustrates the placement of the thermal nodes (indicated by the small circles) used to simulate each of the components, the use of curved elements to represent the 19 fuel plates, and the assumed points of direct contact between the FHE and the inner shell. The right side of the figure includes depiction of the solid elements that are used to simulate the air voids in and around the FHE. The heat transfer between the FHE and the ATR fuel element is computed as conductance through the 0.125 inch thick neoprene rub strips (see Figure 3.5-5) and radiation and conductance through the air voids.

The heat transfer due to direct contact conservatively assumes the FHE has been deformed as a result of the HAC drop event to create 'flat' areas measuring 0.5 inches wide at the lower 2 points of contact, 0.75 inches wide at the top, and extending the entire length of the FHE. Although this type of damage would only occur for the HAC condition (if it occurs at all), it is conservatively assumed for the NCT modeling as well. A conservatively high contact conductance[9] of 1 Btu/min-in^2-ºF is assumed.

A detailed model of the ATR fuel element is used to simulate the heat transfer within the fuel element and between the fuel element and the FHE. The detailed thermal model, illustrated in Figure 3.5-4 and Figure 3.5-5, includes a separate representation of each composite fuel plate, the side plates (including the cutouts), and the upper end box casting. Heat transfer between the individual fuel plates is simulated via conduction and radiation across the air space separating the plates. The curvature and separation distance between the plates is based on the information presented in Section 3.5.2.4, *Determination of Composite Thermal Properties for ATR Fuel Plates*. Each quarter segment of the fuel plates is represented by four thermal nodes in the circumferential direction and 16 nodes along its length.

The thermal modeling for the Loose Fuel Plate Basket uses the same model for the ATR FFSC, but replaces the thermal modeling of the FHE and the ATR fuel element with the thermal modeling for the Loose Fuel Plate Basket depicted in Figure 3.5-6. Approximately 500 nodes, 280 planar elements, and 530 solids are used to simulate the basket. Since the payload for the basket may contain a variable number and size of fuel plates, the thermal modeling is based on an empty basket. This approach is conservative since the addition of a payload will serve to increase the thermal mass of the basket and, thus, reduce its temperature rise under the transient conditions associated with the HAC event. Since the unirradiated fuel plates have essentially zero decay heat, there will be no temperature rise between the loose fuel plates and the basket. As such, modeling of the loose fuel plate payload is both unnecessary and conservative for the purposes of this evaluation.

The ATR FFSC with the ATR U-Mo demonstration element payload is not specifically modeled as part of this evaluation. Instead, its thermal performance is estimated using a qualitative approach based on the thermal characteristics of the other payloads and their associated thermal performance as described in Section 3.5.2.5, *Thermal Properties for ATR U-Mo Demonstration Element*.

The heat transfer from the exterior surfaces of the ATR FFSC is modeled as a combination of convection and radiation exchange. Appendix 3.5.2.3, *Convection Coefficient Calculation*, presents the methodology used to compute the convection coefficients from the various surfaces. The radiation exchange is computed using a Monte Carlo, ray tracing technique and includes the affect of reflection and/or transmission, according to the optical properties assigned to each surface (see Section 3.2.1, *Material Properties*).

In addition, heating of the exterior surfaces due to solar insolation is assumed using a diurnal cycle. A sine wave model is used to simulate the variation in the applied insolation on the surfaces of the package over a 24-hour period, except that when the sine function is negative, the insolation level is set to zero. The timing of the sine wave is set to achieve its peak at 12 pm and peak value of the curve is adjusted to ensure that the total energy delivered matched the regulatory values. As such, the total energy delivered in one day by the sine wave solar model is given by:

$$\int_{6\cdot hr}^{18\cdot hr} Q_{peak}\cdot \sin\left(\frac{\pi\cdot t}{12\cdot hr} - \frac{\pi}{2}\right) dt = \left(\frac{24\cdot hr}{\pi}\right)\cdot Q_{peak}$$

Using the expression above for the peak rate of insolation, the peak rates for top and side insolation may be calculated as follows:

$$Q_{top} = \left(800\frac{cal}{cm^2}\right)\cdot\left(\frac{\pi}{24\ hr}\right) \qquad Q_{top} = 2.68\frac{Btu}{hr\text{ - }in^2} \quad = 0.0447\frac{Btu}{min\text{ - }in^2}$$

$$Q_{side} = \left(200\frac{cal}{cm^2}\right)\cdot\left(\frac{\pi}{24\ hr}\right) \qquad Q_{sside} = 0.67\frac{Btu}{hr\text{ - }in^2} \quad = 0.0112\frac{Btu}{min\text{ - }in^2}$$

Conversion factors of 1 cal/cm^2-hr = 0.0256 Btu/hr-in^2 are used in the above calculations. These peak rates are multiplied by the sine function and the solar absorptivity for Type 304 stainless steel (i.e., 0.52) to create the top and side insolation values as a function of time of day.

3.5.2.2 Description of Thermal Model for HAC Conditions

The thermal evaluations for the hypothetical accident condition (HAC) are conducted using an analytical thermal model of the ATR FFSC. The HAC thermal model is a modified version of the quarter symmetry NCT model described in Section 3.5.2.1, *Description of Thermal Model for NCT Conditions*, with the principal model modifications consisting of simulating the expected package damage resulting from the drop events that are assumed to precede the HAC fire and changing the package surface emissivities to reflect the assumed presence of soot and/or surface oxidization.

Physical testing using full scale certified test units (CTUs) is used to establish the expected level of damage sustained by the ATR FFSC package from the 10 CFR 71.73 prescribed free and puncture drops that are assumed to precede the HAC fire event. Appendix 2.12.1, *Certification Tests on CTU-1* and Appendix 2.12.2, *Certification Tests on CTU-2* document the configuration and initial conditions of the test articles, the test facilities, the instrumentation used, and the test results. The drop tests covered a range of hypothetical free drop orientations and puncture bar drops. The results from both sets of CTU drop tests showed the following:

1) The worst case physical damage to the exterior of the package occurs from a CG over corner drop. The resulting damage (depicted in Figure 3.5-7) is thermally insignificant in that there is no breach in the outer shell and the compaction of the underlying insulation is minor and offset by an increase in the gap between the outer shell and the insulation in other areas.
2) The oblique, CG over side puncture bar drop caused a 0.5 inch indentation to the side of the package at the center of the impact region and less near the edges. No tearing of the outer shell occurred.
3) The end drops caused the ceramic fiber insulation to slide axially between each set of ribs, as depicted in Figure 3.5-9. The amount of re-positioning varied from approximately 1 to 1.75 inches and results in the compression of the insulation in the axial direction by 6 to 10%. No compression or shifting of the insulation in the radial direction was noted from the drop tests. While the insulation jacket showed some crimping at the edges, it was essentially undamaged.

Based on the above observations, the NCT was modified for the HAC evaluations via the following steps:

1) A 1.85 inch long segment of insulation was removed between each set of ribs. This degree of insulation re-positioning/compression conservatively bounds the maximum observed distance of 1.75 inches. Heat transfer across the vacated segments of insulation is then computed as radiation and conduction across an air filled space. Figure 3.5-10 illustrates the change made to the NCT thermal model to capture the expected insulation re-positioning. The change in the insulation's thermal conductivity as a result of the compression is conservatively ignored since thermal conductivity decreases with density at temperatures in excess of approximately 500°F (see Table 3.2-3).
2) All other geometric aspects of the NCT thermal model are assumed to be unchanged for the HAC evaluations since the observed damage to the outer shell resulting from the free and puncture drops has a superficial impact to the thermal protection offered by the ATR FFSC to the HAC fire event.
3) The surface emissivities for the various components of the package are revised as presented in Table 3.2-6 vs. that given in Table 3.2-5.

3.5.2.3 Convection Coefficient Calculation

The convective heat transfer coefficient, h_c, has a form of: $h_c = \text{Nu}\frac{k}{L}$, where k is the thermal conductivity of the gas at the mean film temperature and L is the characteristic length of the vertical or horizontal surface.

Natural convection from each surface is computed based on semi-empirical relationships using the local Rayleigh number and the characteristic length for the surface. The Rayleigh number is defined as:

$$Ra_L = \frac{\rho^2 g_c \beta L^3 \Delta T}{\mu^2} \times Pr$$

where:

g_c = gravitational acceleration, 32.174 ft/s^2
ΔT = temperature difference, °F
μ = dynamic viscosity, lb$_m$/ft-s
L = characteristic length, ft
c_p = specific heat, Btu/lb$_m$-hr-°F
β = coefficient of thermal expansion, °R^{-1}
ρ = density of air at the film temperature, lb$_m$/ft^3
Pr = Prandtl number = (c_p μ) / k
k = thermal conductivity at film temperature
Ra_L = Rayleigh #, based on length 'L'

Note that k, c_p, and μ are each a function of air temperature as taken from Table 3.2-4. Values for ρ are computed using the ideal gas law, β for an ideal gas is simply the inverse of the absolute temperature of the gas, and Pr is computed using the values for k, c_p, and μ from Table 3.2-4. Unit conversion factors are used as required to reconcile the units for the various properties used.

The natural convection from a discrete vertical surface is computed using Equation 6.39 to 6.42 of Rohsenow, et. al.[9], which is applicable over the range 1 < Rayleigh number (Ra) < 10^{12}:

$$Nu^T = \overline{C}_L Ra^{1/4}$$

$$\overline{C}_L = \frac{0.671}{\left(1 + (0.492/Pr)^{9/16}\right)^{4/9}}$$

$$Nu_L = \frac{2.8}{\ln(1 + 2.8/Nu^T)}$$

$$Nu_t = C_t^V Ra^{1/3}$$

$$C_t^V = \frac{0.13\, Pr^{0.22}}{\left(1 + 0.61\, Pr^{0.81}\right)^{0.42}}$$

$$Nu = \frac{h_c L}{k} = \left[(Nu_L)^6 + (Nu_t)^6\right]^{1/6}$$

Natural convection from horizontal surfaces is computed from Equations 4.39 and 4.40 of Rohsenow, et. al.[9], and Equations 3.34 to 3.36 of Guyer[24], where the characteristic dimension (L) is equal to the plate surface area divided by the plate perimeter. For a heated surface facing upwards or a cooled surface facing downwards and Ra > 1:

$$Nu = \frac{h_c L}{k} = \left[(Nu_L)^{10} + (Nu_t)^{10}\right]^{1/10}$$

[24] Guyer, E.C., *Handbook of Applied Thermal Design*, McGraw-Hill, Inc., 1989.

$$\mathrm{Nu_L} = \frac{1.4}{\ln\left(1 + 1.677/\left(\overline{\mathrm{C_L}}\,\mathrm{Ra}^{1/4}\right)\right)}$$

$$\overline{\mathrm{C_L}} = \frac{0.671}{\left[1 + \left(0.492/\mathrm{Pr}\right)^{9/16}\right]^{4/9}}$$

$$\mathrm{Nu_t} = 0.14\mathrm{Ra}^{1/3}$$

For a heated surface facing downwards or a cooled surface facing upwards and $10^3 < \mathrm{Ra} < 10^{10}$, the correlation is as follows:

$$\mathrm{Nu} = \mathrm{Nu_L} = \frac{2.5}{\ln\left(1 + 2.5/\mathrm{Nu^T}\right)}$$

$$\mathrm{Nu^T} = \frac{0.527}{\left(1 + \left(1.9/\mathrm{Pr}\right)^{9/10}\right)^{2/9}}\mathrm{Ra}^{1/5}$$

The forced convection coefficients applied during the HAC fire event are computed using the relationships in Table 6-5 of Kreith[25] for a flat surface, where the characteristic dimension (L) is equal to the length along the surface and the free stream flow velocity is V. The heat transfer coefficient is computed based on the local Reynolds number, where the Reynolds number is defined as:

$$\mathrm{Re_L} = \frac{\mathrm{V} \times \rho \times \mathrm{L}}{\mu}$$

For Reynolds number (Re) < $5\mathrm{x}10^5$ and Prandtl number (Pr) > 0.1:

$$Nu = 0.664\,\mathrm{Re}_L^{\;0.5}\,\mathrm{Pr}^{0.33}$$

For Reynolds number (Re) > $5\mathrm{x}10^5$ and Prandtl number (Pr) > 0.5:

$$Nu = 0.036\,\mathrm{Pr}^{0.33}[\mathrm{Re}_L^{\;0.8} - 23{,}200]$$

Given the turbulent nature of the 30-minute fire event, a characteristic length of 0.25 feet is used for all surfaces to define the probable limited distance for boundary growth. The turbulent heat transfer coefficient relationship used for HAC modeling is a modified version of the Colburn relation recommended by the advisory material for the IAEA (see *Advisory Material for the IAEA Regulations for the Safe Transport of Radioactive Material*, TS-G-1.1, Rev. 1, International Atomic Energy Agency, 2008). The same advisory material states that "pool fire gas velocities are generally found to be in the range of 5–10 m/s". The above forced convection relationships yields a convection heat transfer rate of approximately 40 $\mathrm{W/m^2}$-K, which matches that obtained with the IAEA recommended Colburn relation and conservatively bounds the experimental values in large pool fires.

3.5.2.4 Determination of Composite Thermal Properties for ATR Fuel Plates

[25] Kreith, Frank, *Principles of Heat Transfer*, 3rd edition, Harper & Row, 1973.

The ATR fuel plates are a composite material consisting of a fissile fuel matrix sandwiched within aluminum cladding. For the purposes of this calculation, the fuel composite is treated as a homogenous material with lumped thermal properties as defined below. This modeling approach is justified since the thermal gradient within the fuel element will be very low given that the un-irradiated fuel has essentially no decay heat.

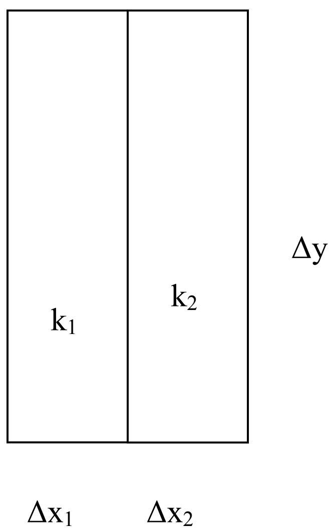

Because of the thinness of the plates, the average conductivity is required only for the axial and circumferential direction. Conductivity through the plates is not required as this analysis assumes a zero temperature gradient in that direction. Mean density and specific heat values are also defined below.

Circumferential and Axial Conductivity

Ignoring the affect of curvature, the heat flow can be written as,

$$q = -\Delta x \Delta z\, \bar{k}\, \frac{\Delta T}{\Delta y} = -\Delta x_1 \Delta z\, k_1 \frac{\Delta T}{\Delta y} - \Delta x_2 \Delta z\, k_2 \frac{\Delta T}{\Delta y} \quad \text{where}$$

$$\Delta x = \sum_i \Delta x_i$$

From which,

$$\bar{k} = \frac{\Delta x_1 k_1 + \Delta x_2 k_2}{\Delta x}$$

Mean Density

The mean density of the fuel plates is computed from:

$Mass = \Delta x \Delta y \Delta z\, \bar{\rho} = \Delta x_1 \Delta y \Delta z\, \rho_1 + \Delta x_2 \Delta y \Delta z\, \rho_2$, from which we get $\bar{\rho} = \dfrac{\Delta x_1 \rho_1 + \Delta x_2 \rho_2}{\Delta x}$

Mean Specific Heat

In the same manner used to define the mean density, the mean specific heat for the fuel plates is computed as;

$\bar{\rho}\, \bar{c}_p \Delta x \Delta y \Delta z = \rho_1 c_{p_1} \Delta x_1 \Delta y \Delta z + \rho_2 c_{p_2} \Delta x_2 \Delta y \Delta z$ from which we get, $\bar{c}_p = \dfrac{\rho_1 c_{p_1} \Delta x_1 + \rho_2 c_{p_2} \Delta x_2}{\bar{\rho}\, \Delta x}$

The thermal properties for the individual plates making up the ATR fuel element are computed using the above approach and thermophysical and geometric data[6,5] for the ATR fuel element.

Based on these data sources, the radius of the inner plate is 3.015 inches, while the radius of the outer plate is 5.44 inches. The gap between the plates is 0.078 inches. The thickness of the aluminum cladding is 0.015 inches.

While the thermal properties for the aluminum cladding and the fissile fuel matrix material will vary with temperature, for the purposes of this evaluation, fixed material properties are assumed in order to simplify the calculation. To provide conservatism for this modeling approach conservatively low value is assumed for the specific heat for each component, while a conservatively high thermal conductivity value is used. This methodology will result in over-predicting the temperature rise within the composite material during the HAC fire event.

The thermal properties used in this calculation are:

1) Aluminum cladding thermal conductivity = 191 W/m-K, conservatively high value from [6], page 18
2) Fissile fuel matrix (UAl_x) conductivity:
    a. 53 W/m-K, conservatively high based on Table 2.3 from [6], at 300K for fuel plates 1, 2, 18, & 19
    b. 43 W/m-K, conservatively high based on Table 2.3 from [6], at 300K for fuel plates 3, 4, 16, & 17
    c. 36.1 W/m-K, conservatively high based on Table 2.3 from [6], at 300K for fuel plates 5 to 15
3) Aluminum cladding density = 2702 kg/m^3, from [6], page 16
4) Fissile fuel matrix (UAl_x) density:
    a. 3409 kg/m^3, from [6], Table 2.5, for fuel plates 1, 2, 18, & 19
    b. 3671 kg/m^3, from [6], Table 2.5, for fuel plates 3, 4, 16, & 17
    c. 3933 kg/m^3, from [6], Table 2.5, for fuel plates 5 to 15
5) Aluminum cladding specific heat = 896 and 1080 J/kg-K, from [6], Table 3.2, at 300 & 600K, respectively
6) Fissile fuel matrix (UAl_x) specific heat:
    a. 666 & 803 J/kg-K, from [6], Table 2.4, value at 300 & 700K, respectively, for fuel plates 1, 2, 18, & 19
    b. 616 & 743 J/kg-K, from [6], Table 2.4, value at 300 & 700K, respectively, for fuel plates 3, 4, 16, & 17
    c. 573 & 692 J/kg-K, from [6], Table 2.4, value at 300 & 700K, respectively, fuel plates 5 to 15

Table 3.5-1 presents the composite thermal conductivity, specific heat, and density values for each of the nineteen (19) fuel plates making up the ATR fuel element. These composite values are based on the thermal property values given above and the geometry depicted in Figure 3.5-11.

3.5.2.5 Thermal Properties for ATR U-Mo Demonstration Element

The external geometry of the ATR U-Mo demonstration element is essentially identical to the ATR Mark VII YA fuel element. The demonstration element contains 18 fueled plates (plate 19 is a solid aluminum alloy plate). The demonstration element contains a mixture of UAl_x (HEU) and U-Mo (LEU) fuel plates, with a maximum U-235 mass of 1,240 g. Plates 1 through 4 and 16 through 18 are UAl_x plates identical in construction and composition to a standard HEU ATR fuel element, except boron is included in the UAl_x plates as a burnable poison. Plates 5 through 15 are fueled with an alloy of LEU uranium and molybdenum. The U-Mo fuel meat is nominally

10% molybdenum by weight, and the U-235 is enriched up to 20.0%. For the LEU fuel, the maximum weight percent for U-234 and U-236 are 0.26% and 0.46%, respectively.

The U-Mo fuel meat is nominally 0.013-in thick, and a nominal 0.001-in thick zirconium interlayer is present between the fuel meat and the aluminum alloy cladding. The fuel element weighs 32 lbs or less, is bagged in protective polyethylene sleeve, and is enclosed in the ATR FHE weighing 15 lbs.

The ATR U-Mo demonstration element is not explicitly modeled for this evaluation, but is considered to be bounded by the ATR fuel element. This modeling approach is based data in Creasy[26] and ECAR-841[27], and on the following facts:

1) the thermal characteristics of plates 1 to 4 and 16 to 18 of each element are essentially identical,
2) plates 5 to 15 of the ATR U-Mo demonstration element have lower fuel matrix thermal conductivity, but a slightly higher plate conductivity due to thicker aluminum alloy cladding used. The thermal mass of the plates are essentially the same as plates 5 to 15 of the ATR element (see Table 3.5-2, *Comparison of ATR and ATR U-Mo Demonstration Element Properties*),
3) the solid aluminum alloy plate 19 of the ATR U-Mo demonstration element has a higher thermal mass than the fueled plate 19 of the ATR element. While the thermal conductivity of a solid plate is higher than a fueled plate, the transient response is dominated by the plate's thermal mass, and
4) since the thermal mass dominates the heat transfer relations, the effect of changes in the conductivity are negligible, and the higher combined thermal mass of the ATR U-Mo fuel plates damps the thermal transient response in the model. This will result in a lower peak temperature in the ATR U-Mo demonstration element.

---

[26] Creasy, J.T., M.S. Thesis, Texas A&M University, *Thermal Properties of Uranium-Molybdenum Alloys: Phase Decomposition Effects of Heat Treatments*, December 2011, pp. 14-16.

[27] ECAR-841, *Density of Uranium Molybdenum Alloys*, Idaho National Laboratory, December 17, 2009.

Table 3.5-1 – Composite ATR Fuel Plate Thermal Properties

Plate	Plate Thickness, in	UAlx Thickness, in	Circumferential Conductivity (W/m-K)	Inner radius, in	Outer radius, in	Mean radius, in	Mean density, kg/m^3	Mean specific heat, J/(kg K) @ 300 K	Mean specific heat, J/(kg K) @ 700 K
1	0.08	0.05①	104.8	3.015	3.095	3.055	3143.9	740.1	892.3
2	0.05	0.02	135.8	3.173	3.223	3.198	2984.8	790.9	953.5
3	0.05	0.02	131.8	3.301	3.351	3.326	3089.6	762.9	919.8
4	0.05	0.02	131.8	3.429	3.479	3.454	3089.6	762.9	919.8
5	0.05	0.02	129.0	3.557	3.607	3.582	3194.4	736.9	888.9
6	0.05	0.02	129.0	3.685	3.735	3.710	3194.4	736.9	888.9
7	0.05	0.02	129.0	3.813	3.863	3.838	3194.4	736.9	888.9
8	0.05	0.02	129.0	3.941	3.991	3.966	3194.4	736.9	888.9
9	0.05	0.02	129.0	4.069	4.119	4.094	3194.4	736.9	888.9
10	0.05	0.02	129.0	4.197	4.247	4.222	3194.4	736.9	888.9
11	0.05	0.02	129.0	4.325	4.375	4.350	3194.4	736.9	888.9
12	0.05	0.02	129.0	4.453	4.503	4.478	3194.4	736.9	888.9
13	0.05	0.02	129.0	4.581	4.631	4.606	3194.4	736.9	888.9
14	0.05	0.02	129.0	4.709	4.759	4.734	3194.4	736.9	888.9
15	0.05	0.02	129.0	4.837	4.887	4.862	3194.4	736.9	888.9
16	0.05	0.02	131.8	4.965	5.015	4.990	3089.6	762.9	919.8
17	0.05	0.02	131.8	5.093	5.143	5.118	3089.6	762.9	919.8
18	0.05	0.02	135.8	5.221	5.271	5.246	2984.8	790.9	953.5
19	0.1	0.07①	94.4	5.349	5.449	5.399	3196.9	724.3	873.2

① An average UAlx thickness of 0.020 inches exists for Plates 1 an 19 vs. the 0.05 and 0.07 inches assumed by this analysis based on the assumption of a constant cladding thickness. However, for the purposes of developing composite fuel plate properties for this evaluation, the UAlx thicknesses identified in the table yield conservative bounding thermal property values.

Table 3.5-2 – Comparison of ATR and ATR U-Mo Demonstration Element Properties

Property for Plates 5 to 15	**UAl_x-Al Fuel Matrix**	**U-Mo Fuel Matrix**
Density (kg/m^3)	3933	17,200
Specific Heat (J/kg-K) @ 600 K	660	155
Thermal Conductivity (W/m-K)	36.1 to 34.8 (273<T<800 K)	11.7 to 26.9 (298 K<T< 773 K)
Heat Capacity (J/m^3-K) – calculated from values above	2.60×10^6	2.67×10^6

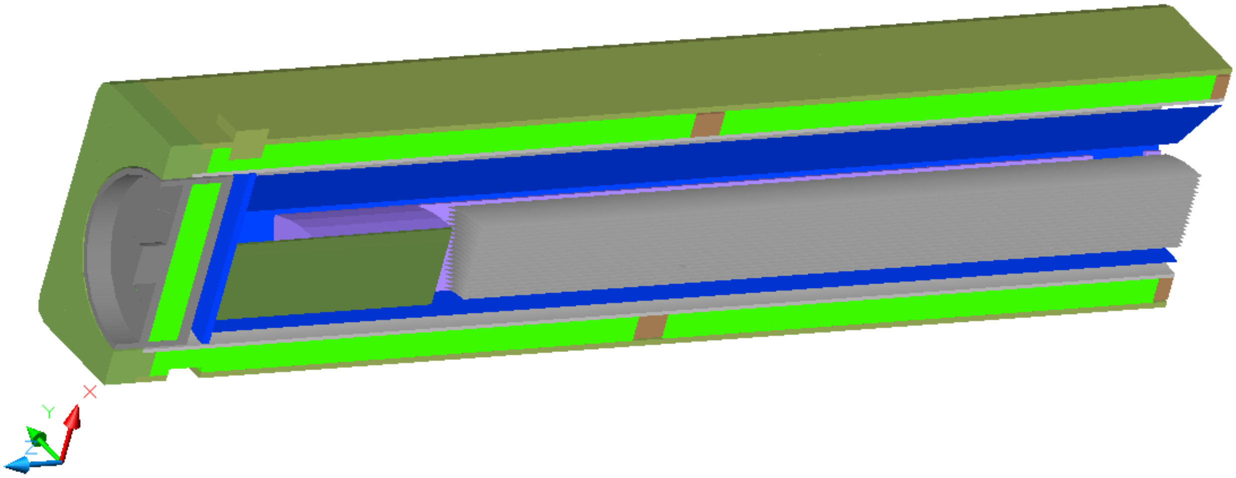

(Note: the positive x-axis is oriented towards the top of the package and the positive z-axis towards the package closure end)

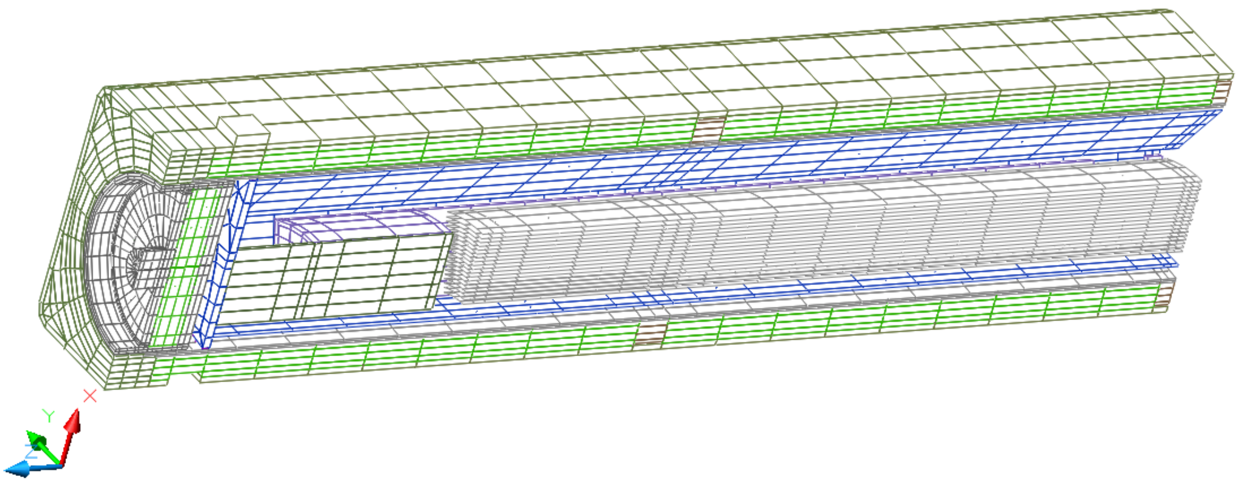

(Note: the positive x-axis is oriented towards the top of the package and the positive z-axis towards the package closure end)

Figure 3.5-1 – 'Solid' and & 'Hidden Line' Views of Package Quarter Symmetry Thermal Model

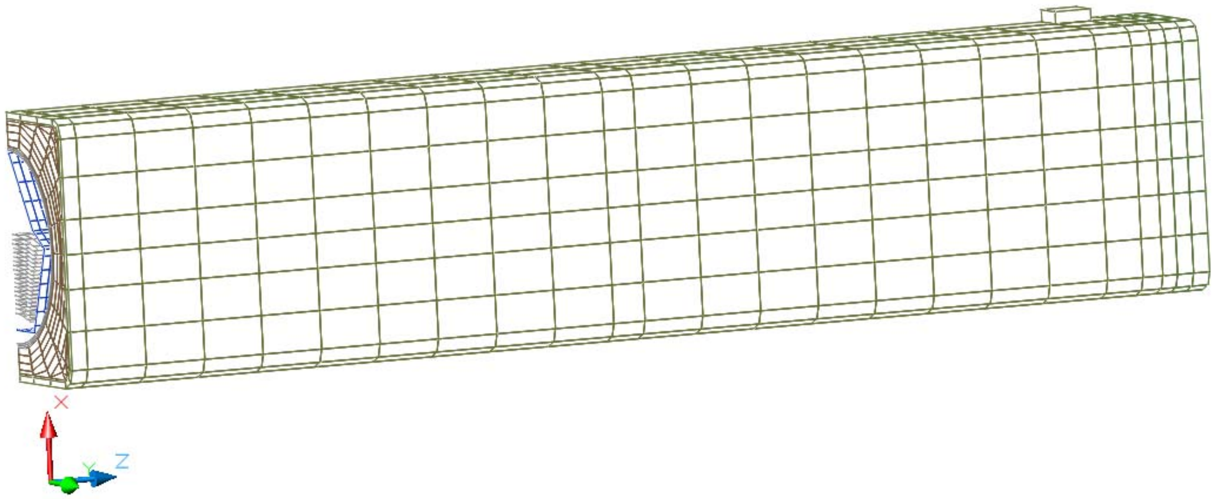

(Note: the positive x-axis is oriented towards the top of the package and the positive z-axis towards the package closure end)

Figure 3.5-2 – Reverse, 'Hidden Line' View of Package Quarter Symmetry Thermal Model

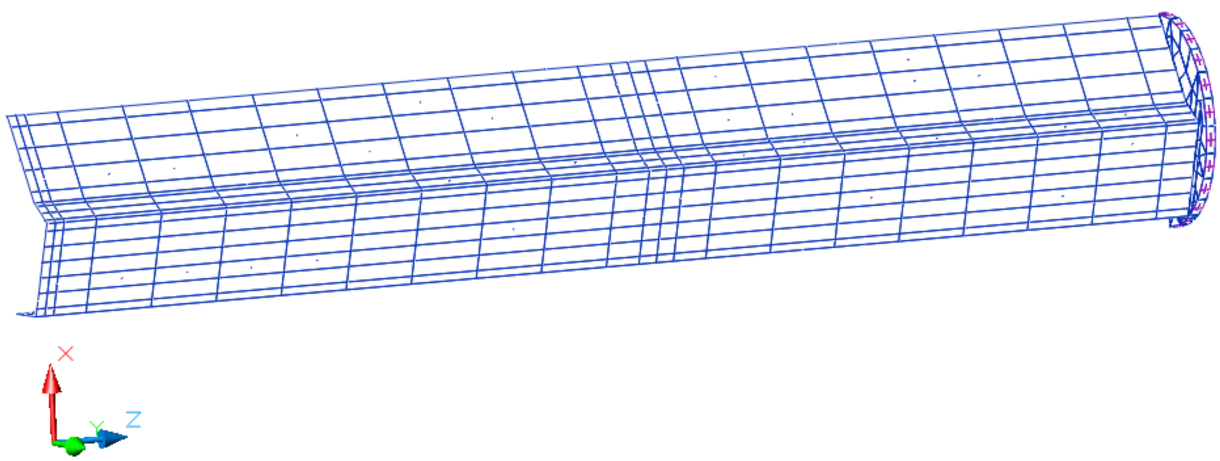

(Note: the positive x-axis is oriented towards the top of the package and the positive z-axis towards the package closure end)

Figure 3.5-3 – Reverse, 'Hidden Line' View of FHE Quarter Symmetry Thermal Model

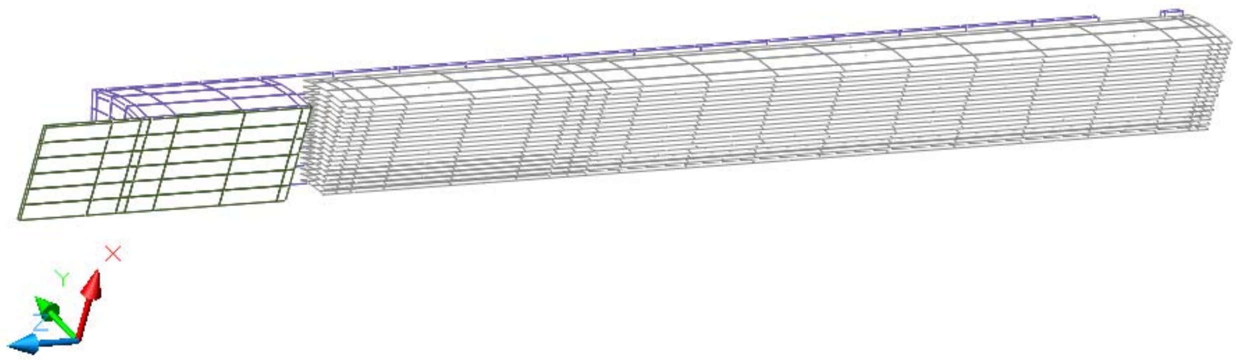

ATR Fuel Element Modeling, View Along Centerline of Element

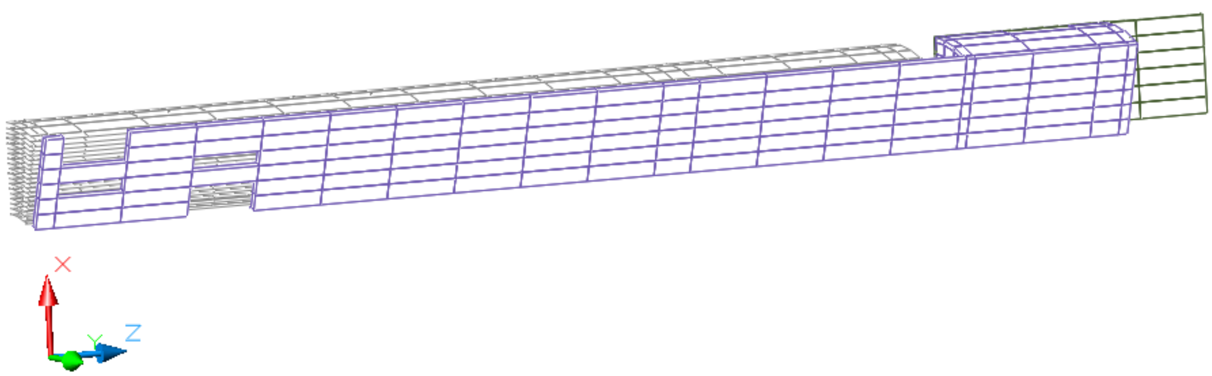

ATR Fuel Element Modeling, View Along Outside of Element

(Note: the positive x-axis is oriented towards the top of the package and the positive z-axis towards the package closure end)

Figure 3.5-4 – Centerline and Side Views of ATR Fuel Element Thermal Model

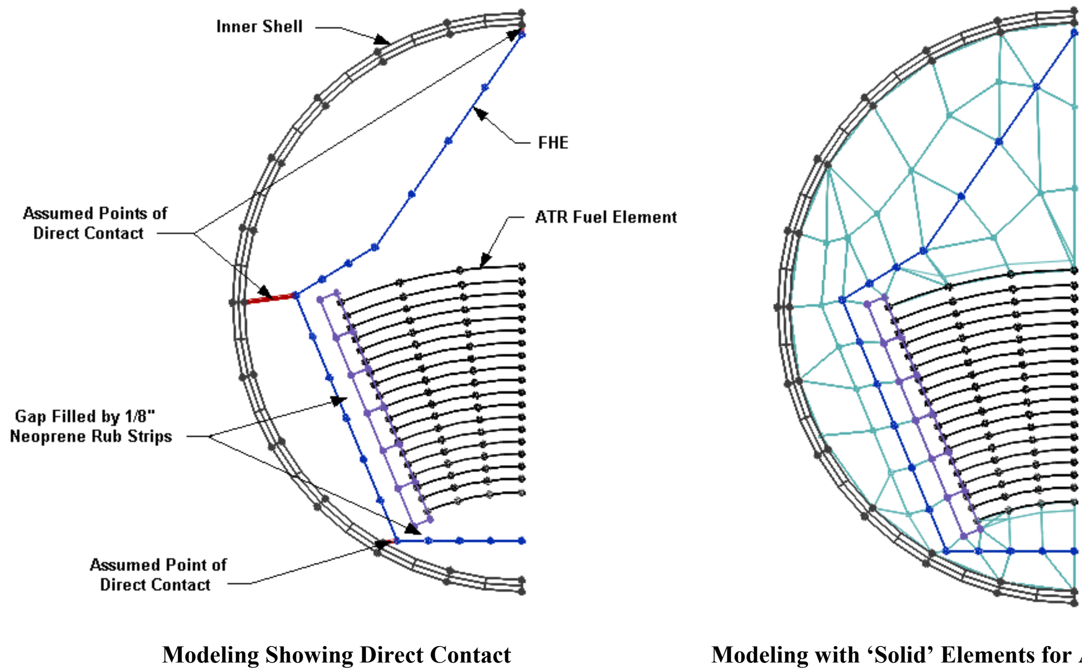

Figure 3.5-5 – Thermal Model of ATR Fuel Element and FHE within Inner Shell

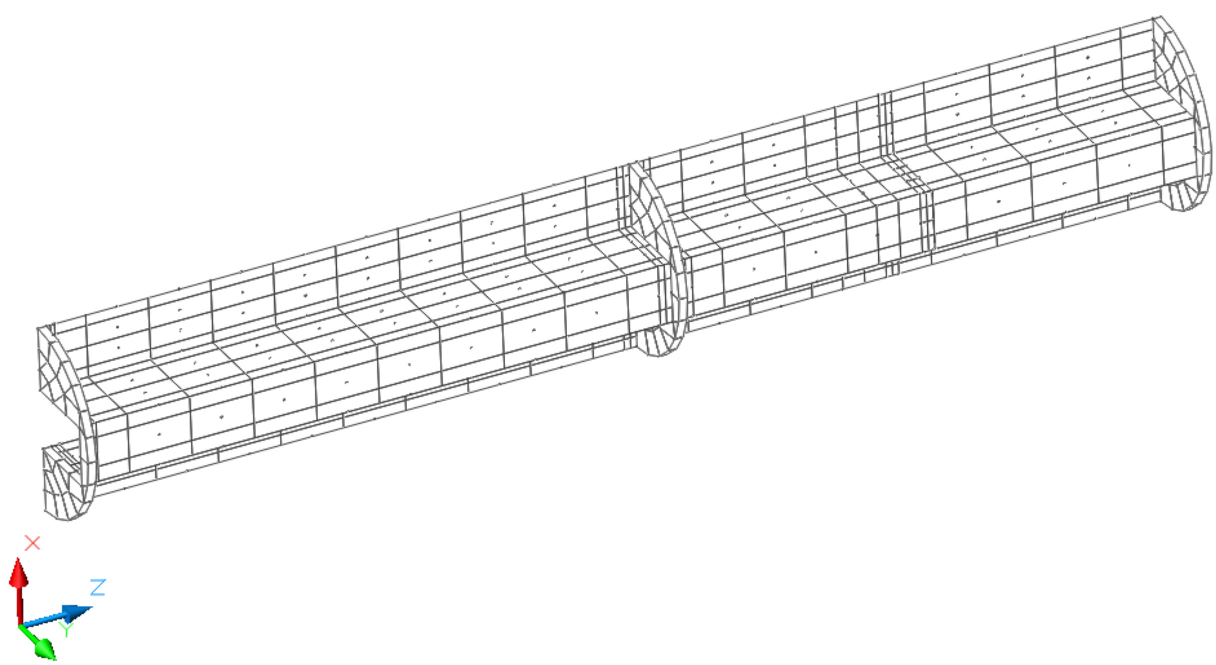

(Note: the positive x-axis is oriented towards the top of the package and the positive z-axis towards the package closure end)

Figure 3.5-6 – Thermal Model of Loose Fuel Plate Basket (LFPB)

Figure 3.5-7 – Worst Case Package Damage Arising from Corner Drop

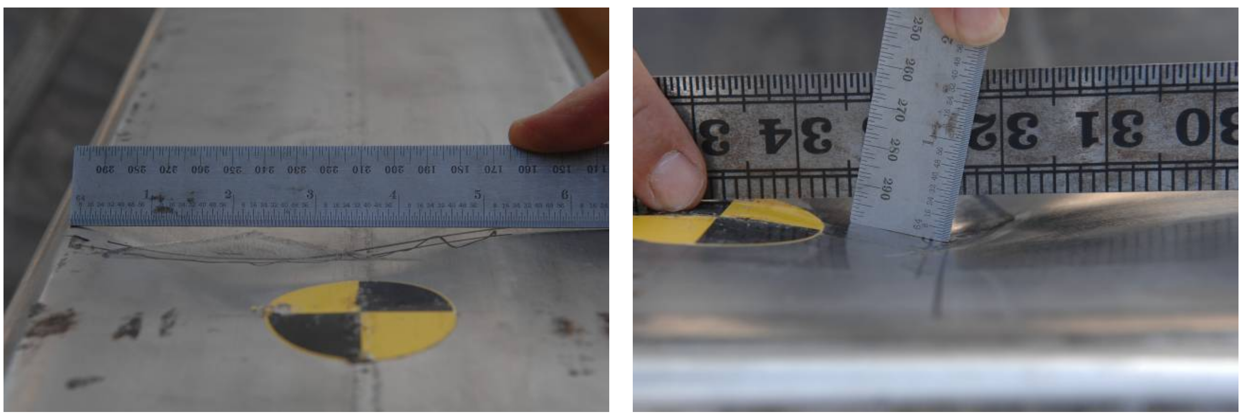

Figure 3.5-8 – Worst Case Package Damage Arising from Oblique Puncture Drop

Figure 3.5-9 – Insulation Re-positioning Arising from End Drop

Security-Related Information Figure Withheld Under 10 CFR 2.390.

Figure 3.5-10 – Thermal Modeling of Insulation Re-positioning for HAC Conditions

Security-Related Information Figure Withheld Under 10 CFR 2.390.

Figure 3.5-11 – ATR Fuel Element Cross Section

3.5.3 Thermal Decomposition/Combustion of Package Organics

The organic material in the ATR FFSC subject to thermal decomposition and/or combustion is limited to polyethylene, neoprene, and the adhesive used to attach the neoprene. The fuel elements and, optionally, the loose fuel plates are enclosed in polyethylene bags prior to their placement in the FHEs and loose plate basket. The bags serve no safety function beyond providing investment protection of the payload material. Similarly, neoprene (polychloroprene) rub strips are attached via adhesive to the FHEs to provide investment protection against fretting on the elements and loose plates. As such, the loss of the organic material under either NCT or HAC conditions has no safety implication beyond the potential for gas and heat generation. The following sections provide a bounding assessment on the potential safety impact associated with the loss of organic material within the ATR FFSC package.

3.5.3.1 Organic Material Within Package

The amount of organic material in the package varies with the payload configuration. While the bounding amount of polyethylene is constant at 100 g, the amount of neoprene varies with payload configuration. The sections below identify the quantity and important thermal properties associated with the organic materials present in the ATR FFSC package.

<u>Polyethylene</u>
Properties of polyethylene related to its thermal decomposition/combustion are as follows:

a) chemical formulation[7]: $-[CH_2- CH_2]_n-$,
b) heat of combustion (ΔH_c)[28]: 46,500 kJ/kg,
c) oxygen index[29,30]: 17.4%,
d) melting temperature[30]: 109-135°C
e) temperature for 1% decomposition[30]: 275°C
f) autoignition temperature[31]: 330 to 410°C

Oxygen index (OI) is the minimum oxygen concentration required to support self-sustaining combustion of the polymer. Since piloted conditions do not exist within the ATR FFSC payload cavity, self-sustaining combustion of the polyethylene can't occur when the oxygen concentration drops below 17.4%. Low oxygen concentrations will not only prevent self-sustaining combustion, but will raise the autoignition temperature. Combustion of polyethylene in air is governed by the following equation:

$$C_2H_4 + 3(O_2 + 3.76N_2) \rightarrow 2CO_2 + 2H_2O + 11.28N_2$$

The above equation demonstrates that complete combustion of a mole of polyethylene requires 3 moles of oxygen and, since oxygen constitutes approximately 21% of air, 14.28 moles of air. The total quantity of gas generated is 15.28 moles, or an increase of 7% over the original gas

---

[28] NUREG-1805, Fire Dynamics Tools, Nuclear Regulatory Commission, Washington, D.C.

[29] office.wendallhull.com/matdb/

[30] *SFPE Handbook of Fire Protection Engineering*, 3rd Edition, Section 1, Chapter 7, Table 1.7-4, NFPA, 2003.

[31] *MSDS for Polyethylene,* #1488, prepared by International Programme on Chemical Safety, 2004.

quantity existing before combustion. Per SAR section 1.2.2, the amount of polyethylene in the package is limited to 100 g or less. Based on a molecular weight of approximately 28 g/g-mole of polyethylene, the 3.57 g-moles of polyethylene represented by the 100 g would require 3.57 x 14.28 = 50.98 g-moles of air for complete combustion.

Neoprene

Properties of neoprene (polychloroprene) related to its thermal decomposition/combustion are as follows:

a) chemical formulation[7]: -[CH_2-Cl-C=CH-CH_2]$_n$-,
b) heat of combustion (ΔH_c)[28]: 10,300 kJ/kg,
c) oxygen index[29,32]: 32-35% at one atmosphere,
d) melting temperature: N/A - thermoset material
e) temperature for initial decomposition[30]: 342°C
f) autoignition temperature[32]: >380°C in a 21% oxygen concentration environment.

As a thermoset plastic, uncontrolled heating of neoprene will result in reaching the decomposition temperature before the melting point is obtained. The high oxygen index demonstrates why neoprene can't support combustion without an external ignition source. The typical adhesives[33] used to bond the rub strips to the FHEs consist of principally of solvents that outgas during the curing process. The non-volatile components consist of polymers, including polychloroprene, and cure and vulcanization agents. As a result, the cured adhesive layer exhibits properties[33] similar to neoprene.

Combustion of neoprene in air is governed by the following equation:

$$C_4H_5Cl + 5.25(O_2 + 3.76N_2) \rightarrow 4CO_2 + 2.5H_2O + Cl + 19.74N_2$$

From the above equation, complete combustion of a mole of neoprene is seen to require 5.25 moles of oxygen and, since oxygen constitutes approximately 21% of air, 24.99 moles of air. The total quantity of gas generated is 27.24 moles, or an increase of 9% over the original gas quantity existing before combustion.

Based on the surface area of rub strips depicted on each SAR drawing, a thickness of 0.125 in, and an adhesive layer thickness of 2 mils, the total quantity of neoprene and neoprene like material used in each FHE is summarized in Table 3.5-3. With a molecular weight of approximately 88.5 g/g-mole of neoprene, the 4.62 g-moles of neoprene represented by the minimum 409 g of neoprene contained within the 60501-40 FHE assembly would require 4.62 x 24.99 = 115.5 g-moles of air for complete combustion.

The same limitation on package oxygen that prevents significant combustion of polyethylene will also prevent combustion of the neoprene. Further, given the higher oxygen index and autoignition temperature for neoprene versus polyethylene, there is a low probability any neoprene material will be involved in combustion. Instead, it is expected that the only damage to be incurred by the neoprene will be a de-bonding from the FHE surfaces and a small amount of

[32] *Safe Use of Oxygen and Oxygen Systems*, ASTM, 2nd Edition.

[33] Product and MSDS sheets for 3M™ Spray 80 Neoprene Contact Adhesive or 3M™ Scotch-Weld Neoprene Contact Adhesive 1357.

thermal decomposition. Since thermal decomposition is an endothermic process, the loss of the material will act to lower the temperatures predicted within the FHE.

3.5.3.2 Air Quantity Within Package

Since the ATR FFSC payload cavity is not sealed, the quantity of gas filling the cavity volume will vary with time as a function of the cavity's bulk gas temperature, the thermal decomposition of the enclosed organic material, and diffusion of gas through the package closure gaps. The following sections address these various mechanisms affecting the air/oxygen content within the package.

Potential Combustion Due to Resident Air Quantity

The ATR FFSC payload cavity has a length of 67.88 in and a diameter of 5.76 in. The gross cavity volume is 1768.8 in^3. The ATR fuel element and the ATR FHE have volumes of approximately 155 and 223 in^3, based on weights of 25 and 15 lbs, respectively, and mean densities of 0.112 and 0.097 lbs/ in^3, respectively. The net cavity space is therefore approximately 1,391 in^3 (22.8 liters). Table 3.5-4 summarizes the net cavity volume existing for all payload configurations. As seen from the table, only the MIT FHE (SAR drawing 60501-40) loaded with a MIT fuel element results in a larger net cavity volume than the ATR FHE (SAR drawing 60501-30) loaded with an ATR fuel element. Given the substantially higher HAC temperature predicted for the ATR FHE (see Section 3.4, *Thermal Evaluation for Hypothetical Accident Conditions*) versus that for the MIT FHE (see Section 3.6, *Thermal Evaluation for MIT, MURR, and Small Quantity Payloads*) and the larger quantity of neoprene used (see Table 3.5-3), the ATR FHE is the appropriate payload configuration for assessing the thermal safety related to the organic material in the package.

At 100°F, approximately 0.9 g-moles of air are required to fill a 1,391 in^3 (22.8 liters) cavity space to a pressure of 14.7 psia, while at 626°F (330°C, i.e., the lower autoignition temperature for polyethylene), the quantity of air required to fill the cavity space drops to approximately 0.5 g-mole. As such, the resident air quantity in the payload cavity is sufficient to support combustion of less than 1% of the polyethylene (i.e., 0.5 g-mole/50.98 g-mole air per 100 g polyethylene). The potential heat release from this quantity of polyethylene is: 1% x 100 g x 46,500 kJ/kg = 46,500 J = 44 Btu. Based on a combined ATR payload weight of 40 lbs and a specific heat of approximately 0.2 Btu/lb_m-°F[34], the net increase in the mean payload temperature would be less than 6°F even if this heat release occurred instantaneously. The use of the combined payload weight for this calculation is appropriate since the combustion occurs in the vapor space and not on a surface. Further, combustion of the limiting 1% of the polyethylene can neither occur instantaneously nor in only one concentrated area since the availability of the oxygen within the cavity will be rate limited by the diffusion process from reaching the potential site(s) of polyethylene combustion. In fact, oxygen diffusion will also prevent the entire resident oxygen quantity from being consumed. As such, the estimated 6°F rise in payload temperature is highly conservative.

[34] Approximate specific heat of ATR fuel plates per Table 3.2-2

Given the lower heat of combustion of neoprene versus that for polyethylene and the greater air quantity needed for complete combustion, the potential temperature rise from the combustion of polyethylene bounds that for neoprene by a factor of over 3.

Potential Combustion Due to Air Induced Via Pressure Forces

Once the residual air existing in the payload cavity prior to the start of the HAC event is consumed, further combustion will require additional air to enter the cavity via pressure and diffusion forces. The pressure forces will arise due to the balance between ideal gas expansion/contraction and gas generation within the package versus the pressure resistance associated with gas flow through the gaps around the package closure. Heatup of the package during the 30-minute fire event will result in elevated cavity pressure and a continuous outflow of gas from the cavity. This gas flow will switch to an inflow condition once the peak bulk gas temperature is reached and the package begins to cool down.

While an accurate estimate of the gas flow due to pressure forces requires a detailed modeling of the flow paths and resistance factors, a bounding estimate on the rate of gas flow into the package due to pressure differential can be made by assuming zero vent resistance and zero internal gas generation. These assumptions assure that the minimum gas quantity is achieved at the point where packaging cooling begins, thus maximizing the potential for the reverse gas flow necessary to restore atmospheric pressure within the package.

Assuming that the bulk average gas temperature within the package is represented by the mean of the average temperatures over the length of the package's inner shell and the FHE, the cavity gas quantity within the package can be estimated as a function of time during the HAC transient. Figure 3.5-12 presents the predicted package gas quantity for the HAC transient depicted in Figure 3.4-1 for the ATR fuel element. As seen, the package gas quantity rapidly drops during the 30-minute fire event as the cavity gas expands under HAC heating. Shortly after the cessation of the fire event, the package begins to cool and the gas flow switches to an inflow. However, due to the rate of package cooldown, greater than 10 hours are required to restore the approximately 0.5 g-moles of gas expelled during package heatup. The calculated reverse gas flow peaks at 0.0025 g-moles per minute. The potential polyethylene combustion supported by this flow rate is 0.0025 g-moles per minute x 100 g polyethylene per 50.98 g-mole air x 46,500 kJ/kg = 228.1 J/min = 0.22 Btu/min. Clearly this flow rate is too low to permit any significant rate of combustion, especially when considering the facts that the reverse gas flowrate decreases rapidly from this peak rate and that accounting for flow resistance through the vent geometry will reduce this potential heat gain even more.

When the above discussion is added to the fact that the oxygen concentration at the start of the inflow condition will be well below the oxygen index of 17.5% required to support combustion, the fact that oxygen diffusion within the package will extend the time for the entering air to reach the site of elevated polyethylene temperatures, and as seen in Figure 3.5-12, that the package temperatures will fall below the lower autoignition temperature for polyethylene after 90 minutes, it is reasonable to conclude that the contribution to package heatup from airflow due to pressure differential is essentially zero.

Potential Combustion Due to Air Induced Via Diffusion

Beside pressure differential, the other force available to drive oxygen inflow to the package cavity is diffusion. Assuming that the oxygen inside the package cavity is consumed as fast as it enters, the rate of oxygen diffusion can be determined via Fick's first law or:

$$\mathrm{J} = -\rho \times \mathrm{D} \times \frac{\partial w}{\partial y}$$

where: J = mass flux of oxygen per area, g/cm^2

D = diffusion coefficient of oxygen in nitrogen, cm^2/sec

ρ = density of air, g/cm^3

$\frac{\partial w}{\partial y}$ = change in mass fraction of oxygen over diffusion path

While diffusion of oxygen in nitrogen is used to reflect that fact that the environment within the payload cavity is assumed to be oxygen depleted, in reality there is little difference between diffusion in air or nitrogen. The diffusion coefficient is a function of temperature and pressure. Diffusion increases with increasing temperature since the molecules move rapidly and decreases with increasing pressure since higher fluid density increases the number of molecules per unit volume, increasing the number of collisions, thus slowing the speed of transport. The diffusion coefficient for oxygen in air at 1 atm and 25°C is 0.206 cm^2/sec[35]. Since the fluid pressure is assumed to remain near atmospheric throughout the HAC event, there is no need to adjust the diffusion coefficient for pressure effects. However, the temperature of the fluid both within and exterior to the package will increase significantly during the HAC transient, thus necessitating an adjustment[36] in the diffusion coefficient via:

$$\mathrm{D_{O\text{-}N}} = 0.0018583 \sqrt{\mathrm{T}^3 \times \left(\frac{1}{\mathrm{M_O}} + \frac{1}{\mathrm{M_N}}\right)} \times \frac{1}{\mathrm{P} \times \sigma^2_{\mathrm{O\text{-}N}} \times \Omega_{\mathrm{D,O\text{-}N}}}$$

where: D = diffusion coefficient of oxygen in air, cm^2/sec

T = temperature, K

M = molecular mass of oxygen and nitrogen

P = pressure, atm

$\Omega_{D,O\text{-}N}$ = collision integral for molecular diffusion of oxygen in nitrogen

$\sigma_{O\text{-}N}$ = collision diameter, Angstroms

From Table E.1 and the equations provided in Transport Phenomena[36], M_O = 31.999, M_N = 28.013, σ_O = 3.433, σ_N = 3.667, ε_O/κ = 113, and ε_N/κ = 99.8. $\sigma_{O\text{-}N}$ = 0.5x(3.433 + 3.667) = 3.55. $\varepsilon_{O\text{-}N}/\kappa = (113 \text{ x } 99.8)^{0.5}$ = 106.2. Assuming the maximum flame temperature of 1475°F (1075K), the dimensionless temperature is $\kappa T/\varepsilon_{O\text{-}N}$ = 1075/106.2 = 10.1. From Table E.2[36], $\Omega_{D,O\text{-}N}$ = 0.741. Thus, $D_{O\text{-}N}$ at a pressure of 1 atm and 1475°F is 1.815 cm^2/sec.

[35] *CRC Handbook of Engineering Tables*, Dorf, R. editor, CRC Press LLC, 2004.

[36] *Transport Phenomena*, 2nd Ed., Eqn 17.3-12 and Appendix E, Bird, R., Stewart, W, and Lightfoot, E., John Wiley & Sons, Inc., 2002.

The bayonet type closure plug for the ATR FFSC package results in a labyrinth like leakage path (see Figure 3.5-13). To conservatively bound the available leakage area for air exchange via diffusion, the closure plug geometry can be simplified as simply the barrel portion (i.e., flow path over segment A-B, Figure 3.5-13). Per the Table 3.5-5, the maximum diffusion area represented by this flow path is 1.71 in^2 (11 cm^2). Based on the derived diffusion coefficient, an air density of 0.000325 g/cm^3at 1475°F (1075K), and a total diffusion path length of 2.5 in (6.4 cm, i.e., the total length of the closure plug), the maximum diffusion rate during the 30-minute fire event is calculated as:

$$\mathrm{J} \times \mathrm{Area} = -\,0.000325\,\mathrm{g/cm^3} \times 1.815\,\mathrm{cm^2/sec} \times \frac{0.21-0}{6.4} \times 11\,\mathrm{cm^2}$$

J x Area = 0.00021 g/sec = 0.0004 g-mole/min

Following the fire event, the ambient temperature will drop to 100°F and the ambient density will rise to 0.001128 g/cm^3. The diffusion coefficient for oxygen in air at 1 atm and 25°C is 0.206 cm^2/sec[35], or approximately 11% of the diffusion coefficient determined for the fire conditions. The net effect of the higher density and lower diffusion coefficient is a diffusion rate of 0.00008 g/sec, or 38% of the rate determined at fire conditions.

Based on the 0.22 Btu/min temperature rise determined in the previous section for the 0.0026 g-mole/min oxygen flow associated with the pressure differential, the 0.0004 g-mole/min oxygen diffusion rate would generate a maximum 0.03 Btu/min temperature rise, dropping to less than 0.013 Btu/min following the end of the fire event. Since accounting for the diffusion resistance within the payload cavity will reduce the potential heat generation rate even more, a reasonable conclusion is that the contribution to package heatup from oxygen diffusion can be ignored.

3.5.3.3 Pressure Loss Across Closure Leakage Path

The ATR FFSC package is not sealed, but uses a bayonet type closure plug that results in a labyrinth like leakage path, see Figure 3.5-13. The size of the various pathways illustrated in the figure are listed in Table 3.5-5. The maximum pressure rise within the package is associated with the minimum flow area and the maximum gas generation and thermal expansion, with the total pressure loss estimated from a summation of the individual pressure losses associated with each portion of the flow path. Normalizing the individual pressure losses to the flow velocity in the A-B channel allows direct addition of the individual loss coefficients and eases the calculation of the pressure loss based on a single flow velocity. The normalizing to flow velocity involves multiplying the calculated loss coefficient by the square of the area ratio.

The entrance loss at the beveled portion of the closure plug can be estimated using a conical inlet with adjoining wall (i.e, Diagram 3-7[37]). Based on a 15° bevel angle on closure plug and L/D_h > 0.6, the total loss coefficient at the entrance is:

$$\xi_1 = \frac{\Delta P}{0.5 \rho v^2} = 0.13$$

---

[37] *Handbook of Hydraulic Resistance*, 3rd Ed., Idelchik, I.E., Begell House Publishers, 1996.

where v is the flow velocity upstream of the inlet area. This value is conservatively increased to $\xi_1 = 0.50$ for a blunt, flush inlet (Diagram 3-1[37]). Since the loss coefficient is based on the flow velocity after entering the gap, no adjustment for flow area in A-B is necessary:

$$K_1 = \xi_1 = 0.5$$

The pressure loss associated with flow in the A-B channel is a function of wall friction losses. Given the short path length and smooth wall surfaces, the associated pressure loss will be insignificant and can be ignored.

Flow between B-B' can be approximated as a 90-degree turn with sharp corners (Diagram 6-6[37]). Here the rectangular side length ratio (a_o/b_o) is equal to (5.64 x pi)/((5.76-5.64)/2) = 295.3 and the ratio of cross section areas (b_1/b_0) is equal to 0.006/0.06 = 0.1 (based on the minimum gap width after the turn). With these values, the loss factor extrapolated from Diagram 6-6 is $\xi_2 = 3.1$. Given uncertainties in the extrapolation, the computed value is doubled to 6.2 for conservatism[38]. Since the loss coefficient is based on the flow velocity in the gap approaching the turn, no adjustment for flow area in A-B is necessary:

$$K_2 = \xi_2 = 6.2$$

Flow between B'-E can also be approximated as a 90-degree sharp corner turn (Diagram 6-6[37]). Again, the rectangular side length ratio (a_o/b_o) is equal to (5.967 x pi)/(0.006 min gap) = 3124 and the ratio of cross section areas (b_1/b_0) is equal to 0.235/0.006 = 39. With these values, the loss factor can be conservatively estimated from Diagram 6-6 as $\xi_3 = 0.55$. Converting to the loss coefficient based on the gap area for flow path A-B yields:

$$K_3 = \xi_3 \left(\frac{0.45}{0.11} \right)^2 = 9.20$$

Flow between E-F can also be approximated as a sudden expansion with a discharge to ambient. A loss factor of 1 is used to account for these losses. Converting to the loss coefficient based on the gap area for flow path A-B yields:

$$K_4 = \xi_4 \left(\frac{0.45}{1.77} \right)^2 = 0.06$$

The parallel flow path to B'-E consisting of B'-C, C-D, and D-E can be conservatively ignored as its inclusion will serve to lower the estimated total pressure loss. Therefore, a bounding estimate of the total loss factor associated with the minimum expected flow path areas is calculated as $K_1 + K_2 + K_3 + K_4 = 0.5 + 6.2 + 9.2 + 0.06 = 16$.

The pressure loss for flow through the closure plug leakage path can be computed as a function of velocity and density via $\Delta P = 16 \times 0.5 \dfrac{\rho v^2}{g_c}$. Since mass flow is also a function of velocity and

[38] This flow loss is a reasonable upper bound given a worst case assumption that the flow comes to a complete stop before the turn and then needs to re-accelerate into the smaller gap. When adjusted for velocity differences, the flow loss under this worst case scenario would be approximately (0.45 in^2/0.11 in^2)^2 x 0.5 = 8.4, where 0.5 is the loss factor associated with a blunt inlet fitting.

density, $\dot{m} = \rho \times v \times \text{Area}$, the pressure loss relationship can be re-formulated as a function of mass flow via:

$$\Delta P = 16 \times 0.5 \frac{\rho \left[\dot{m} / (\rho \times \text{Area}) \right]^2}{g_c}$$

where Area is the flow area in the path A-B (0.45 in^2 minimum) and the density is for the bulk gas temperature. From the data used to develop Figure 3.5-12, the maximum gas flow required to maintain atmospheric pressure within the ATR FFSC cavity due to only ideal gas expansion occurs during package heatup. The peak flowrate of 0.035 g-mole/min occurs approximately 8 minutes after the start of the 30-minute HAC fire and when the bulk gas temperature within the payload cavity has reached 230°F (110°C). Based on a molecular weight of 28.96 g/g-mole for air, the associated mass flow and density are 1.01 g/min (0.00004 lb_m/sec) and the gas density is 0.00091 g/cm^3 (0.057 lb_m/ft^3. Substituting these values into the above equation yields a ΔP = 0.1 psi for the conservative assumption of minimum flow areas within all vent gaps. The pressure loss at nominal gap dimensions will be even lower.

This maximum pressure rise due to thermal expansion of the cavity gas is too low to create an issue. Thermal decomposition of polyethylene and neoprene will generate additional gases that would need to be vented. While only a small fraction of the material is expected to be thermally decomposed due to a combination of the temperature levels achieved and the time above the thermal decomposition temperature level, a bounding maximum pressure rise can be estimated assuming the entire inventory of both polyethylene and neoprene decomposes over a 60 minute period. The potential gas quantity associated with the total decomposition of the 100 g of polyethylene is 100 g/(28 g/g-mole) x 2 g-moles H_2 per g-mole polyethylene = 7.14 g-moles H_2. Similarly, the 1,926 g of neoprene associated with the SAR 60501-70 FHE assembly will generate 1926 g/(88.5 g/g-mole) x (2 g-moles H_2 + 1 g-moles HCl) per g-mole neoprene = 65.3 g-moles H_2 and HCl. The combined gas generation rate is therefore (7.14 + 65.3 g-mole)/60 minutes, or 1.21 g-moles/minute.

Based on the pressure loss associated with the 1.01 g/min flow rate due to gas expansion, the combined pressure loss of thermal decomposition and gas expansion would be:

$$\Delta P = 0.1\,\text{psi} \times \left(\frac{1.01 + 1.21\,\text{g-moles}}{1.01\,\text{g-moles}} \right)^2 = 0.5\,\text{psi}$$

This bounding pressure rise is also insignificant, especially given the conservative assumption of minimum flow areas within all vent gaps. As such, the assumption of a 0 psig pressure throughout the HAC event is valid for the purposes of determining the safety basis of the design.

Based on the level of and type of damage noted in Appendix 2.12.1, *Certification Tests on CTU-1* and Appendix 2.12.2, *Certification Tests on CTU-2,* no change to the net vent areas based on the assumed minimum gaps is expected. Thus the above conclusions remain valid for the damaged package configuration as well.

Table 3.5-3 – Neoprene Quantity Per Assembly

SAR Drawing	Neoprene Surface Area, in^2	Neoprene Volume, in^3	Neoprene Adhesive Volume, in^3	Neoprene Quantity, g①
60501-10	N/A	N/A	N/A	N/A
60501-20	N/A	N/A	N/A	N/A
60501-30	475	59	1.0	1210 g
60501-40	162	20	0.3	409 g
60501-50	266	33	0.5	676 g
60501-60	547	68	1.1	1393 g
60501-70	748	94	1.5	1926 g

Notes: ① Based on density of 1.23 g/cm^3 (76.8 lb/ft^3 per Table 3.2-3)

Table 3.5-4 – Net Cavity Volume vs. Payload Assembly

SAR Drawing	Gross Cavity Volume, in^3	FHE Volume, in^3	Payload Volume, in^3	Net Cavity Volume, in^3	Comments
60501-20	1768.8	307.4①	168.1②	1293.3	ATR Loose Plate FHE
60501-30	"	154.6③	223.2④	1390.9	ATR FHE - Design basis selection due to combination of net cavity size and peak HAC temperature for FHE
60501-40	"	256.1⑤	88.5⑥	1424.1	MIT FHE
60501-50	"	307.4⑦	126.1⑧	1335.4	MURR FHE
60501-60	"	286.9⑨	142.9⑩	1339.0	RINSC FHE
60501-70	"	307.4①	168.1②	1293.3	Small Quantity FHE

Notes: ① Based on 30 lb weight and density of 0.0976 in^3 per Tables 2.1-1 and 3.2-2
② Based on 20 lb weight and density of 0.112 in^3 per Tables 2.1-1 and 3.2-2
③ Based on 15 lb weight and density of 0.097 in^3 per Tables 2.1-1 and 3.2-1
④ Based on 25 lb weight and density of 0.112 in^3 per Tables 2.1-1 and 3.2-2
⑤ Based on 25 lb weight and density of 0.0976 in^3 per Tables 2.1-1 and 3.2-2
⑥ Based on 10 lb weight and density of 0.113 in^3 per Tables 2.1-1 and 3.6-4
⑦ Based on 30 lb weight and density of 0.0976 in^3 per Tables 2.1-1 and 3.2-2
⑧ Based on 15 lb weight and density of 0.119 in^3 per Tables 2.1-1 and 3.6-4
⑨ Based on 28 lb weight and density of 0.0976 in^3 per Tables 2.1-1 and 3.2-2
⑩ Based on 17 lb weight and density of 0.119 in^3 per Tables 2.1-1 and 3.6-4

Table 3.5-5 – Closure Leakage Path Areas

Flow Path	Inner/Outer Diameter, in	Gap Width/Length, in	Flow Path Area, in^2
A to B	5.64 $\pm$ 0.01 5.76 $\pm$ 0.06①	1.69	Max: 1.71 Min: 0.45
B to B'	5.70 (mean)	0.006 to 0.03②	Max: 0.54 Min: 0.11
B' to C	5.967 (min)	0.006 to 0.03②	Max: 0.56 Min: 0.11
C to D	6.38 $\pm$ 0.02 6.44 $\pm$ 0.01	0.281	Max: 0.91 Min: 0.30
D to E	6.21 (mean)	0.006 to 0.03②	Max: 0.59 Min: 0.12
B' to E	5.967 $\pm$ 0.01 6.44 $\pm$ 0.01	0.281	Max: 1.92③ Min: 1.77③
E to F	5.967 $\pm$ 0.01 6.44 $\pm$ 0.01	0.56	Max: 1.92③ Min: 1.77③

Notes: ① Tolerance from ASTM A269
② Based on bayonet tab of width of 0.25 in. centered in slot width of 0.281 in., and tolerances of +0.01 on both parts.
③ Based on 40% of gross area accounting for area of bayonet tabs and ignoring additional smaller gaps

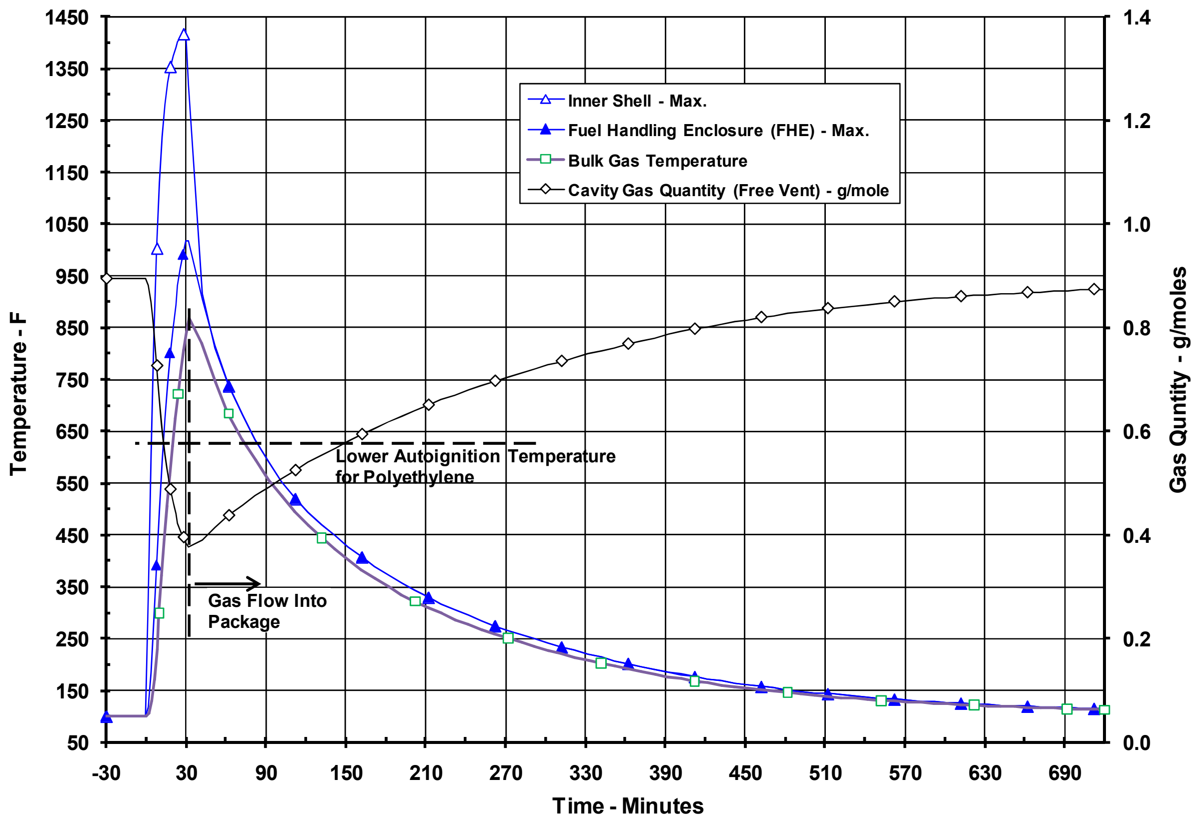

Figure 3.5-12 – Free Vent Gas Flow During HAC Transient

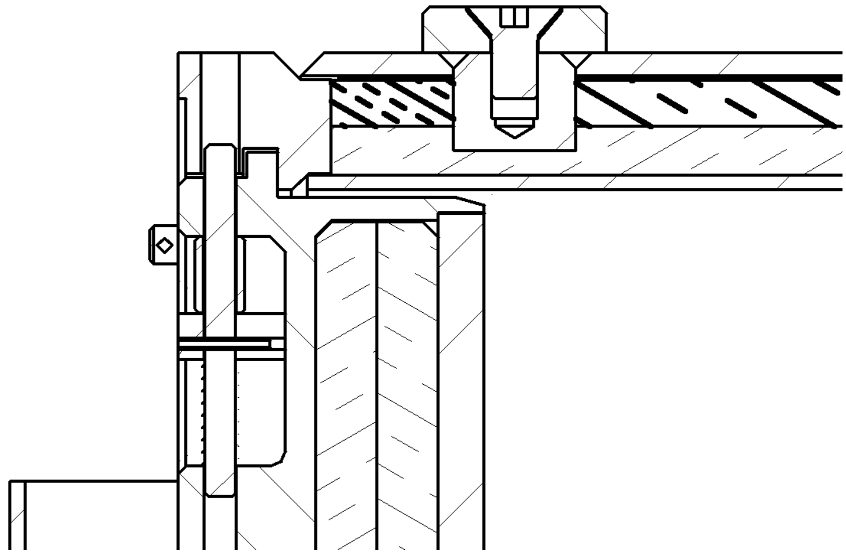

a) Package Closure

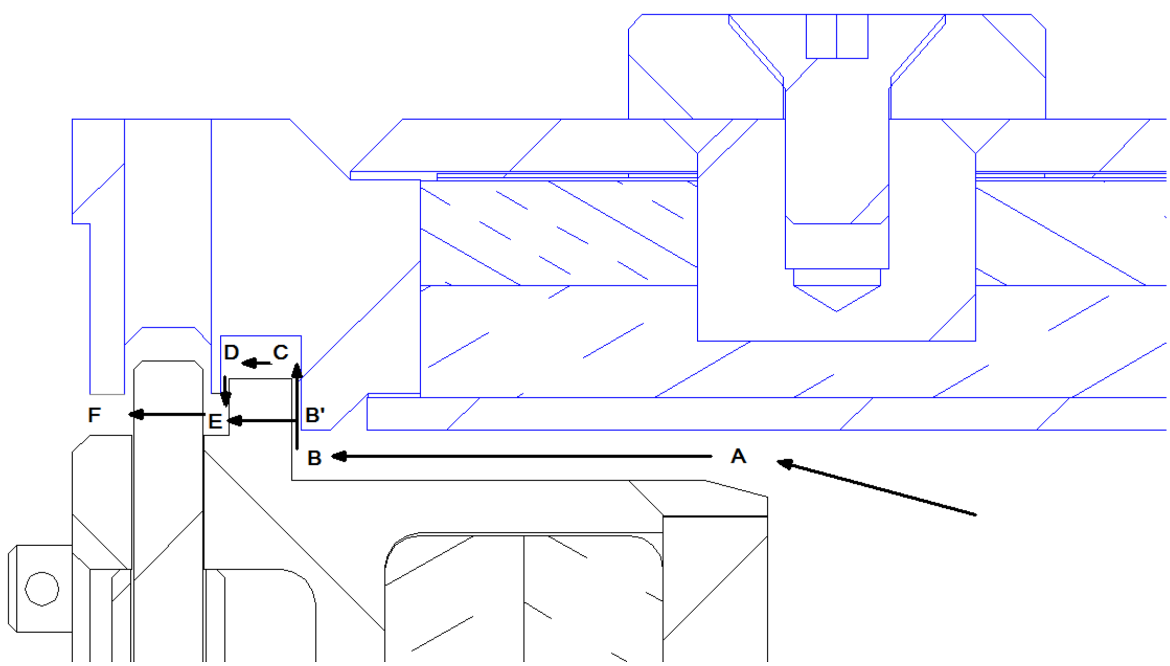

b) Enlarged Flow Paths at Package Closure

Figure 3.5-13 – Free Vent Gas Flow Path

This page intentionally left blank.

3.6 Thermal Evaluation for MIT, MURR, Cobra, and Small Quantity Payloads

This section identifies and describes the principal thermal design aspects of the ATR FFSC for the transport of one assembled MIT fuel element, one MURR fuel element, one Cobra fuel element, or small quantity payloads as described in Section 1.2.2.4, *Small Quantity Payload*. The evaluation presented herein demonstrates that the thermal performance of the ATR FFSC when transporting these payloads is bounded by the temperatures reported for the transport of the ATR fuel element payload. Specifically, the evaluations presented herein demonstrate the thermal safety of the ATR FFSC package[1] complies with the thermal requirements of 10 CFR 71[2] when transporting a payload consisting of either an assembled, unirradiated fuel element, or loose, unirradiated fuel plates, or other small quantity payloads as described in Section 1.2.2, *Contents*.

All package components are shown to remain within their respective temperature limits under the normal conditions of transport (NCT). Further, per 10 CFR §71.43(g), the maximum temperature of the accessible package surfaces is demonstrated to be less than 122 °F for the maximum decay heat loading, an ambient temperature of 100 °F, and no insolation. Finally, the ATR FFSC package is shown to retain sufficient thermal protection following the HAC free and puncture drop scenarios to maintain all package component temperatures within their respective short term limits during the regulatory fire event and subsequent package cool-down.

3.6.1 Description of Thermal Design

The ATR FFSC package, as described and illustrated in Chapter 1.0, *General Information*, consists of three basic components: 1) a Body assembly, 2) a Closure assembly, and 3) either a Fuel Handling Enclosure (FHE) or a Loose Fuel Plate Basket (LFPB). The FHE is configured to house an assembled MIT, MURR, or Cobra fuel element, while the LFPB is configured to house loose fuel element plates. The maximum gross weight of the fully loaded package is approximately 290 lbs.

The ATR FFSC is designed as a Type AF packaging. The packaging is rectangular in shape and is intended to be transported in racks of multiple packages by highway truck. Since the payload generates essentially no decay heat, the worst case thermal conditions will occur with an individual package fully exposed to ambient conditions. The package performance when configured in a rack of multiple packages will be bounded by that seen for an individual package.

The thermal design aspects of the principal components of the packaging are described in more detail in Section 3.1, *Description of Thermal Design*. The paragraphs below present the thermal design features of the MIT, MURR, RINSC, Cobra, and small quantity payloads and their associated FHEs.

3.6.2 Fuel Handling Enclosures

Fuel handling enclosures are used with the MIT, MURR, RINSC, Cobra, Small Quantity Payloads, and associated loose fuel element plates. The FHE are machined, two-piece aluminum enclosures used to protect the fuel element from damage during loading and unloading operations. The FHE consist of two identical segments machined from 6061 aluminum plate or bar stock. The FHE features neoprene rub strips to further protect the fuel. The FHE is neither anodized nor coated, but is left as unfinished aluminum. Spacer weldments on either end of the enclosure halves are used to position and support the FHE within the ATR FFSC cavity. The spacers are also fabricated of 6061 aluminum. A polyethylene bag may be used as a protective sleeve over the fuel elements. The following table presents a directory of figure depictions of the FHE and fuel elements, and design weights of the FHE. Note, the MIT, MURR, and Cobra loose fuel element plates are shipped in the Small Quantity FHE (SQFHE). Loose plates may be shipped with kraft paper and adhesive tape for property protection, and aluminum or cellulosic dunnage, as described in Section 1.2.1.1.8, *Small Quantity Payload FHE*.

Fuel	Exploded View of FHE	Fuel Element Figure	FHE Design Weight, lb
MIT	Figure 1.2-6	Figure 1.2-13	25
MURR	Figure 1.2-7	Figure 1.2-14	30
RINSC	Figure 1.2-8	Figure 1.2-15	28
Small Quantity	Figure 1.2-9	Figure 1.2-17 to Figure 1.2-20	30
Cobra	Figure 1.2-10	Figure 1.2-22	28

3.6.3 Content's Decay Heat

The ATR FFSC is designed as a Type AF packaging for transportation of an unirradiated fuel elements or a bundle of loose, unirradiated fuel plates. The decay heat associated with un-irradiated fuel is negligible. Therefore, no special devices or features are needed or utilized in the ATR FFSC packaging to dissipate the decay heat. Section 1.2.2, *Contents*, provides additional details regarding the potential contents of the ATR FFSC.

3.6.4 Summary Tables of Temperatures

Table 3.6-1 provides a summary of the maximum package component temperatures achieved under NCT and HAC conditions for either the MIT or MURR fuel element payloads. These temperatures are either bounded by or similar to those reported in Table 3.1-1 for the transport of the ATR fuel element payload. Those values unbounded by the values found in Table 3.6-1 remain well below the maximum allowable temperatures. Based on the results for the MURR fuel element, the maximum temperatures achieved under NCT and HAC conditions for the Cobra fuel element and small quantity payloads (including the RINSC fuel element) are shown by qualitative analysis below to also be bounded by the results presented in Table 3.1-1.

The MIT and MURR payload temperatures for NCT are based on an analytical model of the ATR FFSC package under extended operation with an ambient temperature of 100°F and a diurnal cycle for the insolation loading. The temperatures for HAC are based on an analytical model of the ATR FFSC package with the worst-case, hypothetical pre-fire damage as predicted based on drop tests using full-scale certification test units (CTUs). The ATR FFSC with the Cobra fuel element or small quantity payloads was not specifically modeled as part of this evaluation. Instead, their thermal performance is estimated using a qualitative approach based on the thermal characteristics of the other payloads and their associated thermal performance.

The MIT and MURR payload results for NCT demonstrate that significant thermal margin exists for all package components. This is expected since the only significant thermal loads on the package arise from insolation and ambient temperature changes. The payload dissipates essentially zero decay heat. Further, the evaluations for NCT demonstrate that the package skin temperature will be below the maximum temperature of 122°F permitted by 10 CFR §71.43(g) for accessible surface temperature in an nonexclusive use shipment when transported in a 100°F environment with no insolation. Given the significant thermal margin existing for the other payloads and the similar materials of fabrication, the Cobra fuel element and small quantity payloads are also predicted to exhibit large thermal margins.

The MIT and MURR payload results for HAC conditions demonstrate that the design of the ATR FFSC package provides sufficient thermal protection to yield component temperatures that are significantly below the acceptable limits defined for each component. While the neoprene rubber and polyethylene plastic material used to protect the fuel element from damage are expected to reach a sufficient temperature level during the HAC fire event to induce thermal decomposition, the loss of these components is not critical to the safety of the package. As demonstrated in Section 3.5.3, *Thermal Decomposition/Combustion of Package Organics*, the available oxygen in the package, plus that which may enter the package under pressure differential and gas diffusion forces, is insufficient to result in any significant heat generation due to combustion. Given the similar materials of fabrication and equivalent thermal mass as the MURR payload, the Cobra fuel element and small quantity payloads are also predicted to exhibit large thermal margins under HAC conditions.

3.6.5 Summary Tables of Maximum Pressures

Table 3.6-2 presents a summary of the maximum pressures achieved under NCT and HAC conditions. Since the ATR FFSC package is a vented package, both the maximum normal operating pressure (MNOP) and the maximum pressure developed within the payload compartment under the HAC condition are 0 psig. Section 3.5.3, *Thermal Decomposition/Combustion of Package Organics*, provides the justification for assuming a 0 psig package pressure for the HAC event.

Although the volume between the outer and inner shells is sealed, it does not contain organic or other materials that may outgas or thermally decompose. Therefore, the maximum pressure that may develop within the space will be limited to that achieved due to ideal gas expansion. The maximum pressure rise under NCT will be less than 4 psig, while the pressure rise under HAC conditions will be 39 psig.

Table 3.6-1 – Maximum Temperatures for NCT and HAC Conditions

Location / Component	NCT Hot Conditions	Accident Conditions	Maximum Allowable ①	
			Normal	Accident
Fuel Element Fuel Plate	143°F	640°F	400°F	1,100°F
Fuel Element Side Plate	143°F	644°F	400°F	1,100°F
Neoprene Rub Strips/Polyethylene Bag	143°F ②	710°F	225°F	N/A
Fuel Handling Enclosure (FHE)	143°F	710°F	400°F	1,100°F
Inner Shell	157°F	1,417°F	800°F	2,700°F
Ceramic Fiber Insulation, Body				
- Maximum	184°F	1,462°F	2,300°F	2,300°F
- Average	149°F	1,253°F	2,300°F	2,300°F
Ceramic Fiber Insulation, Closure				
- Maximum	145°F	1,402°F	2,300°F	2,300°F
- Average	143°F	1,236°F	2,300°F	2,300°F
Closure	145°F	1,439°F	800°F	2,700°F
Outer Shell	184°F	1,475°F	800°F	2,700°F

Table Notes:

① Maximum allowable temperatures are defined in Section 3.2.2, *Technical Specifications of Components*.

② Component temperature assumed to be equal to that of the FHE.

Table 3.6-2 – Summary of Maximum Pressures

Condition	Fuel Cavity Pressure	Outer/Inner Shell Cavity Pressure
NCT Hot	0 psi gauge	4 psi gauge
HAC Hot	0 psi gauge	39 psi gauge

3.6.6 Material Properties and Component Specifications

The ATR FFSC is fabricated primarily of Type 304 stainless steel, 5052-H32 and 6061-T651 aluminum, ceramic fiber insulation, and neoprene rubber. The payload materials include 6061-T6 and/or 6061-0 aluminum, uranium aluminide (UAl_x), uranium silicide (U_3Si_2), and uranium molybdenum (U-7Mo in an aluminum-silicon matrix or U-10Mo in a foil coated with thin zirconium interlayers). A polyethylene plastic bag is used as a protective sleeve over the fuel element.

3.6.6.1 Material Properties

The material specifications for the ATR FFSC package are defined in Section 3.2.1, *Material Properties*. Table 3.6-3 presents the thermal properties for 6061 aluminum used for the MIT and MURR FHEs, as taken from Table TCD of the ASME Boiler and Pressure Vessel Code[3]. Although the design permits a variety of aluminum tempers to be used, a single data set is provided since the material temper has little to no effect on its thermal properties. Further, because the HAC analysis requires thermal properties in excess of the maximum temperature point of 400°F provided in Table TCD, the property values at 1100°F (i.e., the approximate melting point for aluminum) are assumed to be the same as those at 400°F. This approach is appropriate for estimating the temperature rise within the fuel basket during the HAC event since the thermal conductivity of aluminum alloys tends to decrease with temperature while the specific heat tends to increase. The density values listed in the table are taken from an on-line database[4]. Properties between the tabulated values are calculated via linear interpolation within the heat transfer code.

Table 3.6-4 presents the thermal properties for the MIT and MURR fuel elements. For analysis purposes, the material used for the side plates and end fittings are assumed to be 6061-0 aluminum. The thermal properties for the fuel plates are determined as a composite of the cladding and the fuel core materials based on the geometry data for the MIT and MURR fuel element[39,40] and the thermal properties for the ATR fuel element materials[6]. This approach is the same as used for the ATR fuel element. The details of the computed values are presented in Appendix 3.6.9.2.3, *Determination of Composite Thermal Properties for MIT and MURR Fuel Plates*. For simplicity, the thermal properties are assumed to be constant with temperature based on the use of conservatively high thermal conductivity and conservatively low specific heat values. This approach maximizes the heat transfer into the fuel components during the HAC event, while under-estimating the ability of the components to store the heat.

The RINSC fuel elements are fabricated with a nominally 0.020-in thick mixture of uranium silicide (U_3Si_2) and aluminum powder as the fuel "meat" and a nominally 0.015-in thick aluminum alloy cladding. The twenty-two (22) flat fuel plates have a 2.8-in width, an overall length of 25-in, and an active fuel region of 22.5 to 24.0-in. These fuel plate meat and cladding

[39] *Massachusetts Institute of Technology, Test Research Training Reactor 3 Fuel Plate*, EG&G, Idaho, Inc., Drawing No. 410368, Rev. A.

[40] *University of Missouri at Columbia, Test Research Training Reactor 4 MURR Fuel Plate*, EG&G, Idaho, Inc., Drawing No. 409406, Rev. E.

thicknesses match those of the interior plates for the ATR fuel element and are similar to those for the MURR fuel plates. The side plates are fabricated of ASTM B 209, aluminum alloy 6061-T6 and 6061-T651 and are approximately 0.188-in thick. This is similar to the side plate thicknesses of the ATR, MIT, and MURR fuel elements.

The thermal conductivity of the RINSC fuel plates are similar to data obtained in the measurements of the thermal conductivities for the uranium aluminide (UAl_x) based fuels[41]. Similarly, the thermal mass of the fuel plates are comparable despite the higher density of uranium silicide versus uranium aluminide since the ratio of the specific heats of the two materials is nearly the inverse of the density ratio.

The Cobra fuel elements are fabricated with a nominally 0.025-in thick mixture of Uranium and either aluminum as UAl_x (HEU) or with silicon as U_3Si_2 (LEU) as the fuel "meat" and a nominally 0.014-in thick aluminum alloy cladding. The fuel is constructed using six concentric circular layers of fuel plates, divided into three equal segments by radial, aluminum alloy separator plates. The fuel plates are approximately 38 inches long. The entire fuel element, including aluminum alloy end fittings, is approximately 61 inches long. The diameter of the element (outside edge of the separator plates) is approximately 3.25 inches. The remarks above concerning thermal conductivity and thermal mass for the RINSC fuel elements apply to the Cobra fuel elements as well.

The additional small quantity payloads, including AFIP elements, U-Mo foils, DDEs, MIT, MURR, and Cobra loose fuel plates, and other fresh fuels with total U-235 loading ≤ 400 g and U-235 enrichment ≤ 94% are fabricated as described in Section 1.2.2.4, *Small Quantity Payload*. Small quantity payloads may be shipped with aluminum or cellulosic dunnage.

The thermal properties for air and for the non-metallic materials used in the ATR FFSC are presented in Section 3.2.1, *Material Properties*, as is the assumed emissivity (ε) for each radiating surface and the solar absorptivity (α) value for the exterior surface. The 6061-0 aluminum used for the MIT and MURR fuel components are assumed to have a surface coating of boehmite ($Al_2O_3H_2O$). A 25 μm boehmite film will exhibit a surface emissivity of approximately 0.92[13]. While a fresh fuel element may have a lower surface emissivity, the use of the higher value will provide a conservative estimate of the temperatures achieved during the HAC event.

3.6.6.2 Technical Specifications of Components

The materials used in the ATR FFSC that are considered temperature sensitive include the aluminum used for the FHEs, the LFPB, and the fuel elements, the neoprene rubber, and the polyethylene wrap used as a protective sleeve around the fuel elements. Of these materials, only the aluminum used for the fuel elements is considered critical to the safety of the package. The other materials either have temperature limits above the maximum expected temperatures or are not considered essential to the function of the package.

Section 3.2.2, *Technical Specifications of Components*, presents the basis for the temperature limits of the various components. These temperature limits are applicable to this safety

[41] IAEA-TECDOC-643, *Research Reactor Core Conversion Guidebook*, Volume 4: Fuels (Appendices I-K), International Atomic Energy Agency, Vienna, Austria.

evaluation as well.

Table 3.6-3 – Thermal Properties of Package Metallic Materials

Material	Temperature (ºF)	Thermal Conductivity (Btu/hr-ft-ºF)	Specific Heat (Btu/lb_m-ºF)	Density (lb_m/in^3)
Aluminum Type 6061-T651 / T6511	70	96.1	0.214	0.098
	100	96.9	0.216	
	150	98.0	0.220	
	200	99.0	0.222	
	250	99.8	0.224	
	300	100.6	0.227	
	350	101.3	0.230	
	400	101.9	0.231	
	1100 ①	101.9	0.231	

Notes:

① Values for 1100°F are assumed equal to values at 400°F.

Table 3.6-4 – Thermal Properties of MIT and MURR Fuel Materials

Material	Temperature (°F)	Thermal Conductivity (Btu/hr-ft-°F)	Specific Heat (Btu/lb_m-°F)	Density (lb_m/in^3)
Aluminum Type 6061-0	32	102.3	-	0.0976
	62	-	0.214	
	80	104.0	-	
	170	107.5	-	
	260	109.2	0.225	
	350	109.8	-	
	440	110.4	0.236	
	530	110.4	-	
	620	109.8	0.247	
	710	108.6	-	
	800	106.9	0.258	
	890	105.2	-	
	980	103.4	0.269	
	1080	101.1	0.275	
MURR Fuel Plate①	80	57.9	0.165	0.121
	800		0.200	
MIT Fuel Plate①	80	72.6	0.176	0.115
	800		0.212	

Notes:

① Values determined based on composite value of aluminum cladding and fuel core material (see Appendix 3.5.2.4). Thermal conductivity value is valid for axial and circumferential heat transfer within fuel plate.

3.6.7 Thermal Evaluation for Normal Conditions of Transport

The ATR FFSC with the MIT or MURR fuel element payloads is transported horizontally under normal conditions of transport (NCT). This establishes the orientation of the exterior surfaces of the package for determining the free convection heat transfer coefficients and insolation loading. While the package would normally be transported in tiered stacks of multiple packages, the evaluation for NCT is conservatively based on a single, isolated package since this approach will yield the bounding maximum and minimum temperatures achieved by any of the packages. Further, since the surface of the transport trailer is conservatively assumed to prevent heat exchange between the package and the ambient, the bottom of the ATR FFSC is treated as an adiabatic surface.

The details of the thermal modeling used to simulate the ATR FFSC package under NCT conditions are provided in Appendix 3.5.2, *Analytical Thermal Model*, while details of the thermal modeling of the MIT and MURR FHEs and fuel elements are provided in Appendix 3.6.9.2.1, *Description of MIT and MURR Payload Thermal Models for NCT Conditions*. The ATR FFSC with Cobra fuel elements or small quantity payloads was not specifically modeled as part of this evaluation. Instead, their thermal performance is estimated using a qualitative approach based on the thermal characteristics of the other payloads and their associated thermal performance. See below for the details of this qualitative basis.

3.6.7.1 Heat and Cold

3.6.7.1.1 Maximum Temperatures

The maximum temperature distribution for the ATR FFSC occurs with a diurnal cycle for insolation loading and an ambient air temperature of 100°F, per 10 CFR §71.71(c)(1). The evaluation of this condition is conducted as a transient using the thermal model of an undamaged ATR FFSC described in Appendix 3.6.9.2.1, *Description of MIT and MURR Payload Thermal Models for NCT Conditions*. Figure 3.6-1 illustrates the expected heat-up transient for an ATR FFSC loaded with a MIT fuel element. The transient analysis assumes a uniform temperature condition of 70ºF for all components prior to loading and exposure to the specified NCT condition at time = 0.

The figures demonstrate that the ATR FFSC package will respond rapidly to changes in the level of insolation and will reach it peak temperatures within the first day or two after loading. The higher thermal mass of the MIT FHE on a unit length basis versus that of the ATR FHE is reflected in the delayed response of the MIT FHE to changes in the inner shell temperature, whereas the ATR FHE was seen in Figure 3.3-1 to respond more rapidly. A similar temperature response curve is seen for the MURR FHE.

Table 3.6-5 presents the maximum temperatures reached for various components of the package. As seen from the table, all components are within in their respective temperature limits. Figure 3.6-2 illustrates the predicted temperature distribution within the ATR FFSC package with a MIT fuel element payload at the end of the evaluated transient heat up period and near the time of peak temperature. Figure 3.6-3 presents the temperature distribution within the ATR FFSC package with a MURR fuel element payload.

The maximum temperature distribution for the ATR FFSC without insolation loads occurs with an ambient air temperature of 100°F. Since the package payload dissipates essentially zero watts of decay heat, the thermal analysis of this condition represents a trivial case and no thermal calculations are performed. Instead, it is assumed that all package components achieve the 100°F temperature under steady-state conditions. The resulting 100°F package skin temperature is below the maximum temperature of 122°F permitted by 10 CFR §71.43(g) for accessible surface temperature in a nonexclusive use shipment.

The ATR FFSC with the small quantity payload was not specifically modeled as part of this evaluation. Instead, its thermal performance is estimated using a qualitative approach based on the thermal characteristics of the other payloads and their associated thermal performance. Using this approach, it is estimated that the maximum temperatures attained for the transportation of the small quantity payload within the ATR FFSC will be bounded by that presented for the MURR payload. This conclusion is based on the facts that the combined weight of the small quantity payload and MURR FHE's with their enclosed fuel elements, plates, or foils are similar (see Section 1.2.2.3, *MURR Fuel Element*, and Section 1.2.2.4, *Small Quantity Payload*), the FHE's are both fabricated of 6061 aluminum, and the fuel elements have similar thermal properties (see Section 3.6.6.1). This conclusion is further supported by the fact that Table 3.6-5 demonstrates that the MIT and MURR fuel elements produce essentially the same peak NCT temperatures despite their design differences. As such, the limited design differences between the MURR and small quantity payloads will not yield a significant difference in their NCT thermal response.

The ATR FFSC with the RINSC fuel element payload and the Cobra fuel element payload are not specifically modeled as part of this evaluation. Instead, their thermal performance is estimated using a qualitive approach based on the thermal characteristics of the other payloads and their associated thermal performance. (See Section 3.6.9.2.4, *Determination of Thermal Properties for RINSC Element* and Section 3.6.9.2.5, *Determination of Thermal Properties for Cobra Element* for details). Using this approach, it is estimated that the maximum temperatures attained for the transportation of the RINSC and Cobra fuel elements are considered bounded by the analysis of the MURR payload and no additional analysis is required.

3.6.7.1.2 Minimum Temperatures

The minimum temperature distribution for the ATR FFSC occurs with a zero decay heat load and an ambient air temperature of -40°F per 10 CFR §71.71(c)(2). The thermal analysis of this condition also represents a trivial case and no thermal calculations are performed. Instead, it is assumed that all package components achieve the -40°F temperature under steady-state conditions. As discussed in Section 3.2.2, *Technical Specifications of Components*, the -40°F temperature is within the allowable operating temperature range for all ATR FFSC package components.

3.6.7.2 Maximum Normal Operating Pressure

The payload cavity of the ATR FFSC is vented to the atmosphere. As such, the maximum normal operating pressure (MNOP) for the package is 0 psig.

While the volume between the outer and inner shells is sealed, it does not contain organic or other materials that may outgas or thermally decompose. Therefore, the maximum pressure that may develop within the space will be limited to that achieved due to ideal gas expansion.

Assuming a temperature of 70°F at the time of assembly and a maximum operating temperature of 190°F (based on the outer shell temperature, see Table 3.6-5, conservatively rounded up), the maximum pressure rise within the sealed volume will be less than 4 psi.

Table 3.6-5 - Maximum Package NCT Temperatures

Location / Component	MIT Fuel Payload	MURR Fuel Payload	Maximum Allowable ①
Fuel Element Fuel Plate	143°F	142°F	400°F
Fuel Element Side Plate	143°F	142°F	400°F
Neoprene Rub Strips/Polyethylene Bag	143°F ②	142°F ②	225°F
Fuel Handling Enclosure (FHE)	143°F	142°F	400°F
Inner Shell	157°F	157°F	800°F
Ceramic Fiber Insulation, Body			
- Maximum	184°F	184°F	2,300°F
- Average	149°F	148°F	2,300°F
Ceramic Fiber Insulation, Closure			
- Maximum	145°F	145°F	2,300°F
- Average	143°F	143°F	2,300°F
Closure	145°F	145°F	800°F
Outer Shell	184°F	184°F	800°F

Table Notes:
① The maximum allowable temperatures under NCT conditions are provided in Section 3.2.2, *Technical Specifications of Components*.
② Component temperature assumed to be equal to that of the FHE.

.

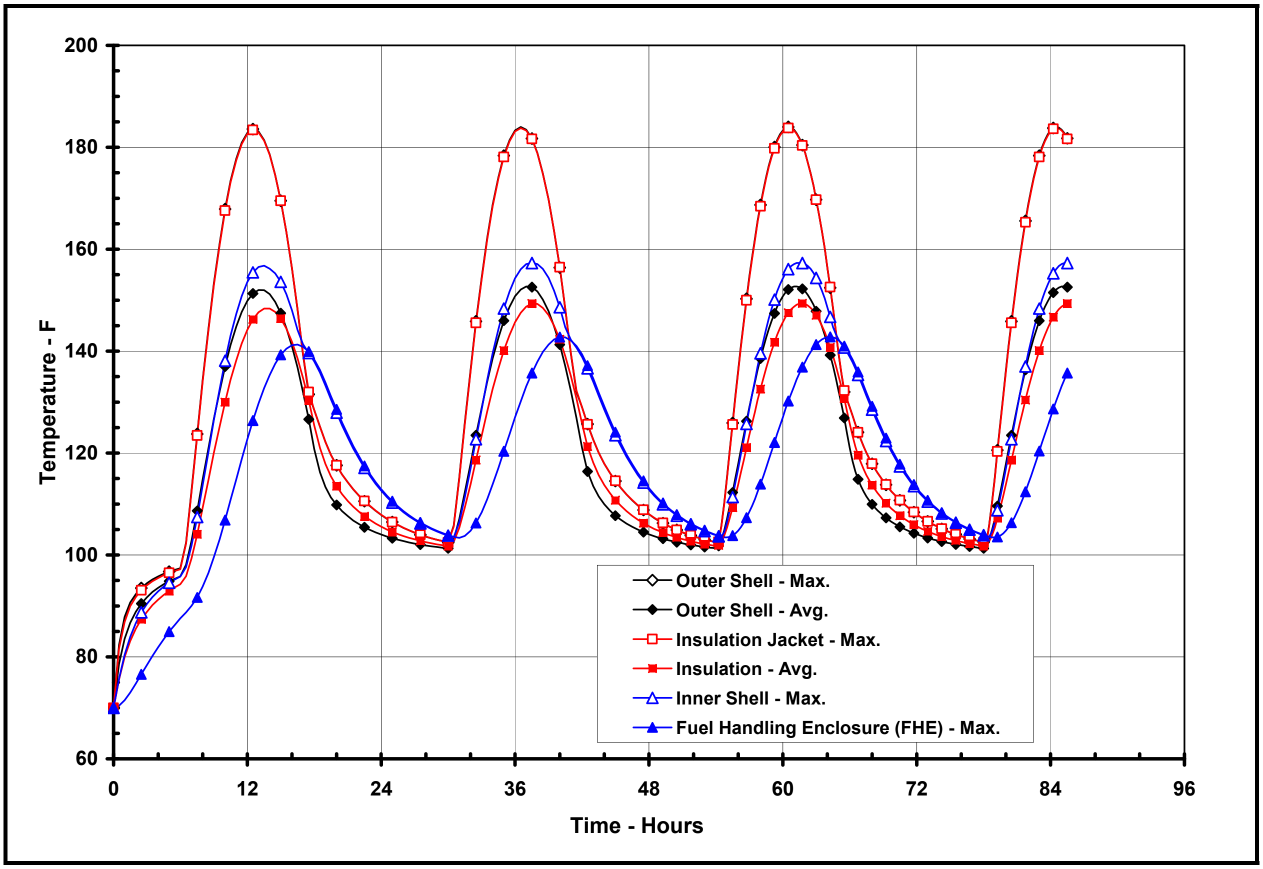

Figure 3.6-1 – ATR FFSC Package Heat-up with MIT Payload, NCT Hot Conditions

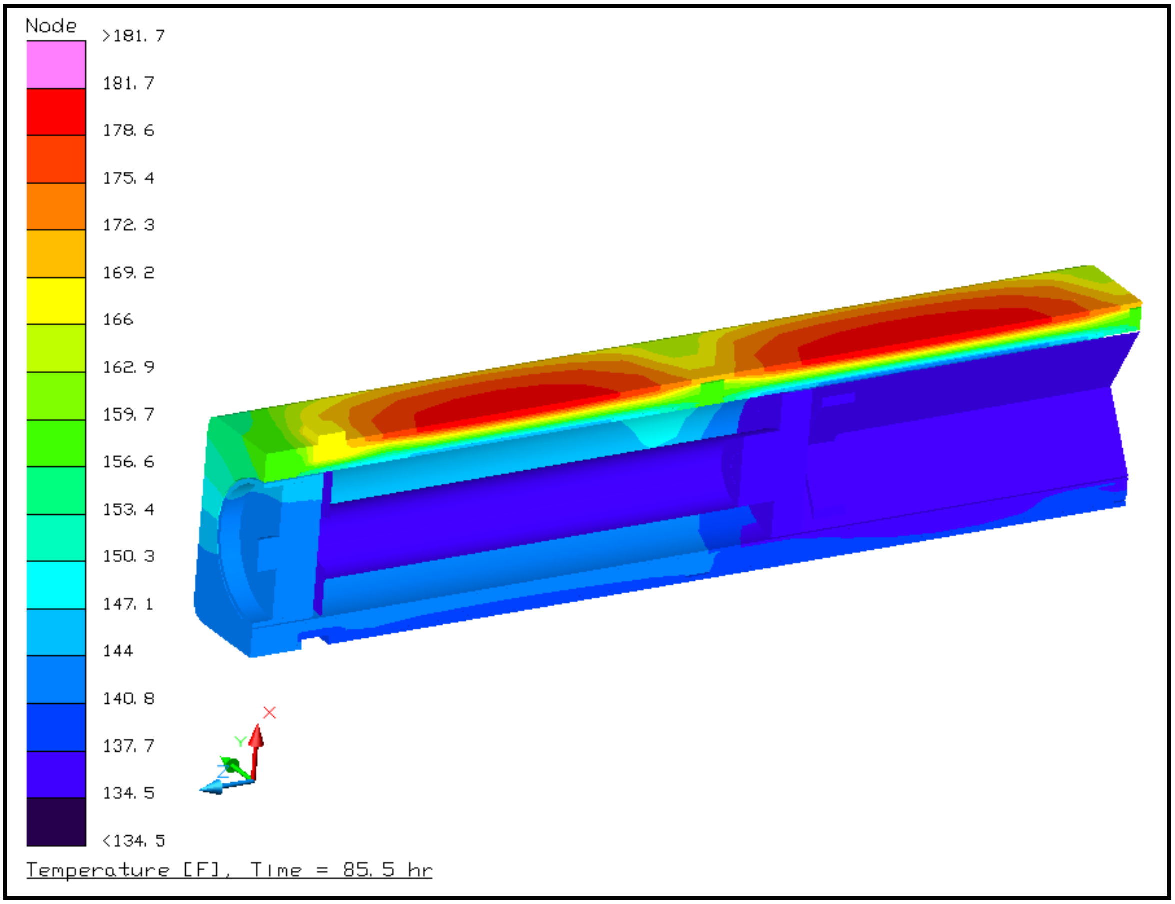

Figure 3.6-2 – Package NCT Temperature Distribution for MIT Payload

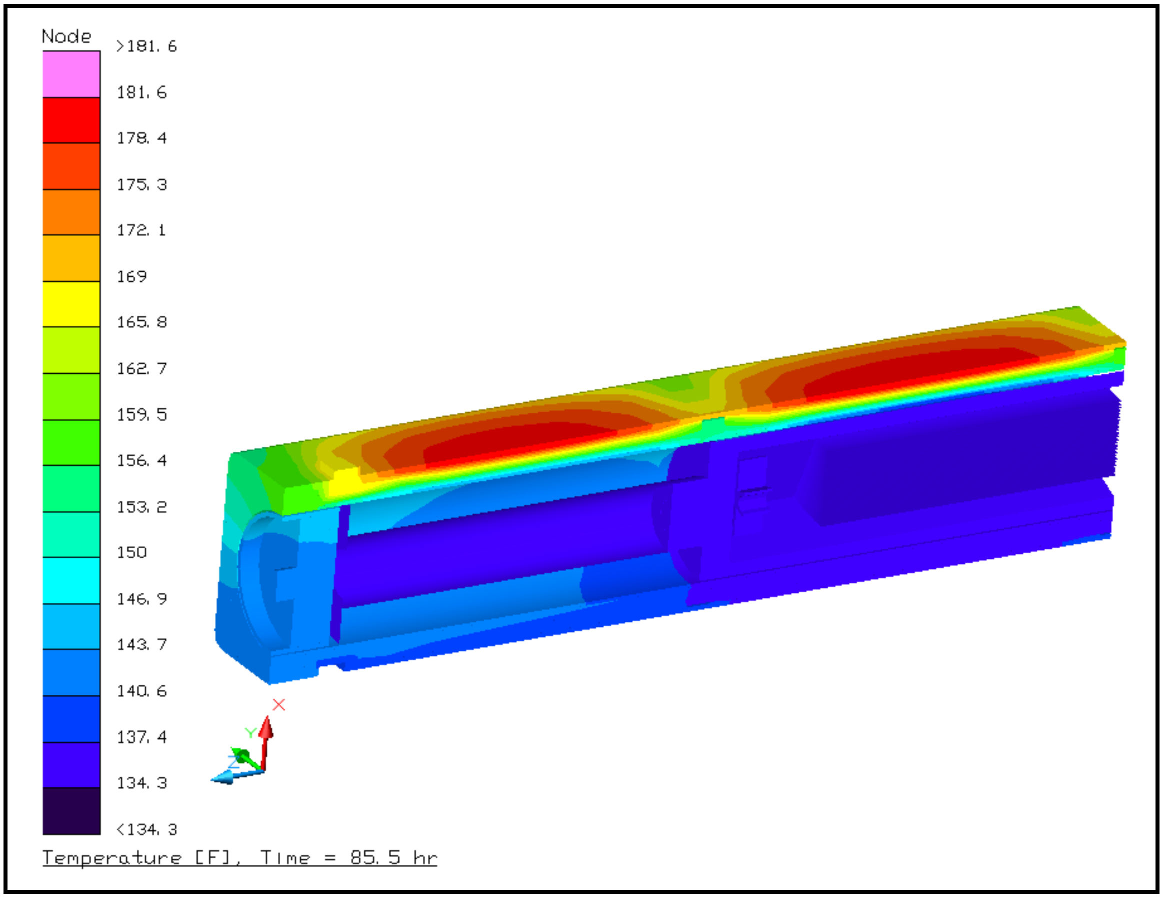

Figure 3.6-3 – Package NCT Temperature Distribution for MURR Payload

3.6.8 Thermal Evaluation for Hypothetical Accident Conditions

This section presents the thermal evaluation of the ATR FFSC package under the hypothetical accident condition (HAC) specified in 10 CFR §71.73(c)(4)[2] based on an analytical thermal model. The analytical model of the ATR FFSC for HAC is a modified version of the quarter symmetry NCT model described in Appendix 3.5.2.1, *Description of Thermal Model for NCT Conditions*, with the principal model modifications consisting of simulating the expected package damage resulting from the drop events that are assumed to precede the HAC fire and changing the package surface emissivities to reflect the assumed presence of soot and/or surface oxidization. The analytical model of the MIT and MURR fuel elements are the same as those described in Appendix 3.6.9.2.1, *Description of MIT and MURR Payload Thermal Models for NCT Conditions*. The evaluations of the ATR FFSC with a small quantity payload and RINSC and Cobra payloads under HAC conditions are accomplished using a qualitative approach in the same manner as accomplished for NCT conditions (see Section 3.6.7.1.1, *Maximum Temperatures*).

Physical testing using full scale certified test units (CTUs) is used to establish the expected level of damage sustained by the ATR FFSC package from the 10 CFR 71.73 prescribed free and puncture drops that are assumed to precede the HAC fire event. Appendix 3.5.2.2, *Description of Thermal Model for HAC Conditions*, provides an overview of the test results, the rationale for selecting the worst-case damage scenario, and the details of the thermal modeling used to simulate the package conditions during the HAC fire event.

3.6.8.1 Initial Conditions

The initial conditions assumed for the package prior to the HAC event are described below in terms of the modifications made to the NCT thermal model to simulate the assumed package conditions prior to and during the HAC event. These modifications are:

- Simulated the worst-case damage arising from the postulated HAC free and puncture drops as described in Appendix 3.5.2.2, *Description of Thermal Model for HAC Conditions*,
- Assume an initial, uniform temperature distribution of 100ºF based on a zero decay heat package at steady-state conditions with a 100ºF ambient with no insolation. This assumption complies with the requirement of 10 CFR §71.73(b)[2] and NUREG-1609[17],
- Increased the emissivity of the external surfaces from 0.45 to 0.8 to account for possible soot accumulation on the surfaces, per 10 CFR §71.73(c)(4),
- Increased the emissivity of the interior surfaces of the outer shell from 0.30 to 0.45 to account for possible oxidization of the surfaces during the HAC event,

Following the free and puncture bar drops, the ATR FFSC package is assumed come to rest in a horizontal position prior to the initiation of the fire event. Given that the package geometry is essentially symmetrical about its axial axis, there are no significant thermal differences whether the package is right-side up, up-side down, or on its side. The MIT, MURR, RINSC, Cobra, and small quantity payloads are not expected to be re-positioned as a result of the pre-fire drop and puncture bar events based on the limited damage seen for the ATR FHE as a result of the drop tests conducted on the ATR FFSC presented in Section 2.12.1, *Certification Tests on CTU-1*, and given the greater robustness of the MIT, MURR, RINSC, Cobra, and small quantity payload FHEs. However, even if the end spacers are conservatively assumed to buckle as a result of the HAC drop event, no significant temperature increase will occur since direct contact between the FHE and the closure plug will be prevented and because the average radial heat transfer through the sides of the package does not change significantly as a function of axial position. Therefore, the peak package temperatures predicted under this evaluation based on no payload re-positioning or reconfiguration are representative of those achieved for any package orientation and/or credible re-positioning of the enclosed payloads.

3.6.8.2 Fire Test Conditions

The fire test conditions analyzed to address the 10 CFR §71.73(c) requirements are as follows:

- The initial ambient conditions are assumed to be 100ºF ambient with no insolation,
- At time = 0, a fully engulfing fire environment consisting of a 1,475ºF ambient with an emissivity of 1.0 is used to simulate the hydrocarbon fuel/air fire event. The assumption of a flame emissivity of 1.0 bounds the minimum average flame emissivity coefficient of 0.9 specified by 10 CFR §71.73(c)(4),
- The convection heat transfer coefficients between the package and the ambient during the 30-minute fire event are based on an average gas velocity[18] of 10 m/sec. Following the 30-minute fire event the convection coefficients are based on still air,
- The ambient condition of 100ºF with insolation is assumed following the 30-minute fire event. Since a diurnal cycle is used for insolation, the evaluation assumes that the 30-minute fire begins at noon so as to maximize the insolation heating during the post-fire cool down period. A solar absorptivity of 0.9 is assumed for the exterior surfaces to account for potential soot accumulation on the package surfaces.

The transient analysis is continued for 11.5 hours after the end of the 30-minute fire to ensure that the peak package temperatures are captured.

3.6.8.3 Maximum Temperatures and Pressure

3.6.8.3.1 Maximum HAC Temperatures

The thermal performance of the ATR FFSC package loaded with a MIT fuel element payload is summarized in Table 3.6-6, while Table 3.6-7 presents a summation of the results with a MURR fuel element payload. With the exception of the neoprene rub strips and the polyethylene bag used as a protective sleeve around the fuel elements, all other components of the package are seen to remain well below their allowable short term temperature limits. As with the ATR payload, the thermal decomposition of the neoprene strips and polyethylene bag will not impact the safety of the package and any associated out-gassing will not contribute to package pressurization since the package is vented. As demonstrated in Section 3.5.3, *Thermal Decomposition/Combustion of Package Organics*, the available oxygen in the package is sufficient for consumption of less than 1% of the polyethylene and the quantity of air that enters the cavity under pressure differential and gas diffusion forces is insignificant. The discussion in Section 3.5.3 also provides validation of a 0 psig package pressure for the HAC event.

The outer shell and the ceramic fiber insulation provide thermal protection to the ATR FFSC package during the HAC fire event. The level of thermal protection can be seen via the thermal response curves presented in Figure 3.6-4 and Figure 3.6-5 for the ATR FFSC package loaded with a MIT and MURR fuel element payload, respectively. As seen from the figures, while the exterior of the package quickly rises to nearly the temperature of the fire, the heat flow to the FHE and its enclosed fuel element payloads is sufficiently restricted to limit the maximum temperatures of both the FHE and the fuel element to well below the melting point of aluminum. The higher thermal mass of the MIT and MURR FHEs in comparison with that of the ATR FHE is reflected in their correspondingly slower heat up and longer cool down during the fire transient when compared to that see in Figure 3.4-1 for the ATR FHE. The higher temperature reached by the MURR FHE versus that seen for the MIT FHE is due to the conservative assumption of direct contact between the FHE and the inner shell along two line locations for the MURR FHE versus one line location for the MIT FHE. Similarly, the difference in the shape of the FHE temperature response curve seen for the MIT FHE between 30 minutes and 60 minutes versus that seen for the MURR FHE for the same time period is related to the fact that the top end of the shorter MIT FHE lies below one of the package's support ribs while the top of the MURR FHE is adjacent to it (see Figures 3.6-6 and 3.6-7).

Although the peak temperature achieved by the MURR FHE is about 20ºF hotter than that achieved by the MIT FHE, the peak temperatures reached by the MIT and MURR fuel elements are approximately the same. This results from a combination of the higher thermal mass and greater separation distance between the end of the fuel element and the start fuel plates associated with the MURR fuel element versus that for the MIT fuel element.

The results demonstrate that thermal performance is similar to that achieved with the transport of a LFPB payload (see Section 3.4.3, *Maximum Temperature and Pressure*) due to the fact that these FHE have a thermal mass similar to that of the LFPB. The result of the higher thermal mass is that the MIT and MURR FHEs have a peak temperature that is approximately 300ºF cooler than that seen for the ATR FHE and the enclosed fuel elements reach peak temperatures that are 90 to 180ºF cooler than that seen for the ATR fuel element. The thermal performance of the ATR FFSC packaging with either the MIT or MURR payload is similar to that seen for the ATR payload.

The results presented above also demonstrate that inclusion of insolation effects prior to the fire would not have affected the safety basis of the design. As documented in Section 3.4.3.1, *Maximum HAC Temperatures*, consideration of the maximum insolation loading raises the package component temperatures by approximately 50°F above the initial 100°F level assumed by the HAC evaluation. Since all package components exhibit thermal margins significantly greater than 50°F, the inclusion of insolation effects prior to the fire event would not have impacted the safety basis for the design.

As with the evaluation for NCT, the thermal performance of the ATR FFSC with the small quantity payload, RINSC, and Cobra fuel elements under HAC conditions was not specifically modeled as part of this evaluation. Instead, based on the similarity between the MURR and small quantity payloads, the thermal performance is qualitatively estimated to be bounded by that presented for the MURR payload. Since the combined weight of the small quantity payload and MURR FHE's with their enclosed fuel elements, plates, or foils are similar (see Section 1.2.2.3, *MURR Fuel Element*, and Section 1.2.2.4, *Small Quantity Payload*) and the thermal mass of the two payloads are similar, the transient response of the small quantity payload can be expected to be similar to that presented for the MURR payload. This conclusion is further supported by the fact that Table 3.6-6 and Table 3.6-7 show that similar transient results occur for the MIT and MURR fuel element payloads despite their design differences. As such, the limited design differences between the MURR and small quantity payloads will not yield a significant difference in their HAC thermal response. This same logic applies to the RINSC and Cobra fuel elements as further discussed in Section 3.6.9.2.4, *Determination of Thermal Properties for RINSC Element* and Section 3.6.9.2.5, *Determination of Thermal Properties for Cobra Element*. Additionally, the SQFHE thermal response without its small quantity payload is expected to be similar with the conservative ATR LFPB thermal response. The empty SQFHE and LFPB are constructed of similar materials and have the same thermal mass of 30 lbs. The LFPB thermal evaluation is conservatively performed without its loose fuel plate payload, see Sections 3.4.3.1 and 3.5.2.1 for discussion of the LFPB thermal evaluation. Therefore, use of the SQFHE for any payload amount up to the maximum loaded SQFHE weight of 50 lbs is bounded by the thermal response of the LFPB evaluation. The addition of any small quantity payload mass to the SQFHE will increase the thermal mass and thereby increase the conservatism of the thermal response with respect to the empty LFPB thermal evaluation results.

3.6.8.3.2 Maximum HAC Pressures

The payload cavity of the ATR FFSC is vented to the atmosphere. As such, the maximum pressure achieved under the HAC event will be 0 psig. Section 3.5.3, *Thermal Decomposition/Combustion of Package Organics*, provides the justification for assuming a 0-psig package pressure for the HAC event.

Although the volume between the outer and inner shells is sealed, it does not contain organic or other materials that may outgas or thermally decompose. Assuming a temperature of 70°F at the time of assembly and a maximum temperature of 1,475°F (based on the outer shell temperature, see Table 3.6-6), the maximum pressure rise within the sealed volume due to ideal gas expansion will be less than 39 psig. This level of pressurization will occur for only a few minutes and then quickly reduce as the package cools.

3.6.8.4 Maximum Thermal Stresses

The ATR FFSC package is fabricated principally of sheet metal and relatively thin structural steel shapes. As such, the thermal stresses developed within each component during the HAC fire event will be low and not significant to the safety of the package.

The temperature difference that exists between the inner and outer shells during the HAC event (see the average inner and outer shell temperatures presented in Figure 3.6-4) will result in differential thermal expansion between the shells. The thermal impact related to the potential package geometry displacement due to this differential thermal expansion was evaluated in

Section 3.4.4, *Maximum Thermal Stresses*, and found not to be significant to the safety of the package.

Table 3.6-6 – HAC Temperatures with MIT Payload

Location / Component	Pre-fire	End of Fire	Peak	Maximum Allowable ①
MIT Fuel Element Fuel Plate	100°F	345°F	640°F	1,100°F
MIT Fuel Element Side Plate	100°F	346°F	643°F	1,100°F
Neoprene Rub Strips/Polyethylene Bag	100°F	599°F	690°F	N/A
Fuel Handling Enclosure (FHE)	100°F	599°F	690°F	1,100°F
Inner Shell	100°F	1,417°F	1,417°F	2,700°F
Ceramic Fiber Insulation, Body				
- Maximum	100°F	1,462°F	1,462°F	2,300°F
- Average	100°F	1,253°F	1,253°F	2,300°F
Ceramic Fiber Insulation, Closure				
- Maximum	100°F	1,401°F	1,401°F	2,300°F
- Average	100°F	1,233°F	1,233°F	2,300°F
Closure	100°F	1,439°F	1,439°F	2,700°F
Outer Shell	100°F	1,475°F	1,475°F	2,700°F

Table Notes:

① The maximum allowable temperatures under HAC conditions are provided in Section 3.2.2, *Technical Specifications of Components*.

Table 3.6-7 – HAC Temperatures with MURR Payload

Location / Component	Pre-fire	End of Fire	Peak	Maximum Allowable ①
MURR Fuel Element Fuel Plate	100°F	371°F	636°F	1,100°F
MURR Fuel Element Side Plate	100°F	380°F	644°F	1,100°F
Neoprene Rub Strips/Polyethylene Bag	100°F	648°F	710°F	N/A
Fuel Handling Enclosure (FHE)	100°F	648°F	710°F	1,100°F
Inner Shell	100°F	1,417°F	1,417°F	2,700°F
Ceramic Fiber Insulation, Body - Maximum - Average	 100°F 100°F	 1,462°F 1,222°F	 1,462°F 1,222°F	 2,300°F 2,300°F
Ceramic Fiber Insulation, Closure - Maximum - Average	 100°F 100°F	 1,402°F 1,236°F	 1,402°F 1,236°F	 2,300°F 2,300°F
Closure	100°F	1,439°F	1,439°F	2,700°F
Outer Shell	100°F	1,475°F	1,475°F	2,700°F

Table Notes:

① The maximum allowable temperatures under HAC conditions are provided in Section 3.2.2, *Technical Specifications of Components*.

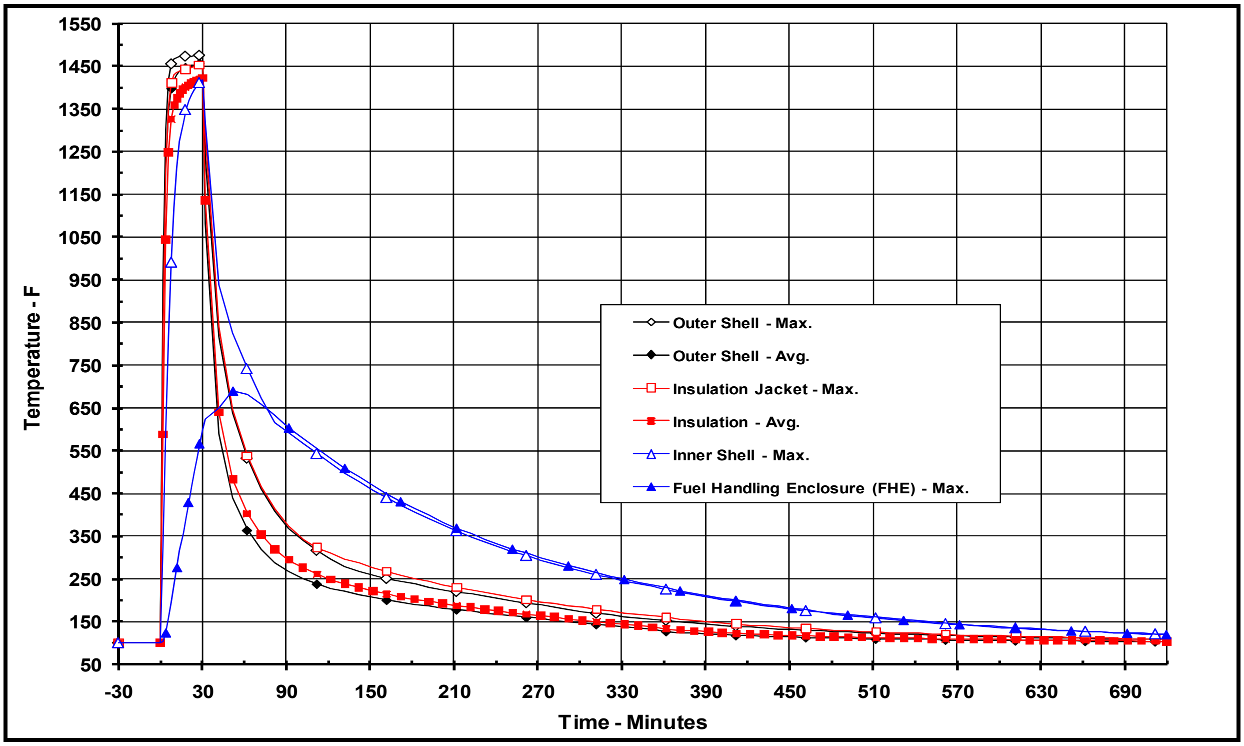

Figure 3.6-4 – ATR FFSC Package Thermal Response to HAC Event with MIT Payload

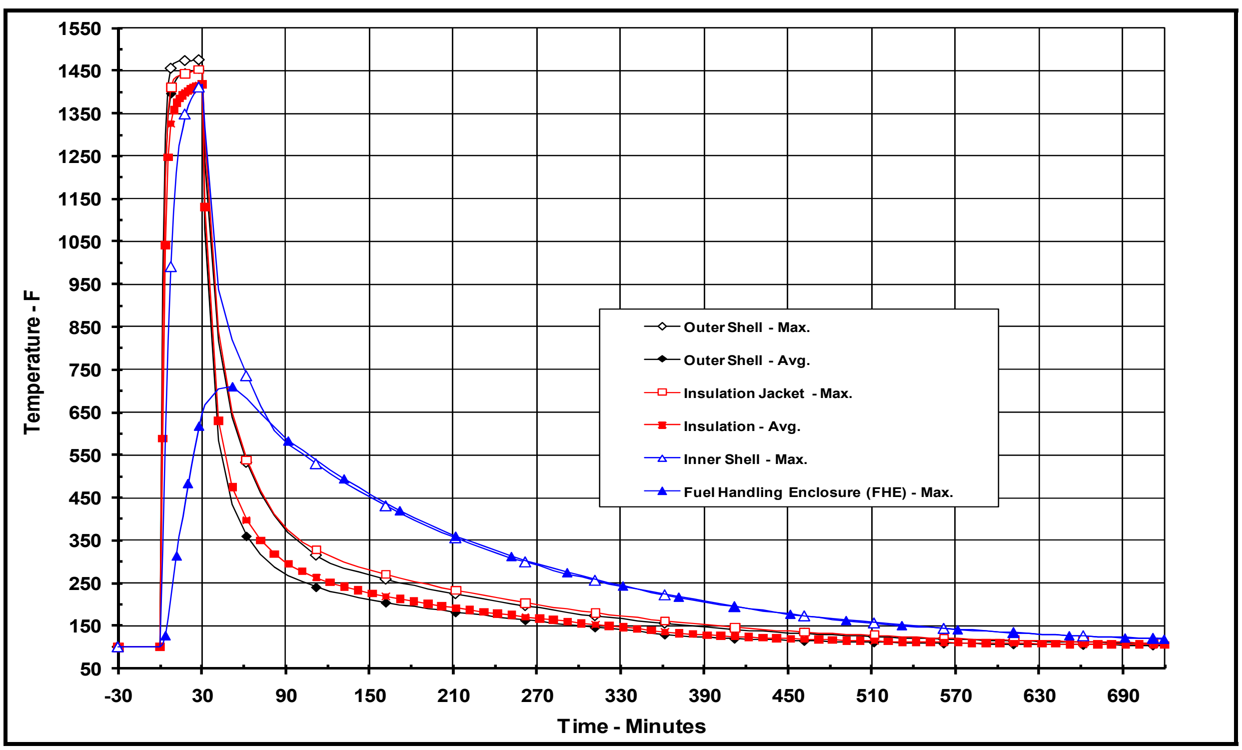

Figure 3.6-5 – ATR FFSC Package Thermal Response to HAC Event with MURR Payload

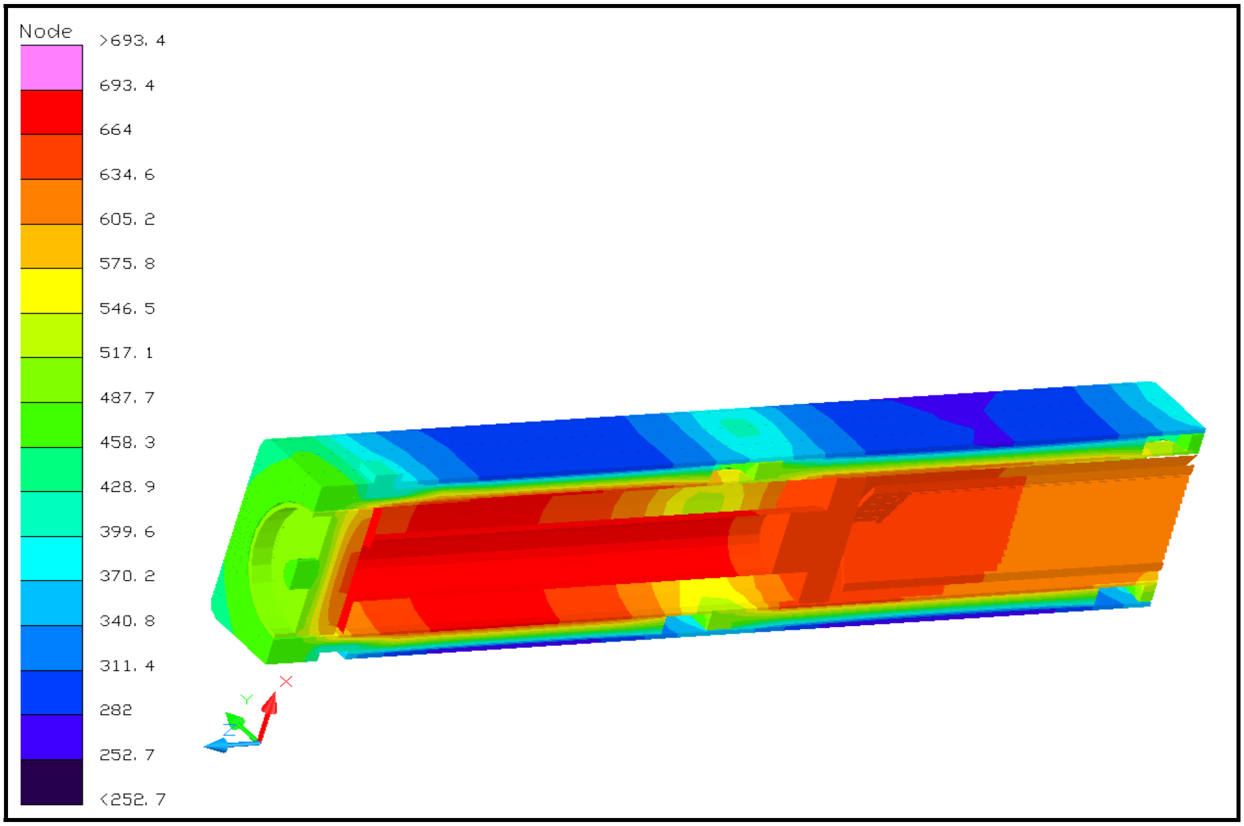

(Note: the positive x-axis is oriented towards the top of the package and the positive z-axis towards the package closure end)

Figure 3.6-6 –Temperature Distribution at Time of Peak MIT Fuel Element Temperature

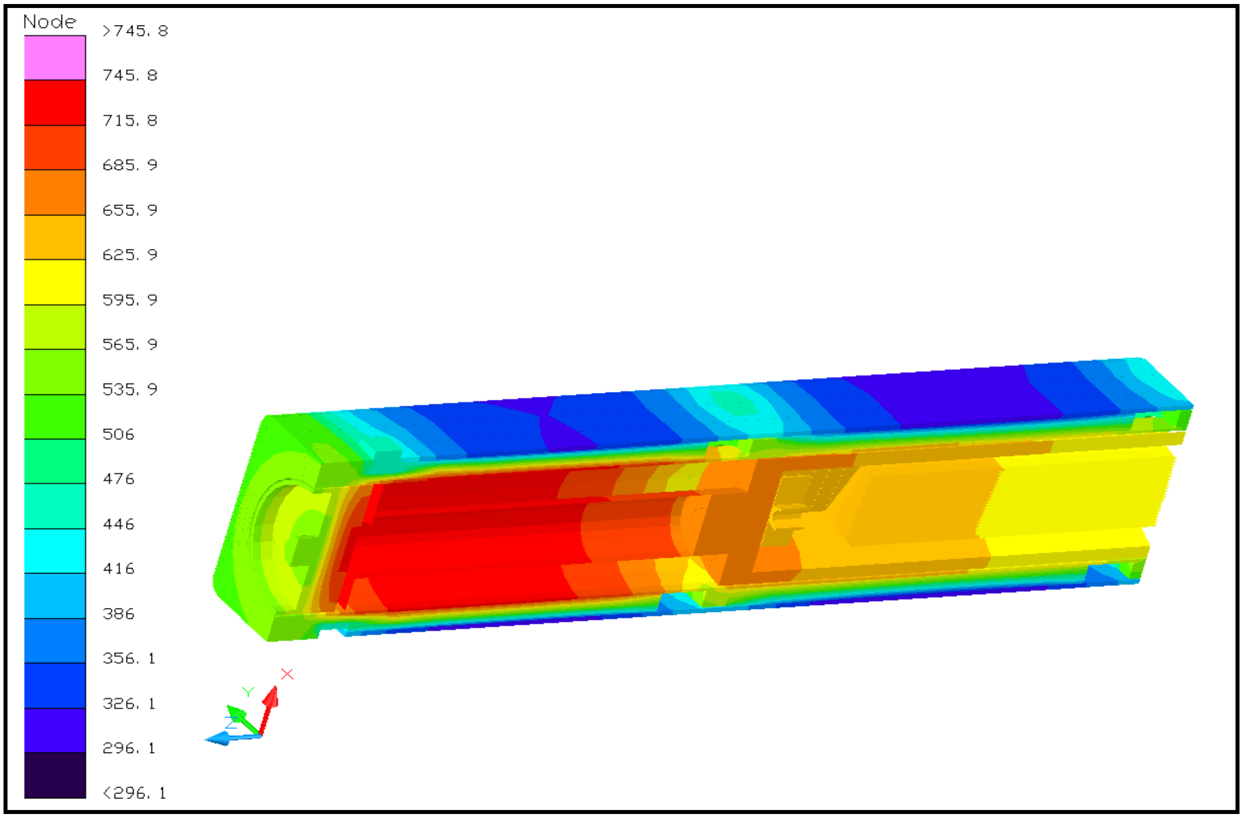

(Note: the positive x-axis is oriented towards the top of the package and the positive z-axis towards the package closure end)

Figure 3.6-7 –Temperature Distribution at Time of Peak MURR Fuel Element Temperature

3.6.9 Appendices

3.6.9.1 Computer Analysis Results

3.6.9.2 Analytical Thermal Model

3.6.9.1 Computer Analysis Results

Due to the size and number of the output files associated with each analyzed condition, results from the computer analysis are provided on a CD-ROM.

3.6.9.2 Analytical Thermal Model

The analytical thermal model of the ATR FFSC package and the MIT and MURR fuel element payloads were developed for use with the Thermal Desktop®[20] and SINDA/FLUINT[21] computer programs. These programs are designed to function together to build, exercise, and post-process a thermal model. Appendix 3.5.2, *Analytical Thermal Model*, provides an overview of the capability and functionality of these programs. The SINDA/FLUINT and Thermal Desktop® computer programs have been validated for safety basis calculations for nuclear related projects[22]. The ATR FFSC with the small quantity payload was not specifically modeled as part of this evaluation. Instead, its thermal performance is estimated using a qualitative approach based on the thermal characteristics of the other payloads and their associated thermal performance.

3.6.9.2.1 Description of MIT and MURR Payload Thermal Models for NCT Conditions

A 3-dimensional, one-quarter symmetry thermal model of the ATR FFSC is used for the NCT evaluation. The model simulates one-quarter of the package, extending from the closure to the axial centerline of the package. Symmetry conditions are assumed about the package's vertical axis and at the axial centerline. This modeling choice captures the full height of the package components and allows the incorporation of the varying insolation loads that will occur at the top and sides of the package. Program features within the Thermal Desktop® computer program automatically compute the various areas, lengths, thermal conductors, and view factors involved in determining the individual elements that make up the thermal model of the complete assembly. Details of the thermal modeling of the ATR FFSC packaging are provided in Appendix 3.5.2.1, *Description of Thermal Model for NCT Conditions*.

A detailed model of the MIT and MURR fuel elements are used to simulate the heat transfer within the fuel elements and between the fuel element and their associated FHEs and spacer weldments. The detailed thermal models, illustrated in Figure 3.6-8 to Figure 3.6-13, include a separate representation of each composite fuel plate, the side plates, and the end fittings. Heat transfer between the individual fuel plates is simulated via conduction and radiation across the air space separating the plates. The curvature and separation distance between the plates is based on the information presented in Appendix 3.6.9.2.3, *Determination of Composite Thermal Properties for MIT and MURR* Fuel Plates.

The thermal modeling for the MIT fuel element and FHE is similar to that described for the ATR fuel element payload. Figure 3.6-8 illustrates the quarter symmetry thermal model of the MIT FHE and one of the two spacer weldments. The FHE thermal model uses planar elements to represent the 0.19 inch thick sides of the enclosure and the 0.25 inch thick elements of the spacer weldment. Solid elements are used to represent the ends of the FHE. Heat transfer between the FHE and the inner shell of the package is modeled as a combination of radiation and conduction across the air-filled void space, as well as via direct contact along 1 edge of the FHE. The contact conductance simulates a conservative idealized physical contact (i.e., a flat, smooth interface and that the FHE is oriented within the package such that the edge is aligned with the vertical axis of the package) between the FHE and the inner shell. Due to the robustness of the MIT FHE, no change to the direct contact between the FHE and the inner shell conservatively assumed for the NCT condition is expected as a result of the HAC drop event.

Figure 3.6-9 illustrates a cross-section through the combined modeling for the inner shell, the FHE, and the MIT fuel element. The left side of the figure illustrates the placement of the thermal nodes (indicated by the small circles) used to simulate each of the components, the use of planar elements to represent the 15 fuel plates, and the assumed points of direct contact between the FHE and the inner shell. The right side of the figure includes depiction of the solid elements that are used to simulate the air voids around the FHE. The heat transfer between the FHE and the MIT fuel element is computed as conductance through the 0.125 inch thick neoprene rub strips and radiation and conductance through the air voids.

Figure 3.6-10 illustrates a side and end view of the thermal model of the MIT fuel element as it would be for a complete fuel element. Approximately 1,140 nodes, 350 planar elements, and 445 solids are used to represent the quarter symmetry thermal model of the MIT fuel element, FHE, and the spacer weldment.

The thermal modeling for the MURR fuel element and FHE is similar to that described above for the MIT fuel element payload. Figure 3.6-11 illustrates the quarter symmetry thermal model of the MURR FHE and one of the two spacer weldments. The FHE thermal model uses planar elements to represent the 0.19 inch thick sides of the enclosure and the 0.25 inch thick elements of the spacer weldment. Solid elements are used to represent the ends of the FHE. Heat transfer between the FHE and the inner shell of the package is modeled as a combination of radiation and conduction across the air-filled void space, as well as via direct contact along 2 edges of the FHE. The contact conductance simulates a conservative idealized physical contact (i.e., a flat, smooth interface and an alignment that places 2 edges of the FHE in contact) between the FHE and the inner shell. Due to the robustness of the MURR FHE, no change to the direct contact between the FHE and the inner shell conservatively assumed for the NCT condition is expected as a result of the HAC drop event.

Figure 3.6-12 illustrates a cross-section through the combined modeling for the inner shell, the FHE, and the MURR fuel element. The left side of the figure illustrates the placement of the thermal nodes (indicated by the small circles) used to simulate each of the components, the use of curved, planar elements to represent the 24 fuel plates, and the assumed points of direct contact between the FHE and the inner shell. The right side of the figure includes depiction of the solid elements that are used to simulate the air voids around the FHE. The heat transfer between the FHE and the MURR fuel element is computed as conductance through the 0.125 inch thick neoprene rub strips and radiation and conductance through the air voids.

Figure 3.6-13 illustrates a side and end view of the quarter symmetry thermal modeling used for the MURR fuel element. Approximately 1,400 nodes, 700 planar elements, and 340 solids are used to represent the quarter symmetry thermal model of the MURR fuel element, FHE, and the spacer weldment.

The heat transfer from the exterior surfaces of the ATR FFSC is modeled in the same manner as that used for the evaluation of the ATR fuel element payload and assumes a combination of convection and radiation exchange. Appendix 3.5.2.3, *Convection Coefficient Calculation*, presents the methodology used to compute the convection coefficients from the various surfaces. The radiation exchange is computed using a Monte Carlo, ray tracing technique and includes the affect of reflection and/or transmission, according to the optical properties assigned to each surface (see Section 3.2.1, *Material Properties*).

In addition, heating of the exterior surfaces due to solar insolation is assumed using a diurnal cycle. The methodology used to simulate and apply the insolation loading is described in Appendix 3.5.2.1, *Description of Thermal Model for NCT Conditions*.

3.6.9.2.2 Description of Thermal Model for HAC Conditions

The thermal evaluations for the hypothetical accident condition (HAC) are conducted in the same manner and using the same methodology as that described in Appendix 3.6.9.2.1, *Description of MIT and MURR Payload Thermal Models for NCT Conditions*. No change to the geometry or position of the MIT and MURR fuel element payloads are expected as a result of the drop and puncture bar events that are assumed to precede the HAC fire event.

3.6.9.2.3 Determination of Composite Thermal Properties for MIT and MURR Fuel Plates

The MIT and MURR fuel plates are a composite material consisting of a fissile fuel matrix sandwiched within aluminum cladding. For the purposes of this calculation, the fuel composite is treated as a homogenous material with lumped thermal properties. The methodology used to compute the composite thermal properties for each fuel element is the same as that described in Appendix 3.5.2.4, *Determination of Composite Thermal Properties for ATR Fuel Plates*.

Each MIT element contains up to 515 g U-235, enriched up to 94 wt.%, which equates to a density of approximately 1.5 g U/cc in the fuel matrix. The thermal properties for the individual plates making up the MIT fuel element are computed using the approach used with the ATR Fuel Plates and the geometric data[39,42] for the MIT fuel element. Each of the fifteen (15) fuel plates contained in the MIT fuel element has a thickness of 0.08 inches and a width of 2.526 inches. The nominal gap between the plates is 0.078 inches. Since the aluminum cladding contains 110 grooves on each side of the plate, the effective thickness of the cladding is reduced from 0.025 inches to 0.02 inches. Table 3.6-8 presents the composite thermal conductivity, specific heat, and density values for the fuel plates. These composite values are based on the described geometry of the fuel plates and the same thermophysical data[6] used for the ATR fuel plates.

The thermal properties for the MIT element used are:

1) Aluminum cladding thermal conductivity = 191 W/m-K, conservatively high value from [6], page 18
2) Fissile fuel matrix (UAl_x) conductivity = 38.5 W/m-K, conservatively high based on Table 2.3 from [6] at 300K for 1.5 g U/cc
3) Aluminum cladding density = 2702 kg/m^3, from [6], page 16
4) Fissile fuel matrix (UAl_x) density = 3846 kg/m^3, from [6], Table 2.5 for 1.5 g U/cc
5) Aluminum cladding specific heat = 896 & 1080 J/kg-K, from [6], Table 3.2 at 300 & 700K, respectively
6) Fissile fuel matrix (UAl_x) specific heat = 587 & 709 J/kg-K, from [6], Table 2.4, value at 300 & 700K, respectively, for 1.5 g U/cc

[42] *Massachusetts Institute of Technology, Test Research Training Reactor 3 Welded Fuel Element Assembly,* EG&G Idaho, Inc. Drawing No. DWG-419486, Rev. A.

Each MURR element contains up to 785 g U-235, enriched up to 94 wt.%, which equates to a density of approximately 1.44 g U/cc in the fuel matrix. The thermal properties for the individual plates making up the MURR fuel element are also computed using the approach used with the ATR Fuel Plates and the geometric data[40,43] for the MURR fuel element. Due to the curved geometry of the twenty-four (24) fuel plates contained in the MURR fuel element, each plate has a different geometry. The inner plate has an inner radius of 2.77 inches and an arc length of 1.993 inches, while the outer plate has an inner radius of 5.76 inches and an arc length of 4.342 inches. The nominal gap between the plates is 0.08 inches. The thickness of the aluminum cladding is 0.01 inches. Table 3.6-9 presents the composite thermal conductivity, specific heat, and density values for the twenty four (24) fuel plates making up the MURR fuel element. These composite values are based on the described geometry of the fuel plates and the same thermophysical data[6] used for the ATR fuel plates.

The thermal properties for the MURR fuel element used in this calculation are:

1) Aluminum cladding thermal conductivity = 191 W/m-K, conservatively high value from [6], page 18
2) Fissile fuel matrix (UAl_x) conductivity = 39.8 W/m-K, conservatively high based on Table 2.3 from [6], at 300K for 1.44 g U/cc
3) Aluminum cladding density = 2702 kg/m^3, from [6], page 16
4) Fissile fuel matrix (UAl_x) density = 3793 kg/m^3, from [6], Table 2.5 for 1.44 g U/cc
5) Aluminum cladding specific heat = 896 & 1080 J/kg-K, from [6], Table 3.2, at 300 & 700K, respectively
6) Fissile fuel matrix (UAl_x) specific heat = 596 & 719 J/kg-K, from [6], Table2.4, value at 300 & 700K, respectively, for 1.44 g U/cc

3.6.9.2.4 Determination of Thermal Properties for RINSC Element

The RINSC fuel elements are fabricated with a nominally 0.020-in thick mixture of uranium silicide (U_3Si_2) and aluminum powder as the fuel "meat" and a nominally 0.015-in thick aluminum alloy cladding. The twenty-two (22) flat fuel plates have a 2.8-in width, an overall length of 25-in, and an active fuel region of 22.5 to 24.0-in. The fuel plate meat and cladding thicknesses match those of the interior plates for the ATR fuel element and are similar to those for the MURR fuel plates. The side plates are fabricated of ASTM B 209, aluminum alloy 6061-T6 and 6061-T651 and are approximately 0.188-in thick. This is similar to the side plate thicknesses of the ATR, MITR, and MURR fuel elements.

The thermal conductivity of the RINSC fuel plates[41] are similar to data obtained in the measurements of the thermal conductivities for the uranium aluminide (UAl_x) based fuels[6]. Similarly, the thermal mass of the fuel plates are comparable despite the higher density of uranium silicide versus uranium aluminide since the ratio of the specific heats of the two materials is nearly the inverse of the density ratio.

[43] *University of Missouri at Columbia, MURR UAlx Fuel Element Assembly,* EG&G Idaho, Inc. Drawing No. DWG-409407, Rev. N.

The ATR FFSC with the RINSC fuel element payload is not specifically modeled as part of this evaluation. Instead, its thermal performance is estimated using a qualitative approach based on the maximum temperatures attained for the transportation of the MURR fuel element within the ATR FFSC. This conclusion is based on the facts that the combined weight of the RINSC and MURR FHE's with their enclosed fuel elements are the same, the FHE's are both fabricated of 6061 aluminum, and the fuel elements have similar thermal properties (see above). This conclusion is further supported by the fact that the MIT and MURR fuel elements produce essentially the same peak temperatures despite their design differences. As such, the limited design differences between the MURR and RINSC payloads will not yield a significant difference in their thermal response.

3.6.9.2.5 Determination of Thermal Properties for Cobra Element

As with the MURR and MIT fuel elements, the temperature of the Cobra fuel element will vary based on the heat that flows into the ATR FFSC package from insolation (NCT) and the hypothetical fire (HAC). The temperature of the fuel element will depend primarily on the nature of the dominant resistances in the heat path between the fuel and the environment, and on the heat capacity or thermal mass of the package. A comparison can be made between the Cobra fuel element case and the MURR case, whose resulting temperatures are given in Table 3.6-5 (NCT) and Table 3.6-7 (HAC). The dominant resistances consist of the non-metallic links in the heat path from the outside to the inside (such as air gaps and rubber); the resistance through the metallic elements is comparatively negligible (such as steel and aluminum), and will be neglected in what follows. The non-metallic elements in the heat path are:

- The insulation between the inner and outer shells of the package, based on the thermal conductivity, thickness, and area of the insulation
- The air gap between the inner shell and the FHE, based on the radiative heat transfer properties and the area
- The contact conductance of the FHE resting on the inner shell
- The neoprene rubber between the FHE and the fuel element
- The air gap between the FHE and the fuel element
- The contact conductance of the fuel element resting on the rubber

Because the Cobra fuel element is transported within a FHE having a design very similar to that of the MURR fuel element, the dominant heat transfer resistances will be very similar, including the same number and approximate size of air gaps, emissivities, contact conductances, and rubber thickness. The thermal behavior in transient heat transfer also depends on the thermal mass of the components. From Table 2.1-1, the weight of the MURR fuel element and its FHE are 15 lb and 30 lb, respectively, for a total of 45 lb; and the weight of the Cobra fuel element and its FHE are 18 lb and 28 lb, respectively, for a total of 46 lb. Since the heat capacity of all aluminum alloys is very similar, and since the total weight of each fuel element plus FHE is essentially the same, the thermal mass will be essentially the same. Thus, the Cobra fuel element case will have essentially the same thermal behavior in NCT and HAC to the MURR fuel element case. In addition, the temperatures calculated for the MURR case show significant margins to the limiting temperatures for the various components.

Table 3.6-8 – Composite MIT Fuel Plate Thermal Properties

Plate	Plate Thickness, in	UAlx Thickness, in	Axial and Circumferential Conductivity (W/m-K)	Plate Width, in	Mean density, kg/m^3	Mean specific heat, J/(kg K) @ 300 K	Mean specific heat, J/(kg K) @ 700 K
1 to 15	0.08*	0.03	125.6	2.314	3192.3	736.5	888.4

* - mean plate thickness estimated at 0.07 inches after allowance for ribbing

Table 3.6-9 – Composite MURR Fuel Plate Thermal Properties

Plate	Plate Thickness, in	UAlx Thickness, in	Axial and Circumferential Conductivity (W/m-K)	Inner radius, in	Outer radius, in	Plate Arc Length, in	Mean density, kg/m^3	Mean specific heat, J/(kg K) @ 300K	Mean specific heat, J/(kg K) @ 700 K
1	0.05	0.03	100.3	2.77	2.82	1.993	3288.8	692.6	835.2
2	0.05	0.03	100.3	2.9	2.95	2.095	3288.8	692.6	835.2
3	0.05	0.03	100.3	3.03	3.08	2.197	3288.8	692.6	835.2
4	0.05	0.03	100.3	3.16	3.21	2.300	3288.8	692.6	835.2
5	0.05	0.03	100.3	3.29	3.34	2.402	3288.8	692.6	835.2
6	0.05	0.03	100.3	3.42	3.47	2.504	3288.8	692.6	835.2
7	0.05	0.03	100.3	3.55	3.6	2.606	3288.8	692.6	835.2
8	0.05	0.03	100.3	3.68	3.73	2.708	3288.8	692.6	835.2
9	0.05	0.03	100.3	3.81	3.86	2.810	3288.8	692.6	835.2
10	0.05	0.03	100.3	3.94	3.99	2.912	3288.8	692.6	835.2
11	0.05	0.03	100.3	4.07	4.12	3.014	3288.8	692.6	835.2
12	0.05	0.03	100.3	4.2	4.25	3.116	3288.8	692.6	835.2
13	0.05	0.03	100.3	4.33	4.38	3.218	3288.8	692.6	835.2
14	0.05	0.03	100.3	4.46	4.51	3.321	3288.8	692.6	835.2
15	0.05	0.03	100.3	4.59	4.64	3.423	3288.8	692.6	835.2
16	0.05	0.03	100.3	4.72	4.77	3.525	3288.8	692.6	835.2
17	0.05	0.03	100.3	4.85	4.9	3.627	3288.8	692.6	835.2
18	0.05	0.03	100.3	4.98	5.03	3.729	3288.8	692.6	835.2
19	0.05	0.03	100.3	5.11	5.16	3.831	3288.8	692.6	835.2
20	0.05	0.03	100.3	5.24	5.29	3.933	3288.8	692.6	835.2
21	0.05	0.03	100.3	5.37	5.42	4.035	3288.8	692.6	835.2
22	0.05	0.03	100.3	5.5	5.55	4.137	3288.8	692.6	835.2
23	0.05	0.03	100.3	5.63	5.68	4.239	3288.8	692.6	835.2
24	0.05	0.03	100.3	5.76	5.81	4.342	3288.8	692.6	835.2

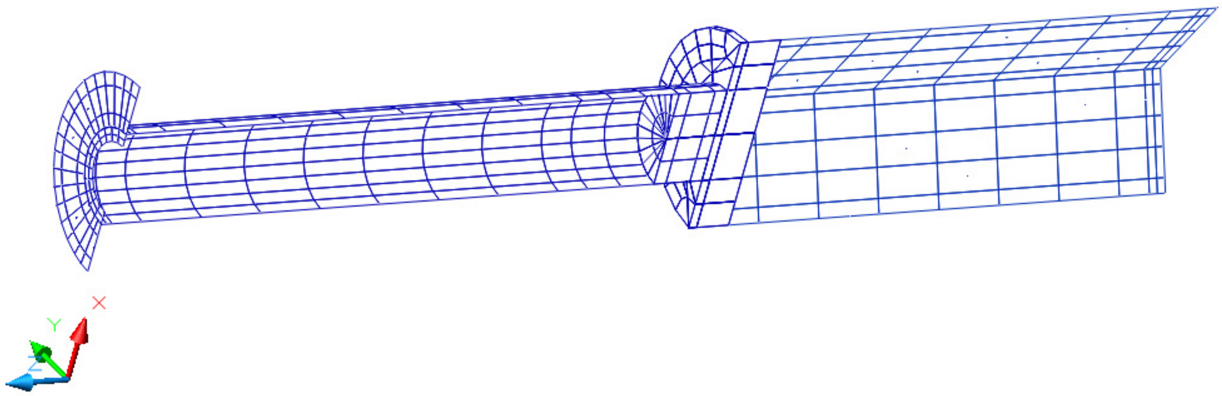

(Note: the positive x-axis is oriented towards the top of the package and the positive z-axis towards the package closure end)

Figure 3.6-8 – ‘Hidden Line’ View of MIT FHE and Spacer Quarter Symmetry Thermal Model

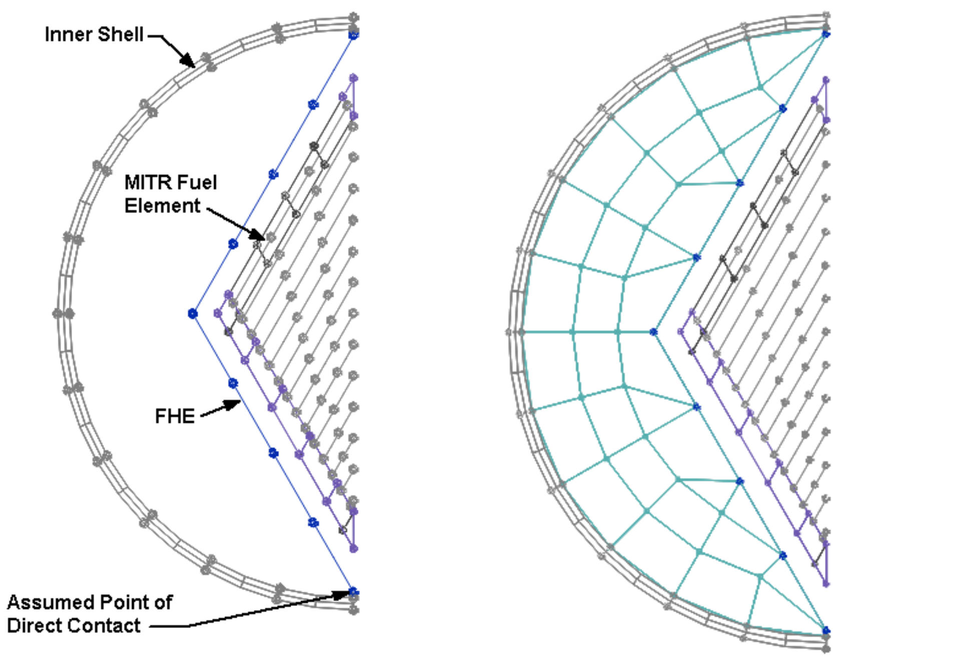

Modeling Showing Direct Contact **Modeling with ‘Solid’ Elements for Air**

Figure 3.6-9 – Thermal Model of MIT Fuel Element and FHE within Inner Shell

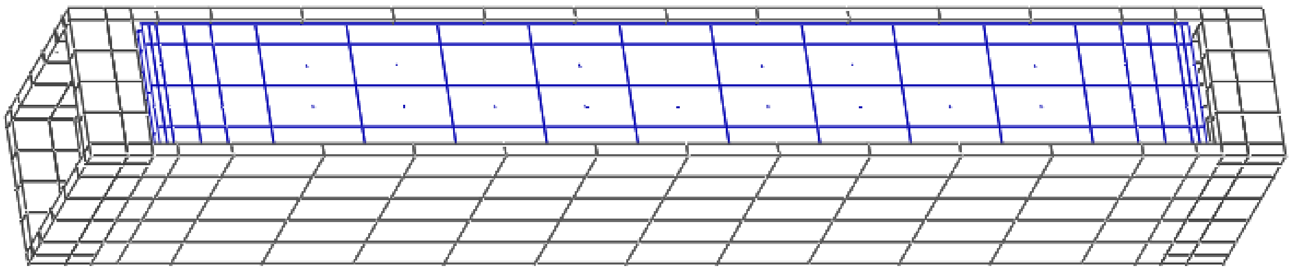

MIT Fuel Element Model, Side View of Full Element

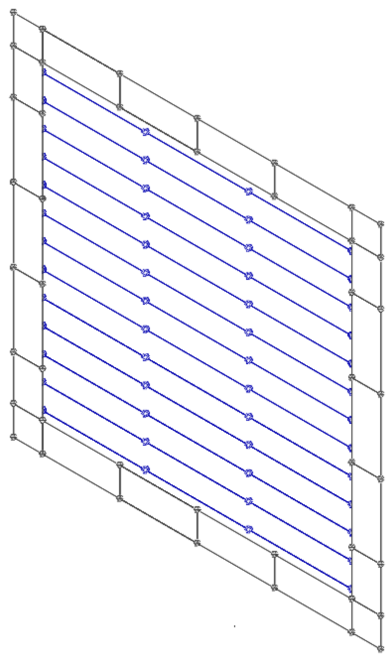

MIT Fuel Element Model, End View of Full Element

Figure 3.6-10 – Side and End Views of MIT Fuel Element Thermal Model

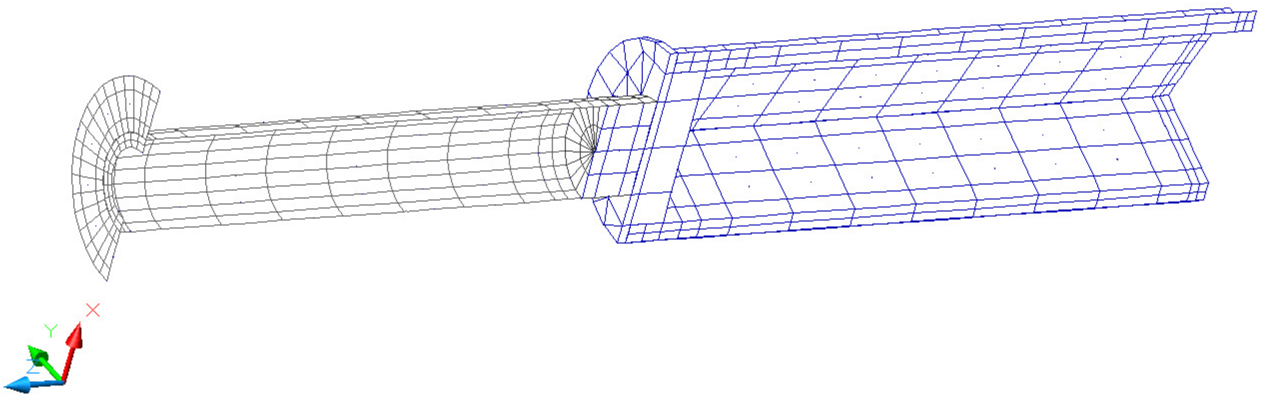

(Note: the positive x-axis is oriented towards the top of the package and the positive z-axis towards the package closure end)

Figure 3.6-11 – 'Hidden Line' View of MURR FHE and Spacer Quarter Symmetry Thermal Model

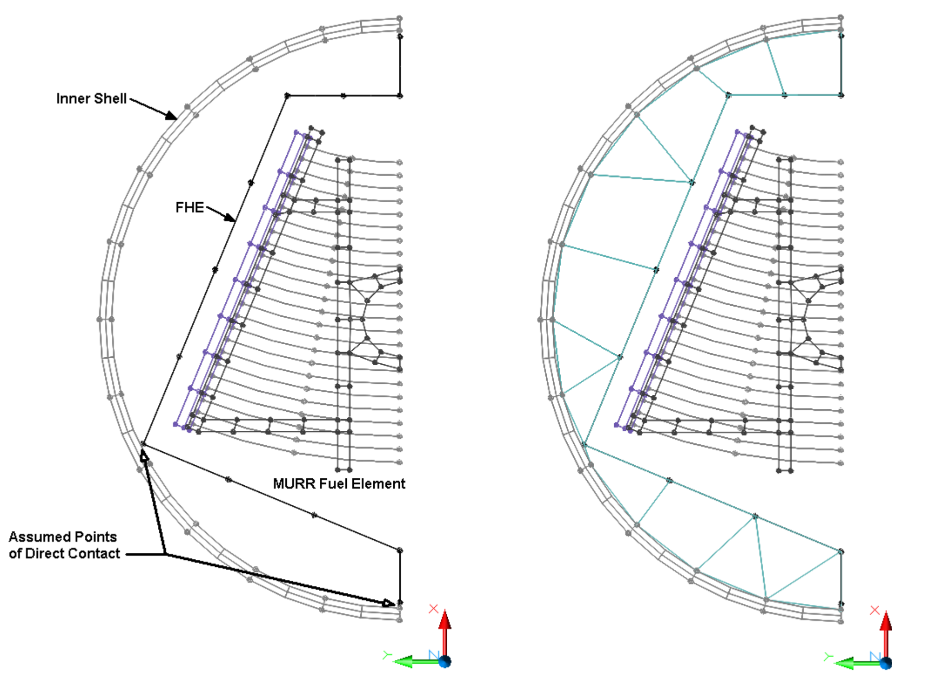

Modeling Showing Direct Contact **Modeling with 'Solid' Elements for Air**

Figure 3.6-12 – Thermal Model of MURR Fuel Element and FHE within Inner Shell

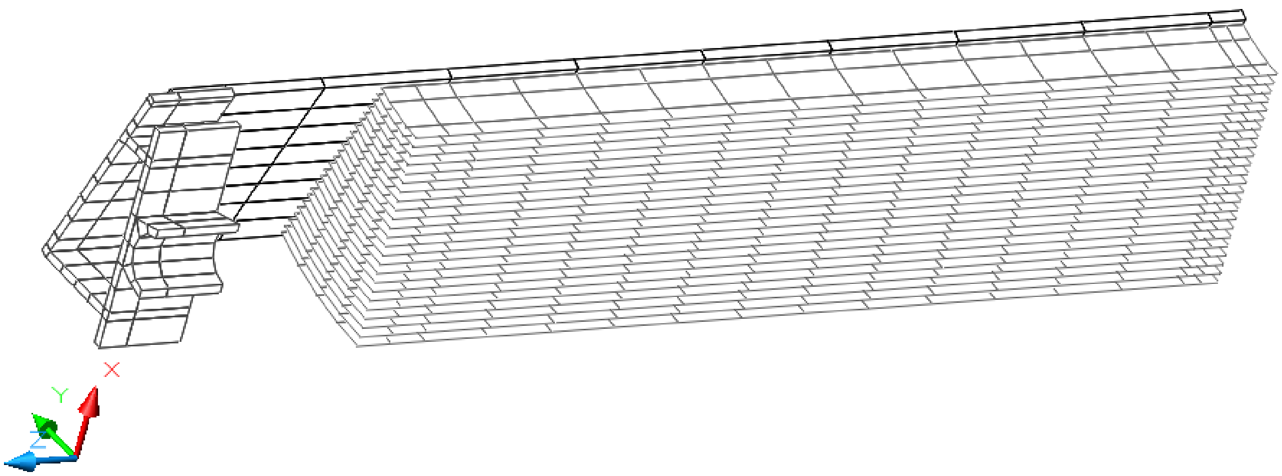

MURR Fuel Element Model, Side View of Quarter Symmetry Model

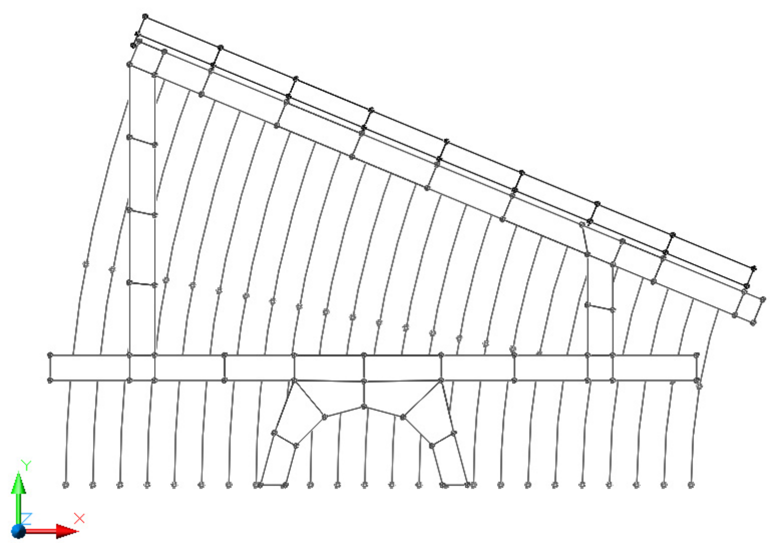

MURR Fuel Element Model, End View of Quarter Symmetry Model

Figure 3.6-13 – Side and End Views of MURR Fuel Element Thermal Model

4.0 CONTAINMENT

4.1 Description of the Containment System

The containment function of the ATR FFSC is to confine the fuel elements or loose plates within the packaging during Normal Conditions of Transport (NCT) and Hypothetical Accident Conditions (HAC).

The package body is a stainless steel weldment that consists of two nested shells. The outer shell is an 8-in square stainless steel tube with a 3/16-in thick wall, and the inner shell is a 6-in diameter stainless steel tube with a 0.120-in thick wall. Components are joined using full-thickness fillet welds (i.e., fillet welds whose leg size is nominally equal to the lesser thickness of the parts joined) and full and partial penetration groove welds. The end of the body is welded closed with 0.88-in plate.

The lid end of the package is closed with a simple closure device. The closure engages with the body using a bayonet style design. There are four lugs, uniformly spaced on the closure, that engage with four slots in the mating body fixture. The closure is secured by two retracting spring loaded pins, rotating the closure through 45°, and releasing the spring loaded pins such that the pins engage with the mating holes on the body. When the pins are properly engaged with the mating holes the closure is locked and cannot be removed unintentionally.

The containment boundary is defined as the boundary of the cavity formed by the closure and inner stainless steel tube. For criticality control purposes, the fuel element must remain within this boundary during NCT and HAC. No seals or gaskets are utilized within the package.

To prevent unauthorized operation, a small post on the closure is drilled to receive a tamper indicating device (TID) wire. An identical post is located on the body and is also drilled for the TID wire. For ease in operation, there are two TID posts on the body. There are only two possible angular orientations for the closure installation and the duplicate TID post on the body enables TID installation in both positions.

4.1.1 Type A Fissile Packages

The ATR FFSC is classified as a Type A Fissile package. The Type A Fissile package is constructed and prepared for shipment so that there is no loss or dispersal of the radioactive contents, and no significant increase in external surface radiation levels, and no substantial reduction in the effectiveness of the packaging during normal conditions of transport. The fissile material is contained within the containment boundary. Chapter 6.0, *Criticality Evaluation*, demonstrates that the package remains subcritical under normal and hypothetical accident conditions.

The ATR FFSC contains four radioactive isotopes: U-234, U-235, U-236, and U-238. The A_2 value for U-235 and U-238 is unlimited, while the minimum A_2 value for U-234 and U-236 is 0.16 Ci for slow lung absorption. To compute the mixture A_2 for the HEU payloads, the maximum value of 1200 g U-235 is assumed, with a low weight fraction of 90% to maximize the mass of uranium. Therefore, the total mass of uranium is 1200/0.9 = 1333 g U. The maximum weight percents of U-234 (1.2%) and U-236 (0.7%) are assumed to maximize the mass of these isotopes. The balance is treated as U-238. For this conservative isotopic mix, the mixture A_2 is

0.164 Ci. The package activity for this mixture is 0.103 Ci (mostly due to U-234); therefore, the package contains approximately $0.6A_2$.

For the U-Mo demonstration element, the maximum value of 1240 g U-235 is utilized. Plates 1 through 4 and 16 through 18 are HEU with U-234 and U-236 compositions as defined in the previous paragraph. Plates 5 through 15 are LEU with a U-235 weight fraction of 20%. For these plates, the maximum weight percents of U-234 (0.26%) and U-236 (0.46%) are utilized to maximize the mass of these isotopes. Although the A_2 value for uranium enriched to 20% or less is unlimited, the mixture A_2 is conservatively computed using the total mass of U-234 and U-236 in the element. The mixture A_2 and package activity are essentially identical to the standard ATR element, and the package contains approximately $0.6A_2$ when transporting the U-Mo demonstration element.

4.1.2 Type B Packages

The content of the ATR FFSC package is high-enriched uranium with approximately $0.6A_2$ for release purposes. As a fissile package the ATR FFSC must meet the release rates for Type B packages when required by the total amount of radioactive material. However, because the A_2 value of the contents is less than 1 A_2, the package is classified as Type A and there are no release limits except as necessary for criticality control.

4.2 Containment under Normal Conditions of Transport

The ATR FFSC payloads listed in Section 1.2.2, *Contents*, are confined within the packaging under NCT. This is verified by full-scale testing, as discussed in Section 2.6, *Normal Conditions of Transport*. The test units survived the NCT drop tests with minimal damage to the packaging and no damage to the fuel elements. The maximum internal pressure in the package does not exceed atmospheric pressure because the closure is not sealed with a gasket or other sealing material. Because the ATR FFSC is a Type A Fissile package, leakage rate testing is not required.

4.3 Containment under Hypothetical Accident Conditions

The radioactive material contents of the ATR FFSC package must meet the containment requirements of 10 CFR §71.55(e) such that the package would be subcritical under the HAC.

The test program demonstrates that the package contains the fuel elements or loose fuel plates under the HAC events sufficient to maintain criticality control. The full-scale HAC drop tests summarized in Section 2.7, *Hypothetical Accident Conditions*, confirm the HAC performance of the package. The closure remained intact throughout all the drop sequences, and the fuel element remained confined within the inner stainless steel tube. The non-fissile end boxes on the fuel element shattered as expected but the fueled portion of the element remained intact and retained its geometry. There was no dispersal of fissile material. The criticality evaluation presented in Section 6.0, *Criticality Evaluation*, evaluates the contents in the most reactive credible configuration and with water moderation as required.

Because the ATR FFSC package is a Type A Fissile package and the contents are less than 1 A_2, the performance requirements of 10 CFR §71.51 do not apply.

4.4 Leakage Rate Tests for Type B Packages

The ATR FFSC is a Type A Fissile package; therefore, this section does not apply.

This page left intentionally blank.

5.0 SHIELDING EVALUATION

Compliance of the ATR FFSC with respect to the dose rate limits established by 10 CFR §71.47[1] for normal conditions of transport (NCT) or 10 CFR §71.51(a)(2) for hypothetical accident conditions (HAC) are satisfied when limiting the package to the contents specified in Section 1.2.2, *Contents*, and verified by measurement.

Prior to transport, the ATR FFSC shall be monitored for both gamma and neutron radiation to demonstrate compliance with 10 CFR §71.47. Although the ATR FFSC will likely be shipped exclusive use, dose rates will be sufficiently low to allow non-exclusive use transport, if desired.

Shielding materials are not specifically provided by the ATR FFSC. Because the contents are essentially unshielded, the HAC dose rates at one meter will not be significantly different from the NCT dose rates at one meter. This result ensures that the post-HAC, allowable dose rate of 1 rem/hr a distance of one meter from the package surface per 10 CFR §71.51(a)(2) will be met.

[1] Title 10, Code of Federal Regu1ations, Part 71 (10 CFR 71), *Packaging and Transportation of Radioactive Material*.

This page left intentionally blank.

6.0 CRITICALITY EVALUATION

The following analyses demonstrate that the ATR FFSC complies with the requirements of 10 CFR §71.55[1] and §71.59.

The analysis in the main body of Chapter 6 (Sections 6.2 through 6.6, 6.8, and 6.9) pertains only to the ATR fuel element and ATR loose plate basket. Additional payloads are added as appendices.

The analysis for MIT and MURR fuel is contained in Appendix B (Section 6.10, *Criticality Analysis for MIT and MURR Fuel*).

The analysis for the small quantity payloads is contained in Appendix C (Section 6.11, *Criticality Analysis for Small Quantity Payloads*).

The analysis for the ATR U-Mo demonstration element is contained in Appendix D (Section 6.12, *Criticality Analysis for the U-Mo Demonstration Element*).

The analysis for the Cobra fuel element is contained in Appendix E (Section 6.13, *Criticality Analysis for the Cobra Fuel Element*).

The air transport analysis in Section 6.7 applies to all payloads.

6.1 Description of Criticality Design

The results presented in this section are for all payload types.

6.1.1 Design Features Important for Criticality

A comprehensive description of the ATR FFSC is provided in Section 1.2, *Packaging Description*, and in the drawings in Appendix 1.3.2, *Packaging General Arrangement Drawings*. This section summarizes those design features important for criticality.

No poisons are utilized in the package.

For the ATR fuel element payload (including the ATR U-Mo demonstration element), the separation provided by the packaging (outer tube minimum flat-to-flat dimension of 7.9-in, inner tube maximum inner diameter of 5.814-in), along with the limit on the number of packages per shipment, is sufficient to maintain criticality safety.

For the ATR loose plate payload, in addition to the packaging design features noted above, moderation of the loose plates is controlled by the loose plate basket, which confines the fuel plates to a rectangular area.

For the MURR/MIT payload, in addition to the packaging design features noted above, the MURR and MIT fuel handling enclosures (FHEs) restrict postulated fuel element pitch expansion under hypothetical accident conditions.

For the small quantity payload and Cobra fuel element analyses, the fuel is modeled as a homogenized mixture of uranium and water. Therefore, the packaging itself is sufficient to

[1] Title 10, Code of Federal Regulations, Part 71 (10 CFR 71), *Packaging and Transportation of Radioactive Material*.

maintain criticality safety, as the fuel handling enclosures and fuel structural materials are not credited in the analyses.

6.1.2 Summary Table of Criticality Evaluation

The upper subcritical limit (USL) for ensuring that the ATR FFSC (single package or package array) is acceptably subcritical, as determined in Section 6.8 (for plate-fuel), Section 6.11.8 (for the small quantity payload), Section 6.12.8 (for the U-Mo demonstration element), and Section 6.13.8 (for the Cobra fuel element) is:

$$USL = 0.9209$$

The package is considered to be acceptably subcritical if the computed k_{safe} (k_s), which is defined as $k_{effective}$ (k_{eff}) plus twice the statistical uncertainty (σ), is less than or equal to the USL, or:

$$k_s = k_{eff} + 2\sigma \leq USL$$

The USL is determined on the basis of a benchmark analysis and incorporates the combined effects of code computational bias, the uncertainty in the bias based on both benchmark-model and computational uncertainties, and an administrative margin. The results of the benchmark analysis indicate that the USL is adequate to ensure subcriticality of the package.

<u>ATR Fuel Element and ATR Loose Plate Basket</u>

The packaging design is shown to meet the requirements of 10 CFR 71.55(b) when the package is limited to either one 1200 g U-235 ATR fuel element, or 600 g U-235 in the form of ATR loose fuel plates. Moderation by water in the most reactive credible extent is utilized in both the NCT and HAC analyses. In the single package NCT models, full-density water fills the accessible cavity, while in the single package HAC models, full-density water fills all cavities. In the fuel element models, the most reactive credible configuration is utilized by maximizing the gap between the fuel plates. Maximizing this gap maximizes the moderation and hence the reactivity because the system is under moderated. In the loose plate model, no credit is taken for the dunnage plates and the optimal pitch and fuel arrangement is utilized. In all single package models, 12-in of water reflection is utilized.

In the NCT and HAC array cases, partial moderation is considered to maximize array interaction effects. A 9x9x1 array is utilized for the NCT array, while a 5x5x1 array is utilized in the HAC array. In all array models, 12-in of water reflection is utilized.

The maximum results of the ATR fuel element criticality calculations are summarized in Table 6.1-1. The maximum calculated k_s is 0.8362, which occurs for the optimally moderated NCT array case. The NCT array is more reactive than the HAC array because the NCT array is larger, and moderation is allowed in both conditions. In this case, the fuel element is moderated with full-density water, the inner tube is moderated with 0.3 g/cm^3 water, and void is modeled between the insulation and outer tube.

The maximum results of the loose plate basket criticality calculations are summarized in Table 6.1-2. The maximum calculated k_s is 0.7747, which occurs for the optimally moderated NCT array case. The NCT array is more reactive than the HAC array because the NCT array is larger, and moderation is allowed in both conditions. In this case, the loose fuel plate basket is moderated with full-density water, the inner tube is moderated with 0.5 g/cm^3 water, and void is modeled between the insulation and outer tube.

It may be noted when comparing Table 6.1-1 and Table 6.1-2 the fuel element payload is more reactive than the loose plate basket payload.

MURR and MIT Fuel Element

A summary of the MURR and MIT fuel element analysis is provided in Section 6.10.1.2. The summary table is also provided as Table 6.1-3 for convenience.

Small Quantity Payload

A summary of the small quantity payload analysis is provided in Section 6.11.1.2. The summary table is also provided as Table 6.1-4 for convenience.

U-Mo Demonstration Element

A summary of the U-Mo demonstration analysis is provided in Section 6.12.1.2. The summary table is also provided as Table 6.1-5 for convenience.

Cobra Element

A summary of the Cobra element analysis is provided in Section 6.13.1.2. The summary table is also provided as Table 6.1-6 for convenience.

Air Transport Analysis

The air transport analysis applies to all licensed payloads. In the air transport analysis, 2000 g U-235 is modeled as a sphere moderated with the hydrogenous packaging materials and reflected with 20 cm of water. The hydrogenous packaging materials include 100 g polyethylene and 4000 g neoprene. Maximum reactivity is achieved when the fissile material is divided into a 1500 g U-235 inner sphere moderated with polyethylene and neoprene and an outer sphere consisting of 500 g U-235 uranium metal. The maximum calculated k_s is 0.6074 for the most reactive air transport case, which is far below the USL.

Table 6.1-1 – Summary of Criticality Evaluation (ATR Fuel Element Payload)

Normal Conditions of Transport (NCT)	
Case	k_s
Single Unit Maximum	0.4224
9x9 Array Maximum	0.8362
Hypothetical Accident Conditions (HAC)	
Case	k_s
Single Unit Maximum	0.4524
5x5 Array Maximum	0.7453
USL = 0.9209	

Table 6.1-2 – Summary of Criticality Evaluation (ATR Loose Plate Payload)

Normal Conditions of Transport (NCT)	
Case	k_s
Single Unit Maximum	0.4020
9x9 Array Maximum	0.7747
Hypothetical Accident Conditions (HAC)	
Case	k_s
Single Unit Maximum	0.4363
5x5 Array Maximum	0.6979
USL = 0.9209	

Table 6.1-3 – Summary of Criticality Evaluation (MURR/MIT Payload)

	MURR	**MIT**
Normal Conditions of Transport (NCT)		
Case	k_s	k_s
Single Unit Maximum	0.44807	0.36978
9x9 Array Maximum	0.85643	0.65658
Hypothetical Accident Conditions (HAC)		
Case	k_s	k_s
Single Unit Maximum	0.54584	0.43666
5x5 Array Maximum	0.85881	0.67309
USL = 0.9209		

Table 6.1-4 – Summary of Criticality Evaluation (Small Quantity Payload)

Normal Conditions of Transport (NCT)	
Case	k_s
Single Unit Maximum	0.6478
10 Package Array Maximum	0.8943
Hypothetical Accident Conditions (HAC)	
Case	k_s
Single Unit Maximum	0.7244
4 Package Array Maximum	0.8222
USL = 0.9209	

Table 6.1-5 – Summary of Criticality Evaluation (U-Mo Demonstration Element)

Normal Conditions of Transport (NCT)	
Case	k_s
Single Unit Maximum	0.4055
9x9 Array Maximum	0.7879
Hypothetical Accident Conditions (HAC)	
Case	k_s
Single Unit Maximum	0.4344
5x5 Array Maximum	0.7054
USL = 0.9209	

Table 6.1-6 – Summary of Criticality Evaluation (Cobra Element)

Normal Conditions of Transport (NCT)	
Case	k_s
Single Unit Maximum	0.6622
8 Package Array Maximum	0.8952
Hypothetical Accident Conditions (HAC)	
Case	k_s
Single Unit Maximum	0.7409
4 Package Array Maximum	0.8400
USL = 0.9209	

6.1.3 Criticality Safety Index

The HAC array calculations are performed for 2N packages and the NCT array calculations are performed for at least 5N packages. The number of packages modeled for each payload type is summarized in Table 6.1-7, along with the value of N. Note that for many of the NCT array cases, the number of packages modeled conservatively exceeds the 5N value. The 10 CFR §71.59 criticality safety index (CSI) is computed as 50/N and is provided in Table 6.1-7 for each payload type.

Table 6.1-7 – Summary of Criticality Safety Indices

Payload	NCT Array (# Packages)	HAC Array (# Packages)	N	CSI
ATR fuel element	81 (exceeds 5N)	25	12.5	4.0
ATR loose plates				
ATR U-Mo Demonstration element				
MIT fuel element				
MURR fuel element				
Small Quantity Payload	10	4	2.0	25.0
Cobra fuel element	8	4	1.6	31.3

6.2 Fissile Material Contents

The package can accommodate either (i) one ATR Mark VII fuel element, or (ii) a loose plate basket filled with ATR Mark VII fuel plates.

6.2.1 Fuel Element

Four different ATR Mark VII fuel element types are available: standard (7F), non-borated (7NB), non-borated hybrid (7NBH), and non-fueled plate 19 (YA). These fuel element types are described in Section 1.2.2, *Contents*. The 7NB fuel element is the only fuel element that does not contain boron, and is conservatively utilized in the criticality analysis.

Each fuel element contains up to 1200 g U-235, enriched up to 94 wt.%. The U-235 mass per plate is provided in Table 6.2-1. These values are generated by scaling up the U-235 loading for a 1075 g U-235 fuel element, as the 1200 g limit has been selected to envelope future increases in the loading. The weight percents of the remaining uranium isotopes are 1.2 wt.% U-234 (max), 0.7 wt.% U-236 (max), and 5.0-7.0 wt.% U-238. Each fuel element contains 19 curved fuel plates. Fuel plate 1 has the smallest radius, while fuel plate 19 has the largest radius, as shown in Figure 6.2-1. The as-modeled fuel element is shown in Figure 6.2-2. The fuel "meat" is uranium aluminide (UAl_x) mixed with additional aluminum. In the following paragraphs, the details of the fuel element are provided.

The key fuel element dimensions and tolerances utilized in the criticality models are summarized on Figure 6.2-1. Fuel plate 1 is nominally 0.080-in thick, fuel plates 2 through 18 are nominally 0.050-in thick, and fuel plate 19 is nominally 0.100-in thick. The plate thickness tolerance is +0.000/-0.002-in for all plates. The fuel meat is nominally 0.02-in thick for all 19 plates. The plate cladding material is aluminum ASTM B 209, 6061-0. Fuel element side plates are fabricated of ASTM B 209, aluminum alloy 6061-T6 or 6061-T651. All aluminum alloys are modeled as pure aluminum. The fuel element side plates have a minimum thickness of 0.182-in. Channels 2 through 10 have a width of 0.078 ± 0.007-in, while channels 11 through 19 have a width of 0.077 +0.008/-0.006-in. These tolerances represent average and not localized channel width. Therefore, the maximum average channel width is 0.085-in. For an actual fuel element, the channel width may exceed these tolerances in localized areas. The local maximum is 0.087-in.

The arc length of the fuel meat changes from plate to plate. This arc length varies based on the distance from the edge of the fuel meat to the fuel element side plate, as defined for each plate on Figure 6.2-1. This dimension is 0.245-in (max)/0.145-in (min) for fuel plates 1 and 19, 0.145-in (max)/0.045-in (min) for fuel plates 2 through 17, and 0.165-in (max)/0.065-in (min) for fuel plate 18. The smaller this dimension, the larger the arc length of the fuel meat.

The active fuel length varies between a minimum of 47.245-in (= 49.485 – 2*1.12) and a maximum of 48.775-in (= 49.515 – 2*0.37) for all fuel plates.

It is demonstrated in Section 6.4.1.2.1, *Fuel Element Payload Parametric Evaluation*, that reactivity increases with increasing meat arc length. Therefore, the arc length is modeled at the maximum value. To determine the number densities of the fuel meat, it is first necessary to compute the volume of the fuel meat. The volume of the fuel meat for each plate is the maximum arc length of the meat multiplied by the fuel length (48-in) and meat thickness (0.02-

in). The fuel length and meat thickness are treated as fixed quantities in all fuel element models, and the use of these dimensions is justified in Section 6.4.1.2.1.

The fuel meat volume for each of the 19 fuel plates is provided in Table 6.2-1. The mass of U-235 per plate utilized in the analysis is also provided in Table 6.2-1. The U-235 gram density for each fuel plate is also computed. Note that the U-235 gram density is higher in the inner plates compared to the outer plates.

The fuel itself is a mixture of UAl_x and aluminum. The density of this mixture is proportional to the U-235 gram density, as shown in Table 6.2-2. These data are perfectly linear, and a linear fit of the data is $\rho_2 = 0.8733\rho_1 + 2.5357$, where ρ_2 is the total gram density of the mixture, and ρ_1 is the gram density of the U-235 in the mixture. This equation is used to compute the total mixture gram density provided as the last column in Table 6.2-1.

From the fuel volumes, U-235 gram densities, and total mixture densities provided in Table 6.2-1, the number densities for the fuel region of each fuel plate may be computed. These number densities are provided in Table 6.2-3. The U-235 weight percent is assumed to be the maximum value of 94%. Representative weight percents of 0.6% and 0.35% are assumed for U-234 and U-236, respectively, and the balance (5.05%) is modeled as U-238.

6.2.2 Loose Fuel Plates

The loose plate basket may transport up to 600 g of U-235 in the form of ATR Mark VII fuel plates. These plates are described in Section 6.2.1, *Fuel Element*, although the loose plates may be flat as well as curved. The widths of the fuel meat for flat plates are the same as the fuel meat arc lengths provided in Table 6.2-1.

Because an integer number of plates will be transported, for computational purposes it is useful to modify the mass of U-235 per plate so that the total U-235 mass per package adds to 600 g. The column labeled “Number of Plates to 600 g” in Table 6.2-4 is simply the total desired mass (600 g) divided by the mass of U-235 per plate (from Table 6.2-1) and gives an estimate of the number of plates of each type required to reach 600 g U-235. Detailed models are developed for only four plates: 3, 5, 8, and 15. It is demonstrated in the analysis that it is sufficient to bound all of the plates by modeling these four. The number of plates modeled and the modeled mass of U-235 per plate are provided as the last two columns in Table 6.2-4.

In fuel element calculations, it has been determined that the fuel element is the most reactive when the arc length of the fuel “meat” is maximized. Therefore, all loose plate models utilize fuel plates with maximized fuel meat arc length. Also, because it has been determined that nominal fuel meat thickness (0.02-in) and nominal active fuel length (48.0-in) may be utilized with negligible effect on the reactivity, all loose plate models utilize these nominal dimensions. The overall plate thickness tolerance is +0.000/-0.002-in, and the loose plates are modeled at the minimum thickness of 0.048-in by reducing the cladding thickness by 0.001-in.

The number densities utilized in the models are provided in Table 6.2-5. These number densities are computed using the same method utilized in the fuel element models, although the U-235 mass per plate has been slightly adjusted as necessary so that the models always have 600 g U-235.

The active fuel length is modeled as 48-in for all fuel plates, consistent with the treatment of the fuel elements. The axial regions outside the active fuel region are conservatively ignored. The width of cladding from the fuel meat to the edge of the plate is modeled as 0.045-in for all of the fuel plates, which is the minimum dimension from the fuel meat to the fuel element support structure. The actual plates are wider than modeled because the plates extend into the fuel element support structure and this additional width is neglected.

Table 6.2-1 – Fuel Element Volume and Gram Densities

Plate	Fuel Meat Arc Length (cm)	Fuel Meat Volume (cm^3)	U-235 Mass Per Plate (g)	U-235 density, ρ_1 (g/cm^3)	Total UAl_x + Al Density, ρ_2 (g/cm^3)
1	4.2247	26.2	27.1	1.04	3.44
2	5.0209	31.1	32.5	1.04	3.45
3	5.2764	32.7	43.2	1.32	3.69
4	5.5319	34.3	45.1	1.32	3.69
5	5.7873	35.8	58.2	1.62	3.95
6	6.0427	37.4	60.9	1.63	3.96
7	6.2982	39.0	63.6	1.63	3.96
8	6.5536	40.6	66.3	1.63	3.96
9	6.8090	42.2	69.0	1.64	3.96
10	7.0644	43.8	71.7	1.64	3.97
11	7.3198	45.3	74.3	1.64	3.97
12	7.5752	46.9	77.0	1.64	3.97
13	7.8306	48.5	79.7	1.64	3.97
14	8.0860	50.1	82.4	1.64	3.97
15	8.3414	51.7	85.2	1.65	3.98
16	8.5968	53.2	71.4	1.34	3.71
17	8.8521	54.8	73.6	1.34	3.71
18	9.0058	55.8	60.1	1.08	3.48
19	8.9039	55.1	58.7	1.06	3.47
Total	--	824.5	1200.0	--	--

Table 6.2-2 – Fuel Density Equation

U-235 Density (g/cm^3) ρ_1	Total Fuel Density (g/cm^3) ρ_2
1.00	3.409
1.30	3.671
1.60	3.933
Linear Fit: $\rho_2 = 0.8733\rho_1 + 2.5357$	

Table 6.2-3 – Fuel Element Number Densities

Plate	U-234 (atom/b-cm)	U-235 (atom/b-cm)	U-236 (atom/b-cm)	U-238 (atom/b-cm)	Aluminum (atom/b-cm)	Total (atom/b-cm)
1	1.7026E-05	2.6560E-03	9.8475E-06	1.4089E-04	5.2187E-02	5.5010E-02
2	1.7156E-05	2.6763E-03	9.9226E-06	1.4196E-04	5.2153E-02	5.4998E-02
3	2.1711E-05	3.3869E-03	1.2557E-05	1.7966E-04	5.0974E-02	5.4574E-02
4	2.1618E-05	3.3724E-03	1.2503E-05	1.7889E-04	5.0998E-02	5.4583E-02
5	2.6648E-05	4.1571E-03	1.5413E-05	2.2051E-04	4.9696E-02	5.4115E-02
6	2.6746E-05	4.1724E-03	1.5470E-05	2.2132E-04	4.9670E-02	5.4106E-02
7	2.6790E-05	4.1791E-03	1.5495E-05	2.2168E-04	4.9659E-02	5.4102E-02
8	2.6830E-05	4.1854E-03	1.5518E-05	2.2201E-04	4.9649E-02	5.4098E-02
9	2.6867E-05	4.1911E-03	1.5539E-05	2.2232E-04	4.9639E-02	5.4095E-02
10	2.6901E-05	4.1965E-03	1.5559E-05	2.2260E-04	4.9630E-02	5.4092E-02
11	2.6933E-05	4.2015E-03	1.5577E-05	2.2287E-04	4.9622E-02	5.4089E-02
12	2.6963E-05	4.2061E-03	1.5595E-05	2.2311E-04	4.9614E-02	5.4086E-02
13	2.6990E-05	4.2105E-03	1.5611E-05	2.2334E-04	4.9607E-02	5.4083E-02
14	2.7017E-05	4.2145E-03	1.5626E-05	2.2356E-04	4.9600E-02	5.4081E-02
15	2.7077E-05	4.2239E-03	1.5661E-05	2.2406E-04	4.9585E-02	5.4075E-02
16	2.2037E-05	3.4377E-03	1.2746E-05	1.8235E-04	5.0889E-02	5.4544E-02
17	2.2037E-05	3.4377E-03	1.2745E-05	1.8235E-04	5.0889E-02	5.4544E-02
18	1.7683E-05	2.7586E-03	1.0228E-05	1.4633E-04	5.2016E-02	5.4949E-02
19	1.7487E-05	2.7279E-03	1.0114E-05	1.4470E-04	5.2067E-02	5.4967E-02

Table 6.2-4 – Loose Plate Data

Plate	Number of Plates to 600 g U-235	Modeled Number of Plates	Modeled U-235 Mass Per Plate (g)
1	22.12	-	-
2	18.47	-	-
3	13.89	14	42.9
4	13.30	-	-
5	10.32	10	60.0
6	9.84	-	-
7	9.43	-	-
8	9.05	9	66.7
9	8.70	-	-
10	8.37	-	-
11	8.07	-	-
12	7.79	-	-
13	7.53	-	-
14	7.28	-	-
15	7.04	7	85.7
16	8.40	-	-
17	8.16	-	-
18	9.99	-	-
19	10.22	-	-

Table 6.2-5 – Loose Plate Number Densities (as-modeled)

Plate	U-234 (atom/b-cm)	U-235 (atom/b-cm)	U-236 (atom/b-cm)	U-238 (atom/b-cm)	Aluminum (atom/b-cm)	Total (atom/b-cm)
3	2.1539E-05	3.3600E-03	1.2458E-05	1.7823E-04	5.1018E-02	5.4591E-02
5	2.7492E-05	4.2887E-03	1.5901E-05	2.2749E-04	4.9477E-02	5.4037E-02
8	2.6975E-05	4.2081E-03	1.5602E-05	2.2322E-04	4.9611E-02	5.4085E-02
15	2.7249E-05	4.2508E-03	1.5760E-05	2.2548E-04	4.9540E-02	5.4059E-02

This page left intentionally blank.

Security-Related Information Figure Withheld Under 10 CFR 2.390.

Figure 6.2-1 – ATR Fuel Element Dimensions

This page left intentionally blank.

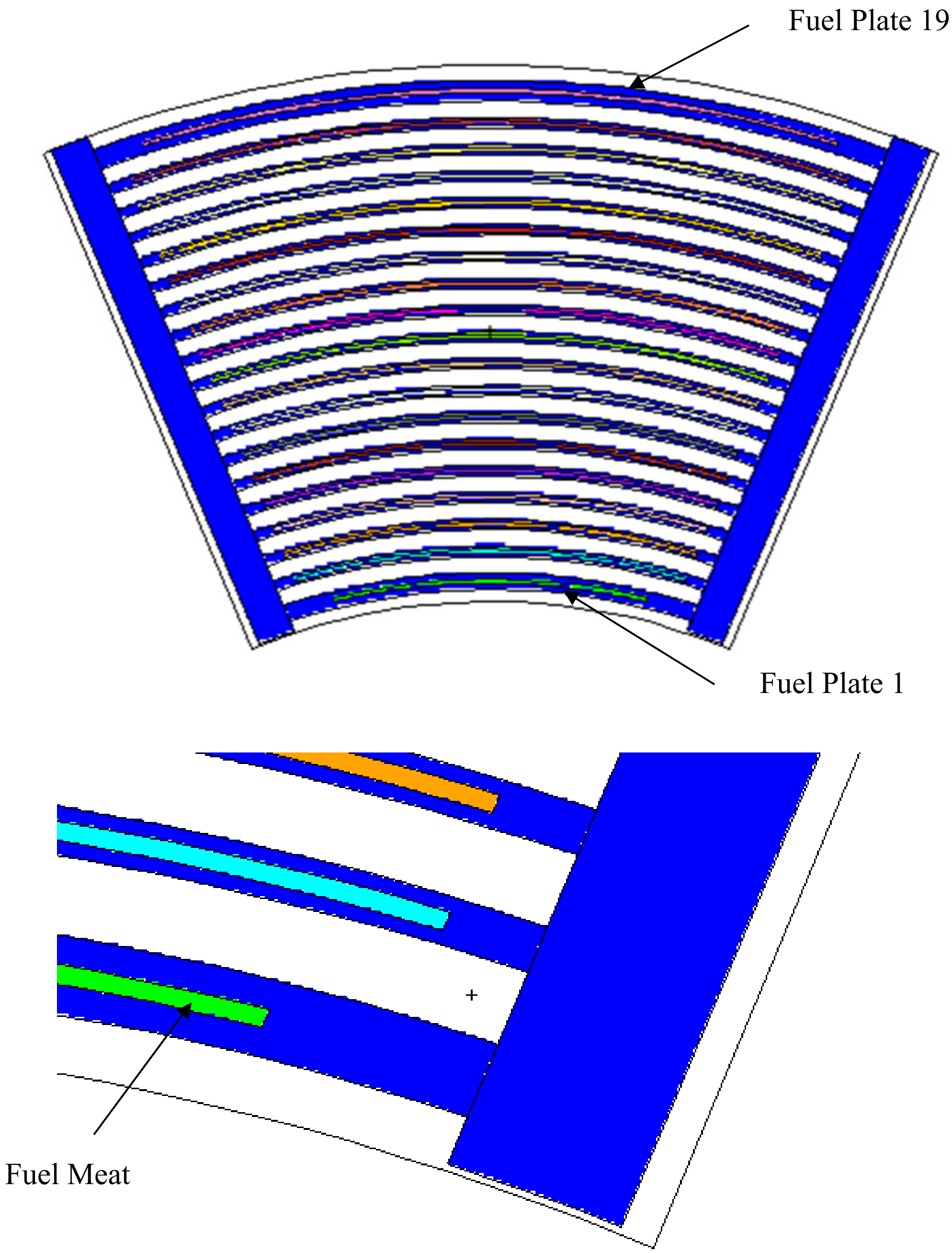

Figure 6.2-2 – Fuel Element Model

6.3 General Considerations

Criticality calculations for the ATR FFSC are performed using the three-dimensional Monte Carlo computer code MCNP5[2]. Descriptions of the fuel assembly geometric models are given in Section 6.3.1, *Model Configuration*. The material properties for all materials used in the models are provided in Section 6.3.2, *Material Properties*. The computer code and cross section libraries used are provided in Section 6.3.3, *Computer Codes and Cross-Section Libraries*. Finally, the most reactive configuration is provided in Section 6.3.4, *Demonstration of Maximum Reactivity*.

6.3.1 Model Configuration

Models are developed for both the fuel element and loose plate basket payloads.

6.3.1.1 Fuel Element Payload

The model configuration is relatively simple. Most packaging details are conservatively ignored, particularly at the ends. Because the package is long and narrow, array configurations will stack only in the lateral directions (e.g., 5x5x1). Therefore, the end details, for both the package and the fuel element, are conservatively ignored external to the active fuel region, and these end regions are simply modeled as full-density water.

The package consists of two primary structural components, a circular inner tube and a square outer tube, as shown in Appendix 1.3.2, *Packaging General Arrangement Drawings*. The inner tube has a nominal outer diameter of 6-in and a nominal thickness of 0.12-in. The outer tube has a nominal outer dimension of 8-in and a nominal thickness of 0.188-in. A layer of insulating material 1-in thick is wrapped around the inner tube.

For the inner tube, tolerances are based upon ASTM A269[3]. The tolerance on the outer diameter (OD) is ± 0.030-in, and the tolerance on the wall thickness is ±10%. Tolerances are selected to minimize the spacing between the fuel elements in the array configuration. This spacing is minimized using the maximum OD and minimum wall thickness. Using the minimum wall thickness also reduces parasitic neutron absorption in the steel. Therefore, the modeled tube OD is 6.03-in, the modeled wall thickness is 0.108-in, and the modeled tube ID is 5.814-in.

For the outer tube, the wall thickness tolerance is ±10% based upon ASTM A554[4] (the tolerance for the optional use of ASTM A240[5] also falls within this value). Using the minimum wall thickness of 0.169-in reduces parasitic neutron absorption in the steel. Reactivity in the array cases is maximized by minimizing the outer dimensions of the square. A bounding tolerance of 0.1-in is assumed for this dimension based on drawing tolerance in Appendix 1.3.2, *Packaging General Arrangement Drawings*, for a modeled OD of 7.9-in. The as-fabricated packages will meet this tolerance.

---

[2] MCNP5, "*MCNP – A General Monte Carlo N-Particle Transport Code, Version 5; Volume II: User's Guide*," LA-CP-03-0245, Los Alamos National Laboratory, April, 2003.

[3] ASTM A269-02a, *Standard Specification for Seamless and Welded Austenitic Stainless Steel Tubing for General Service*.

[4] ASTM A554-03, *Standard Specification for Welded Stainless Steel Mechanical Tubing*.

[5] ASTM A240-03, *Standard Specification for Chromium and Chromium-Nickel Stainless Steel Plate, Sheet, and Strip for Pressure Vessels and for General Applications*.

In the NCT single package models, the inner tube, insulation, and outer tube are modeled explicitly, as shown in Figure 6.3-1 and Figure 6.3-2. Although negligible water ingress is expected during NCT, the inner cavity of the package is assumed to be flooded with water because the package lid does not contain a seal. However, the region between the insulation and the outer tube will remain dry because water cannot enter this region. The Fuel Handling Enclosure (FHE) is conservatively ignored. Modeling the FHE would decrease water reflection in the single package model. However, the neoprene along the sides of the FHE is modeled explicitly using a thickness of 1/8-in. Because neoprene will reduce the reactivity due to parasitic absorption in chlorine, chlorine is removed from the neoprene, and the density is reduced accordingly. In the model, the fuel element is conservatively positioned at the radial center of the inner tube to maximize neutron reflection. The package is reflected with 12-in of full-density water.

The HAC single package model is essentially the same as the NCT single package model. Damage in the drop tests was shown to be negligible and concentrated at the ends of the package (See Section 2.12.1). As the ends of the package are not modeled, this end damage does not affect the modeling. The various side drops resulted in only minor localized damage to the outer tube, and no observable bulk deformation of the package. Therefore, the minor damage observed will not impact the reactivity. The insulation is replaced with full-density water, and the region between the insulation and outer tube is also filled with full-density water (see Figure 6.3-3). The treatment of the FHE is the same as the NCT single package model. Cases are developed both with and without the FHE neoprene, and with and without chlorine in the neoprene.

As a result of the drop tests, limited damage to the fuel element was observed. The bottom end box sheared off from the main body, although this condition has no effect on the criticality models because the fuel element is not modeled beyond the active fuel region. Limited damage to the fuel element plates was observed at the ends, although this damage is over a short length in a region of low reactivity worth. Slight localized buckling of the fuel plates was also observed in the region of the fuel element side plate vent openings, as the fuel plates are not as well supported in these regions. Because the observed fuel element damage is minor and will have only a negligible effect on reactivity, no damaged fuel element models are developed.

In the NCT array models, a 9x9x1 array is utilized. Although the FHE would survive NCT events with no damage, the FHE is conservatively ignored and the fuel elements are pushed toward the center of the array. Because the fuel elements are transported in a thin (~0.01-in) plastic bag, this plastic bag is assumed to act as a boundary for partial moderation effects. The plastic bag is not modeled explicitly, because it is too thin to have an appreciable effect on the reactivity. Therefore, it is postulated that the fuel element channels may fill with full-density water, while the region between the fuel element and inner tube fills with variable density water. The partial moderation effects that could be achieved by modeling the FHE explicitly are essentially addressed by the partial moderation analysis using the plastic bag. Also, modeling the FHE explicitly would result in the fuel elements being significantly pushed apart, which is a less reactive condition. Axial movement of the fuel elements is not considered because axial movement would increase the effective active height of the system and reduce the reactivity due to increased leakage. The presence of chlorine-free neoprene is also considered.

In the HAC array models, a 5x5x1 array is utilized. The HAC array models are essentially the same as the NCT array models, except additional cases are developed to determine the reactivity effect of allowing variable density water in the region between the inner and outer tubes. Cases are also developed with and without the insulation, and with and without chlorine-free neoprene. The FHE is conservatively ignored for the reasons stated in the previous paragraph. Because the NCT and HAC models are very similar and the NCT models utilize a larger array, the NCT array models are more reactive than the HAC array models.

The detailed moderation assumptions for the array cases are discussed more fully in Section 6.5, *Evaluation of Package Arrays under Normal Conditions of Transport*, and Section 6.6, *Package Arrays under Hypothetical Accident Conditions*.

6.3.1.2 Loose Plate Basket Payload

The NCT and HAC single package models are shown in Figure 6.3-4 and Figure 6.3-5, respectively. The NCT and HAC packaging models, including tolerances, are consistent with the values used in the fuel element analysis. The difference is that the aluminum loose plate basket and payload of fuel plates is inserted into the cavity. The loose plate basket does not contain neoprene.

The dimensions of the loose plate basket are provided on the packaging general arrangement drawings. The wall thickness of the basket in the central rectangular region is 0.19 ± 0.06-in. The cavity width is 4.5 ± 0.06-in, and the cavity height is 1.62 ± 0.06-in. The basket wall thickness is modeled at the minimum thickness of 0.13-in to minimize absorption in the aluminum. The inner dimensions of the basket are modeled at the maximum values of 4.56-in x 1.68-in to maximize the volume available for moderation. The radial supports are neglected in the MCNP models.

In the actual loaded configuration, the loose plates are bundled so that the plates are in close contact, and aluminum dunnage plates are used to fill the void space to prevent lateral movement. In the criticality models, the dunnage plates are conservatively ignored. Modeling the dunnage plates would severely restrict the volume available for water moderation. Because no dunnage plates are modeled, the fuel plates are allowed to arrange in the most reactive geometry, including non-regular pitches. Flat plates are modeled rather than curved plates because flat plates are much simpler to model. It is demonstrated that flat plates and curved plates are neutronically equivalent.

Axial movement of the fuel plates is not considered, because this motion would be negligible and is precluded by the basket design, which has a cavity length of 50.5-in. The fuel plates are approximately 49.5-in long, although only the 48-in active length is modeled.

In the NCT and HAC single package models, the fuel basket is centered in the cavity to maximize water reflection, and all water is at full density to maximize moderation and reflection.

In the NCT array analysis, four different plate types are examined: 3, 5, 8, and 15. Plate type 5 is shown to be the most reactive. A number of both regular and non-regular pitches are utilized in order to find the most reactive condition. Plate type 5 is used in all single package and array analyses.

In the NCT array models, a 9x9x1 array is utilized. Water is assumed to be present inside the cavity at a density that maximizes reactivity. To bound any potential damage to the loose plate basket, the rectangular region of each basket is pushed toward the radial center of the array until contact is made with the circular tube. This geometry is not considered credible because the ribs will maintain concentricity between the basket and cavity.

In the HAC array models, a 5x5x1 array is utilized. Water is assumed to be present inside the cavity and between the inner and outer tubes at a density that maximizes reactivity. The detailed moderation assumptions for the array cases are discussed more fully in Section 6.5, *Evaluation of Package Arrays under Normal Conditions of Transport*, and Section 6.6, *Package Arrays under Hypothetical Accident Conditions.*

The fuel plates are modeled as undamaged in both the NCT and HAC models. As a result of the drop tests, limited buckling of the fuel plates was observed at the end, although this damage is over a short length in a region of low reactivity worth. Because the observed fuel plate damage is minor and will have only a negligible effect on reactivity, no damaged fuel plate models are developed. Also, any anticipated damage is bounded because the most reactive pitch is modeled for both uniform and non-uniform conditions, and the damaged condition is essentially a subset of the conditions already modeled.

6.3.2 Material Properties

The fuel meat compositions are provided in Table 6.2-3 and Table 6.2-5 for the fuel element and loose plates, respectively. The fuel plate cladding is aluminum alloy 6061-0, while the side plates may be either aluminum alloy 6061-T6 or 6061-T651. From a criticality perspective, these alloys are essentially aluminum, and in the MCNP models all aluminum alloy structural materials are modeled as pure aluminum with a density of 2.7 g/cm^3. The material properties of the remaining packaging and moderating materials are described in the following paragraphs.

The inner and outer tubes of the package are constructed from stainless steel 304. Although MCNP is used in the calculations, the standard compositions for stainless steel 304 are obtained from the SCALE material library[6], which is a standard set accepted for use in criticality analyses. The stainless steel composition and density utilized in the MCNP models are provided in Table 6.3-1.

The insulation material utilized in the NCT models has a density of 6 pounds per cubic foot (0.096 g/cm^3). The insulation is composed of Al_2O_3 and SiO_2 in approximately equal quantities, with small (<1 wt%) quantities of other minor constituents. It is assumed in this analysis that the material is simply 50% Al_2O_3 and 50% SiO_2 by weight and the impurities are neglected. Insulation material properties are provided in Table 6.3-2.

Neoprene (C_4H_5Cl) has a density of 1.23 g/cm^3, and the chemical composition is provided in Table 6.3-3. Because chlorine is a neutron absorber, for models in which the chlorine has been deleted, a density of 0.737 g/cm^3 is utilized.

Water is modeled with a density ranging up to 1.0 g/cm^3 and the chemical formula H_2O. The $S(\alpha,\beta)$ card LWTR.60T is used to simulate hydrogen bound to oxygen in water.

[6] *Standard Composition Library*, NUREG/CR-0200, Rev. 6, Volume 3, Section M8, ORNL/NUREG/CSD-2/V3/R6, September 1998.

6.3.3 Computer Codes and Cross-Section Libraries

MCNP5 v1.30 is used for the criticality analysis[7]. All cross sections utilized are at room temperature (293.6 K). The uranium isotopes utilize preliminary ENDF/B-VII cross section data that are considered by Los Alamos National Laboratory to be more accurate than ENDF/B-VI cross sections. ENDF/B-V cross sections are utilized for chromium, nickel, and iron because natural composition ENDF/B-VI cross sections are not available for these elements. The remaining isotopes utilize ENDF/B-VI cross sections. Titles of the cross sections utilized in the models have been extracted from the MCNP output and provided in Table 6.3-4. As discussed in Section 6.3.2, the S(α,β) card LWTR.60T is also used to simulate hydrogen bound to water.

Cases are run with a minimum 2500 neutrons per generation for 250 generations, skipping the first 50. The 1-sigma uncertainty is approximately 0.001 for most cases.

6.3.4 Demonstration of Maximum Reactivity

Fuel Element Payload

The reactivities of the NCT and HAC single package cases are small, with $k_s < 0.5$.

The NCT and HAC array cases are similar. For the NCT array, a 9x9x1 array is utilized, while in the HAC array, a smaller 5x5x1 array is utilized. Because negligible damage was observed in the drop tests, the package dimensions are the same between the NCT and HAC models. Dimensions of both the fuel element and packaging are selected to maximize reactivity, and close-water reflection is utilized. In the fuel element, the fuel meat width and channel width are maximized, as this condition is the most reactive. In both NCT and HAC array cases, flooding with partial moderation is allowed in the central cavity, and the fuel elements are pushed toward the center of the array. In the fuel element models, the FHE is not modeled explicitly because the FHE would increase the fuel element spacing and decrease the reactivity. Any partial moderation effects of the FHE are essentially addressed by the partial moderation analysis for the fuel element itself.

In the NCT array models, insulation is modeled between the inner and outer tubes, while in the HAC array models, this region may have water, void, or insulation. In both sets of models, chlorine-free neoprene is modeled adjacent to the fuel element side plates, although the effect on the reactivity is small. No models in which the neoprene is allowed to decompose and homogeneously mix with the water are developed, as this scenario is already bounded by the variable water density search.

The NCT array is more reactive than the HAC array, primarily because the NCT array is significantly larger. The most reactive case (Case E23) results in a $k_s = 0.8362$, which is below the USL of 0.9209.

Loose Plate Basket Payload

The reactivities of the NCT and HAC single package cases are small, with $k_s < 0.5$.

To facilitate model preparation, only four different plate types are examined: 3, 5, 8, and 15. The fuel meat width is maximized in all loose plate models, as this condition has been shown to

[7] MCNP5, "*MCNP – A General Monte Carlo N-Particle Transport Code, Version 5; Volume II: User's Guide*," LA-CP-03-0245, Los Alamos National Laboratory, April 2003.

maximize reactivity. For simplicity, plate types are not mixed in the same model. An optimum pitch search is performed to determine the most reactive condition. Both regular and non-regular pitches are examined. Plate 5 is the most reactive because its small width allows this plate to “double stack” along the width of the basket, resulting in a higher level of moderation compared to the larger plates. Plates 1 through 4 are smaller than Plate 5, but the low uranium loading of these plates results in a higher number of plates to achieve 600 g U-235, and the larger number of plates results in less moderation. In actual practice, plates of any type may be combined in a single loose plate basket, although random combinations of plates would be less reactive than modeling all plates as type 5.

The actual loose plate basket may accept either flat or curved plates. However, plates are modeled as flat rather than curved to facilitate model preparation. It is demonstrated that flat plates are neutronically equivalent to curved plates.

The array geometry and modeling assumption for the loose plate basket payload are similar to those described above for the fuel element payload. The NCT array is more reactive than the HAC array, primarily because the NCT array is significantly larger. The most reactive NCT configuration is with full-water density between the fuel plates, a water density of 0.5 g/cm^3 between the basket and the inner pipe, and void between the insulation and the outer tube. The axial regions beyond the active fuel are modeled as water to maximize reflection. The most reactive case (Case LG5) results in a $k_s = 0.7747$, which is below the USL of 0.9209. Note that the most reactive loose plate basket case is less reactive than the most reactive fuel element payload case.

Table 6.3-1 – SS304 Composition

Component	Wt.%
C	0.08
Si	1.0
P	0.045
Cr	19.0
Mn	2.0
Fe	68.375
Ni	9.5
Density = 7.94 g/cm^3	

Table 6.3-2 – Insulation Composition

Component	Wt.%
Al	26.5
Si	23.4
O	50.2
Density = 0.096 g/cm^3	

Table 6.3-3 – Neoprene Composition

Component	Wt.%
H	5.7
C	54.3
Cl	40.0
Density = 1.23 g/cm^3	

Table 6.3-4 – Cross Section Libraries Utilized

Isotope/Element	Cross Section Label (from MCNP output)
1001.62c	1-h-1 at 293.6K from endf-vi.8 njoy99.50
6000.66c	6-c-0 at 293.6K from endf-vi.6 njoy99.50
8016.62c	8-o-16 at 293.6K from endf-vi.8 njoy99.50
13027.62c	13-al-27 at 293.6K from endf-vi.8 njoy99.50
14000.60c	14-si-nat from endf/b-vi
15031.66c	15-p-31 at 293.6K from endf-vi.6 njoy99.50
17000.66c	17-cl-0 at 293.6K from endf-vi.0 njoy99.50
24000.50c	njoy
25055.62c	25-mn-55 at 293.6K from endf/b-vi.8 njoy99.50
26000.55c	njoy
28000.50c	njoy
92234.69c	92-u-234 at 293.6K from t16 u234la4 njoy99.50
92235.69c	92-u-235 at 293.6K from t16 u235la9d njoy99.50
92236.69c	92-u-236 at 293.6K from t16 u236la2d njoy99.50
92238.69c	92-u-238 at 293.6K from t16 u238la8h njoy99.50

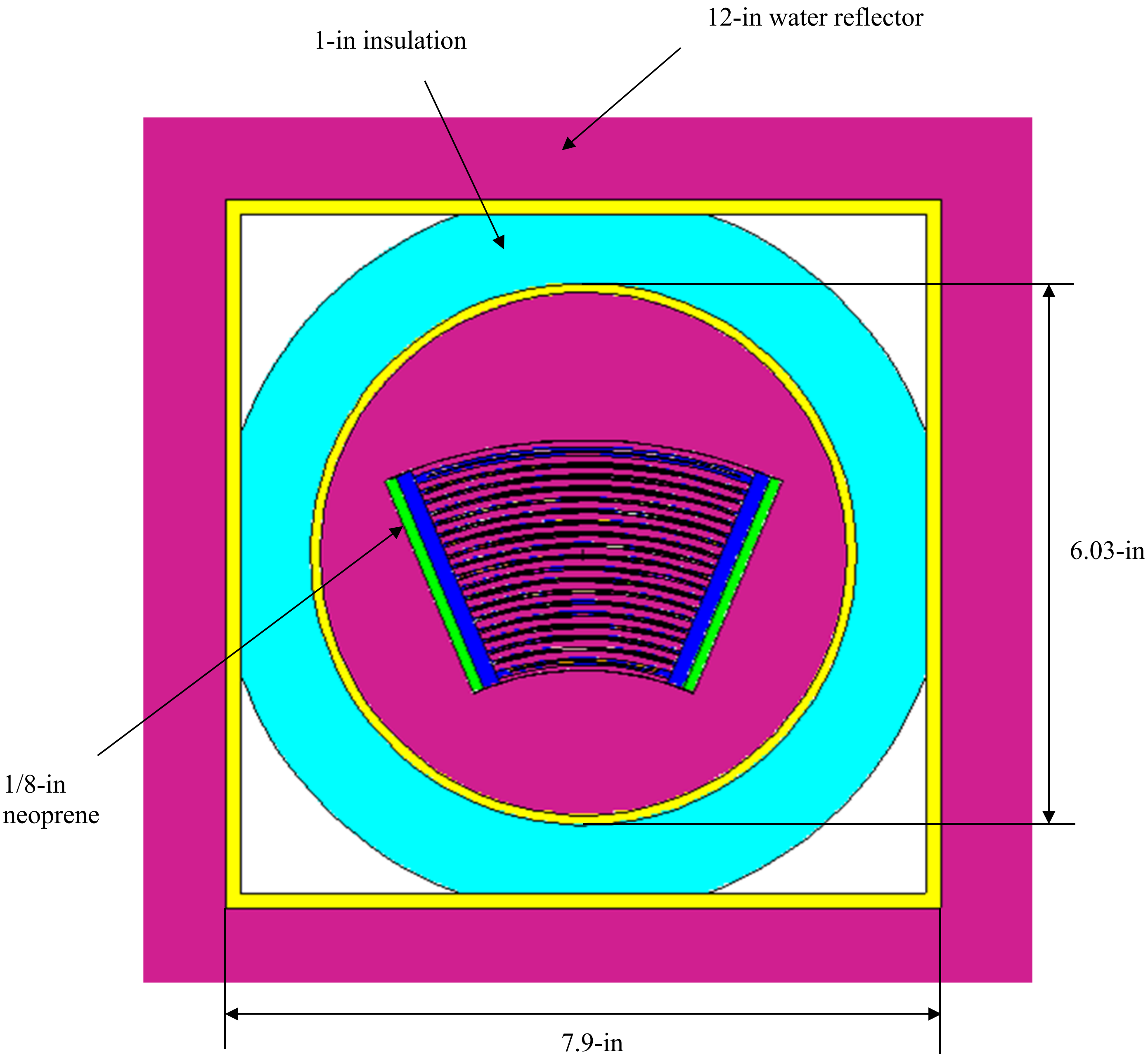

Figure 6.3-1 – NCT Single Package Model, Fuel Element (planar view)

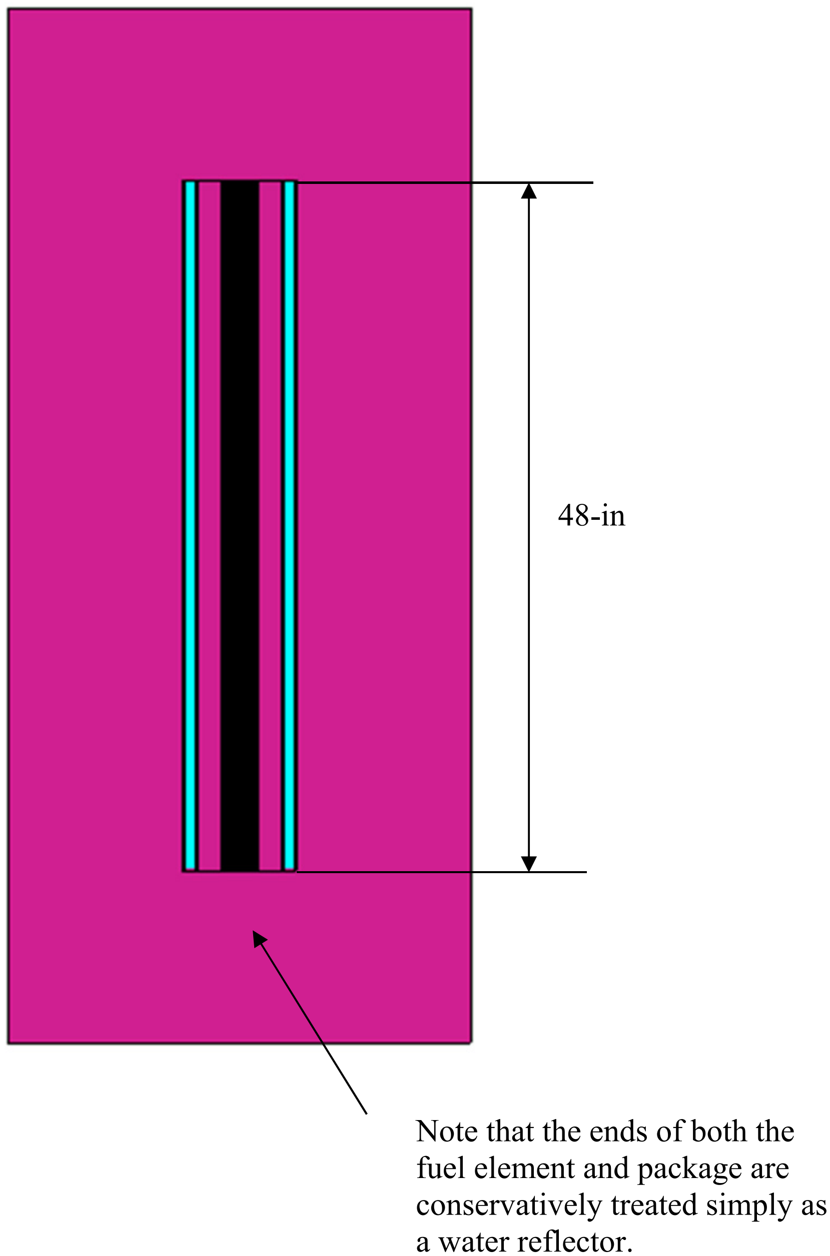

Figure 6.3-2 – NCT Single Package Model, Fuel Element (axial view)

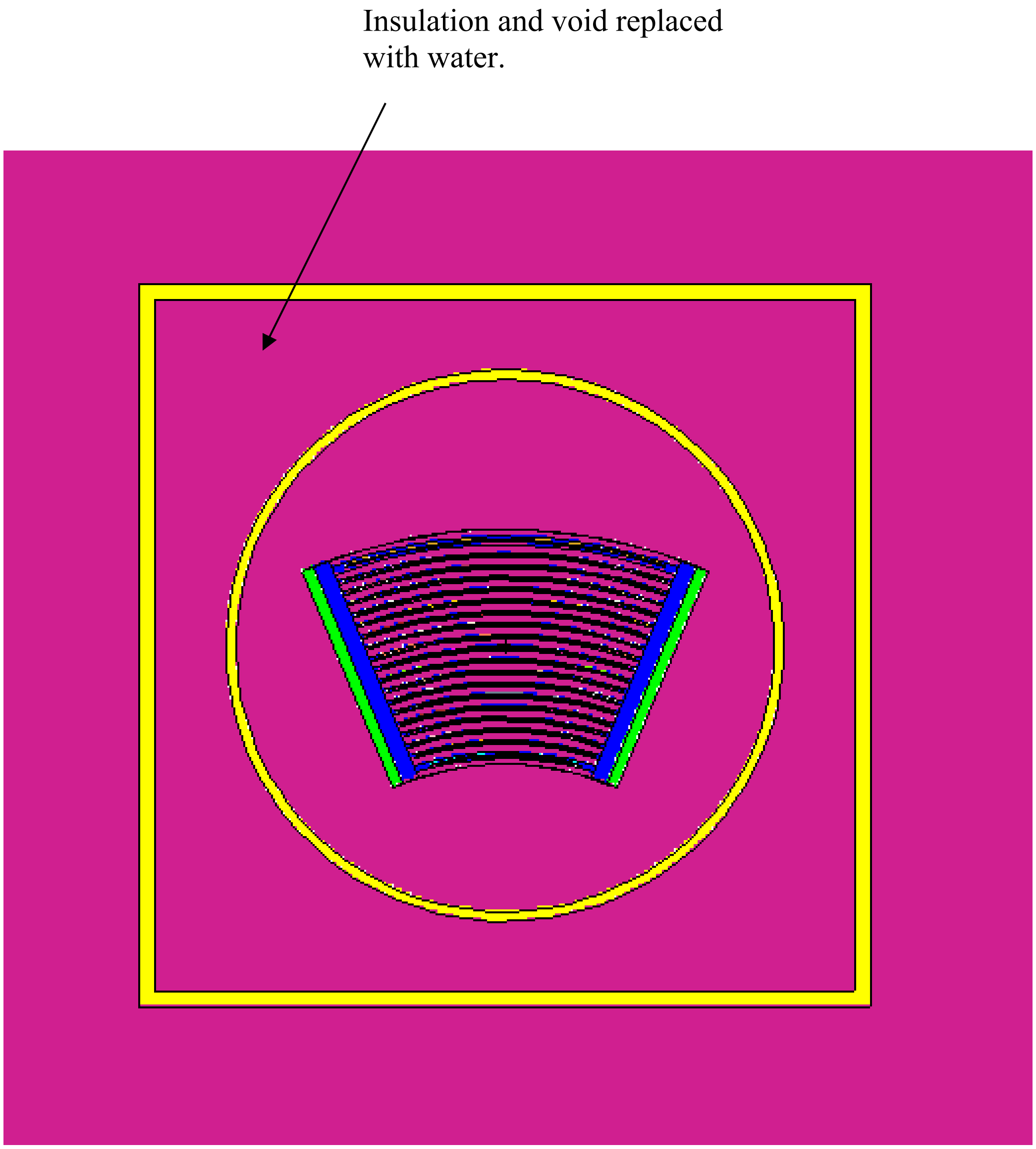

Figure 6.3-3 – HAC Single Package Model, Fuel Element (planar view)

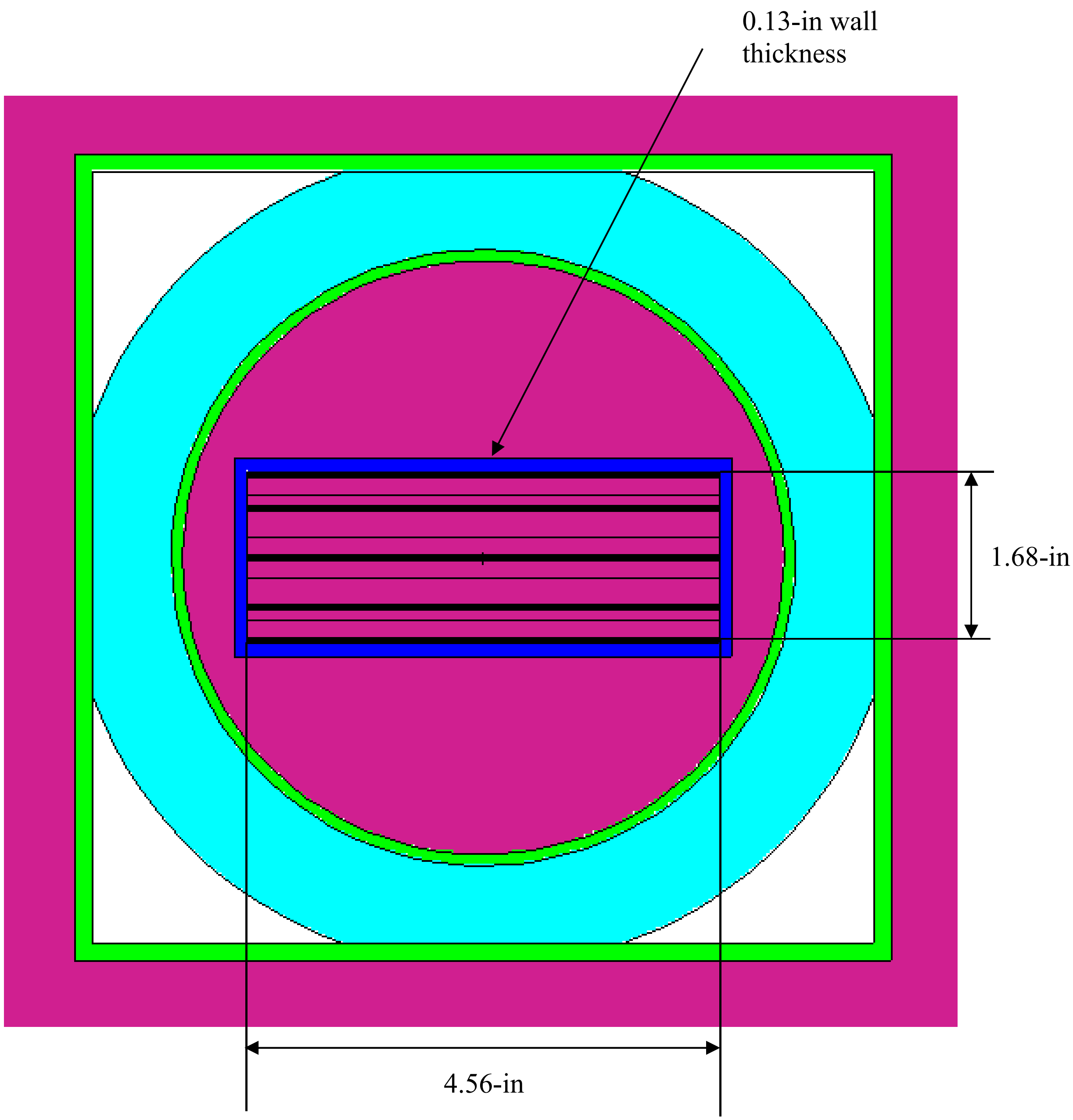

Figure 6.3-4 – NCT Single Package Model, Basket (planar view)

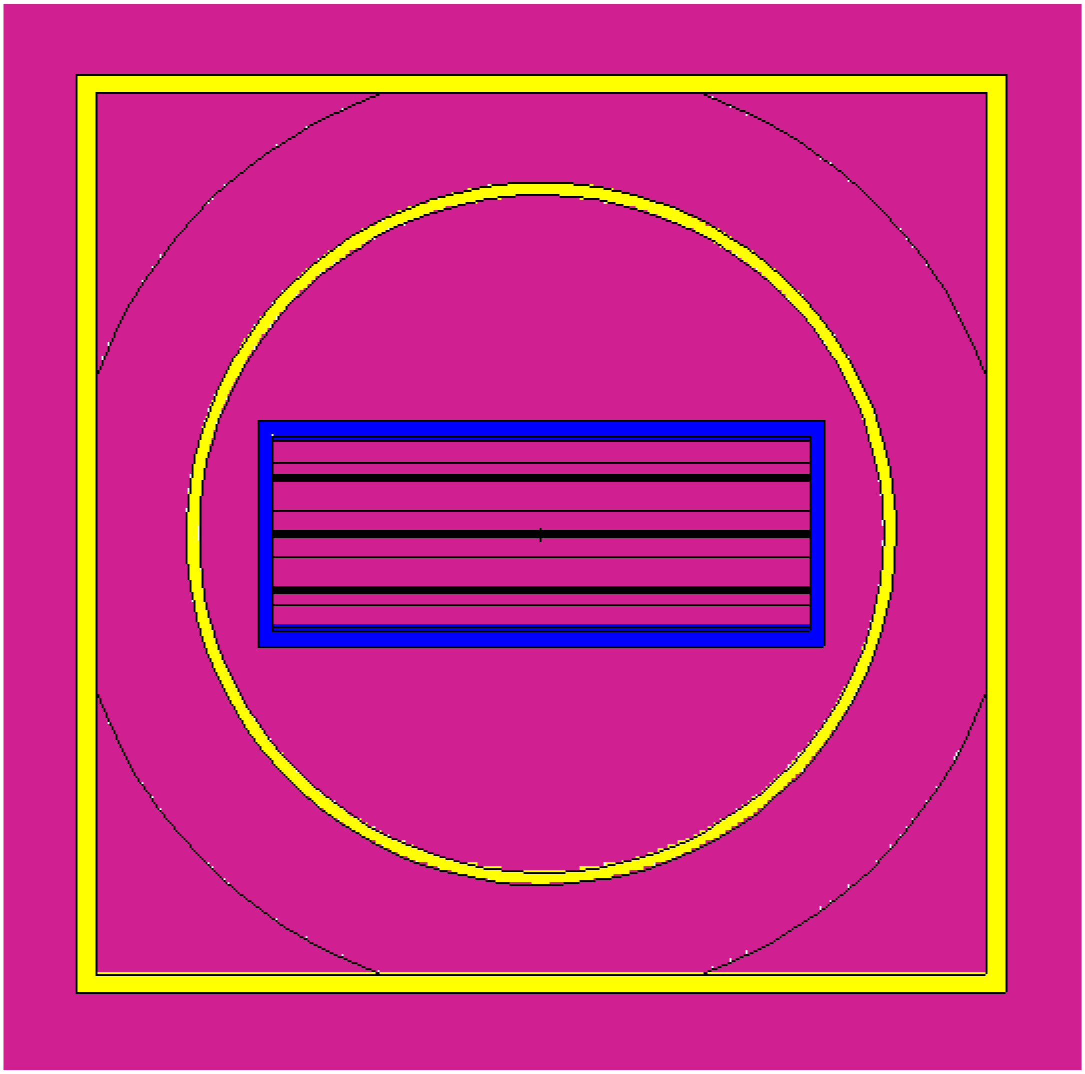

Case LB3

Figure 6.3-5 – HAC Single Package Model, Basket (planar view)

6.4 Single Package Evaluation

Compliance with the requirements of 10 CFR §71.55 is demonstrated by analyzing an optimally moderated damaged and undamaged, single-unit ATR FFSC. The figures and descriptions provided in Section 6.3.1, *Model Configuration*, describe the basic geometry of the single-unit models.

6.4.1 Single Package Configuration

6.4.1.1 NCT Configuration

6.4.1.1.1 Fuel Element Payload

The geometry of the NCT single package configuration is discussed in Section 6.3.1, *Model Configuration*. The inner tube is flooded with full-density water. The fuel element geometry is consistent with the most reactive fuel element model, including tolerances, as determined in Section 6.4.1.2.1, *Fuel Element Payload Parametric Evaluation*. Consistent with the most reactive HAC single package model, neoprene from the FHE is modeled at the sides of the fuel element. Chlorine is conservatively removed from the neoprene because chlorine acts as a poison. The package is reflected with 12-in of water.

Two cases are developed. In Case A1, the modeled channel width is 0.085-in, and in Case A2, the modeled channel width is 0.089-in. A channel width of 0.089-in is the maximum local channel width (0.087-in) with an additional margin of 0.002-in. The larger channel width is achieved by reducing the cladding thickness. Case A2 is more reactive, although the reactivity is low, with k_s = 0.42239. This result is below the USL of 0.9209. Results are provided in Table 6.4-1.

6.4.1.1.2 Loose Plate Basket Payload

The selection of the bounding fuel plate and development of the various plate arrangements are presented in conjunction with the NCT array analysis in Section 6.5.1.2, *Loose Plate Basket Payload*. It is determined that Plate 5 may be used as a bounding plate type for criticality purposes. Because the aluminum dunnage has not been credited, the plates are allowed to become arranged in the most reactive configuration within the loose plate container. The most reactive fuel plate arrangements determined in the NCT array analysis are used in the NCT single package analysis. The NCT single package models are reflected with 12-in of water.

The 10 Type 5 plates are modeled as 5 plates of double fuel meat width to allow two plates to be present side by side. The top and bottom plates are in contact with the fuel basket inner surfaces, and the center plate is always in the center of the basket. The two off-center plates are shifted in 0.1-cm increments away from the center plate so that the pitch is non-regular. When the pitch is non-regular, the maximum pitch is given as a "max" value in the results table.

A figure showing the general NCT model geometry is provided in Figure 6.3-4. Results are provided in Table 6.4-2. Six cases are run, with small variations in the plate arrangement. The maximum reactivity occurs for Case LA4, with k_s = 0.40199. This result is below the USL of 0.9209. The pitch of this case is non-regular. The top, center, and bottom plates are centered in the lattice locations with a base pitch of 1.036-cm, while the off-center plates are shifted 0.3-cm from the center plate. Note that the most reactive NCT array case peaks with the off-center plates shifted 0.2-cm rather than 0.3-cm, although this difference is most likely due to statistical fluctuation.

6.4.1.2 HAC Configuration

6.4.1.2.1 Fuel Element Payload Parametric Evaluation

Prior to development of a single package model, a parametric analysis is performed to determine the impacts of various fuel element tolerances on the reactivity. This parametric analysis considers the effects of a number of parameters, such as fuel meat arc length, fuel meat thickness, channel width, and active fuel length.

Because the ATR fuel element is complex, with 19 unique fuel plates and 19 unique fuel material descriptions, performing this parametric study on an actual fuel element would be cumbersome. Rather, the approach utilized is to perform the parametric study on a system of 19 identical flat plates. This geometry mimics the ATR fuel element to determine trends in the data. Note that the reactivity of the 19 flat plate model is not identical to the reactivity of an actual ATR fuel element due to geometrical and material differences, although the trends are the same. The most reactive model variations are then incorporated into the ATR fuel element model.

In the parametric models, 1200 g U-235 is equally distributed between 19 identical flat plates. The base configuration consists of plates with a fuel meat width of 2.65-in (6.7355 cm; the average nominal meat arc length), active fuel height of 48-in, fuel meat thickness of 0.02-in, fuel cladding thickness of 0.015-in (total plate thickness of 0.050-in), and fuel channel thickness of 0.078-in. The geometry of Case B1 is shown in Figure 6.4-1. A total of 12 parametric models are developed, as summarized below.

Case ID	Case Description
B1	Base case
B2	Increase width of fuel meat by 0.1-in
B3	Decrease width of fuel meat by 0.1-in
B4	Increase thickness of fuel meat by 0.002-in
B5	Decrease thickness of fuel meat by 0.002-in
B6	Increase thickness of fuel meat by 0.002-in but decrease the cladding thickness to maintain a nominal plate thickness
B7	Decrease thickness of fuel meat by 0.002-in but increase the cladding thickness to maintain a nominal plate thickness
B8	Increase water channel thickness to 0.085-in
B9	Increase water channel thickness to 0.085-in by reducing the cladding thickness
B10	Decrease active fuel length to 47.0-in
B11	Reduce cladding thickness to the minimum value of 0.008-in
B12	Combine cases B2 and B9

In Cases B2 through B12, each case is identical to the base case B1 with the exception of the changes identified in the table above. The pitch, which is the sum of the plate thickness and channel thickness, is treated as a dependant variable and is allowed to vary as the independent parameters are changed. For example, in Case B5, decreasing the thickness of the fuel meat decreases the pitch, although the channel thickness remains constant. The detailed model description of the parametric cases is summarized in Table 6.4-3.

The results of the parametric analysis are summarized in Table 6.4-4. Because the uncertainty in the calculation is ~0.001, a difference of at least 0.002 (2 milli-k, abbreviated mk) between the various cases is required in order to distinguish a real effect from statistical fluctuation. The results indicate a reactivity increase of 4.3 mk for Case B2, when the width of the fuel meat is increased, and a decrease of 5.4 mk for Case B3, when the width of the fuel meat is decreased. Therefore, reactivity increases when the width of the fuel meat is maximized.

The nominal thickness of the fuel meat is 0.02-in. No tolerance on the fuel meat is defined because the fuel plates are fabricated using a rolling process. A thickness tolerance of 0.002-in (±10%) is assumed for computational purposes. In Cases B4 and B5, the fuel meat thickness is adjusted for constant channel thickness and variable pitch, while for Cases B6 and B7 the fuel meat thickness is adjusted for constant plate thickness and nominal pitch. The reactivity fluctuations are within 2 mk in all four cases, and it is concluded that a nominal fuel meat thickness of 0.02-in is acceptable for modeling purposes.

In Case B8, the water channel thickness is increased to 0.085-in (increase in pitch), while in Case B9 the water channel thickness is increased to the maximum by artificially reducing the cladding thickness (nominal pitch). Both cases B8 and B9 show large reactivity gains of 9.6 and 12.9 mk, respectively, indicating that reactivity increases when the water channel thickness increases.

In Case B10, the active fuel length is reduced to a lower bound value of 47.0-in. The reactivity increase is within statistical fluctuation. It may be inferred that increasing the active fuel length would also result in a reactivity effect within statistical fluctuation.

In Case B11, the cladding is reduced to the minimum value of 0.008-in, and the reactivity increases by 5.5 mk. This reactivity gain is likely due to the more compact geometry, as the pitch reduces considerably. This scenario is not directly applicable to an ATR fuel element because the pitch is fixed by the side plates and such a minimum pitch is not possible.

The only cases that show a statistically significant increase are B2, B8, B9, and B11. In Case B12, the increased fuel meat width of Case B2 and increased channel width of Case B9 are combined. This model geometry bounds Case B8, and Case B11 is incorporated in an approximate manner because the cladding thickness has been reduced to accommodate the larger channel. The reactivity of Case B12 represents an increase of 19.5 mk over base Case B1.

6.4.1.2.2 Fuel Element Payload

The geometry of the HAC single package configuration is discussed in Section 6.3.1, *Model Configuration*. Based on the parametric evaluation, three HAC single package ATR fuel element models are developed in order to verify the trends indicated in the parametric analysis: (1) Case C1, a nominal (base) model, (2) Case C2, a conservative model with the increased channel width consistent with Case B9, and (3) Case C3, an optimized model with both increased channel width and increased meat arc length. In all three models, the FHE neoprene is ignored and a nominal pitch is utilized (i.e., the centerline radial locations of the 19 plates are the same in each model). Note that in Cases C1 and C2, the fuel number densities are computed using nominal fuel meat arc lengths and thus do not correspond to the values in Table 6.2-3. In the increased channel width models, the channel width is increased by removing cladding. This approach is highly conservative, because it is unlikely (if not impossible) to maximize the channel width between each plate. In an actual fuel element, maximizing the channel width between two plates would likely minimize the channel width between the next two plates, as the overall plate thickness is held to a rather tight tolerance.

The HAC single package results are provided in Table 6.4-5. As expected from the parametric analysis, Case C2 is more reactive than Case C1 (by 13.7 mk), and Case C3 is more reactive than Case C1 (by 17.2 mk). Therefore, it may be concluded that reactivity is maximized in the ATR fuel element by maximizing the fuel meat arc length and maximizing the channel width between the fuel plates. This optimized fuel element is used in all models using the fuel element payload (including NCT single package, NCT array, and HAC array models).

In Cases C1, C2, and C3, the neoprene of the FHE is ignored and treated as full-density water. In Cases C4 and C5, the effect of neoprene is evaluated. Neoprene is a hydrocarbon with the chemical formula C_4H_5Cl. Neoprene is present on the FHE and is used to cushion the fuel element. In Case C4, 1/8-in of neoprene is modeled along the sides of the fuel element (see Figure 6.3-3). The small strips of neoprene above and below the fuel element are neglected because these strips are of insufficient mass to affect the reactivity in any appreciable manner. Inclusion of the neoprene has a pronounced negative effect on the reactivity, presumably due to absorption in the chlorine. In Case C5, the chlorine is deleted from the neoprene, and the density is reduced accordingly. Eliminating the chlorine from the neoprene may be postulated to be a result of decomposition during a fire, although such a scenario is not credible. Case C5 is slightly more reactive than Case C3, although the effect may simply be statistical fluctuation. It may be concluded that chlorine-free neoprene has a negligible effect on the reactivity.

Because the fuel may be transported inside of a plastic bag, it is conservatively assumed that the water density inside of the inner tube can vary independently of the water density inside of the fuel element. To maximize neutron reflection, full-density water is always modeled inside of the tube external to the fuel element, and the fuel element is centered laterally within the tube. In Cases C6 through C10, Case C5 is run with a range of water densities between the fuel plates, and maximum water density in all other regions of the model. Reactivity drops as the water density is reduced between the fuel plates, indicating that the system is under moderated.

Case C5 is the most reactive case when comparing Cases C1 through C10. In Case C11, Case C5 is rerun with the channel width increased from 0.085-in to 0.089-in. A channel width of 0.089-in is the maximum local channel width (0.087-in) with an additional margin of 0.002-in. The larger channel width is achieved by reducing the cladding thickness. Case C11 is the most reactive, with k_s = 0.45237. This result is below the USL of 0.9209.

6.4.1.2.3 Loose Plate Basket Payload

The selection of the bounding fuel plate and development of the various plate arrangements are presented in conjunction with the NCT array analysis in Section 6.5.1.2, *Loose Plate Basket Payload*. The most reactive fuel plate arrangements determined in the NCT array analysis are used in the HAC single package analysis. This arrangement will also be the most reactive in the HAC single package models because both the NCT and HAC models are flooded and behave in a similar manner.

A figure showing the general HAC model geometry is provided in Figure 6.3-5. Results are provided in Table 6.4-6. Six cases are run, with small variations in the plate arrangement. The maximum reactivity occurs for Case LB3, with k_s = 0.43629. This result is below the USL of 0.9209. The pitch of this case is non-regular. The top, center, and bottom plates are centered in the lattice locations with a base pitch of 1.036-cm, while the off-center plates are shifted 0.2-cm from the center plate.

6.4.2 Single Package Results

Following are the tabulated results for the single package cases. The most reactive configurations are listed in boldface.

Table 6.4-1 – NCT Single Package Results, Fuel Element

NCT Case					
Case ID	**Filename**	**Moderator Density (g/cm^3)**	**k_{eff}**	**σ**	**k_s (k+2σ)**
A1	NS_M100	1.0	0.41068	0.00097	0.41262
A2	**NS_M100_C89**	**1.0**	**0.42021**	**0.00109**	**0.42239**

Table 6.4-2 – NCT Single Package Results, Loose Plate Basket

Case ID	Filename	Pitch (cm)	k_{eff}	σ	k_s (k+2σ)
LA1	NS_N5P52	1.036	0.39898	0.00091	0.40080
LA2	NS_N5P52A	1.136 (max)	0.39847	0.00096	0.40039
LA3	NS_N5P52B	1.236 (max)	0.39856	0.00097	0.40050
LA4	**NS_N5P52C**	**1.336 (max)**	**0.40007**	**0.00096**	**0.40199**
LA5	NS_N5P52D	1.436 (max)	0.39881	0.00095	0.40071
LA6	NS_N5P52E	1.491 (max)	0.39751	0.00095	0.39941

Table 6.4-3 – Parametric Analysis Input Data, Fuel Element

Parameter	B1	B2	B3	B4	B5	B6
Fuel Arc (cm)	6.7355	6.9895	6.4815	6.7355	6.7355	6.7355
Meat thickness (in)	0.02	0.02	0.02	0.022	0.018	0.022
Active fuel height (in)	48	48	48	48	48	48
Channel (in)	0.078	0.078	0.078	0.078	0.078	0.078
Cladding (in)	0.015	0.015	0.015	0.015	0.015	0.014
Total plate (in)	0.050	0.050	0.050	0.052	0.048	0.050
Pitch (in)	0.128	0.128	0.128	0.130	0.126	0.128
Volume (cm^3)	41.7164	43.2895	40.1432	45.8880	37.5447	45.8880
U-235 (g)	63.2	63.2	63.2	63.2	63.2	63.2
U-235 density (g/cm^3)	1.51	1.46	1.57	1.38	1.68	1.38
UAlx+Al density (g/cm^3)	3.86	3.81	3.91	3.74	4.00	3.74
N U-234	2.4865E-05	2.3962E-05	2.5840E-05	2.2605E-05	2.7628E-05	2.2605E-05
N U-235	3.8789E-03	3.7380E-03	4.0309E-03	3.5263E-03	4.3099E-03	3.5263E-03
N U-236	1.4382E-05	1.3859E-05	1.4945E-05	1.3074E-05	1.5980E-05	1.3074E-05
N U-238	2.0576E-04	1.9828E-04	2.1382E-04	1.8705E-04	2.2862E-04	1.8705E-04
N U-Al	5.0157E-02	5.0391E-02	4.9905E-02	5.0742E-02	4.9442E-02	5.0742E-02
Total	5.4281E-02	5.4365E-02	5.4190E-02	5.4491E-02	5.4024E-02	5.4491E-02

Parameter	B7	B8	B9	B10	B11	B12
Fuel Arc (cm)	6.7355	6.7355	6.7355	6.7355	6.7355	6.9895
Meat thickness (in)	0.018	0.02	0.02	0.02	0.02	0.02
Active fuel height (in)	48	48	48	47	48	48
Channel (in)	0.078	0.085	0.085	0.078	0.078	0.085
Cladding (in)	0.016	0.015	0.0115	0.015	0.008	0.0115
Total plate (in)	0.050	0.050	0.0430	0.050	0.036	0.0430
Pitch (in)	0.128	0.135	0.128	0.128	0.114	0.128
Volume (cm^3)	37.5447	41.7164	41.7164	40.8473	41.7164	43.2895
U-235 (g)	63.2	63.2	63.2	63.2	63.2	63.2
U-235 density (g/cm^3)	1.68	1.51	1.51	1.55	1.51	1.46
UAlx+Al density (g/cm^3)	4.00	3.86	3.86	3.89	3.86	3.81
N U-234	2.7628E-05	2.4865E-05	2.4865E-05	2.5394E-05	2.4865E-05	2.3962E-05
N U-235	4.3099E-03	3.8789E-03	3.8789E-03	3.9615E-03	3.8789E-03	3.7380E-03
N U-236	1.5980E-05	1.4382E-05	1.4382E-05	1.4688E-05	1.4382E-05	1.3859E-05
N U-238	2.2862E-04	2.0576E-04	2.0576E-04	2.1014E-04	2.0576E-04	1.9828E-04
N U-Al	4.9442E-02	5.0157E-02	5.0157E-02	5.0020E-02	5.0157E-02	5.0391E-02
Total	5.4024E-02	5.4281E-02	5.4281E-02	5.4232E-02	5.4281E-02	5.4365E-02

Table 6.4-4 – Parametric Analysis Results, Fuel Element

Case ID	Filename	k_{eff}	σ	k_s ($k+2\sigma$)	Δ from B1 (mk)
B1	P1	0.46601	0.00096	0.46793	--
B2	P2	0.47015	0.00102	0.47219	4.3
B3	P3	0.46045	0.00102	0.46249	-5.4
B4	P5	0.46403	0.00101	0.46605	-1.9
B5	P4	0.46442	0.00111	0.46664	-1.3
B6	P10	0.46753	0.00105	0.46963	1.7
B7	P9	0.46683	0.00101	0.46885	0.9
B8	P6	0.47528	0.00112	0.47752	9.6
B9	P7	0.47879	0.00100	0.48079	12.9
B10	P8	0.46704	0.00106	0.46916	1.2
B11	P11	0.47123	0.00108	0.47339	5.5
B12	P12	0.48534	0.00104	0.48742	19.5

Table 6.4-5 – HAC Single Package Results, Fuel Element

Case ID	Filename	Water Density Between Plates (g/cm^3)	k_{eff}	σ	k_s (k+2σ)
C1	HS_M100_NOM	1.0	0.42274	0.00095	0.42464
C2	HS_M100_TOL	1.0	0.43639	0.00099	0.43837
C3	HS_M100_TOLW	1.0	0.43991	0.00097	0.44185
C4	HS_M100_TOLW_N1	1.0	0.41002	0.00102	0.41206
C5	HS_M100_TOLW_N2	1.0	0.44040	0.00104	0.44248
C6	HS_M050	0.5	0.35396	0.00088	0.35572
C7	HS_M060	0.6	0.36994	0.00095	0.37184
C8	HS_M070	0.7	0.38607	0.00099	0.38805
C9	HS_M080	0.8	0.40411	0.00102	0.40615
C10	HS_M090	0.9	0.42092	0.00096	0.42284
C11	**HS_M100_TOLW_N2_C89**	**1.0**	**0.45029**	**0.00104**	**0.45237**

Table 6.4-6 – HAC Single Package Results, Loose Plate Basket

Case ID	Filename	Pitch (cm)	k_{eff}	σ	k_s (k+2σ)
LB1	HS_N5P52	1.036	0.43263	0.00097	0.43457
LB2	HS_N5P52A	1.136 (max)	0.43350	0.00092	0.43534
LB3	**HS_N5P52B**	**1.236 (max)**	**0.43443**	**0.00093**	**0.43629**
LB4	HS_N5P52C	1.336 (max)	0.43388	0.00096	0.43580
LB5	HS_N5P52D	1.436 (max)	0.43328	0.00091	0.43510
LB6	HS_N5P52E	1.491 (max)	0.43169	0.00089	0.43347

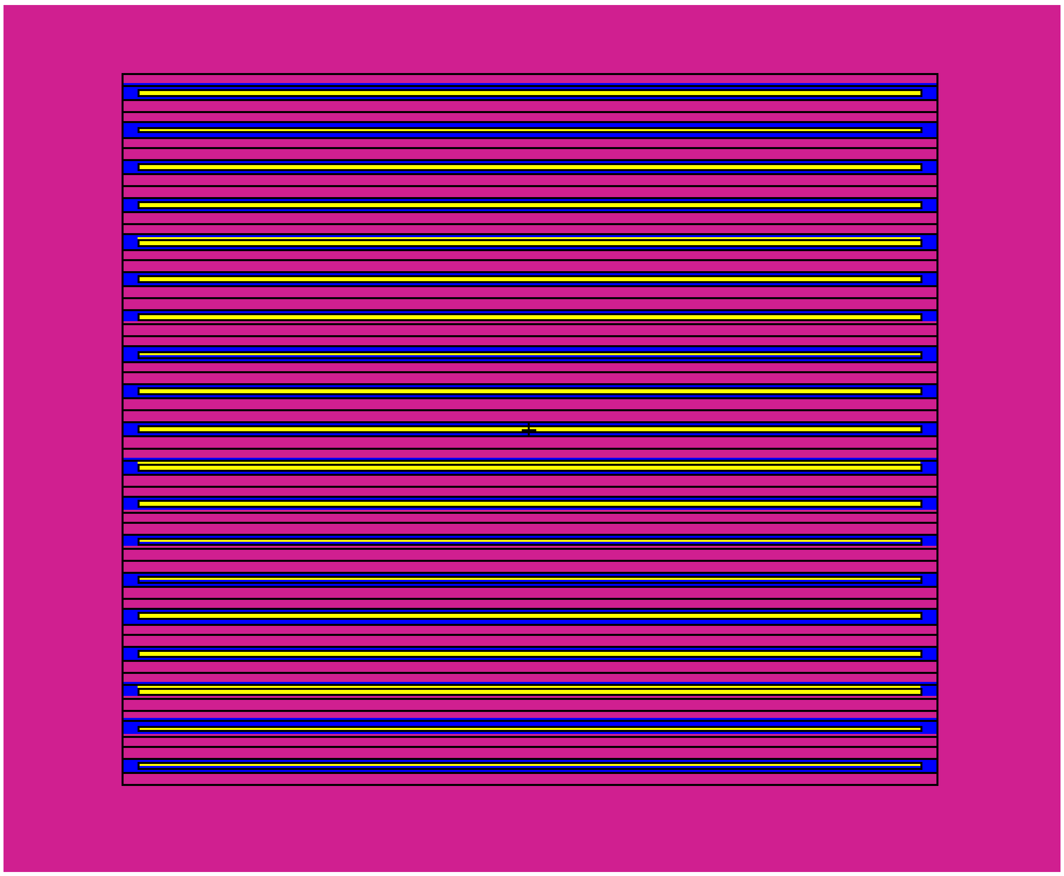

Figure 6.4-1 – Base Parametric Model (Case B1)

6.5 Evaluation of Package Arrays under Normal Conditions of Transport

6.5.1 NCT Array Configuration

6.5.1.1 Fuel Element Payload

The NCT array model is a 9x9x1 array of the NCT single package model, see Figure 6.5-1. Although an 8x8x1 array is of sufficient size to justify a CSI = 4.0, the larger 9x9x1 array is utilized simply for modeling convenience. Neoprene is modeled without chlorine in all models. It is demonstrated in Section 6.6.1.1, *Fuel Element Payload*, that chlorine-free neoprene may have a slight positive effect on the reactivity, although the effect is small. The entire array is reflected with 12-in of full-density water.

The fuel elements are pushed to the center of the array and rotated to minimize the distance between the fuel elements. This geometry is not feasible for NCT, because the FHE would force the fuel elements to remain in the center of the package, although the FHE does allow rotation. Therefore, it is conservative to ignore the FHE to minimize the separation distance. In addition, a small notch is added to the neoprene so that the fuel element may be translated to the maximum extent without interfering with the inner tube geometry. This notch is not present in the single package models.

Three calculational series are developed. In Series 1, the water density is fixed at 1.0 g/cm^3 between the fuel plates and the water density is allowed to vary inside the inner tube. The channel width is modeled at 0.085-in. Series 2 is the same as Series 1, although the density within the fuel plates is at a reduced density of 0.9 g/cm^3. Void is always present between the insulation and the outer tube, as this region is water-tight. Series 3 is a repeat of Series 1, although with the channel width increased to 0.089-in. A channel width of 0.089-in is the maximum local channel width (0.087-in) with an additional margin of 0.002-in. The larger channel width is achieved by reducing the cladding thickness. The results are provided in Table 6.5-1.

Reactivity is at a maximum for Case E23, which has full-density water between the fuel plates, and 0.3 g/cm^3 water inside the inner tube, and a channel width of 0.089-in, with k_s = 0.83616. As expected, the reactivity drops when the water density between the fuel plates is reduced, as the system is under moderated. The maximum result is far below the USL of 0.9209.

As a point of interest, an additional case (Case D12) is developed in which the fuel elements are centered in the cavity and not rotated, using the moderation and channel width assumptions of Case D4 (see the lower figure of Figure 6.5-1). The reactivity drops by 18.5 mk, which essentially represents the additional conservatism of pushing the fuel elements to the center of the array.

6.5.1.2 Loose Plate Basket Payload

The NCT array model is a 9x9x1 array of the NCT single package model. For the NCT single package cases, it was sufficient to laterally center the fuel basket within the inner tube to maximize reflection by the water in the tube. However, in the NCT array configuration, it is expected that reactivity would be maximized by pushing the fuel baskets to the center of the array, as shown in the top sketch of Figure 6.5-2. The fuel elements may be packed closer by rotating them as shown in the figure. Therefore, unless otherwise noted, all NCT array models have the baskets pushed toward the center of the array. Although this assumption bounds any anticipated basket damage, this arrangement is not credible, because the structural ribs that center the baskets within the inner tube will not deform in this manner.

The loose plate payload consists of 19 different plate types. Each plate type has a different width and uranium mass, although the lengths are the same. Each plate may be either flat or curved, for a total of 19*2 = 38 different variations. However, flat and curved plates will not be mixed in the same basket (to facilitate packaging). Within each loose plate basket, any combination of plate types may be present, with the only limitation that the total U-235 mass present in the basket must not exceed 600 g.

Clearly, there are a large number of possible combinations of plates that may be present within the basket. The objective is to determine a simplified configuration that bounds any random collection of plates. Fortunately, calculations may be performed using only flat plates, because the neutronic behavior of flat and curved plates is demonstrated to be nearly identical. Therefore, the flat plate results also apply to the curved plates. Flat plates allow easy geometry setup using MCNP repeated structures, while curved plates generally cannot be modeled using repeated structures unless the plate pitch is rather large.

Basic data for the 19 plate types are provided in Table 6.2-1. It is not necessary to model each of the 19 different plate types. Rather, from examination of these data, a subset of plates is selected for further analysis. Plates 5 through 15 have a U-235 density of approximately 1.64 g/cm^3, while the remaining plates have a significantly lower U-235 density. Plate 5 is the smallest plate in this range, and Plate 15 is the largest plate in this range; both are selected for further evaluation. Plate 8 is also selected as a representative plate between these two extremes, and should result in reactivity values between Plate 5 and 15. It is demonstrated that the smaller plate configuration (Plate 5) is more reactive than the larger plate configurations (Plates 8 and 15). Plate 3 is also selected for further evaluation because it is smaller than Plate 5, although the reduced U-235 density will result in a larger number of plates.

For simplicity, only one plate type is modeled within each basket. Randomly mixing different plate types would result in a less reactive condition that the most reactive single plate configuration. Also, number densities of the selected plates have been slightly adjusted so that the total mass of U-235 is always 600 g. For plates 5, 8, and 15, the number densities are increased, while for plate 3 the number densities are decreased.

Four initial series of calculations are performed, one series for each of the four plate types under consideration. The goal of these initial calculations is to simply determine the bounding plate type. Once the bounding plate type has been determined, additional series of calculations are performed on the bounding plate type. For all of the initial models, full-density water is modeled between the plates, 0.3 g/cm^3 water is modeled between the plate array and basket (this region is not present once the plate array fills the entire basket area), 0.3 g/cm^3 water is modeled between the basket and inner tube, and insulation/void is modeled between the inner and outer tubes. The water density of 0.3 g/cm^3 is selected based upon the most reactive moderation condition of the ATR fuel element analysis, and will be optimized once the bounding plate is selected.

Fuel Plate 5 Series: Fuel plate 5 is the first plate type examined. Ten plates are required to achieve a mass of 600 g U-235. The plate arrangements for a number of the configurations are shown in Figure 6.5-3 through Figure 6.5-5. Results are provided in Table 6.5-2. In cases LC1 through LC9, the plates are arranged in a 1x10 array at the center of the basket. Reactivity is low when the pitch is small, and reactivity increases as the pitch increases. In cases LC10 and LC11, the reactivity increases as the plates are alternately shifted to the right and left because moderation increases. In case LC12, plates are alternately shifted up and down until they contact each other.

Because fuel plate 5 is rather narrow, it is possible to further increase the moderation by modeling the plates in a 2x5 array in cases LC13 through LC29. Because the plate is slightly too wide to fit two side-by-side, the two side-by-side plates are modeled as a single plate by doubling the fuel meat width. The reactivity continues to increase with increasing pitch. Case LC19 has the largest reactivity obtained with a constant pitch.

However, moderation can be further increased if a non-regular pitch is utilized. In cases LC20 through LC29, non-regular pitches are examined. In these cases, the plates at the top, center, and bottom of the basket remain fixed, while the two off-center plates are shifted away from the center plate in 0.1-cm increments. Because the pitches in these cases are non-regular, the pitches provided in the results table are noted as “max” values. Case LC21 is the most reactive, with k_s=0.76806, although the reactivity gain resulting from a non-regular pitch is relatively small and within statistical fluctuation. For case LC21, the top, center, and bottom plates are centered in the lattice locations with a base pitch of 1.036 cm, while the off-center plates are shifted 0.2-cm from the center plate (maximum pitch of 1.236 cm).

Fuel Plate 8 Series: Nine plates are required to achieve a mass of 600 g U-235. The plate arrangements for a number of configurations are shown in Figure 6.5-6 and Figure 6.5-7. Results are provided in Table 6.5-3. Considerably fewer cases are generated compared to fuel plate 5 because it has been established that the plates are highly under moderated when packed tightly.

In cases LD1 through LD3, the plates are modeled in a simple 1x9 array. In cases LD4 though LD11, the plates are alternately shifted left and right to increase moderation. In cases LD6 through LD11, the top, bottom, and center plates remain fixed, while the remaining plates are progressively shifted up or down in 0.1-cm increments. Case LD7 is the most reactive, with k_s=0.75241, although the reactivity is less than the most reactive plate 5 case. For case LC7, the base lattice pitch is 0.574-cm, and the off-center plates are shifted 0.2-cm from the center plate.

Fuel Plate 15 Series: Seven plates are required to achieve a mass of 600 g U-235. The plate arrangements for a number of the configurations are shown in Figure 6.5-8. Results are provided in Table 6.5-3. Using the same methodology as plates 5 and 8, case LE8 is the most reactive, with k_s=0.74548. This case also features a non-regular pitch. For case LE8, the base lattice pitch is 0.804 cm, and the off-center plates are shifted 0.1 cm from the center plate.

Comparing the maximum k_s values for plates 5, 8, and 15, plate 5 is the most reactive (k_s=0.76806), plate 15 is the least reactive (k_s=0.74548), and plate 8 falls between the two (k_s=0.75241). In fact, the reactivities of plates 8 and 15 are fairly close, despite the difference in the width and number of plates. Plate 5 is somewhat more reactive than either plate 8 or 15, most likely because its narrow width allows “double stacking” of this plate along the width of the basket, which results in a more advantageous moderation and geometry conditions. Therefore, the trend is that for a fixed U-235 mass per basket, the smaller plates are more reactive than the larger plates.

Of course, plates 1 through 4 are smaller than plate 5. However, these plates have a lower U-235 density so that more plates are required to achieve 600 g U-235. More plates would provide less volume for moderation, so it is expected that plate 5 would bound plates 1 through 4. This is confirmed by running several cases for plate 3.

Fuel Plate 3 Series: Fourteen plates are required to achieve a mass of 600 g U-235. The plate arrangements for the configurations are shown in Figure 6.5-9. Results are provided in Table 6.5-3. All cases are for a 2x7 arrangement and non-regular pitches, as similar arrangements have been shown to be the most reactive for the other plates. Two side-by-side plates are modeled as a single plate with double fuel meat width, consistent with the treatment of the Type 5 plate. Case LF2 is the most reactive, with k_s=0.75904, although this case is less reactive than the Type 5 plate. For case LF2, the pitch is 0.796 cm.

Criticality Analysis Using Plate 5: From the analysis of plate types 3, 5, 8, and 15, Type 5 is shown to be the most reactive. Therefore, the remaining analysis uses only this plate type. An additional two series of cases are performed using fuel plate 5 in which the water densities in the various model regions are allowed to vary. The primary regions of interest are within the basket and between the basket and the inner tube.

In Series 1, full-density water is modeled within the basket, while the water density between the basket and the inner tube is varied from 0 to 1.0 g/cm^3. The results are provided in Table 6.5-4. The maximum reactivity occurs for Case LG5, with k_s = 0.77469. A water density of 0.5 g/cm^3 within the inner tube is utilized in the most reactive case.

In Series 2, the water density inside the basket is reduced to 0.9 g/cm^3, while the water density between the basket and the inner tube is varied from 0 to 1.0 g/cm^3. The reactivity clearly drops when reduced density water is modeled inside the basket.

Several miscellaneous cases are run to validate the assumptions noted above. In Case LJ1, the most reactive case (Case LG5) is run with the fuel baskets centered inside of the tubes (see the lower sketch of Figure 6.5-2). The reactivity drops as the fuel elements are pushed apart, k_s = 0.76237 for Case LJ1, compared to k_s = 0.77469 for Case LG5.

It has been implicitly assumed the maximum reactivity is obtained for the maximum fissile mass of 600 g U-235. In general, the maximum allowable fissile loading is not necessarily the most reactive condition if the volume of fissile material is so large that little volume is available for moderating material. That is not the case for the loose plate analysis, as the fuel plates are thin and only a small number of plates are required to achieve a mass of 600 g U-235. Removing plates might increase moderation slightly as water is added to the system, although reducing the fissile mass more than compensates for the additional moderation and lowers the reactivity. To demonstrate this effect, the arrangement of Case LC9, which has ten type 5 plates in a 1x10 evenly spaced array (see Figure 6.5-3), is repeated with ten, nine, eight, and seven evenly spaced plates (Cases LJ2, LJ3, LJ4, and LJ5, see Figure 6.5-10) with an inner tube water density of 0.5 g/cm^3. The reactivity drops as each successive plate is removed (0.62333 for Case LJ2 to 0.57579 for Case LJ5), despite the fact that the plates are spaced farther and farther apart and moderation is improved. If plates are removed from the most reactive models, for which the pitch is already non-regular to maximize reactivity, the reactivity drop resulting from removing plates would be more pronounced.

It is stated that modeling the plates as flat is neutronically equivalent to modeling the plates as curved. This modeling assumption is verified by modeling both flat and curved plates with a constant pitch of 0.80 cm. This pitch is selected because it is large and constant and the curved plates may be modeled with repeated structures. Case LJ6 is the flat plate model, and Case LJ7 is the curved plate model. Case LJ6 is geometrically identical to case LC13 (see Figure 6.5-4) except the water density inside the basket is 1.0 g/cm^3 between the plate array and the basket. Case LJ7 is shown in Figure 6.5-10. Flat plate Case LJ6 has k_s=0.73021, while curved plate Case LJ7 has k_s=0.73022. The difference between these cases is negligible, and the statement that flat plates are neutronically equivalent to curved plates is verified.

In conclusion, Case LG5 is the most reactive loose plate basket model, with k_s = 0.77469. This result is below the USL of 0.9209. Case LG5 has fully moderated fuel plates, 0.5 g/cm^3 water inside the inner tube, and fuel plate baskets that have been rotated and moved to the center of the array.

6.5.2 NCT Array Results

The results for the NCT array cases are provided in the following table. The most reactive configuration is listed in boldface.

Table 6.5-1 – NCT Array Results, Fuel Element Payload

Case ID	Filename	Water Density Between Tubes (g/cm^3)	Water Density Inside Inner Tube (g/cm^3)	Water Density Between Plates (g/cm^3)	k_{eff}	σ	k_s (k+2σ)
Series 1: Variable water density inside inner tube, full density water between plates.							
D1	NA_P000	0	0	1.0	0.76716	0.00120	0.76956
D2	NA_P010	0	0.1	1.0	0.80349	0.00123	0.80595
D3	NA_P020	0	0.2	1.0	0.81928	0.00112	0.82152
D4	**NA_P030**	**0**	**0.3**	**1.0**	**0.82605**	**0.00117**	**0.82839**
D5	NA_P040	0	0.4	1.0	0.82149	0.00119	0.82387
D6	NA_P050	0	0.5	1.0	0.81420	0.00118	0.81656
D7	NA_P060	0	0.6	1.0	0.80521	0.00108	0.80737
D8	NA_P070	0	0.7	1.0	0.79216	0.00121	0.79458
D9	NA_P080	0	0.8	1.0	0.78130	0.00132	0.78394
D10	NA_P090	0	0.9	1.0	0.76905	0.00120	0.77145
D11	NA_P100	0	1.0	1.0	0.75603	0.00124	0.75851
D12	NA_P030C	0	0.3	1.0	0.80743	0.00122	0.80987
Series 2: Variable water density inside inner tube, 0.9 g/cm^3 density water between plates.							
E1	NA_M90P000	0	0	0.9	0.72938	0.00111	0.73160
E2	NA_M90P010	0	0.1	0.9	0.77108	0.00120	0.77348
E3	NA_M90P020	0	0.2	0.9	0.79299	0.00116	0.79531
E4	NA_M90P030	0	0.3	0.9	0.79943	0.00123	0.80189
E5	**NA_M90P040**	**0**	**0.4**	**0.9**	**0.80192**	**0.00108**	**0.80408**
E6	NA_M90P050	0	0.5	0.9	0.79378	0.00108	0.79594
E7	NA_M90P060	0	0.6	0.9	0.78539	0.00111	0.78761
E8	NA_M90P070	0	0.7	0.9	0.77658	0.00118	0.77894
E9	NA_M90P080	0	0.8	0.9	0.76496	0.00117	0.76730
E10	NA_M90P090	0	0.9	0.9	0.75315	0.00121	0.75557
E11	NA_M90P100	0	1.0	0.9	0.74334	0.00126	0.74586
Series 3: Variable water density inside inner tube, full density water between plates, channel width increased to 0.089-in							
E20	NA_P000_C89	0	0	1.0	0.78147	0.00115	0.78377
E21	NA_P010_C89	0	0.1	1.0	0.81601	0.00119	0.81839
E22	NA_P020_C89	0	0.2	1.0	0.83027	0.00119	0.83265
E23	**NA_P030_C89**	**0**	**0.3**	**1.0**	**0.83372**	**0.00122**	**0.83616**
E24	NA_P040_C89	0	0.4	1.0	0.82984	0.00118	0.83220
E25	NA_P050_C89	0	0.5	1.0	0.82481	0.00125	0.82731
E26	NA_P060_C89	0	0.6	1.0	0.81462	0.00119	0.81700

Table 6.5-2 – NCT Array Results, Pitch Variations, Plate 5

Case ID	Filename	Pitch (cm)	k_{eff}	σ	k_s (k+2σ)
LC1	NA_N5P08	0.160	0.41955	0.00093	0.42141
LC2	NA_N5P10	0.200	0.44783	0.00091	0.44965
LC3	NA_N5P12	0.240	0.47653	0.00104	0.47861
LC4	NA_N5P14	0.280	0.50372	0.00104	0.50580
LC5	NA_N5P16	0.320	0.53109	0.00103	0.53315
LC6	NA_N5P18	0.360	0.55470	0.00109	0.55688
LC7	NA_N5P20	0.400	0.57669	0.00104	0.57877
LC8	NA_N5P22	0.440	0.59930	0.00111	0.60152
LC9	NA_N5P23	0.460	0.61120	0.00102	0.61324
LC10	NA_N5P23A	0.460	0.69108	0.00118	0.69344
LC11	NA_N5P23B	0.460	0.74866	0.00109	0.75084
LC12	NA_N5P23C	0.460	0.74714	0.00102	0.74918
LC13	NA_N5P40	0.800	0.71462	0.00107	0.71676
LC14	NA_N5P42	0.840	0.72319	0.00108	0.72535
LC15	NA_N5P44	0.880	0.73353	0.00102	0.73557
LC16	NA_N5P46	0.920	0.74169	0.00107	0.74383
LC17	NA_N5P48	0.960	0.74962	0.00112	0.75186
LC18	NA_N5P50	1.000	0.75920	0.00109	0.76138
LC19	NA_N5P52	1.036	0.76423	0.00118	0.76659
LC20	NA_N5P52A	1.136 (max)	0.76520	0.00102	0.76724
LC21	**NA_N5P52B**	**1.236 (max)**	**0.76582**	**0.00112**	**0.76806**
LC22	NA_N5P52C	1.336 (max)	0.76393	0.00107	0.76607
LC23	NA_N5P52D	1.436 (max)	0.76254	0.00096	0.76446
LC24	NA_N5P52E	1.493 (max)	0.75949	0.00093	0.76135
LC25	NA_N5P67	1.540 (max)	0.75942	0.00101	0.76144
LC26	NA_N5P67A	1.640 (max)	0.75508	0.00105	0.75718
LC27	NA_N5P67B	1.740 (max)	0.74803	0.00106	0.75015
LC28	NA_N5P67C	1.840 (max)	0.73839	0.00107	0.74053
LC29	NA_N5P67D	1.940 (max)	0.72412	0.00105	0.72622

Table 6.5-3 – NCT Array Results, Pitch Variations, Plates 8, 15, and 3

Case ID	Filename	Pitch (cm)	k_{eff}	σ	k_s ($k+2\sigma$)
Plate 8					
LD1	NA_N8P22	0.440	0.60412	0.00106	0.60624
LD2	NA_N8P24	0.480	0.62588	0.00106	0.62800
LD3	NA_N8P26	0.518	0.64309	0.00112	0.64533
LD4	NA_N8P26A	0.518	0.74015	0.00102	0.74219
LD5	NA_N8P29	0.574	0.74719	0.00105	0.74929
LD6	NA_N8P29A	0.674 (max)	0.74875	0.00112	0.75099
LD7	**NA_N8P29B**	**0.774 (max)**	**0.75035**	**0.00103**	**0.75241**
LD8	NA_N8P29C	0.874 (max)	0.74896	0.00099	0.75094
LD9	NA_N8P29D	0.974 (max)	0.74574	0.00102	0.74778
LD10	NA_N8P29E	1.074 (max)	0.74373	0.00092	0.74557
LD11	NA_N8P29F	1.174 (max)	0.73494	0.00106	0.73706
Plate 15					
LE1	NA_N15P32	0.640	0.68653	0.00107	0.68867
LE2	NA_N15P34	0.690	0.70200	0.00113	0.70426
LE3	NA_N15P34A	0.690	0.73590	0.00114	0.73818
LE4	NA_N15P34B	0.790 (max)	0.74090	0.00110	0.74310
LE5	NA_N15P34C	0.890 (max)	0.74003	0.00111	0.74225
LE6	NA_N15P34D	0.970 (max)	0.74209	0.00108	0.74425
LE7	NA_N15P40	0.804	0.74153	0.00115	0.74383
LE8	**NA_N15P40A**	**0.904 (max)**	**0.74322**	**0.00113**	**0.74548**
LE9	NA_N15P40B	1.004 (max)	0.74089	0.00118	0.74325
LE10	NA_N15P40C	1.104 (max)	0.73801	0.00100	0.74001
Plate 3					
LF1	NA_N3P40	0.796	0.75062	0.00102	0.75266
LF2	**NA_N3P40A**	**0.796**	**0.75696**	**0.00104**	**0.75904**
LF3	NA_N3P40B	0.896 (max)	0.75655	0.00107	0.75869
LF4	NA_N3P40C	0.996 (max)	0.75365	0.00094	0.75553
LF5	NA_N3P40D	1.096 (max)	0.75155	0.00106	0.75367

Table 6.5-4 – NCT Array Results, Plate 5

Case ID	Filename	Water Density Between Tubes (g/cm^3)	Water Density Inside Inner Tube (g/cm^3)	Water Density Between Plates (g/cm^3)	k_{eff}	σ	k_s ($k+2\sigma$)
Series 1: Variable water density inside inner tube, full-density water in basket.							
LG1	NA_N5P000	0	0	1.0	0.66797	0.00097	0.66991
LG2	NA_N5P010	0	0.1	1.0	0.71859	0.00100	0.72059
LG3	NA_N5P020	0	0.2	1.0	0.74925	0.00104	0.75133
LC21	NA_N5P52B	0	0.3	1.0	0.76582	0.00112	0.76806
LG4	NA_N5P040	0	0.4	1.0	0.77225	0.00117	0.77459
LG5	**NA_N5P050**	**0**	**0.5**	**1.0**	**0.77251**	**0.00109**	**0.77469**
LG6	NA_N5P060	0	0.6	1.0	0.76738	0.00099	0.76936
LG7	NA_N5P070	0	0.7	1.0	0.75998	0.00100	0.76198
LG8	NA_N5P080	0	0.8	1.0	0.75086	0.00114	0.75314
LG9	NA_N5P090	0	0.9	1.0	0.74066	0.00111	0.74288
LG10	NA_N5P100	0	1.0	1.0	0.72764	0.00111	0.72986
Series 2: Variable water density inside inner tube, reduced density water in basket.							
LH1	NA_N5M090P000	0	0	0.9	0.63496	0.00098	0.63692
LH2	NA_N5M090P010	0	0.1	0.9	0.69390	0.00093	0.69576
LH3	NA_N5M090P020	0	0.2	0.9	0.72793	0.00095	0.72983
LH4	NA_N5M090P030	0	0.3	0.9	0.74560	0.00108	0.74776
LH5	NA_N5M090P040	0	0.4	0.9	0.75402	0.00108	0.75618
LH6	**NA_N5M090P050**	**0**	**0.5**	**0.9**	**0.75480**	**0.00109**	**0.75698**
LH7	NA_N5M090P060	0	0.6	0.9	0.75429	0.00110	0.75649
LH8	NA_N5M090P070	0	0.7	0.9	0.74414	0.00100	0.74614
LH9	NA_N5M090P080	0	0.8	0.9	0.73639	0.00104	0.73847
LH10	NA_N5M090P090	0	0.9	0.9	0.72573	0.00095	0.72763
LH11	NA_N5M090P100	0	1.0	0.9	0.71549	0.00107	0.71763
Miscellaneous Cases							
LJ1	NA_N5P050C	0	0.5	1.0	0.76003	0.00117	0.76237
LJ2	NA_N5P23_10	0	0.5	1.0	0.62119	0.00107	0.62333
LJ3	NA_N5P23_9	0	0.5	1.0	0.60657	0.00106	0.60869
LJ4	NA_N5P23_8	0	0.5	1.0	0.59251	0.00114	0.59479
LJ5	NA_N5P23_7	0	0.5	1.0	0.57369	0.00105	0.57579
LJ6	NA_N5P40_F	0	0.5	1.0	0.72815	0.00103	0.73021
LJ7	NA_N5P40_C	0	0.5	1.0	0.72810	0.00106	0.73022

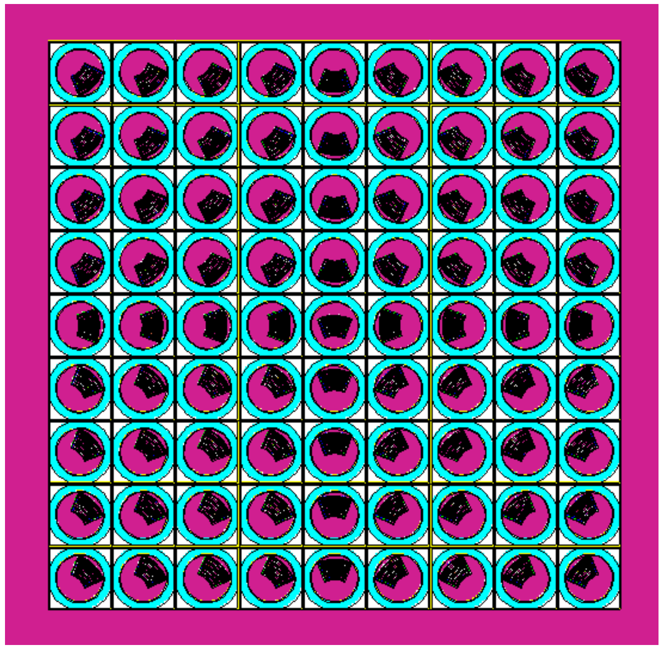

Pushed to center of array

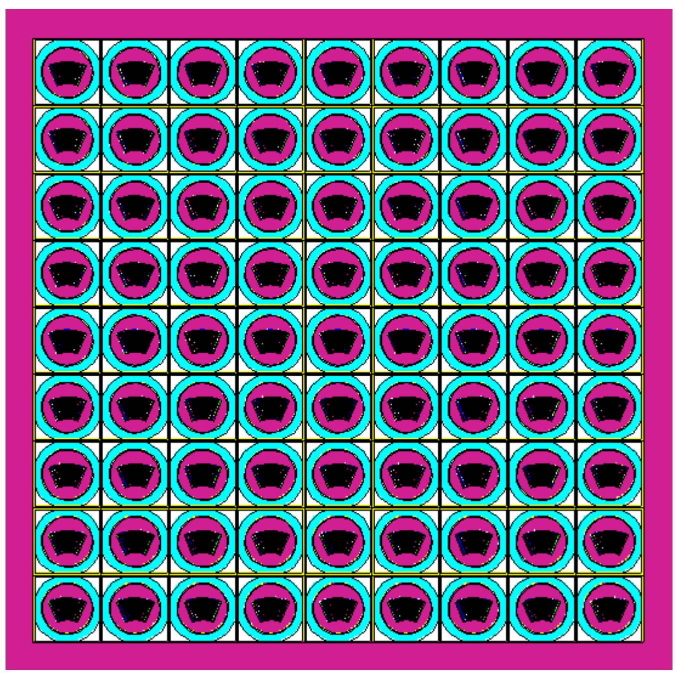

Centered in each tube (D12)

Figure 6.5-1 – NCT Array Geometry, Fuel Element Payload

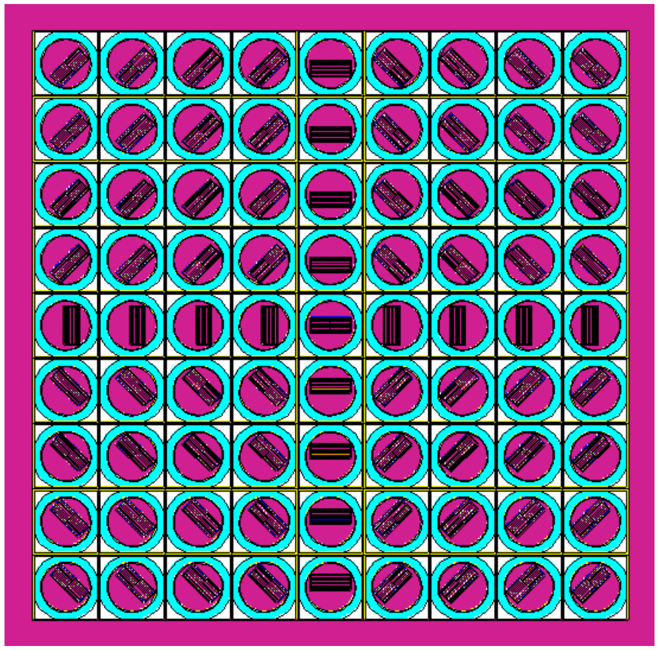

Pushed to center of array

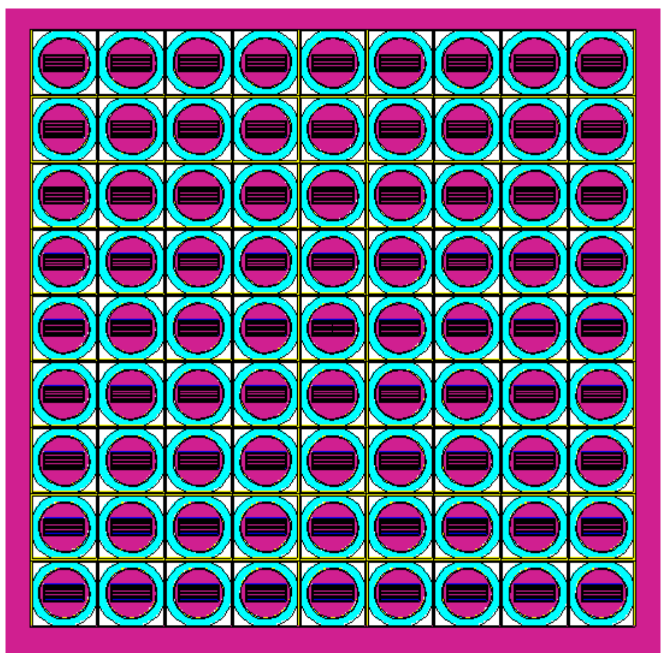

Centered in each tube (LJ1)

Figure 6.5-2 – NCT Array Geometry, Loose Plate Basket Payload

LC1

LC9

LC10

LC11

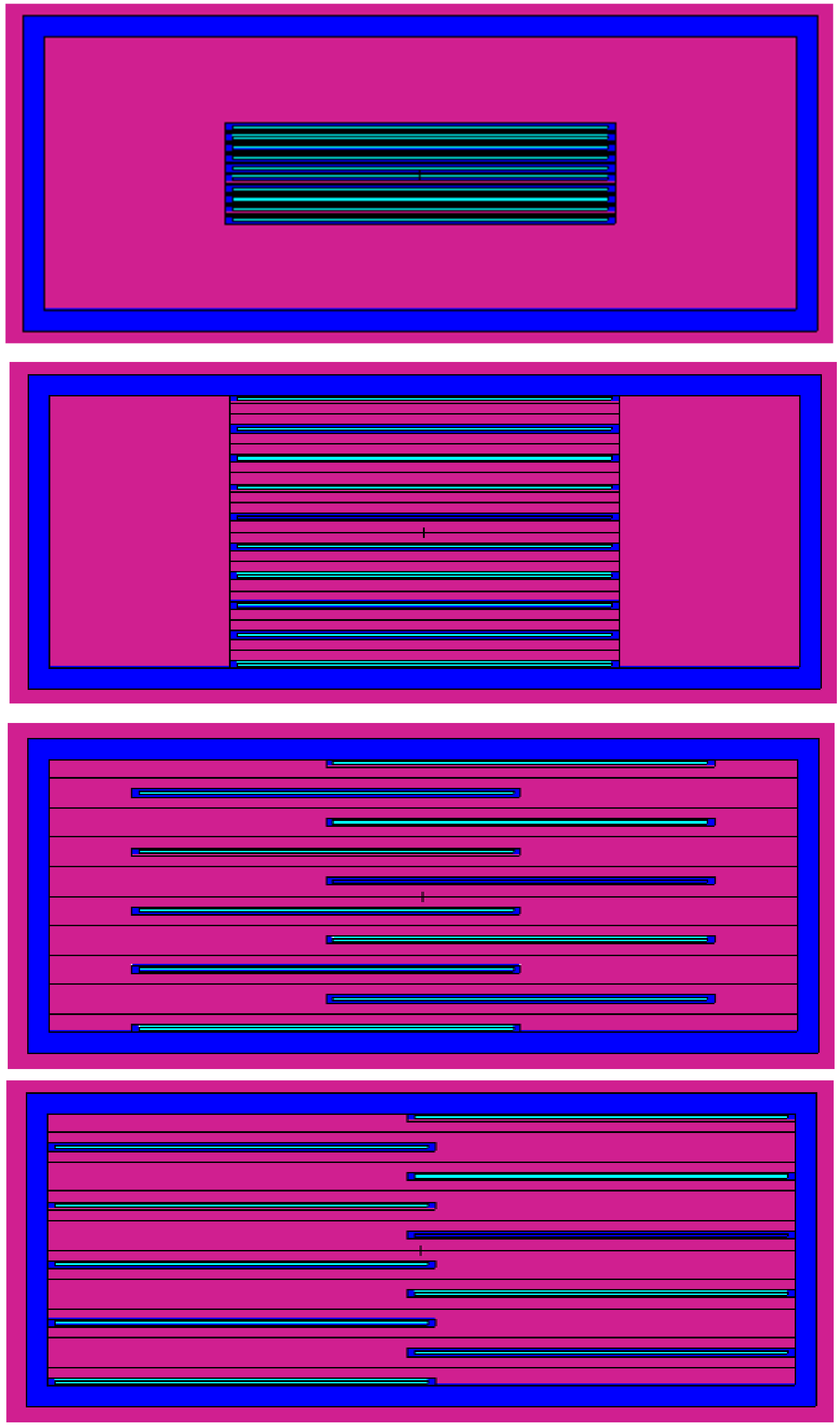

Figure 6.5-3 – NCT Array Geometry, Plate 5 (LC1, LC9, LC10, LC11)

LC12

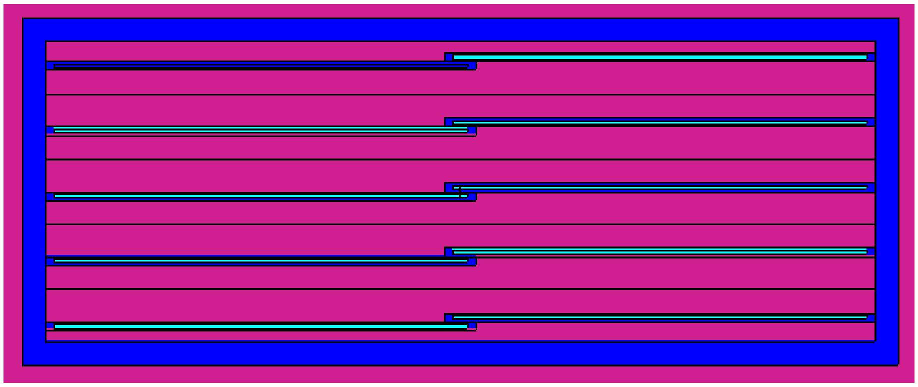

LC13

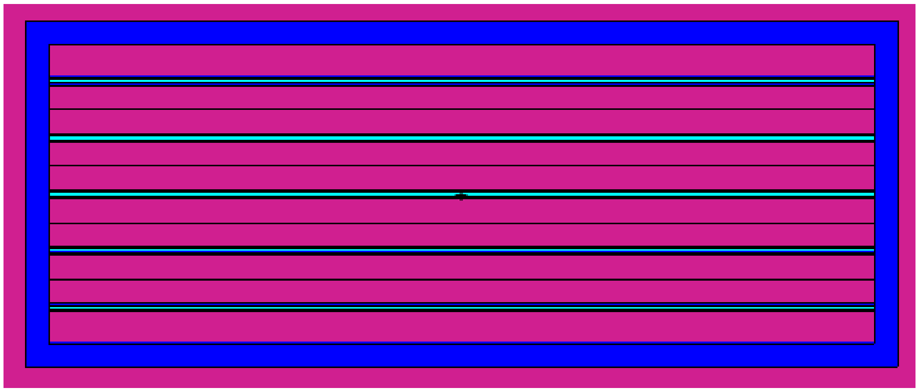

LC19

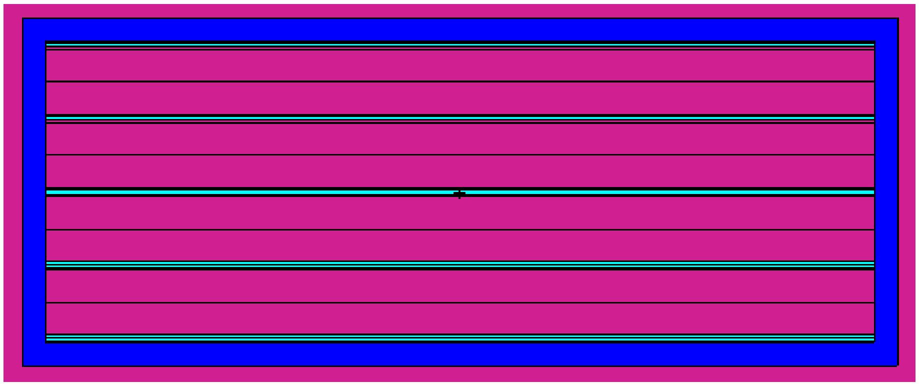

LC21

Figure 6.5-4 – NCT Array Geometry, Plate 5 (LC12, LC13, LC19, LC21)

LC22

LC24

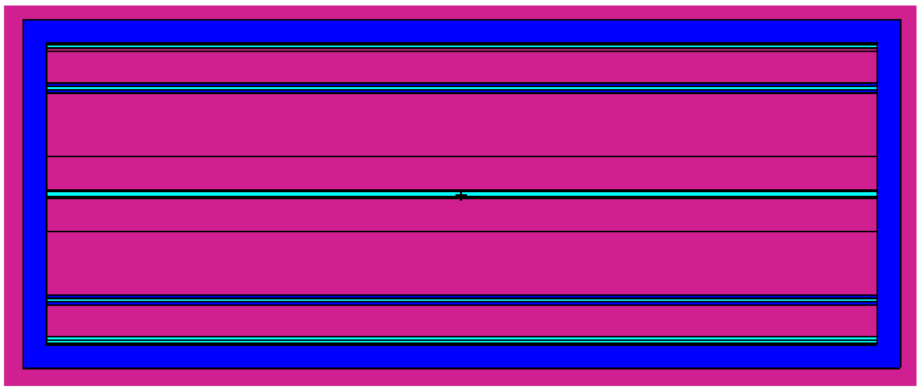

LC26

LC29

Figure 6.5-5 – NCT Array Geometry, Plate 5 (LC22, LC24, LC26, LC29)

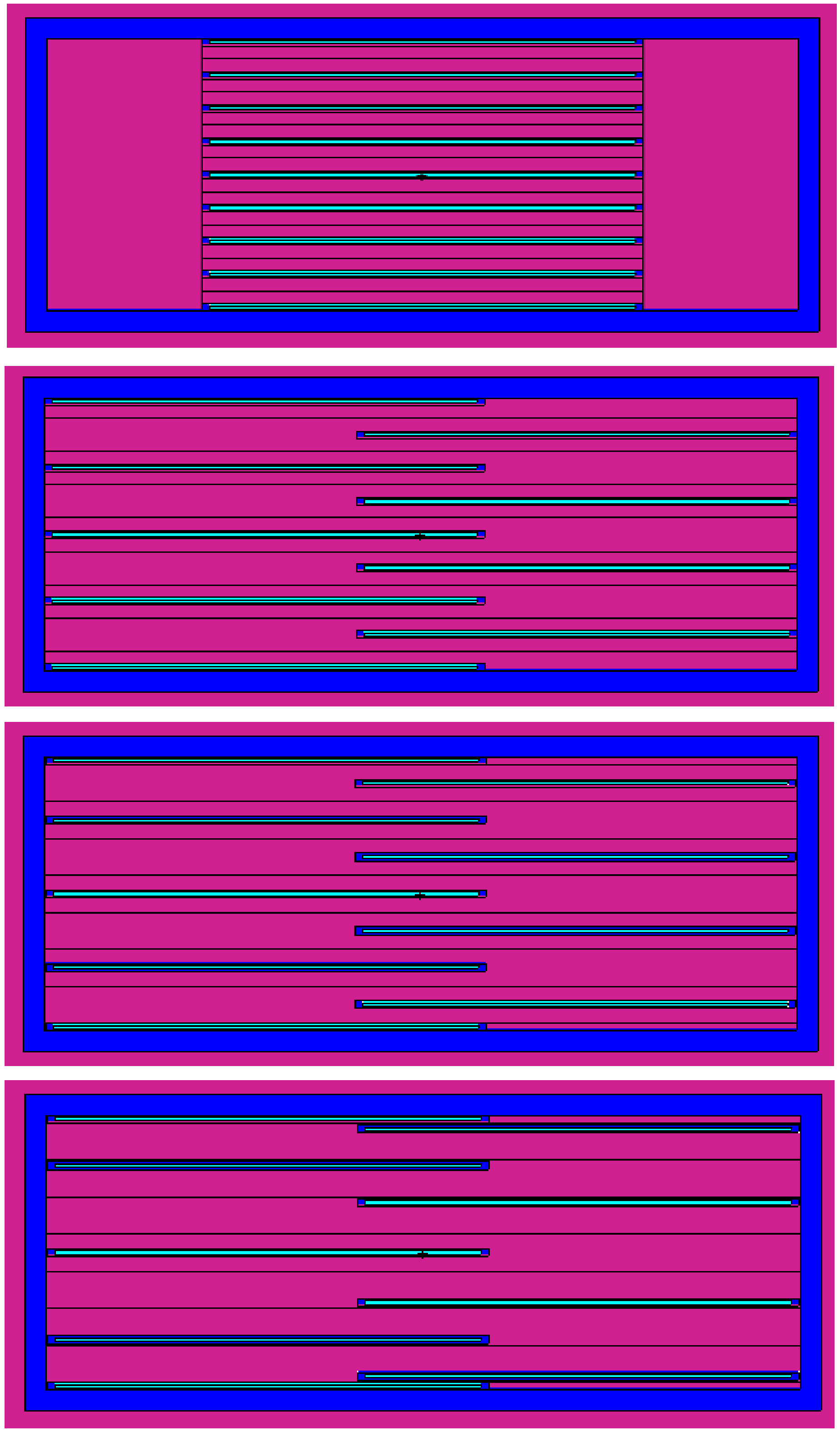

Figure 6.5-6 – NCT Array Geometry, Plate 8 (LD3, LD4, LD5, LD7)

LD8

LD9

LD10

LD11

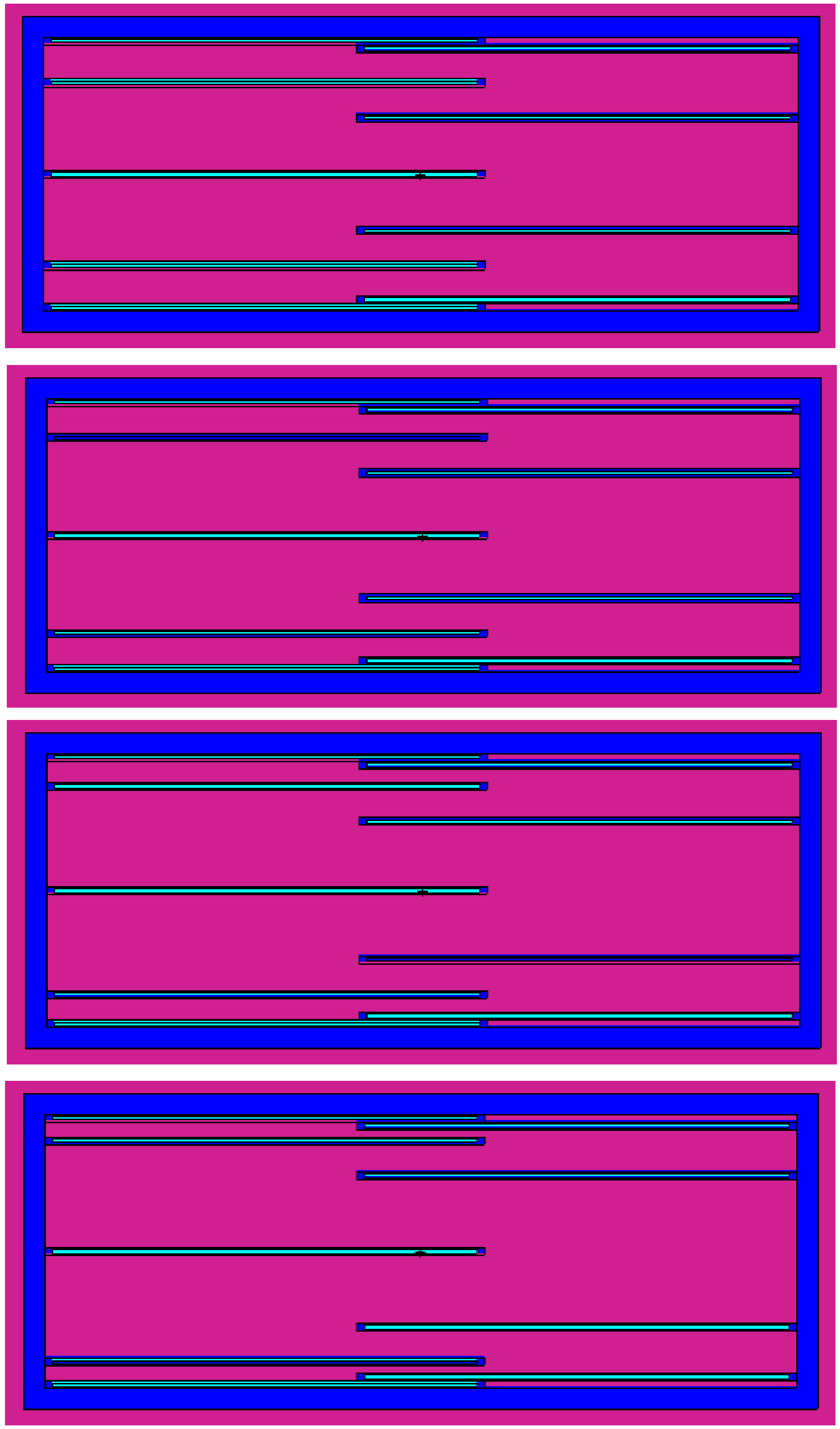

Figure 6.5-7 – NCT Array Geometry, Plate 8 (LD8, LD9, LD10, LD11)

LE2

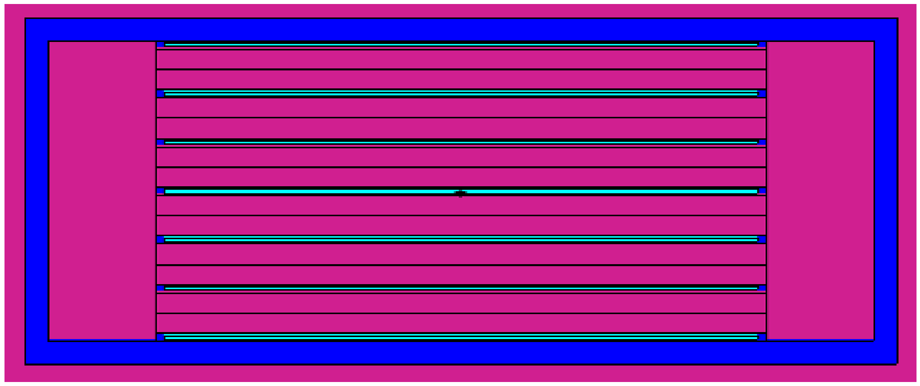

LE3

LE6

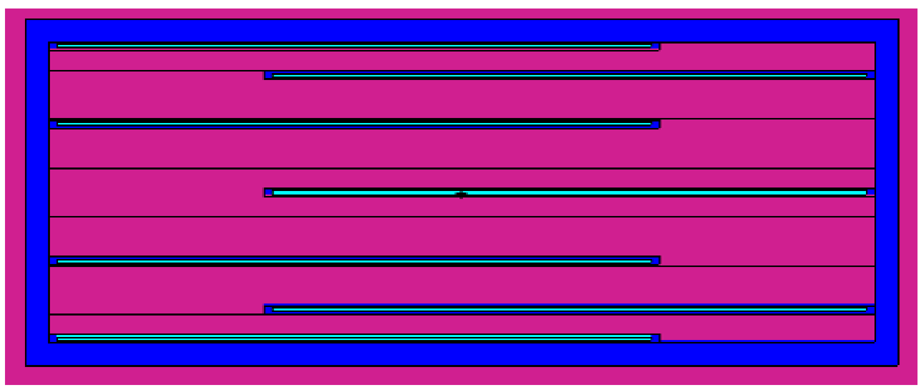

LE8

Figure 6.5-8 – NCT Array Geometry, Plate 15 (LE2, LE3, LE6, LE8)

LF1

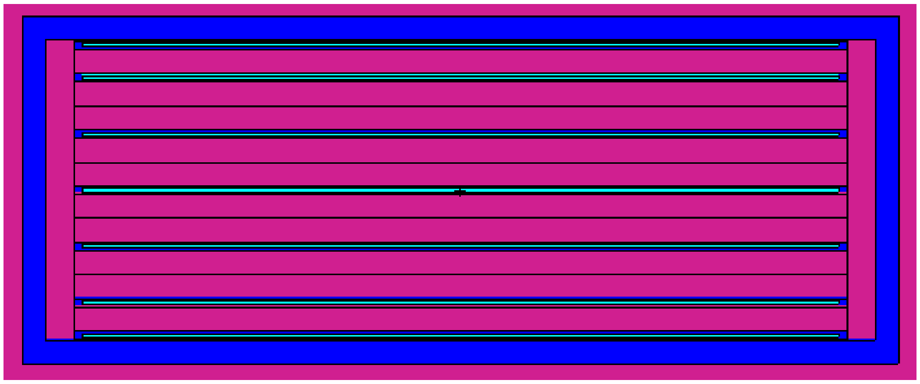

LF2

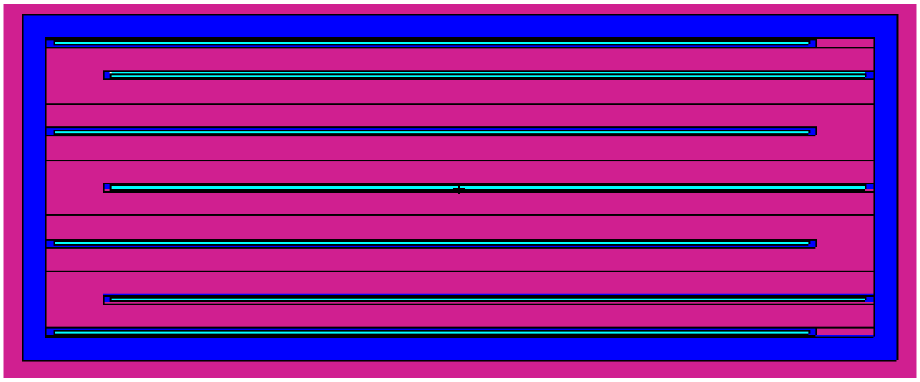

LF4

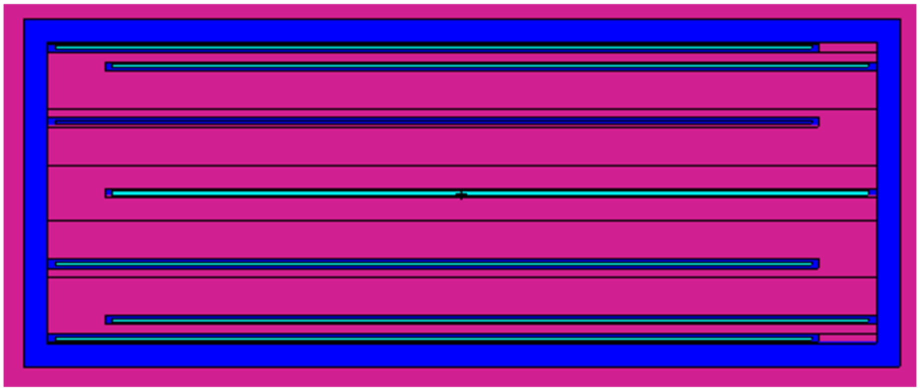

LF5

Figure 6.5-9 – NCT Array Geometry, Plate 3 (LF1, LF2, LF4, LF5)

LJ3

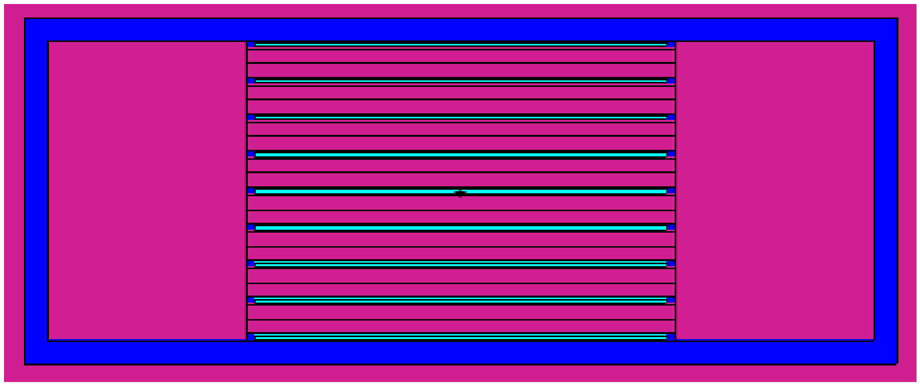

LJ4

LJ5

LJ7

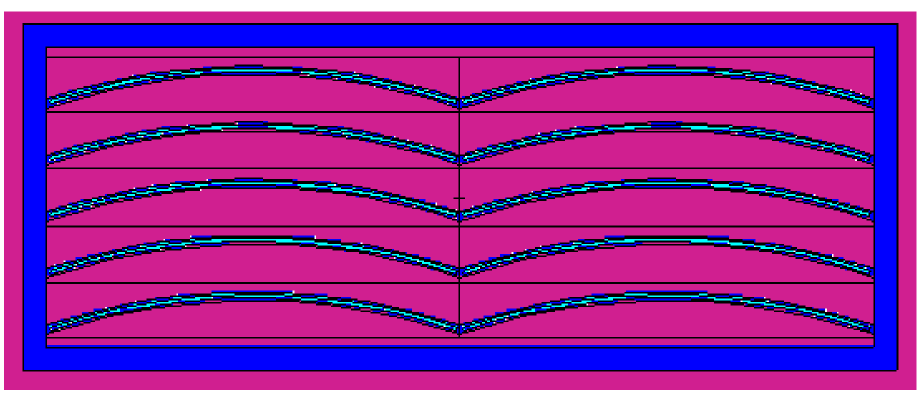

Figure 6.5-10 – NCT Array Geometry, Miscellaneous (LJ3, LJ4, LJ5, LJ7)

6.6 Package Arrays under Hypothetical Accident Conditions

6.6.1 HAC Array Configuration

6.6.1.1 Fuel Element Payload

The HAC array model is a 5x5x1 array of the HAC single package model. As the FHE is assumed to be damaged, the fuel is free to move laterally within the package. To minimize the distance between the fuel elements, in all HAC array models the fuel elements are rotated and moved toward the center of the array, consistent with the NCT array configuration. The FHE is not modeled, because modeling the FHE in any capacity would push the fuel elements apart and lower the reactivity.

From the HAC single package analysis and NCT array analysis, it is known that reactivity is maximized with full-density water between the fuel plates, because the fuel elements are under moderated. Therefore, all HAC array models have full-density water between the fuel plates. Because the fuel elements may be transported in a plastic bag, it is assumed that the water density between the plates may vary independently from the water density inside the inner tube. This partial moderation effect is similar to the partial moderation effect that could be achieved by modeling the FHE explicitly.

Nine computational series are performed. The variables addressed are (1) water density inside inner tube, (2) water density between tubes, (3) presence of insulation, and (4) presence of FHE neoprene. The geometries of two of these series are shown in Figure 6.6-1, and the geometries of the other configurations are similar. These nine computational series are described in the following paragraphs. The full results are provided in Table 6.6-1.

In Series 1, the water density inside the inner tube is varied from 0 to 1.0 g/cm^3, while void is modeled between the tubes. The modeled channel width is 0.085-in. The insulation and FHE neoprene are not modeled. The maximum reactivity occurs for Case F9, with k_s = 0.72933. A water density of 0.8 g/cm^3 within the inner tube is utilized in the most reactive case.

In Series 2, the most reactive case from Series 1 (Case F9) is modified so that the water density between the tubes is varied between 0 and 1.0 g/cm^3, while the water density within the inner tube remains fixed at 0.8 g/cm^3. The reactivity reduces as water is added to this region, indicating that the most reactive condition is with void between the tubes.

In Series 3, the water density both inside and between the tubes is assumed to be exactly the same and varied between 0 and 1.0 g/cm^3. These cases are less reactive than Case F9 in Series 1.

In Series 4, the moderation conditions of Series 1 are repeated except with the insulation modeled. The maximum reactivity occurs for Case J7 for a water density of 0.6 g/cm^3, with a maximum k_s = 0.73476. This case is slightly more reactive than Case F9, in which no insulation was modeled.

In Series 5, the most reactive case from Series 4 (Case J7) is modified so that the water density between the insulation and the outer tube is varied between 0 and 1.0 g/cm^3, while the water density within the inner tube remains fixed at 0.6 g/cm^3. The reactivity decreases as water is added to this region.

In Series 6, the moderation conditions of Series 1 are repeated except with the FHE neoprene modeled. It was determined in the HAC single package analysis that neoprene will lower the reactivity due to absorption in the chlorine. Therefore, the neoprene is conservatively modeled without chlorine. The maximum reactivity occurs for Case L8, with k_s = 0.73297, an increase of 3.6 mk when compared to Case F9. This increase is only slightly above statistical fluctuation, so it may be concluded that the presence of neoprene has at most a small effect on the reactivity. A water density of 0.7 g/cm^3 within the inner tube is utilized in the most reactive case. No cases are performed with the neoprene homogeneously mixed into the water because this scenario is already implicitly considered using the variable water density search within the inner tube.

In Series 7, insulation and neoprene are combined in the same model with variable density water inside the inner pipe, as the presence of both insulation and neoprene slightly increased the reactivity when treated separately. The maximum reactivity occurs for Case M8, with k_s = 0.73599. This case is slightly more reactive than the cases in which insulation and neoprene are addressed separately.

In Series 8, for completeness, void is modeled in the inner tube, while the water density is allowed to vary between the tubes. Chlorine-free neoprene is utilized to increase moderation in the inner tube, but insulation is ignored to maximize the amount of water between the tubes. The peak reactivity for Series 8 is the lowest of all nine series of calculations.

In Series 9, Series 7 is repeated with the channel width increased to 0.089-in. A channel width of 0.089-in is the maximum local channel width (0.087-in) with an additional margin of 0.002-in. The larger channel width is achieved by reducing the cladding thickness. Case O5 is the most reactive of all computational series.

In conclusion, Case O5 is the most reactive, with k_s = 0.74531. This result is below the USL of 0.9209. Case O5 has fully moderated fuel elements, 0.7 g/cm^3 water in the inner tube, insulation and chlorine-free neoprene, void between the insulation and outer tube, fuel elements that have been rotated and moved to the center of the array, and a channel width of 0.089-in. Note that this result is lower than the maximum NCT array case because the HAC and NCT array models are quite similar, except the NCT array uses a much larger 9x9x1 configuration.

6.6.1.2 Loose Plate Basket Payload

It was established in the criticality analysis for the ATR fuel element that the NCT array calculations bound the HAC array calculations. This result is obtained because a 9x9x1 array is utilized in the NCT calculations, while a smaller 5x5x1 array is utilized in the HAC array calculations. Water moderation is modeled in both the NCT and HAC array calculations within the inner tube, although additional moderation is allowed in the HAC cases between the inner and outer tubes. Therefore, the HAC array calculations are performed only for completeness, as these calculations will not be bounding.

In all the HAC array models, the loose plate basket is filled with full-density water, as it has been established in the NCT array analysis that full-density water moderation within the basket maximizes the reactivity. The internal plate arrangement determined in the NCT array calculations to be the most reactive (Case LC21 for plate type 5) is used in all HAC array models. Also, the loose plate basket is modeled pushed to the center of the array to maximize reactivity, as shown in Figure 6.6-2.

Four series of calculations are performed that utilize different moderations conditions. Results for all cases are provided in Table 6.6-2.

Series 1: In Series 1, the insulation is modeled, and void is modeled between the insulation and the outer tube. The water density between the basket and the inner tube is varied between 0 and 1.0 g/cm^3. The maximum reactivity is achieved for Case LK9, with k_s = 0.69792. The water density for this case is 0.8 g/cm^3.

Series 2: In Series 2, the most reactive case from Series 1 (Case LK9) is run with variable density water between the insulation and the outer tube. The reactivity decreases when water is added to this region.

Series 3: In Series 3, Series 1 is repeated, except the insulation is replaced with void. The maximum reactivity is close to but bounded by the maximum reactivity from Series 1.

Series 4: In Series 4, the insulation is not modeled, and the same water density is modeled both between the inner and outer tubes, and between the basket and inner tube. The maximum reactivity is significantly less than the maximum reactivity from Series 1.

In conclusion, the maximum reactivity is from Case LK9, with k_s = 0.69792, in which full-density water is modeled within the basket, 0.8 g/cm^3 water is modeled between the basket and the inner tube, and void between the insulation and the outer tube. This value is less than the USL of 0.9209.

6.6.2 HAC Array Results

Following are the tabulated results for the HAC array cases. The most reactive configuration in each series is listed in boldface.

Table 6.6-1 – HAC Array Results, Fuel Element

Case ID	Filename	Water Density Between Tubes (g/cm^3)	Water Density Inside Inner Tube (g/cm^3)	Water Density Between Plates (g/cm^3)	k_{eff}	σ	k_s ($k+2\sigma$)
Series 1: Variable water density in inner tube (no insulation, no neoprene)							
F1	HA_S0P000	0	0	1.0	0.57908	0.00102	0.58112
F2	HA_S0P010	0	0.1	1.0	0.63182	0.00112	0.63406
F3	HA_S0P020	0	0.2	1.0	0.66922	0.00124	0.67170
F4	HA_S0P030	0	0.3	1.0	0.69357	0.00121	0.69599
F5	HA_S0P040	0	0.4	1.0	0.71180	0.00116	0.71412
F6	HA_S0P050	0	0.5	1.0	0.72106	0.00120	0.72346
F7	HA_S0P060	0	0.6	1.0	0.72553	0.00122	0.72797
F8	HA_S0P070	0	0.7	1.0	0.72706	0.00112	0.72930
F9	**HA_S0P080**	**0**	**0.8**	**1.0**	**0.72695**	**0.00119**	**0.72933**
F10	HA_S0P090	0	0.9	1.0	0.72116	0.00110	0.72336
F11	HA_S0P100	0	1.0	1.0	0.71826	0.00123	0.72072
Series 2: Case F9 with variable density water between tubes							
F9	**HA_S0P080**	**0**	**0.8**	**1.0**	**0.72695**	**0.00119**	**0.72933**
G1	HA_P80S010	0.1	0.8	1.0	0.70205	0.00112	0.70429
G2	HA_P80S020	0.2	0.8	1.0	0.67677	0.00125	0.67927
G3	HA_P80S030	0.3	0.8	1.0	0.65374	0.00113	0.65600
G4	HA_P80S040	0.4	0.8	1.0	0.63121	0.00114	0.63349
G5	HA_P80S050	0.5	0.8	1.0	0.60791	0.00104	0.60999
G6	HA_P80S060	0.6	0.8	1.0	0.59303	0.00111	0.59525
G7	HA_P80S070	0.7	0.8	1.0	0.57461	0.00109	0.57679
G8	HA_P80S080	0.8	0.8	1.0	0.56082	0.00110	0.56302
G9	HA_P80S090	0.9	0.8	1.0	0.54767	0.00102	0.54971
G10	HA_P80S100	1.0	0.8	1.0	0.53613	0.00108	0.53829
Series 3: Matching water density inside and between tubes							
F1	HA_S0P000	0	0	1.0	0.57908	0.00102	0.58112
H1	HA_SP010	0.1	0.1	1.0	0.64719	0.00115	0.64949
H2	**HA_SP020**	**0.2**	**0.2**	**1.0**	**0.66047**	**0.00115**	**0.66277**
H3	HA_SP030	0.3	0.3	1.0	0.64457	0.00112	0.64681
H4	HA_SP040	0.4	0.4	1.0	0.62648	0.00117	0.62882
H5	HA_SP050	0.5	0.5	1.0	0.60286	0.00112	0.60510
H6	HA_SP060	0.6	0.6	1.0	0.58814	0.00116	0.59046
H7	HA_SP070	0.7	0.7	1.0	0.57337	0.00106	0.57549
H8	HA_SP080	0.8	0.8	1.0	0.56082	0.00110	0.56302
H9	HA_SP090	0.9	0.9	1.0	0.55245	0.00122	0.55489
H10	HA_SP100	1.0	1.0	1.0	0.54360	0.00100	0.54560

(continued)

Table 6.6-1 – HAC Array Results, Fuel Element (continued)

Case ID	Filename	Water Density Between Tubes (g/cm^3)	Water Density Inside Inner Tube (g/cm^3)	Water Density Between Plates (g/cm^3)	k_{eff}	σ	k_s (k+2σ)
Series 4: Repeat of Series 1 with insulation							
J1	HA_DS0P000	0	0	1.0	0.58824	0.00116	0.59056
J2	HA_DS0P010	0	0.1	1.0	0.63716	0.00111	0.63938
J3	HA_DS0P020	0	0.2	1.0	0.67403	0.00118	0.67639
J4	HA_DS0P030	0	0.3	1.0	0.69920	0.00130	0.70180
J5	HA_DS0P040	0	0.4	1.0	0.71665	0.00116	0.71897
J6	HA_DS0P050	0	0.5	1.0	0.72388	0.00117	0.72622
J7	**HA_DS0P060**	**0**	**0.6**	**1.0**	**0.73230**	**0.00123**	**0.73476**
J8	HA_DS0P070	0	0.7	1.0	0.73178	0.00112	0.73402
J9	HA_DS0P080	0	0.8	1.0	0.72965	0.00124	0.73213
J10	HA_DS0P090	0	0.9	1.0	0.72638	0.00107	0.72852
J11	HA_DS0P100	0	1.0	1.0	0.71985	0.00113	0.72211
Series 5: Case J7 with variable density water between insulation and outer tube							
J7	**HA_DS0P090**	**0**	**0.6**	**1.0**	**0.73230**	**0.00123**	**0.73476**
K1	HA_DP60S010	0.1	0.6	1.0	0.72284	0.00123	0.72530
K2	HA_DP60S020	0.2	0.6	1.0	0.71587	0.00120	0.71827
K3	HA_DP60S030	0.3	0.6	1.0	0.71029	0.00118	0.71265
K4	HA_DP60S040	0.4	0.6	1.0	0.70002	0.00117	0.70236
K5	HA_DP60S050	0.5	0.6	1.0	0.69370	0.00122	0.69614
K6	HA_DP60S060	0.6	0.6	1.0	0.68266	0.00111	0.68488
K7	HA_DP60S070	0.7	0.6	1.0	0.67122	0.00112	0.67346
K8	HA_DP60S080	0.8	0.6	1.0	0.66359	0.00115	0.66589
K9	HA_DP60S090	0.9	0.6	1.0	0.65393	0.00111	0.65615
K10	HA_DP60S100	1.0	0.6	1.0	0.64595	0.00116	0.64827
Series 6: Repeat of Series 1 with neoprene							
L1	HA_N2S0P000	0	0	1.0	0.60058	0.00113	0.60284
L2	HA_N2S0P010	0	0.1	1.0	0.64323	0.00119	0.64561
L3	HA_N2S0P020	0	0.2	1.0	0.68153	0.00118	0.68389
L4	HA_N2S0P030	0	0.3	1.0	0.70640	0.00120	0.70880
L5	HA_N2S0P040	0	0.4	1.0	0.71669	0.00124	0.71917
L6	HA_N2S0P050	0	0.5	1.0	0.72733	0.00117	0.72967
L7	HA_N2S0P060	0	0.6	1.0	0.72872	0.00122	0.73116
L8	**HA_N2S0P070**	**0**	**0.7**	**1.0**	**0.73069**	**0.00114**	**0.73297**
L9	HA_N2S0P080	0	0.8	1.0	0.73081	0.00107	0.73295
L10	HA_N2S0P090	0	0.9	1.0	0.72692	0.00129	0.72950
L11	HA_N2S0P100	0	1.0	1.0	0.72371	0.00122	0.72615

(continued)

Table 6.6-1 – HAC Array Results, Fuel Element (concluded)

Case ID	Filename	Water Density Between Tubes (g/cm^3)	Water Density Inside Inner Tube (g/cm^3)	Water Density Between Plates (g/cm^3)	k_{eff}	σ	k_s (k+2σ)
Series 7: Repeat of Series 1 with insulation and neoprene							
M1	HA_DNS0P000	0	0	1.0	0.60377	0.00107	0.60591
M2	HA_DNS0P010	0	0.1	1.0	0.64940	0.00107	0.65154
M3	HA_DNS0P020	0	0.2	1.0	0.68596	0.00110	0.68816
M4	HA_DNS0P030	0	0.3	1.0	0.70846	0.00115	0.71076
M5	HA_DNS0P040	0	0.4	1.0	0.72168	0.00122	0.72412
M6	HA_DNS0P050	0	0.5	1.0	0.73000	0.00124	0.73248
M7	HA_DNS0P060	0	0.6	1.0	0.73182	0.00122	0.73426
M8	**HA_DNS0P070**	**0**	**0.7**	**1.0**	**0.73365**	**0.00117**	**0.73599**
M9	HA_DNS0P080	0	0.8	1.0	0.73187	0.00127	0.73441
M10	HA_DNS0P090	0	0.9	1.0	0.73006	0.00112	0.73230
M11	HA_DNS0P100	0	1.0	1.0	0.72332	0.00122	0.72576
Series 8: Case L1 with variable density water between tubes							
L1	HA_N2S0P000	0	0	1.0	0.60058	0.00113	0.60284
N1	**HA_N2P0S010**	**0.1**	**0**	**1.0**	**0.63054**	**0.00107**	**0.63268**
N2	HA_N2P0S020	0.2	0	1.0	0.62961	0.00118	0.63197
N3	HA_N2P0S030	0.3	0	1.0	0.61939	0.00113	0.62165
N4	HA_N2P0S040	0.4	0	1.0	0.60776	0.00108	0.60992
N5	HA_N2P0S050	0.5	0	1.0	0.58874	0.00108	0.59090
N6	HA_N2P0S060	0.6	0	1.0	0.57308	0.00109	0.57526
N7	HA_N2P0S070	0.7	0	1.0	0.55837	0.00107	0.56051
N8	HA_N2P0S080	0.8	0	1.0	0.54139	0.00101	0.54341
N9	HA_N2P0S090	0.9	0	1.0	0.52714	0.00106	0.52926
N10	HA_N2P0S100	1.0	0	1.0	0.51600	0.00114	0.51828
Series 9: Repeat of Series 7 with a channel width of 0.089-in							
O1	HA_DNS0P030_C89	0	0.3	1.0	0.71885	0.00118	0.72121
O2	HA_DNS0P040_C89	0	0.4	1.0	0.73301	0.00114	0.73529
O3	HA_DNS0P050_C89	0	0.5	1.0	0.73889	0.00124	0.74137
O4	HA_DNS0P060_C89	0	0.6	1.0	0.74172	0.00121	0.74414
O5	**HA_DNS0P070_C89**	**0**	**0.7**	**1.0**	**0.74299**	**0.00116**	**0.74531**
O6	HA_DNS0P080_C89	0	0.8	1.0	0.74192	0.00125	0.74442
O7	HA_DNS0P090_C89	0	0.9	1.0	0.73527	0.00105	0.73737
O8	HA_DNS0P100_C89	0	1.0	1.0	0.73282	0.00110	0.73502

Table 6.6-2 – HAC Array Results, Plate 5

Case ID	Filename	Water Density Between Tubes (g/cm³)	Water Density Inside Inner Tube (g/cm³)	Water Density Between Plates (g/cm³)	k_{eff}	σ	k_s (k+2σ)
Series 1: Variable water density in inner tube, with insulation							
LK1	HA_N5DS0P000	0	0	1.0	0.53784	0.00096	0.53976
LK2	HA_N5DS0P010	0	0.1	1.0	0.58878	0.00098	0.59074
LK3	HA_N5DS0P020	0	0.2	1.0	0.62946	0.00101	0.63148
LK4	HA_N5DS0P030	0	0.3	1.0	0.65858	0.00102	0.66062
LK5	HA_N5DS0P040	0	0.4	1.0	0.67685	0.00100	0.67885
LK6	HA_N5DS0P050	0	0.5	1.0	0.68901	0.00102	0.69105
LK7	HA_N5DS0P060	0	0.6	1.0	0.69483	0.00107	0.69697
LK8	HA_N5DS0P070	0	0.7	1.0	0.69266	0.00120	0.69506
LK9	**HA_N5DS0P080**	**0**	**0.8**	**1.0**	**0.69576**	**0.00108**	**0.69792**
LK10	HA_N5DS0P090	0	0.9	1.0	0.69250	0.00105	0.69460
LK11	HA_N5DS0P100	0	1.0	1.0	0.68585	0.00104	0.68793
Series 2: Case LK9 with variable density water between tubes.							
LK9	**HA_N5DS0P080**	**0**	**0.8**	**1.0**	**0.69576**	**0.00108**	**0.69792**
LM1	HA_N5DP80S010	0.1	0.8	1.0	0.68989	0.00106	0.69201
LM2	HA_N5DP80S020	0.2	0.8	1.0	0.67989	0.00107	0.68203
LM3	HA_N5DP80S030	0.3	0.8	1.0	0.67352	0.00098	0.67548
LM4	HA_N5DP80S040	0.4	0.8	1.0	0.66658	0.00105	0.66868
LM5	HA_N5DP80S050	0.5	0.8	1.0	0.65700	0.00105	0.65910
LM6	HA_N5DP80S060	0.6	0.8	1.0	0.64893	0.00118	0.65129
LM7	HA_N5DP80S070	0.7	0.8	1.0	0.64141	0.00106	0.64353
LM8	HA_N5DP80S080	0.8	0.8	1.0	0.63415	0.00099	0.63613
LM9	HA_N5DP80S090	0.9	0.8	1.0	0.62748	0.00103	0.62954
LM10	HA_N5DP80S100	1.0	0.8	1.0	0.62100	0.00094	0.62288
Series 3: Repeat of Series 1, no insulation							
LN1	HA_N5S0P000	0	0	1.0	0.53334	0.00092	0.53518
LN2	HA_N5S0P010	0	0.1	1.0	0.58456	0.00091	0.58638
LN3	HA_N5S0P020	0	0.2	1.0	0.62421	0.00108	0.62637
LN4	HA_N5S0P030	0	0.3	1.0	0.65402	0.00109	0.65620
LN5	HA_N5S0P040	0	0.4	1.0	0.67129	0.00108	0.67345
LN6	HA_N5S0P050	0	0.5	1.0	0.68550	0.00108	0.68766
LN7	HA_N5S0P060	0	0.6	1.0	0.69042	0.00106	0.69254
LN8	**HA_N5S0P070**	**0**	**0.7**	**1.0**	**0.69145**	**0.00104**	**0.69353**
LN9	HA_N5S0P080	0	0.8	1.0	0.69071	0.00101	0.69273
LN10	HA_N5S0P090	0	0.9	1.0	0.68925	0.00102	0.69129
LN11	HA_N5S0P100	0	1.0	1.0	0.68493	0.00116	0.68725

(continued)

Table 6.6-2 – HAC Array Results, Plate 5 (concluded)

Case ID	Filename	Water Density Between Packages (g/cm^3)	Water Density Inside Pipe (g/cm^3)	Water Density Between Plates (g/cm^3)	k_{eff}	σ	k_s ($k+2\sigma$)
Series 4: No insulation, matching water densities inside and between tubes							
LN1	HA_N5S0P000	0	0	1.0	0.53334	0.00092	0.53518
LO1	HA_N5SP010	0.1	0.1	1.0	0.59685	0.00097	0.59879
LO2	**HA_N5SP020**	**0.2**	**0.2**	**1.0**	**0.61533**	**0.00096**	**0.61725**
LO3	HA_N5SP030	0.3	0.3	1.0	0.60844	0.00108	0.61060
LO4	HA_N5SP040	0.4	0.4	1.0	0.59462	0.00099	0.59660
LO5	HA_N5SP050	0.5	0.5	1.0	0.57802	0.00107	0.58016
LO6	HA_N5SP060	0.6	0.6	1.0	0.56514	0.00107	0.56728
LO7	HA_N5SP070	0.7	0.7	1.0	0.55116	0.00106	0.55328
LO8	HA_N5SP080	0.8	0.8	1.0	0.54262	0.00093	0.54448
LO9	HA_N5SP090	0.9	0.9	1.0	0.53400	0.00102	0.53604
LO10	HA_N5SP100	1.0	1.0	1.0	0.52785	0.00106	0.52997

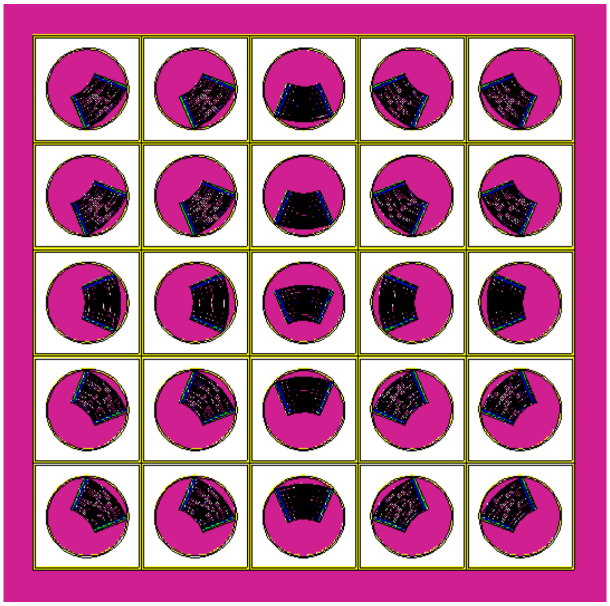

Series 1: Array with variable density water in inner tube, and void between tubes. No insulation modeled.

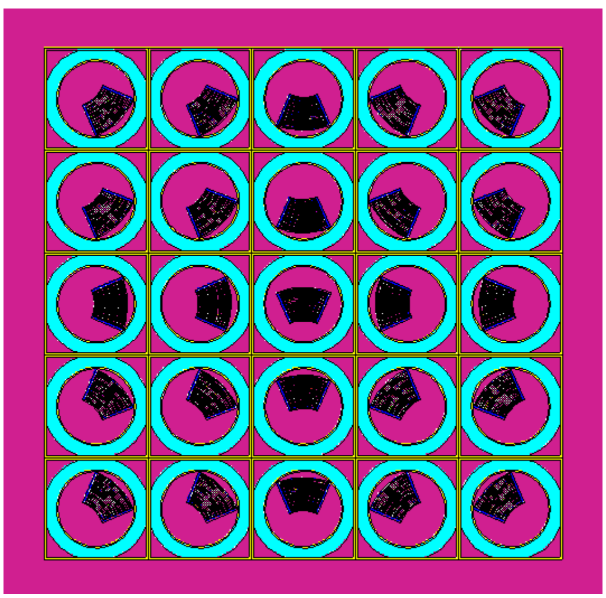

Series 5: Array with 0.6 g/cm^3 water in inner tube and variable density water between tubes. Insulation is modeled.

Figure 6.6-1 – HAC Array Geometry Examples, Fuel Element

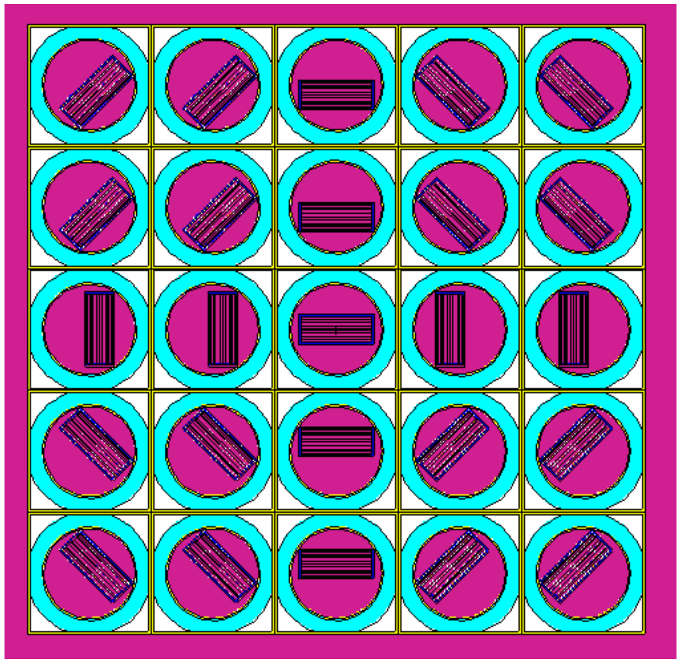

Series 1: Array with variable density water in inner tube, and void between tubes. Insulation is modeled.

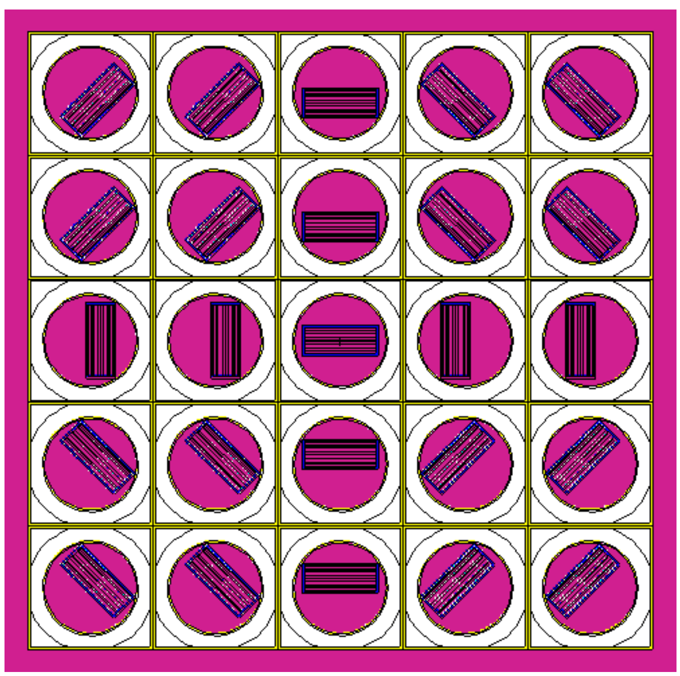

Series 3: Array with variable density water in inner tube, and void between tubes. No insulation modeled.

Figure 6.6-2 – HAC Array Geometry Examples, Loose Plate Basket

6.7 Fissile Material Packages for Air Transport

The applicable licensing requirements for air transport of fissile material are contained in 10 CFR 71.55(f) and IAEA Safety Standard SSR-6, paragraph 683. For air transport, no structural integrity is credited for the hypothetical accident conditions. Rather, the fissile material from a single package is modeled as a sphere that is optimally moderated and reflected by the packaging materials. The sphere is reflected with 20 cm of water. Per the licensing requirements of 10 CFR 71.55(f) and IAEA Safety Standard SSR-6, paragraph 683, environmental water is not included in the fissile sphere.

The air transport analysis is intended to bound all current and projected future payloads. The ATR U-Mo demonstration element has the largest fissile mass (1240 g U-235) of the currently licensed ATR payloads (see Chapter 1, Table 1.1-1). To bound the 1240 g U-235 payload and provide additional margin for potential future payloads, 2000 g U-235 in HEU is conservatively modeled. The non-uranium elements that may be present in the fuel matrix (e.g., aluminum, silicon, molybdenum), and structural materials of the fuel elements and package (e.g., aluminum, steel) are conservatively neglected within the fissile mixture, which minimizes parasitic neutron absorption. Omitting these materials from the fissile sphere also minimizes the size of the fissile sphere, which minimizes neutron leakage. Both of these effects conservatively maximize the reactivity. The U-235 weight percent is modeled at the maximum value of 94%. Consistent with the ATR fuel element analysis, representative weight percents of 0.6% and 0.35% are utilized for U-234 and U-236, respectively, and the balance (5.05%) is modeled as U-238.

The package contains up to 100 g polyethylene (CH_2), and the sum of neoprene (C_4H_5Cl) and cellulosic material ($C_6H_{10}O_5$) (such as kraft paper and cardboard) is limited to 4000 g. Because polyethylene, neoprene, and cellulosic material contain hydrogen, these materials act as a moderator and are explicitly addressed in the analysis.

The fissile sphere is modeled as a mixture of uranium, polyethylene, neoprene and/or cellulosic material. For an air transport analysis, environmental water is not included. The total mass of uranium based on 94% enrichment is 2000 g U-235 / 0.94 = 2127.7 g uranium. The theoretical material densities are 19.0 g/cm^3 uranium metal, 0.92 g/cm^3 polyethylene, 1.23 g/cm^3 neoprene, and 0.44 g/cm^3 for cellulosic material (density of kraft paper). Based upon the mass inputs and the material densities, the volume of uranium, polyethylene, neoprene, and cellulosic material are summed to create the total volume for the fissile sphere, which is used to compute atom densities for each isotope.

The atom densities for several different example mixtures are provided in Table 6.7-1. The total volume V is computed as $V = V_U + V_{poly} + V_{cellulosic} + V_{neoprene}$, and the radius R of the fissile material is then:

$$R = \sqrt[3]{\frac{3V}{4\pi}}$$

The gram density for each material within the sphere is computed as the mass of the material divided by the total volume (V), which is then used to compute the atom density of each material. These atom densities are then summed to create the overall mixture atom densities presented in Table 6.7-1.

In the first series of cases, the uranium is homogeneously mixed with various quantities of polyethylene, neoprene, and cellulosic material in a single fissile sphere reflected with 20 cm of water, see Figure 6.7-1. These results are summarized in Table 6.7-2. Case AIR01 is pure uranium with no hydrogenous material, with k_s = 0.51683. Cases AIR02 through AIR06 include increasing amounts of polyethylene (no neoprene or cellulosic material) up to the maximum value of 100 g polyethylene. The reactivity decreases compared to Case AIR01 when < 80 g polyethylene is added, but reactivity is maximized with the full 100 g polyethylene, with k_s = 0.52233.

Cases AIR07 through AIR14 include increasing amounts of neoprene (no polyethylene or cellulosic material) up to the maximum value of 4000 g neoprene. The reactivity decreases compared to Case AIR01 when < 1500 g of neoprene is added, but reactivity is maximized with the full 4000 g neoprene, with k_s = 0.57035.

Cases AIR15 through AIR22 include increasing amounts of cellulosic material (no polyethylene or neoprene) up to the maximum value of 4000 g cellulosic material. The reactivity decreases compared to Case AIR01 when < 3000 g of cellulosic material is added, but reactivity is maximized with the full 4000 g cellulosic material, with k_s = 0.55065.

For all three hydrogenous materials, reactivity initially decreases for smaller amounts of moderating material. The most likely reason that reactivity initially decreases when small amounts of hydrogenous material are added is that adding moderator greatly enlarges the volume of the fissile sphere. For small amounts of moderator, the increase in neutron leakage due to the larger sphere results in a net reduction in reactivity despite the increase in moderation. For larger quantities of moderator, the enhanced moderation increases the reactivity despite the increased leakage.

The sum of neoprene and cellulosic material is limited to 4000 g. Comparing Cases AIR14 and AIR22, it is concluded that neoprene is a superior moderator than cellulosic material. Therefore, it is conservative to model the 4000 g of neoprene/cellulosic material as 4000 g neoprene. In Case AIR23, both 100 g polyethylene and 4000 g neoprene are included in the fissile sphere, with k_s = 0.58222. This is the most reactive single fissile sphere case.

The above models do not include the packaging structural materials, which may also act as a reflector. The maximum weight of a loaded package is 290 lbs (see Section 1.2.1.2). This weight includes the fuel, stainless steel structural members, aluminum fuel support structures, insulation, etc. Therefore, 300 lbs (136 kg) bounds the total mass of stainless steel in the package by a large margin and is used as a reflector outside the fissile sphere. The stainless steel density is 7.94 g/cm^3, resulting in a steel reflector thickness of 7.61 cm (see Figure 6.7-2) if added to the most reactive single fissile sphere model (Case AIR23). A 20 cm water reflector is modeled outside the steel reflector. When the steel reflector is added (Case AIR24), k_s = 0.55311, which is less reactive than without the steel reflector. Therefore, the reflection provided by the structural materials of the packaging may be neglected.

The single fissile sphere is undermoderated with 4000 g neoprene and 100 g polyethylene. Moderation may be further enhanced by modeling the fissile material in two regions, an inner sphere and outer shell, with all of the moderating material in the inner sphere (see Figure 6.7-3). The inner sphere contains a mass “M” grams U-235, 4000 g neoprene, and 100 g polyethylene. The outer shell contains (2000 – M) grams U-235 with no moderating material. Therefore, the system always contains 2000 g U-235. The inner sphere in the two region model achieves greater moderation than the single sphere model because less U-235 is moderated with the full mass of moderating material.

The atom densities are computed using the same method developed for the single region model, although the mass of U-235 is now varied. Sample atom densities for the moderated inner sphere for several different U-235 masses are summarized in Table 6.7-3, as well as the outer shell composition.

The two-region model results are summarized in Table 6.7-4. The two-region model achieves a higher reactivity than the single-region model. The reactivity is maximized with 1500 g U-235 in the inner sphere and 500 g U-235 in the outer shell (Case AIR40), with k_s = 0.60739. The most reactive air transport case is far below the USL.

A limited quantity of moderating material is used in the air transport analysis. As a result, the system is closer to an intermediate or fast system and is generally outside the bounds of either the plate-fuel benchmark experiments (see Section 6.8) or the thermal benchmark experiments from the small quantity payload analysis (see Section 6.11.8). The most reactive air transport case (Case AIR40) has an EALF = 6.9045×10^{-7} MeV and H/U-235 = 38. While these parameters are outside of the range of applicability shown in either Table 6.8-2 or Table 6.11-12, the maximum reactivity is relatively low (highest k_s = 0.60739) and addition of intermediate and fast benchmark experiments is not warranted.

Table 6.7-1 – Example Atom Densities, Single Fissile Sphere

Isotope	2000 g U-235 0 g polyethylene 0 g neoprene 0 g cellulosic (atom/b-cm)	2000 g U-235 100 g polyethylene 0 g neoprene 0 g cellulosic (atom/b-cm)	2000 g U-235 0 g polyethylene 4000 g neoprene 0 g cellulosic (atom/b-cm)	2000 g U-235 0 g polyethylene 0 g neoprene 4000 g cellulosic (atom/b-cm)
U-234	2.9333E-04	1.4885E-04	9.7644E-06	3.5650E-06
U-235	4.5759E-02	2.3220E-02	1.5232E-03	5.5614E-04
U-236	1.6965E-04	8.6091E-05	5.6475E-06	2.0619E-06
U-238	2.4273E-03	1.2317E-03	8.0799E-05	2.9500E-05
H	-	3.8910E-02	4.0439E-02	1.6124E-02
C	-	1.9455E-02	3.2351E-02	9.6743E-03
O	-	-	-	8.0619E-03
Cl	-	-	8.0877E-03	-
Total	4.8649E-02	8.3052E-02	8.2497E-02	3.4451E-02

Table 6.7-2 – Air Transport Results, Single Fissile Sphere

Case ID	Filename	Radius (cm)	Poly-ethylene Mass (g)	Neoprene Mass (g)	Cellulosic Mass (g)	k	σ	k_s (k+2σ)
AIR01	AIR_P0_N0_K0	2.9901	0	0	0	0.51621	0.00031	0.51683
AIR02	AIR_P020	3.1723	20	0	0	0.50988	0.00031	0.51050
AIR03	AIR_P040	3.3356	40	0	0	0.50946	0.00032	0.51010
AIR04	AIR_P060	3.4844	60	0	0	0.51250	0.00033	0.51316
AIR05	AIR_P080	3.6214	80	0	0	0.51649	0.00033	0.51715
AIR06	AIR_P100	3.7488	100	0	0	0.52167	0.00033	0.52233
AIR07	AIR_N0500	4.9837	0	500	0	0.48059	0.00034	0.48127
AIR08	AIR_N1000	6.0443	0	1000	0	0.50801	0.00035	0.50871
AIR09	AIR_N1500	6.8247	0	1500	0	0.52854	0.00036	0.52926
AIR10	AIR_N2000	7.4585	0	2000	0	0.54342	0.00038	0.54418
AIR11	AIR_N2500	7.9998	0	2500	0	0.55460	0.00036	0.55532
AIR12	AIR_N3000	8.4763	0	3000	0	0.56208	0.00036	0.56280
AIR13	AIR_N3500	8.9046	0	3500	0	0.56762	0.00035	0.56832
AIR14	AIR_N4000	9.2952	0	4000	0	0.56965	0.00035	0.57035
Note: All models reflected with 20 cm water.								

(continued)

Table 6.7-2 – Air Transport Results, Single Fissile Sphere (concluded)

Case ID	Filename	Radius (cm)	Poly-ethylene Mass (g)	Neoprene Mass (g)	Cellulosic Mass (g)	k	σ	k_s (k+2σ)
AIR15	AIR_K0500	6.6820	0	0	500	0.43112	0.00034	0.43180
AIR16	AIR_K1000	8.2912	0	0	1000	0.45924	0.00036	0.45996
AIR17	AIR_K1500	9.4413	0	0	1500	0.48136	0.00036	0.48208
AIR18	AIR_K2000	10.3639	0	0	2000	0.49829	0.00037	0.49903
AIR19	AIR_K2500	11.1463	0	0	2500	0.51439	0.00038	0.51515
AIR20	AIR_K3000	11.8319	0	0	3000	0.52755	0.00039	0.52833
AIR21	AIR_K3500	12.4462	0	0	3500	0.53825	0.0004	0.53905
AIR22	AIR_K4000	13.0052	0	0	4000	0.54989	0.00038	0.55065
AIR23	**AIR_NP**	**9.3942**	**100**	**4000**	**0**	**0.58148**	**0.00037**	**0.58222**
Case AIR24 features a steel reflector between the fissile sphere and outer water reflector								
AIR24	AIR_NP_RSS	9.3942	100	4000	0	0.55239	0.00036	0.55311
Note: All models reflected with 20 cm water.								

Table 6.7-3 – Example Atom Densities, Two-Region Model

	Inner Region			Outer Region
Isotope	**500 g U-235 100 g polyethylene 4000 g neoprene (atom/b-cm)**	**1000 g U-235 100 g polyethylene 4000 g neoprene (atom/b-cm)**	**1500 g U-235 100 g polyethylene 4000 g neoprene (atom/b-cm)**	**Uranium Metal**
U-234	2.4233E-06	4.8069E-06	7.1517E-06	2.9333E-04
U-235	3.7803E-04	7.4986E-04	1.1157E-03	4.5759E-02
U-236	1.4016E-06	2.7802E-06	4.1364E-06	1.6965E-04
U-238	2.0052E-05	3.9776E-05	5.9180E-05	2.4273E-03
H	4.2678E-02	4.2328E-02	4.1984E-02	-
C	3.3382E-02	3.3108E-02	3.2839E-02	-
Cl	8.0288E-03	7.9630E-03	7.8983E-03	-
Total	8.4490E-02	8.4197E-02	8.3908E-02	4.8649E-02

Table 6.7-4 – Air Transport Results, Two-Region Model

Case ID	Filename	Radius Inner (cm)	U-235 Mass Inner (g)	U-235 Mass Outer (g)	k	σ	k_s (k+2σ)
AIR30	AIR_MI0500	9.3179	500	1500	0.55303	0.00035	0.55373
AIR31	AIR_MI0600	9.3230	600	1400	0.56436	0.00035	0.56506
AIR32	AIR_MI0700	9.3281	700	1300	0.57413	0.00035	0.57483
AIR33	AIR_MI0800	9.3332	800	1200	0.58213	0.00037	0.58287
AIR34	AIR_MI0900	9.3383	900	1100	0.58823	0.00036	0.58895
AIR35	AIR_MI1000	9.3434	1000	1000	0.59313	0.00036	0.59385
AIR36	AIR_MI1100	9.3485	1100	900	0.59856	0.00037	0.59930
AIR37	AIR_MI1200	9.3536	1200	800	0.60211	0.00038	0.60287
AIR38	AIR_MI1300	9.3587	1300	700	0.60424	0.00038	0.60500
AIR39	AIR_MI1400	9.3638	1400	600	0.60641	0.00038	0.60717
AIR40	**AIR_MI1500**	**9.3689**	**1500**	**500**	**0.60663**	**0.00038**	**0.60739**
AIR41	AIR_MI1600	9.3740	1600	400	0.60610	0.00035	0.60680
AIR42	AIR_MI1700	9.3790	1700	300	0.60433	0.00037	0.60507
AIR43	AIR_MI1800	9.3841	1800	200	0.60075	0.00039	0.60153
AIR44	AIR_MI1900	9.3892	1900	100	0.59442	0.00039	0.59520
AIR45	AIR_MI1995	9.3940	1995	5	0.58274	0.00036	0.58346

Notes:
(1) The total U-235 mass is 2000 g in all models.
(2) All models contain 4000 g neoprene and 100 g polyethylene in the inner sphere. The outer shell is uranium metal.
(3) The outer radius of the outer fissile shell is 9.3942 cm in all models.
(4) All cases reflected with 20 cm water.

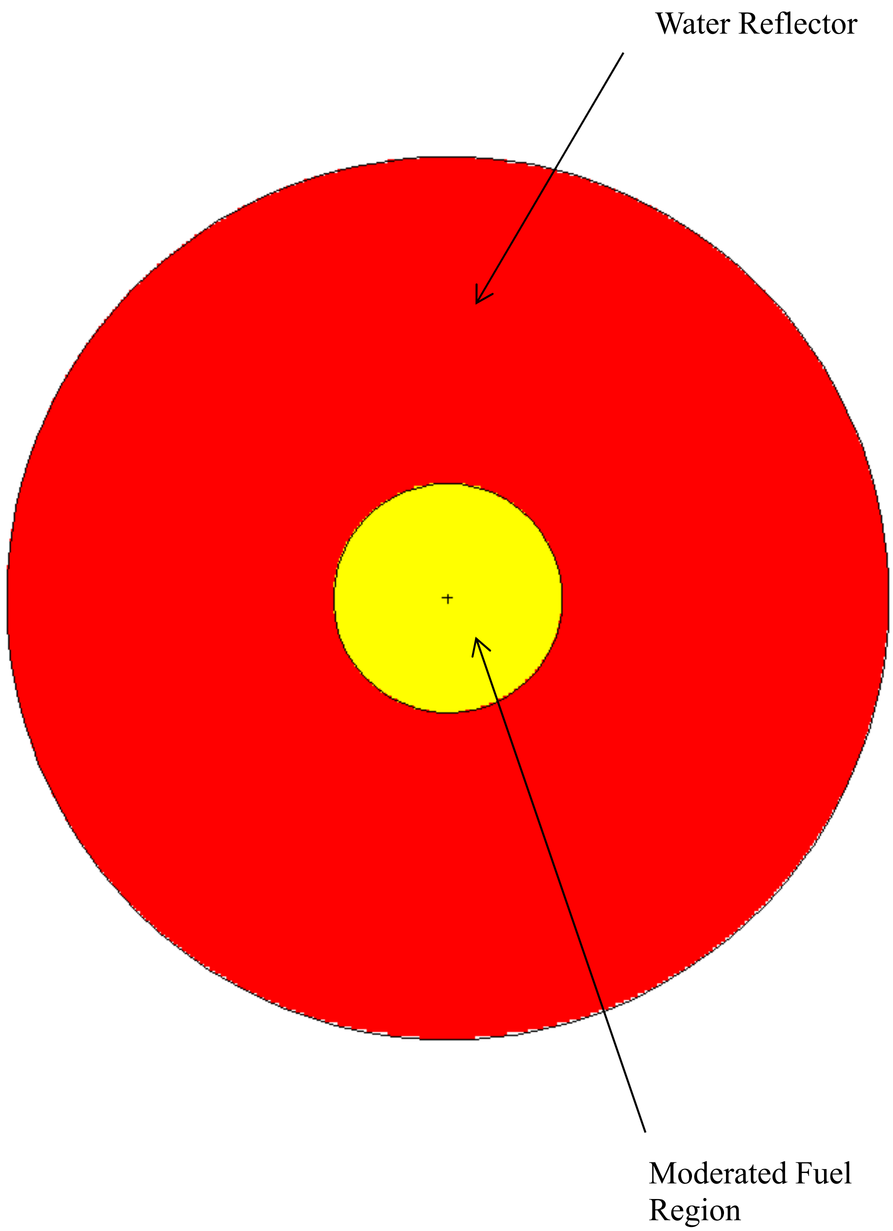

Figure 6.7-1 – Air Transport Model, Single Region Model

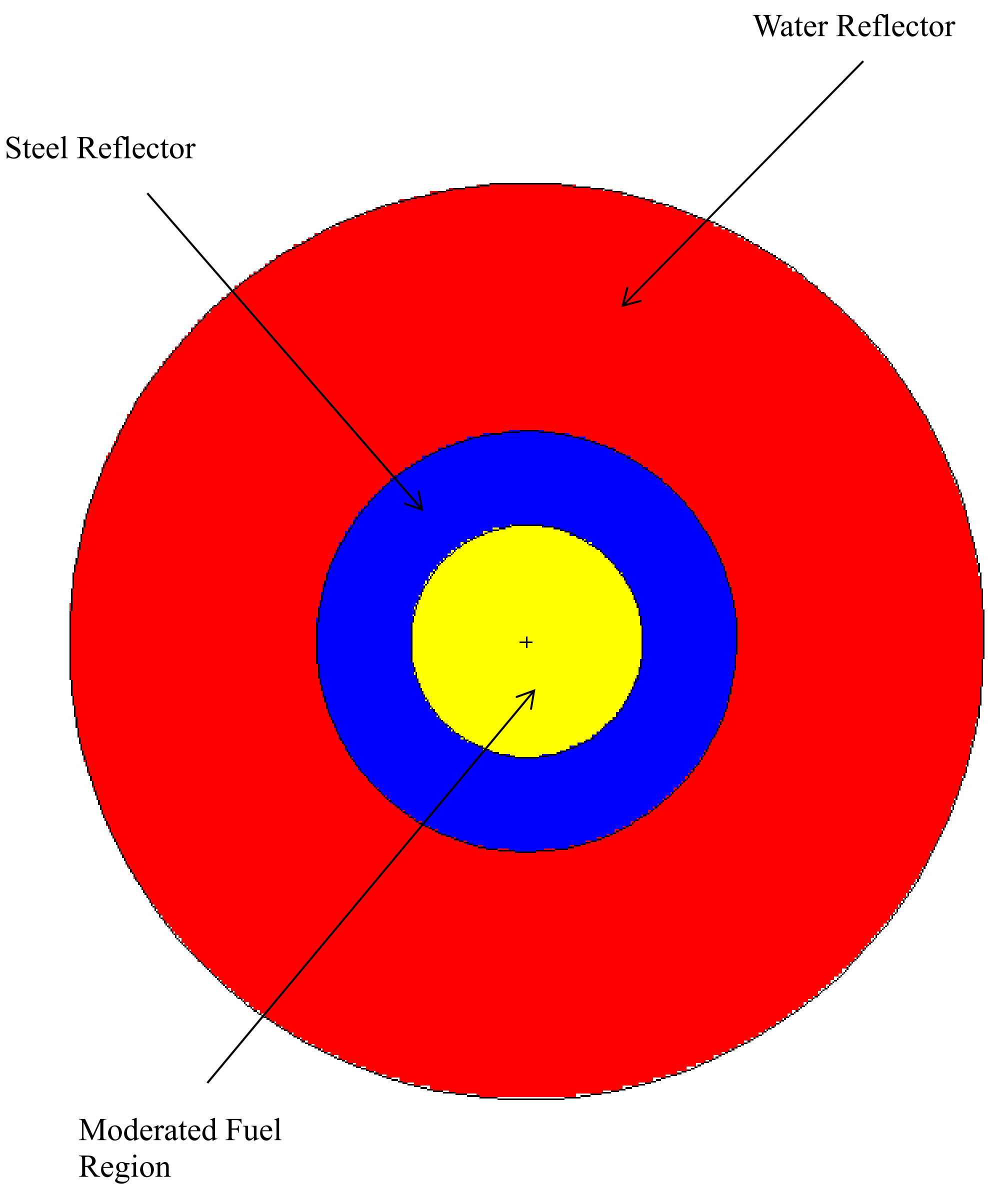

Figure 6.7-2 – Air Transport Model with Steel Reflector

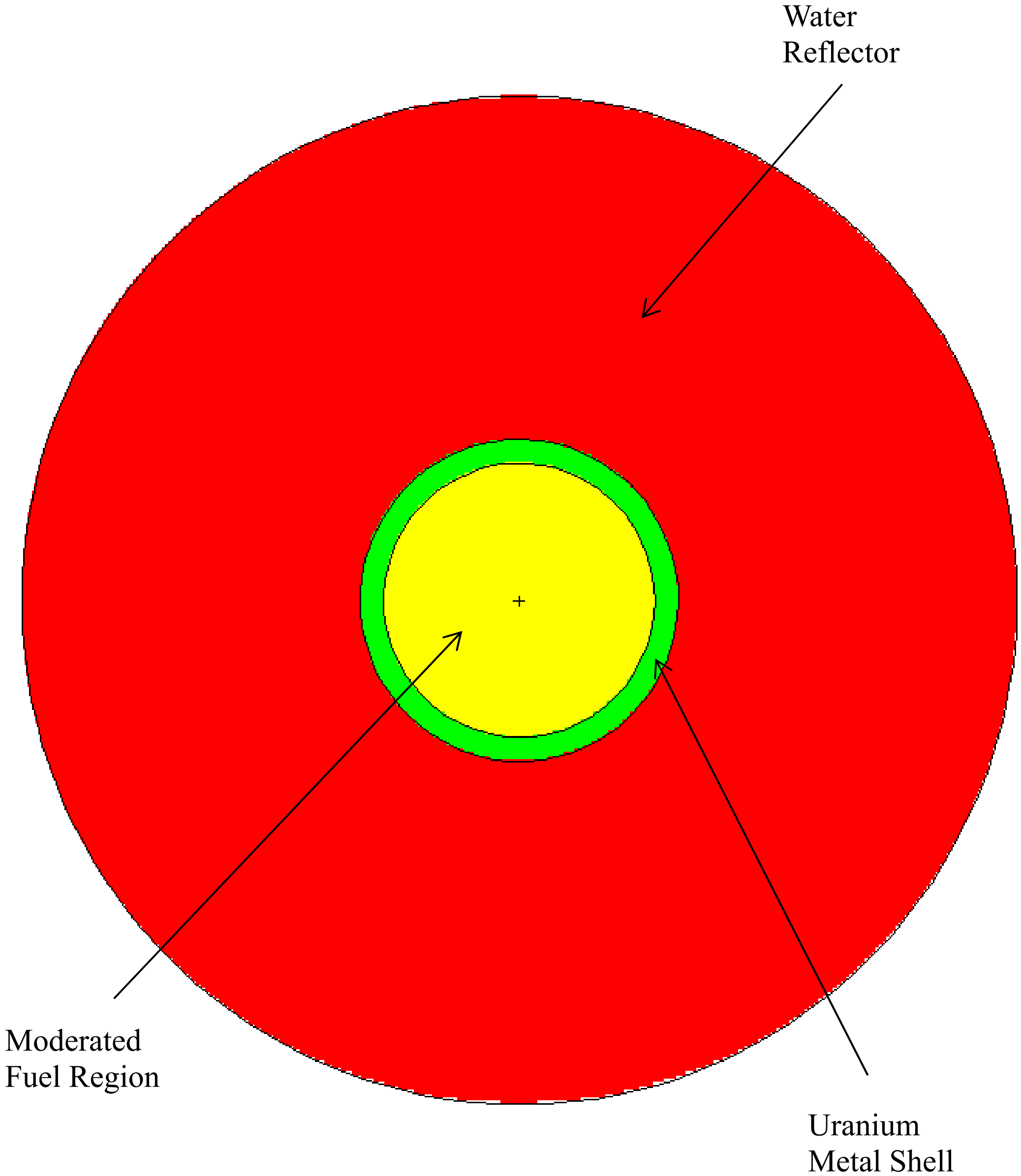

Note: This figure is not to scale. The thickness of the uranium metal shell has been exaggerated for illustrative purposes.

Figure 6.7-3 – Air Transport Model, Two-Region Model

6.8 Benchmark Evaluations

The MCNP, Version 5, Monte Carlo computer code[8] with point-wise ENDF/B-V, -VI, and -VII cross sections has been used extensively in criticality evaluations. The uranium isotopes utilize preliminary ENDF/B-VII cross section data that are considered by Los Alamos National Laboratory to be more accurate than ENDF/B-VI cross sections. ENDF/B-V cross sections are utilized for chromium, nickel, and iron because natural composition ENDF/B-VI cross sections are not available for these elements. The remaining isotopes utilize ENDF/B-VI cross sections. This section justifies the validity of this computation tool and data library combination for application to the ATR FFSC criticality analysis and a bias factor is obtained from these calculations of the critical experiments.

The MCNP code uses room temperature continuous-energy (point-wise) cross sections that are thoroughly documented in Appendix G of the manual. These cross sections are defined with a high-energy resolution that describes each resolved cross section resonance for the isotope. All of the cross-sections used for these analyses were generated from the U.S. Evaluated Nuclear Data Files (ENDF/B).

The validation of the point-wise cross sections is conducted using 35 experimental criticality benchmarks applicable to the ATR FFSC. The statistical analysis of the benchmark experiments results in a USL of 0.9209.

6.8.1 Applicability of Benchmark Experiments

The experimental benchmarks are summarized in the OECD Nuclear Energy Agency's *International Handbook of Evaluated Criticality Safety Benchmark Experiments*[9]. Each experiment is discussed in detail in the *Handbook*. It includes estimates of the uncertainty in the measurements, detailed information regarding dimensions and material compositions, comparisons between the multiplication factor calculated by various computer codes, and a list of input files that were used in their calculations.

The critical experiment benchmarks are selected based upon their similarity to the ATR FFSC and contents. The important selection parameters are high-enriched uranium plate-type fuel with a thermal spectrum. Thirty-five (35) benchmarks that meet these criteria are selected from the *Handbook*. The titles for all utilized experiments are listed in Table 6.8-1. Note that the benchmark from HEU-MET-THERM-022 is for the Advanced Test Reactor itself, so the fuel configuration in this benchmark is essentially the same as the fuel modeled in the packaging analysis.

Ideally, benchmarks would be limited to those with a fuel matrix of UAl_x and aluminum, aluminum cladding, and no absorbers, consistent with the ATR criticality models. Experiment set HEU-MET-THERM-006 consists of 23 benchmark experiments. The first 16 experiments are directly applicable, although experiments 17 and 18 utilize thin cadmium sheets, and experiments 19 through 23 utilize uranium in solution in addition to the fuel plates. Experiment set HEU-COMP-THERM-022 consists of 11 benchmark experiments that utilize UO_2 powder

---

[8] MCNP5, "*MCNP – A General Monte Carlo N-Particle Transport Code, Version 5; Volume II: User's Guide*," LA-CP-03-0245, Los Alamos National Laboratory, April, 2003.

[9] OECD Nuclear Energy Agency, *International Handbook of Evaluated Criticality Safety Benchmark Experiments*, NEA/NSC/DOC(95)03, September, 2006.

sintered with stainless steel, and stainless steel cladding. Experiments 1 through 5 do not utilize control rods, while experiments 6 through 11 utilize boron control rods. HEU-MET-THERM-022 is a detailed model of the ATR core using explicit ATR fuel elements very similar to the ATR fuel element model utilized in the criticality analysis. However, this full-core model necessarily contains absorber materials. Despite the presence of absorbers, because this benchmark utilizes ATR fuel, it is considered directly applicable to the ATR criticality analysis.

Therefore, of these 35 benchmarks, 17 benchmarks are directly applicable, while 18 benchmarks are applicable to a lesser degree. To compensate for the benchmarks that are not directly applicable, trending will be performed both on all 35 benchmark experiments and on the subset of 17 directly applicable benchmark experiments. The USL selected is the minimum of both experimental sets.

Benchmark input files are either obtained from the *Handbook* or directly from Idaho National Laboratory (INL). The only changes made to the input files involve changing to a consistent set of cross section libraries, as needed. Review of the input files indicates that standard MCNP modeling techniques are employed. All but one of the input files consists of simple flat plates in various arrangements. The only benchmark that deviates from simple flat plates is the Advanced Test Reactor full-core model, which is directly applicable to the current analysis. These benchmark input files were developed by INL and have been used extensively for their internal criticality evaluations and are considered to be acceptable. Because the geometry and materials are modeled explicitly, any analyst properly modeling the experimental configuration in MCNP5 would obtain the same result within statistical fluctuation.

6.8.2 Bias Determination

The USL is calculated by application of the USLSTATS computer program[10]. USLSTATS receives as input the k_{eff} as calculated by MCNP, the total 1-σ uncertainty (combined benchmark and MCNP uncertainties), and a trending parameter. Five trending parameters have been selected: (1) Energy of the Average neutron Lethargy causing Fission (EALF), (2) U-235 number density, (3) channel width, (4) ratio of the number of hydrogen atoms in a unit cell to the number of U-235 atoms in a unit cell (H/U-235), and (5) plate pitch.

The uncertainty value, σ_{total}, assigned to each case is a combination of the benchmark uncertainty for each experiment, σ_{bench}, and the Monte Carlo uncertainty associated with the particular computational evaluation of the case, σ_{MCNP}, or:

$$\sigma_{total} = (\sigma_{bench}^2 + \sigma_{MCNP}^2)^{½}$$

These values are input into the USLSTATS program in addition to the following parameters, which are the values recommended by the USLSTATS user's manual:

- P, proportion of population falling above lower tolerance level = 0.995 (note that this parameter is required input but is not utilized in the calculation of USL Method 1)
- 1-γ, confidence on fit = 0.95

[10] USLSTATS, "*USLSTATS: A Utility To Calculate Upper Subcritical Limits For Criticality Safety Applications,"* Version 1.4.2, Oak Ridge National Laboratory, April 23, 2003.

- α, confidence on proportion P = 0.95 (note that this parameter is required input but is not utilized in the calculation of USL Method 1)
- Δk_m, administrative margin used to ensure subcriticality = 0.05.

These data are followed by triplets of trending parameter value, computed k_{eff}, and uncertainty for each case. A confidence band analysis is performed on the data for each trending parameter using USL Method 1. The USL generated for each of the trending parameters utilized is provided in Table 6.8-2. All benchmark data used as input to USLSTATS are reported in Table 6.8-3.

In the following sections, the minimum USL computed for each parameter is identified, and the range of applicability is compared to the fuel element and loose plate models.

6.8.2.1 Energy of the Average neutron Lethargy causing Fission (EALF)

The EALF is used as the first trending parameter for the benchmark cases. The EALF comparison provides a means to observe neutron spectral dependencies or trends. The data for all 35 experiments are plotted in Figure 6.8-1. Over the range of applicability, the minimum USL is 0.9254 for the full benchmark set, and 0.9212 for the subset of directly applicable benchmarks.

Range of Applicability, Fuel element models: All of the single package models and most of the NCT and HAC array models fall within the range of the applicability. The EALF of the most reactive fuel element model (Case E23) has an EALF of 1.39E-07 MeV, which is within the range of applicability. Models with significantly more void spaces or low water densities sometimes exceed the range of applicability (maximum EALF = 2.73E-07 MeV for Case E1), although these cases are not the most reactive. Therefore, the EALF of the most reactive models is acceptably within the range of applicability of the benchmarks.

Range of Applicability, Loose plate models: The loose plate analysis is highly moderated, and the EALF of the models fall within the range of applicability of the benchmark experiments with few exceptions. The only cases that fall outside the range of applicability are the very-small pitch cases for Plate 5, because these cases are insufficiently moderated and also thus have low reactivity. Therefore, the EALF is acceptably within the range of applicability of the benchmarks.

6.8.2.2 U-235 Number Density

The U-235 number density is used as the second trending parameter for the benchmark cases. The data for all 35 experiments are plotted in Figure 6.8-2. Over the range of applicability, the minimum USL is 0.9240 for the full benchmark set, and 0.9209 for the subset of directly applicable benchmarks.

Range of Applicability, Fuel element models: For the optimized fuel element model, the U-235 number densities for plates 1 through 4 and 16 through 19 fall within the range of applicability, while the number densities for plates 5 through 15 exceed the range of applicability (maximum value = 4.22E-03 atom/b-cm). The maximum range of applicability is 3.92E-03 atom/b-cm, so range is exceeded only slightly. If the minimum USL is extrapolated to this larger number density, the minimum USL of 0.9209 does not change. Also, the average U-235 number density for the fuel element is 3.73E-03 atom/b-cm, which is within the allowable range. Therefore, application of this USL to the fuel element criticality models is considered acceptable.

Range of Applicability, Loose plate models: Of the four plate types modeled, the U-235 number densities for plate type 3 fall within the range of applicability, while the number densities for plate types 5, 8, and 15 exceed the range of applicability (maximum value = 4.29E-03 atom/b-cm). The maximum range of applicability is 3.92E-03 atom/b-cm, so the range is exceeded only slightly. If the minimum USL is extrapolated to this larger number density, the minimum USL of 0.9209 does not change. Therefore, application of this USL to the loose plate basket criticality models is considered acceptable.

6.8.2.3 Channel Width

The channel width is used as the third trending parameter for the benchmark cases. The data for all 35 experiments are plotted in Figure 6.8-3. Over the range of applicability, the minimum USL is 0.9225 for the full benchmark set, and 0.9209 for the subset of directly applicable benchmarks.

Range of Applicability, Fuel element models: The channel width is fixed at 0.089-in for the most reactive fuel element models, which exceeds the maximum channel width of 0.078-in of the benchmark experiments. However, this parameter is only slightly larger than the maximum benchmark experiment channel width, and was maximized in order to maximize model reactivity. Extrapolation of the USL to the channel width of 0.089-in yields a USL of 0.9208, which is essentially the same as the minimum USL of 0.9209 over the range of applicability. Therefore, application of this USL to the fuel element criticality models is considered acceptable.

Range of Applicability, Loose plate models: The maximum channel width of the benchmark models is 0.078-in, while the channel width of the most reactive loose plate model is 0.439-in. Clearly, the loose plate models are well outside the bounds of the benchmark models and extrapolation of the USL would not be appropriate over such a wide range. However, the channel width is directly related to system moderation, and the acceptability of the EALF indicator demonstrates that MCNP is performing acceptably for thermal conditions.

6.8.2.4 H/U-235 Atom Ratio

The H/U-235 atom ratio is used as the fourth trending parameter for the benchmark cases. The H/U-235 atom ratio is defined here as the ratio of hydrogen atoms to U-235 atoms in a unit cell. This parameter is computed by the following equation:

NH*C/(NU235*M)

where,

NH is the hydrogen number density

C is the channel width

NU235 is the U-235 number density

M is the fuel meat width

The data for all 35 experiments are plotted in Figure 6.8-4. Over the range of applicability, the minimum USL is 0.9257 for the full benchmark set, and 0.9209 for the subset of directly applicable benchmarks.

Range of Applicability, Fuel element models: Using the maximum fuel element plate U-235 number density for the optimized fuel element model, the H/U-235 value may be computed as:

6.687E-02*0.089/(4.224E-03*0.02) = 70.4

Therefore, H/U-235 of the models is acceptably within the range of applicability of the benchmarks.

Range of Applicability, Loose plate models: The H/U-235 atom ratio for the most reactive model may be computed as:

6.687E-02*0.439/(4.2887E-03*0.02) = 342

The maximum H/U-235 atom ratio of the benchmark models is 116.5. Clearly, the loose plate models are well outside the bounds of the benchmark models and extrapolation of the USL would not be appropriate over such a wide range. However, the H/U-235 atom ratio is directly related to system moderation, and the acceptability of the EALF indicator demonstrates that MCNP is performing acceptably for thermal conditions.

6.8.2.5 Pitch

The fuel plate pitch is used as the fifth trending parameter for the benchmark cases. The data for all 35 experiments is plotted in Figure 6.8-5. Over the range of applicability, the minimum USL is 0.9225 for the full benchmark set, and 0.9209 for the subset of directly applicable benchmarks.

Range of Applicability, Fuel element models: The fuel plate pitch is fixed at 0.128-in for all fuel element models (excluding the pitch for plates 1 and 19, which is slightly bigger because these plates are thicker). This pitch falls within the range of the benchmark experiments.

Range of Applicability, Loose plate models: The maximum pitch of the benchmark models is 0.128-in, while the pitch of the most reactive loose plate model is 0.487-in (1.236 cm). Clearly, the loose plate models are well outside the bounds of the benchmark models and extrapolation of the USL would not be appropriate over such a wide range. However, the pitch is directly related to system moderation, and the acceptability of the EALF indicator demonstrates that MCNP is performing acceptably for thermal conditions.

6.8.2.6 Recommended USL

For the full benchmark set, the minimum USL is 0.9225, while for the subset of directly applicable benchmarks, the minimum USL is 0.9209. Therefore, the USL is trending lower for the subset of directly applicable benchmarks. Note, however, that the average k_{eff} = 0.992 for both the full benchmark set and directly applicable subset. The USL could likely be improved by development of additional benchmark models, but given the large margins to the most reactive case, the lower value (0.9209) is conservatively selected as the USL for this analysis.

Table 6.8-1 – Benchmark Experiments Utilized

Series	Title
HEU-COMP-THERM-022	SPERT III Stainless-Steel-Clad Plate-Type Fuel in Water
HEU-MET-THERM-006	SPERT-D Aluminum-Clad Plate-Type Fuel in Water, Dilute Uranyl Nitrate, or Borated Uranyl Nitrate
HEU-MET-THERM-022	Advanced Test Reactor: Serpentine Arrangement of Highly Enriched Water-Moderated Uranium-Aluminide Fuel Plates Reflected by Beryllium

Table 6.8-2 – USL Results

Trending Parameter (X)	Minimum USL Over Range of Applicability	Range of Applicability
35 Experiment Set		
EALF (MeV)	0.9254	5.22210E-08 <= X <= 1.58510E-07
U-235 Number Density (atom/b-cm)	0.9240	1.84900E-03 <= X <= 3.92600E-03
Channel width (in)	0.9225	6.45700E-02 <= X <= 7.80000E-02
H/U-235	0.9257	65.100 <= X <= 116.50
Pitch (in)	0.9225	0.12457 <= X <= 0.12800
17 Experiment Set		
EALF (MeV)	0.9212	5.22210E-08 <= X <= 1.58510E-07
U-235 Number Density (atom/b-cm)	0.9209	1.84900E-03 <= X <= 3.92600E-03
Channel width (in)	0.9209	6.45700E-02 <= X <= 7.80000E-02
H/U-235	0.9209	66.0 <= X <= 116.50
Pitch (in)	0.9209	0.12457 <= X <= 0.12800

This page left intentionally blank.

Table 6.8-3 – Benchmark Experiment Data

No	Case	k	σ_{mcnp}	σ_{bench}	σ_{total}	EALF (MeV)	U-235 (atom/b-cm)	Chanel Width (in)	H/U-235	Pitch (in)
1	hct022_c01	0.98895	0.00060	0.0081	0.0081	9.528E-08	3.3155E-03	0.06457	65.1	0.12457
2	hct022_c02	0.98980	0.00061	0.0081	0.0081	9.665E-08	3.3155E-03	0.06457	65.1	0.12457
3	hct022_c03	0.98985	0.00063	0.0081	0.0081	9.809E-08	3.3155E-03	0.06457	65.1	0.12457
4	hct022_c04	0.98856	0.00060	0.0081	0.0081	9.917E-08	3.3155E-03	0.06457	65.1	0.12457
5	hct022_c05	0.98909	0.00063	0.0081	0.0081	9.587E-08	3.3155E-03	0.06457	65.1	0.12457
6	hct022_c06	0.98902	0.00059	0.0081	0.0081	9.840E-08	3.3155E-03	0.06457	65.1	0.12457
7	hct022_c07	0.98963	0.00056	0.0081	0.0081	9.890E-08	3.3155E-03	0.06457	65.1	0.12457
8	hct022_c08	0.98908	0.00057	0.0081	0.0081	9.951E-08	3.3155E-03	0.06457	65.1	0.12457
9	hct022_c09	0.98840	0.00056	0.0081	0.0081	9.589E-08	3.3155E-03	0.06457	65.1	0.12457
10	hct022_c10	0.98845	0.00060	0.0081	0.0081	9.963E-08	3.3155E-03	0.06457	65.1	0.12457
11	hct022_c11	0.98930	0.00060	0.0081	0.0081	1.001E-07	3.3155E-03	0.06457	65.1	0.12457
12	hmt006_c01	0.99240	0.00082	0.0044	0.0045	8.481E-08	1.8490E-03	0.06457	116.5	0.12457
13	hmt006_c02	0.99331	0.00088	0.0040	0.0041	7.044E-08	1.8490E-03	0.06457	116.5	0.12457
14	hmt006_c03	0.99740	0.00072	0.0040	0.0041	6.338E-08	1.8490E-03	0.06457	116.5	0.12457
15	hmt006_c04	0.99282	0.00081	0.0040	0.0041	6.185E-08	1.8490E-03	0.06457	116.5	0.12457
16	hmt006_c05	0.99230	0.00079	0.0040	0.0041	5.852E-08	1.8490E-03	0.06457	116.5	0.12457
17	hmt006_c06	0.99010	0.00071	0.0040	0.0041	5.615E-08	1.8490E-03	0.06457	116.5	0.12457
18	hmt006_c07	0.98783	0.00073	0.0040	0.0041	5.432E-08	1.8490E-03	0.06457	116.5	0.12457
19	hmt006_c08	0.98428	0.00076	0.0040	0.0041	5.245E-08	1.8490E-03	0.06457	116.5	0.12457
20	hmt006_c09	0.98657	0.00072	0.0040	0.0041	5.222E-08	1.8490E-03	0.06457	116.5	0.12457
21	hmt006_c10	0.99885	0.00085	0.0040	0.0041	8.220E-08	1.8490E-03	0.06457	116.5	0.12457
22	hmt006_c11	0.98965	0.00081	0.0040	0.0041	6.236E-08	1.8490E-03	0.06457	116.5	0.12457
23	hmt006_c12	0.99403	0.00070	0.0040	0.0041	5.415E-08	1.8490E-03	0.06457	116.5	0.12457
24	hmt006_c13	1.01283	0.00086	0.0040	0.0041	8.231E-08	1.8490E-03	0.06457	116.5	0.12457
25	hmt006_c14	0.98495	0.00071	0.0061	0.0061	5.715E-08	1.8490E-03	0.06457	116.5	0.12457

(continued)

Table 6.8-3 – Benchmark Experiment Data (concluded)

No	Case	k	σ_{mcnp}	σ_{bench}	σ_{total}	EALF (MeV)	U-235 (atom/b-cm)	Chanel Width (in)	H/U-235	Pitch (in)
26	hmt006_c15	0.98128	0.00077	0.0040	0.0041	5.654E-08	1.8490E-03	0.06457	116.5	0.12457
27	hmt006_c16	0.99241	0.00078	0.0040	0.0041	6.330E-08	1.8490E-03	0.06457	116.5	0.12457
28	hmt006_c17	0.98934	0.00082	0.0040	0.0041	7.405E-08	1.8490E-03	0.06457	116.5	0.12457
29	hmt006_c18	0.99282	0.00087	0.0040	0.0041	8.003E-08	1.8490E-03	0.06457	116.5	0.12457
30	hmt006_c19	0.99360	0.00068	0.0040	0.0041	5.243E-08	1.8490E-03	0.06457	113.9	0.12457
31	hmt006_c20	0.99275	0.00076	0.0040	0.0041	6.471E-08	1.8490E-03	0.06457	113.7	0.12457
32	hmt006_c21	0.99469	0.00077	0.0040	0.0041	6.917E-08	1.8490E-03	0.06457	113.7	0.12457
33	hmt006_c22	0.99670	0.00080	0.0040	0.0041	7.407E-08	1.8490E-03	0.06457	113.6	0.12457
34	hmt006_c23	1.00132	0.00080	0.0040	0.0041	7.670E-08	1.8490E-03	0.06457	113.5	0.12457
35	hmt022_c01	0.99179	0.00013	0.0035	0.0035	1.585E-07	3.9260E-03	0.078	66.0	0.12800

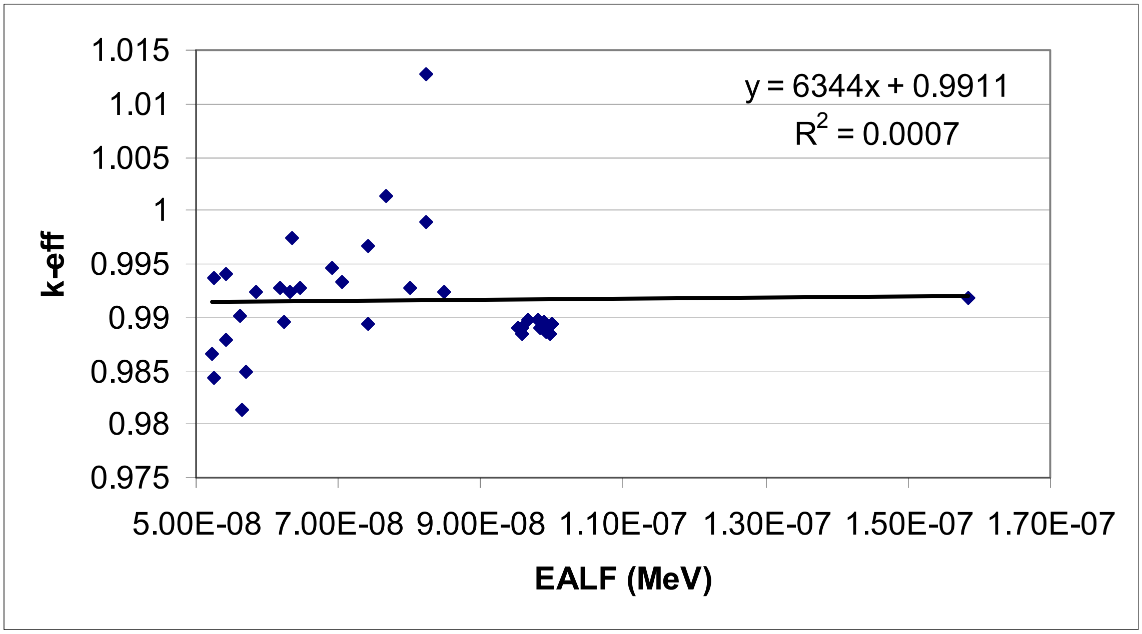

Figure 6.8-1 – Benchmark Data Trend for EALF

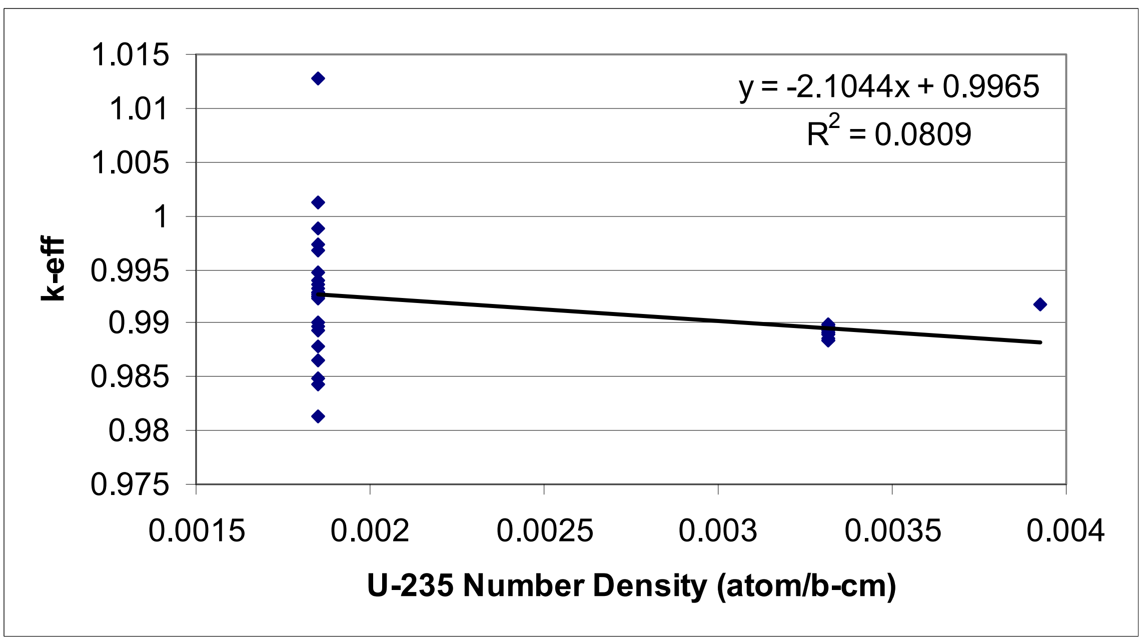

Figure 6.8-2 – Benchmark Data Trend for U-235 Number Density

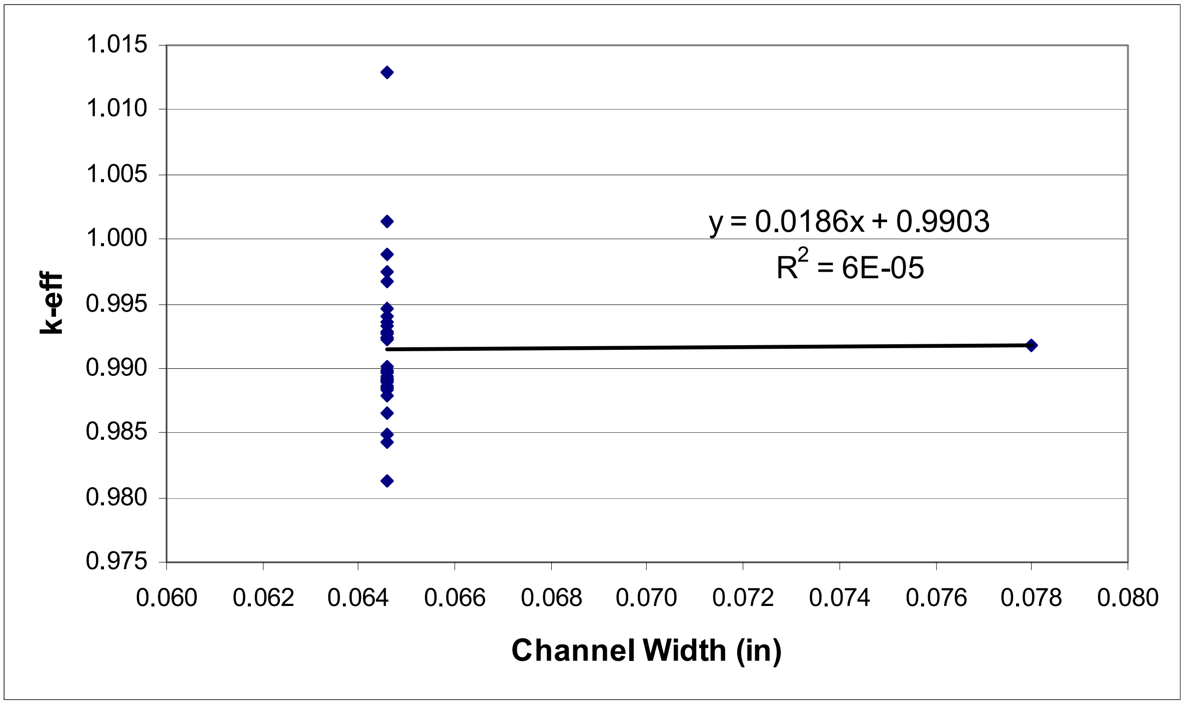

Figure 6.8-3 – Benchmark Data Trend for Channel Width

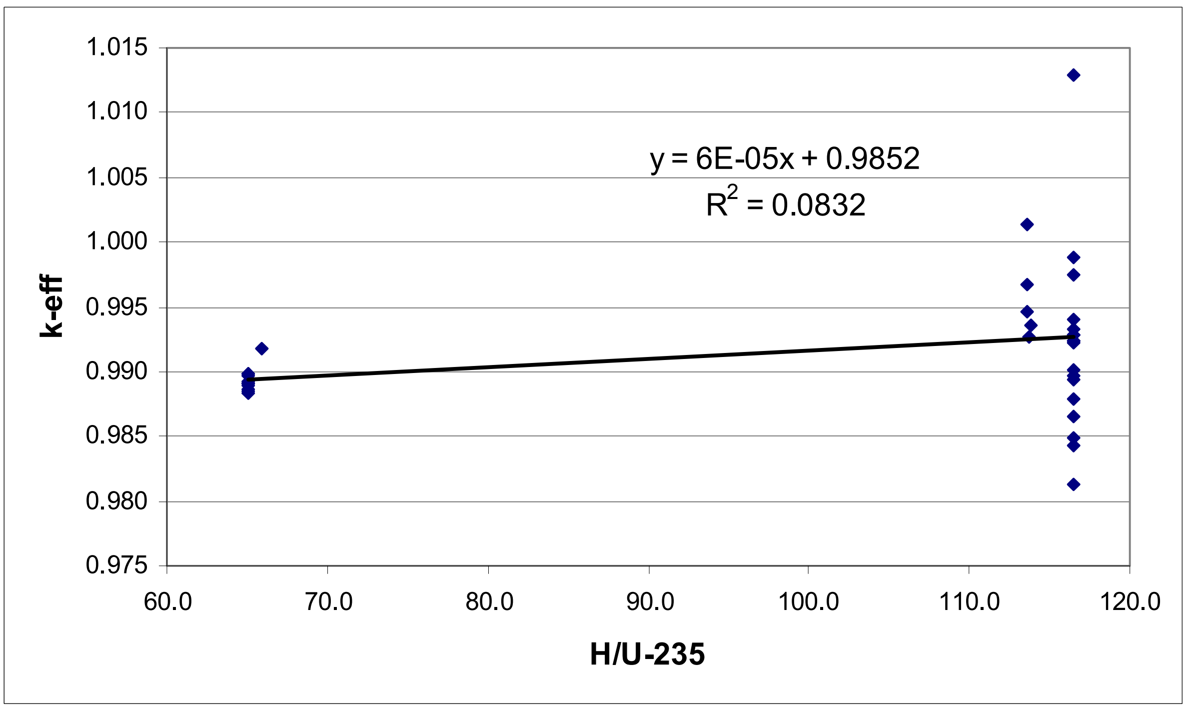

Figure 6.8-4 – Benchmark Data Trend for H/U-235

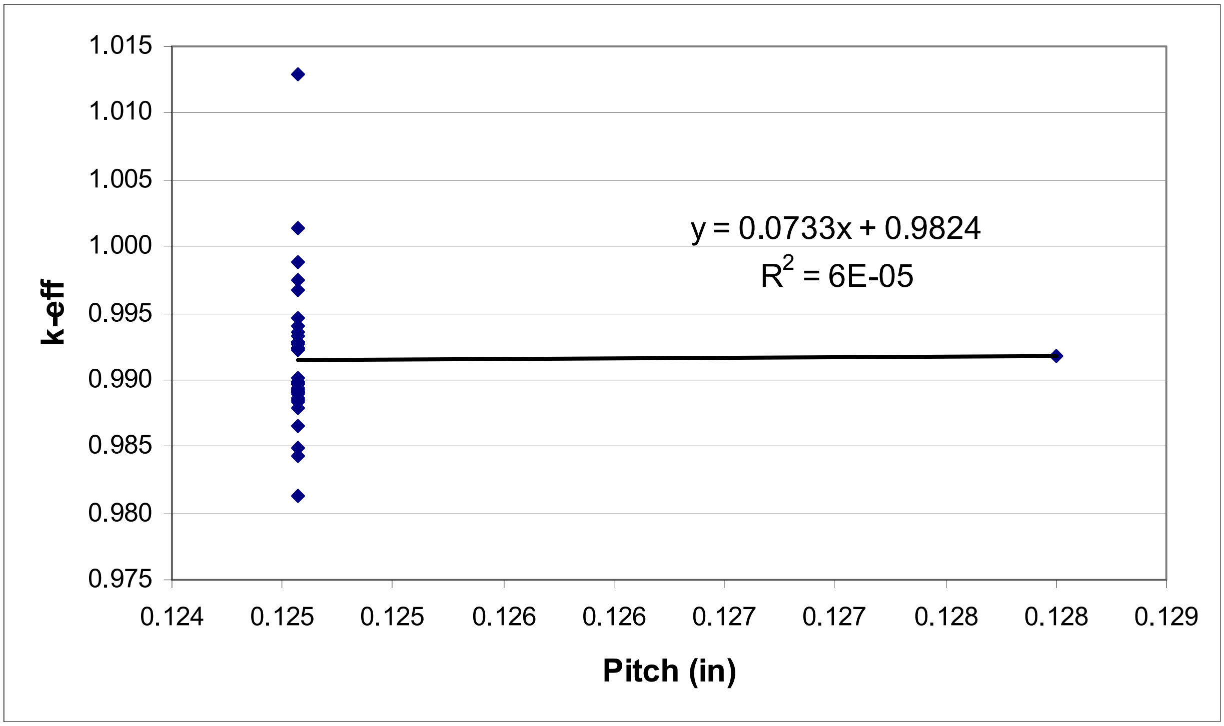

Figure 6.8-5 – Benchmark Data Trend for Pitch

6.9 Appendix A: Sample Input Files

Sample input files are provided for the most reactive NCT array case for both the fuel element payload (Case E23) and the loose plate basket payload (Case LG5).

Case E23 (NA_P030_C89)

```
ATR
999     0       -320:321:-322:323:-324:325                  imp:n=0
900     0       310 -311 312 -313 24 -25     fill=3         imp:n=1
901     2 -1.0 (311:-310:313:-312:-24:25) 320 -321 322 -323 324 -325  imp:n=1
c
c       Universe 1: ATR Fuel Element (infinitely long)
c
2       3 -2.7         -6 8 9 -10                   u=1 imp:n=1 $ left Al piece
4       3 -2.7         -5 7 9 -10                   u=1 imp:n=1 $ right Al piece
6       10 5.5010E-02  52 -53 -14 -13               u=1 imp:n=1 $ plate 1
8       3 -2.7         51 -54   -7 -8          #6   u=1 imp:n=1
10      2 -1.00        54 -55   -7 -8               u=1 imp:n=1
12      11 5.4998E-02  56 -57 -16 -15               u=1 imp:n=1 $ plate 2
14      3 -2.7         55 -58   -7 -8          #12  u=1 imp:n=1
16      2 -1.00        58 -59   -7 -8               u=1 imp:n=1
18      12 5.4574E-02  60 -61 -16 -15               u=1 imp:n=1 $ plate 3
20      3 -2.7         59 -62   -7 -8          #18  u=1 imp:n=1
22      2 -1.00        62 -63   -7 -8               u=1 imp:n=1
24      13 5.4583E-02  64 -65 -16 -15               u=1 imp:n=1 $ plate 4
26      3 -2.7         63 -66   -7 -8          #24  u=1 imp:n=1
28      2 -1.00        66 -67   -7 -8               u=1 imp:n=1
30      14 5.4115E-02  68 -69 -16 -15               u=1 imp:n=1 $ plate 5
32      3 -2.7         67 -70   -7 -8          #30  u=1 imp:n=1
34      2 -1.00        70 -71   -7 -8               u=1 imp:n=1
36      15 5.4106E-02  72 -73 -16 -15               u=1 imp:n=1 $ plate 6
38      3 -2.7         71 -74   -7 -8          #36  u=1 imp:n=1
40      2 -1.00        74 -75   -7 -8               u=1 imp:n=1
42      16 5.4102E-02  76 -77 -16 -15               u=1 imp:n=1 $ plate 7
44      3 -2.7         75 -78   -7 -8          #42  u=1 imp:n=1
46      2 -1.00        78 -79   -7 -8               u=1 imp:n=1
48      17 5.4098E-02  80 -81 -16 -15               u=1 imp:n=1 $ plate 8
50      3 -2.7         79 -82   -7 -8          #48  u=1 imp:n=1
52      2 -1.00        82 -83   -7 -8               u=1 imp:n=1
54      18 5.4095E-02  84 -85 -16 -15               u=1 imp:n=1 $ plate 9
56      3 -2.7         83 -86   -7 -8          #54  u=1 imp:n=1
58      2 -1.00        86 -87   -7 -8               u=1 imp:n=1
60      19 5.4092E-02  88 -89 -16 -15               u=1 imp:n=1 $ plate 10
62      3 -2.7         87 -90   -7 -8          #60  u=1 imp:n=1
64      2 -1.00        90 -91   -7 -8               u=1 imp:n=1
66      20 5.4089E-02  92 -93 -16 -15               u=1 imp:n=1 $ plate 11
68      3 -2.7         91 -94   -7 -8          #66  u=1 imp:n=1
70      2 -1.00        94 -95   -7 -8               u=1 imp:n=1
72      21 5.4086E-02  96 -97 -16 -15               u=1 imp:n=1 $ plate 12
74      3 -2.7         95 -98   -7 -8          #72  u=1 imp:n=1
76      2 -1.00        98 -99   -7 -8               u=1 imp:n=1
78      22 5.4083E-02  100 -101 -16 -15             u=1 imp:n=1 $ plate 13
80      3 -2.7          99 -102   -7 -8        #78  u=1 imp:n=1
82      2 -1.00        102 -103   -7 -8             u=1 imp:n=1
84      23 5.4081E-02  104 -105 -16 -15             u=1 imp:n=1 $ plate 14
```

```
86      3 -2.7          103 -106   -7 -8     #84  u=1 imp:n=1
88      2 -1.00         106 -107   -7 -8          u=1 imp:n=1
90      24 5.4075E-02  108 -109 -16 -15           u=1 imp:n=1 $ plate 15
92      3 -2.7          107 -110   -7 -8     #90  u=1 imp:n=1
94      2 -1.00         110 -111   -7 -8          u=1 imp:n=1
96      25 5.4544E-02  112 -113 -16 -15           u=1 imp:n=1 $ plate 16
98      3 -2.7          111 -114   -7 -8     #96  u=1 imp:n=1
100     2 -1.00         114 -115   -7 -8          u=1 imp:n=1
102     26 5.4544E-02  116 -117 -16 -15           u=1 imp:n=1 $ plate 17
104     3 -2.7          115 -118   -7 -8     #102 u=1 imp:n=1
106     2 -1.00         118 -119   -7 -8          u=1 imp:n=1
108     27 5.4949E-02  120 -121 -18 -17           u=1 imp:n=1 $ plate 18
110     3 -2.7          119 -122   -7 -8     #108 u=1 imp:n=1
112     2 -1.00         122 -123   -7 -8          u=1 imp:n=1
114     28 5.4967E-02  124 -125 -14 -13           u=1 imp:n=1 $ plate 19
116     3 -2.7          123 -126   -7 -8     #114 u=1 imp:n=1
c 122     2 -1.00       6:5:-9:10:9 -51 -8 -7:126 -10 -8 -7 u=1 imp:n=1
120     2 -1.00         126 -10 -8 -7             u=1 imp:n=1 $ above 19
121     2 -1.00         9 -51 -8 -7               u=1 imp:n=1 $ below 1
122     5 -0.737        5 -11 9 -10               u=1 imp:n=1 $ right neoprene
123     5 -0.737      -12 6 9 -10                 u=1 imp:n=1 $ left neoprene
125     2 -1.0         12:11:-9:10                u=1 imp:n=1
c
c       Universe 20: ATR with pipe (center)
c
200     0  -27 -26 22 -23:26 -20 22 -28:27 -21 22 -28  trcl=1
             fill=1  u=20 imp:n=1
201     2 -0.3     #200 -200                    u=20 imp:n=1 $ between
ATR/pipe
202     4 -7.94     200 -201                    u=20 imp:n=1 $ pipe
203     6 -0.096    201 -203 250 -251 252 -253 u=20 imp:n=1 $ insulation
204     0           203 250 -251 252 -253      u=20 imp:n=1 $ insulation to
tube
205     4 -7.94     -250:251:-252:253          u=20 imp:n=1 $ tube to inf
c
c       Universe 21: ATR with pipe (down)
c
210     0  -27 -26 22 -23:26 -20 22 -28:27 -21 22 -28  trcl=2
             fill=1  u=21 imp:n=1
211     2 -0.3     #210 -200                    u=21 imp:n=1 $ between
ATR/pipe
212     4 -7.94     200 -201                    u=21 imp:n=1 $ pipe
213     6 -0.096    201 -203 250 -251 252 -253 u=21 imp:n=1 $ insulation
214     0           203 250 -251 252 -253      u=21 imp:n=1 $ insulation to
tube
215     4 -7.94     -250:251:-252:253          u=21 imp:n=1 $ tube to inf
c
c       Universe 22: ATR with pipe (up)
c
220     0  -27 -26 22 -23:26 -20 22 -28:27 -21 22 -28  trcl=3
             fill=1  u=22 imp:n=1
221     2 -0.3     #220 -200                    u=22 imp:n=1 $ between
ATR/pipe
222     4 -7.94     200 -201                    u=22 imp:n=1 $ pipe
223     6 -0.096    201 -203 250 -251 252 -253 u=22 imp:n=1 $ insulation
224     0           203 250 -251 252 -253      u=22 imp:n=1 $ insulation to
tube
```

```
225     4 -7.94     -250:251:-252:253          u=22 imp:n=1 $ tube to inf
c
c       Universe 23: ATR with pipe (right)
c
230     0  -27 -26 22 -23:26 -20 22 -28:27 -21 22 -28  trcl=4
             fill=1  u=23 imp:n=1
231     2 -0.3     #230 -200                   u=23 imp:n=1 $ between
ATR/pipe
232     4 -7.94     200 -201                   u=23 imp:n=1 $ pipe
233     6 -0.096    201 -203 250 -251 252 -253 u=23 imp:n=1 $ insulation
234     0           203 250 -251 252 -253      u=23 imp:n=1 $ insulation to
tube
235     4 -7.94     -250:251:-252:253          u=23 imp:n=1 $ tube to inf
c
c       Universe 24: ATR with pipe (left)
c
240     0  -27 -26 22 -23:26 -20 22 -28:27 -21 22 -28  trcl=5
             fill=1  u=24 imp:n=1
241     2 -0.3     #240 -200                   u=24 imp:n=1 $ between
ATR/pipe
242     4 -7.94     200 -201                   u=24 imp:n=1 $ pipe
243     6 -0.096    201 -203 250 -251 252 -253 u=24 imp:n=1 $ insulation
244     0           203 250 -251 252 -253      u=24 imp:n=1 $ insulation to
tube
245     4 -7.94     -250:251:-252:253          u=24 imp:n=1 $ tube to inf
c
c       Universe 25: ATR with pipe (up right)
c
250     0  -27 -26 22 -23:26 -20 22 -28:27 -21 22 -28  trcl=6
             fill=1  u=25 imp:n=1
251     2 -0.3     #250 -200                   u=25 imp:n=1 $ between
ATR/pipe
252     4 -7.94     200 -201                   u=25 imp:n=1 $ pipe
253     6 -0.096    201 -203 250 -251 252 -253 u=25 imp:n=1 $ insulation
254     0           203 250 -251 252 -253      u=25 imp:n=1 $ insulation to
tube
255     4 -7.94     -250:251:-252:253          u=25 imp:n=1 $ tube to inf
c
c       Universe 26: ATR with pipe (up left)
c
260     0  -27 -26 22 -23:26 -20 22 -28:27 -21 22 -28  trcl=7
             fill=1  u=26 imp:n=1
261     2 -0.3     #260 -200                   u=26 imp:n=1 $ between
ATR/pipe
262     4 -7.94     200 -201                   u=26 imp:n=1 $ pipe
263     6 -0.096    201 -203 250 -251 252 -253 u=26 imp:n=1 $ insulation
264     0           203 250 -251 252 -253      u=26 imp:n=1 $ insulation to
tube
265     4 -7.94     -250:251:-252:253          u=26 imp:n=1 $ tube to inf
c
c       Universe 27: ATR with pipe (down right)
c
270     0  -27 -26 22 -23:26 -20 22 -28:27 -21 22 -28  trcl=8
             fill=1  u=27 imp:n=1
271     2 -0.3     #270 -200                   u=27 imp:n=1 $ between
ATR/pipe
272     4 -7.94     200 -201                   u=27 imp:n=1 $ pipe
```

```
273     6 -0.096    201 -203 250 -251 252 -253 u=27 imp:n=1 $ insulation
274     0           203 250 -251 252 -253      u=27 imp:n=1 $ insulation to
tube
275     4 -7.94     -250:251:-252:253          u=27 imp:n=1 $ tube to inf
c
c       Universe 28: ATR with pipe (down left)
c
280     0  -27 -26 22 -23:26 -20 22 -28:27 -21 22 -28  trcl=9
             fill=1  u=28 imp:n=1
281     2 -0.3     #280 -200                   u=28 imp:n=1 $ between
ATR/pipe
282     4 -7.94     200 -201                   u=28 imp:n=1 $ pipe
283     6 -0.096    201 -203 250 -251 252 -253 u=28 imp:n=1 $ insulation
284     0           203 250 -251 252 -253      u=28 imp:n=1 $ insulation to
tube
285     4 -7.94     -250:251:-252:253          u=28 imp:n=1 $ tube to inf
c
c       Universe 3: Array of Packages
c
300   0    -300 301 -302 303 imp:n=1 u=3 lat=1 fill=-4:4 -4:4 0:0
             25 25 25 25 22 26 26 26 26
             25 25 25 25 22 26 26 26 26
             25 25 25 25 22 26 26 26 26
             25 25 25 25 22 26 26 26 26
             23 23 23 23 20 24 24 24 24
             27 27 27 27 21 28 28 28 28
             27 27 27 27 21 28 28 28 28
             27 27 27 27 21 28 28 28 28
             27 27 27 27 21 28 28 28 28

5       p  2.4142136 -1 0 -0.2665911 $ right Al outer
6       p -2.4142136 -1 0 -0.2665911 $ left Al outer
7       p  2.4142136 -1 0 -1.474587  $ right Al inner
8       p -2.4142136 -1 0 -1.474587  $ left Al inner
9       cz 7.52856                   $ Al boundary
10      cz 14.015466                 $ Al boundary
11      p  2.4142136 -1 0  0.563076  $ right neoprene
12      p -2.4142136 -1 0  0.563076  $ left neoprene
c
13      p  2.4142136 -1 0 -2.4370013 $ plate 1 & 19 meat
14      p -2.4142136 -1 0 -2.4370013 $ plate 1 & 19 meat
15      p  2.4142136 -1 0 -1.7732672 $ plate 2-17 meat
16      p -2.4142136 -1 0 -1.7732672 $ plate 2-17 meat
17      p  2.4142136 -1 0 -1.9060140 $ plate 18 meat
18      p -2.4142136 -1 0 -1.9060140 $ plate 18 meat
c
20      p  2.4142136 -1 0   0.6      $ right u0 boundary
21      p -2.4142136 -1 0   0.6      $ left u0 boundary
22      cz 7.51                      $ u0 boundary
23      cz 14.02                     $ u0 boundary
24      pz -60.96                    $ bottom of fuel
25      pz  60.96                    $ top of fuel (48")
26      p  2.4142136 -1 0  0.0       $ neoprene notch
27      p -2.4142136 -1 0  0.0       $ neoprene notch
28      cz 13.9                      $ neoprene notch
c
51      cz 7.67207  $ fuel plate 1 (0.089)
```

```
52      cz 7.7343
53      cz 7.7851
54      cz 7.84733
c
55      cz 8.07339  $ fuel plate 2
56      cz 8.09752
57      cz 8.14832
58      cz 8.17245
c
59      cz 8.39851  $ fuel plate 3
60      cz 8.42264
61      cz 8.47344
62      cz 8.49757
c
63      cz 8.72363  $ fuel plate 4
64      cz 8.74776
65      cz 8.79856
66      cz 8.82269
c
67      cz 9.04875  $ fuel plate 5
68      cz 9.07288
69      cz 9.12368
70      cz 9.14781
c
71      cz 9.37387  $ fuel plate 6
72      cz 9.398
73      cz 9.4488
74      cz 9.47293
c
75      cz 9.69899  $ fuel plate 7
76      cz 9.72312
77      cz 9.77392
78      cz 9.79805
c
79      cz 10.02411  $ fuel plate 8
80      cz 10.04824
81      cz 10.09904
82      cz 10.12317
c
83      cz 10.34923  $ fuel plate 9
84      cz 10.37336
85      cz 10.42416
86      cz 10.44829
c
87      cz 10.67435  $ fuel plate 10
88      cz 10.69848
89      cz 10.74928
90      cz 10.77341
c
91      cz 10.99947  $ fuel plate 11
92      cz 11.0236
93      cz 11.0744
94      cz 11.09853
c
95      cz 11.32459  $ fuel plate 12
96      cz 11.34872
97      cz 11.39952
```

```
98      cz 11.42365
c
99       cz 11.64971  $ fuel plate 13
100      cz 11.67384
101      cz 11.72464
102      cz 11.74877
c
103      cz 11.97483  $ fuel plate 14
104      cz 11.99896
105      cz 12.04976
106      cz 12.07389
c
107      cz 12.29995  $ fuel plate 15
108      cz 12.32408
109      cz 12.37488
110      cz 12.39901
c
111      cz 12.62507  $ fuel plate 16
112      cz 12.6492
113      cz 12.7
114      cz 12.72413
c
115      cz 12.95019  $ fuel plate 17
116      cz 12.97432
117      cz 13.02512
118      cz 13.04925
c
119      cz 13.27531  $ fuel plate 18
120      cz 13.29944
121      cz 13.35024
122      cz 13.37437
c
123      cz 13.60043  $ fuel plate 19 (0.089)
124      cz 13.68806
125      cz 13.73886
126      cz 13.82649
c
200      cz 7.3838 $ IR pipe
201      cz 7.6581 $ OR pipe
202      cz 38.1   $ 12" water
203      cz 10.1981 $ 1" insulation
c
250      px  -9.6032 $ square tube
251      px   9.6032
252      py  -9.6032
253      py   9.6032
c
300      px  10.033 $ lattice surfaces/sq. tube
301      px -10.033
302      py  10.033
303      py -10.033
310      px -90.297 $ 9x9 bounds
311      px  90.297
312      py -90.297
313      py  90.297
320      px -120.777 $ outer bounds
321      px  120.777
```

```
322      py -120.777
323      py  120.777
324      pz -91.44
325      pz  91.44

m2      1001.62c  2          $ water
        8016.62c  1
mt2     lwtr.60t
m3      13027.62c 1          $ Al
m4      6000.66c   -0.08     $ SS-304
        14000.60c  -1.0
        15031.66c  -0.045
        24000.50c  -19.0
        25055.62c  -2.0
        26000.55c  -68.375
        28000.50c  -9.5
m5      1001.62c  -0.056920  $ neoprene
        6000.66c  -0.542646
c        17000.66c -0.400434
m6      13027.62c  -26.5     $ insulation material
        14000.60c  -23.4
        8016.62c   -50.2
m10     92234.69c 1.7026E-05 $ fuel plate 1
        92235.69c 2.6560E-03
        92236.69c 9.8475E-06
        92238.69c 1.4089E-04
        13027.62c 5.2187E-02
c       total     5.5010E-02
m11     92234.69c 1.7156E-05 $ fuel plate 2
        92235.69c 2.6763E-03
        92236.69c 9.9226E-06
        92238.69c 1.4196E-04
        13027.62c 5.2153E-02
c       total     5.4998E-02
m12     92234.69c 2.1711E-05 $ fuel plate 3
        92235.69c 3.3869E-03
        92236.69c 1.2557E-05
        92238.69c 1.7966E-04
        13027.62c 5.0974E-02
c       total     5.4574E-02
m13     92234.69c 2.1618E-05 $ fuel plate 4
        92235.69c 3.3724E-03
        92236.69c 1.2503E-05
        92238.69c 1.7889E-04
        13027.62c 5.0998E-02
c       total     5.4583E-02
m14     92234.69c 2.6648E-05 $ fuel plate 5
        92235.69c 4.1571E-03
        92236.69c 1.5413E-05
        92238.69c 2.2051E-04
        13027.62c 4.9696E-02
c       total     5.4115E-02
m15     92234.69c 2.6746E-05 $ fuel plate 6
        92235.69c 4.1724E-03
        92236.69c 1.5470E-05
        92238.69c 2.2132E-04
        13027.62c 4.9670E-02
```

```
c       total     5.4106E-02
m16     92234.69c 2.6790E-05 $ fuel plate 7
        92235.69c 4.1791E-03
        92236.69c 1.5495E-05
        92238.69c 2.2168E-04
        13027.62c 4.9659E-02
c       total     5.4102E-02
m17     92234.69c 2.6830E-05 $ fuel plate 8
        92235.69c 4.1854E-03
        92236.69c 1.5518E-05
        92238.69c 2.2201E-04
        13027.62c 4.9649E-02
c       total     5.4098E-02
m18     92234.69c 2.6867E-05 $ fuel plate 9
        92235.69c 4.1911E-03
        92236.69c 1.5539E-05
        92238.69c 2.2232E-04
        13027.62c 4.9639E-02
c       total     5.4095E-02
m19     92234.69c 2.6901E-05 $ fuel plate 10
        92235.69c 4.1965E-03
        92236.69c 1.5559E-05
        92238.69c 2.2260E-04
        13027.62c 4.9630E-02
c       total     5.4092E-02
m20     92234.69c 2.6933E-05 $ fuel plate 11
        92235.69c 4.2015E-03
        92236.69c 1.5577E-05
        92238.69c 2.2287E-04
        13027.62c 4.9622E-02
c       total     5.4089E-02
m21     92234.69c 2.6963E-05 $ fuel plate 12
        92235.69c 4.2061E-03
        92236.69c 1.5595E-05
        92238.69c 2.2311E-04
        13027.62c 4.9614E-02
c       total     5.4086E-02
m22     92234.69c 2.6990E-05 $ fuel plate 13
        92235.69c 4.2105E-03
        92236.69c 1.5611E-05
        92238.69c 2.2334E-04
        13027.62c 4.9607E-02
c       total     5.4083E-02
m23     92234.69c 2.7017E-05 $ fuel plate 14
        92235.69c 4.2145E-03
        92236.69c 1.5626E-05
        92238.69c 2.2356E-04
        13027.62c 4.9600E-02
c       total     5.4081E-02
m24     92234.69c 2.7077E-05 $ fuel plate 15
        92235.69c 4.2239E-03
        92236.69c 1.5661E-05
        92238.69c 2.2406E-04
        13027.62c 4.9585E-02
c       total     5.4075E-02
m25     92234.69c 2.2037E-05 $ fuel plate 16
        92235.69c 3.4377E-03
```

```
        92236.69c 1.2746E-05
        92238.69c 1.8235E-04
        13027.62c 5.0889E-02
c       total     5.4544E-02
m26     92234.69c 2.2037E-05 $ fuel plate 17
        92235.69c 3.4377E-03
        92236.69c 1.2745E-05
        92238.69c 1.8235E-04
        13027.62c 5.0889E-02
c       total     5.4544E-02
m27     92234.69c 1.7683E-05 $ fuel plate 18
        92235.69c 2.7586E-03
        92236.69c 1.0228E-05
        92238.69c 1.4633E-04
        13027.62c 5.2016E-02
c       total     5.4949E-02
m28     92234.69c 1.7487E-05 $ fuel plate 19
        92235.69c 2.7279E-03
        92236.69c 1.0114E-05
        92238.69c 1.4470E-04
        13027.62c 5.2067E-02
c       total     5.4967E-02
c
*tr1     0 -10.8 0                        $ base to center
*tr2     0 7.9 0    180 90 90 90 180 90   $ down
*tr3     0 -7.9 0                         $ up
*tr4    -7.9 0 0    90 180 90 0 90 90     $ right
*tr5     7.9 0 0    90 0 90 180 90 90     $ left
*tr6    -5.6  -5.6 0 45 135 90 45 45 90   $ up/right
*tr7     5.6  -5.6 0 45 45 90 135 45 90   $ up/left
*tr8    -5.6   5.6 0 135 135 90 45 135 90 $ down/right
*tr9     5.6   5.6 0 135 45 90 135 135 90 $ down/left
c
mode   n
kcode  2500 1.0 50 250
sdef    x=d1 y=d2 z=d3
si1     -90 90
sp1     0 1
si2     -90 90
sp2     0 1
si3     -60 60
sp3     0 1
```

Case LG5 (NA_N5P050)

```
ATR
999     0      -320:321:-322:323:-324:325                imp:n=0
900     0      310 -311 312 -313 24 -25     fill=3       imp:n=1
901     2 -1.0 (311:-310:313:-312:-24:25) 320 -321 322 -323 324 -325  imp:n=1
c
c       Universe 5: Plate 5
c
500     14 5.4037E-02   500 -501 502 -503           u=5 imp:n=1 $ fuel meat
501     3 -2.7         (-500:501:-502:503) 510 -511 512 -513  u=5 imp:n=1 $
cladding
502     2 -1.0         -510:511:-512:513                      u=5 imp:n=1 $
water
```

```
c
c       Universe 6: Lattice
c
600     0  -531 530  lat=1 fill=-2:2 0:0 0:0
           5
           5(0 -0.2 0)
           5
           5(0 0.2 0)
           5
                           imp:n=1 u=6
c
c       Universe 4: Plates and basket (no pipe)
c
400     0          520 -521 522 -523   fill=6(0 0 0)     imp:n=1 u=4 $ fuel
lattice
401     2 -0.5     (-520:521:-522:523) 400 -401 402 -403 imp:n=1 u=4 $ water
between fuel and basket
402     3 -2.7    -400:401:-402:403        imp:n=1 u=4 $ basket (to infinity)
c
c       Universe 20: Plates with pipe (center)
c
200     0         410 -411 412 -413        fill=4 imp:n=1 u=20 $ fuel/basket
201     2 -0.5    #200 -200            imp:n=1 u=20 $ water between basket
and tube
202     4 -7.94   200 -201                        imp:n=1 u=20 $ tube
203     6 -0.096    201 -203 250 -251 252 -253    imp:n=1 u=20 $ insulation
204     0           203 250 -251 252 -253         imp:n=1 u=20 $ insulation
to tube
205     4 -7.94     -250:251:-252:253             imp:n=1 u=20 $ tube to inf
c
c       Universe 21: Plates with pipe (down)
c
210     0         410 -411 412 -413 trcl=2 fill=4 imp:n=1 u=21 $ fuel/basket
211     2 -0.5    #210 -200            imp:n=1 u=21 $ water between basket
and tube
212     4 -7.94   200 -201                        imp:n=1 u=21 $ tube
213     6 -0.096    201 -203 250 -251 252 -253    imp:n=1 u=21 $ insulation
214     0           203 250 -251 252 -253         imp:n=1 u=21 $ insulation
to tube
215     4 -7.94     -250:251:-252:253             imp:n=1 u=21 $ tube to inf
c
c       Universe 22: Plates with pipe (up)
c
220     0         410 -411 412 -413 trcl=3 fill=4 imp:n=1 u=22 $ fuel/basket
221     2 -0.5    #220 -200            imp:n=1 u=22 $ water between basket
and tube
222     4 -7.94   200 -201                        imp:n=1 u=22 $ tube
223     6 -0.096    201 -203 250 -251 252 -253    imp:n=1 u=22 $ insulation
224     0           203 250 -251 252 -253         imp:n=1 u=22 $ insulation
to tube
225     4 -7.94     -250:251:-252:253             imp:n=1 u=22 $ tube to inf
c
c       Universe 23: Plates with pipe (right)
c
230     0         410 -411 412 -413 trcl=4 fill=4 imp:n=1 u=23 $ fuel/basket
231     2 -0.5    #230 -200            imp:n=1 u=23 $ water between basket
and tube
```

```
232     4 -7.94   200 -201                        imp:n=1 u=23 $ tube
233     6 -0.096    201 -203 250 -251 252 -253    imp:n=1 u=23 $ insulation
234     0           203 250 -251 252 -253         imp:n=1 u=23 $ insulation
to tube
235     4 -7.94     -250:251:-252:253             imp:n=1 u=23 $ tube to inf
c
c       Universe 24: Plates with pipe (left)
c
240     0         410 -411 412 -413 trcl=5 fill=4 imp:n=1 u=24 $ fuel/basket
241     2 -0.5    #240 -200             imp:n=1 u=24 $ water between basket
and tube
242     4 -7.94   200 -201                        imp:n=1 u=24 $ tube
243     6 -0.096    201 -203 250 -251 252 -253    imp:n=1 u=24 $ insulation
244     0           203 250 -251 252 -253         imp:n=1 u=24 $ insulation
to tube
245     4 -7.94     -250:251:-252:253             imp:n=1 u=24 $ tube to inf
c
c       Universe 25: Plates with pipe (up right)
c
250     0         410 -411 412 -413 trcl=6 fill=4 imp:n=1 u=25 $ fuel/basket
251     2 -0.5    #250 -200            imp:n=1 u=25 $ water between basket
and tube
252     4 -7.94   200 -201                        imp:n=1 u=25 $ tube
253     6 -0.096    201 -203 250 -251 252 -253    imp:n=1 u=25 $ insulation
254     0           203 250 -251 252 -253         imp:n=1 u=25 $ insulation
to tube
255     4 -7.94     -250:251:-252:253             imp:n=1 u=25 $ tube to inf
c
c       Universe 26: Plates with pipe (up left)
c
260     0         410 -411 412 -413 trcl=7 fill=4 imp:n=1 u=26 $ fuel/basket
261     2 -0.5    #260 -200           imp:n=1 u=26 $ water between basket and
tube
262     4 -7.94   200 -201                        imp:n=1 u=26 $ tube
263     6 -0.096    201 -203 250 -251 252 -253    imp:n=1 u=26 $ insulation
264     0           203 250 -251 252 -253         imp:n=1 u=26 $ insulation
to tube
265     4 -7.94     -250:251:-252:253             imp:n=1 u=26 $ tube to inf
c
c       Universe 27: Plates with pipe (down right)
c
270     0         410 -411 412 -413 trcl=8 fill=4 imp:n=1 u=27 $ fuel/basket
271     2 -0.5    #270 -200            imp:n=1 u=27 $ water between basket
and tube
272     4 -7.94   200 -201                        imp:n=1 u=27 $ tube
273     6 -0.096    201 -203 250 -251 252 -253    imp:n=1 u=27 $ insulation
274     0           203 250 -251 252 -253         imp:n=1 u=27 $ insulation
to tube
275     4 -7.94     -250:251:-252:253             imp:n=1 u=27 $ tube to inf
c
c       Universe 28: Plates with pipe (down left)
c
280     0         410 -411 412 -413 trcl=9 fill=4 imp:n=1 u=28 $ fuel/basket
281     2 -0.5    #280 -200            imp:n=1 u=28 $ water between basket
and tube
282     4 -7.94   200 -201                        imp:n=1 u=28 $ tube
283     6 -0.096    201 -203 250 -251 252 -253    imp:n=1 u=28 $ insulation
```

```
284     0           203 250 -251 252 -253         imp:n=1 u=28 $ insulation
to tube
285     4 -7.94     -250:251:-252:253             imp:n=1 u=28 $ tube to inf
c
c       Universe 3: Array of Packages
c
300   0    -300 301 -302 303 imp:n=1 u=3 lat=1 fill=-4:4 -4:4 0:0
             25 25 25 25 22 26 26 26 26
             25 25 25 25 22 26 26 26 26
             25 25 25 25 22 26 26 26 26
             25 25 25 25 22 26 26 26 26
             23 23 23 23 20 24 24 24 24
             27 27 27 27 21 28 28 28 28
             27 27 27 27 21 28 28 28 28
             27 27 27 27 21 28 28 28 28
             27 27 27 27 21 28 28 28 28

24      pz -60.96                    $ bottom of fuel
25      pz  60.96                    $ top of fuel (48")
c
200      cz 7.3838 $ IR pipe
201      cz 7.6581 $ OR pipe
203      cz 10.1981 $ 1" insulation
c
250      px  -9.6032 $ square tube
251      px   9.6032
252      py  -9.6032
253      py   9.6032
c
300      px  10.033 $ lattice surfaces/sq. tube
301      px -10.033
302      py  10.033
303      py -10.033
310      px -90.297 $ 9x9 bounds
311      px  90.297
312      py -90.297
313      py  90.297
320      px -120.777 $ outer bounds
321      px  120.777
322      py -120.777
323      py  120.777
324      pz -91.44
325      pz  91.44
c
400      px -5.7912  $ inner basket surfaces
401      px  5.7912
402      py -2.1336
403      py  2.1336
410      px -6.1214  $ outer basket surfaces
411      px  6.1214
412      py -2.4638
413      py  2.4638
c
500      px -5.7873 $ fuel meat
501      px  5.7873
502      py -0.0254
503      py  0.0254
```

```
510      px -5.79   $ fuel cladding
511      px  5.79
512      py -0.06096
513      py  0.06096
520      px -5.791  $ array boundary
521      px  5.791
522      py -2.13296
523      py  2.13296
530      py -0.518    $ lattice bounds
531      py  0.518

m2      1001.62c  2          $ water
        8016.62c  1
mt2     lwtr.60t
m3      13027.62c 1          $ Al
m4      6000.66c   -0.08     $ SS-304
        14000.60c  -1.0
        15031.66c  -0.045
        24000.50c  -19.0
        25055.62c  -2.0
        26000.55c  -68.375
        28000.50c  -9.5
m6      13027.62c  -26.5     $ insulation material
        14000.60c  -23.4
        8016.62c   -50.2
m14     92234.69c 2.7492E-05 $ plate 5
        92235.69c 4.2887E-03
        92236.69c 1.5901E-05
        92238.69c 2.2749E-04
        13027.62c 4.9477E-02
c       total     5.4037E-02
c
*tr2     0  -1.6 0                            $ down
*tr3     0   1.6 0                            $ up
*tr4     1.6 0   0       90 180 90 0 90 90     $ right
*tr5    -1.6 0   0       90 0 90 180 90 90     $ left
*tr6     1.13  1.13 0    45 135 90 45 45 90    $ up/right
*tr7    -1.13  1.13 0    45 45 90 135 45 90    $ up/left
*tr8     1.13 -1.13 0    135 135 90 45 135 90  $ down/right
*tr9    -1.13 -1.13 0    135 45 90 135 135 90  $ down/left
c
mode   n
kcode  2500 1.0 50 250
sdef    x=d1 y=d2 z=d3
si1     -90 90
sp1     0 1
si2     -90 90
sp2     0 1
si3     -60 60
sp3     0 1
```

6.10 Appendix B: Criticality Analysis for MIT and MURR Fuel

The ATR FFSC may be utilized to transport MIT fuel and MURR fuel. Both of these fuels are high-enriched plate-type fuels similar to the ATR fuel analyzed in this chapter, although the fuel geometries are different. The following analyses demonstrate that the ATR FFSC with the MIT and MURR fuel complies with the requirements of 10 CFR §71.55 and §71.59. Based on a 5x5 array of damaged packages, the Criticality Safety Index (CSI), per 10 CFR §71.59, is 4.0.

6.10.1 Description of Criticality Design

6.10.1.1 Design Features Important for Criticality

No special design features are required to maintain criticality safety. No poisons are utilized in the package. The MURR and MIT fuel handling enclosures (FHEs) restrict postulated fuel element pitch expansion under hypothetical accident conditions. In addition, the separation provided by the packaging (outer flat-to-flat dimension of 7.9-in), along with the limit on the number of packages per shipment, is sufficient to maintain criticality safety.

6.10.1.2 Summary Table of Criticality Evaluation

The upper subcritical limit (USL) for ensuring that the ATR FFSC (single package or package array) is acceptably subcritical, is:

$$USL = 0.9209$$

The package is considered to be acceptably subcritical if the computed k_{safe} (k_s), which is defined as $k_{effective}$ (k_{eff}) plus twice the statistical uncertainty (σ), is less than or equal to the USL, or:

$$k_s = k_{eff} + 2\sigma \le USL$$

The USL is determined on the basis of a benchmark analysis and incorporates the combined effects of code computational bias, the uncertainty in the bias based on both benchmark-model and computational uncertainties, and an administrative margin. The results of the benchmark analysis indicate that the USL is adequate to ensure subcriticality of the package.

The packaging design is shown to meet the requirements of 10 CFR 71.55(b). Moderation by water in the most reactive credible extent is utilized in both the normal conditions of transport (NCT) and hypothetical accident conditions of transport (HAC) analyses. In the single package NCT models, full-density water fills the accessible cavity, while in the single package HAC models, full-density water fills all cavities. In the NCT fuel element models, the fuel element is modeled as undamaged, although the most reactive credible configuration is utilized by maximizing the gap between the fuel plates. Maximizing this gap maximizes the moderation and hence the reactivity because the system is undermoderated. In the HAC fuel element models, a damaged fuel element is assumed, and the fuel element pitch is allowed to expand until constrained by the FHE, which maximizes moderation. In all single package models, 12-in of water reflection is utilized.

In the NCT and HAC array cases, partial moderation is considered to maximize array interaction effects. A 9x9x1 array is utilized for the NCT array, while a 5x5x1 array is utilized in the HAC array. In all array models, 12-in of water reflection are utilized.

The maximum results of the criticality calculations are summarized in Table 6.10-1. The MURR fuel is significantly more reactive than the MIT fuel. The maximum calculated k_s is 0.85881, which occurs for the optimally moderated MURR HAC array case. In this case, the FHE is moderated with full-density water, the inner tube (outside the FHE) is moderated with 0.8 g/cm^3 water, and void is modeled between the insulation and outer tube.

6.10.1.3 Criticality Safety Index

The criticality safety index of 4.0 for MIT and MURR fuel is unchanged from the value provided in Section 6.1.3, *Criticality Safety Index*.

Table 6.10-1 – Summary of Criticality Evaluation

	MURR	**MIT**
Normal Conditions of Transport (NCT)		
Case	k_s	k_s
Single Unit Maximum	0.44807	0.36978
9x9 Array Maximum	0.85643	0.65658
Hypothetical Accident Conditions (HAC)		
Case	k_s	k_s
Single Unit Maximum	0.54584	0.43666
5x5 Array Maximum	0.85881	0.67309
USL = 0.9209		

6.10.2 Fissile Material Contents

The package can accommodate either one MURR or one MIT fuel element. The geometry and composition of these fuel elements are described in the following sections.

6.10.2.1 MURR Fuel Element

Each MURR element contains up to 785 g U-235, enriched up to 94 wt.%. The weight percents of the remaining uranium isotopes are 1.2 wt.% U-234, 0.7 wt.% U-236, and 5.0-7.0 wt.% U-238. Each fuel element contains 24 curved fuel plates. Fuel plate 1 has the smallest radius, while fuel plate 24 has the largest radius, as shown in Figure 6.10-1 and Figure 6.10-3. The fuel "meat" is a mixture of uranium metal and aluminum, while the cladding and structural materials are an aluminum alloy.

The geometry of the fuel element is defined in Figure 6.10-1. Each fuel plate is nominally 0.05-in thick, with a thickness tolerance of ±0.002-in. The fuel meat is nominally 0.02-in thick, and the cladding is nominally 0.015-in thick. The plate cladding material is aluminum. Fuel element side plates are fabricated of ASTM B 209, aluminum alloy 6061-T6 or 6061-T651. These fuel element side plates have a minimum thickness of 0.145-in. The channel width between the plates is 0.080 ± 0.008-in. This tolerance represents average and not localized channel width.

For an actual fuel element, the channel width may exceed this tolerance in localized areas. The maximum local channel width is 0.090-in.

The arc length of the fuel meat changes from plate to plate. Reference fuel meat arc length and inner radius dimensions for each plate are provided in Table 6.10-2. The active fuel length ranges from 23.25-in to 24.75-in as illustrated in Figure 6.10-1.

It is necessary to determine the number densities of the fuel meat, which are the same for all fuel plates. To determine the number densities of the fuel meat, it is first necessary to compute the volume of the fuel meat. The volume of the fuel meat for each plate is the arc length of the meat (nominal + 0.065-in) multiplied by the active fuel length (24.0-in) and meat thickness (0.02-in). The active fuel length and meat thickness are modeled at nominal values in all final (i.e., non-parametric) fuel element models, and the use of these dimensions is justified in Section 6.10.4.1.2, *HAC Single Package Configuration*. It is demonstrated that reactivity increases with increasing meat arc length. The results of the fuel meat volume computations for all 24 plates are provided in Table 6.10-2 for maximum fuel arc length.

The midpoint radii of the fuel plates are treated as fixed quantities in the NCT models, and are computed based on nominal dimensions. However, the channel width is modeled at the maximum value of 0.088-in between all plates in most NCT fuel element models. To achieve this channel width between all fuel plates, the cladding is artificially reduced to a thickness of 0.011-in, or a total plate thickness of 0.042-in. In the most reactive NCT models, a channel width of 0.092-in is modeled between all fuel plates. This value represents the maximum local channel width (0.090-in) plus an additional 0.002-in. To achieve this channel width between all fuel plates, the cladding is artificially reduced to a thickness of 0.009-in, or a total plate thickness of 0.038-in. These plate thicknesses are impossible to achieve in actual practice because they are below the allowable minimum plate thickness of 0.048-in.

The U-235 gram density for each fuel plate is computed by dividing the U-235 mass by the total volume, or 785 g/556.4 cm^3 = 1.41 g/cm^3. The fuel itself is a mixture of UAl_x and aluminum. The density of this mixture for ATR fuel is proportional to the U-235 gram density, as shown in Table 6.2-2. Because ATR and MURR fuel are of the same type, this equation is also used to develop the MURR fuel matrix density. These data are perfectly linear, and a linear fit of the data is $\rho_2 = 0.8733\rho_1 + 2.5357$, where ρ_2 is the total gram density of the mixture, and ρ_1 is the gram density of the U-235 in the mixture. Therefore, using this equation, the total density of the fuel matrix is computed to be approximately 3.77 g/cm^3.

From the fuel volumes, U-235 gram densities, and total mixture densities provided, the number densities for the fuel region may be computed. These number densities are provided in Table 6.10-3. The U-235 weight percent is modeled at the maximum value of 94%. Representative weight percents of 0.6% and 0.35% are utilized for U-234 and U-236, respectively, and the balance (5.05%) is modeled as U-238.

6.10.2.2 MIT Fuel Element

Each MIT element contains up to 515 g U-235, enriched up to 94 wt.%. The weight percents of the remaining uranium isotopes are 1.2 wt.% U-234, 0.7 wt.% U-236, and 5.0-7.0 wt.% U-238. Each fuel element contains 15 flat fuel plates, as shown in Figure 6.10-2 and Figure 6.10-4. The fuel “meat” is a mixture of uranium metal and aluminum, while the cladding and structural materials are an aluminum alloy.

The geometry of the fuel element is defined in Figure 6.10-2. Each fuel plate is nominally 0.08-in thick, with a thickness tolerance of ±0.003-in. The fuel meat is nominally 0.03-in thick, and the cladding is nominally 0.025-in thick. The plate cladding material is aluminum. Fuel element side plates are fabricated of ASTM B 209, aluminum alloy 6061-T6. These fuel element side plates have a nominal thickness of 0.188-in. The channel width between the plates is 0.078 ± 0.004-in (excluding the thermal grooves). This tolerance represents average and not localized channel width. For an actual fuel element, the channel width may exceed this tolerance in localized areas. The maximum local channel width is 0.090-in (excluding the thermal grooves).

The maximum and minimum active fuel lengths and maximum and minimum active fuel widths may be computed based on Figure 6.10-2:

- Maximum active fuel length = (23.0+0.01)-2(0.125) = 22.76-in
- Minimum active fuel length = (23.0-0.01)-2(0.5) = 21.99-in
- Maximum active fuel width = 2.531 – 2(0.18) = 2.171-in
- Minimum active fuel width = 2.521 – 2(0.27) = 1.981-in.

The nominal active fuel length may be estimated as the average of the maximum and minimum values, or 22.375-in.

It is necessary to determine the number densities of the fuel meat, which are the same for all fuel plates. To determine the number densities of the fuel meat, it is first necessary to compute the volume of the fuel meat. The volume of the fuel meat for each plate is the maximum width of the meat (2.171-in) multiplied by the active fuel length (22.375-in) and meat thickness (0.03-in). The active fuel length and meat thickness are modeled at nominal values in all final (i.e., non-parametric) fuel element models, and the use of these dimensions is justified in Section 6.10.4.1.2, *HAC Single Package Configuration*. It is demonstrated that reactivity increases with increasing meat width. The total meat volume is therefore $(15)(0.03)(22.375)(2.171)(2.54^3)$ = 358.2 cm^3.

The centerlines of the fuel plates are treated as fixed quantities in the NCT models, and are computed based on nominal dimensions. However, the channel width is modeled at 0.094-in between all plates in most NCT fuel element models. This modeled channel width includes half of the thermal groove depth on each cladding plate. The fuel plates have grooves a maximum of 0.012-in deep cut into the surface of the fuel plates to increase heat transfer. Because the grooves cover approximately half the surface area of the cladding, half of the groove depth (i.e., 0.006-in) is removed from each cladding plate, so that a channel width of 0.082+2*0.006 = 0.094-in is modeled. To achieve this channel width between all fuel plates, the cladding is artificially reduced to a thickness of 0.017-in, or a total plate thickness of 0.064-in.

Additional NCT models are developed in which the channel width is modeled at 0.116-in. This value is based upon the local maximum channel width (0.090-in) with an additional margin of 0.002-in, and the full thermal groove depth (0.012-in) removed from each plate (0.090-in + 0.002-in + 2*0.012-in = 0.116-in). To achieve this channel width between all fuel plates, the cladding is artificially reduced to a thickness of 0.006-in, or a total plate thickness of 0.042-in.

The U-235 gram density for each fuel plate is computed by dividing the U-235 mass by the total volume, or 515 g/358.2 cm^3 = 1.44 g/cm^3. The fuel itself is a mixture of UAl_x and aluminum. The density of this mixture for ATR fuel is proportional to the U-235 gram density, as shown in

Table 6.2-2. Because ATR and MIT fuel are of the same type, this equation is also used to develop the MIT fuel matrix density. These data are perfectly linear, and a linear fit of the data is $\rho_2 = 0.8733\rho_1 + 2.5357$, where ρ_2 is the total gram density of the mixture, and ρ_1 is the gram density of the U-235 in the mixture. Therefore, using this equation, the total density of the fuel matrix is computed to be approximately 3.79 g/cm^3.

From the fuel volumes, U-235 gram densities, and total mixture densities provided, the number densities for the fuel region may be computed. These number densities are provided in Table 6.10-4. The U-235 weight percent is modeled at the maximum value of 94%. Representative weight percents of 0.6% and 0.35% are utilized for U-234 and U-236, respectively, and the balance (5.05%) is modeled as U-238.

Table 6.10-2 – MURR Fuel Volume Computation (maximum arc length)

Plate	Midpoint Radius (cm)	Fuel Arc (cm)	Volume (cm^3)
1	7.0993	4.5034	13.9460
2	7.4295	4.7625	14.7484
3	7.7597	5.0216	15.5507
4	8.0899	5.2832	16.3608
5	8.4201	5.5423	17.1632
6	8.7503	5.8014	17.9655
7	9.0805	6.0604	18.7678
8	9.4107	6.3195	19.5701
9	9.7409	6.5786	20.3724
10	10.0711	6.8377	21.1747
11	10.4013	7.0968	21.9770
12	10.7315	7.3558	22.7793
13	11.0617	7.6149	23.5816
14	11.3919	7.8765	24.3918
15	11.7221	8.1356	25.1941
16	12.0523	8.3947	25.9964
17	12.3825	8.6538	26.7987
18	12.7127	8.9129	27.6011
19	13.0429	9.1719	28.4034
20	13.3731	9.4310	29.2057
21	13.7033	9.6901	30.0080
22	14.0335	9.9492	30.8103
23	14.3637	10.2083	31.6126
24	14.6939	10.4699	32.4228
Total			556.4024

Table 6.10-3 – MURR Fuel Number Densities (maximum arc length)

Isotope	Number Density (atom/b-cm)
U-234	2.3171E-05
U-235	3.6147E-03
U-236	1.3402E-05
U-238	1.9174E-04
Al	5.0596E-02
Total	5.4439E-02

Table 6.10-4 – MIT Fuel Number Densities (maximum fuel width)

Isotope	Number Density (atom/b-cm)
U-234	2.3613E-05
U-235	3.6835E-03
U-236	1.3657E-05
U-238	1.9539E-04
Al	5.0481E-02
Total	5.4398E-02

Security-Related Information Figure Withheld Under 10 CFR 2.390.

Figure 6.10-1 – MURR Fuel Element Dimensions

Security-Related Information Figure Withheld Under 10 CFR 2.390.

Figure 6.10-2 – MIT Fuel Element Dimensions

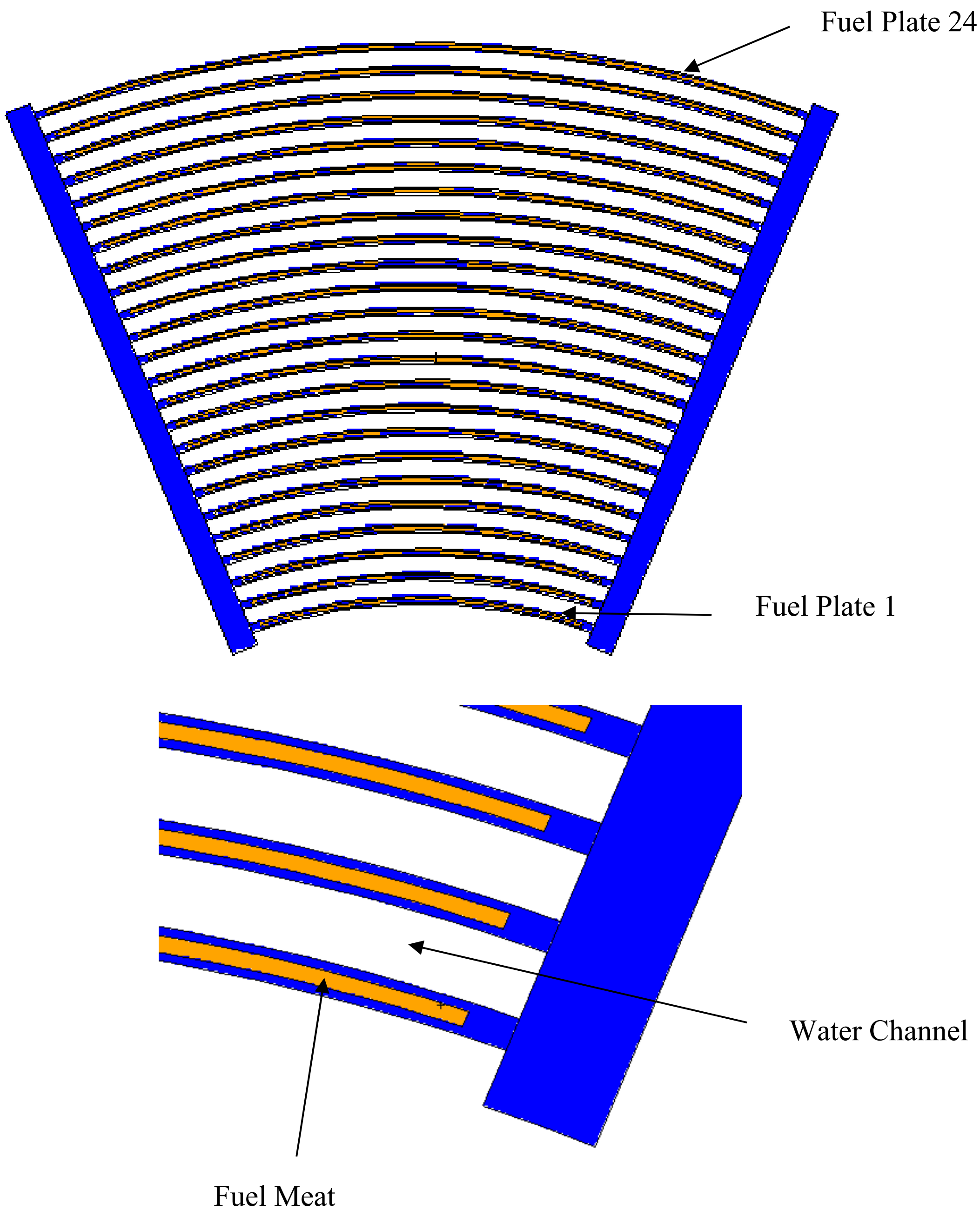

Figure 6.10-3 – MURR Fuel Element Model

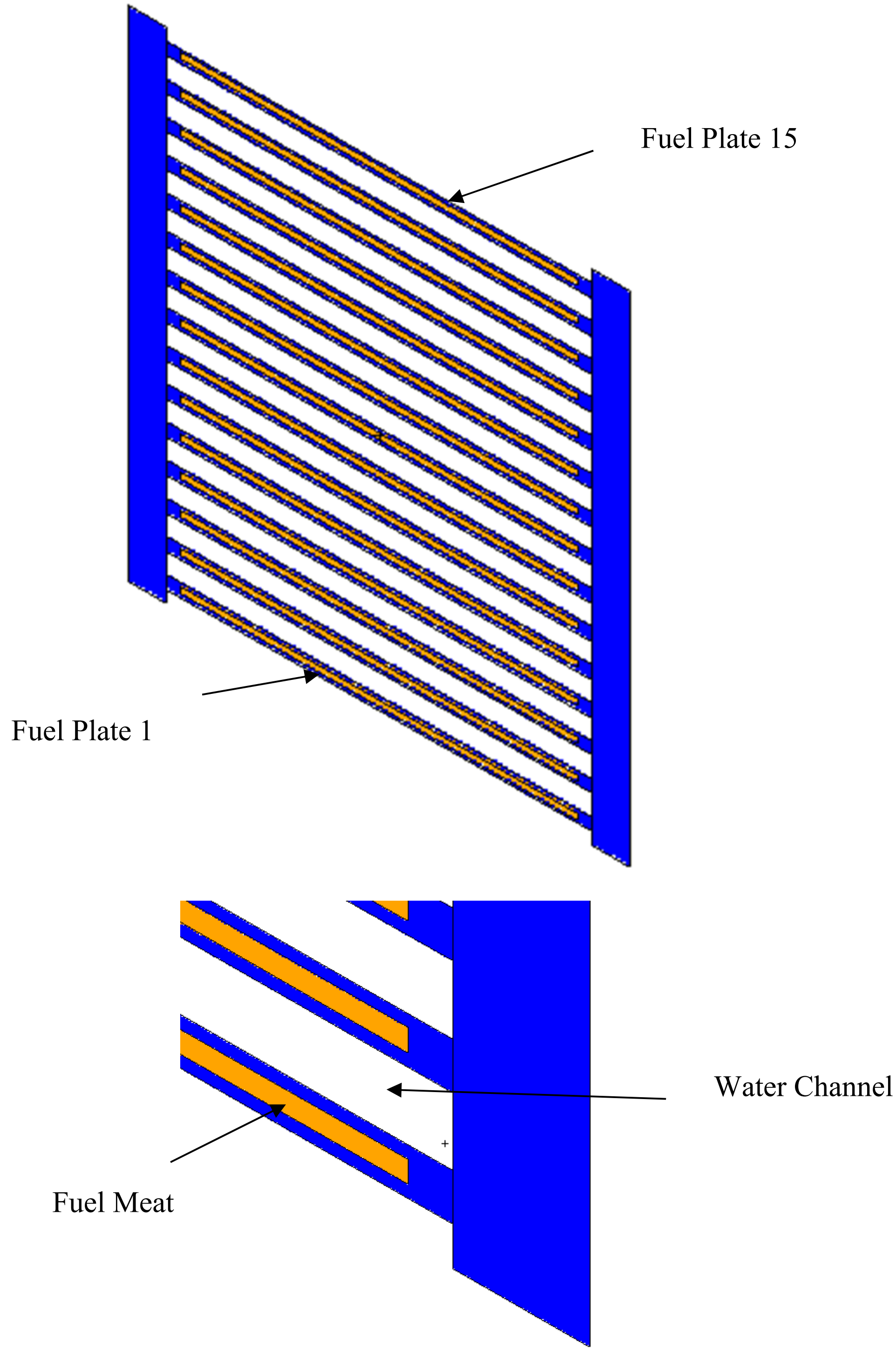

Figure 6.10-4 – MIT Fuel Element Model

6.10.3 General Considerations

6.10.3.1 Model Configuration

The packaging is modeled essentially the same as described in Section 6.3.1, *Model Configuration*, including the number of packages utilized in the NCT and HAC array cases. The only difference is the FHE is modeled explicitly, and the contents are different.

The MURR and MIT FHEs are modeled explicitly over the active fuel length. The FHEs are constructed of aluminum. Maximum dimensional tolerances are selected so that the FHEs are as large as possible, which results in the largest possible pitch expansion in the HAC models. For the MURR FHE, these dimensions are 2.00+0.06-in, 3.56+0.06-in, 1.85+0.06-in, and 22.5°+2° (see the packaging general arrangement drawings for dimension placement). For the MIT FHE, these dimensions are 1.62+0.06-in and 2.82+0.06-in (see the packaging general arrangement drawings for dimension placement). The wall thickness is 0.19 ± 0.06-in for each FHE. The array cases are run with both minimum and maximum wall thickness to determine the most reactive condition. All of the figures in this chapter show minimum wall thickness models. Each FHE is comprised of two pieces held together by ball lock pins. Under NCT, the two FHE halves do not separate.

In the NCT single package models, the inner tube, FHE, insulation, and outer tube are modeled explicitly, as shown in Figure 6.10-5 and Figure 6.10-6 for MURR and MIT, respectively. An axial view is shown in Figure 6.10-7. Note that the thin steel sheet that encases the insulation has been conservatively neglected (the steel sheet would absorb neutrons and lower the reactivity). Although negligible water ingress is expected during NCT, the inner cavity of the package is assumed to be flooded with water because the package lid does not contain a seal. However, the region between the insulation and the outer tube will remain dry because water cannot enter this region. In the models, the fuel element is conservatively positioned at the radial center of the FHE to maximize neutron reflection. The package is reflected with 12-in of full-density water.

The neoprene along the sides of the FHEs is modeled in an approximate manner using a thickness of 1/8-in. In both cases, the neoprene is modeled continuously along two sides for simplicity, rather than modeling the neoprene in detail as narrow strips. Because it was determined in the ATR fuel criticality analysis that neoprene will reduce the reactivity due to parasitic absorption in chlorine, the neoprene is modeled without chlorine, and the density is reduced accordingly.

The HAC single package model is similar to the NCT single package model. Damage in the drop tests was shown to be negligible and concentrated at the ends of the package (See Section 2.12.1, *Certification Tests on CTU-1*). As the ends of the package are not modeled, this end damage does not affect the modeling. The various side drops resulted in only minor localized damage to the outer tube, and no observable bulk deformation of the package. Therefore, the minor damage observed will not impact the reactivity. The insulation is replaced with full-density water, and the region between the insulation and outer tube is also filled with full-density water (see Figure 6.10-8 and Figure 6.10-9 for the MURR and MIT model geometry, respectively). The treatment of the fuel enclosure is the same as the NCT single package models. Cases are developed both with and without the neoprene.

No MURR or MIT fuels were included in the drop tests. Therefore, the damage to the MURR or MIT fuel under HAC is not known precisely. To conservatively bound the potential fuel damage in the HAC models, the fuel plate pitch is allowed to expand uniformly until constrained by the FHE. In addition, the FHEs, which are composed of two halves pinned together, are assumed to separate in a manner that maximizes the space available for pitch expansion. For simplicity, the gap between the two halves is not modeled explicitly in the HAC models. This pitch expansion increases the moderation and the reactivity. In actuality, such a large uniform expansion of the fuel element pitch is not credible, and in the worst case scenario would be localized at one end of the fuel element. Drop tests performed with ATR fuel, which is similar to MURR and MIT fuel, showed no damage that would affect the criticality analysis [See Section 2.12.1, *Certification Tests on CTU-1*]. The modeled damage is intended to bound a damaged fuel element that is otherwise intact.

In the NCT array models, a 9x9x1 array is utilized. To increase the reactivity, fuel elements are pushed toward the center of the array. Because the fuel elements are transported in a thin (~0.01-in) plastic bag, this plastic bag is allowed to act as a boundary for partial moderation effects. The plastic bag is not modeled explicitly, because it is too thin to have an appreciable effect on the reactivity. Therefore, it is postulated that the fuel element channels may fill with full-density water, while the region between the fuel element and FHE fills with variable density water. Different water densities inside and outside the FHE are also addressed. Axial movement of the fuel elements is not considered because axial movement would increase the effective active height of the system (i.e., if some fuel elements shift and others remain in place) and reduce the reactivity due to increased leakage. The presence of chlorine-free neoprene is also considered in the array cases.

In the HAC array models, a 5x5x1 array is utilized, although the moderation conditions considered are similar to the NCT array analysis. Cases in which the insulation is replaced with water are also investigated. The fuel elements are modeled at the maximum pitch, consistent with the most reactive single package models.

The detailed moderation assumptions for these cases are discussed more fully in Section 6.10.5, *Evaluation of Package Arrays under Normal Conditions of Transport*, and Section 6.10.6, *Package Arrays under Hypothetical Accident Conditions*.

6.10.3.2 Material Properties

The fuel meat compositions are provided in Table 6.10-3 and Table 6.10-4 for MURR and MIT fuel, respectively. The material properties of the packaging materials are provided in Section 6.3.2, *Material Properties*. The aluminum of the FHE is modeled as pure with a density of 2.7 g/cm^3.

6.10.3.3 Computer Codes and Cross-Section Libraries

The computer code and cross section libraries utilized are provided in Section 6.3.3, *Computer Codes and Cross-Section Libraries*.

6.10.3.4 Demonstration of Maximum Reactivity

The reactivities of the NCT and HAC single package cases are small, with $k_s < 0.6$.

For the NCT array, a 9x9x1 array is utilized, while for the HAC array, a smaller 5x5x1 array is utilized. Because negligible packaging damage was observed in the drop tests, the package dimensions are the same between the NCT and HAC models. However, the fuel elements are modeled differently between the NCT and HAC models. In the NCT models, the fuel elements are modeled as intact, although with dimensions optimized to maximize the reactivity. In the HAC models, the fuel is assumed to be damaged, and the pitch is allowed to expand until constrained by the FHE. In the HAC cases, the pins connecting the two halves of the FHE are assumed to break, and the two halves are pushed apart to the maximum extent to maximize the available space for pitch expansion. The FHEs and fuel elements are pushed toward the center of the array.

In both NCT and HAC array cases, flooding with partial moderation is allowed in the fuel element itself, between the fuel element and the FHE, and between the FHE and the inner tube. A number of different partial moderation scenarios are considered.

In the NCT array models, insulation is modeled between the inner and outer tubes. In the HAC array models, it is demonstrated that modeling the insulation is more reactive than replacing the insulation with variable density water. In both sets of models, chlorine-free neoprene that is attached to the FHE is modeled, although the effect on the reactivity is small. No models in which the neoprene is allowed to decompose and homogeneously mix with the water are developed, as this scenario is already implicitly included in the search for optimum reactivity using various water densities.

Tolerances of the packaging materials are selected to maximize the reactivity. Both maximum and minimum wall thicknesses for the FHE are modeled to determine the most reactive condition, although the effect on the reactivity of this parameter is not significant.

The MURR fuel is significantly more reactive than the MIT fuel in all scenarios, a difference in k_s of 0.186 comparing the most reactive models. The most reactive case occurs for the HAC array (Case XN9), and results in a k_s = 0.85881, which is below the USL of 0.9209. For this case, full-density water is modeled between the fuel plates and inside the FHE, 0.8 g/cm^3 water is modeled between the FHE and inner tube, the FHE is modeled with a thick wall, and insulation is modeled.

When comparing the reactivities of the three fuel types (ATR, MURR, MIT), MURR is the most reactive, MIT is the least reactive.

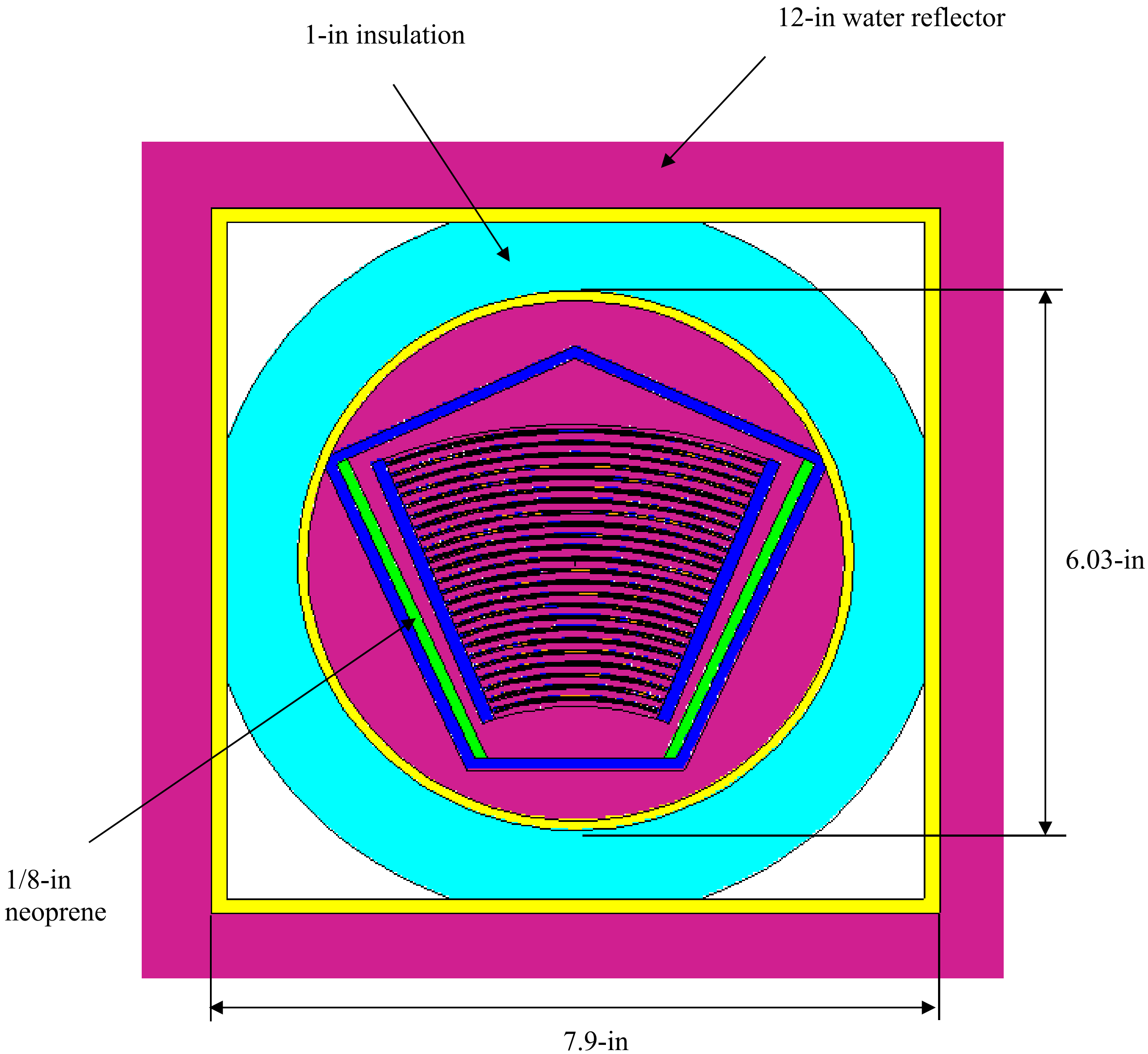

Figure 6.10-5 – MURR NCT Single Package Model (planar view)

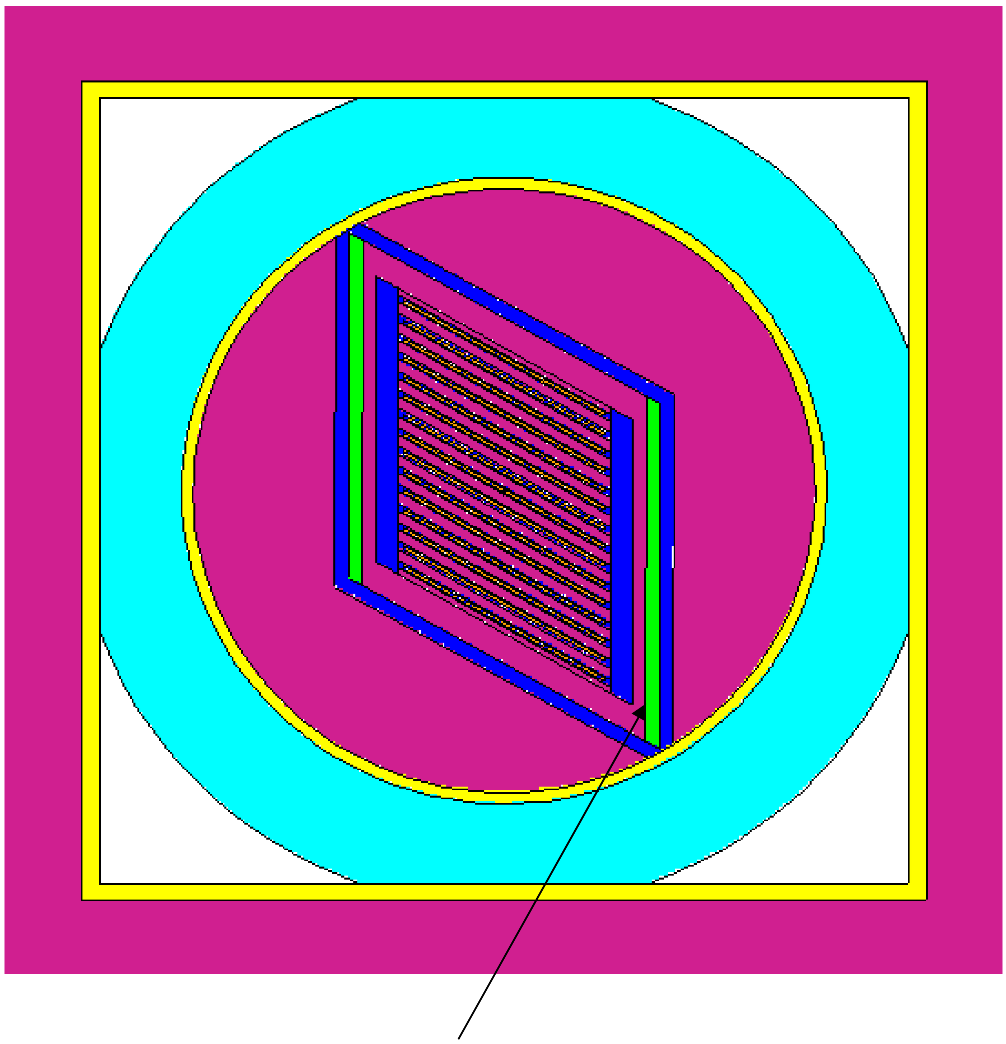

Figure 6.10-6 – MIT NCT Single Package Model (planar view)

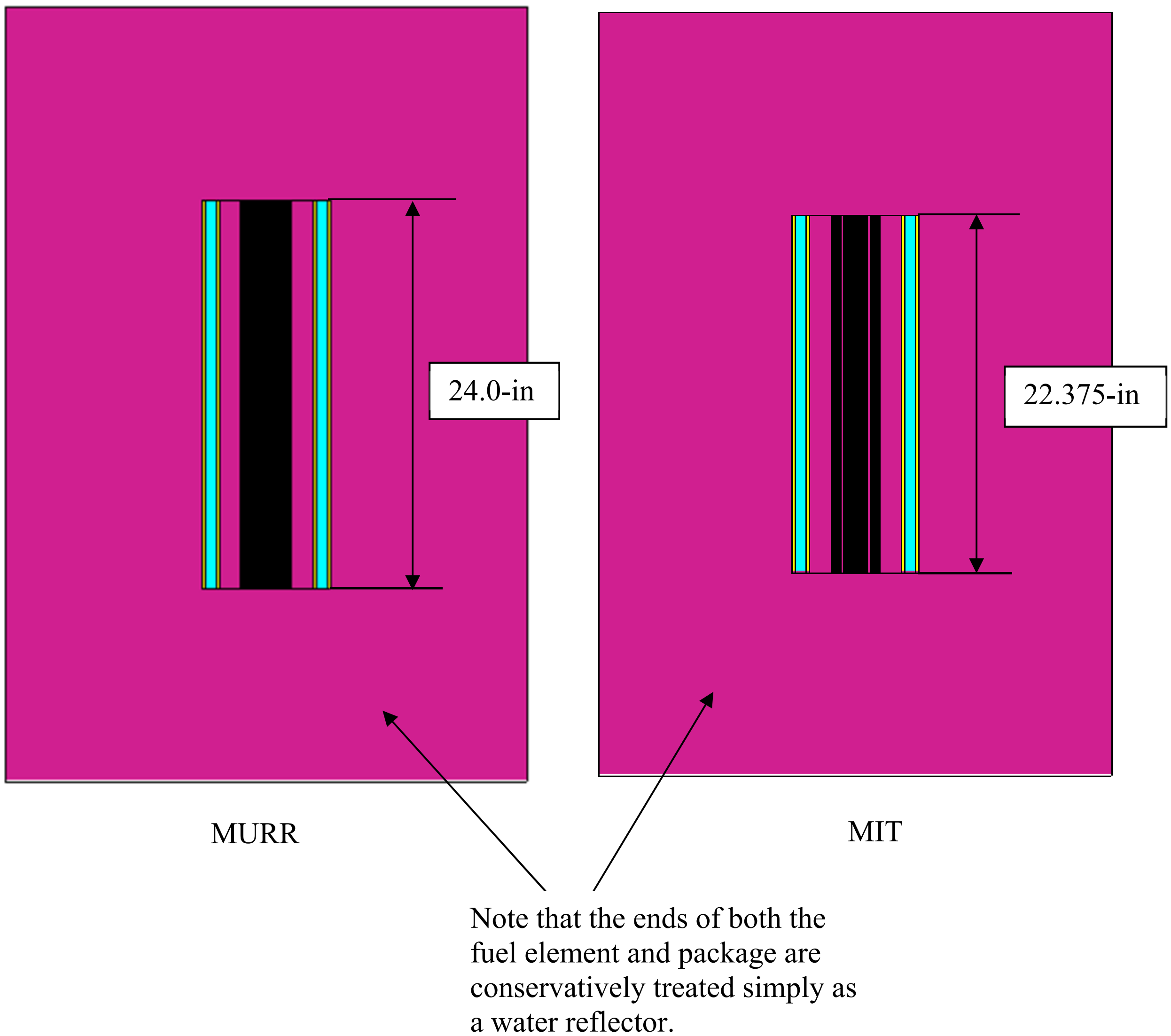

Figure 6.10-7 – MURR/MIT NCT Single Package Models (axial view)

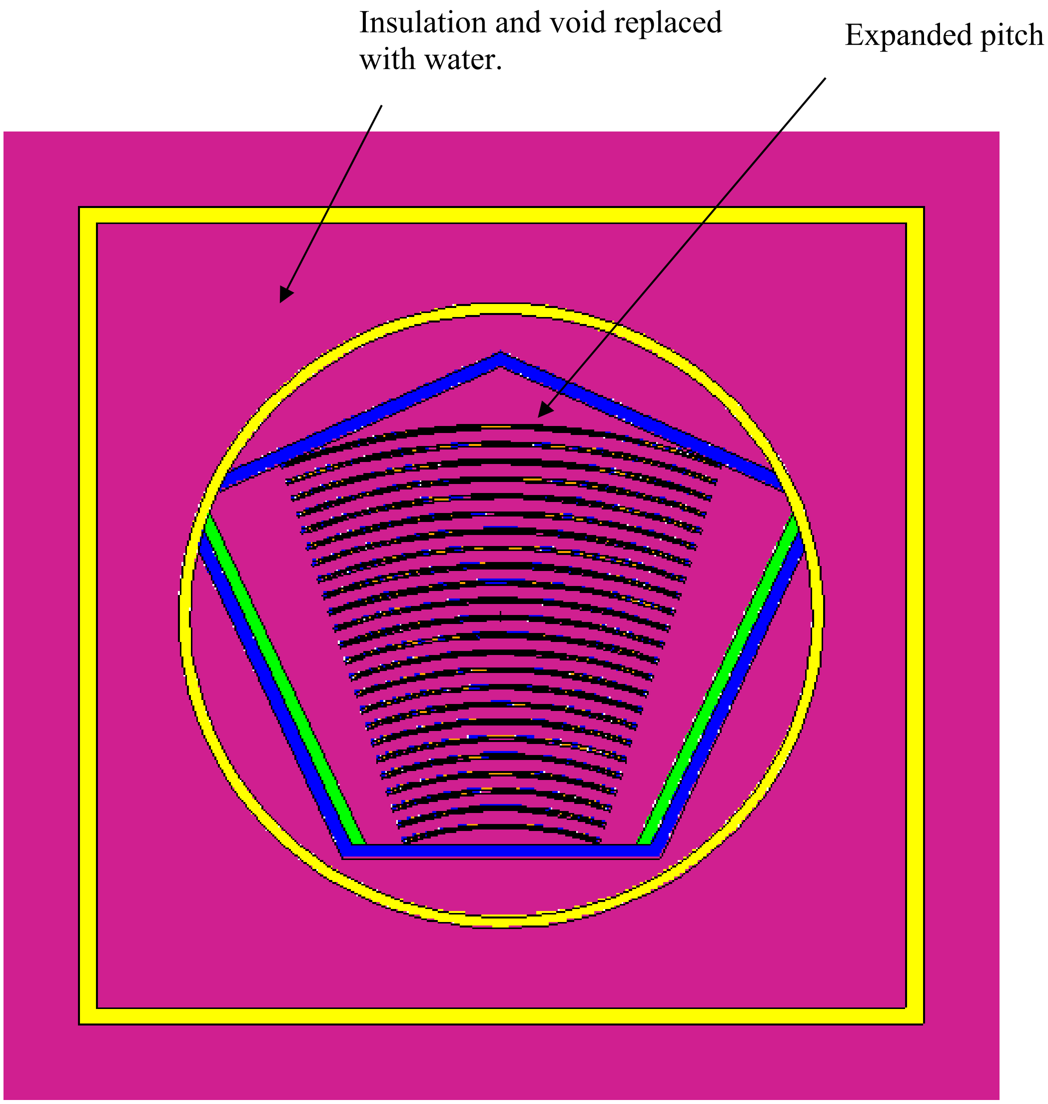

Figure 6.10-8 – MURR HAC Single Package Model (planar view)

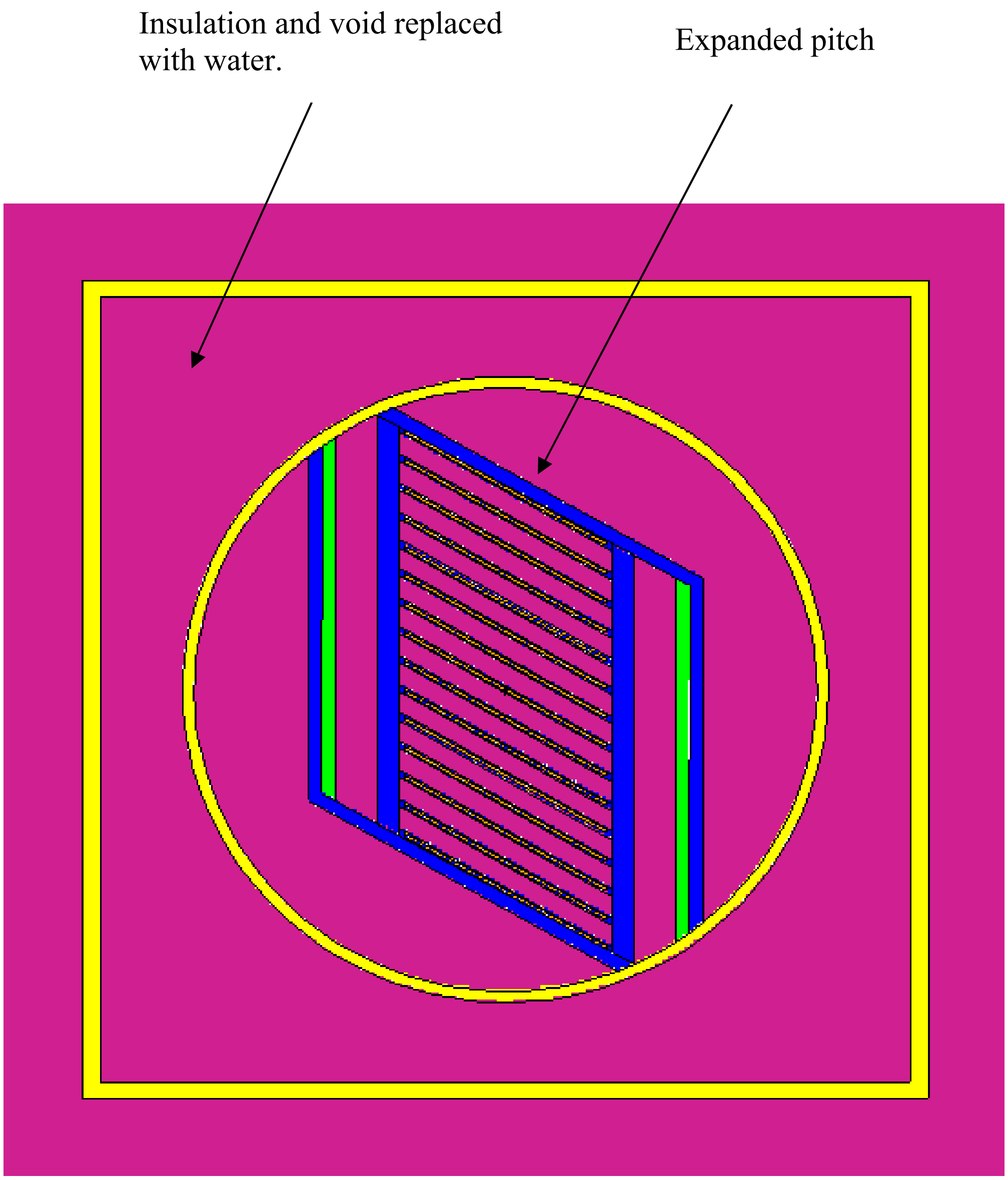

Figure 6.10-9 – MIT HAC Single Package Model (planar view)

6.10.4 Single Package Evaluation

6.10.4.1 Single Package Configuration

Prior to development of a single package model, a parametric analysis is performed to determine the impacts of various fuel element tolerances on the reactivity. In the criticality analysis for ATR fuel (see Section 6.4.1.2.1, *Fuel Element Payload Parametric Evaluation*), it was determined that reactivity was maximized by maximizing the arc length of the fuel meat and the channel thickness. Because ATR, MURR, and MIT fuel are all plate-type and utilize similar enrichments, it is expected that MURR and MIT fuel will also experience maximum reactivity with these parameters maximized. Therefore, the parametric analysis considers the effects of only the following parameters: fuel meat arc length/width, channel width, and active fuel length.

The base configuration for both MURR and MIT consists of plates with a nominal meat arc length/width, nominal active fuel length, and nominal channel width. The minimum, nominal, and maximum meat arc lengths for MURR fuel are provided in Table 6.10-5. The minimum meat arc lengths are obtained directly from Figure 6.10-1 (see dimension B). The maximum meat arc lengths are computed by subtracting twice the fuel-free width (2*0.115-in) from the maximum plate width (dimension C of Figure 6.10-1 + 0.010-in). The nominal value is computed as the average of the minimum and maximum values.

A total of 14 parametric models are developed (7 for each fuel type), as listed in the following table. The detailed model descriptions of the parametric cases are summarized in Table 6.10-6. In each parametric case, the indicated parameter is modified in comparison with the base case. In all parametric models, the fuel element is modeled in the center of an ATR FFSC with the inner tube flooded, and the insulation replaced with full density water. The FHEs are neglected for simplicity.

Case ID	Case Description
XB1	Base MURR case
XB2	Decrease active fuel length to minimum value
XB3	Increase active fuel length to maximum value
XB4	Increase channel width to 0.088-in
XB5	Decrease width of fuel meat to minimum value
XB6	Increase width of fuel meat to maximum value
XB7	Combine cases XB4 and XB6
Case ID	**Case Description**
YB1	Base MIT case
YB2	Decrease active fuel length to minimum value
YB3	Increase active fuel length to maximum value
YB4	Increase channel width to 0.094-in
YB5	Decrease width of fuel meat to minimum value
YB6	Increase width of fuel meat to maximum value
YB7	Combine cases YB4 and YB6

The results of the parametric analysis are summarized in Table 6.10-7. Because the uncertainty in the calculation is ~0.001, a difference of at least 0.002 (2 milli-k, abbreviated mk) between the various cases is required in order to distinguish a real effect from statistical fluctuation. For both MURR and MIT fuel, the variation of the active fuel length has a negligible effect on the results. Also, both MURR and MIT fuel show a positive reactivity increase when the fuel meat is widened and the channel width is increased. For MURR fuel, the increase is 23.5 mk (compare Case XB7 with Case XB1), and for MIT fuel, the increase is 8.8 mk (compare Case YB7 with Case YB1). This result is consistent with the results obtained in the ATR fuel analysis. Therefore, in all subsequent NCT MURR and MIT fuel models, the fuel is modeled with nominal active fuel length and maximum fuel width. Also, in subsequent models, maximizing the channel width is achieved by either reducing the cladding thickness (if the fuel is undamaged) or increasing the plate pitch (if the fuel is damaged).

6.10.4.1.1 NCT Single Package Configuration

The geometry of the NCT single package configuration is discussed in Section 6.10.3.1, *Model Configuration*. In the NCT single package models, the FHEs are modeled explicitly, and the neoprene is modeled in an approximate manner (see Figure 6.10-5 and Figure 6.10-6 for the NCT single package MURR and MIT models, respectively). The inner tube is flooded with full-density water. The fuel element geometry for both MURR and MIT is consistent with the most reactive fuel element model, including tolerances, as determined in the previous section. Neoprene from the FHEs is modeled at the sides of the fuel element. Chlorine is conservatively removed from the neoprene because chlorine acts as a poison. The package is reflected with 12-in of water.

Results are provided in Table 6.10-8 for both MURR and MIT fuel. For MURR, Case XA1 is for a modeled channel width of 0.088-in, and Case XA2 is for a modeled channel width of 0.092-in. The channel width of 0.088-in represents the maximum average channel width, while the channel width of 0.092-in is the local maximum channel width of 0.090-in with an additional 0.002-in of margin. For MIT, Case YA1 is for a modeled channel width of 0.094-in, and Case YA2 is for a modeled channel width of 0.116-in. The channel width of 0.094-in represents the maximum average channel width (0.082-in) plus half of the thermal groove (0.006-in) on each cladding plate. The channel width of 0.116-in represents the local maximum channel width of 0.090-in plus the full thermal groove (0.012-in) on each cladding plate, plus an additional 0.002-in margin.

For both MURR and MIT, reactivity increases with increased channel width. The reactivity is low, with $k_s = 0.44807$ for MURR and $k_s = 0.36978$ for MIT. These results are below the USL of 0.9209.

6.10.4.1.2 HAC Single Package Configuration

The geometry of the HAC single package configuration is discussed in Section 6.10.3.1, *Model Configuration*. In the HAC single package models, the FHEs are modeled explicitly, and the neoprene is modeled in an approximate manner (see Figure 6.10-8 and Figure 6.10-9 for the HAC single package MURR and MIT models, respectively). Chlorine is conservatively removed from the neoprene because chlorine acts as a poison. Eliminating the chlorine from the neoprene may be postulated to be a result of decomposition during a fire, although such a scenario is not credible.

The results are summarized in Table 6.10-9. In both the MURR and MIT models, the pitch is varied from the nominal value to the maximum value allowed by the FHE (Cases XC1 through

XC6 for MURR and YC1 through YC10 for MIT). For both fuel types, the reactivity increases as the plate pitch increases, reaching the maximum reactivity at the maximum pitch. For MURR, the maximum pitch is 0.167-in, which corresponds to a modeled channel spacing of 0.125-in. For MIT, the maximum pitch is 0.240-in, which corresponds to a modeled channel spacing of 0.176-in. Neoprene is included in the variable pitch models. Note that the aluminum fuel element side plates are omitted from the MURR model for simplicity. In the MIT models, the aluminum fuel element side plates are allowed to "stretch" with the model for simplicity.

In Cases XC7 and YC11, the maximum-pitch MURR and MIT cases are repeated without neoprene. In both instances, the reactivity increases slightly when neoprene is modeled as water.

Because the fuel may be transported inside of a plastic bag, it is conservatively assumed that the water density inside of the FHE may vary independently of the water density inside of the fuel element. Note that additional surfaces are added to the MURR model to isolate the water between the fuel plates from the water inside the FHE (in Figure 6.10-8 these regions are combined). To maximize neutron reflection, full-density water is always modeled inside and outside the FHE, and the fuel element is centered laterally within the FHE.

In MURR Cases XC8 and XC9, Case XC7 is run with reduced water densities of 0.8 and 0.9 g/cm^3 between the fuel plates, but maximum water density in all other regions of the model. MIT Cases YC12 and YC13 are similar, except the Case YC11 is used as the base case. In both cases, reactivity drops as the water density is reduced between the fuel plates, indicating that the system is undermoderated.

The results are summarized in Table 6.10-9. Case XC7 is the most reactive MURR model, with k_s = 0.54584, while Case YC11 is the most reactive MIT model, with k_s = 0.43666. Both results are below the USL of 0.9209.

6.10.4.2 Single Package Results

Following are the tabulated results for the single package cases. The most reactive configurations are listed in boldface.

Table 6.10-5 – MURR Meat Arc Lengths

Plate	Minimum (in)	Nominal (in)	Maximum (in)
1	1.643	1.708	1.773
2	1.745	1.810	1.875
3	1.847	1.912	1.977
4	1.950	2.015	2.080
5	2.052	2.117	2.182
6	2.154	2.219	2.284
7	2.256	2.321	2.386
8	2.358	2.423	2.488
9	2.460	2.525	2.590
10	2.562	2.627	2.692
11	2.664	2.729	2.794
12	2.766	2.831	2.896
13	2.868	2.933	2.998
14	2.971	3.036	3.101
15	3.073	3.138	3.203
16	3.175	3.240	3.305
17	3.277	3.342	3.407
18	3.379	3.444	3.509
19	3.481	3.546	3.611
20	3.583	3.648	3.713
21	3.685	3.750	3.815
22	3.787	3.852	3.917
23	3.889	3.954	4.019
24	3.992	4.057	4.122

Table 6.10-6 – Parametric Analysis Input Data

MURR					
Parameter	**XB1/XB4**	**XB2**	**XB3**	**XB5**	**XB6/XB7**
Fuel width (in)	nominal	nominal	nominal	nominal-0.065	nominal+0.065
Meat thickness (in)	0.02	0.02	0.02	0.02	0.02
Active fuel height (in)	24	23.25	24.75	24	24
Channel (in)	0.08/0.088	0.08	0.08	0.08	0.08/0.088
Cladding (in)	0.015/0.011	0.015	0.015	0.015	0.015/0.011
Total plate (in)	0.050/0.042	0.050	0.050	0.050	0.050/0.042
Pitch (in)	0.13	0.13	0.13	0.13	0.13
Meat volume (cm3)	544.13	527.13	561.14	531.86	556.40
U-235 mass (g)	785	785	785	785	785
U-235 den (g/cm3)	1.44	1.49	1.40	1.48	1.41
UAlx+Al den (g/cm3)	3.80	3.84	3.76	3.82	3.77
N-234 (atom/b-cm)	2.3694E-05	2.4458E-05	2.2976E-05	2.4241E-05	2.3171E-05
N-235 (atom/b-cm)	3.6962E-03	3.8154E-03	3.5842E-03	3.7815E-03	3.6147E-03
N-236 (atom/b-cm)	1.3704E-05	1.4146E-05	1.3289E-05	1.4020E-05	1.3402E-05
N-238 (atom/b-cm)	1.9607E-04	2.0239E-04	1.9012E-04	2.0059E-04	1.9174E-04
N-Al (atom/b-cm)	5.0460E-02	5.0262E-02	5.0646E-02	5.0319E-02	5.0596E-02
Total (atom/b-cm)	5.4390E-02	5.4319E-02	5.4457E-02	5.4339E-02	5.4439E-02
MIT					
Parameter	**YB1/YB4**	**YB2**	**YB3**	**YB5**	**YB6/YB7**
Fuel width (in)	2.076	2.076	2.076	1.981	2.171
Meat thickness (in)	0.03	0.03	0.03	0.03	0.03
Active fuel height (in)	22.375	21.99	22.76	22.375	22.375
Channel (in)	0.090/0.094	0.090	0.090	0.090	0.090/0.094
Cladding (in)	0.019/0.017	0.019	0.019	0.019	0.019/0.017
Total plate (in)	0.068/0.064	0.068	0.068	0.068	0.068/0.064
Pitch (in)	0.158	0.158	0.158	0.158	0.158
Meat volume (cm^3)	342.53	336.64	348.43	326.86	358.21
U-235 mass (g)	515	515	515	515	515
U-235 den (g/cm3)	1.503	1.530	1.478	1.576	1.438
UAlx+Al den (g/cm3)	3.85	3.87	3.83	3.91	3.79
N-234 (atom/b-cm)	2.4693E-05	2.5125E-05	2.4275E-05	2.5877E-05	2.3613E-05
N-235 (atom/b-cm)	3.8521E-03	3.9195E-03	3.7869E-03	4.0368E-03	3.6835E-03
N-236 (atom/b-cm)	1.4282E-05	1.4532E-05	1.4040E-05	1.4967E-05	1.3657E-05
N-238 (atom/b-cm)	2.0433E-04	2.0791E-04	2.0088E-04	2.1413E-04	1.9539E-04
N-Al (atom/b-cm)	5.0202E-02	5.0090E-02	5.0310E-02	4.9895E-02	5.0481E-02
Total (atom/b-cm)	5.4297E-02	5.4257E-02	5.4336E-02	5.4187E-02	5.4398E-02

Table 6.10-7 – Parametric Analysis Results

Case ID	Filename	k_{eff}	σ	k_s (k+2σ)	Δ from XB1 (mk)
		MURR			
XB1	HS_MURR2_P1	0.47068	0.00109	0.47286	--
XB2	HS_MURR2_P2	0.47199	0.00114	0.47427	1.4
XB3	HS_MURR2_P3	0.47075	0.00114	0.47303	0.2
XB4	HS_MURR2_P4	0.49257	0.00101	0.49459	21.7
XB5	HS_MURR2_P5	0.46808	0.00116	0.47040	-2.5
XB6	HS_MURR2_P6	0.47465	0.00097	0.47659	3.7
XB7	**HS_MURR2_P7**	**0.49432**	**0.00102**	**0.49636**	**23.5**
		MIT			
Case ID	**Filename**	**k_{eff}**	**σ**	**k_s (k+2σ)**	**Δ from YB1 (mk)**
YB1	HS_MIT_P1	0.37801	0.00089	0.37979	--
YB2	HS_MIT_P2	0.37683	0.00093	0.37869	-1.1
YB3	HS_MIT_P3	0.37722	0.00091	0.37904	-0.8
YB4	HS_MIT_P4	0.38179	0.00095	0.38369	3.9
YB5	HS_MIT_P5	0.37018	0.00087	0.37192	-7.9
YB6	HS_MIT_P6	0.38064	0.00088	0.38240	2.6
YB7	**HS_MIT_P7**	**0.38664**	**0.00097**	**0.38858**	**8.8**

Table 6.10-8 – NCT Single Package Results

Case ID	Filename	Moderator Density (g/cm^3)	k_{eff}	σ	k_s (k+2σ)
		MURR			
XA1	NS_MURR	1.0	0.43268	0.00107	0.43482
XA2	**NS_MURR2C**	**1.0**	**0.44597**	**0.00105**	**0.44807**
		MIT			
YA1	NS_MIT	1.0	0.33434	0.00086	0.33606
YA2	**NS_MITC**	**1.0**	**0.36788**	**0.00095**	**0.36978**

Table 6.10-9 – HAC Single Package Results

Case ID	Filename	Pitch (in)	Water Density Between Plates (g/cm^3)	k	σ	k_s (k+2σ)
MURR						
XC1	HS_MURR2_NP00	0.130	1.0	0.48916	0.00107	0.49130
XC2	HS_MURR2_NP02	0.138	1.0	0.50506	0.00111	0.50728
XC3	HS_MURR2_NP04	0.146	1.0	0.51620	0.00116	0.51852
XC4	HS_MURR2_NP06	0.154	1.0	0.52285	0.00113	0.52511
XC5	HS_MURR2_NP08	0.161	1.0	0.53481	0.00104	0.53689
XC6	HS_MURR2_NP09	0.167	1.0	0.53887	0.00103	0.54093
XC7	**HS_MURR2_P09**	**0.167**	**1.0**	**0.54374**	**0.00105**	**0.54584**
XC8	HS_MURR2_P09_M080	0.167	0.8	0.47997	0.00111	0.48219
XC9	HS_MURR2_P09_M090	0.167	0.9	0.51244	0.00106	0.51456
MIT						
YC1	HS_MIT_NP158	0.158	1.0	0.37316	0.00090	0.37496
YC2	HS_MIT_NP16	0.160	1.0	0.37349	0.00095	0.37539
YC3	HS_MIT_NP17	0.170	1.0	0.38238	0.00088	0.38414
YC4	HS_MIT_NP18	0.180	1.0	0.38957	0.00098	0.39153
YC5	HS_MIT_NP19	0.190	1.0	0.39967	0.00105	0.40177
YC6	HS_MIT_NP20	0.200	1.0	0.40825	0.00095	0.41015
YC7	HS_MIT_NP21	0.210	1.0	0.41309	0.00104	0.41517
YC8	HS_MIT_NP22	0.220	1.0	0.41701	0.00100	0.41901
YC9	HS_MIT_NP23	0.230	1.0	0.42605	0.00093	0.42791
YC10	HS_MIT_NP24	0.240	1.0	0.43051	0.00105	0.43261
YC11	**HS_MIT_P24**	**0.240**	**1.0**	**0.43474**	**0.00096**	**0.43666**
YC12	HS_MIT_P24_M080	0.240	0.8	0.39439	0.00098	0.39635
YC13	HS_MIT_P24_M090	0.240	0.9	0.41226	0.00095	0.41416

6.10.5 Evaluation of Package Arrays under Normal Conditions of Transport

6.10.5.1 NCT Array Configuration

6.10.5.1.1 MURR Fuel Element Models

The NCT array model is a 9x9x1 array of the NCT single package model. Although an 8x8x1 array is of sufficient size to justify a CSI = 4.0, the larger 9x9x1 array is utilized simply for modeling convenience. Void is always present between the insulation and the outer tube, as this region is water-tight. The entire array is reflected with 12-in of full-density water.

The FHEs are pushed to the center of the array and rotated to minimize the distance between the fuel elements, see Figure 6.10-10. The modeled lateral shifting of the FHE inside of the tube is computed assuming the maximum inner diameter of the inner tube (5.814-in, see Section 6.3.1, *Model Configuration*) and minimum outer radius of the FHE (2.8-0.2 = 2.6-in, from the packaging general arrangement drawings), or 0.307-in. The fuel element is also modeled at the lateral "top" of the FHE to minimize the distance between the fuel elements.

Six calculational series are developed, as described below. Results are summarized in Table 6.10-10.

Series 1 (Cases XD1 through XD12): In Series 1, the water density is fixed at 1.0 g/cm^3 between the fuel plates, and the water density inside and outside the FHE is modeled at the same density, which is allowed to vary between 0 and 1.0 g/cm^3. This moderation condition simulates the partial moderation effect of assuming the plastic bag that surrounds the fuel element retains water. The neoprene (without chlorine) from the FHEs is modeled in an approximate manner. The modeled channel width is 0.088-in. Also, the FHE is modeled with the minimum wall thickness.

As a point of interest, an additional case (Case XD12) is developed in which the fuel elements are centered in the cavity and not rotated, using the moderation assumptions of the most reactive case (Case XD7). The reactivity drops by 18.5 mk, which essentially represents the additional conservatism of pushing the fuel elements to the center of the array.

Series 2 (Cases XE1 through XE11): Series 2 is the same as Series 1, although the FHE neoprene is not modeled. The results in Table 6.10-10 indicate that the maximum reactivity occurs when chlorine-free neoprene is modeled (compare Cases XD7 and XE7), although the difference is within statistical fluctuation.

Series 3 (Cases XF1 through XF10): In Series 3, the water density inside the FHE is fixed at 1.0 g/cm^3, while the water density outside the FHE is allowed to vary between 0 and 1.0 g/cm^3. This moderation condition simulates the partial moderation effect of assuming the FHE retains water. The maximum reactivity increases slightly compared to Series 1.

Series 4 (Cases XG1 through XG11): Series 4 is the same as Series 3, although the FHE is modeled with the maximum wall thickness. The reactivity increases slightly, although the difference is within statistical fluctuation.

Series 5 (Cases XH1 through XH11): Series 5 is the same as Series 3, although the density within the fuel plates is modeled at a reduced density of 0.9 g/cm^3. The reactivity drops sharply as the water density between the plates is reduced.

Series 6 (Cases XI1 through XI11) is the same as Series 4, except the channel width is increased from 0.088-in to 0.092-in. The reactivity increases with increasing channel width, consistent with the single package models. Reactivity is at a maximum for Case XI5, with k_s = 0.85643. In this case, the fuel elements are pushed to the center of the array, full-density water is modeled between the plates and inside the FHE, 0.4 g/cm^3 water is modeled outside the FHE, chlorine-free neoprene is included, the FHE is modeled with maximum wall thickness, and the channel width is modeled at 0.092-in. The maximum result is below the USL of 0.9209.

6.10.5.1.2 MIT Fuel Element Models

The NCT array model is a 9x9x1 array of the NCT single package model. Although an 8x8x1 array is of sufficient size to justify a CSI = 4.0, the larger 9x9x1 array is utilized simply for modeling convenience. Void is always present between the insulation and the outer tube, as this region is water-tight. The entire array is reflected with 12-in of full-density water.

The FHEs are pushed to the center of the array and rotated to minimize the distance between the fuel elements, see Figure 6.10-10. The modeled lateral shifting of the FHE inside of the tube is computed assuming the maximum inner diameter of the inner tube (5.814-in, see Section 6.3.1, *Model Configuration*) and minimum outer radius of the FHE (2.8-0.2 = 2.6-in, from the packaging general arrangement drawings), or 0.307-in.

In addition to the lateral shifting of the FHE within the tube, the MIT fuel element is free to move laterally within the FHE. To simplify the model geometry, rather than modeling each fuel element shifted within each FHE, the fuel elements are modeled in the center of the FHE, and the FHE is shifted toward the center of the array an additional 0.13-in (the approximate as-modeled distance between the fuel element and neoprene).

Six calculational series are developed, as described below. Results are summarized in Table 6.10-11.

Series 1 (Cases YD1 through YD12): In Series 1, the water density is fixed at 1.0 g/cm^3 between the fuel plates, and the water density inside and outside the FHE is modeled at the same density, which is allowed to vary between 0 and 1.0 g/cm^3. This moderation condition simulates the partial moderation effect of assuming the plastic bag that surrounds the fuel element retains water. The neoprene (without chlorine) from the FHE is modeled in an approximate manner. The modeled channel width is 0.094-in. Also, the FHE is modeled with the minimum wall thickness.

As a point of interest, an additional case (Case YD12) is developed in which the fuel elements are centered in the cavity and not rotated, using the moderation assumptions of the most reactive case (Case YD7). The reactivity drops by 12.5 mk, which essentially represents the additional conservatism of pushing the fuel elements to the center of the array.

Series 2 (Cases YE1 through YE11): Series 2 is the same as Series 1, although the FHE neoprene is not modeled. Comparing Series 1 to Series 2, the reactivity is slightly higher when chlorine-free neoprene is modeled (compare Cases YD7 and YE7), although the difference is within statistical fluctuation.

Series 3 (Cases YF1 through YF10): In Series 3, the water density inside the FHE is fixed at 1.0 g/cm^3, while the water density outside the FHE is allowed to vary between 0 and 1.0 g/cm^3. This moderation condition simulates the partial moderation effect of assuming the FHE retains water. The maximum reactivity increases slightly compared to Series 1, although the effect is well within statistical fluctuation.

Series 4 (Cases YG1 through YG11): Series 4 is the same as Series 3, although the FHE is modeled with the maximum wall thickness. The reactivity decreases slightly, although the difference may be statistical fluctuation. Note that reactivity increased slightly with the thicker walled FHE in the MURR models.

Series 5 (Cases YH1 through YH11): Series 5 is the same as Series 3, although the density within the fuel plates is modeled at a reduced density of 0.9 g/cm^3. The reactivity drops sharply as the water density between the plates is reduced.

Series 6 (Cases YI1 through YI11): Series 6 is the same as Series 3, although the modeled channel width is increased from 0.094-in to 0.116-in. Reactivity is at a maximum for Case YI6, with $k_s = 0.65658$. In this case, the fuel elements are pushed to the center of the array, full-density water is modeled between the plates and inside the FHE, 0.5 g/cm^3 water is modeled outside the FHE, chlorine-free neoprene is included, the FHE is modeled with minimum wall thickness, and the modeled channel width is 0.116-in. The maximum result is far below the USL of 0.9209.

6.10.5.2 NCT Array Results

The results for the NCT array cases are provided in the following tables. The most reactive configuration in each series is listed in boldface.

Table 6.10-10 – MURR NCT Array Results

Case ID	Filename	Water Density Inside FHE (g/cm^3)	Water Density Outside FHE (g/cm^3)	Water Density Between Plates (g/cm^3)	k_{eff}	σ	k_s (k+2σ)
Series 1: Variable water density inside and outside FHE, with neoprene.							
XD1	NA_MURR2_NW000	0	0	1.0	0.76937	0.00121	0.77179
XD2	NA_MURR2_NW010	0.1	0.1	1.0	0.79729	0.00123	0.79975
XD3	NA_MURR2_NW020	0.2	0.2	1.0	0.81129	0.00129	0.81387
XD4	NA_MURR2_NW030	0.3	0.3	1.0	0.82519	0.00129	0.82777
XD5	NA_MURR2_NW040	0.4	0.4	1.0	0.83449	0.00130	0.83709
XD6	NA_MURR2_NW050	0.5	0.5	1.0	0.83502	0.00123	0.83748
XD7	**NA_MURR2_NW060**	**0.6**	**0.6**	**1.0**	**0.83801**	**0.00124**	**0.84049**
XD8	NA_MURR2_NW070	0.7	0.7	1.0	0.83447	0.00111	0.83669
XD9	NA_MURR2_NW080	0.8	0.8	1.0	0.83185	0.00119	0.83423
XD10	NA_MURR2_NW090	0.9	0.9	1.0	0.82537	0.00123	0.82783
XD11	NA_MURR2_NW100	1.0	1.0	1.0	0.81935	0.00120	0.82175
XD12	NA_MURR2_NW060C	0.6	0.6	1.0	0.81957	0.00123	0.82203
Series 2: Repeat of Series 1 without neoprene							
XE1	NA_MURR2_W000	0	0	1.0	0.75717	0.00117	0.75951
XE2	NA_MURR2_W010	0.1	0.1	1.0	0.78680	0.00103	0.78886
XE3	NA_MURR2_W020	0.2	0.2	1.0	0.80910	0.00116	0.81142
XE4	NA_MURR2_W030	0.3	0.3	1.0	0.82154	0.00114	0.82382
XE5	NA_MURR2_W040	0.4	0.4	1.0	0.83148	0.00129	0.83406
XE6	NA_MURR2_W050	0.5	0.5	1.0	0.83479	0.00111	0.83701
XE7	**NA_MURR2_W060**	**0.6**	**0.6**	**1.0**	**0.83681**	**0.00115**	**0.83911**
XE8	NA_MURR2_W070	0.7	0.7	1.0	0.83504	0.00126	0.83756
XE9	NA_MURR2_W080	0.8	0.8	1.0	0.83138	0.00116	0.83370
XE10	NA_MURR2_W090	0.9	0.9	1.0	0.82487	0.00122	0.82731
XE11	NA_MURR2_W100	1.0	1.0	1.0	0.81734	0.00128	0.81990
Series 3: Variable water density outside FHE, with neoprene.							
XF1	NA_MURR2_FNW000	1.0	0	1.0	0.83204	0.00135	0.83474
XF2	NA_MURR2_FNW010	1.0	0.1	1.0	0.83421	0.00118	0.83657
XF3	NA_MURR2_FNW020	1.0	0.2	1.0	0.84008	0.00131	0.84270
XF4	**NA_MURR2_FNW030**	**1.0**	**0.3**	**1.0**	**0.84082**	**0.00132**	**0.84346**
XF5	NA_MURR2_FNW040	1.0	0.4	1.0	0.84055	0.00120	0.84295
XF6	NA_MURR2_FNW050	1.0	0.5	1.0	0.83832	0.00116	0.84064
XF7	NA_MURR2_FNW060	1.0	0.6	1.0	0.83730	0.00118	0.83966
XF8	NA_MURR2_FNW070	1.0	0.7	1.0	0.83373	0.00130	0.83633
XF9	NA_MURR2_FNW080	1.0	0.8	1.0	0.83100	0.00124	0.83348
XF10	NA_MURR2_FNW090	1.0	0.9	1.0	0.82544	0.00129	0.82802
XD11	NA_MURR2_NW100	1.0	1.0	1.0	0.81935	0.00120	0.82175

(continued)

Table 6.10-10 – MURR NCT Array Results (concluded)

Case ID	Filename	Water Density Inside FHE (g/cm^3)	Water Density Outside FHE (g/cm^3)	Water Density Between Plates (g/cm^3)	k_{eff}	σ	k_s (k+2σ)
Series 4: Same as Series 3 but with maximum thickness FHE.							
XG1	NA_MURR2_TFNW000	1.0	0	1.0	0.83659	0.00121	0.83901
XG2	NA_MURR2_TFNW010	1.0	0.1	1.0	0.83959	0.00114	0.84187
XG3	NA_MURR2_TFNW020	1.0	0.2	1.0	0.84116	0.00126	0.84368
XG4	NA_MURR2_TFNW030	1.0	0.3	1.0	0.84029	0.00128	0.84285
XG5	**NA_MURR2_TFNW040**	**1.0**	**0.4**	**1.0**	**0.84340**	**0.00128**	**0.84596**
XG6	NA_MURR2_TFNW050	1.0	0.5	1.0	0.83927	0.00116	0.84159
XG7	NA_MURR2_TFNW060	1.0	0.6	1.0	0.83816	0.00117	0.84050
XG8	NA_MURR2_TFNW070	1.0	0.7	1.0	0.83704	0.00131	0.83966
XG9	NA_MURR2_TFNW080	1.0	0.8	1.0	0.83199	0.00118	0.83435
XG10	NA_MURR2_TFNW090	1.0	0.9	1.0	0.82930	0.00116	0.83162
XG11	NA_MURR2_TFNW100	1.0	1.0	1.0	0.82461	0.00129	0.82719
Series 5: Same as Series 3 with 0.9 g/cm^3 water between fuel plates.							
XH1	NA_MURR2_M90FNW000	1.0	0	0.9	0.80160	0.00132	0.80424
XH2	NA_MURR2_M90FNW010	1.0	0.1	0.9	0.80747	0.00120	0.80987
XH3	NA_MURR2_M90FNW020	1.0	0.2	0.9	0.81288	0.00127	0.81542
XH4	**NA_MURR2_M90FNW030**	**1.0**	**0.3**	**0.9**	**0.81512**	**0.00127**	**0.81766**
XH5	NA_MURR2_M90FNW040	1.0	0.4	0.9	0.81504	0.00120	0.81744
XH6	NA_MURR2_M90FNW050	1.0	0.5	0.9	0.81382	0.00112	0.81606
XH7	NA_MURR2_M90FNW060	1.0	0.6	0.9	0.81369	0.00121	0.81611
XH8	NA_MURR2_M90FNW070	1.0	0.7	0.9	0.81165	0.00129	0.81423
XH9	NA_MURR2_M90FNW080	1.0	0.8	0.9	0.80950	0.00122	0.81194
XH10	NA_MURR2_M90FNW090	1.0	0.9	0.9	0.80311	0.00124	0.80559
XH11	NA_MURR2_M90FNW100	1.0	1.0	0.9	0.79735	0.00117	0.79969
Series 6: Same as Series 4 but with a modeled channel width of 0.092-in.							
XI1	NA_MURR2_TFNW000C	1.0	0	1.0	0.84994	0.00110	0.85214
XI2	NA_MURR2_TFNW010C	1.0	0.1	1.0	0.85141	0.00120	0.85381
XI3	NA_MURR2_TFNW020C	1.0	0.2	1.0	0.85273	0.00124	0.85521
XI4	NA_MURR2_TFNW030C	1.0	0.3	1.0	0.85209	0.00124	0.85457
XI5	**NA_MURR2_TFNW040C**	**1.0**	**0.4**	**1.0**	**0.85405**	**0.00119**	**0.85643**
XI6	NA_MURR2_TFNW050C	1.0	0.5	1.0	0.84925	0.00127	0.85179
XI7	NA_MURR2_TFNW060C	1.0	0.6	1.0	0.84912	0.00124	0.85160
XI8	NA_MURR2_TFNW070C	1.0	0.7	1.0	0.84584	0.00115	0.84814
XI9	NA_MURR2_TFNW080C	1.0	0.8	1.0	0.84296	0.00127	0.84550
XI10	NA_MURR2_TFNW090C	1.0	0.9	1.0	0.83957	0.00115	0.84187
XI11	NA_MURR2_TFNW100C	1.0	1.0	1.0	0.83490	0.00123	0.83736

Table 6.10-11 – MIT NCT Array Results

Case ID	Filename	Water Density Inside FHE (g/cm^3)	Water Density Outside FHE (g/cm^3)	Water Density Between Plates (g/cm^3)	k_{eff}	σ	k_s (k+2σ)
Series 1: Variable water density and outside FHE, with neoprene							
YD1	NA_MIT_NW000	0	0	1.0	0.48041	0.00096	0.48233
YD2	NA_MIT_NW010	0.1	0.1	1.0	0.52918	0.00105	0.53128
YD3	NA_MIT_NW020	0.2	0.2	1.0	0.56301	0.00103	0.56507
YD4	NA_MIT_NW030	0.3	0.3	1.0	0.59062	0.00105	0.59272
YD5	NA_MIT_NW040	0.4	0.4	1.0	0.60722	0.00122	0.60966
YD6	NA_MIT_NW050	0.5	0.5	1.0	0.61575	0.00118	0.61811
YD7	**NA_MIT_NW060**	**0.6**	**0.6**	**1.0**	**0.61989**	**0.00114**	**0.62217**
YD8	NA_MIT_NW070	0.7	0.7	1.0	0.61723	0.00110	0.61943
YD9	NA_MIT_NW080	0.8	0.8	1.0	0.61618	0.00116	0.61850
YD10	NA_MIT_NW090	0.9	0.9	1.0	0.61352	0.00112	0.61576
YD11	NA_MIT_NW100	1.0	1.0	1.0	0.60885	0.00112	0.61109
YD12	NA_MIT_CNW060	0.6	0.6	1.0	0.60764	0.00103	0.60970
Series 2: Repeat of Series 1 without neoprene							
YE1	NA_MIT_W000	0	0	1.0	0.46154	0.00093	0.46340
YE2	NA_MIT_W010	0.1	0.1	1.0	0.51291	0.00095	0.51481
YE3	NA_MIT_W020	0.2	0.2	1.0	0.55394	0.00103	0.55600
YE4	NA_MIT_W030	0.3	0.3	1.0	0.58160	0.00113	0.58386
YE5	NA_MIT_W040	0.4	0.4	1.0	0.60184	0.00111	0.60406
YE6	NA_MIT_W050	0.5	0.5	1.0	0.61163	0.00119	0.61401
YE7	**NA_MIT_W060**	**0.6**	**0.6**	**1.0**	**0.61746**	**0.00117**	**0.61980**
YE8	NA_MIT_W070	0.7	0.7	1.0	0.61518	0.00116	0.61750
YE9	NA_MIT_W080	0.8	0.8	1.0	0.61215	0.00106	0.61427
YE10	NA_MIT_W090	0.9	0.9	1.0	0.61082	0.00111	0.61304
YE11	NA_MIT_W100	1.0	1.0	1.0	0.60324	0.00110	0.60544
Series 3: Variable water density outside FHE, with neoprene.							
YF1	NA_MIT_FNW000	1.0	0	1.0	0.55417	0.00118	0.55653
YF2	NA_MIT_FNW010	1.0	0.1	1.0	0.57731	0.00104	0.57939
YF3	NA_MIT_FNW020	1.0	0.2	1.0	0.59825	0.00117	0.60059
YF4	NA_MIT_FNW030	1.0	0.3	1.0	0.60830	0.00119	0.61068
YF5	NA_MIT_FNW040	1.0	0.4	1.0	0.61581	0.00116	0.61813
YF6	NA_MIT_FNW050	1.0	0.5	1.0	0.61968	0.00107	0.62182
YF7	**NA_MIT_FNW060**	**1.0**	**0.6**	**1.0**	**0.62059**	**0.00113**	**0.62285**
YF8	NA_MIT_FNW070	1.0	0.7	1.0	0.62035	0.00110	0.62255
YF9	NA_MIT_FNW080	1.0	0.8	1.0	0.61650	0.00110	0.61870
YF10	NA_MIT_FNW090	1.0	0.9	1.0	0.61120	0.00105	0.61330
YD11	NA_MIT_NW100	1.0	1.0	1.0	0.60885	0.00112	0.61109

(continued)

Table 6.10-11 – MIT NCT Array Results (concluded)

Case ID	Filename	Water Density Inside FHE (g/cm^3)	Water Density Outside FHE (g/cm^3)	Water Density Between Plates (g/cm^3)	k_{eff}	σ	k_s ($k+2\sigma$)
Series 4: Same as Series 3 but with maximum thickness FHE.							
YG1	NA_MIT_TFNW000	1.0	0	1.0	0.55951	0.00106	0.56163
YG2	NA_MIT_TFNW010	1.0	0.1	1.0	0.58058	0.00105	0.58268
YG3	NA_MIT_TFNW020	1.0	0.2	1.0	0.59653	0.00105	0.59863
YG4	NA_MIT_TFNW030	1.0	0.3	1.0	0.60581	0.00118	0.60817
YG5	NA_MIT_TFNW040	1.0	0.4	1.0	0.61242	0.00110	0.61462
YG6	NA_MIT_TFNW050	1.0	0.5	1.0	0.61318	0.00104	0.61526
YG7	NA_MIT_TFNW060	1.0	0.6	1.0	0.61463	0.00120	0.61703
YG8	**NA_MIT_TFNW070**	**1.0**	**0.7**	**1.0**	**0.61501**	**0.00111**	**0.61723**
YG9	NA_MIT_TFNW080	1.0	0.8	1.0	0.61394	0.00114	0.61622
YG10	NA_MIT_TFNW090	1.0	0.9	1.0	0.60894	0.00113	0.61120
YG11	NA_MIT_TFNW100	1.0	1.0	1.0	0.60456	0.00120	0.60696
Series 5: Same as Series 3 with 0.9 g/cm^3 water between fuel plates.							
YH1	NA_MIT_M90FNW000	1.0	0	0.9	0.53177	0.00107	0.53391
YH2	NA_MIT_M90FNW010	1.0	0.1	0.9	0.55655	0.00108	0.55871
YH3	NA_MIT_M90FNW020	1.0	0.2	0.9	0.57776	0.00122	0.58020
YH4	NA_MIT_M90FNW030	1.0	0.3	0.9	0.59349	0.00102	0.59553
YH5	NA_MIT_M90FNW040	1.0	0.4	0.9	0.60205	0.00103	0.60411
YH6	NA_MIT_M90FNW050	1.0	0.5	0.9	0.60659	0.00102	0.60863
YH7	NA_MIT_M90FNW060	1.0	0.6	0.9	0.60651	0.00119	0.60889
YH8	**NA_MIT_M90FNW070**	**1.0**	**0.7**	**0.9**	**0.60753**	**0.00121**	**0.60995**
YH9	NA_MIT_M90FNW080	1.0	0.8	0.9	0.60615	0.00112	0.60839
YH10	NA_MIT_M90FNW090	1.0	0.9	0.9	0.60192	0.00100	0.60392
YH11	NA_MIT_M90FNW100	1.0	1.0	0.9	0.59396	0.00111	0.59618
Series 6: Same as Series 3 but with modeled channel width of 0.116-in.							
YI1	NA_MIT_FNW000C	1.0	0	1.0	0.60247	0.00113	0.60473
YI2	NA_MIT_FNW010C	1.0	0.1	1.0	0.62391	0.00116	0.62623
YI3	NA_MIT_FNW020C	1.0	0.2	1.0	0.63710	0.00115	0.63940
YI4	NA_MIT_FNW030C	1.0	0.3	1.0	0.64617	0.00129	0.64875
YI5	NA_MIT_FNW040C	1.0	0.4	1.0	0.65160	0.00119	0.65398
YI6	**NA_MIT_FNW050C**	**1.0**	**0.5**	**1.0**	**0.65414**	**0.00122**	**0.65658**
YI7	NA_MIT_FNW060C	1.0	0.6	1.0	0.65181	0.00119	0.65419
YI8	NA_MIT_FNW070C	1.0	0.7	1.0	0.65016	0.00109	0.65234
YI9	NA_MIT_FNW080C	1.0	0.8	1.0	0.64541	0.00118	0.64777
YI10	NA_MIT_FNW090C	1.0	0.9	1.0	0.64029	0.00106	0.64241
YI11	NA_MIT_FNW100C	1.0	1.0	1.0	0.63436	0.00114	0.63664

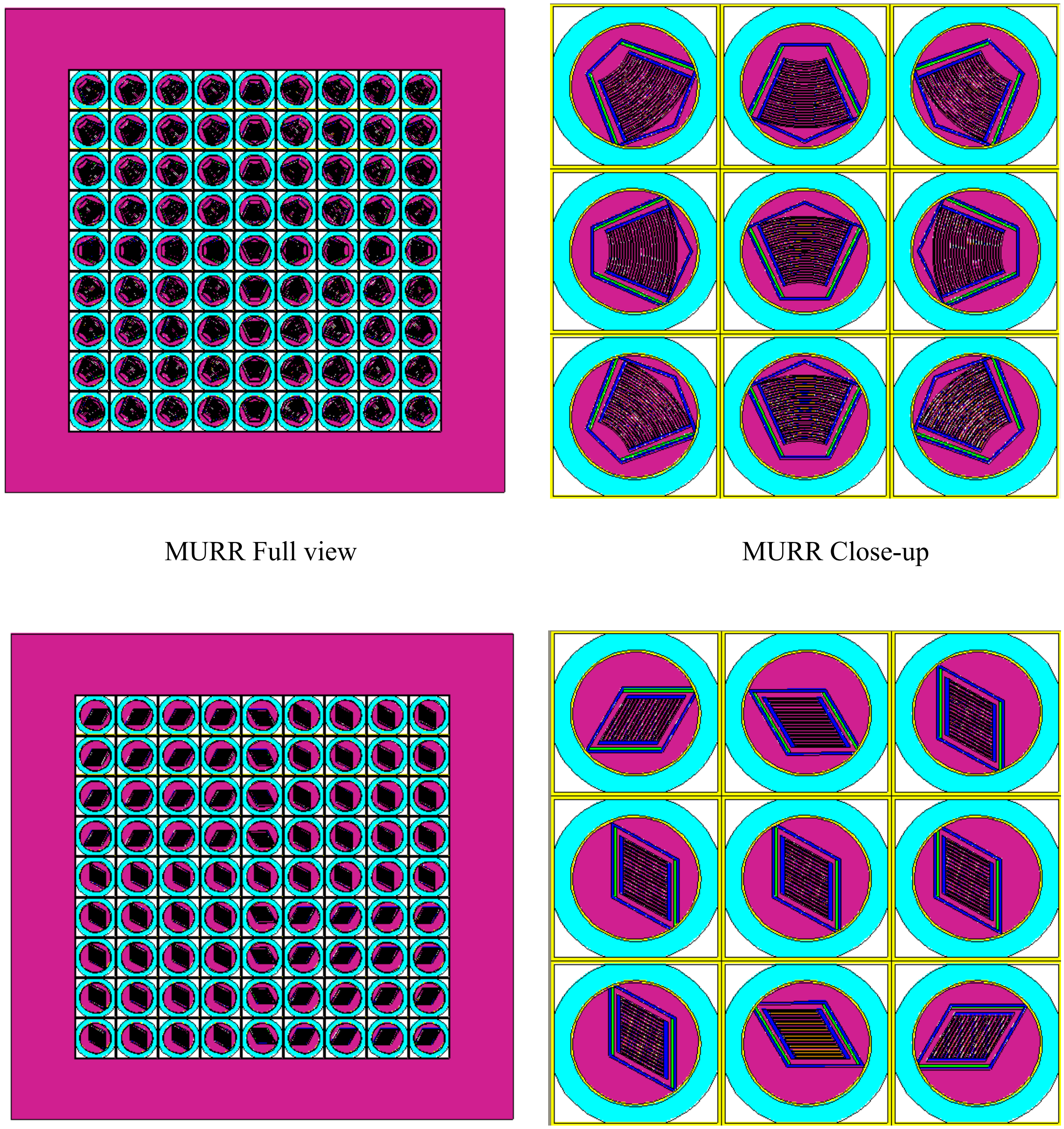

MURR Full view

MURR Close-up

MIT Full view

MIT Close-up

Figure 6.10-10 – MURR/MIT NCT Array Geometry

6.10.6 Package Arrays under Hypothetical Accident Conditions

6.10.6.1 HAC Array Condition

The HAC array model is a 5x5x1 array of packages. The primary difference comparing NCT to HAC is the modeled fuel damage, and separation of the FHE halves. Consistent with the HAC single package models, the two FHE halves are allowed to separate to the maximum possible extent, and the fuel element pitch is allowed to increase to the maximum possible value until constrained by the FHE. It is established in the HAC single package analysis that the reactivity is maximized with the maximum pitch, so all HAC array calculations utilize the maximum pitch.

The moderation conditions for the HAC array cases are largely the same as the NCT array moderation conditions, with the exception of the insulation region. In the HAC models, this region may be filled with variable density water. From the NCT array calculations, it was determined that the neoprene has a statistically insignificant effect on the reactivity, although the results showed a negligible increase. Therefore, neoprene is included in all HAC array models. Also, it has also been established in the HAC single package and NCT array cases that reducing the water density between the fuel plates reduces the reactivity. Therefore, the water between the fuel plates is always modeled at full density.

Although it is not feasible in actual practice to push the FHEs to the center of the array if the two FHE halves are already pushed apart, both the MURR and MIT models are shifted by 0.307-in towards the center of the array, as determined in Section 6.10.5.1, *NCT Array Configuration*. Note in Figure 6.10-11 that the FHEs for both MURR and MIT are “sliced off” in the corners because such a translation is not possible without interference, and the aluminum corners of the MIT element are also “sliced off” slightly for the same reason.

6.10.6.1.1 MURR Fuel Element Models

Five calculational series are developed, as described below. Results are summarized in Table 6.10-12.

Series 1 (Cases XJ1 through XJ11): In Series 1, the water density inside and outside the FHE is modeled at the same density, which is allowed to vary between 0 and 1.0 g/cm^3. This moderation condition simulates the partial moderation effect of assuming the plastic bag that surrounds the fuel element retains water. The region between the circular and square tubes is modeled as insulation/void, and the FHE is modeled with the minimum wall thickness.

Series 2 (Cases XK1 through XK11): In Series 2, the water density inside the FHE is fixed at 1.0 g/cm^3, while the water density outside the FHE is allowed to vary between 0 and 1.0 g/cm^3. This moderation condition simulates the partial moderation effect of assuming the FHE retains water. The region between the circular and square tubes is modeled as insulation/void, and the FHE is modeled with a minimum wall thickness. The maximum reactivity increases slightly compared to Series 1, although the effect is well within statistical fluctuation.

An additional case (Case XK11) is developed in which the insulation is replaced with void for the most reactive Series 2 case (Case XK10). Comparing Cases XK10 and XK11, it is slightly more reactive to model the insulation, which is consistent with the trend in the ATR fuel analysis.

Series 3 (Cases XL1 through XL11): In Series 3, the outer insulation/void region is replaced with variable density water. There are now three regions that contain water: (1) between the circular and square tubes, (2) between FHE and circular tube, and (3) between fuel element and FHE. In this series, each of these regions is modeled with the same water density, which is allowed to vary between 0 and 1.0 g/cm^3. Reactivity is significantly lower in Series 3 compared with either Series 1 or 2.

Series 4 (Cases XM1 through XM10): In Series 4, full-density water is modeled inside the FHE, while variable density water between 0 and 1.0 g/cm^3 is modeled outside the FHE and between the inner and outer tubes. This series is less reactive than either Series 1 or 2.

Series 5 (Cases XN1 through XN11): Series 5 is a repeat of Series 2 except using a thick-walled FHE. The reactivity increases slightly when the thick-walled FHE is used.

Series 1, 2 and 5 result in similar reactivities within the statistical uncertainty of the method. Case XN9 is the most reactive MURR case, with k_s = 0.85881. In this case, the fuel elements are pushed to the center of the array, full-density water is modeled between the plates and inside the FHE, 0.8 g/cm^3 water is modeled outside the FHE, insulation/void is modeled between the inner and outer tubes, chlorine-free neoprene is included, and the FHE is modeled with maximum wall thickness. The maximum result is below the USL of 0.9209.

6.10.6.1.2 MIT Fuel Element Models

Five calculational series are developed, as described below. Results are summarized in Table 6.10-13.

Series 1 (Cases YJ1 through YJ11): In Series 1, the water density inside and outside the FHE is modeled at the same density, which is allowed to vary between 0 and 1.0 g/cm^3. This moderation condition simulates the partial moderation effect of assuming the plastic bag that surrounds the fuel element retains water. The region between the circular and square tubes is modeled as insulation/void, and the FHE is modeled with the minimum wall thickness.

Series 2 (Cases YK1 through YK11): In Series 2, the water density inside the FHE is fixed at 1.0 g/cm^3, while the water density outside the FHE is allowed to vary between 0 and 1.0 g/cm^3. This moderation condition simulates the partial moderation effect of assuming the FHE retains water. The region between the circular and square tubes is modeled as insulation/void, and the FHE is modeled with a minimum wall thickness. The maximum reactivity increases slightly compared to Series 1, although the effect is well within statistical fluctuation.

An additional case (Case YK11) is developed in which the insulation is replaced with void for the most reactive Series 2 case (Case YK9). Comparing Cases YK9 and YK11, it is slightly more reactive to model the insulation, which is consistent with the trend in the ATR fuel analysis.

Series 3 (Cases YL1 through YL11): In Series 3, the outer insulation/void region is replaced with variable density water. There are now three regions that contain water: (1) between the circular and square tubes, (2) between FHE and circular tube, and (3) between fuel element and FHE. In this series, each of these regions is modeled with the same water density, which is allowed to vary between 0 and 1.0 g/cm^3. Reactivity is significantly lower in Series 3 compared with either Series 1 or 2.

Series 4 (Cases YM1 through YM10): In Series 4, full-density water is modeled inside the FHE, while variable density water between 0 and 1.0 g/cm^3 is modeled outside the FHE and between the inner and outer tubes. This series is less reactive than either Series 1 or 2.

Series 5 (Cases YN1 through YN11): Series 5 is a repeat of Series 2 except using a thick-walled FHE. The reactivity decreases slightly when the thick-walled FHE is used, although the decrease is within statistical fluctuation.

Series 1, 2 and 5 result in similar reactivities within the statistical uncertainty of the method. Case YK9 is the most reactive MIT case, with k_s = 0.67309. In this case, the fuel elements are pushed to the center of the array, full-density water is modeled between the plates and inside the FHE, 0.8 g/cm^3 water is modeled outside the FHE, insulation/void is modeled between the inner and outer tubes, chlorine-free neoprene is included, and the FHE is modeled with minimum wall thickness. The maximum result is below the USL of 0.9209.

6.10.6.2 HAC Array Results

Following are the tabulated results for the HAC array cases. The most reactive configuration in each series is listed in boldface.

Table 6.10-12 – MURR HAC Array Results

Case ID	Filename	Water Density Between Tubes (g/cm^3)	Water Density Inside FHE (g/cm^3)	Water Density Outside FHE (g/cm^3)	k_{eff}	σ	k_s ($k+2\sigma$)
Series 1: Insulation modeled, full-density water between plates, variable density water as indicated.							
XJ1	HA_MURR2_NW000	0	0	0	0.76355	0.00115	0.76585
XJ2	HA_MURR2_NW010	0	0.1	0.1	0.78430	0.00122	0.78674
XJ3	HA_MURR2_NW020	0	0.2	0.2	0.80290	0.00111	0.80512
XJ4	HA_MURR2_NW030	0	0.3	0.3	0.81874	0.00124	0.82122
XJ5	HA_MURR2_NW040	0	0.4	0.4	0.83311	0.00127	0.83565
XJ6	HA_MURR2_NW050	0	0.5	0.5	0.84140	0.00122	0.84384
XJ7	HA_MURR2_NW060	0	0.6	0.6	0.84544	0.00124	0.84792
XJ8	HA_MURR2_NW070	0	0.7	0.7	0.85035	0.00118	0.85271
XJ9	HA_MURR2_NW080	0	0.8	0.8	0.84998	0.00127	0.85252
XJ10	**HA_MURR2_NW090**	**0**	**0.9**	**0.9**	**0.85379**	**0.00128**	**0.85635**
XJ11	HA_MURR2_NW100	0	1.0	1.0	0.84975	0.00120	0.85215
Series 2: Insulation modeled, full-density water between plates and inside FHE, variable density water as indicated.							
XK1	HA_MURR2_FNW000	0	1.0	0	0.83610	0.00115	0.83840
XK2	HA_MURR2_FNW010	0	1.0	0.1	0.84001	0.00125	0.84251
XK3	HA_MURR2_FNW020	0	1.0	0.2	0.84152	0.00115	0.84382
XK4	HA_MURR2_FNW030	0	1.0	0.3	0.84875	0.00130	0.85135
XK5	HA_MURR2_FNW040	0	1.0	0.4	0.84946	0.00127	0.85200
XK6	HA_MURR2_FNW050	0	1.0	0.5	0.84850	0.00119	0.85088
XK7	HA_MURR2_FNW060	0	1.0	0.6	0.85141	0.00118	0.85377
XK8	HA_MURR2_FNW070	0	1.0	0.7	0.85076	0.00117	0.85310
XK9	HA_MURR2_FNW080	0	1.0	0.8	0.85054	0.00127	0.85308
XK10	**HA_MURR2_FNW090**	**0**	**1.0**	**0.9**	**0.85391**	**0.00125**	**0.85641**
XJ11	HA_MURR2_NW100	0	1.0	1.0	0.84975	0.0012	0.85215
XK11	HA_MURR2_FNW090X	0	1.0	0.9	0.84922	0.00132	0.85186
Series 3: Insulation not modeled, variable density water as indicated.							
XL1	HA_MURR2_ANW000	0	0	0	0.75710	0.00115	0.75940
XL2	HA_MURR2_ANW010	0.1	0.1	0.1	0.78773	0.00117	0.79007
XL3	**HA_MURR2_ANW020**	**0.2**	**0.2**	**0.2**	**0.78883**	**0.00124**	**0.79131**
XL4	HA_MURR2_ANW030	0.3	0.3	0.3	0.77894	0.00115	0.78124
XL5	HA_MURR2_ANW040	0.4	0.4	0.4	0.75950	0.00114	0.76178
XL6	HA_MURR2_ANW050	0.5	0.5	0.5	0.74010	0.00119	0.74248
XL7	HA_MURR2_ANW060	0.6	0.6	0.6	0.72381	0.00113	0.72607
XL8	HA_MURR2_ANW070	0.7	0.7	0.7	0.70323	0.00130	0.70583
XL9	HA_MURR2_ANW080	0.8	0.8	0.8	0.69154	0.00108	0.69370
XL10	HA_MURR2_ANW090	0.9	0.9	0.9	0.67881	0.00115	0.68111
XL11	HA_MURR2_ANW100	1.0	1.0	1.0	0.67207	0.00113	0.67433

(continued)

Table 6.10-12 – MURR HAC Array Results (concluded)

Case ID	Filename	Water Density Between Tubes (g/cm^3)	Water Density Inside FHE (g/cm^3)	Water Density Outside FHE (g/cm^3)	k_{eff}	σ	k_s (k+2σ)
Series 4: Insulation not modeled, variable density water as indicated.							
XM1	**HA_MURR2_IFNW000**	**0**	**1.0**	**0**	**0.83196**	**0.00121**	**0.83438**
XM2	HA_MURR2_IFNW010	0.1	1.0	0.1	0.82347	0.00123	0.82593
XM3	HA_MURR2_IFNW020	0.2	1.0	0.2	0.80575	0.00127	0.80829
XM4	HA_MURR2_IFNW030	0.3	1.0	0.3	0.78652	0.00109	0.78870
XM5	HA_MURR2_IFNW040	0.4	1.0	0.4	0.76597	0.00108	0.76813
XM6	HA_MURR2_IFNW050	0.5	1.0	0.5	0.74360	0.00124	0.74608
XM7	HA_MURR2_IFNW060	0.6	1.0	0.6	0.72740	0.00119	0.72978
XM8	HA_MURR2_IFNW070	0.7	1.0	0.7	0.70952	0.00112	0.71176
XM9	HA_MURR2_IFNW080	0.8	1.0	0.8	0.69669	0.00115	0.69899
XM10	HA_MURR2_IFNW090	0.9	1.0	0.9	0.68144	0.00119	0.68382
XL11	HA_MURR2_ANW100	1.0	1.0	1.0	0.67207	0.00113	0.67433
Series 5: Repeat of Series 2 with thick-walled FHE.							
XN1	HA_MURR2_TFNW000	0	1.0	0	0.83999	0.00136	0.84271
XN2	HA_MURR2_TFNW010	0	1.0	0.1	0.84169	0.00120	0.84409
XN3	HA_MURR2_TFNW020	0	1.0	0.2	0.84521	0.00115	0.84751
XN4	HA_MURR2_TFNW030	0	1.0	0.3	0.84875	0.00131	0.85137
XN5	HA_MURR2_TFNW040	0	1.0	0.4	0.84997	0.00117	0.85231
XN6	HA_MURR2_TFNW050	0	1.0	0.5	0.85368	0.00128	0.85624
XN7	HA_MURR2_TFNW060	0	1.0	0.6	0.85219	0.00115	0.85449
XN8	HA_MURR2_TFNW070	0	1.0	0.7	0.85204	0.00121	0.85446
XN9	**HA_MURR2_TFNW080**	**0**	**1.0**	**0.8**	**0.85621**	**0.00130**	**0.85881**
XN10	HA_MURR2_TFNW090	0	1.0	0.9	0.85319	0.00126	0.85571
XN11	HA_MURR2_TFNW100	0	1.0	1.0	0.85277	0.00121	0.85519

Table 6.10-13 – MIT HAC Array Results

Case ID	Filename	Water Density Between Tubes (g/cm^3)	Water Density Inside FHE (g/cm^3)	Water Density Outside FHE (g/cm^3)	k_{eff}	σ	k_s (k+2σ)
Series 1: Insulation modeled, full-density water between plates, variable density water as indicated.							
YJ1	HA_MIT_NW000	0	0	0	0.53667	0.00092	0.53851
YJ2	HA_MIT_NW010	0	0.1	0.1	0.56904	0.00111	0.57126
YJ3	HA_MIT_NW020	0	0.2	0.2	0.59837	0.00116	0.60069
YJ4	HA_MIT_NW030	0	0.3	0.3	0.62139	0.00122	0.62383
YJ5	HA_MIT_NW040	0	0.4	0.4	0.63737	0.00108	0.63953
YJ6	HA_MIT_NW050	0	0.5	0.5	0.65014	0.00109	0.65232
YJ7	HA_MIT_NW060	0	0.6	0.6	0.65850	0.00122	0.66094
YJ8	HA_MIT_NW070	0	0.7	0.7	0.66668	0.00115	0.66898
YJ9	**HA_MIT_NW080**	**0**	**0.8**	**0.8**	**0.67043**	**0.00121**	**0.67285**
YJ10	HA_MIT_NW090	0	0.9	0.9	0.67026	0.00112	0.67250
YJ11	HA_MIT_NW100	0	1.0	1.0	0.67058	0.00104	0.67266
Series 2: Insulation modeled, full-density water between plates and inside FHE, variable density water as indicated.							
YK1	HA_MIT_FNW000	0	1.0	0	0.60486	0.00110	0.60706
YK2	HA_MIT_FNW010	0	1.0	0.1	0.62101	0.00117	0.62335
YK3	HA_MIT_FNW020	0	1.0	0.2	0.63436	0.00121	0.63678
YK4	HA_MIT_FNW030	0	1.0	0.3	0.64759	0.00106	0.64971
YK5	HA_MIT_FNW040	0	1.0	0.4	0.65646	0.00117	0.65880
YK6	HA_MIT_FNW050	0	1.0	0.5	0.66078	0.00117	0.66312
YK7	HA_MIT_FNW060	0	1.0	0.6	0.66656	0.00107	0.66870
YK8	HA_MIT_FNW070	0	1.0	0.7	0.67022	0.00114	0.67250
YK9	**HA_MIT_FNW080**	**0**	**1.0**	**0.8**	**0.67105**	**0.00102**	**0.67309**
YK10	HA_MIT_FNW090	0	1.0	0.9	0.66898	0.00113	0.67124
YJ11	HA_MIT_NW100	0	1.0	1.0	0.67058	0.00104	0.67266
YK11	HA_MIT_FNW080X	0	1.0	0.9	0.66684	0.00110	0.66904
Series 3: Insulation not modeled, variable density water as indicated.							
YL1	HA_MIT_ANW000	0	0	0	0.53173	0.00103	0.53379
YL2	HA_MIT_ANW010	0.1	0.1	0.1	0.58121	0.00100	0.58321
YL3	HA_MIT_ANW020	0.2	0.2	0.2	0.59902	0.00119	0.60140
YL4	**HA_MIT_ANW030**	**0.3**	**0.3**	**0.3**	**0.60054**	**0.00105**	**0.60264**
YL5	HA_MIT_ANW040	0.4	0.4	0.4	0.59003	0.00116	0.59235
YL6	HA_MIT_ANW050	0.5	0.5	0.5	0.57811	0.00109	0.58029
YL7	HA_MIT_ANW060	0.6	0.6	0.6	0.56624	0.00114	0.56852
YL8	HA_MIT_ANW070	0.7	0.7	0.7	0.55438	0.00107	0.55652
YL9	HA_MIT_ANW080	0.8	0.8	0.8	0.54409	0.00114	0.54637
YL10	HA_MIT_ANW090	0.9	0.9	0.9	0.53935	0.00105	0.54145
YL11	HA_MIT_ANW100	1.0	1.0	1.0	0.53078	0.00104	0.53286

(continued)

Table 6.10-13 – MIT HAC Array Results (concluded)

Case ID	Filename	Water Density Between Tubes (g/cm^3)	Water Density Inside FHE (g/cm^3)	Water Density Outside FHE (g/cm^3)	k_{eff}	σ	k_s ($k+2\sigma$)
Series 4: Insulation not modeled, variable density water as indicated.							
YM1	HA_MIT_IFNW000	0	1.0	0	0.59996	0.00108	0.60212
YM2	**HA_MIT_IFNW010**	**0.1**	**1.0**	**0.1**	**0.61992**	**0.00112**	**0.62216**
YM3	HA_MIT_IFNW020	0.2	1.0	0.2	0.61899	0.00117	0.62133
YM4	HA_MIT_IFNW030	0.3	1.0	0.3	0.61130	0.00107	0.61344
YM5	HA_MIT_IFNW040	0.4	1.0	0.4	0.59725	0.00106	0.59937
YM6	HA_MIT_IFNW050	0.5	1.0	0.5	0.58253	0.00113	0.58479
YM7	HA_MIT_IFNW060	0.6	1.0	0.6	0.56935	0.00115	0.57165
YM8	HA_MIT_IFNW070	0.7	1.0	0.7	0.56002	0.00118	0.56238
YM9	HA_MIT_IFNW080	0.8	1.0	0.8	0.54870	0.00112	0.55094
YM10	HA_MIT_IFNW090	0.9	1.0	0.9	0.54119	0.00095	0.54309
YL11	HA_MIT_ANW100	1.0	1.0	1.0	0.53078	0.00104	0.53286
Series 5: Repeat of Series 2 with thick-walled FHE.							
YN1	HA_MIT_TFNW000	0	1.0	0	0.61405	0.00116	0.61637
YN2	HA_MIT_TFNW010	0	1.0	0.1	0.62418	0.00114	0.62646
YN3	HA_MIT_TFNW020	0	1.0	0.2	0.63652	0.00110	0.63872
YN4	HA_MIT_TFNW030	0	1.0	0.3	0.64631	0.00101	0.64833
YN5	HA_MIT_TFNW040	0	1.0	0.4	0.65197	0.00108	0.65413
YN6	HA_MIT_TFNW050	0	1.0	0.5	0.65994	0.00114	0.66222
YN7	HA_MIT_TFNW060	0	1.0	0.6	0.66467	0.00118	0.66703
YN8	HA_MIT_TFNW070	0	1.0	0.7	0.66785	0.00120	0.67025
YN9	HA_MIT_TFNW080	0	1.0	0.8	0.66872	0.00123	0.67118
YN10	**HA_MIT_TFNW090**	**0**	**1.0**	**0.9**	**0.66920**	**0.00111**	**0.67142**
YN11	HA_MIT_TFNW100	0	1.0	1.0	0.66847	0.00122	0.67091

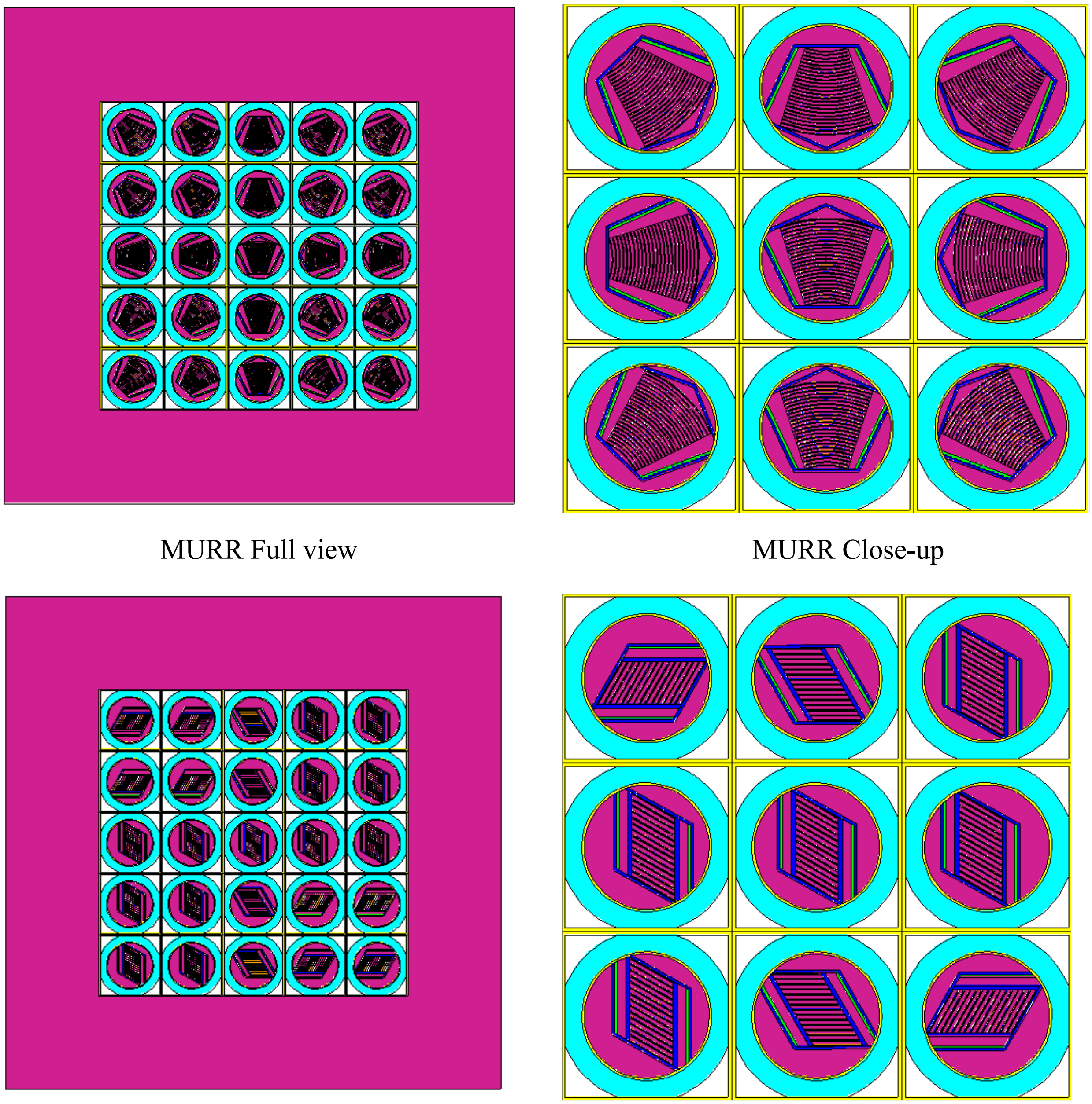

MURR Full view

MURR Close-up

MIT Full view

MIT Close-up

Figure 6.10-11 – MURR/MIT HAC Array Geometry

6.10.7 Fissile Material Packages for Air Transport

See Section 6.7, which applies to all contents.

6.10.8 Benchmark Evaluations

MURR and MIT fuel are both high-enriched aluminum plate-type fuel, similar to ATR fuel. Therefore, the benchmarking evaluation performed for the ATR fuel in Section 6.8, *Benchmark Evaluations*, is applicable to the current analysis, and the USL is 0.9209. The Monte Carlo computer program MCNP5 v1.30 was utilized in the benchmark analysis. MCNP has been used extensively in criticality evaluations for several decades and is considered a standard in the industry.

Five parameters were selected for the benchmark evaluation: (1) energy of the average neutron lethargy causing fission (EALF), (2) U-235 number density, (3) channel width, (4) H/U-235 atom ratio, and (5) pitch. The range of applicability of these parameters for the benchmarks utilized is summarized in Table 6.8-2. In the following sections, the range of applicability of the benchmarks is compared with the MURR and MIT criticality analysis.

6.10.8.1 Energy of the Average neutron Lethargy causing Fission (EALF)

Range of Applicability, MURR models: All of the single package models and most of the NCT and HAC array models fall within the range of the applicability. The EALF of the most reactive MURR fuel element model (Case XN9) has an EALF of 9.26E-08 MeV, which is within the range of applicability. Models with significantly more void spaces or low water densities sometimes exceed the range of applicability (maximum EALF = 2.03E-07 MeV for Case XE1), although these cases are not the most reactive. Therefore, the EALF of the most reactive models is acceptably within the range of applicability of the benchmarks.

Range of Applicability, MIT models: All of the single package models and most of the NCT and HAC array models fall within the range of the applicability. The EALF of the most reactive MIT fuel element model (Case YK9) has an EALF of 8.70E-08 MeV, which is within the range of applicability. Models with significantly more void spaces or low water densities sometimes exceed the range of applicability (maximum EALF = 3.30E-07 MeV for Case YE1), although these cases are not the most reactive. Therefore, the EALF of the most reactive models is acceptably within the range of applicability of the benchmarks.

6.10.8.2 U-235 Number Density

The U-235 number density is 3.61E-03 atom/b-cm in the MURR models and 3.68E-03 atom/b-cm in the MIT models. These number densities are within the range of applicability.

6.10.8.3 Channel Width

The maximum modeled NCT channel width is 0.092-in in the MURR models and 0.116-in in the MIT models. In the HAC models, in which the pitch is allowed to expand, the maximum channel width is 0.125-in in the MURR models and 0.176-in in the MIT models. All of these values exceed the maximum channel width of 0.078-in of the benchmark experiments. However, this parameter was artificially maximized in order to maximize model reactivity. As the channel width is directly related to system moderation, the acceptability of the EALF indicator demonstrates that MCNP is performing acceptably for thermal conditions. Therefore, this parameter is considered to be acceptable.

6.10.8.4 H/U-235 Atom Ratio

The H/U-235 atom ratio is used as the fourth trending parameter for the benchmark cases. The H/U-235 atom ratio is defined here as the ratio of hydrogen atoms to U-235 atoms in a unit cell. This parameter is computed by the following equation:

NH*C/(NU235*M)

where,

NH is the hydrogen number density

C is the channel width

NU235 is the U-235 number density

M is the fuel meat width

Range of Applicability, MURR models: The H/U-235 atom ratio may be computed as:

NCT: 6.687E-02*0.088/(3.6147E-03*0.02) = 81.4

NCT: 6.687E-02*0.092/(3.6147E-03*0.02) = 85.1

HAC: 6.687E-02*0.125/(3.6147E-03*0.02) = 115.6

Therefore, H/U-235 of the MURR cases is acceptably within the range of applicability of the benchmarks.

Range of Applicability, MIT models: The H/U-235 atom ratio may be computed as:

NCT: 6.687E-02*0.094/(3.6835E-03*0.03) = 56.9

NCT: 6.687E-02*0.116/(3.6835E-03*0.03) = 70.2

HAC: 6.687E-02*0.176/(3.6835E-03*0.03) = 106.5

The minimum H/U-235 atom ratio of the benchmark models is 65.1. Therefore, this parameter is slightly outside the range of the benchmark experiments for the 0.094-in channel width NCT cases, although this parameter is in range for the more reactive 0.116-in channel width NCT cases. Therefore, this parameter is considered to be acceptable for the NCT cases. For the HAC cases, which bound the NCT cases, this parameter is acceptably within the range of applicability of the benchmarks.

6.10.8.5 Pitch

The NCT pitch is fixed at 0.13-in in the MURR models and 0.16-in in the MIT models. In the HAC models, in which the pitch is allowed to expand, the maximum pitch is 0.167-in in the MURR models and 0.24-in in the MIT models. The maximum pitch of the benchmark models is 0.128-in, so the pitch in the models exceeds the range of the benchmarks, particularly for the HAC cases. However, this parameter was artificially maximized in order to maximize model reactivity. As the pitch is directly related to system moderation, the acceptability of the EALF indicator demonstrates that MCNP is performing acceptably for thermal conditions. Therefore, this parameter is considered to be acceptable.

6.10.9 Sample Input Files

A sample input file is provided for the most reactive MURR and MIT cases.

MURR Case XN9 (HA_MURR2_TFNW080)

```
MURR
999     0      -320:321:-322:323:-324:325                imp:n=0
900     0      310 -311 312 -313 24 -25     fill=3       imp:n=1
901     2 -1.0 (311:-310:313:-312:-24:25) 320 -321 322 -323 324 -325  imp:n=1
c
c       Universe 1: MURR Fuel Element (infinitely long)
c
10       10 5.4439E-02 52 -53 -16 -15                        u=1 imp:n=1 $
plate 1
11       3 -2.7        (-52:53:16:15) 51 -54 -7 -8           u=1 imp:n=1
12       10 5.4439E-02 401 -402 -406 -407                    u=1 imp:n=1 $
plate 2
13       3 -2.7        (-401:402:406:407) 400 -403 -404 -405 u=1 imp:n=1
14       10 5.4439E-02 411 -412 -416 -417                    u=1 imp:n=1 $
plate 3
15       3 -2.7        (-411:412:416:417) 410 -413 -414 -415 u=1 imp:n=1
16       10 5.4439E-02 421 -422 -426 -427                    u=1 imp:n=1 $
plate 4
17       3 -2.7        (-421:422:426:427) 420 -423 -424 -425 u=1 imp:n=1
18       10 5.4439E-02 431 -432 -436 -437                    u=1 imp:n=1 $
plate 5
19       3 -2.7        (-431:432:436:437) 430 -433 -434 -435 u=1 imp:n=1
20       10 5.4439E-02 441 -442 -446 -447                    u=1 imp:n=1 $
plate 6
21       3 -2.7        (-441:442:446:447) 440 -443 -444 -445 u=1 imp:n=1
22       10 5.4439E-02 451 -452 -456 -457                    u=1 imp:n=1 $
plate 7
23       3 -2.7        (-451:452:456:457) 450 -453 -454 -455 u=1 imp:n=1
24       10 5.4439E-02 461 -462 -466 -467                    u=1 imp:n=1 $
plate 8
25       3 -2.7        (-461:462:466:467) 460 -463 -464 -465 u=1 imp:n=1
26       10 5.4439E-02 471 -472 -476 -477                    u=1 imp:n=1 $
plate 9
27       3 -2.7        (-471:472:476:477) 470 -473 -474 -475 u=1 imp:n=1
28       10 5.4439E-02 481 -482 -486 -487                    u=1 imp:n=1 $
plate 10
29       3 -2.7        (-481:482:486:487) 480 -483 -484 -485 u=1 imp:n=1
30       10 5.4439E-02 491 -492 -496 -497                    u=1 imp:n=1 $
plate 11
31       3 -2.7        (-491:492:496:497) 490 -493 -494 -495 u=1 imp:n=1
32       10 5.4439E-02 501 -502 -506 -507                    u=1 imp:n=1 $
plate 12
33       3 -2.7        (-501:502:506:507) 500 -503 -504 -505 u=1 imp:n=1
34       10 5.4439E-02 511 -512 -516 -517                    u=1 imp:n=1 $
plate 13
35       3 -2.7        (-511:512:516:517) 510 -513 -514 -515 u=1 imp:n=1
36       10 5.4439E-02 521 -522 -526 -527                    u=1 imp:n=1 $
plate 14
37       3 -2.7        (-521:522:526:527) 520 -523 -524 -525 u=1 imp:n=1
38       10 5.4439E-02 531 -532 -536 -537                    u=1 imp:n=1 $
plate 15
```

```
39       3 -2.7        (-531:532:536:537) 530 -533 -534 -535 u=1 imp:n=1
40       10 5.4439E-02 541 -542 -546 -547                    u=1 imp:n=1 $
plate 16
41       3 -2.7        (-541:542:546:547) 540 -543 -544 -545 u=1 imp:n=1
42       10 5.4439E-02 551 -552 -556 -557                    u=1 imp:n=1 $
plate 17
43       3 -2.7        (-551:552:556:557) 550 -553 -554 -555 u=1 imp:n=1
44       10 5.4439E-02 561 -562 -566 -567                    u=1 imp:n=1 $
plate 18
45       3 -2.7        (-561:562:566:567) 560 -563 -564 -565 u=1 imp:n=1
46       10 5.4439E-02 571 -572 -576 -577                    u=1 imp:n=1 $
plate 19
47       3 -2.7        (-571:572:576:577) 570 -573 -574 -575 u=1 imp:n=1
48       10 5.4439E-02 581 -582 -586 -587                    u=1 imp:n=1 $
plate 20
49       3 -2.7        (-581:582:586:587) 580 -583 -584 -585 u=1 imp:n=1
50       10 5.4439E-02 591 -592 -596 -597                    u=1 imp:n=1 $
plate 21
51       3 -2.7        (-591:592:596:597) 590 -593 -594 -595 u=1 imp:n=1
52       10 5.4439E-02 601 -602 -606 -607                    u=1 imp:n=1 $
plate 22
53       3 -2.7        (-601:602:606:607) 600 -603 -604 -605 u=1 imp:n=1
54       10 5.4439E-02 611 -612 -616 -617                    u=1 imp:n=1 $
plate 23
55       3 -2.7        (-611:612:616:617) 610 -613 -614 -615 u=1 imp:n=1
56       10 5.4439E-02 621 -622 -626 -627                    u=1 imp:n=1 $
plate 24
57       3 -2.7        (-621:622:626:627) 620 -623 -624 -625 u=1 imp:n=1
150      2 -1.0  (-51:54:7:8)       (-400:403:404:405) (-410:413:414:415)
                 (-420:423:424:425) (-430:433:434:435) (-440:443:444:445)
                 (-450:453:454:455) (-460:463:464:465) (-470:473:474:475)
                 (-480:483:484:485) (-490:493:494:495) (-500:503:504:505)
                 (-510:513:514:515) (-520:523:524:525) (-530:533:534:535)
                 (-540:543:544:545) (-550:553:554:555) (-560:563:564:565)
                 (-570:573:574:575) (-580:583:584:585) (-590:593:594:595)
                 (-600:603:604:605) (-610:613:614:615) (-620:623:624:625)
                 u=1 imp:n=1
c
c       Universe 19: MURR with FHE
c
200     0          -232 -233 212 213 214 -234 fill=1(1) u=19 imp:n=1
201     5 -0.737  230 -210 212 214                u=19 imp:n=1 $ right
neoprene
202     5 -0.737  231 -211 213 214                u=19 imp:n=1 $ left
neoprene
203     2 -1.0    213 212 234                     u=19 imp:n=1 $ top water
outside bag
204     2 -1.0    -230 232 214 212                u=19 imp:n=1 $ side water
outside bag
205     2 -1.0    -231 233 214 213                u=19 imp:n=1 $ side water
outside bag
206     3 -2.7    (210:211:-212:-213:-214) -220 -221 222 223 224 u=19 imp:n=1
$ FHE
207     2 -0.8     220:221:-222:-223:-224        u=19 imp:n=1 $ water
c
c       Universe 20: MURR with pipe (center)
c
```

```
210     0           -200 fill=19                 u=20 imp:n=1
211     4 -7.94     200 -201                     u=20 imp:n=1 $ pipe
212     6 -0.096    201 -203 250 -251 252 -253  u=20 imp:n=1 $ insulation
213     0           203 250 -251 252 -253       u=20 imp:n=1 $ insulation to
tube
214     4 -7.94     -250:251:-252:253           u=20 imp:n=1 $ tube to inf
c
c       Universe 21: MURR with pipe (down)
c
220     0           -200 fill=19(2)              u=21 imp:n=1
221     4 -7.94     200 -201                     u=21 imp:n=1 $ pipe
222     6 -0.096    201 -203 250 -251 252 -253  u=21 imp:n=1 $ insulation
223     0           203 250 -251 252 -253       u=21 imp:n=1 $ insulation to
tube
224     4 -7.94     -250:251:-252:253           u=21 imp:n=1 $ tube to inf
c
c       Universe 22: MURR with pipe (up)
c
230     0           -200 fill=19(3)              u=22 imp:n=1
231     4 -7.94     200 -201                     u=22 imp:n=1 $ pipe
232     6 -0.096    201 -203 250 -251 252 -253  u=22 imp:n=1 $ insulation
233     0           203 250 -251 252 -253       u=22 imp:n=1 $ insulation to
tube
234     4 -7.94     -250:251:-252:253           u=22 imp:n=1 $ tube to inf
c
c       Universe 23: MURR with pipe (right)
c
240     0           -200 fill=19(4)              u=23 imp:n=1
241     4 -7.94     200 -201                     u=23 imp:n=1 $ pipe
242     6 -0.096    201 -203 250 -251 252 -253  u=23 imp:n=1 $ insulation
243     0           203 250 -251 252 -253       u=23 imp:n=1 $ insulation to
tube
244     4 -7.94     -250:251:-252:253           u=23 imp:n=1 $ tube to inf
c
c       Universe 24: MURR with pipe (left)
c
250     0           -200 fill=19(5)              u=24 imp:n=1
251     4 -7.94     200 -201                     u=24 imp:n=1 $ pipe
252     6 -0.096    201 -203 250 -251 252 -253  u=24 imp:n=1 $ insulation
253     0           203 250 -251 252 -253       u=24 imp:n=1 $ insulation to
tube
254     4 -7.94     -250:251:-252:253           u=24 imp:n=1 $ tube to inf
c
c       Universe 25: MURR with pipe (up right)
c
260     0           -200 fill=19(6)              u=25 imp:n=1
261     4 -7.94     200 -201                     u=25 imp:n=1 $ pipe
262     6 -0.096    201 -203 250 -251 252 -253  u=25 imp:n=1 $ insulation
263     0           203 250 -251 252 -253       u=25 imp:n=1 $ insulation to
tube
264     4 -7.94     -250:251:-252:253           u=25 imp:n=1 $ tube to inf
c
c       Universe 26: MURR with pipe (up left)
c
270     0           -200 fill=19(7)              u=26 imp:n=1
271     4 -7.94     200 -201                     u=26 imp:n=1 $ pipe
272     6 -0.096    201 -203 250 -251 252 -253  u=26 imp:n=1 $ insulation
```

```
273     0           203 250 -251 252 -253       u=26 imp:n=1 $ insulation to
tube
274     4 -7.94     -250:251:-252:253           u=26 imp:n=1 $ tube to inf
c
c       Universe 27: MURR with pipe (down right)
c
280     0           -200 fill=19(8)             u=27 imp:n=1
281     4 -7.94     200 -201                    u=27 imp:n=1 $ pipe
282     6 -0.096    201 -203 250 -251 252 -253  u=27 imp:n=1 $ insulation
283     0           203 250 -251 252 -253       u=27 imp:n=1 $ insulation to
tube
284     4 -7.94     -250:251:-252:253           u=27 imp:n=1 $ tube to inf
c
c       Universe 28: MURR with pipe (down left)
c
290     0           -200 fill=19(9)             u=28 imp:n=1
291     4 -7.94     200 -201                    u=28 imp:n=1 $ pipe
292     6 -0.096    201 -203 250 -251 252 -253  u=28 imp:n=1 $ insulation
293     0           203 250 -251 252 -253       u=28 imp:n=1 $ insulation to
tube
294     4 -7.94     -250:251:-252:253           u=28 imp:n=1 $ tube to inf
c
c       Universe 3: Array of Packages
c
300   0    -300 301 -302 303 imp:n=1 u=3 lat=1 fill=-2:2 -2:2 0:0
             25 25 22 26 26
             25 25 22 26 26
             23 23 20 24 24
             27 27 21 28 28
             27 27 21 28 28

c 5       p  2.4142136 -1 0 -0.13275   $ right Al outer
c 6       p -2.4142136 -1 0 -0.13275   $ left Al outer
7       p  2.4142136 -1 0 -1.09516   $ right Al inner
8       p -2.4142136 -1 0 -1.09516   $ left Al inner
c 9       cz 6.858                     $ Al boundary
c 10      cz 14.884                    $ Al boundary
c
15      p  2.4142136 -1 0 -1.39997   $ plate meat boundary
16      p -2.4142136 -1 0 -1.39997   $ plate meat boundary
c
24      pz -30.48                    $ bottom of fuel
25      pz  30.48                    $ top of fuel (24")
c
51      cz 7.0460 $ fuel plate 1
52      cz 7.0739
53      cz 7.1247
54      cz 7.1526
c
400 22    cz 7.3762 $ fuel plate 2
401 22    cz 7.4041
402 22    cz 7.4549
403 22    cz 7.4828
404 22    p  2.4142136 -1 0 -1.09516   $ right Al inner
405 22    p -2.4142136 -1 0 -1.09516   $ left Al inner
406 22    p  2.4142136 -1 0 -1.39997   $ plate meat boundary
407 22    p -2.4142136 -1 0 -1.39997   $ plate meat boundary
```

```
c
410 23  cz 7.7064 $ fuel plate 3
411 23  cz 7.7343
412 23  cz 7.7851
413 23  cz 7.8130
414 23    p  2.4142136 -1 0 -1.09516   $ right Al inner
415 23    p -2.4142136 -1 0 -1.09516   $ left Al inner
416 23    p  2.4142136 -1 0 -1.39997   $ plate meat boundary
417 23    p -2.4142136 -1 0 -1.39997   $ plate meat boundary
c
420 24  cz 8.0366 $ fuel plate 4
421 24  cz 8.0645
422 24  cz 8.1153
423 24  cz 8.1432
424 24    p  2.4142136 -1 0 -1.09516   $ right Al inner
425 24    p -2.4142136 -1 0 -1.09516   $ left Al inner
426 24    p  2.4142136 -1 0 -1.39997   $ plate meat boundary
427 24    p -2.4142136 -1 0 -1.39997   $ plate meat boundary
c
430 25  cz 8.3668 $ fuel plate 5
431 25  cz 8.3947
432 25  cz 8.4455
433 25  cz 8.4734
434 25    p  2.4142136 -1 0 -1.09516   $ right Al inner
435 25    p -2.4142136 -1 0 -1.09516   $ left Al inner
436 25    p  2.4142136 -1 0 -1.39997   $ plate meat boundary
437 25    p -2.4142136 -1 0 -1.39997   $ plate meat boundary
c
440 26  cz 8.6970 $ fuel plate 6
441 26  cz 8.7249
442 26  cz 8.7757
443 26  cz 8.8036
444 26    p  2.4142136 -1 0 -1.09516   $ right Al inner
445 26    p -2.4142136 -1 0 -1.09516   $ left Al inner
446 26    p  2.4142136 -1 0 -1.39997   $ plate meat boundary
447 26    p -2.4142136 -1 0 -1.39997   $ plate meat boundary
c
450 27  cz 9.0272 $ fuel plate 7
451 27  cz 9.0551
452 27  cz 9.1059
453 27  cz 9.1338
454 27    p  2.4142136 -1 0 -1.09516   $ right Al inner
455 27    p -2.4142136 -1 0 -1.09516   $ left Al inner
456 27    p  2.4142136 -1 0 -1.39997   $ plate meat boundary
457 27    p -2.4142136 -1 0 -1.39997   $ plate meat boundary
c
460 28  cz 9.3574 $ fuel plate 8
461 28  cz 9.3853
462 28  cz 9.4361
463 28  cz 9.4640
464 28    p  2.4142136 -1 0 -1.09516   $ right Al inner
465 28    p -2.4142136 -1 0 -1.09516   $ left Al inner
466 28    p  2.4142136 -1 0 -1.39997   $ plate meat boundary
467 28    p -2.4142136 -1 0 -1.39997   $ plate meat boundary
c
470 29  cz 9.6876 $ fuel plate 9
471 29  cz 9.7155
```

```
472 29  cz 9.7663
473 29  cz 9.7942
474 29    p  2.4142136 -1 0 -1.09516   $ right Al inner
475 29    p -2.4142136 -1 0 -1.09516   $ left Al inner
476 29    p  2.4142136 -1 0 -1.39997   $ plate meat boundary
477 29    p -2.4142136 -1 0 -1.39997   $ plate meat boundary
c
480 30  cz 10.0178 $ fuel plate 10
481 30  cz 10.0457
482 30  cz 10.0965
483 30  cz 10.1244
484 30    p  2.4142136 -1 0 -1.09516   $ right Al inner
485 30    p -2.4142136 -1 0 -1.09516   $ left Al inner
486 30    p  2.4142136 -1 0 -1.39997   $ plate meat boundary
487 30    p -2.4142136 -1 0 -1.39997   $ plate meat boundary
c
490 31  cz 10.3480 $ fuel plate 11
491 31  cz 10.3759
492 31  cz 10.4267
493 31  cz 10.4546
494 31    p  2.4142136 -1 0 -1.09516   $ right Al inner
495 31    p -2.4142136 -1 0 -1.09516   $ left Al inner
496 31    p  2.4142136 -1 0 -1.39997   $ plate meat boundary
497 31    p -2.4142136 -1 0 -1.39997   $ plate meat boundary
c
500 32  cz 10.6782 $ fuel plate 12
501 32  cz 10.7061
502 32  cz 10.7569
503 32  cz 10.7848
504 32    p  2.4142136 -1 0 -1.09516   $ right Al inner
505 32    p -2.4142136 -1 0 -1.09516   $ left Al inner
506 32    p  2.4142136 -1 0 -1.39997   $ plate meat boundary
507 32    p -2.4142136 -1 0 -1.39997   $ plate meat boundary
c
510 33  cz 11.0084 $ fuel plate 13
511 33  cz 11.0363
512 33  cz 11.0871
513 33  cz 11.1150
514 33    p  2.4142136 -1 0 -1.09516   $ right Al inner
515 33    p -2.4142136 -1 0 -1.09516   $ left Al inner
516 33    p  2.4142136 -1 0 -1.39997   $ plate meat boundary
517 33    p -2.4142136 -1 0 -1.39997   $ plate meat boundary
c
520 34  cz 11.3386 $ fuel plate 14
521 34  cz 11.3665
522 34  cz 11.4173
523 34  cz 11.4452
524 34    p  2.4142136 -1 0 -1.09516   $ right Al inner
525 34    p -2.4142136 -1 0 -1.09516   $ left Al inner
526 34    p  2.4142136 -1 0 -1.39997   $ plate meat boundary
527 34    p -2.4142136 -1 0 -1.39997   $ plate meat boundary
c
530 35  cz 11.6688 $ fuel plate 15
531 35  cz 11.6967
532 35  cz 11.7475
533 35  cz 11.7754
534 35    p  2.4142136 -1 0 -1.09516   $ right Al inner
```

```
535 35    p -2.4142136 -1 0 -1.09516   $ left Al inner
536 35    p  2.4142136 -1 0 -1.39997   $ plate meat boundary
537 35    p -2.4142136 -1 0 -1.39997   $ plate meat boundary
c
540 36  cz 11.9990 $ fuel plate 16
541 36  cz 12.0269
542 36  cz 12.0777
543 36  cz 12.1056
544 36    p  2.4142136 -1 0 -1.09516   $ right Al inner
545 36    p -2.4142136 -1 0 -1.09516   $ left Al inner
546 36    p  2.4142136 -1 0 -1.39997   $ plate meat boundary
547 36    p -2.4142136 -1 0 -1.39997   $ plate meat boundary
c
550 37  cz 12.3292 $ fuel plate 17
551 37  cz 12.3571
552 37  cz 12.4079
553 37  cz 12.4358
554 37    p  2.4142136 -1 0 -1.09516   $ right Al inner
555 37    p -2.4142136 -1 0 -1.09516   $ left Al inner
556 37    p  2.4142136 -1 0 -1.39997   $ plate meat boundary
557 37    p -2.4142136 -1 0 -1.39997   $ plate meat boundary
c
560 38  cz 12.6594 $ fuel plate 18
561 38  cz 12.6873
562 38  cz 12.7381
563 38  cz 12.7660
564 38    p  2.4142136 -1 0 -1.09516   $ right Al inner
565 38    p -2.4142136 -1 0 -1.09516   $ left Al inner
566 38    p  2.4142136 -1 0 -1.39997   $ plate meat boundary
567 38    p -2.4142136 -1 0 -1.39997   $ plate meat boundary
c
570 39  cz 12.9896 $ fuel plate 19
571 39  cz 13.0175
572 39  cz 13.0683
573 39  cz 13.0962
574 39    p  2.4142136 -1 0 -1.09516   $ right Al inner
575 39    p -2.4142136 -1 0 -1.09516   $ left Al inner
576 39    p  2.4142136 -1 0 -1.39997   $ plate meat boundary
577 39    p -2.4142136 -1 0 -1.39997   $ plate meat boundary
c
580 40  cz 13.3198 $ fuel plate 20
581 40  cz 13.3477
582 40  cz 13.3985
583 40  cz 13.4264
584 40    p  2.4142136 -1 0 -1.09516   $ right Al inner
585 40    p -2.4142136 -1 0 -1.09516   $ left Al inner
586 40    p  2.4142136 -1 0 -1.39997   $ plate meat boundary
587 40    p -2.4142136 -1 0 -1.39997   $ plate meat boundary
c
590 41  cz 13.6500 $ fuel plate 21
591 41  cz 13.6779
592 41  cz 13.7287
593 41  cz 13.7566
594 41    p  2.4142136 -1 0 -1.09516   $ right Al inner
595 41    p -2.4142136 -1 0 -1.09516   $ left Al inner
596 41    p  2.4142136 -1 0 -1.39997   $ plate meat boundary
597 41    p -2.4142136 -1 0 -1.39997   $ plate meat boundary
```

```
c
600 42  cz 13.9802 $ fuel plate 22
601 42  cz 14.0081
602 42  cz 14.0589
603 42  cz 14.0868
604 42    p  2.4142136 -1 0 -1.09516   $ right Al inner
605 42    p -2.4142136 -1 0 -1.09516   $ left Al inner
606 42    p  2.4142136 -1 0 -1.39997   $ plate meat boundary
607 42    p -2.4142136 -1 0 -1.39997   $ plate meat boundary
c
610 43  cz 14.3104 $ fuel plate 23
611 43  cz 14.3383
612 43  cz 14.3891
613 43  cz 14.4170
614 43    p  2.4142136 -1 0 -1.09516   $ right Al inner
615 43    p -2.4142136 -1 0 -1.09516   $ left Al inner
616 43    p  2.4142136 -1 0 -1.39997   $ plate meat boundary
617 43    p -2.4142136 -1 0 -1.39997   $ plate meat boundary
c
620 44  cz 14.6406 $ fuel plate 24
621 44  cz 14.6685
622 44  cz 14.7193
623 44  cz 14.7472
624 44    p  2.4142136 -1 0 -1.09516   $ right Al inner
625 44    p -2.4142136 -1 0 -1.09516   $ left Al inner
626 44    p  2.4142136 -1 0 -1.39997   $ plate meat boundary
627 44    p -2.4142136 -1 0 -1.39997   $ plate meat boundary
c
200      cz 7.3838 $ IR pipe
201      cz 7.6581 $ OR pipe
c 202      cz 38.1   $ 12" water
203      cz 10.1981 $ 1" insulation
c
210 50     p  2.194300 -1 0 11.6987 $ right lower inner
211 51     p -2.194300 -1 0 11.6987 $ left lower inner
212 50     p -0.455726 -1 0 -5.7501 $ right upper inner
213 51     p  0.455726 -1 0 -5.7501 $ left upper inner
214        py -5.6175               $ bottom inner
220 50     p  2.194300 -1 0 13.2300 $ right lower outer
221 51     p -2.194300 -1 0 13.2300 $ left lower outer
222 50     p -0.455726 -1 0 -6.4479 $ right upper outer
223 51     p  0.455726 -1 0 -6.4479 $ left upper outer
224        py -6.2525               $ bottom outer
230 50     p  2.194300 -1 0 10.9331 $ right neoprene
231 51     p -2.194300 -1 0 10.9331 $ left neoprene
232        p  3.1993   -1 0 13.2244 $ right plastic bag
233        p -3.1993   -1 0 13.2244 $ left plastic bag
234        c/z 0 -10.065 14.8       $ top of plastic bag
c
250      px  -9.6032 $ square tube
251      px   9.6032
252      py  -9.6032
253      py   9.6032
c
300      px  10.033 $ lattice surfaces/sq. tube
301      px -10.033
302      py  10.033
```

```
303      py -10.033
310      px -50.165 $ 5x5 bounds
311      px  50.165
312      py -50.165
313      py  50.165
320      px -80.645 $ outer bounds
321      px  80.645
322      py -80.645
323      py  80.645
324      pz -60.96
325      pz  60.96

m2      1001.62c  2          $ water
        8016.62c  1
mt2     lwtr.60t
m3      13027.62c 1          $ Al
m4      6000.66c   -0.08     $ SS-304
        14000.60c  -1.0
        15031.66c  -0.045
        24000.50c  -19.0
        25055.62c  -2.0
        26000.55c  -68.375
        28000.50c  -9.5
m5      1001.62c  -0.056920  $ neoprene (no Cl)
        6000.66c  -0.542646
c        17000.66c -0.400434
m6      13027.62c  -26.5     $ insulation material
        14000.60c  -23.4
        8016.62c   -50.2
m10     92234.69c 2.3171E-05
        92235.69c 3.6147E-03
        92236.69c 1.3402E-05
        92238.69c 1.9174E-04
        13027.62c 5.0596E-02
c           total 5.4439E-02
c
*tr1     0 -12.25 0                        $ base to center
*tr2     0 -0.7798 0  180 90 90 90 180 90  $ down
*tr3     0  0.7798 0                       $ up
*tr4     0.7798 0 0  90 180 90 0 90 90     $ right
*tr5    -0.7798 0 0  90 0 90 180 90 90     $ left
*tr6     0.5514   0.5514  0  45 135 90 45 45 90     $ up/right
*tr7    -0.5514   0.5514  0  45 45 90 135 45 90     $ up/left
*tr8     0.5514  -0.5514  0  135 135 90 45 135 90   $ down/right
*tr9    -0.5514  -0.5514  0  135 45 90 135 135 90   $ down/left
tr22 0 0.095 0 $ plate 2
tr23 0 0.190 0 $ plate 3
tr24 0 0.285 0 $ plate 4
tr25 0 0.380 0 $ plate 5
tr26 0 0.475 0 $ plate 6
tr27 0 0.570 0 $ plate 7
tr28 0 0.665 0 $ plate 8
tr29 0 0.760 0 $ plate 9
tr30 0 0.855 0 $ plate 10
tr31 0 0.950 0 $ plate 11
tr32 0 1.045 0 $ plate 12
tr33 0 1.140 0 $ plate 13
```

```
tr34 0 1.235 0 $ plate 14
tr35 0 1.330 0 $ plate 15
tr36 0 1.425 0 $ plate 16
tr37 0 1.520 0 $ plate 17
tr38 0 1.615 0 $ plate 18
tr39 0 1.710 0 $ plate 19
tr40 0 1.805 0 $ plate 20
tr41 0 1.900 0 $ plate 21
tr42 0 1.995 0 $ plate 22
tr43 0 2.090 0 $ plate 23
tr44 0 2.185 0 $ plate 24
tr50   0.7798 0 0  $ shift FHE right
tr51  -0.7798 0 0  $ shift FHE left
c
mode   n
kcode  2500 1.0 50 250
sdef    x=d1 y=d2 z=d3
si1     -50 50
sp1     0 1
si2     -50 50
sp2     0 1
si3     -31 31
sp3     0 1
```

MIT Case YK9 (HA_MIT_FNW080)

```
MIT
999     0      -320:321:-322:323:-324:325                imp:n=0
900     0      310 -311 312 -313 24 -25     fill=3       imp:n=1
901     2 -1.0 (311:-310:313:-312:-24:25) 320 -321 322 -323 324 -325  imp:n=1
c
c       Universe 1: MIT Fuel Element (infinitely long)
c
10      3 -2.7        10 -11 50 -124            u=1 imp:n=1 $ right Al piece
11      3 -2.7        13 -12 50 -124            u=1 imp:n=1 $ left Al piece
c 12      2 -1.0        12 -10 18 -50             u=1 imp:n=1
20      10 5.4398E-02 40 -41 70 -90             u=1 imp:n=1 $ plate 1
21      3 -2.7        12 -10 50 -110 #20        u=1 imp:n=1
22      2 -1.0        12 -10 110 -51            u=1 imp:n=1
30      10 5.4398E-02 40 -41 71 -91             u=1 imp:n=1 $ plate 2
31      3 -2.7        12 -10 51 -111 #30        u=1 imp:n=1
32      2 -1.0        12 -10 111 -52            u=1 imp:n=1
40      10 5.4398E-02 40 -41 72 -92             u=1 imp:n=1 $ plate 3
41      3 -2.7        12 -10 52 -112 #40        u=1 imp:n=1
42      2 -1.0        12 -10 112 -53            u=1 imp:n=1
50      10 5.4398E-02 40 -41 73 -93             u=1 imp:n=1 $ plate 4
51      3 -2.7        12 -10 53 -113 #50        u=1 imp:n=1
52      2 -1.0        12 -10 113 -54            u=1 imp:n=1
60      10 5.4398E-02 40 -41 74 -94             u=1 imp:n=1 $ plate 5
61      3 -2.7        12 -10 54 -114 #60        u=1 imp:n=1
62      2 -1.0        12 -10 114 -55            u=1 imp:n=1
70      10 5.4398E-02 40 -41 75 -95             u=1 imp:n=1 $ plate 6
71      3 -2.7        12 -10 55 -115 #70        u=1 imp:n=1
72      2 -1.0        12 -10 115 -56            u=1 imp:n=1
80      10 5.4398E-02 40 -41 76 -96             u=1 imp:n=1 $ plate 7
81      3 -2.7        12 -10 56 -116 #80        u=1 imp:n=1
```

```
82       2 -1.0         12 -10 116 -57            u=1 imp:n=1
90       10 5.4398E-02 40 -41 77 -97              u=1 imp:n=1 $ plate 8
91       3 -2.7         12 -10 57 -117 #90        u=1 imp:n=1
92       2 -1.0         12 -10 117 -58            u=1 imp:n=1
100       10 5.4398E-02 40 -41 78 -98              u=1 imp:n=1 $ plate 9
101       3 -2.7         12 -10 58 -118 #100       u=1 imp:n=1
102       2 -1.0         12 -10 118 -59            u=1 imp:n=1
110       10 5.4398E-02 40 -41 79 -99              u=1 imp:n=1 $ plate 10
111       3 -2.7         12 -10 59 -119 #110       u=1 imp:n=1
112       2 -1.0         12 -10 119 -60            u=1 imp:n=1
120       10 5.4398E-02 40 -41 80 -100             u=1 imp:n=1 $ plate 11
121       3 -2.7         12 -10 60 -120 #120       u=1 imp:n=1
122       2 -1.0         12 -10 120 -61            u=1 imp:n=1
130       10 5.4398E-02 40 -41 81 -101             u=1 imp:n=1 $ plate 12
131       3 -2.7         12 -10 61 -121 #130       u=1 imp:n=1
132       2 -1.0         12 -10 121 -62            u=1 imp:n=1
140       10 5.4398E-02 40 -41 82 -102             u=1 imp:n=1 $ plate 13
141       3 -2.7         12 -10 62 -122 #140       u=1 imp:n=1
142       2 -1.0         12 -10 122 -63            u=1 imp:n=1
150       10 5.4398E-02 40 -41 83 -103             u=1 imp:n=1 $ plate 14
151       3 -2.7         12 -10 63 -123 #150       u=1 imp:n=1
152       2 -1.0         12 -10 123 -64            u=1 imp:n=1
160       10 5.4398E-02 40 -41 84 -104             u=1 imp:n=1 $ plate 15
161       3 -2.7         12 -10 64 -124 #160       u=1 imp:n=1
c 162       2 -1.0         12 -10 124 -19            u=1 imp:n=1
170       2 -1.0         -13:11:-50:124            u=1 imp:n=1 $ water between
fuel and enclosure
c
c       Universe 19: MIT with FHE
c
201     0           30 38 -32 -39 fill=1                u=19 imp:n=1
202     5 -0.737    -33 39 -32 30                       u=19 imp:n=1 $ right
neo
203     5 -0.737    31 -38 -32 30                       u=19 imp:n=1 $ left
neo
204     3 -2.7      (-30:-31:32:33) 34 35 -36 -37       u=19 imp:n=1 $
enclosure
205     2 -0.8      -34:-35:36:37                       u=19 imp:n=1 $ water
outside FHE
c
c       Universe 20: FHE in tube (center)
c
210     2 -0.9     -200           fill=19               u=20 imp:n=1 $ inside
pipe
211     4 -7.94     200 -201                            u=20 imp:n=1 $ pipe
212     6 -0.096    201 -203 250 -251 252 -253          u=20 imp:n=1 $
insulation
213     0           203 250 -251 252 -253               u=20 imp:n=1 $ pipe to
tube
214     4 -7.94     -250:251:-252:253                   u=20 imp:n=1 $ tube to
inf
c
c       Universe 21: FHE in tube (down)
c
220     2 -0.9     -200           fill=19(2)            u=21 imp:n=1 $ inside
pipe
221     4 -7.94     200 -201                            u=21 imp:n=1 $ pipe
```

```
222     6 -0.096    201 -203 250 -251 252 -253         u=21 imp:n=1 $
insulation
223     0           203 250 -251 252 -253              u=21 imp:n=1 $ pipe to
tube
224     4 -7.94     -250:251:-252:253                  u=21 imp:n=1 $ tube to
inf
c
c       Universe 22: FHE in tube (up)
c
230     2 -0.9     -200           fill=19(3)           u=22 imp:n=1 $ inside
pipe
231     4 -7.94     200 -201                           u=22 imp:n=1 $ pipe
232     6 -0.096    201 -203 250 -251 252 -253         u=22 imp:n=1 $
insulation
233     0           203 250 -251 252 -253              u=22 imp:n=1 $ pipe to
tube
234     4 -7.94     -250:251:-252:253                  u=22 imp:n=1 $ tube to
inf
c
c       Universe 23: FHE in tube (right)
c
240     2 -0.9     -200           fill=19(4)           u=23 imp:n=1 $ inside
pipe
241     4 -7.94     200 -201                           u=23 imp:n=1 $ pipe
242     6 -0.096    201 -203 250 -251 252 -253         u=23 imp:n=1 $
insulation
243     0           203 250 -251 252 -253              u=23 imp:n=1 $ pipe to
tube
244     4 -7.94     -250:251:-252:253                  u=23 imp:n=1 $ tube to
inf
c
c       Universe 24: FHE in tube (left)
c
250     2 -0.9     -200           fill=19(5)           u=24 imp:n=1 $ inside
pipe
251     4 -7.94     200 -201                           u=24 imp:n=1 $ pipe
252     6 -0.096    201 -203 250 -251 252 -253         u=24 imp:n=1 $
insulation
253     0           203 250 -251 252 -253              u=24 imp:n=1 $ pipe to
tube
254     4 -7.94     -250:251:-252:253                  u=24 imp:n=1 $ tube to
inf
c
c       Universe 25: FHE in tube (up/right)
c
260     2 -0.9     -200           fill=19(6)           u=25 imp:n=1 $ inside
pipe
261     4 -7.94     200 -201                           u=25 imp:n=1 $ pipe
262     6 -0.096    201 -203 250 -251 252 -253         u=25 imp:n=1 $
insulation
263     0           203 250 -251 252 -253              u=25 imp:n=1 $ pipe to
tube
264     4 -7.94     -250:251:-252:253                  u=25 imp:n=1 $ tube to
inf
c
c       Universe 26: FHE in tube (up/left)
c
```

```
270     2 -0.9     -200          fill=19(7)          u=26 imp:n=1 $ inside
pipe
271     4 -7.94     200 -201                         u=26 imp:n=1 $ pipe
272     6 -0.096    201 -203 250 -251 252 -253       u=26 imp:n=1 $
insulation
273     0           203 250 -251 252 -253            u=26 imp:n=1 $ pipe to
tube
274     4 -7.94     -250:251:-252:253                u=26 imp:n=1 $ tube to
inf
c
c       Universe 27: FHE in tube (down/right)
c
280     2 -0.9     -200          fill=19(8)          u=27 imp:n=1 $ inside
pipe
281     4 -7.94     200 -201                         u=27 imp:n=1 $ pipe
282     6 -0.096    201 -203 250 -251 252 -253       u=27 imp:n=1 $
insulation
283     0           203 250 -251 252 -253            u=27 imp:n=1 $ pipe to
tube
284     4 -7.94     -250:251:-252:253                u=27 imp:n=1 $ tube to
inf
c
c       Universe 28: FHE in tube (down/left)
c
290     2 -0.9     -200          fill=19(9)          u=28 imp:n=1 $ inside
pipe
291     4 -7.94     200 -201                         u=28 imp:n=1 $ pipe
292     6 -0.096    201 -203 250 -251 252 -253       u=28 imp:n=1 $
insulation
293     0           203 250 -251 252 -253            u=28 imp:n=1 $ pipe to
tube
294     4 -7.94     -250:251:-252:253                u=28 imp:n=1 $ tube to
inf
c
c       Universe 3: Array of Packages
c
300   0    -300 301 -302 303 imp:n=1 u=3 lat=1 fill=-2:2 -2:2 0:0
             25 25 22 26 26
             25 25 22 26 26
             23 23 20 24 24
             27 27 21 28 28
             27 27 21 28 28

10      px  2.5451   $ Al side
11      px  3.0226   $ Al side
12      px -2.5451   $ Al side
13      px -3.0226   $ Al side
18  10  py -3.02768  $ Al bottom
19  10  py 3.02768   $ Al top
20  10  py -3.34518  $ neoprene
21  10  py  3.34518  $ neoprene
c
24      pz -28.41625  $ bottom of fuel
25      pz  28.41625  $ top of fuel (22.375")
30 20   p -1.71429 -1 0 -7.3152 $ inner FHE
31 21   p  1.71429 -1 0 -7.3152 $ inner FHE
32 21   p -1.71429 -1 0  7.3152 $ inner FHE
```

```
33 20   p  1.71429 -1 0  7.3152 $ inner FHE
34 20   p -1.71429 -1 0 -7.9697 $ outer FHE
35 21   p  1.71429 -1 0 -7.9697 $ outer FHE
36 21   p -1.71429 -1 0  7.9697 $ outer FHE
37 20   p  1.71429 -1 0  7.9697 $ outer FHE
38 21   p  1.71429 -1 0 -6.6859 $ left neo
39 20   p  1.71429 -1 0  6.6859 $ right neo
c
40      px -2.3878 $ meat width (w/2*cos(30))
41      px  2.3878 $ meat width
c
50 10   py -4.34848
51 10   py -3.73888
52 10   py -3.12928
53 10   py -2.51968
54 10   py -1.91008
55 10   py -1.30048
56 10   py -0.69088
57 10   py -0.08128
58 10   py 0.52832
59 10   py 1.13792
60 10   py 1.74752
61 10   py 2.35712
62 10   py 2.96672
63 10   py 3.57632
64 10   py 4.18592
c
70 10   py -4.30530
71 10   py -3.69570
72 10   py -3.08610
73 10   py -2.47650
74 10   py -1.86690
75 10   py -1.25730
76 10   py -0.64770
77 10   py -0.03810
78 10   py 0.57150
79 10   py 1.18110
80 10   py 1.79070
81 10   py 2.40030
82 10   py 3.00990
83 10   py 3.61950
84 10   py 4.22910
c
90 10   py -4.22910
91 10   py -3.61950
92 10   py -3.00990
93 10   py -2.40030
94 10   py -1.79070
95 10   py -1.18110
96 10   py -0.57150
97 10   py 0.03810
98 10   py 0.64770
99 10   py 1.25730
100 10   py 1.86690
101 10   py 2.47650
102 10   py 3.08610
103 10   py 3.69570
```

```
104 10   py 4.30530
c
110 10   py -4.18592
111 10   py -3.57632
112 10   py -2.96672
113 10   py -2.35712
114 10   py -1.74752
115 10   py -1.13792
116 10   py -0.52832
117 10   py 0.08128
118 10   py 0.69088
119 10   py 1.30048
120 10   py 1.91008
121 10   py 2.51968
122 10   py 3.12928
123 10   py 3.73888
124 10   py 4.34848
c
199      cz 6.9012 $ Al
200      cz 7.3838 $ IR pipe
201      cz 7.6581 $ OR pipe
203      cz 10.1981 $ 1" insulation
c
250      px  -9.6032 $ square tube
251      px   9.6032
252      py  -9.6032
253      py   9.6032
c
300      px  10.033 $ lattice surfaces/sq. tube
301      px -10.033
302      py  10.033
303      py -10.033
310      px -50.165 $ 5x5 bounds
311      px  50.165
312      py -50.165
313      py  50.165
320      px -80.645 $ outer bounds
321      px  80.645
322      py -80.645
323      py  80.645
324      pz -58.8963
325      pz  58.8963

m2      1001.62c  2          $ water
        8016.62c  1
mt2     lwtr.60t
m3      13027.62c 1          $ Al
m4      6000.66c   -0.08     $ SS-304
        14000.60c  -1.0
        15031.66c  -0.045
        24000.50c  -19.0
        25055.62c  -2.0
        26000.55c  -68.375
        28000.50c  -9.5
m5      1001.62c  -0.056920  $ neoprene (no Cl)
        6000.66c  -0.542646
c        17000.66c -0.400434
```

```
m6      13027.62c  -26.5     $ insulation material
        14000.60c  -23.4
        8016.62c   -50.2
m10     92234.69c 2.3613E-05 $ fuel
        92235.69c 3.6835E-03
        92236.69c 1.3657E-05
        92238.69c 1.9539E-04
        13027.62c 5.0481E-02
c           total 5.4398E-02
c
*tr2     0 -0.7798 0  30 60 90 120 30 90   $ down
*tr3     0  0.7798 0  30 60 90 120 30 90   $ up
*tr4     0.7798 0 0                        $ right
*tr5    -0.7798 0 0                        $ left
*tr6     0.5514    0.5514  0                      $ up/right
*tr7    -0.5514    0.5514  0  90 0 90 180 90 90   $ up/left
*tr8     0.5514   -0.5514  0  90 0 90 180 90 90   $ down/right
*tr9    -0.5514   -0.5514  0                      $ down/left
*tr10    0 0 0  30 120 90 60 30 90 $ rotate fuel surfaces 30 deg CCW
*tr20    -0.7798 0 0  30.2 59.8 90 120.2 30.2 90 j j j -1 $ rotate right FHE
30.2 deg CCW
*tr21     0.7798 0 0  30.2 59.8 90 120.2 30.2 90 j j j -1 $ rotate left FHE
30.2 deg CCW
c
mode   n
kcode  2500 1.0 50 250
sdef    x=d1 y=d2 z=d3
si1     -50 50
sp1     0 1
si2     -50 50
sp2     0 1
si3     -31 31
sp3     0 1
```

6.11 Appendix C: Criticality Analysis for Small Quantity Payloads

The ATR FFSC may be utilized to transport fuel with a small U-235 fissile loading (≤ 400 g U-235). This fuel may be enriched up to 94% U-235. The intent is to bound in a generic manner several classes of research and development fuel types, as the geometry and fissile loading of such fuels is subject to change. These fuel types include AFIP elements, U-Mo foils, and design demonstration elements (DDEs). In addition, some standard fuel elements, such as RINSC, classify for transport as a small quantity payload, as well as individual plates used to fabricate MURR, MIT, and Cobra fuel. The following analysis demonstrates that the ATR FFSC with small quantity payload fuel complies with the requirements of 10 CFR 71.55 and 71.59. Based on a 3x4 array of 10 undamaged packages and a 2x2 array of four damaged packages, the Criticality Safety Index (CSI), per 10 CFR 71.59, is 25.0.

6.11.1 Description of Criticality Design

6.11.1.1 Design Features Important for Criticality

No special design features are required to maintain criticality safety. No poisons are utilized in the package. The separation provided by the packaging (outer flat-to-flat dimension of 7.9-in), along with the limit on the number of packages per shipment, is sufficient to maintain criticality safety.

6.11.1.2 Summary Table of Criticality Evaluation

The upper subcritical limit (USL) for ensuring that the ATR FFSC (single package or package array) is acceptably subcritical, as determined in Section 6.11.8, *Benchmark Evaluations*, is:

$$USL = 0.9209$$

The package is considered to be acceptably subcritical if the computed k_{safe} (k_s), which is defined as $k_{effective}$ (k_{eff}) plus twice the statistical uncertainty (σ), is less than or equal to the USL, or:

$$k_s = k_{eff} + 2\sigma \leq USL$$

The USL is determined on the basis of a benchmark analysis and incorporates the combined effects of code computational bias, the uncertainty in the bias based on both benchmark-model and computational uncertainties, and an administrative margin. The results of the benchmark analysis indicate that the USL is adequate to ensure subcriticality of the package.

The packaging design is shown to meet the requirements of 10 CFR 71.55(b). Moderation by water in the most reactive credible extent is utilized in both the normal conditions of transport (NCT) and hypothetical accident conditions of transport (HAC) analyses. In the single package NCT models, full-density water fills the accessible cavity, while in the single package HAC models, full-density water fills all cavities. In all single package models, 12-in of water reflection is utilized.

A 3x4x1 array of 10 packages (2 empty locations) is utilized for the NCT array, while a 2x2x1 array of 4 packages is utilized in the HAC array. In the HAC array cases, partial moderation is considered to maximize array interaction effects. In all array models, 12-in of water reflection is utilized external to the array.

The maximum results of the criticality calculations are summarized in Table 6.11-1. The maximum calculated k_s is 0.8943, which occurs for the optimally moderated NCT array case. The NCT array is more reactive than the HAC array because the NCT array is larger, and moderation is allowed in both conditions. In this case, the fuel mixture is modeled with a height of 32.5 cm, and void is modeled between the insulation and outer tube.

6.11.1.3 Criticality Safety Index

The criticality safety index is defined in 10 CFR 71.59 as 50/N, where 5N packages are used in the NCT array configuration, and 2N packages are used in the HAC array configuration. A 2x2 array (2N = 4, or N = 2) is utilized for the HAC array calculations, while a 3x4 array of 10 packages (5N = 10, or N = 2) is utilized for the NCT array calculations. Therefore, the criticality safety index is 50/N = 50/2 = 25.0. With a CSI = 25.0, a maximum of four packages is allowed per exclusive use shipment.

Table 6.11-1 – Summary of Small Quantity Payloads Criticality Evaluation

Normal Conditions of Transport (NCT)	
Case	k_s
Single Unit Maximum	0.6478
Array Maximum	0.8943
Hypothetical Accident Conditions (HAC)	
Case	k_s
Single Unit Maximum	0.7244
Array Maximum	0.8222
USL = 0.9209	

6.11.2 Fissile Material Contents

The fissile material content is up to 400 g U-235 enriched up to 94% as a general payload material. Because HEU is modeled in the analysis, the results also apply to medium enriched uranium (MEU) and low enriched uranium (LEU) fuels. The analysis also applies to any generic fuel with U-235 as the fissile isotope. The objective is to bound research and development fuels with designs that are subject to change. The full list of anticipated contents bounded by this analysis is summarized in Section 1.2.2.4, *Small Quantity Payload*.

In general, for enrichments greater than 5% U-235, a system is more reactive using a homogenized mixture rather than an explicit heterogeneous representation[11]. Therefore, to simplify the modeling approach, the fuel is modeled as a homogenized mixture of uranium and water. Note that the homogenized representation is simply a conservative representation, and it is not implied that the actual fuel would behave in this manner. The fuel, even in accident conditions, would remain largely intact.

[11] JJ Duderstadt and LJ Hamilton, *Nuclear Reactor Analysis*, p. 405, John Wiley & Sons, Inc., 1976.

This fuel mixture is assumed to conform to the cylindrical geometry constraint of the inner circular tube of the ATR FFSC. The fuel element structural materials (i.e., aluminum, silicon, etc.) are conservatively ignored, as well as the fuel handling enclosure (FHE) that supports the fuel element (either the RINSC FHE for RINSC fuel, or the small payload FHE for the remaining fuels). Modeling the structural materials would increase parasitic neutron absorption, as well as enlarge the size of the fissile volume to achieve the same hydrogen/U-235 ratio, and both effects would decrease the reactivity. A polyethylene limit of 100 g is justified in the analysis.

The contents may contain burnable absorbers, such as gadolinium, samarium, or boron. All burnable absorbers are conservatively neglected in the analysis.

The isotopic distribution of HEU fuel used in the analysis is listed in Table 6.11-2. The U-235 enrichment is conservatively modeled at 94%, which bounds the approximately 20% enrichment of LEU fuel, and 40-80% enrichment of MEU fuel. The remaining uranium isotopic values are representative and are consistent with the values used in the ATR criticality analysis (see Section 6.2, *Fissile Material Contents*). The fuel is modeled as homogenized mixture of uranium and water. Optimum reactivity is achieved by varying the height of the fissile mixture. A useful index of moderation for homogeneous systems is the hydrogen to U-235 ratio, abbreviated as H/U-235. This parameter is adjusted by varying the height of the fissile mixture. Increasing the height of the fissile mixture increases H/U-235.

The number densities of the homogenized mixture are computed in the following manner. A U-235 mass of 400 g is modeled, which bounds the masses of the small quantity payload items. The weight percent of U-235 is 94.0%. Therefore, the total mass of uranium M_U for 400 g U-235 is 400/0.94 = 425.5 g U. The theoretical density of uranium is 19.0 g/cm^3, so the solid-volume V_U of 425.5 g U is 425.5/19.0 = 22.4 cm^3. The homogenized volume V is $\pi R^2 H$, where R is the inner radius of the ATR FFSC circular tube (7.3838 cm) and H is the height of the fissile mixture. The gram density of uranium in the mixture is then M_U/V, and if water of density 1.0 g/cm^3 fills the remaining volume, the water density in the mixture is $(V- V_U)/V$. The number densities of uranium and water may then be computed from the mixture densities. An example set of fuel mixture number densities for a height of 40 cm is provided in Table 6.11-3.

The ATR FFSC may contain hydrogenous materials. Fuel elements may be transported in a polyethylene (CH_2) bag with a mass of approximately 3 oz, or 85 g. Neoprene (C_4H_5Cl) is used as a padding material in the fuel holders, and cellulosic material ($C_6H_{10}O_5$) (e.g., kraft paper, cardboard) may be used as a cushioning material. The total mass of neoprene and cellulosic material is limited to a sum of 4000 g. Fiberglass reinforced tape may also be used to secure bundles of loose plates, and the mass of tape is conservatively treated as polyethylene. Homogenized mixtures are developed that include either polyethylene, neoprene, cellulosic material, or structural material (such as aluminum) using the same method described above. For these computations, the density of polyethylene is 0.92 g/cm^3, the density of neoprene is 1.23 g/cm^3, the density of cellulosic material is 0.44 g/cm^3, and the density of aluminum is 2.6989 g/cm^3. As an example, fuel mixture number densities are provided in Table 6.11-3 for a height of 40 cm. Mixture number densities for other heights may be computed using the methodology described above.

Table 6.11-2 – Uranium Isotopics

Isotope	Modeled HEU Isotopics (Wt. %)
U-234	0.60
U-235	94.0
U-236	0.35
U-238	5.05

This page left intentionally blank.

Table 6.11-3 – Example Fissile Mixture Number Densities for Height = 40 cm

Isotope	Fuel/Water Number Densities (atom/b-cm)	Fuel/Water Number Densities (atom/b-cm) with 100 g of Polyethylene	Fuel/Water Number Densities (atom/b-cm) with 1500 g of Neoprene	Fuel/Water Number Densities (atom/b-cm) with 1500 g of Cellulosic Material	Fuel/Water Number Densities (atom/b-cm) with 1500 g of Aluminum
U-234	9.5888E-07	9.5888E-07	9.5888E-07	9.5888E-07	9.5888E-07
U-235	1.4958E-04	1.4958E-04	1.4958E-04	1.4958E-04	1.4958E-04
U-236	5.5459E-07	5.5459E-07	5.5459E-07	5.5459E-07	5.5459E-07
U-238	7.9346E-06	7.9346E-06	7.9346E-06	7.9346E-06	7.9346E-06
H	6.6636E-02	6.6828E-02	6.2182E-02	4.1461E-02	6.1213E-02
O	3.3318E-02	3.2788E-02	2.7368E-02	2.0731E-02	3.0606E-02
C	-	6.2664E-04	5.9567E-03	4.8789E-03	-
Cl	-	-	1.4892E-03	-	-
Al	-	-	-	-	4.8865E-03
Total	1.0011E-01	1.0040E-01	9.7155E-02	6.7230E-02	9.6864E-02

This page left intentionally blank.

6.11.3 General Considerations

6.11.3.1 Model Configuration

The packaging is modeled essentially the same as described in Section 6.3.1, *Model Configuration*. Refer to that section for details of the packaging model. The package length is modeled as 48-in long to be consistent with the original criticality models using ATR fuel (which has an active length of 48-in), although this length is somewhat arbitrary and is conservatively shorter than the actual inner cavity length of 67.88-in. The package is reflected with 12-in of full-density water.

In the NCT single package models, the inner tube, insulation, and outer tube are modeled explicitly, as shown in Figure 6.11-1 and Figure 6.11-2. Although negligible water ingress is expected during NCT, the inner cavity of the package is assumed to be flooded with water because the package lid does not contain a seal. However, the region between the insulation and the outer tube will remain dry because water cannot enter this region. The fuel is transported in a Fuel Handling Enclosure (FHE), which is conservatively ignored because the fuel is homogenized with water. Modeling the FHE would decrease the reactivity significantly if it is assumed that the fuel is homogenized within the constraint of the FHE. If it is assumed that the homogenized mixture could flow out of the FHE, modeling the FHE would still be less reactive than ignoring it because it would displace fissile material and increase the size of the fissile cylinder.

Although the FHE is not modeled, hydrogenous neoprene cushioning material along the sides of the enclosure is included in the fissile mixture in the NCT array models to demonstrate the poisoning effect of neoprene. The combined mass of neoprene and cellulosic material is limited to 4000 g.

The fuel elements may be transported in a polyethylene bag with an approximate mass of 3 oz, or 85 g. A polyethylene mass of 100 g is conservatively homogenized with the fuel/water mixture when indicated. The mass of fiberglass reinforced tape, which may be used to bind loose plates, shall be included in the polyethylene mass.

The HAC single package model is essentially the same as the NCT single package model. Damage in the drop tests was shown to be negligible and concentrated at the ends of the package [See Section 2.12.1, *Certification Tests on CTU-1*]. As the ends of the package are not modeled, this end damage does not affect the modeling. The various side drops resulted in only minor localized damage to the outer tube, and no observable bulk deformation of the package. Therefore, the minor damage observed will not impact the reactivity. The insulation is replaced with full-density water, and the region between the insulation and outer tube is also filled with full-density water (see Figure 6.11-3). The treatment of the FHE is the same as the NCT single package model.

In the NCT array models, a 3x4x1 array is utilized, although two array positions are empty, for a total of 10 packages. The geometry of a package in the NCT array is the same as the NCT single package models. In the HAC array models, a 2x2x1 array is utilized. The HAC array models are essentially the same as the NCT array models, except additional cases are developed to determine the reactivity effect of allowing variable density water in the region between the inner and outer tubes. Cases are also developed with and without the insulation. The FHE is conservatively ignored for the reasons stated in the previous paragraphs. Because the NCT and HAC models are very similar and the NCT models utilize a larger array, the NCT array models are more reactive than the HAC array models.

The detailed moderation assumptions for these cases are discussed more fully in Section 6.11.5, *Evaluation of Package Arrays under Normal Conditions of Transport*, and Section 6.11.6, *Package Arrays under Hypothetical Accident Conditions*.

6.11.3.2 Material Properties

An example fissile material composition is provided in Table 6.11-3. The material properties of the packaging materials are provided in Section 6.3.2, *Material Properties*.

6.11.3.3 Computer Codes and Cross-Section Libraries

The computer codes and cross-section libraries utilized are provided in Section 6.3.3, *Computer Codes and Cross-Section Libraries*.

6.11.3.4 Demonstration of Maximum Reactivity

A number of conservative assumptions are utilized to obtain the maximum reactivity:

- The fuel is modeled as a homogeneous mixture of uranium and water, which is a significantly more reactive configuration than modeling the fuel explicitly. Fuel element structural materials are ignored in the most reactive case.
- 400 g of U-235 is modeled, which bounds the U-235 loading of the proposed contents.
- The U-235 enrichment is modeled as 94%, which bounds the enrichment of the proposed contents.

The fissile mixture is assumed to fill the inner tube of the ATR FFSC, and moderation is varied by running cases with different fissile mixture heights. No credit is taken for fuel handling enclosures that would maintain the fuel in a more favorable geometry. Note that the homogenized representation is simply a conservative representation, and it is not implied that the actual fuel would behave in this manner. The fuel, even in accident conditions, would remain largely intact.

In the NCT cases, water fills only the inner tube, because water would not enter the region between the inner circular tube and outer square tube. In the HAC cases, water is allowed in the region between the inner circular tube and outer square tube. Also, insulation may be replaced with water in the HAC cases. All single package cases are reflected with 12-in of water.

For the NCT array, 10 packages are modeled in a 3x4x1 array (with 2 empty locations), while in the HAC array, a smaller 2x2x1 array is utilized. Because negligible damage was observed in the drop tests, the package dimensions are the same between the NCT and HAC models. Dimensions of the packaging are selected to maximize reactivity, and 12-in of close-water reflection is utilized.

The NCT array analysis is rather straightforward, because the only variable is the height of the fissile mixture. In the HAC array analysis, variables include the height of the fissile mixture, the presence or absence of insulation, and the water density of the region between the circular and square tubes. These parameters are varied to find the most reactive HAC condition.

Because fuel elements may be transported in polyethylene bags, 100 g of polyethylene is included in the fissile mixture. Polyethylene has a small, but positive, effect on the reactivity. The hydrogenous materials neoprene and cellulosic material are shown to have a negative effect on reactivity because they are less effective at moderating the fissile mixture than the water that is displaced. Therefore, it is conservative to ignore neoprene and cellulosic material in the models. It is also explicitly demonstrated that modeling inert structural materials, such as aluminum, has a negative effect on the reactivity.

The NCT array is more reactive than the HAC array, primarily because the NCT array is significantly larger, and both cases use a homogenized fuel assumption. The most reactive NCT array case (Case HC16) has a fissile mixture height of 32.5 cm and results in a $k_s = 0.89427$, which is below the USL of 0.9209. The most reactive HAC array case (Case HD34) results in a $k_s = 0.82217$.

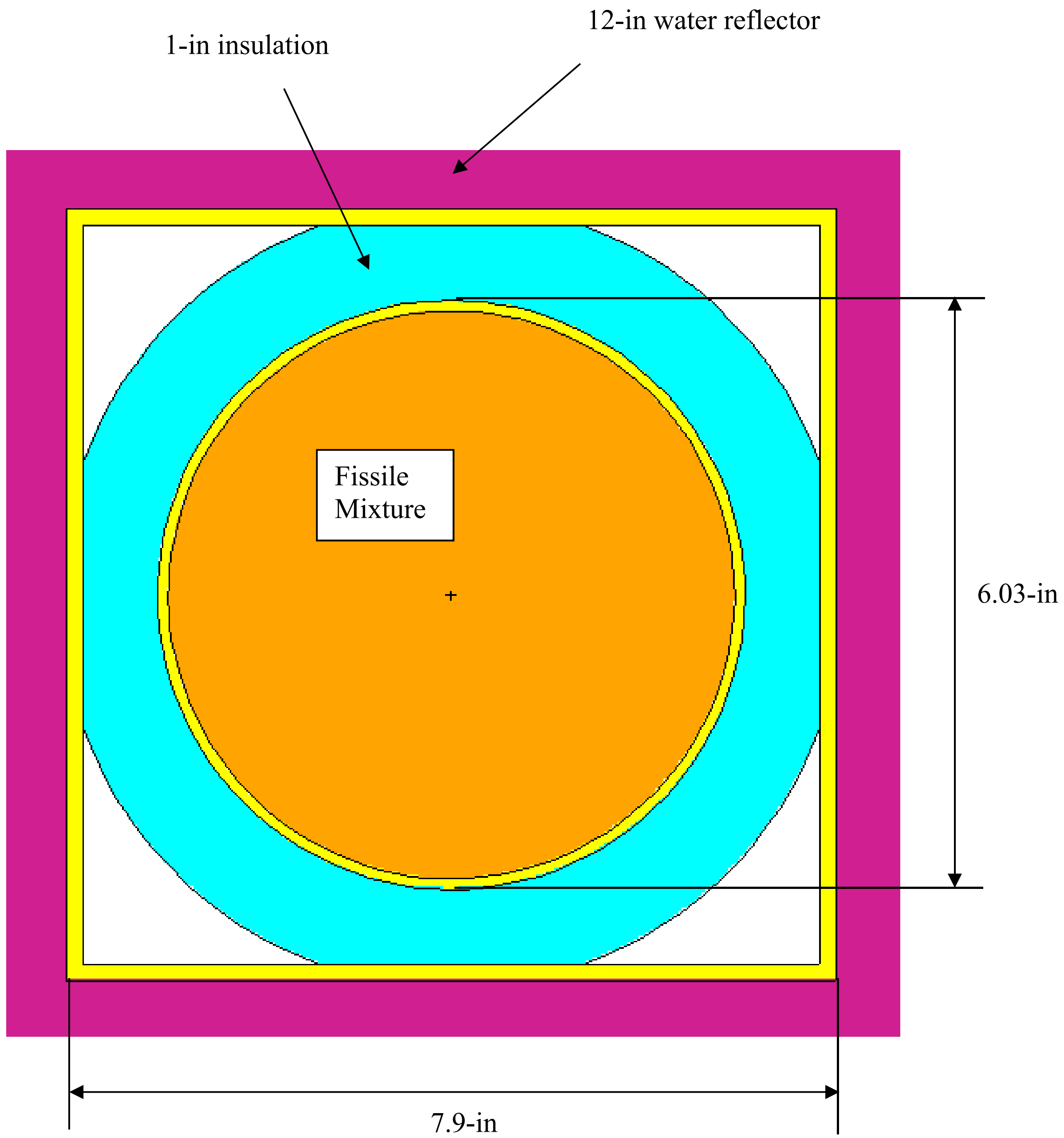

Figure 6.11-1 – NCT Single Package Model (planar view)

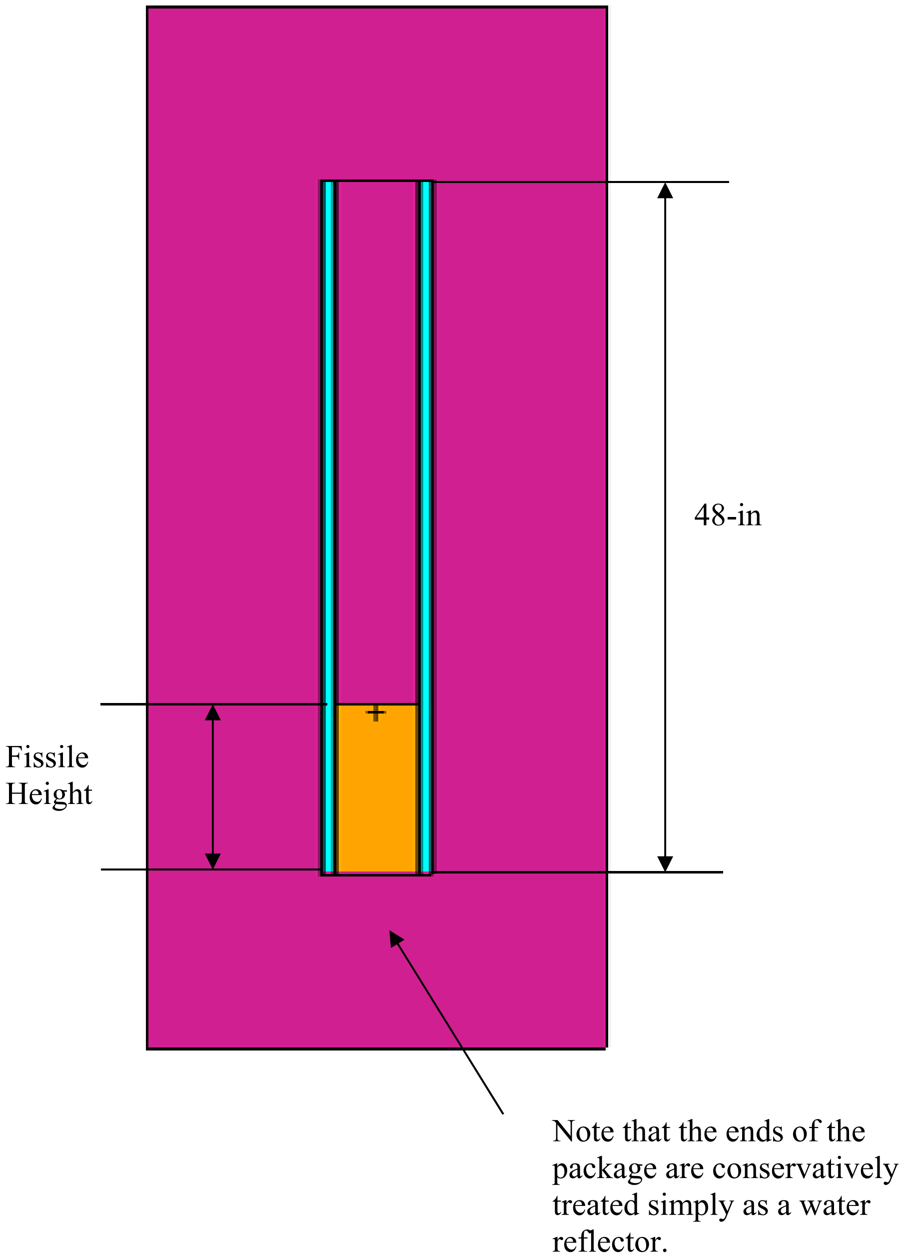

Figure 6.11-2 – NCT Single Package Model (axial view)

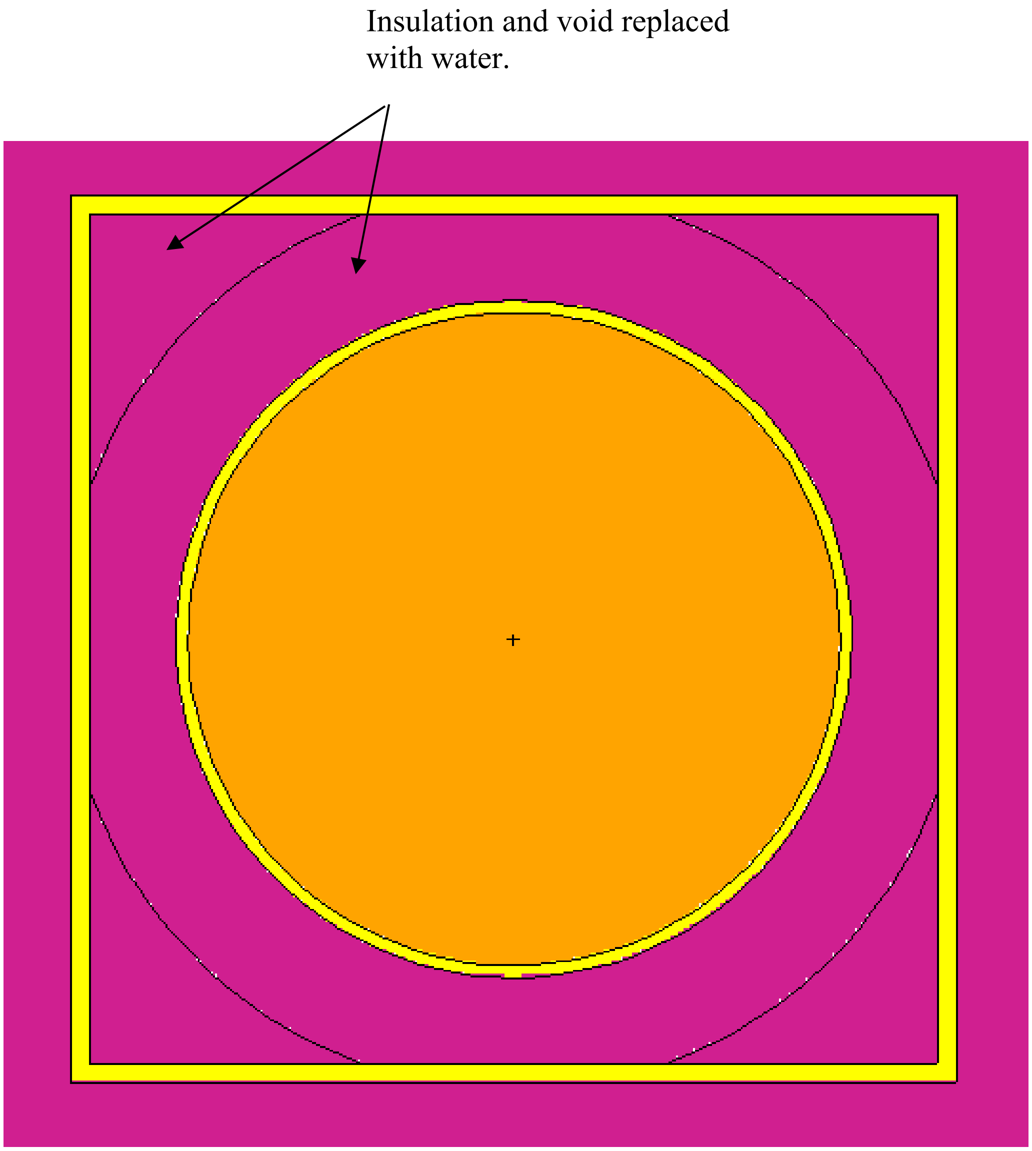

Figure 6.11-3 – HAC Single Package Model (planar view)

6.11.4 Single Package Evaluation

6.11.4.1 Single Package Configuration

6.11.4.1.1 NCT Single Package Configuration

The geometry of the NCT single package configuration is discussed in Section 6.11.3.1, *Model Configuration*. The fissile material is homogenized with water for a variety of fissile mixture heights. The water above the fissile mixture is modeled at full-density to maximize reflection. The package is reflected with 12-in of water.

It is demonstrated in Section 6.11.5 that including neoprene, cellulosic material, or structural materials in the fissile mixture reduces the reactivity, so these materials are conservatively neglected in the NCT single package configuration.

Results are provided in Table 6.11-4. Cases HA1 through HA10 are without polyethylene, and Cases HA11 through HA20 include 100 g of polyethylene. The cases with polyethylene are slightly more reactive, although the effect is small. Maximum reactivity is achieved for Case HA13, with a fissile mixture height of 25.0 cm. The reactivity of this case is low, with k_s = 0.64775. This result is below the USL of 0.9209.

6.11.4.1.2 HAC Singe Package Configuration

The geometry of the HAC single package configuration is discussed in Section 6.11.3.1, *Model Configuration*. The fissile material is homogenized with water for a variety of fissile mixture heights. The water above the fissile mixture is modeled at full-density to maximize reflection. The insulation is replaced with full-density water, and full-density water is also modeled between the inner and outer tubes. The package is reflected with 12-in of water.

It is demonstrated in Section 6.11.5 that including neoprene, cellulosic material, or structural materials in the fissile mixture reduces the reactivity, so these materials are conservatively neglected in the HAC single package configuration.

Results are provided in Table 6.11-5. Cases HB1 through HB10 are without polyethylene, and Cases HB11 through HB20 include 100 g of polyethylene. The cases with polyethylene are slightly more reactive, although the effect is small. Maximum reactivity is achieved for Case HB15, with a fissile mixture height of 27.5 cm. The reactivity of this case is low, with k_s = 0.72441. This result is below the USL of 0.9209.

6.11.4.2 Single Package Results

Following are the tabulated results for the single package cases. The most reactive configurations are listed in boldface.

Table 6.11-4 – NCT Single Package Results

Case ID	Filename	Fissile Mixture Height (cm)	k_{eff}	σ	k_s ($k+2\sigma$)
No Polyethylene					
HA1	NS_HEU_H15	15.0	0.61609	0.00130	0.61869
HA2	NS_HEU_H20	20.0	0.63614	0.00115	0.63844
HA3	NS_HEU_H25	25.0	0.64046	0.00116	0.64278
HA4	**NS_HEU_H275**	**27.5**	**0.64251**	**0.00114**	**0.64479**
HA5	NS_HEU_H30	30.0	0.64189	0.00116	0.64421
HA6	NS_HEU_H325	32.5	0.63773	0.00111	0.63995
HA7	NS_HEU_H35	35.0	0.62944	0.00106	0.63156
HA8	NS_HEU_H40	40.0	0.62060	0.00105	0.62270
HA9	NS_HEU_H45	45.0	0.60913	0.00110	0.61133
HA10	NS_HEU_H50	50.0	0.59328	0.00104	0.59536
With 100 g Polyethylene					
HA11	NS_HEUP_H15	15.0	0.62298	0.00128	0.62554
HA12	NS_HEUP_H20	20.0	0.64179	0.00112	0.64403
HA13	**NS_HEUP_H25**	**25.0**	**0.64531**	**0.00122**	**0.64775**
HA14	NS_HEUP_H275	27.5	0.64503	0.00114	0.64731
HA15	NS_HEUP_H30	30.0	0.64193	0.00113	0.64419
HA16	NS_HEUP_H325	32.5	0.63741	0.00116	0.63973
HA17	NS_HEUP_H35	35.0	0.63154	0.00113	0.63380
HA18	NS_HEUP_H40	40.0	0.62058	0.00108	0.62274
HA19	NS_HEUP_H45	45.0	0.60798	0.00109	0.61016
HA20	NS_HEUP_H50	50.0	0.59553	0.00101	0.59755

Table 6.11-5 – HAC Single Package Results

Case ID	Filename	Fissile Mixture Height (cm)	k_{eff}	σ	k_s ($k+2\sigma$)
No Polyethylene					
HB1	HS_HEU_H15	15.0	0.69170	0.00124	0.69418
HB2	HS_HEU_H20	20.0	0.71519	0.00122	0.71763
HB3	HS_HEU_H225	22.5	0.72038	0.00131	0.72300
HB4	**HS_HEU_H25**	**25.0**	**0.72067**	**0.00126**	**0.72319**
HB5	HS_HEU_H275	27.5	0.71817	0.00114	0.72045
HB6	HS_HEU_H30	30.0	0.71422	0.00120	0.71662
HB7	HS_HEU_H325	32.5	0.70809	0.00116	0.71041
HB8	HS_HEU_H35	35.0	0.70653	0.00121	0.70895
HB9	HS_HEU_H40	40.0	0.69450	0.00111	0.69672
HB10	HS_HEU_H45	45.0	0.67855	0.00120	0.68095
With 100 g Polyethylene					
HB11	HS_HEUP_H15	15.0	0.69905	0.00128	0.70161
HB12	HS_HEUP_H20	20.0	0.71848	0.00128	0.72104
HB13	HS_HEUP_H225	22.5	0.72122	0.00125	0.72372
HB14	HS_HEUP_H25	25.0	0.72136	0.00120	0.72376
HB15	**HS_HEUP_H275**	**27.5**	**0.72189**	**0.00126**	**0.72441**
HB16	HS_HEUP_H30	30.0	0.71679	0.00130	0.71939
HB17	HS_HEUP_H325	32.5	0.71212	0.00123	0.71458
HB18	HS_HEUP_H35	35.0	0.70759	0.00119	0.70997
HB19	HS_HEUP_H40	40.0	0.69424	0.00111	0.69646
HB20	HS_HEUP_H45	45.0	0.67857	0.00112	0.68081

6.11.5 Evaluation of Package Arrays under Normal Conditions of Transport

6.11.5.1 NCT Array Configuration

The NCT array model is a 3x4x1 array with two empty locations, for a total of 10 packages. The array configuration utilized is the most reactive 10 package configuration, with 9 packages in a 3x3 configuration, and one package at the center of a side, see Figure 6.11-4. Axial stacking configurations, such as 2x3x2 with two empty locations, would lower the reactivity and are not investigated. The geometry of the individual packages is the same as the NCT single package model. The entire array is reflected with 12-in of full-density water. Moderation is varied by adjusting the height of the fissile mixture. The region above the fissile mixture is filled with full density water to maximize reflection.

The following series of cases are run:

- Table 6.11-6: Moderator as pure water or water with 100 g polyethylene
- Table 6.11-7: Moderator as water with 100 g or 1500 g neoprene
- Table 6.11-8: Moderator as water with 100 g or 1500 g cellulosic material
- Table 6.11-9: Moderator as water with 100 g or 1500 g aluminum

The results for pure water and water with 100 g polyethylene are provided in Table 6.11-6. For a pure water moderator, k_s = 0.89381 at a fissile mixture height of 30 cm (Case HC5). When 100 g of polyethylene is added, k_s = 0.89427 at a fissile mixture height of 32.5 cm (Case HC16). While polyethylene is a superior moderator than water, the results with polyethylene are statistically identical to the results with pure water because the mass of added polyethylene is small.

While neoprene and cellulosic material both contain hydrogen, these materials are less effective moderators than pure water and the reactivity decreases when these materials are added to the fissile mixture, as shown in Table 6.11-7 and Table 6.11-8. The chlorine in the neoprene also acts as a poison. Therefore, it is conservative to neglect neoprene and cellulosic material in the models. A combined mass limit for neoprene plus cellulosic material of 4000 g is therefore justified.

When aluminum is added to the fissile mixture, the reactivity also decreases, as shown in Table 6.11-9. There is a sizable quantity of aluminum within the package cavity due to both the fuel cladding and FHE structural materials. Therefore, the modeling approach is inherently conservative because all metallic structural materials are neglected. Inert materials in the fuel meat, such as molybdenum or silicon, are also conservatively neglected.

The most reactive condition is Case HC16, which includes 100 g polyethylene and has a fissile height of 32.5 cm. For this case, k_s = 0.89427, which is below the USL of 0.9209.

6.11.5.2 NCT Array Results

The results for the NCT array cases are provided in the following tables. The most reactive configurations are listed in boldface.

Table 6.11-6 – NCT Array Results with Polyethylene

Case ID	Filename	Fissile Mixture Height (cm)	k_{eff}	σ	k_s ($k+2\sigma$)
Moderator: Water					
HC1	NA_HEU_H15	15.0	0.81375	0.00130	0.81635
HC2	NA_HEU_H20	20.0	0.86031	0.00130	0.86291
HC3	NA_HEU_H25	25.0	0.88140	0.00120	0.88380
HC4	NA_HEU_H275	27.5	0.88591	0.00129	0.88849
HC5	**NA_HEU_H30**	**30.0**	**0.89141**	**0.00120**	**0.89381**
HC6	NA_HEU_H325	32.5	0.89089	0.00123	0.89335
HC7	NA_HEU_H35	35.0	0.89028	0.00114	0.89256
HC8	NA_HEU_H40	40.0	0.88126	0.00116	0.88358
HC9	NA_HEU_H45	45.0	0.87387	0.00116	0.87619
HC10	NA_HEU_H50	50.0	0.85981	0.00104	0.86189
Moderator: Water with 100 g Polyethylene					
HC11	NA_HEUP_H15	15.0	0.81856	0.00130	0.82116
HC12	NA_HEUP_H20	20.0	0.86138	0.00129	0.86396
HC13	NA_HEUP_H25	25.0	0.88386	0.00119	0.88624
HC14	NA_HEUP_H275	27.5	0.88818	0.00113	0.89044
HC15	NA_HEUP_H30	30.0	0.88873	0.00122	0.89117
HC16	**NA_HEUP_H325**	**32.5**	**0.89207**	**0.00110**	**0.89427**
HC17	NA_HEUP_H35	35.0	0.88988	0.00113	0.89214
HC18	NA_HEUP_H40	40.0	0.88439	0.00110	0.88659
HC19	NA_HEUP_H45	45.0	0.87352	0.00106	0.87564
HC20	NA_HEUP_H50	50.0	0.86011	0.00110	0.86231

Table 6.11-7 – NCT Array Results with Neoprene

Case ID	Filename	Fissile Mixture Height (cm)	k_{eff}	σ	k_s ($k+2\sigma$)
Moderator: Water with 100 g Neoprene					
HC30	NA_N100_H15	15.0	0.78812	0.00045	0.78902
HC31	NA_N100_H20	20.0	0.83258	0.00043	0.83344
HC32	NA_N100_H25	25.0	0.85690	0.00044	0.85778
HC33	NA_N100_H30	30.0	0.86748	0.00042	0.86832
HC34	**NA_N100_H35**	**35.0**	**0.86790**	**0.00040**	**0.86870**
HC35	NA_N100_H40	40.0	0.86268	0.00039	0.86346
HC36	NA_N100_H45	45.0	0.85398	0.00040	0.85478
HC37	NA_N100_H50	50.0	0.84194	0.00039	0.84272
Moderator: Water with 1500 g Neoprene					
HC40	NA_HEUN_H30	30.0	0.62595	0.00096	0.62787
HC41	NA_HEUN_H35	35.0	0.63410	0.00092	0.63594
HC42	NA_HEUN_H40	40.0	0.63992	0.00099	0.64190
HC43	**NA_HEUN_H45**	**45.0**	**0.64188**	**0.00091**	**0.64370**
HC44	NA_HEUN_H50	50.0	0.63611	0.00086	0.63783
HC45	NA_HEUN_H55	55.0	0.63358	0.00079	0.63516
HC46	NA_HEUN_H60	60.0	0.62747	0.00087	0.62921

Table 6.11-8 – NCT Array Results with Cellulosic Material

Case ID	Filename	Fissile Mixture Height (cm)	k_{eff}	σ	k_s ($k+2\sigma$)
Moderator: Water with 100 g Cellulosic Material					
HC50	NA_K100_H15	15.0	0.78017	0.00044	0.78105
HC51	NA_K100_H20	20.0	0.83462	0.00047	0.83556
HC52	NA_K100_H25	25.0	0.86375	0.00043	0.86461
HC53	NA_K100_H30	30.0	0.87624	0.00045	0.87714
HC54	**NA_K100_H35**	**35.0**	**0.87873**	**0.00041**	**0.87955**
HC55	NA_K100_H40	40.0	0.87524	0.00042	0.87608
HC56	NA_K100_H45	45.0	0.86633	0.00041	0.86715
HC57	NA_K100_H50	50.0	0.85509	0.00038	0.85585
Moderator: Water with 1500 g Cellulosic Material					
HC60	NA_K1500_H40	40.0	0.69615	0.00040	0.69695
HC61	NA_K1500_H45	45.0	0.72143	0.00039	0.72221
HC62	NA_K1500_H50	50.0	0.73626	0.00039	0.73704
HC63	NA_K1500_H55	55.0	0.74237	0.00038	0.74313
HC64	**NA_K1500_H60**	**60.0**	**0.74390**	**0.00037**	**0.74464**
HC65	NA_K1500_H65	65.0	0.74255	0.00037	0.74329
HC66	NA_K1500_H70	70.0	0.73673	0.00037	0.73747
HC67	NA_K1500_H75	75.0	0.72883	0.00034	0.72951
HC68	NA_K1500_H80	80.0	0.72050	0.00033	0.72116

Table 6.11-9 – NCT Array Results with Aluminum

Case ID	Filename	Fissile Mixture Height (cm)	k_{eff}	σ	k_s (k+2σ)
Moderator: Water with 100 g Aluminum					
HC70	NA_A100_H15	15.0	0.80807	0.00047	0.80901
HC71	NA_A100_H20	20.0	0.85445	0.00045	0.85535
HC72	NA_A100_H25	25.0	0.87889	0.00043	0.87975
HC73	NA_A100_H30	30.0	0.88745	0.00043	0.88831
HC74	**NA_A100_H325**	**32.5**	**0.88880**	**0.00043**	**0.88966**
HC75	NA_A100_H35	35.0	0.88808	0.00040	0.88888
HC76	NA_A100_H40	40.0	0.88135	0.00041	0.88217
HC77	NA_A100_H45	45.0	0.87218	0.00038	0.87294
HC78	NA_A100_H50	50.0	0.86069	0.00038	0.86145
Moderator: Water with 1500 g Aluminum					
HC80	NA_A1500_H20	20.0	0.78043	0.00045	0.78133
HC81	NA_A1500_H25	25.0	0.82043	0.00044	0.82131
HC82	NA_A1500_H30	30.0	0.84233	0.00044	0.84321
HC83	NA_A1500_H35	35.0	0.85139	0.00042	0.85223
HC84	**NA_A1500_H40**	**40.0**	**0.85197**	**0.00040**	**0.85277**
HC85	NA_A1500_H45	45.0	0.84700	0.00038	0.84776
HC86	NA_A1500_H50	50.0	0.83791	0.00039	0.83869
HC87	NA_A1500_H55	55.0	0.82724	0.00036	0.82796
HC88	NA_A1500_H60	60.0	0.81461	0.00038	0.81537

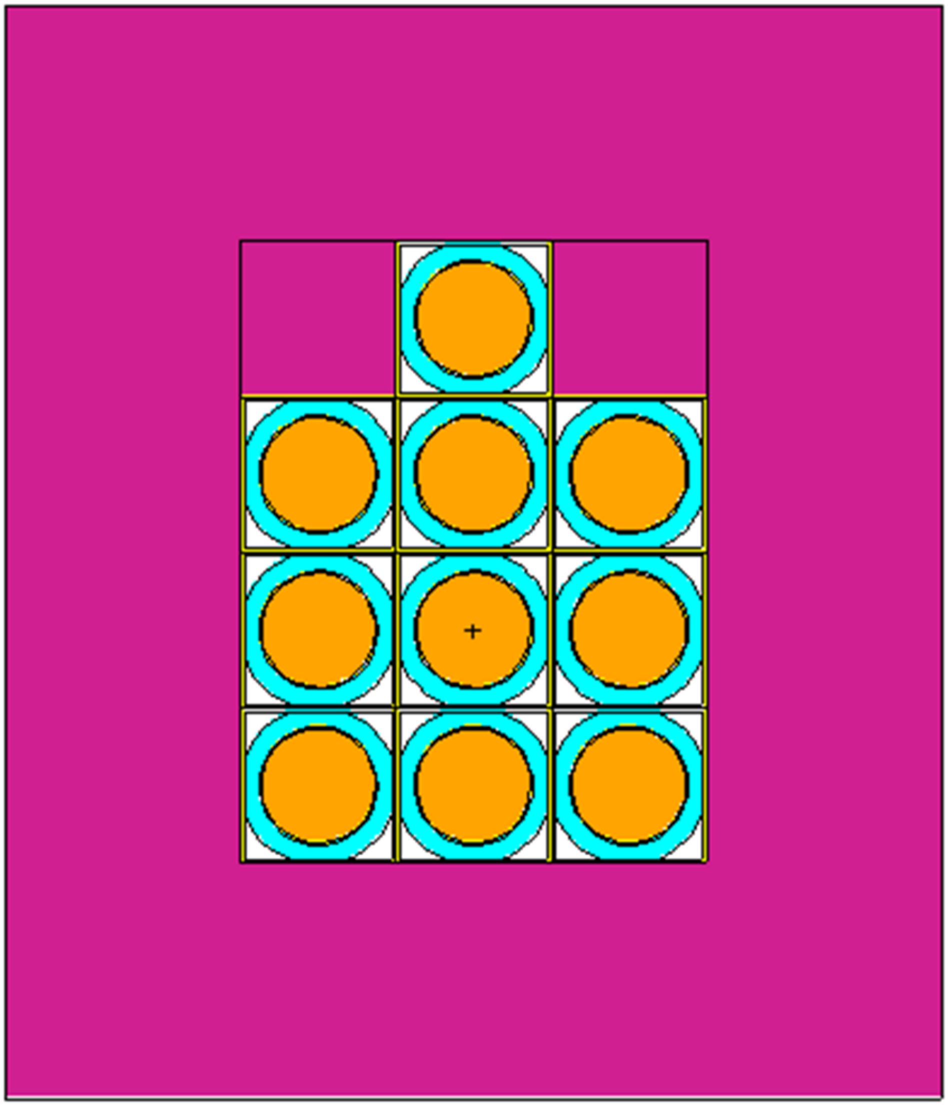

Figure 6.11-4 – NCT Array Geometry

6.11.6 Package Arrays under Hypothetical Accident Conditions

6.11.6.1 HAC Array Configuration

The HAC array model is a 2x2x1 array of the HAC single package model, as shown in Figure 6.11-5. Results are provided in Table 6.11-10. Because it has been demonstrated in the NCT single package, HAC single package, and NCT array cases that adding 100 g of polyethylene to the fissile mixture slightly increases the reactivity, all HAC array cases include 100 g of polyethylene.

In Cases HD1 through HD10, the region between the inner circular tube and outer square tube is filled with full-density water. Therefore, the insulation is replaced with water. The fissile mixture height is varied to find the optimum moderation, and the region above the fissile mixture is filled with full-density water. Of these 10 cases, Case HD4 is the most reactive, with a fissile mixture height of 25.0 cm.

In Cases HD11 through HD15, the most reactive fissile mixture height of 25.0 cm is modeled. The insulation is modeled explicitly, and a range of water densities are modeled between the insulation and outer square tube. These cases are less reactive than Case HD4, indicating that it is conservative to ignore the insulation in the HAC array models.

In Cases HD16 through HD25, Case HD4 is modified for a range of water densities between the inner circular tube and outer square tube. Case HD22 is the most reactive, with $k_s = 0.81981$ and a water density between tubes of 0.6 g/cm^3. This case is slightly more reactive than Case HD4, for which $k_s = 0.81502$. However, the reactivity gain by using a reduced water density between the tubes is small.

The most reactive fissile mixture height may change based on the water density between the tubes. For this reason, a limited number of additional cases are run for fissile mixture heights of 22.5 cm, 27.5 cm, and 30.0 cm. In Cases HD26 through HD31, the fissile mixture height is 22.5 cm and the water density is varied between 0.3 and 0.8 g/cm^3. Cases HD32 through HD37 are similar except the fissile mixture height is 27.5 cm, and in Cases HD38 through HD43 the fissile mixture height is 30.0 cm. The most reactive case is Case HD34, which is slightly more reactive than Case HD22.

Therefore, Case HD34 is the most reactive, with $k_s = 0.82217$. This case has a fissile mixture height of 27.5 cm, the insulation has been replaced with water, and the water density between the inner circular tube and outer square tube is 0.5 g/cm^3. This case is below the USL of 0.9209. Note that the most reactive HAC array case is less reactive than the most reactive NCT array case (Case HC16) because the NCT array uses 10 packages, while the HAC array uses only 4 packages.

6.11.6.2 HAC Array Results

Following are the tabulated results for the HAC array cases. The most reactive configurations are listed in boldface.

Table 6.11-10 – HAC Array Results

Case ID	Filename	Fissile Mixture Height (cm)	Water Density Between Tubes (g/cm^3)	Insulation	k_{eff}	σ	k_s (k+2σ)
HD1	HA_HEUP_H15	15.0	1.0	No	0.77954	0.00115	0.78184
HD2	HA_HEUP_H20	20.0	1.0	No	0.80655	0.00123	0.80901
HD3	HA_HEUP_H225	22.5	1.0	No	0.80899	0.00130	0.81159
HD4	**HA_HEUP_H25**	**25.0**	**1.0**	**No**	**0.81254**	**0.00124**	**0.81502**
HD5	HA_HEUP_H275	27.5	1.0	No	0.81232	0.00124	0.81480
HD6	HA_HEUP_H30	30.0	1.0	No	0.80789	0.00116	0.81021
HD7	HA_HEUP_H325	32.5	1.0	No	0.80247	0.00114	0.80475
HD8	HA_HEUP_H35	35.0	1.0	No	0.79682	0.00119	0.79920
HD9	HA_HEUP_H40	40.0	1.0	No	0.78144	0.00114	0.78372
HD10	HA_HEUP_H45	45.0	1.0	No	0.76909	0.00110	0.77129
HD11	HA_HEUP_H25_IW000	25.0	0	Yes	0.79417	0.00131	0.79679
HD12	HA_HEUP_H25_IW025	25.0	0.25	Yes	0.79759	0.00128	0.80015
HD13	HA_HEUP_H25_IW050	25.0	0.50	Yes	0.80131	0.00121	0.80373
HD14	HA_HEUP_H25_IW075	25.0	0.75	Yes	0.80017	0.00121	0.80259
HD15	HA_HEUP_H25_IW100	25.0	1.0	Yes	0.80331	0.00118	0.80567
HD16	HA_HEUP_H25_W000	25.0	0	No	0.79115	0.00126	0.79367
HD17	HA_HEUP_H25_W010	25.0	0.1	No	0.79794	0.00117	0.80028
HD18	HA_HEUP_H25_W020	25.0	0.2	No	0.80884	0.00133	0.81150
HD19	HA_HEUP_H25_W030	25.0	0.3	No	0.81008	0.00123	0.81254
HD20	HA_HEUP_H25_W040	25.0	0.4	No	0.81535	0.00116	0.81767
HD21	HA_HEUP_H25_W050	25.0	0.5	No	0.81666	0.00129	0.81924
HD22	**HA_HEUP_H25_W060**	**25.0**	**0.6**	**No**	**0.81733**	**0.00124**	**0.81981**
HD23	HA_HEUP_H25_W070	25.0	0.7	No	0.81576	0.00130	0.81836
HD24	HA_HEUP_H25_W080	25.0	0.8	No	0.81435	0.00121	0.81677
HD25	HA_HEUP_H25_W090	25.0	0.9	No	0.81266	0.00130	0.81526
HD26	HA_HEUP_H225_W030	22.5	0.3	No	0.80656	0.00134	0.80924
HD27	HA_HEUP_H225_W040	22.5	0.4	No	0.80968	0.00135	0.81238
HD28	HA_HEUP_H225_W050	22.5	0.5	No	0.81297	0.00126	0.81549
HD29	HA_HEUP_H225_W060	22.5	0.6	No	0.81408	0.00113	0.81634
HD30	HA_HEUP_H225_W070	22.5	0.7	No	0.81343	0.00114	0.81571
HD31	HA_HEUP_H225_W080	22.5	0.8	No	0.81282	0.00123	0.81528
HD32	HA_HEUP_H275_W030	27.5	0.3	No	0.81386	0.00118	0.81622
HD33	HA_HEUP_H275_W040	27.5	0.4	No	0.81679	0.00123	0.81925
HD34	**HA_HEUP_H275_W050**	**27.5**	**0.5**	**No**	**0.81993**	**0.00112**	**0.82217**
HD35	HA_HEUP_H275_W060	27.5	0.6	No	0.81757	0.00123	0.82003
HD36	HA_HEUP_H275_W070	27.5	0.7	No	0.81559	0.00114	0.81787
HD37	HA_HEUP_H275_W080	27.5	0.8	No	0.81315	0.00125	0.81565

(continued)

Table 6.11-10 – HAC Array Results (concluded)

Case ID	Filename	Fissile Mixture Height (cm)	Water Density Between Tubes (g/cm^3)	Insulation	k_{eff}	σ	k_s ($k+2\sigma$)
HD38	HA_HEUP_H30_W030	30.0	0.3	No	0.81016	0.00115	0.81246
HD39	HA_HEUP_H30_W040	30.0	0.4	No	0.81437	0.00121	0.81679
HD40	HA_HEUP_H30_W050	30.0	0.5	No	0.81585	0.00121	0.81827
HD41	HA_HEUP_H30_W060	30.0	0.6	No	0.81631	0.00113	0.81857
HD42	HA_HEUP_H30_W070	30.0	0.7	No	0.81257	0.00108	0.81473
HD43	HA_HEUP_H30_W080	30.0	0.8	No	0.81328	0.00113	0.81554

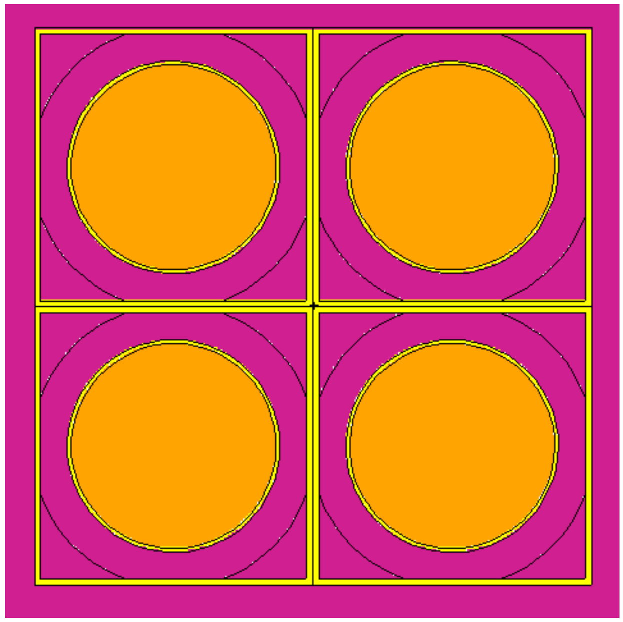

Without insulation

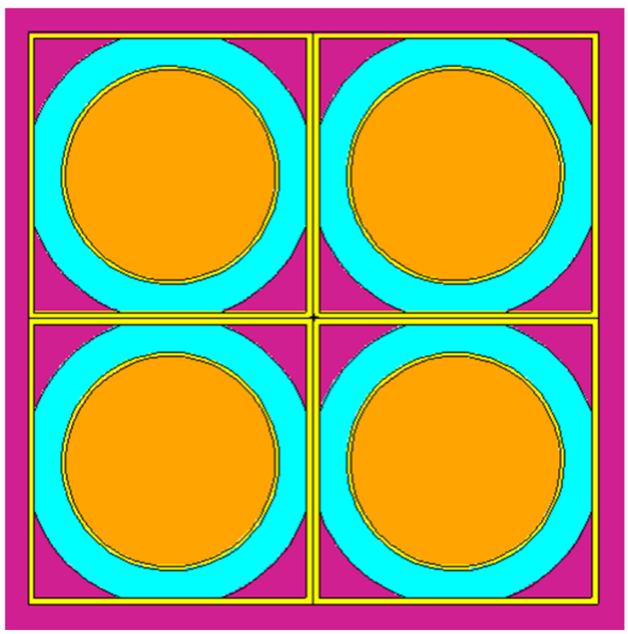

With insulation

Figure 6.11-5 – HAC Array Geometry

6.11.7 Fissile Material Packages for Air Transport

See Section 6.7, which applies to all contents.

6.11.8 Benchmark Evaluations

The Monte Carlo computer program MCNP5 v1.30[12] is utilized for this benchmark analysis. MCNP has been used extensively in criticality evaluations for several decades and is considered a standard in the industry.

The uranium isotopes utilize preliminary ENDF/B-VII cross section data that are considered by Los Alamos National Laboratory to be more accurate than ENDF/B-VI cross sections. ENDF/B-V cross sections are utilized for chromium, nickel, and iron because natural composition ENDF/B-VI cross sections are not available for these elements. The remaining isotopes utilize ENDF/B-VI cross sections. All cross sections utilized are at room temperature. A listing of the cross section libraries used in the ATR FFSC analysis is provided in Table 6.3-4. These cross sections are consistent with the cross sections utilized in the benchmarks.

The ORNL USLSTATS code[13] is used to establish a USL for the analysis. USLSTATS provides a simple means of evaluating and combining the statistical error of the calculation, code biases, and benchmark uncertainties. The USLSTATS calculation uses the combined uncertainties and data to provide a linear trend and an overall uncertainty. Computed multiplication factors, k_{eff}, for the package are deemed to be adequately subcritical if the computed value of k_s is less than or equal to the USL as follows:

$$k_s = k_{eff} + 2\sigma \leq USL$$

The USL includes the combined effects of code bias, uncertainty in the benchmark experiments, uncertainty in the computational evaluation of the benchmark experiments, and an administrative margin. This methodology has accepted precedence in establishing criticality safety limits for transportation packages complying with 10 CFR 71.

6.11.8.1 Applicability of Benchmark Experiments

The critical experiment benchmarks are selected from the *International Handbook of Evaluated Criticality Safety Benchmark Experiments*[14] based upon their similarity to the ATR FFSC and contents. The important selection parameters are high enriched uranium solutions with a thermal spectrum and no strong absorbers such as boron. Ten benchmarks are available that meet this criteria. Because this is a small benchmark set, to supplement these benchmark cases, an additional 45 benchmarks are used for high enriched uranium solutions with boron or cadmium, as well as 42 low enriched (10%) solutions without poisons. The titles for all utilized experiments are listed in Table 6.11-11.

[12] MCNP5, "*MCNP – A General Monte Carlo N-Particle Transport Code, Version 5; Volume II: User's Guide*," LA-CP-03-0245, Los Alamos National Laboratory, April, 2003.

[13] USLSTATS, "*USLSTATS: A Utility To Calculate Upper Subcritical Limits For Criticality Safety Applications,*" Version 1.4.2, Oak Ridge National Laboratory, April 23, 2003.

[14] OECD Nuclear Energy Agency, *International Handbook of Evaluated Criticality Safety Benchmark Experiments*, NEA/NSC/DOC(95)03, September, 2006.

6.11.8.2 Bias Determination

The USL is calculated by application of the USLSTATS computer program. USLSTATS receives as input the k_{eff} as calculated by MCNP, the total 1-σ uncertainty (combined benchmark and MCNP uncertainties), and a trending parameter. Two trending parameters have been selected: (1) Energy of the Average neutron Lethargy causing Fission (EALF), and (2) the ratio of the hydrogen to U-235 number density (H/U-235).

The uncertainty value, σ_{total}, assigned to each case is a combination of the benchmark uncertainty for each experiment, σ_{bench}, and the Monte Carlo uncertainty associated with the particular computational evaluation of the case, σ_{MCNP}, or:

$$\sigma_{total} = (\sigma_{bench}^2 + \sigma_{MCNP}^2)^{½}$$

These values are input into the USLSTATS program in addition to the following parameters, which are the values recommended by the USLSTATS user's manual:

- P, proportion of population falling above lower tolerance level = 0.995 (note that this parameter is required input but is not utilized in the calculation of USL Method 1)
- 1-γ, confidence on fit = 0.95
- α, confidence on proportion P = 0.95 (note that this parameter is required input but is not utilized in the calculation of USL Method 1)
- Δk_m, administrative margin used to ensure subcriticality = 0.05.

These data are followed by triplets of trending parameter value, computed k_{eff}, and uncertainty for each case. A confidence band analysis is performed on the data for each trending parameter using USL Method 1. The USL generated for each of the trending parameters utilized is provided in Table 6.11-12. All benchmark data used as input to USLSTATS are reported in Table 6.11-13.

Energy of the Average neutron Lethargy causing Fission (EALF)

The EALF is used as the first trending parameter for the benchmark cases. The EALF comparison provides a means to observe neutron spectral dependencies or trends. USLSTATS is run for all experiments, as well as the subset of experiments that do not contain poisons. The data for the subset of experiments without poisons are plotted in Figure 6.11-6, while the data for all experiments is plotted in Figure 6.11-7. Over the range of applicability, the minimum USL is 0.9344 for the subset of benchmarks that do not contain poisons, and is 0.9309 when all benchmarks are considered. In both cases the USL is trending downward for increasing EALF. Note that for the benchmarks that do not contain poison, the data tests not normal by a small margin (chi = 12.4231, upper bound = 9.49). This behavior is judged to be acceptable, both because the deviation from normal is not large, and the USL generated from this data is bounded by the USL with poison.

EALF for all ATR FFSC small quantity payload cases falls within the range of applicability. The EALF is 4.98E-08 MeV for the most reactive case (Case HC16).

H/U-235 Atom Ratio

The H/U-235 atom ratio is used as the second trending parameter for the benchmark cases. The data for the subset of experiments without poisons are plotted in Figure 6.11-8, while the data for all experiments is plotted in Figure 6.11-9. Over the range of applicability, the minimum USL is 0.9401 for the subset of benchmarks that do not contain poisons, and is 0.9359 when all benchmarks are considered. The USL is relatively constant over the range of applicability when no poisons are considered, and is trending downward for decreasing H/U-235 when all benchmarks are considered. Note that for the benchmarks that do not contain poison, the data tests not normal by a small margin (chi = 12.4231, upper bound = 9.49). This behavior is judged to be acceptable, both because the deviation from normal is not large, and the USL generated from this data is bounded by the USL with poison.

The H/U-235 atom ratio for all ATR FFSC small quantity payload cases falls within the range of applicability. The H/U-235 atom ratio is 363 for the most reactive case (Case HC16).

Recommended USL

For the H/U-235 trending parameter, the minimum USL is 0.9359, while for the EALF trending parameter, the USL is 0.9309. Therefore, a USL of 0.9309 could be justified. However, a benchmark analysis was also performed for high-enriched plate fuel for the original ATR FFSC criticality analysis (see Section 6.8, *Benchmark Evaluations*). In that section, a USL of 0.9209 is justified. Therefore, a USL of 0.9209 is conservatively selected as the USL for this analysis for consistency.

Table 6.11-11 – Benchmark Experiments Utilized

Series	Title
HEU-SOL-THERM-001	Minimally Reflected Cylinders of Highly Enriched Solutions of Uranyl Nitrate
HEU-SOL-THERM-027	Uranium (89% ^{235}U) Nitrate Solution with Central Boron Carbide or Cadmium Absorber Rod
HEU-SOL-THERM-028	Uranium (89% ^{235}U) Nitrate Solutions with Central Boron Carbide Absorber Rod
HEU-SOL-THERM-029	Uranium (89% ^{235}U) Nitrate Solution with Cluster of Seven Boron Carbide Absorber Rods
HEU-SOL-THERM-030	Uranium (89% ^{235}U) Nitrate Solution with Cluster of Several Boron Carbide Absorber Rods
HEU-SOL-THERM-036	Square-Pitched Lattices of Boron Carbide Absorber Rods In Uranium (89% ^{235}U) Nitrate Solutions
LEU-SOL-THERM-003	Full and Truncated Bare Spheres of 10% Enriched Uranyl Nitrate Water Solutions
LEU-SOL-THERM-004	Stacy: Water-Reflected 10%-Enriched Uranyl Nitrate Solution in a 60-cm-Diameter Cylindrical Tank
LEU-SOL-THERM-007	Stacy: Unreflected 10%-Enriched Uranyl Nitrate Solution in a 60-cm-Diameter Cylindrical Tank
LEU-SOL-THERM-016	Stacy: 28-cm-Thick Slabs of 10%-Enriched Uranyl Nitrate Solutions, Water-Reflected
LEU-SOL-THERM-017	Stacy: 28-cm-Thick Slabs of 10%-Enriched Uranyl Nitrate Solutions, Unreflected
LEU-SOL-THERM-020	Stacy: 80-cm-Diameter Cylindrical Tank of 10%-Enriched Uranyl Nitrate Solutions, Water-Reflected
LEU-SOL-THERM-021	Stacy: 80-cm-Diameter Cylindrical Tank of 10%-Enriched Uranyl Nitrate Solutions, Unreflected

Table 6.11-12 – USL Results

Trending Parameter (X)	Experiment Set	Minimum USL Over Range of Applicability	Range of Applicability
EALF (MeV)	No poison (1-10, 56-97)	0.9344	3.43E-08 ≤ x ≤ 2.95E-07
EALF (MeV)	All	0.9309	3.43E-08 ≤ x ≤ 2.95E-07
H/U-235	No poison (1-10, 56-97)	0.9401	68.2 ≤ x ≤ 1437.5
H/U-235	All	0.9359	68.2 ≤ x ≤ 1437.5

Table 6.11-13 – Benchmark Experiment Data

No	Case	k	σ_{mcnp}	σ_{bench}	σ_{total}	EALF (MeV)	H/U-235
1	HST001_C01	0.99661	0.00100	0.0060	0.0061	8.17E-08	181.8
2	HST001_C02	0.99185	0.00096	0.0072	0.0073	2.76E-07	70.6
3	HST001_C03	0.99921	0.00090	0.0035	0.0036	8.00E-08	185.7
4	HST001_C04	0.99586	0.00094	0.0053	0.0054	2.93E-07	68.2
5	HST001_C05	0.99785	0.00079	0.0049	0.0050	4.28E-08	499.4
6	HST001_C06	1.00159	0.00081	0.0046	0.0047	4.45E-08	458.8
7	HST001_C07	0.99693	0.00092	0.0040	0.0041	7.70E-08	193.3
8	HST001_C08	0.99696	0.00094	0.0038	0.0039	8.18E-08	181.8
9	HST001_C09	0.99087	0.00101	0.0054	0.0055	2.95E-07	68.2
10	HST001_C10	0.99005	0.00086	0.0054	0.0055	4.61E-08	427.4
11	HST027_C01	0.99609	0.00093	0.0046	0.0047	7.42E-08	203.6
12	HST027_C02	0.99522	0.00090	0.0043	0.0044	7.49E-08	203.6
13	HST027_C03	0.99626	0.00089	0.0037	0.0038	7.52E-08	203.6
14	HST027_C04	0.99780	0.00093	0.0037	0.0038	7.53E-08	203.6
15	HST027_C05	0.99563	0.00086	0.0044	0.0045	7.58E-08	203.6
16	HST027_C06	0.99028	0.00095	0.0043	0.0044	7.50E-08	203.6
17	HST027_C07	0.99604	0.00094	0.0038	0.0039	7.50E-08	203.6
18	HST027_C08	0.99772	0.00091	0.0035	0.0036	7.48E-08	203.6
19	HST027_C09	0.99517	0.00090	0.0039	0.0040	7.49E-08	203.6
20	HST028_C01	0.99350	0.00080	0.0023	0.0024	4.72E-08	374.6
21	HST028_C02	0.99332	0.00078	0.0034	0.0035	4.77E-08	374.6
22	HST028_C03	0.99596	0.00080	0.0026	0.0027	4.71E-08	374.6
23	HST028_C04	0.99814	0.00078	0.0028	0.0029	4.76E-08	374.6
24	HST028_C05	0.99070	0.00077	0.0031	0.0032	4.74E-08	374.6
25	HST028_C06	0.99492	0.00080	0.0023	0.0024	4.77E-08	374.6
26	HST028_C07	0.99497	0.00082	0.0038	0.0039	4.77E-08	374.6
27	HST028_C08	0.99433	0.00083	0.0027	0.0028	4.81E-08	374.6
28	HST028_C09	0.99179	0.00088	0.0049	0.0050	1.45E-07	91.5
29	HST028_C10	0.99032	0.00086	0.0053	0.0054	1.46E-07	91.5
30	HST028_C11	0.99179	0.00090	0.0051	0.0052	1.47E-07	91.5
31	HST028_C12	0.99009	0.00083	0.0046	0.0047	1.49E-07	91.5
32	HST028_C13	0.99102	0.00089	0.0058	0.0059	1.49E-07	91.5
33	HST028_C14	0.99180	0.00086	0.0046	0.0047	1.51E-07	91.5
34	HST028_C15	1.00006	0.00092	0.0064	0.0065	1.50E-07	91.5
35	HST028_C16	0.99561	0.00084	0.0052	0.0053	1.52E-07	91.5
36	HST028_C17	0.99144	0.00087	0.0066	0.0067	1.53E-07	91.5
37	HST028_C18	0.99322	0.00085	0.0060	0.0061	1.54E-07	91.5
38	HST029_C01	0.99468	0.00088	0.0066	0.0067	1.58E-07	91.5

(continued)

Table 6.11-13 – Benchmark Experiment Data

No	Case	k	σ_{mcnp}	σ_{bench}	σ_{total}	EALF (MeV)	H/U-235
39	HST029_C02	0.99722	0.00085	0.0058	0.0059	1.58E-07	91.5
40	HST029_C03	0.99112	0.00090	0.0068	0.0069	1.59E-07	91.5
41	HST029_C04	0.99158	0.00087	0.0074	0.0075	1.67E-07	91.5
42	HST029_C05	0.99602	0.00085	0.0067	0.0068	1.69E-07	91.5
43	HST029_C06	0.99484	0.00092	0.0065	0.0066	1.69E-07	91.5
44	HST029_C07	0.99381	0.00089	0.0063	0.0064	1.68E-07	91.5
45	HST030_C01	0.99405	0.00078	0.0039	0.0040	4.78E-08	374.6
46	HST030_C02	0.99786	0.00079	0.0032	0.0033	4.85E-08	374.6
47	HST030_C03	0.99465	0.00075	0.0031	0.0032	4.88E-08	374.6
48	HST030_C04	0.99533	0.00092	0.0064	0.0065	1.58E-07	91.1
49	HST030_C05	0.99334	0.00085	0.0058	0.0059	1.60E-07	91.1
50	HST030_C06	0.99430	0.00084	0.0059	0.0060	1.61E-07	91.1
51	HST030_C07	0.99458	0.00082	0.0064	0.0065	1.65E-07	91.1
52	HST036_C01	0.99355	0.00086	0.0045	0.0046	5.58E-08	302.5
53	HST036_C02	0.99779	0.00084	0.0039	0.0040	5.79E-08	302.5
54	HST036_C03	0.99834	0.00084	0.0044	0.0045	6.05E-08	302.5
55	HST036_C04	0.99971	0.00078	0.0062	0.0062	6.31E-08	302.5
56	LST003_C01	0.99621	0.00040	0.0039	0.0039	4.10E-08	770.3
57	LST003_C02	0.99383	0.00038	0.0042	0.0042	3.91E-08	877.6
58	LST003_C03	0.99926	0.00038	0.0042	0.0042	3.89E-08	897.0
59	LST003_C04	0.99292	0.00036	0.0042	0.0042	3.87E-08	913.2
60	LST003_C05	0.99641	0.00032	0.0048	0.0048	3.59E-08	1173.4
61	LST003_C06	0.99695	0.00030	0.0049	0.0049	3.57E-08	1213.1
62	LST003_C07	0.99535	0.00030	0.0049	0.0049	3.55E-08	1239.8
63	LST003_C08	0.99894	0.00027	0.0052	0.0052	3.45E-08	1411.6
64	LST003_C09	0.99697	0.00025	0.0052	0.0052	3.43E-08	1437.5
65	LST004_C01	1.00136	0.00067	0.0008	0.0010	4.17E-08	719.0
66	LST004_C29	1.00057	0.00065	0.0009	0.0011	4.08E-08	771.3
67	LST004_C33	0.99847	0.00059	0.0009	0.0011	3.96E-08	842.2
68	LST004_C34	1.00148	0.00061	0.0010	0.0012	3.88E-08	895.8
69	LST004_C46	1.00196	0.00052	0.0010	0.0011	3.82E-08	941.7
70	LST004_C51	0.99877	0.00056	0.0011	0.0012	3.78E-08	982.5
71	LST004_C54	1.00160	0.00052	0.0011	0.0012	3.73E-08	1017.5
72	LST007_C01	0.99414	0.00045	0.0009	0.0010	4.25E-08	709.2
73	LST007_C02	0.99734	0.00044	0.0009	0.0010	4.11E-08	770.0
74	LST007_C03	0.99472	0.00041	0.0010	0.0011	3.99E-08	842.2
75	LST007_C04	0.99791	0.00038	0.0011	0.0012	3.91E-08	896.0
76	LST007_C05	0.99628	0.00038	0.0011	0.0012	3.85E-08	942.2
77	LST016_C105	1.00345	0.00047	0.0013	0.0014	5.14E-08	468.7
78	LST016_C113	1.00438	0.00049	0.0013	0.0014	4.89E-08	514.2
79	LST016_C125	1.00368	0.00045	0.0014	0.0015	4.51E-08	608.4
80	LST016_C129	1.00225	0.00041	0.0014	0.0015	4.39E-08	650.2

(continued)

Table 6.11-13 – Benchmark Experiment Data (concluded)

No	Case	k	σ_{mcnp}	σ_{bench}	σ_{total}	EALF (MeV)	H/U-235
81	LST016_C131	1.00227	0.00044	0.0014	0.0015	4.26E-08	699.1
82	LST016_C140	1.00142	0.00041	0.0015	0.0016	4.17E-08	738.9
83	LST016_C196	1.00218	0.00041	0.0015	0.0016	4.11E-08	771.8
84	LST017_C104	1.00273	0.00050	0.0013	0.0014	5.15E-08	468.7
85	LST017_C122	1.00223	0.00049	0.0013	0.0014	4.94E-08	510.8
86	LST017_C123	1.00095	0.00045	0.0014	0.0015	4.52E-08	610.9
87	LST017_C126	1.00158	0.00044	0.0014	0.0015	4.39E-08	650.1
88	LST017_C130	1.00164	0.00046	0.0015	0.0016	4.27E-08	699.2
89	LST017_C147	1.00152	0.00042	0.0015	0.0016	4.20E-08	729.0
90	LST020_C01	0.99867	0.00038	0.0010	0.0011	3.78E-08	971.0
91	LST020_C02	0.99796	0.00034	0.0010	0.0011	3.69E-08	1053.9
92	LST020_C03	0.99807	0.00033	0.0012	0.0012	3.60E-08	1168.0
93	LST020_C04	0.99839	0.00031	0.0012	0.0012	3.54E-08	1239.3
94	LST021_C01	0.99672	0.00038	0.0009	0.0010	3.79E-08	971.0
95	LST021_C02	0.99767	0.00035	0.0010	0.0011	3.71E-08	1052.7
96	LST021_C03	0.99630	0.00034	0.0011	0.0012	3.61E-08	1168.0
97	LST021_C04	0.99786	0.00032	0.0012	0.0012	3.57E-08	1238.9

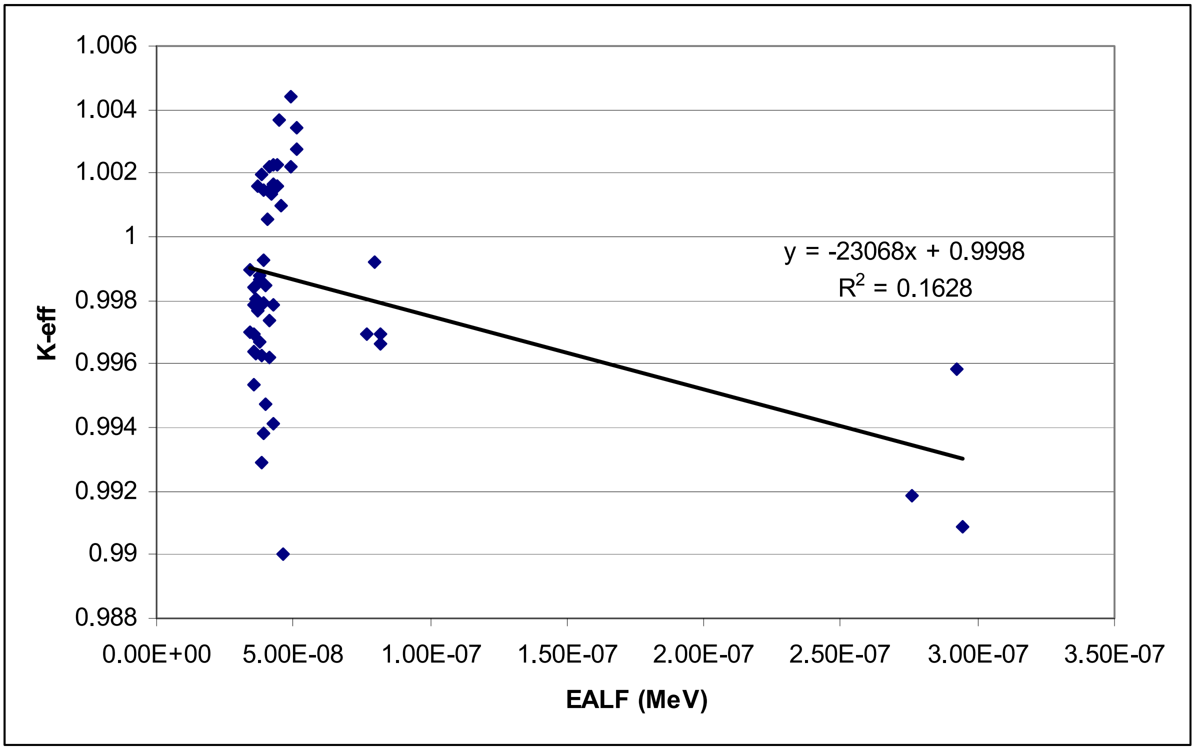

Figure 6.11-6 – Benchmark Data Trend for EALF (no poisons)

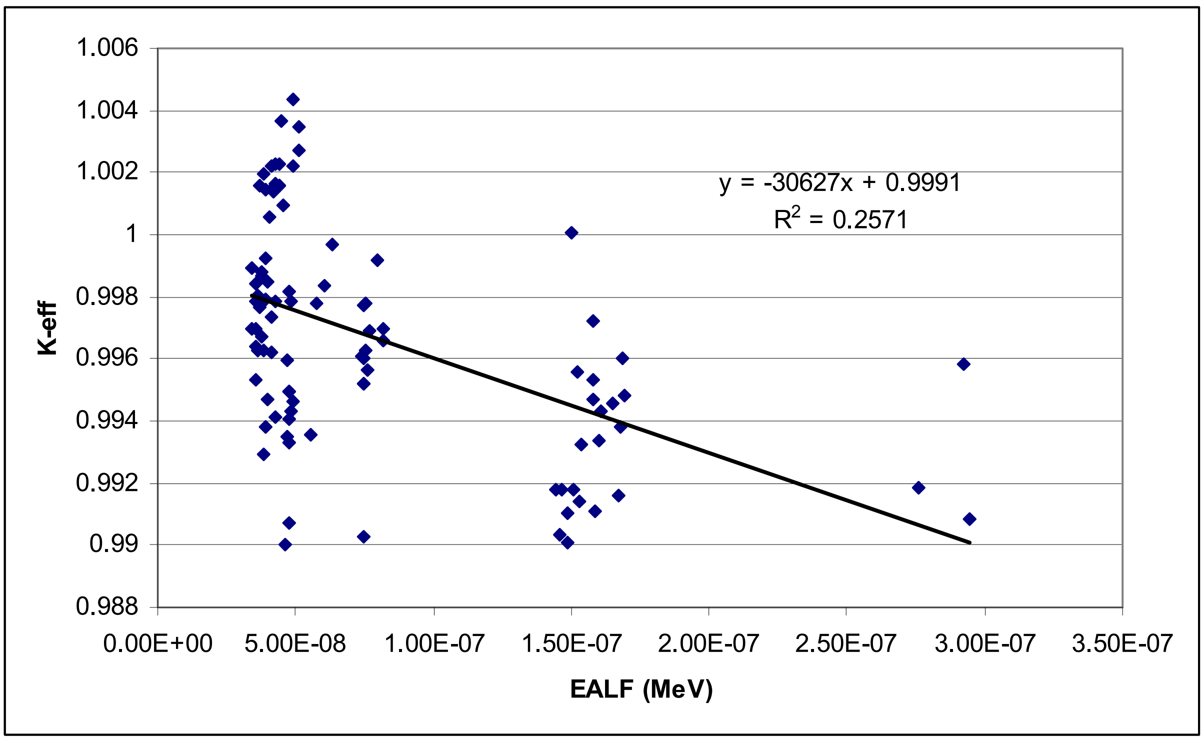

Figure 6.11-7 – Benchmark Data Trend for EALF (all)

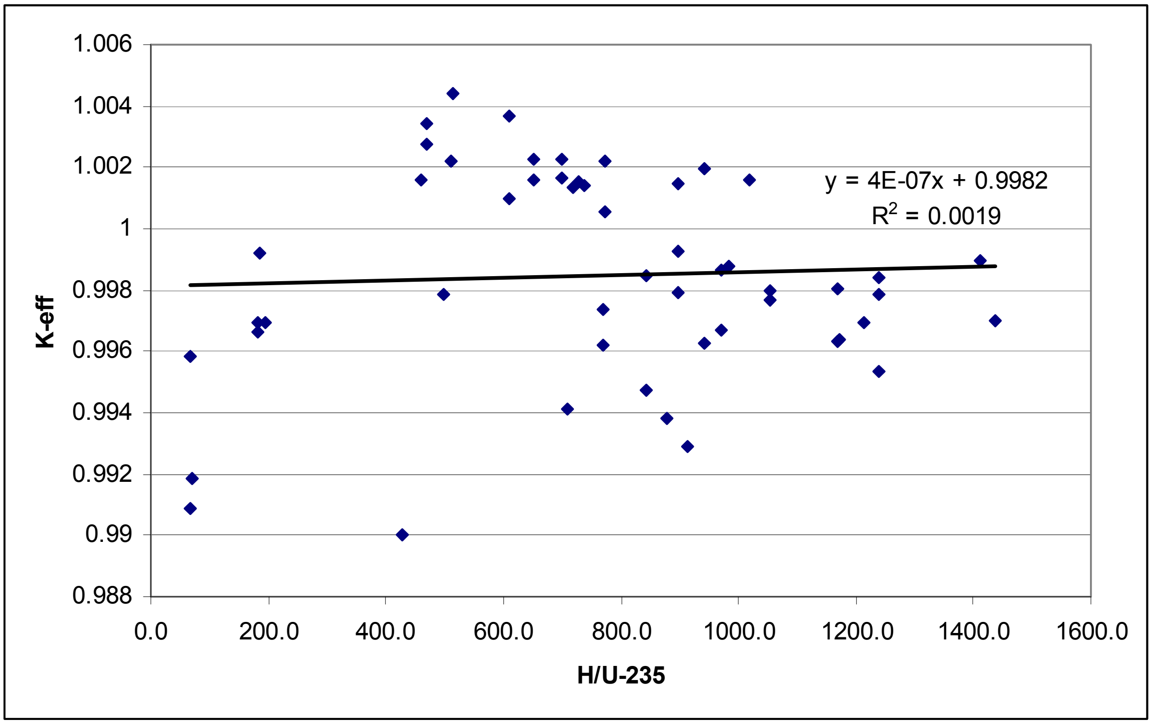

Figure 6.11-8 – Benchmark Data Trend for H/U-235 (no poisons)

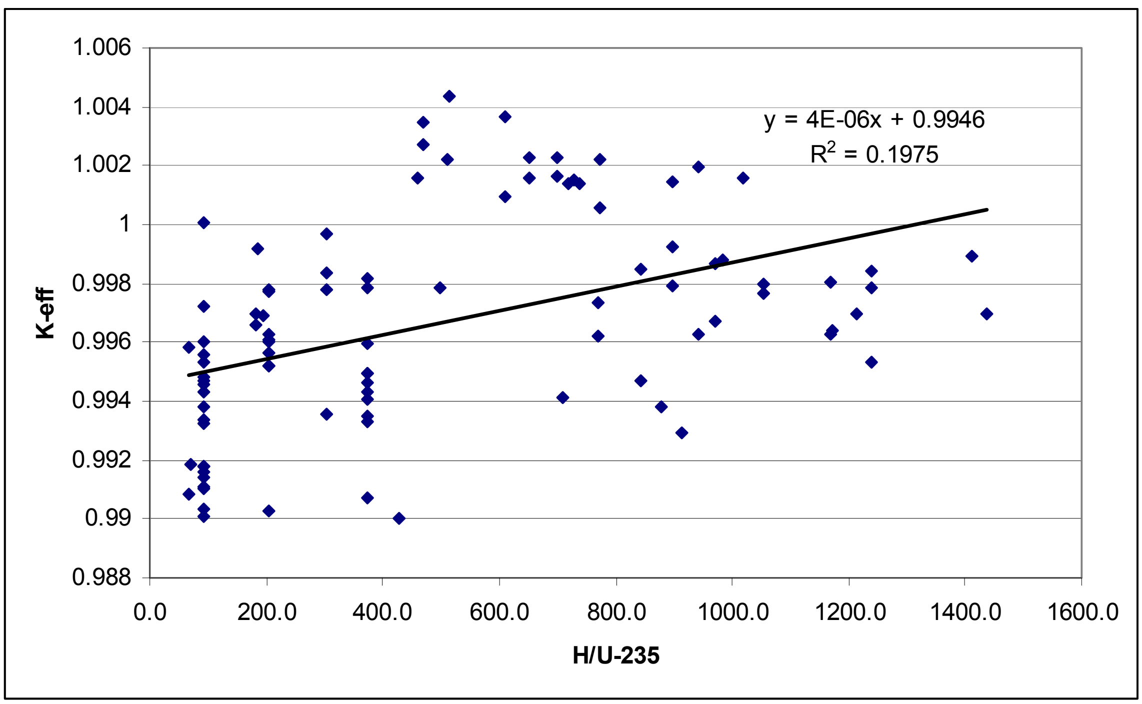

Figure 6.11-9 – Benchmark Data Trend for H/U-235 (all)

6.11.9 Sample Input Files

A sample input file (NA_HEUP_H325) is provided for the most reactive case (Case HC16).

```
ATR Package
999     0      -320:321:-322:323:-324:325                imp:n=0
900     0      310 -311 312 -313 24 -25     fill=3       imp:n=1
901     2 -1.0 (311:-310:313:-312:-24:25) 320 -321 322 -323 324 -325  imp:n=1
c
c       Universe 20: Fuel mixture with pipe
c
200     10 1.0043E-01 -26 -200                   u=20 imp:n=1 $ fuel mix
201     2 -1.0         26 -200                   u=20 imp:n=1 $ water above
fuel
202     4 -7.94     200 -201                     u=20 imp:n=1 $ pipe
203     6 -0.096    201 -203 250 -251 252 -253 u=20 imp:n=1 $ insulation
204     0           203 250 -251 252 -253      u=20 imp:n=1 $ insulation to
tube
205     4 -7.94     -250:251:-252:253          u=20 imp:n=1 $ tube to inf
c
c       Universe 21: Water
c
210     2 -1.0      -204                       u=21 imp:n=1
c
c       Universe 3: Array of Packages
c
300   0    -300 301 -302 303 imp:n=1 u=3 lat=1 fill=-1:1 -1:2 0:0
             20 20 20
             20 20 20
             20 20 20
             21 20 21

24      pz  0             $ bottom of fuel
25      pz  121.92        $ top of cavity (48")
26      pz  32.5          $ top of fuel mix
c
200      cz 7.3838  $ IR pipe
201      cz 7.6581  $ OR pipe
203      cz 10.1981 $ 1" insulation
204      pz 1000    $ dummy
c
250      px  -9.6032 $ square tube
251      px   9.6032
252      py  -9.6032
253      py   9.6032
c
300      px  10.033 $ lattice surfaces/sq. tube
301      px -10.033
302      py  10.033
303      py -10.033
310      px -30.099 $ 3x4 bounds
311      px  30.099
312      py -30.099
313      py  50.165
320      px -60.579 $ outer bounds
321      px  60.579
```

```
322      py -60.579
323      py  80.645
324      pz -30.48
325      pz  152.4

m2      1001.62c  2          $ water
        8016.62c  1
mt2     lwtr.60t
m3      13027.62c 1          $ Al
m4      6000.66c   -0.08     $ SS-304
        14000.60c  -1.0
        15031.66c  -0.045
        24000.50c  -19.0
        25055.62c  -2.0
        26000.55c  -68.375
        28000.50c  -9.5
m5      1001.62c  -0.056920  $ neoprene
        6000.66c  -0.542646
c       17000.66c -0.400434
m6      13027.62c  -26.5     $ insulation material
        14000.60c  -23.4
        8016.62c   -50.2
m10    92234.69c 1.1802E-06 $ HEU fuel H=32.5 M235=400.0 100g Poly
       92235.69c 1.8410E-04
       92236.69c 6.8258E-07
       92238.69c 9.7657E-06
        1001.62c 6.6822E-02
        6000.66c 7.7125E-04
        8016.62c 3.2640E-02
c          Total 1.0043E-01
mt10    lwtr.60t
c
mode   n
kcode  2500 1.0 50 250
sdef    x=d1 y=d2 z=d3
si1     -30 30
sp1     0 1
si2     -30 50
sp2     0 1
si3     0 32.5
sp3     0 1
```

6.12 Appendix D: Criticality Analysis for the U-Mo Demonstration Element

The Advanced Test Reactor (ATR) Fresh Fuel Shipping Container (FFSC) is used to transport a single high-enriched uranium ATR fuel element. A demonstration element has been developed using low-enriched uranium (LEU) for several of the fuel plates. To achieve the necessary fissile mass in the LEU fuel plates, the fuel matrix for these plates is being changed from UAl_x to U-Mo, which allows a much higher uranium density. Several full-sized U-Mo demonstration elements are to be tested in the ATR. Therefore, a criticality analysis is performed for the U-Mo demonstration element to allow shipment in the ATR FFSC. The following analyses demonstrate that the ATR FFSC complies with the requirements of 10 CFR §71.55 and §71.59. Based on the analysis, the Criticality Safety Index (CSI), per 10 CFR §71.59, is 4.0.

6.12.1 Description of Criticality Design

6.12.1.1 Design Features

No special design features are required to maintain criticality safety. No poisons are utilized in the package. The separation provided by the packaging (outer flat-to-flat dimension of 7.9-in), along with the limit on the number of packages per shipment, is sufficient to maintain criticality safety.

6.12.1.2 Summary Table of Criticality Evaluation

The upper subcritical limit (USL) for ensuring that the ATR FFSC (single package or package array) is acceptably subcritical, as determined in Section 6.12.8, *Benchmark Evaluations*, is:

$$USL = 0.9209$$

The package is considered to be acceptably subcritical if the computed k_{safe} (k_s), which is defined as $k_{effective}$ (k_{eff}) plus twice the statistical uncertainty (σ), is less than or equal to the USL, or:

$$k_s = k_{eff} + 2\sigma \leq USL$$

The USL is determined on the basis of a benchmark analysis and incorporates the combined effects of code computational bias, the uncertainty in the bias based on both benchmark-model and computational uncertainties, and an administrative margin. The results of the benchmark analysis indicate that the USL is adequate to ensure subcriticality of the package.

The packaging design is shown to meet the requirements of 10 CFR 71.55(b). Moderation by water in the most reactive credible extent is utilized in both the normal conditions of transport (NCT) and hypothetical accident conditions of transport (HAC) analyses. In the single package NCT models, full-density water fills the accessible cavity, while in the single package HAC models, full-density water fills all cavities. In the fuel element models, the most reactive credible configuration is utilized by maximizing the gap between the fuel plates. Maximizing this gap maximizes the moderation and hence the reactivity because the system is undermoderated. In all single package models, 12-in of water reflection is utilized.

In the NCT and HAC array cases, partial moderation is considered to maximize array interaction effects. A 9x9x1 array is utilized for the NCT array, while a 5x5x1 array is utilized in the HAC array. In all array models, 12-in of water reflection is utilized.

The maximum results of the criticality calculations are summarized in Table 6.12-1. The maximum calculated k_s is 0.7879, which occurs for the optimally moderated NCT array case. The NCT array is more reactive than the HAC array because the NCT array is larger, and moderation is allowed in both conditions. In this case, the fuel element is moderated with full-density water, the inner tube is moderated with 0.3 g/cm^3 water, and void is modeled between the insulation and outer tube.

Table 6.12-1 – Summary of Criticality Evaluation, U-Mo Demonstration Element

Normal Conditions of Transport (NCT)	
Case	k_s
Single Unit Maximum	0.4055
9x9 Array Maximum	0.7879
Hypothetical Accident Conditions (HAC)	
Case	k_s
Single Unit Maximum	0.4344
5x5 Array Maximum	0.7054
USL = 0.9209	

6.12.1.3 Criticality Safety Index

A 5x5 array (2N = 25, or N = 12.5) is utilized for the HAC array calculations, while a 9x9 array (5N = 81, or N = 16.2) is utilized for the NCT array calculations. Therefore, the criticality safety index is computed with the smaller value of N, or 50/N = 50/12.5 = 4.0. With a CSI = 4.0, a maximum of twenty-five (25) packages are allowed per exclusive use shipment.

6.12.2 Fissile Material Contents

The package can accommodate one ATR U-Mo demonstration element. A schematic of the demonstration element is provided in Figure 6.12-1. The demonstration element contains 19 plates. Plates 1-4 and 16-18 are standard UAl_x, plates 5-15 are U-Mo, and plate 19 is solid aluminum (no fuel). Each element contains 1215.73 ± 21.15 g U-235.

For the UAl_x plates, the U-235 is enriched up to 94%, with 1.2 wt.% U-234 (max), and 0.7 wt.% U-236 (max). For the U-Mo plates, the U-235 is enriched up to 19.95%, with 0.26 wt.% U-234 (max), and 0.46 wt.% U-236 (max).

The external geometry of the demonstration element is essentially identical to the external geometry of a standard ATR element shown on Figure 6.2-1. The width (or arc length) of the U-Mo fuel meat is also the same as a standard UAl_x element. However, the U-Mo fuel meat thickness is 0.013-in, and a 0.001-in zirconium interlayer is present between the fuel meat and the cladding. The cladding material is aluminum 6061 for all fuel plates.

The standard ATR fuel element models are modified to be consistent with the U-Mo demonstration element. It was determined in Section 6.4.1.2.1, *Fuel Element Payload Parametric Evaluation*, that reactivity for an ATR element is maximized when the arc length of the fuel meat is maximized, so the maximum fuel meat arc lengths for a standard ATR element are used without modification.

It is necessary to determine the number densities of the fuel meat. To determine the number densities of the fuel meat, it is first necessary to compute the volume of the fuel meat. The volume of the fuel meat for each plate is the arc length of the meat multiplied by the fuel length (48-in) and meat thickness (0.02-in for UAl_x, and 0.013-in for U-Mo). The fuel meat volumes are provided in Table 6.12-2.

The mass of U-235 varies for each fuel plate. The nominal U-235 loading for each plate is provided in Table 6.12-3. The tolerance on the U-235 mass in each plate is ±2%. A bounding U-235 mass for each plate is developed by applying the maximum tolerance to each plate, as indicated in Table 6.12-3. The total as-modeled U-235 mass for the demonstration element is then 1240.0 g. This conservatively exceeds the maximum value of 1215.73 + 21.15 = 1236.88 g U-235.

From the fuel meat volumes and U-235 mass per plate, the fuel number densities for each plate are computed and are provided in Table 6.12-4. The UAl_x fuel meat composition is based on a conservative enrichment of 94%, and the U-Mo fuel meat composition is based on a conservative enrichment of 20.0%. The U-234 and U-236 weight percents utilized in the calculations are representative values based on half of the maximum values for each fuel meat type.

The number densities for the UAl_x fuel meat are computed using the same methodology as described in Section 6.2, *Fissile Material Contents*. The number densities for the U-Mo fuel meat are computed by first determining the U-235 gram density for each plate. Using a conservative enrichment of 20.0%, the total uranium density is computed as $\rho_{U235}/0.2$. Because the U-Mo alloy is 10 wt.% molybdenum, the total U-Mo density is computed as $\rho_U/0.9$. The number densities of all constituents are then computed based upon the computed gram densities for each plate.

The demonstration element is modeled explicitly in MCNP, including the 0.001-in thick zirconium interlayers. The MCNP representation of the demonstration element is shown in Figure 6.12-2.

Table 6.12-2 – Fuel Volume Computation (maximum arc length)

Plate	Fuel Meat	Fuel Meat Arc Length (cm)	Fuel Meat Thickness (cm)	Fuel Length (cm)	Fuel Meat Volume (cm^3)
1	UAl_x	4.2247	0.0508	121.92	26.1660
2	UAl_x	5.0209	0.0508	121.92	31.0974
3	UAl_x	5.2764	0.0508	121.92	32.6796
4	UAl_x	5.5319	0.0508	121.92	34.2618
5	U-Mo	5.7873	0.0330	121.92	23.2985
6	U-Mo	6.0427	0.0330	121.92	24.3269
7	U-Mo	6.2982	0.0330	121.92	25.3551
8	U-Mo	6.5536	0.0330	121.92	26.3834
9	U-Mo	6.8090	0.0330	121.92	27.4116
10	U-Mo	7.0644	0.0330	121.92	28.4399
11	U-Mo	7.3198	0.0330	121.92	29.4681
12	U-Mo	7.5752	0.0330	121.92	30.4962
13	U-Mo	7.8306	0.0330	121.92	31.5244
14	U-Mo	8.0860	0.0330	121.92	32.5525
15	U-Mo	8.3414	0.0330	121.92	33.5807
16	UAl_x	8.5968	0.0508	121.92	53.2443
17	UAl_x	8.8521	0.0508	121.92	54.8260
18	UAl_x	9.0058	0.0508	121.92	55.7776
19	Plate 19 is solid aluminum				

Table 6.12-3 – U-235 Mass per Plate

Plate	Nominal U-235 Mass Per Plate (g)	Maximum U-235 Mass Per Plate (g)
1	24.3	24.79
2	29.1	29.68
3	38.7	39.47
4	40.4	41.21
5	66.35	67.68
6	69.45	70.84
7	72.52	73.97
8	75.62	77.13
9	78.69	80.26
10	81.78	83.42
11	84.85	86.55
12	87.95	89.71
13	91.02	92.84
14	94.12	96.00
15	97.18	99.12
16	64.0	65.28
17	65.9	67.22
18	53.8	54.88
19	0	0
Total	1215.73	1240.0

Table 6.12-4 – Fuel Number Densities

Plate	U-234	U-235	U-236	U-238	Al	Mo	Total
	(atom/b-cm)						
1	1.5558E-05	2.4269E-03	8.9982E-06	1.2874E-04	5.2567E-02	-	5.5147E-02
2	1.5676E-05	2.4455E-03	9.0668E-06	1.2972E-04	5.2536E-02	-	5.5136E-02
3	1.9838E-05	3.0947E-03	1.1474E-05	1.6416E-04	5.1458E-02	-	5.4749E-02
4	1.9753E-05	3.0815E-03	1.1425E-05	1.6346E-04	5.1480E-02	-	5.4757E-02
5	4.8582E-05	7.4422E-03	8.5223E-05	2.9261E-02	-	1.0129E-02	4.6966E-02
6	4.8702E-05	7.4607E-03	8.5434E-05	2.9333E-02	-	1.0154E-02	4.7082E-02
7	4.8793E-05	7.4745E-03	8.5592E-05	2.9388E-02	-	1.0173E-02	4.7170E-02
8	4.8895E-05	7.4903E-03	8.5773E-05	2.9450E-02	-	1.0195E-02	4.7269E-02
9	4.8972E-05	7.5020E-03	8.5907E-05	2.9496E-02	-	1.0211E-02	4.7343E-02
10	4.9055E-05	7.5147E-03	8.6052E-05	2.9546E-02	-	1.0228E-02	4.7423E-02
11	4.9120E-05	7.5248E-03	8.6167E-05	2.9585E-02	-	1.0242E-02	4.7487E-02
12	4.9199E-05	7.5367E-03	8.6304E-05	2.9632E-02	-	1.0258E-02	4.7562E-02
13	4.9255E-05	7.5454E-03	8.6404E-05	2.9666E-02	-	1.0270E-02	4.7617E-02
14	4.9324E-05	7.5559E-03	8.6525E-05	2.9708E-02	-	1.0284E-02	4.7684E-02
15	4.9368E-05	7.5627E-03	8.6602E-05	2.9734E-02	-	1.0293E-02	4.7726E-02
16	2.0136E-05	3.1412E-03	1.1646E-05	1.6663E-04	5.1381E-02	-	5.4721E-02
17	2.0136E-05	3.1412E-03	1.1646E-05	1.6662E-04	5.1381E-02	-	5.4721E-02
18	1.6158E-05	2.5207E-03	9.3456E-06	1.3371E-04	5.2411E-02	-	5.5091E-02
19	Plate 19 is solid aluminum						

Security-Related Information Figure Withheld Under 10 CFR 2.390.

Figure 6.12-1 – U-Mo Demonstration Element

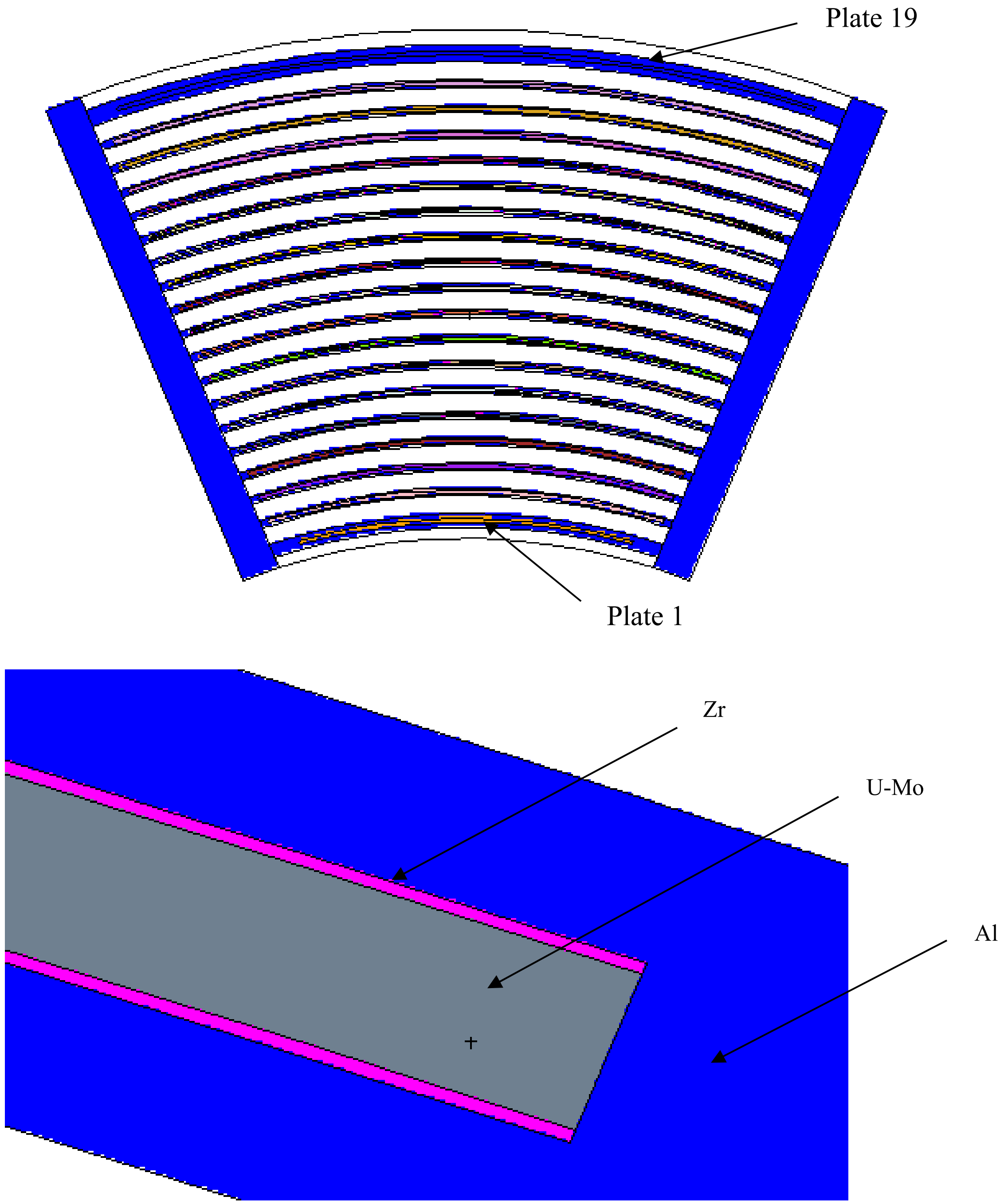

Close-up of U-Mo Plate

Figure 6.12-2 – U-Mo Demonstration Element MCNP Model

6.12.3 General Considerations

6.12.3.1 Model Configuration

The model configuration is relatively simple. Most packaging details are conservatively ignored, particularly at the ends. Because the package is long and narrow, array configurations will stack only in the lateral directions (e.g., 5x5x1). Therefore, the end details, for both the package and the fuel element, are conservatively ignored external to the active fuel region, and these end regions are simply modeled as full-density water.

Tolerances on the packaging are selected to result in the most reactive condition, as described in Section 6.3.1, *Model Configuration*. The standard ATR models are utilized with no change to the packaging descriptions.

The package consists of two primary structural components, a circular inner tube and a square outer tube. The modeled tube OD is 6.03-in, the modeled wall thickness is 0.108-in, and the modeled tube ID is 5.814-in. The outer tube is modeled with a wall thickness of 0.169-in and outer dimension of 7.9-in.

In the NCT single package models, the inner tube, insulation, and outer tube are modeled explicitly, as shown in Figure 6.12-3 and Figure 6.12-4. Although negligible water ingress is expected during NCT, the inner cavity of the package is assumed to be flooded with water because the package lid does not contain a seal. However, the region between the insulation and the outer tube will remain dry because water cannot enter this region. The Fuel Handling Enclosure (FHE) is conservatively ignored. Modeling the FHE would decrease water reflection in the single package model. However, the neoprene along the sides of the FHE is modeled explicitly using a thickness of 1/8-in. Because neoprene will reduce the reactivity due to parasitic absorption in chlorine, chlorine is removed from the neoprene, and the density is reduced accordingly. In the model, the fuel element is conservatively positioned at the radial center of the inner tube to maximize neutron reflection. The package is reflected with 12-in of full-density water.

The HAC single package model is essentially the same as the NCT single package model. Damage in the drop tests was shown to be negligible and concentrated at the ends of the package. As the ends of the package are not modeled, this end damage does not affect the modeling. The various side drops resulted in only minor localized damage to the outer tube, and no observable bulk deformation of the package. Therefore, the minor damage observed will not impact the reactivity. The insulation is replaced with full-density water, and the region between the insulation and outer tube is also filled with full-density water (see Figure 6.12-5). The treatment of the FHE is the same as the NCT single package model.

In the NCT array models, a 9x9x1 array is utilized. Although the FHE would survive NCT events with no damage, the FHE is conservatively ignored and the fuel elements are pushed toward the center of the array. Because the fuel elements are transported in a thin (~0.01-in) plastic bag, this plastic bag is assumed to act as a boundary for partial moderation effects. The plastic bag is not modeled explicitly, because it is too thin to have an appreciable effect on the reactivity. Therefore, it is postulated that the fuel element channels may fill with full-density water, while the region between the fuel element and inner tube fills with variable density water. The partial moderation effects that could be achieved by modeling the FHE explicitly are essentially addressed by the partial moderation analysis using the plastic bag. Also, modeling the FHE explicitly would result in the fuel elements being significantly pushed apart, which is a less reactive condition. Axial movement of the fuel elements is not considered because axial movement would increase the effective active height of the system and reduce the reactivity due to increased leakage.

In the HAC array models, a 5x5x1 array is utilized. The HAC array models are essentially the same as the NCT array models, except additional cases are developed to determine the reactivity effect of allowing variable density water in the region between the inner and outer tubes. The FHE is conservatively ignored for the reasons stated in the previous paragraph. Because the NCT and HAC models are very similar and the NCT models utilize a larger array, the NCT array models are more reactive than the HAC array models.

The detailed moderation assumptions for these cases are discussed more fully in Section 6.12.5, *Evaluation of Package Arrays under Normal Conditions of Transport*, and Section 6.12.6, *Package Arrays under Hypothetical Accident Conditions*.

6.12.3.2 Material Properties

The fuel meat compositions are provided in Table 6.12-4. For the U-Mo plates, the zirconium interlayer is modeled as pure zirconium with a density of 6.506 g/cm^3. All aluminum alloy structural materials are modeled as pure aluminum with a density of 2.7 g/cm^3. The material properties of the packaging materials are provided in Section 6.3.2, *Material Properties*.

6.12.3.3 Computer Codes and Cross-Section Libraries

MCNP5 v1.30 is used for the criticality analysis. All cross sections utilized are at room temperature (293.6 K). The uranium isotopes utilize preliminary ENDF/B-VII cross section data that are considered by Los Alamos National Laboratory to be more accurate than ENDF/B-VI cross sections. ENDF/B-V cross sections are utilized for chromium, nickel, and iron because natural composition ENDF/B-VI cross sections are not available for these elements. The remaining isotopes utilize ENDF/B-VI cross sections. Titles of the cross sections utilized in the models have been extracted from the MCNP output (when available) and provided in Table 6.12-5. The $S(\alpha,\beta)$ card LWTR.60T is used to simulate hydrogen bound to water.

All cases are run with 2500 neutrons per generation for 250 generations, skipping the first 50. The 1-sigma uncertainty is approximately 0.001 for all cases.

6.12.3.4 Demonstration of Maximum Reactivity

The reactivities of the NCT and HAC single package cases are small, with $k_s < 0.5$.

The NCT and HAC array cases are similar. For the NCT array, a 9x9x1 array is utilized, while in the HAC array, a smaller 5x5x1 array is utilized. Because negligible damage was observed in the drop tests, the package dimensions are the same between the NCT and HAC models. Dimensions of both the fuel element and packaging are selected to maximize reactivity, and close-water reflection is utilized. In both NCT and HAC array cases, flooding with partial moderation is allowed in the central cavity, and the fuel elements are pushed toward the center of the array. The FHE is not modeled explicitly because the FHE would increase the fuel element spacing and decrease the reactivity. Any partial moderation effects of the FHE are essentially addressed by the partial moderation analysis for the fuel element itself.

In the NCT array models, insulation is modeled between the inner and outer tubes. In the HAC array models for the standard ATR fuel element, it was determined in Section 6.6, *Package Arrays under Hypothetical Accident Conditions*, that it is conservative to model the insulation rather than treating this region as void or water. Therefore, in the demonstration element HAC models, insulation is modeled in all cases. In both sets of models, chlorine-free neoprene is modeled adjacent to the fuel element side plates, although the effect on the reactivity is small. No models in which the neoprene is allowed to decompose and homogeneously mix with the water are developed, as this scenario is already bounded by the variable water density search.

The NCT array is more reactive than the HAC array, primarily because the NCT array is significantly larger. The most reactive case (Case MO13) results in a k_s = 0.78785, which is below the USL of 0.9209. Note that the demonstration element is less reactive than a standard ATR fuel element.

Table 6.12-5 – Cross Section Libraries Utilized

Isotope/Element	Cross Section Label (from MCNP output)
1001.62c	1-h-1 at 293.6K from endf-vi.8 njoy99.50
6000.66c	6-c-0 at 293.6K from endf-vi.6 njoy99.50
8016.62c	8-o-16 at 293.6K from endf-vi.8 njoy99.50
13027.62c	13-al-27 at 293.6K from endf-vi.8 njoy99.50
14000.60c	14-si-nat from endf/b-vi
15031.66c	15-p-31 at 293.6K from endf-vi.6 njoy99.50
17000.66c	17-cl-0 at 293.6K from endf-vi.0 njoy99.50
24000.50c	njoy
25055.62c	25-mn-55 at 293.6K from endf/b-vi.8 njoy99.50
26000.55c	njoy
28000.50c	njoy
40000.66c	40-zr-0 at 293.6K from endf-vi.1 njoy99.50
42000.66c	42-mo-0 at 293.6K from endf-vi.0 njoy99.50
92234.69c	92-u-234 at 293.6K from t16 u234la4 njoy99.50
92235.69c	92-u-235 at 293.6K from t16 u235la9d njoy99.50
92236.69c	92-u-236 at 293.6K from t16 u236la2d njoy99.50
92238.69c	92-u-238 at 293.6K from t16 u238la8h njoy99.50

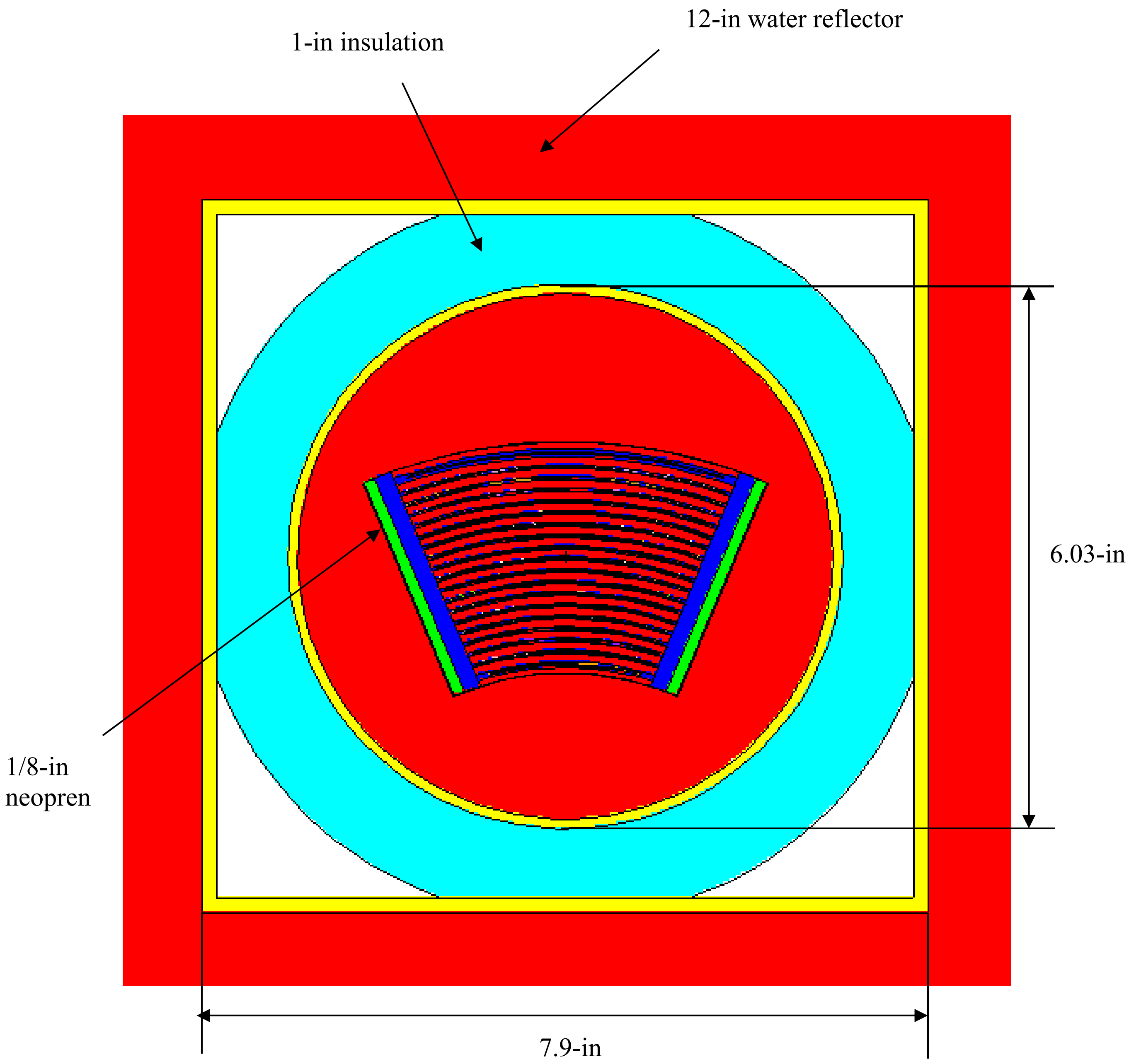

Figure 6.12-3 – NCT Single Package Model (planar view)

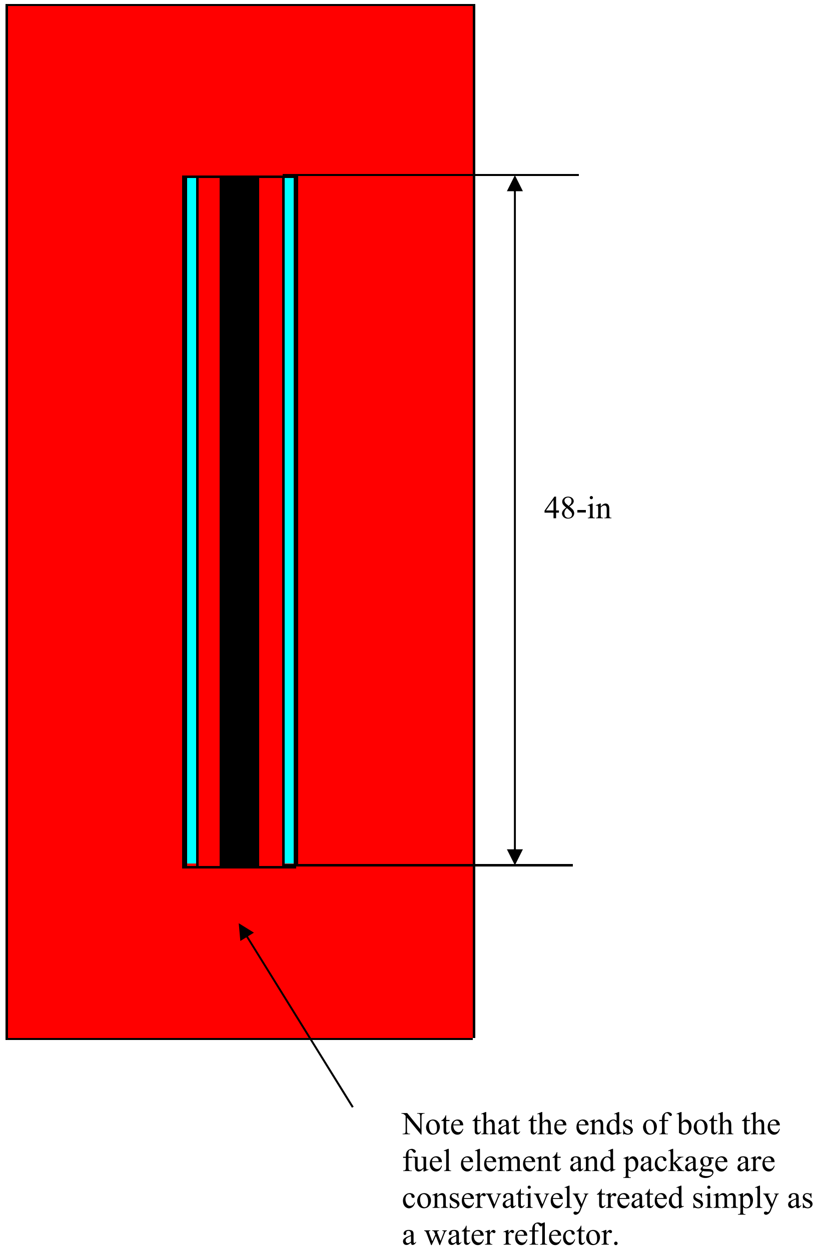

Figure 6.12-4 – NCT Single Package Model (axial view)

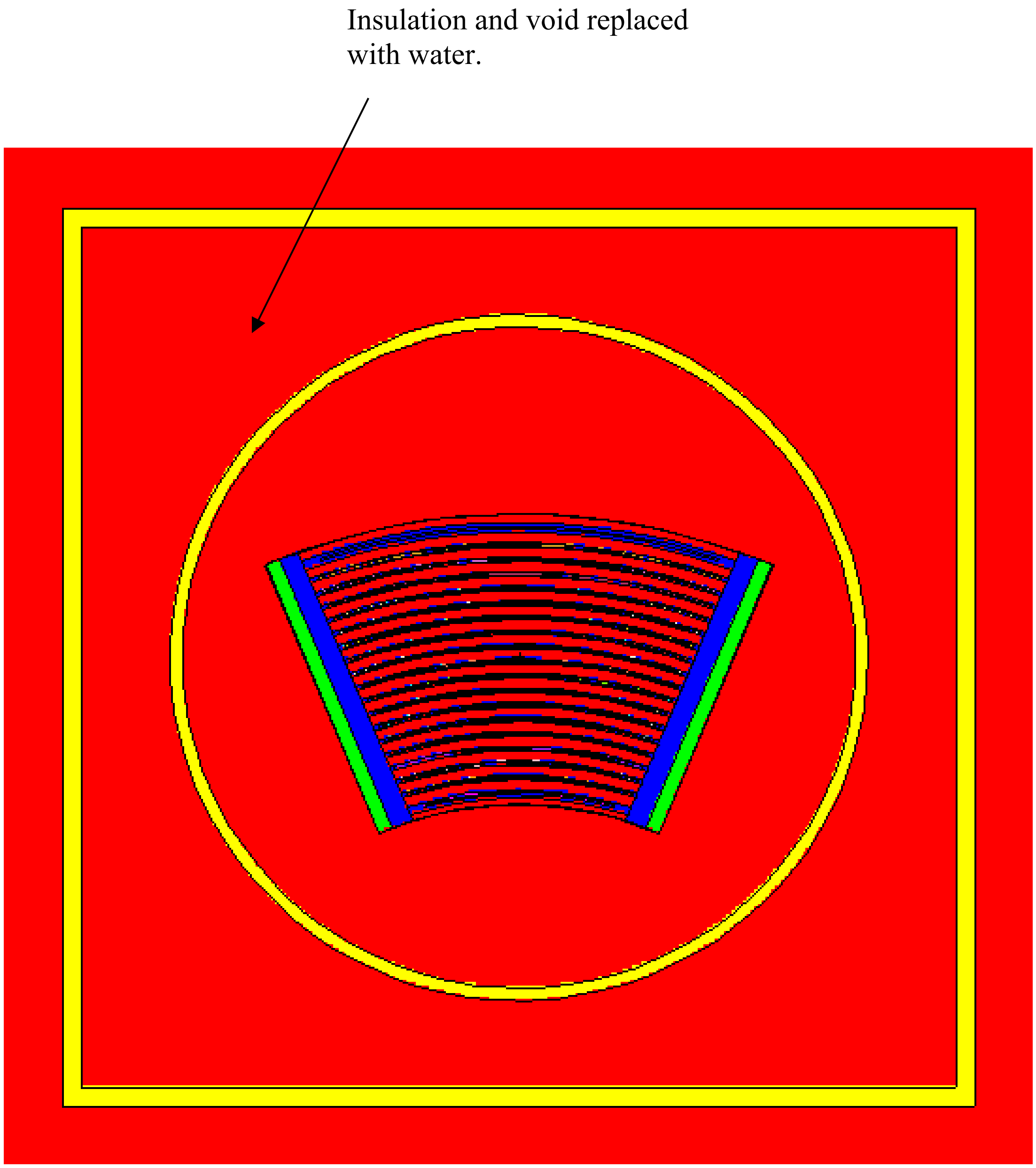

Figure 6.12-5 – HAC Single Package Model (planar view)

6.12.4 Single Package Evaluation

6.12.4.1 Single Package Configuration

6.12.4.1.1 NCT Single Package Configuration

The geometry of the NCT single package configuration is discussed in Section 6.12.3.1, *Model Configuration*. A detailed parametric analysis of standard ATR fuel was performed in Section 6.4.1.2.1, *Fuel Element Payload Parametric Evaluation*. It was determined that reactivity for ATR-type fuel is maximized by maximizing the arc length of the fuel meat and maximizing the channel spacing between fuel plates. These conclusions are applicable to the U-Mo demonstration element because the fuel element geometry is the same and the fissile loading per plate is very similar to the standard ATR fuel element. Therefore, the demonstration elements are modeled with the maximum fuel meat arc lengths and a bounding channel spacing of 0.089-in. A channel spacing of 0.089-in is the maximum local channel spacing (0.087-in) with an additional margin of 0.002-in. This channel spacing is achieved by artificially reducing the cladding thickness.

Only the most reactive NCT single package configuration for a standard ATR fuel element is repeated with the U-Mo demonstration element. Results are provided in Table 6.12-6, Case MO1. This case features an inner tube flooded with full-density water. Neoprene is modeled, but chlorine is conservatively removed from the neoprene because chlorine acts as a poison. The package is reflected with 12-in of water. For this case, k_s = 0.40552, which is below the USL of 0.9209.

6.12.4.1.2 HAC Single Package Configuration

The packaging and fuel geometry of the HAC single package configuration is discussed in Section 6.12.3.1, *Model Configuration*. The HAC single package geometry is the same as the NCT single package geometry, except the insulation and region between the inner and outer tubes is replaced with water.

Only the most reactive HAC single package configuration for a standard ATR fuel element is repeated with the U-Mo demonstration element because the fuel element geometry is the same and the fissile loading per plate is very similar to the standard ATR fuel element. Results are provided in Table 6.12-6, Case MO2. This case features an inner tube flooded with full-density water. Neoprene is modeled, but chlorine is conservatively removed from the neoprene because chlorine acts as a poison. The package is reflected with 12-in of water. For this case, k_s = 0.43443, which is below the USL of 0.9209.

Note that the most reactive HAC single package case for a standard HEU ATR fuel element has k_s = 0.45237 (see Table 6.4-5). Therefore, the U-Mo demonstration element is less reactive than a standard HEU ATR fuel element.

6.12.4.2 Single Package Results

Following are the tabulated results for the single package cases.

Table 6.12-6 – Single Package Results

Case ID	Filename	k_{eff}	σ	k_s ($k+2\sigma$)
NCT				
MO1	NS_MO	0.40358	0.00097	0.40552
HAC				
MO2	HS_MO	0.43257	0.00093	0.43443

6.12.5 Evaluation of Package Arrays under Normal Conditions of Transport

6.12.5.1 NCT Array Configuration

The NCT array model is a 9x9x1 array of the NCT single package model, see Figure 6.12-6. Although an 8x8x1 array is of sufficient size to justify a CSI = 4.0, the larger 9x9x1 array is utilized simply for modeling convenience. The entire array is reflected with 12-in of full-density water.

The fuel elements are pushed to the center of the array and rotated to minimize the distance between the fuel elements. This geometry is not feasible for NCT, because the FHE would force the fuel elements to remain in the center of the package, although the FHE does allow rotation. Therefore, it is conservative to ignore the FHE to minimize the separation distance. In addition, a small notch is added to the neoprene so that the fuel element may be translated to the maximum extent without interfering with the inner tube geometry. This notch is not present in the single package models.

It was determined in the analysis for the standard ATR fuel element that the most reactive NCT array configuration has full-density water between fuel plates, variable density water inside the inner tube, and a channel spacing of 0.089-in. Therefore, only this configuration is investigated for the demonstration element because the fuel element geometry is the same and the fissile loading per plate is very similar to the standard ATR fuel element.

The results are provided in Table 6.12-7. Reactivity is at a maximum for Case MO13, which has 0.3 g/cm^3 water inside the inner tube, and k_s = 0.78785. The maximum result is far below the USL of 0.9209.

Case MO13 is the most reactive demonstration element case. Note that is it significantly less reactive than the equivalent standard ATR NCT array case, which has k_s = 0.83616 (see Table 6.5-1). To determine if the molybdenum in the fuel could potentially be acting as a poison, an additional case (Case MO21) is run "for information only" with no molybdenum in the fuel matrix. For Case MO21, k_s = 0.79228, which is a negligible increase from Case MO13 compared to the USL of 0.9209. Therefore, it is concluded that molybdenum has little effect on the system reactivity. It is inferred that reactivity differences between the demonstration element and a standard ATR element are largely related to increased parasitic absorption in U-238.

6.12.5.2 NCT Array Results

The results for the NCT array cases are provided in the following table.

Table 6.12-7 – NCT Array Results

Case ID	Filename	Water Density Between Tubes (g/cm^3)	Water Density Inside Inner Tube (g/cm^3)	Water Density Between Plates (g/cm^3)	k_{eff}	σ	k_s ($k+2\sigma$)
MO10	NA_MO_P000	0	0	1.0	0.73196	0.00116	0.73428
MO11	NA_MO_P010	0	0.1	1.0	0.76638	0.00107	0.76852
MO12	NA_MO_P020	0	0.2	1.0	0.77779	0.00126	0.78031
MO13	**NA_MO_P030**	**0**	**0.3**	**1.0**	**0.78557**	**0.00114**	**0.78785**
MO14	NA_MO_P040	0	0.4	1.0	0.78312	0.00110	0.78532
MO15	NA_MO_P050	0	0.5	1.0	0.77669	0.00111	0.77891
MO16	NA_MO_P060	0	0.6	1.0	0.76518	0.00114	0.76746
MO17	NA_MO_P070	0	0.7	1.0	0.75554	0.00102	0.75758
MO18	NA_MO_P080	0	0.8	1.0	0.74778	0.00113	0.75004
MO19	NA_MO_P090	0	0.9	1.0	0.73366	0.00112	0.73590
MO20	NA_MO_P100	0	1.0	1.0	0.72399	0.00114	0.72627
Case MO13 without Molybdenum in Fuel - For Information Only							
MO21	NA_NOMO_P030	0	0.3	1.0	0.78990	0.00119	0.79228

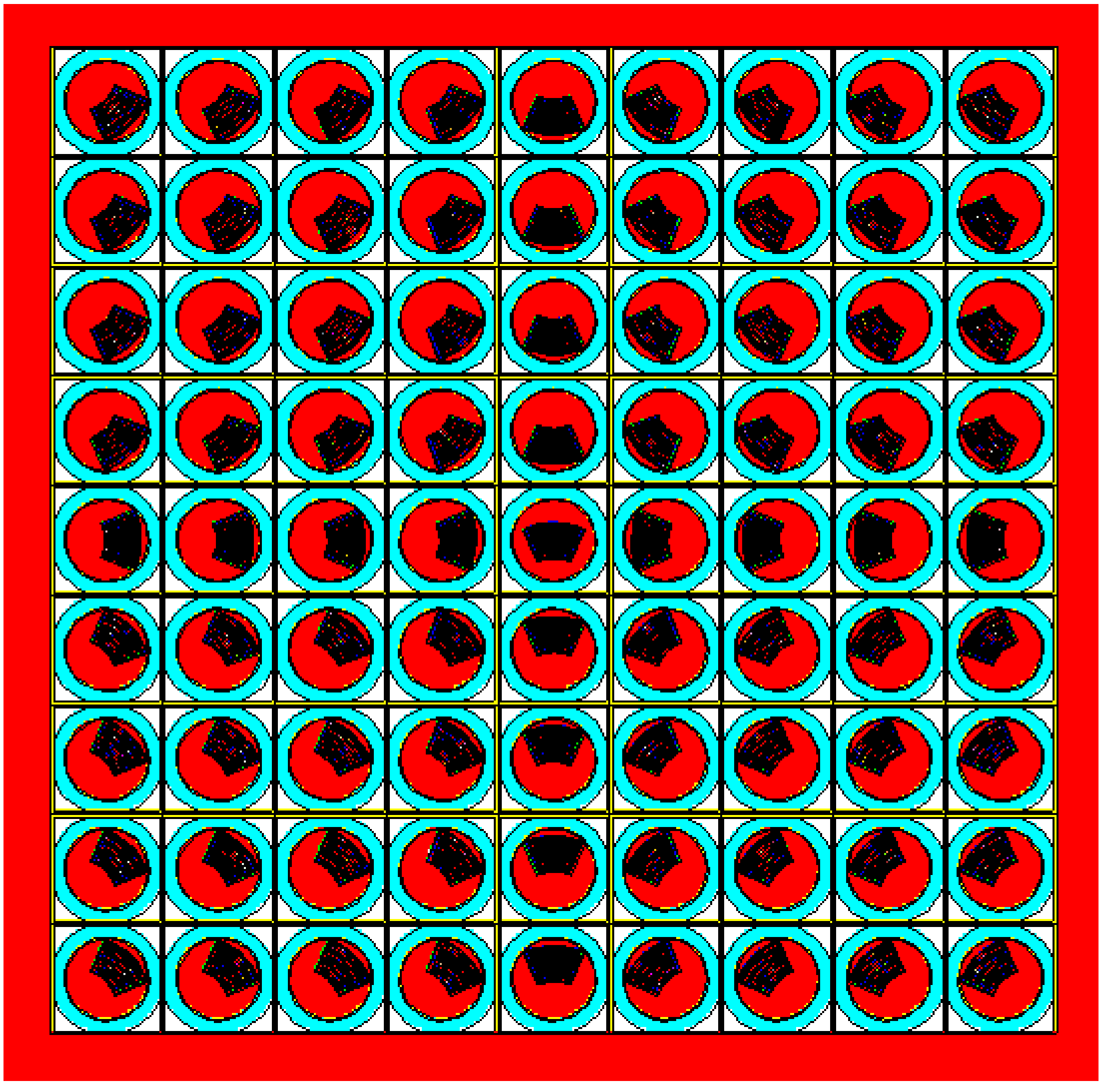

Figure 6.12-6 – NCT Array Geometry

6.12.6 Package Arrays under Hypothetical Accident Conditions

6.12.6.1 HAC Array Configuration

The HAC array model is a 5x5x1 array of the HAC single package model. It was determined in the analysis for the standard ATR element that the most reactive HAC array configuration features full-density water between the fuel plates, a channel spacing of 0.089-in, variable density water inside the inner tube, insulation modeled with void present between the insulation and outer tube, and neoprene modeled without chlorine. Therefore, only this configuration is investigated for the demonstration element because the fuel element geometry is the same and the fissile loading per plate is very similar to the standard ATR fuel element. This configuration is shown in Figure 6.12-7.

The results are provided in Table 6.12-8. Case MO36 is the most reactive, with a water density of 0.6 g/cm^3 inside the inner tube and k_s = 0.70543. This result is below the USL of 0.9209. Note that this result is lower than the maximum NCT array case because the HAC and NCT array models are quite similar, except the NCT array uses a much larger 9x9x1 configuration.

6.12.6.2 HAC Array Results

Following are the tabulated results for the HAC array cases.

Table 6.12-8 – HAC Array Results

Case ID	Filename	Water Density Between Tubes (g/cm^3)	Water Density Inside Inner Tube (g/cm^3)	Water Density Between Plates (g/cm^3)	k_{eff}	σ	k_s (k+2σ)
MO30	HA_MO_P000	0	0	1.0	0.58525	0.00099	0.58723
MO31	HA_MO_P010	0	0.1	1.0	0.62456	0.00105	0.62666
MO32	HA_MO_P020	0	0.2	1.0	0.65775	0.00116	0.66007
MO33	HA_MO_P030	0	0.3	1.0	0.67626	0.00119	0.67864
MO34	HA_MO_P040	0	0.4	1.0	0.69053	0.00115	0.69283
MO35	HA_MO_P050	0	0.5	1.0	0.69590	0.00117	0.69824
MO36	**HA_MO_P060**	**0**	**0.6**	**1.0**	**0.70311**	**0.00116**	**0.70543**
MO37	HA_MO_P070	0	0.7	1.0	0.70183	0.00113	0.70409
MO38	HA_MO_P080	0	0.8	1.0	0.70024	0.00121	0.70266
MO39	HA_MO_P090	0	0.9	1.0	0.69510	0.00121	0.69752
MO40	HA_MO_P100	0	1.0	1.0	0.69183	0.00109	0.69401

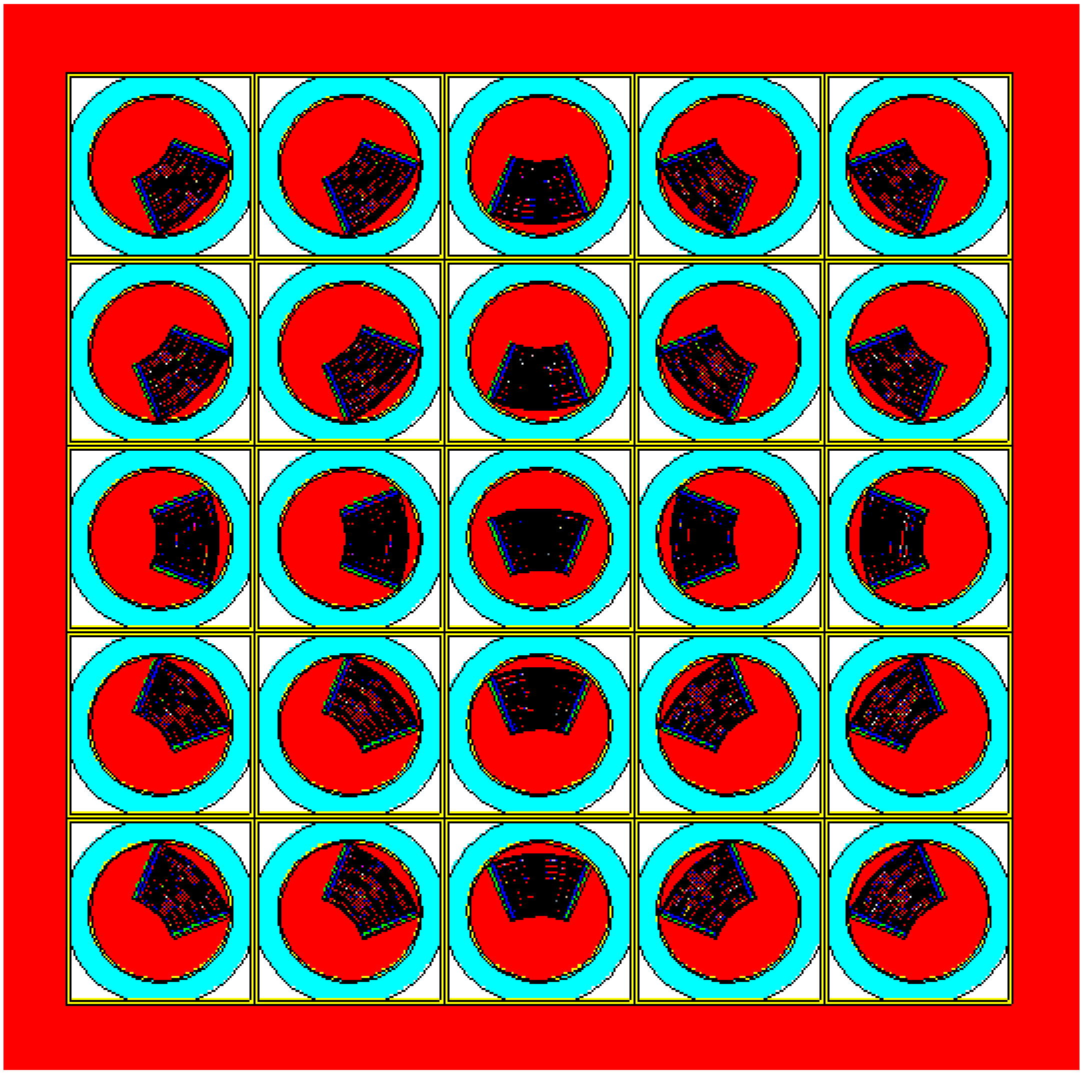

Figure 6.12-7 – HAC Array Geometry

6.12.7 Fissile Material Packages for Air Transport

See Section 6.7, which applies to all contents.

6.12.8 Benchmark Evaluations

The Monte Carlo computer program MCNP5 v1.30[15] is utilized for this analysis. MCNP has been used extensively in criticality evaluations for several decades and is considered a standard in the industry.

The ORNL USLSTATS code[16] is used to establish a USL for the analysis. USLSTATS provides a simple means of evaluating and combining the statistical error of the calculation, code biases, and benchmark uncertainties. The USLSTATS calculation uses the combined uncertainties and data to provide a linear trend and an overall uncertainty. Computed multiplication factors, k_{eff}, for the package are deemed to be adequately subcritical if the computed value of k_s is less than or equal to the USL as follows:

$$k_s = k_{eff} + 2\sigma \leq USL$$

The USL includes the combined effects of code bias, uncertainty in the benchmark experiments, uncertainty in the computational evaluation of the benchmark experiments, and an administrative margin. This methodology has accepted precedence in establishing criticality safety limits for transportation packages complying with 10 CFR 71.

6.12.8.1 Applicability of Benchmark Experiments

The critical experiment benchmarks are selected from the *International Handbook of Evaluated Criticality Safety Benchmark Experiments*[17] based upon their similarity to the ATR Fresh Fuel Shipping Container and contents. The important selection parameters are HEU and LEU uranium plate-type fuels with a thermal spectrum. Thirty-five benchmarks are available for HEU plate fuel, while only one is available for LEU plate fuel. Therefore, the plate-type benchmarks are supplemented with 54 LEU rod benchmarks, for a total of 90 benchmarks. The titles for all utilized experiments are listed in Table 6.12-9.

Ideally, benchmarks would be limited to those with a fuel matrix of HEU UAl_x and LEU U-Mo, aluminum cladding, and no absorbers, consistent with the ATR demonstration element criticality models. However, no experiment set is available that meets all of these criteria since U-Mo fuel is in a research and development stage, and benchmarks for U-Mo fuel designs are not available. Therefore, the selected experiments are subdivided into two general subsets, plate-type benchmarks and LEU rod benchmarks. Trending is performed for both subsets of benchmarks and the entire benchmark set. The USL selected is the minimum of all sets.

[15] MCNP5, "*MCNP – A General Monte Carlo N-Particle Transport Code, Version 5; Volume II: User's Guide*," LA-CP-03-0245, Los Alamos National Laboratory, April, 2003.

[16] USLSTATS, "*USLSTATS: A Utility To Calculate Upper Subcritical Limits For Criticality Safety Applications,"* Version 1.4.2, Oak Ridge National Laboratory, April 23, 2003.

[17] OECD Nuclear Energy Agency, *International Handbook of Evaluated Criticality Safety Benchmark Experiments*, NEA/NSC/DOC(95)03, September, 2010.

The primary difference between the U-Mo demonstration element and a standard ATR element is the presence of molybdenum rather than aluminum in the fuel matrix. It is demonstrated in Section 6.12.5, *Evaluation of Package Arrays under Normal Conditions of Transport*, that deletion of molybdenum from the MCNP model has very little effect on the reactivity. Therefore, because molybdenum has little effect on the reactivity and margins to the USL are very large, the lack of U-Mo benchmarks has little effect on the USL and is acceptable.

LEU-COMP-THERM-009 uses various separator plates. Only cases 1-8 (steel separators) and 24-27 (aluminum and/or zircaloy separators) are utilized, and the rest are considered not applicable. LEU-COMP-THERM-010 uses various reflector plates. Only cases 9-19 (steel reflectors) are utilized, and the rest are considered not applicable.

Note that IEU-COMP-THERM-014 consists of a single LEU plate-type benchmark with U_3Si_2-Al fuel meat and is the experiment that is closest to meeting all of the desired criteria.

6.12.8.2 Bias Determination

The USL is calculated by application of the USLSTATS computer program. USLSTATS receives as input the k_{eff} as calculated by MCNP, the total 1-σ uncertainty (combined benchmark and MCNP uncertainties), and a trending parameter. Six trending parameters have been selected: (1) Energy of the Average neutron Lethargy causing Fission (EALF), (2) U-235 number density, (3) channel spacing, (4) ratio of the number of hydrogen atoms in a unit cell to the number of U-235 atoms in a unit cell (H/U-235), (5) plate pitch, and (6) U-235 enrichment. The channel spacing and plate pitch parameters are applied only to the plate-type benchmarks.

The uncertainty value, σ_{total}, assigned to each case is a combination of the benchmark uncertainty for each experiment, σ_{bench}, and the Monte Carlo uncertainty associated with the particular computational evaluation of the case, σ_{MCNP}, or:

$$\sigma_{total} = (\sigma_{bench}^2 + \sigma_{MCNP}^2)^{½}$$

These values are input into the USLSTATS program in addition to the following parameters, which are the values recommended by the USLSTATS user's manual:

- P, proportion of population falling above lower tolerance level = 0.995 (note that this parameter is required input but is not utilized in the calculation of USL Method 1)
- 1-γ, confidence on fit = 0.95
- α, confidence on proportion P = 0.95 (note that this parameter is required input but is not utilized in the calculation of USL Method 1)
- Δk_m, administrative margin used to ensure subcriticality = 0.05.

These data are followed by triplets of trending parameter value, computed k_{eff}, and uncertainty for each case. A confidence band analysis is performed on the data for each trending parameter using USL Method 1. The USL generated for each of the trending parameters utilized is provided in Table 6.12-10. All benchmark data used as input to USLSTATS are reported in Table 6.12-11. The results for each trending parameter are discussed in the following paragraphs.

Energy of the Average neutron Lethargy causing Fission (EALF)

The EALF is used as the first trending parameter for the benchmark cases. The EALF comparison provides a means to observe neutron spectral dependencies or trends. The range of applicability for the benchmarks is 5.222E-08 MeV ≤ EALF ≤ 3.217E-07 MeV. The ATR demonstration element cases fall within the range of applicability. This parameter is trended on all benchmarks and the subset of plate and rod-type benchmarks. A minimum USL based on EALF of 0.9254 occurs for the plate-type benchmarks.

U-235 Number Density

The U-235 number density is used as the second trending parameter for the benchmark cases. The range of applicability for the benchmarks is 4.879E-04 atom/b-cm ≤ U-235 ≤ 3.926E-03 atom/b-cm. The U-235 number densities for UAl_x plates 1 through 4 and 16 through 18 fall within the range of applicability, while the number densities for U-Mo plates 5 through 15 exceed the range of applicability (maximum value = 7.563E-03 atom/b-cm). However, the average U-235 number density for the fuel element is 4.843E-03 atom/b-cm.

This parameter is trended on all benchmarks and the subset of plate and rod-type benchmarks. A minimum USL based on U-235 number density of 0.9239 occurs for the plate-type benchmarks. If this USL is extrapolated based on the average value, the estimated USL is 0.9219. Note that it is not expected that the U-235 number density trend is a truly physical trend because MCNP performs no special cross-section processing.

Channel Spacing

The channel spacing is used as the third trending parameter for the benchmark cases. The range of applicability for the benchmarks is 6.457E-02 in ≤ channel spacing ≤ 0.107 in. The ATR demonstration element channel spacing of 0.089-in falls within the range of applicability. Trending is performed only over the plate-type benchmarks, and the minimum USL over the range of applicability is 0.9228.

H/U-235 Atom Ratio

The H/U-235 atom ratio is used as the fourth trending parameter for the benchmark cases. The H/U-235 atom ratio is defined here as the ratio of hydrogen atoms to U-235 atoms in a unit cell. The range of applicability for the benchmarks is 65.100 ≤ H/U235 ≤ 399.0. This parameter for the demonstration element is computed by the following equation:

$$N_H*C/(N_{U235}*M)$$

where,

N_H is the hydrogen number density (6.687E-02 atom/b-cm)

C is the channel spacing (0.089-in)

N_{U235} is the U-235 number density (variable)

M is the fuel meat width (0.02-in for UAl_x and 0.013-in for U-Mo)

The benchmark cases are a mixture of plate and rod-type benchmarks. The H/U-235 ratios for the plate-type benchmarks are computed as shown above, while the H/U-235 ratios for the rod-type benchmarks are computed using the area of a fuel pellet in place of “M” and water area inside a unit cell in place of “C.”

If this parameter is computed for all 18 fueled plates, the ratio ranges from 60.5 to 122.6 for the demonstration element fuel plates. This parameter is trended on all benchmarks and the subset of plate and rod-type benchmarks. The minimum USL for this parameter over the range of applicability is 0.9251. This range is only slightly outside the range of applicability at the lower end (60.5 vs. 65.1) and is considered acceptable.

Plate Pitch

The fuel plate pitch is used as the fifth trending parameter for the benchmark cases. The range of applicability for the benchmarks is 0.12457-in ≤ P ≤ 0.165-in. The fuel plate pitch is fixed at 0.128-in for all models (excluding the pitch for plate 1, which is slightly bigger because this plate is thicker). This pitch falls within the range of the benchmark experiments. Trending is performed only over the plate-type benchmarks, and the minimum USL over the range of applicability is 0.9225.

Enrichment

The U-235 enrichment is used as the sixth trending parameter for the benchmark cases. The range of applicability for the benchmarks is 2.35% ≤ E ≤ 93.2%. The U-Mo demonstration element is comprised of U-Mo plates with an enrichment of 20%, and UAl_x plates with an enrichment of 94%. The enrichment of the U-Mo plates is within the range of applicability, and the enrichment of the UAl_x plates is only slightly outside the range of applicability and is considered acceptable. This parameter is trended on all benchmarks and the subset of plate and rod-type benchmarks. A minimum USL based on enrichment of 0.9224 occurs for the plate-type benchmarks.

Recommended USL

Based on the trending over six parameters, a minimum USL of 0.9224 occurs for the enrichment parameter. However, the benchmarking analysis documented in Section 6.8, *Benchmark Evaluations*, for the standard HEU element resulted in a USL of 0.9209. Both for consistency and added conservatism, a USL of 0.9209 is selected for this analysis.

Table 6.12-9 – Benchmark Experiments Utilized

Series	Title
Plate-Type Benchmarks	
HEU-COMP-THERM-022	SPERT III Stainless-Steel-Clad Plate-Type Fuel in Water
HEU-MET-THERM-006	SPERT-D Aluminum-Clad Plate-Type Fuel in Water, Dilute Uranyl Nitrate, or Borated Uranyl Nitrate
HEU-MET-THERM-022	Advanced Test Reactor: Serpentine Arrangement of Highly Enriched Water-Moderated Uranium-Aluminide Fuel Plates Reflected by Beryllium
IEU-COMP-THERM-014	RA-6 Reactor: Water Reflected, Water Moderated $U(19.77)_3Si_2$-Al Fuel Plates
Rod-Type Benchmarks	
LEU-COMP-THERM-001	Water-Moderated $U(2.35)O_2$ Fuel Rods in 2.032-cm Square-Pitched Arrays
LEU-COMP-THERM-002	Water-Moderated $U(4.31)O_2$ Fuel Rods in 2.54-cm Square-Pitched Arrays
LEU-COMP-THERM-006	Critical Arrays of Low-Enriched UO_2 Fuel Rods with Water-to-Fuel Volume Ratios Ranging From 1.5 to 3.0
LEU-COMP-THERM-009	Water-Moderated Rectangular Clusters of $U(4.31)O_2$ Fuel Rods (2.54-cm Pitch) Separated by Steel, Boral, Copper, Cadmium, Aluminum, or Zircaloy-4 Plates (Cases 1-8 and 24-27 only)
LEU-COMP-THERM-010	Water-Moderated $U(4.31)O_2$ Fuel Rods Reflected by Two Lead, Uranium, or Steel Walls (Cases 9-19 only)

Table 6.12-10 – USL Results

Trending Parameter (X)	Minimum USL Over Range of Applicability	Range of Applicability
All Benchmarks (90)		
EALF (MeV)	0.9323	5.22170E-08 <= X <= 3.21670E-07
U-235 Number Density (atom/b-cm)	0.9285	4.87850E-04 <= X <= 3.92600E-03
H/U-235	0.9325	65.100 <= X <= 399.00
Enrichment (%)	0.9321	2.35 <= X <= 93.2
Plate-Type Benchmarks (36)		
EALF (MeV)	0.9254	5.22170E-08 <= X <= 1.58510E-07
U-235 Number Density (atom/b-cm)	0.9239	1.84900E-03 <= X <= 3.92600E-03
Channel spacing (in)	0.9228	6.45700E-02 <= X <= 0.10669
H/U-235	0.9251	65.100 <= X <= 147.00
Plate Pitch (in)	0.9225	0.12457 <= X <= 0.16535
Enrichment (%)	0.9224	19.77 <= X <= 93.2
Rod-Type Benchmarks (54)		
EALF (MeV)	0.9400	9.65510E-08 <= X <= 3.21670E-07
U-235 Number Density (atom/b-cm)	0.9403	4.87850E-04 <= X <= 1.01020E-03
H/U-235	0.9396	105.50 <= X <= 399.00
Enrichment (%)	0.9404	2.35 <= X <= 4.31

This page left intentionally blank.

Table 6.12-11 – Benchmark Experiment Data

No	Case	k	σ_{mcnp}	σ_{bench}	σ_{total}	EALF (MeV)	U-235 (atom/b-cm)	Channel Spacing (in)	H/U-235	Plate Pitch (in)	Enrichment (%)
1	hct022_c01	0.98862	0.00059	0.0081	0.0081	9.542E-08	3.3155E-03	0.06457	65.1	0.12457	93.2
2	hct022_c02	0.98860	0.00055	0.0081	0.0081	9.677E-08	3.3155E-03	0.06457	65.1	0.12457	93.2
3	hct022_c03	0.98924	0.00061	0.0081	0.0081	9.861E-08	3.3155E-03	0.06457	65.1	0.12457	93.2
4	hct022_c04	0.98919	0.00062	0.0081	0.0081	9.920E-08	3.3155E-03	0.06457	65.1	0.12457	93.2
5	hct022_c05	0.98706	0.00062	0.0081	0.0081	9.543E-08	3.3155E-03	0.06457	65.1	0.12457	93.2
6	hct022_c06	0.99001	0.00061	0.0081	0.0081	9.857E-08	3.3155E-03	0.06457	65.1	0.12457	93.2
7	hct022_c07	0.98892	0.00063	0.0081	0.0081	9.872E-08	3.3155E-03	0.06457	65.1	0.12457	93.2
8	hct022_c08	0.98824	0.00063	0.0081	0.0081	9.964E-08	3.3155E-03	0.06457	65.1	0.12457	93.2
9	hct022_c09	0.98797	0.00061	0.0081	0.0081	9.634E-08	3.3155E-03	0.06457	65.1	0.12457	93.2
10	hct022_c10	0.98867	0.00061	0.0081	0.0081	9.925E-08	3.3155E-03	0.06457	65.1	0.12457	93.2
11	hct022_c11	0.98967	0.00060	0.0081	0.0081	9.997E-08	3.3155E-03	0.06457	65.1	0.12457	93.2
12	hmt006_c01	0.99240	0.00082	0.0044	0.0045	8.481E-08	1.8490E-03	0.06457	116.5	0.12457	93.17
13	hmt006_c02	0.99333	0.00088	0.0040	0.0041	7.043E-08	1.8490E-03	0.06457	116.5	0.12457	93.17
14	hmt006_c03	0.99705	0.00077	0.0040	0.0041	6.317E-08	1.8490E-03	0.06457	116.5	0.12457	93.17
15	hmt006_c04	0.99113	0.00078	0.0040	0.0041	6.202E-08	1.8490E-03	0.06457	116.5	0.12457	93.17
16	hmt006_c05	0.99230	0.00079	0.0040	0.0041	5.852E-08	1.8490E-03	0.06457	116.5	0.12457	93.17
17	hmt006_c06	0.99010	0.00071	0.0040	0.0041	5.615E-08	1.8490E-03	0.06457	116.5	0.12457	93.17
18	hmt006_c07	0.98783	0.00073	0.0040	0.0041	5.432E-08	1.8490E-03	0.06457	116.5	0.12457	93.17
19	hmt006_c08	0.98246	0.00071	0.0040	0.0041	5.256E-08	1.8490E-03	0.06457	116.5	0.12457	93.17
20	hmt006_c09	0.98657	0.00072	0.0040	0.0041	5.222E-08	1.8490E-03	0.06457	116.5	0.12457	93.17
21	hmt006_c10	0.99885	0.00085	0.0040	0.0041	8.220E-08	1.8490E-03	0.06457	116.5	0.12457	93.17
22	hmt006_c11	0.98965	0.00081	0.0040	0.0041	6.236E-08	1.8490E-03	0.06457	116.5	0.12457	93.17
23	hmt006_c12	0.99425	0.00071	0.0040	0.0041	5.428E-08	1.8490E-03	0.06457	116.5	0.12457	93.17
24	hmt006_c13	1.01283	0.00086	0.0040	0.0041	8.231E-08	1.8490E-03	0.06457	116.5	0.12457	93.17
25	hmt006_c14	0.98495	0.00071	0.0061	0.0061	5.715E-08	1.8490E-03	0.06457	116.5	0.12457	93.17

(continued)

Table 6.12-11 – Benchmark Experiment Data

No	Case	k	σ_{mcnp}	σ_{bench}	σ_{total}	EALF (MeV)	U-235 (atom/b-cm)	Channel Spacing (in)	H/U-235	Plate Pitch (in)	Enrichment (%)
26	hmt006_c15	0.98155	0.00073	0.0040	0.0041	5.638E-08	1.8490E-03	0.06457	116.5	0.12457	93.17
27	hmt006_c16	0.99241	0.00078	0.0040	0.0041	6.330E-08	1.8490E-03	0.06457	116.5	0.12457	93.17
28	hmt006_c17	0.98946	0.00082	0.0040	0.0041	7.384E-08	1.8490E-03	0.06457	116.5	0.12457	93.17
29	hmt006_c18	0.99252	0.00088	0.0040	0.0041	8.009E-08	1.8490E-03	0.06457	116.5	0.12457	93.17
30	hmt006_c19	0.99442	0.00070	0.0040	0.0041	5.222E-08	1.8490E-03	0.06457	113.9	0.12457	93.17
31	hmt006_c20	0.99319	0.00082	0.0040	0.0041	6.461E-08	1.8490E-03	0.06457	113.7	0.12457	93.17
32	hmt006_c21	0.99604	0.00076	0.0040	0.0041	6.923E-08	1.8490E-03	0.06457	113.7	0.12457	93.17
33	hmt006_c22	0.99552	0.00079	0.0040	0.0041	7.408E-08	1.8490E-03	0.06457	113.6	0.12457	93.17
34	hmt006_c23	1.00066	0.00078	0.0040	0.0041	7.637E-08	1.8490E-03	0.06457	113.5	0.12457	93.17
35	hmt022_c01	0.99179	0.00013	0.0035	0.0035	1.585E-07	3.9260E-03	0.078	66.0	0.12800	93.0
36	ict014	0.99647	0.00059	0.0014	0.0015	8.821E-08	2.4170E-03	0.10669	147.0	0.16535	19.77
37	lct001_c01	0.99562	0.00076	0.0030	0.0031	1.007E-07	4.8785E-04	na	399.0	na	2.35
38	lct001_c02	0.99637	0.00079	0.0030	0.0031	9.962E-08	4.8785E-04	na	399.0	na	2.35
39	lct001_c03	0.99385	0.00071	0.0030	0.0031	9.883E-08	4.8785E-04	na	399.0	na	2.35
40	lct001_c04	0.99543	0.00075	0.0030	0.0031	9.956E-08	4.8785E-04	na	399.0	na	2.35
41	lct001_c05	0.99271	0.00075	0.0030	0.0031	9.795E-08	4.8785E-04	na	399.0	na	2.35
42	lct001_c06	0.99376	0.00079	0.0030	0.0031	9.917E-08	4.8785E-04	na	399.0	na	2.35
43	lct001_c07	0.99561	0.00074	0.0031	0.0032	9.655E-08	4.8785E-04	na	399.0	na	2.35
44	lct001_c08	0.99224	0.00072	0.0030	0.0031	9.843E-08	4.8785E-04	na	399.0	na	2.35
45	lct002_c01	0.99550	0.00072	0.0020	0.0021	1.181E-07	1.0102E-03	na	271.0	na	4.31
46	lct002_c02	0.99611	0.00073	0.0020	0.0021	1.175E-07	1.0102E-03	na	271.0	na	4.31
47	lct002_c03	0.99499	0.00071	0.0020	0.0021	1.172E-07	1.0102E-03	na	271.0	na	4.31
48	lct002_c04	0.99486	0.00072	0.0018	0.0019	1.171E-07	1.0102E-03	na	271.0	na	4.31
49	lct002_c05	0.99254	0.00078	0.0019	0.0021	1.145E-07	1.0102E-03	na	271.0	na	4.31
50	lct006_c01	0.99488	0.00077	0.0020	0.0021	2.482E-07	6.0830E-04	na	164.7	na	2.596

(continued)

Table 6.12-11 – Benchmark Experiment Data

No	Case	k	σ_{mcnp}	σ_{bench}	σ_{total}	EALF (MeV)	U-235 (atom/b-cm)	Channel Spacing (in)	H/U-235	Plate Pitch (in)	Enrichment (%)
51	lct006_c02	0.99547	0.00074	0.0020	0.0021	2.550E-07	6.0830E-04	na	164.7	na	2.596
52	lct006_c03	0.99481	0.00083	0.0020	0.0022	2.626E-07	6.0830E-04	na	164.7	na	2.596
53	lct006_c04	0.99708	0.00069	0.0020	0.0021	1.903E-07	6.0830E-04	na	201.1	na	2.596
54	lct006_c05	0.99634	0.00076	0.0020	0.0021	1.958E-07	6.0830E-04	na	201.1	na	2.596
55	lct006_c06	0.99599	0.00066	0.0020	0.0021	2.012E-07	6.0830E-04	na	201.1	na	2.596
56	lct006_c07	0.99464	0.00070	0.0020	0.0021	2.061E-07	6.0830E-04	na	201.1	na	2.596
57	lct006_c08	0.99551	0.00077	0.0020	0.0021	2.109E-07	6.0830E-04	na	201.1	na	2.596
58	lct006_c09	0.99613	0.00075	0.0020	0.0021	1.419E-07	6.0830E-04	na	272.3	na	2.596
59	lct006_c10	0.99722	0.00069	0.0020	0.0021	1.446E-07	6.0830E-04	na	272.3	na	2.596
60	lct006_c11	0.99622	0.00068	0.0020	0.0021	1.489E-07	6.0830E-04	na	272.3	na	2.596
61	lct006_c12	0.99640	0.00068	0.0020	0.0021	1.523E-07	6.0830E-04	na	272.3	na	2.596
62	lct006_c13	0.99655	0.00074	0.0020	0.0021	1.557E-07	6.0830E-04	na	272.3	na	2.596
63	lct006_c14	0.99497	0.00070	0.0020	0.0021	1.196E-07	6.0830E-04	na	329.1	na	2.596
64	lct006_c15	0.99717	0.00068	0.0020	0.0021	1.222E-07	6.0830E-04	na	329.1	na	2.596
65	lct006_c16	0.99617	0.00069	0.0020	0.0021	1.250E-07	6.0830E-04	na	329.1	na	2.596
66	lct006_c17	0.99542	0.00070	0.0020	0.0021	1.289E-07	6.0830E-04	na	329.1	na	2.596
67	lct006_c18	0.99593	0.00071	0.0020	0.0021	1.310E-07	6.0830E-04	na	329.1	na	2.596
68	lct009_c01	0.99386	0.00075	0.0021	0.0022	1.175E-07	1.0102E-03	na	256.2	na	4.31
69	lct009_c02	0.99508	0.00073	0.0021	0.0022	1.170E-07	1.0102E-03	na	256.2	na	4.31
70	lct009_c03	0.99365	0.00077	0.0021	0.0022	1.172E-07	1.0102E-03	na	256.2	na	4.31
71	lct009_c04	0.99535	0.00069	0.0021	0.0022	1.168E-07	1.0102E-03	na	256.2	na	4.31
72	lct009_c05	0.99609	0.00063	0.0021	0.0022	1.187E-07	1.0102E-03	na	256.2	na	4.31
73	lct009_c06	0.99539	0.00074	0.0021	0.0022	1.169E-07	1.0102E-03	na	256.2	na	4.31
74	lct009_c07	0.99676	0.00073	0.0021	0.0022	1.187E-07	1.0102E-03	na	256.2	na	4.31
75	lct009_c08	0.99309	0.00074	0.0021	0.0022	1.172E-07	1.0102E-03	na	256.2	na	4.31

(continued)

Table 6.12-11 – Benchmark Experiment Data (concluded)

No	Case	k	σ_{mcnp}	σ_{bench}	σ_{total}	EALF (MeV)	U-235 (atom/b-cm)	Channel Spacing (in)	H/U-235	Plate Pitch (in)	Enrichment (%)
76	lct009_c24	0.99520	0.00070	0.0021	0.0022	1.168E-07	1.0102E-03	na	256.2	na	4.31
77	lct009_c25	0.99492	0.00067	0.0021	0.0022	1.167E-07	1.0102E-03	na	256.2	na	4.31
78	lct009_c26	0.99480	0.00077	0.0021	0.0022	1.166E-07	1.0102E-03	na	256.2	na	4.31
79	lct009_c27	0.99491	0.00085	0.0021	0.0023	1.164E-07	1.0102E-03	na	256.2	na	4.31
80	lct010_c09	0.99797	0.00077	0.0021	0.0022	1.267E-07	1.0102E-03	na	256.3	na	4.31
81	lct010_c10	0.99775	0.00078	0.0021	0.0022	1.232E-07	1.0102E-03	na	256.3	na	4.31
82	lct010_c11	1.00076	0.00069	0.0021	0.0022	1.197E-07	1.0102E-03	na	256.3	na	4.31
83	lct010_c12	0.99679	0.00078	0.0021	0.0022	1.165E-07	1.0102E-03	na	256.3	na	4.31
84	lct010_c13	0.99366	0.00070	0.0021	0.0022	1.155E-07	1.0102E-03	na	256.3	na	4.31
85	lct010_c14	0.99729	0.00075	0.0028	0.0029	3.217E-07	1.0102E-03	na	105.5	na	4.31
86	lct010_c15	0.99775	0.00079	0.0028	0.0029	3.072E-07	1.0102E-03	na	105.5	na	4.31
87	lct010_c16	0.99823	0.00077	0.0028	0.0029	2.997E-07	1.0102E-03	na	105.5	na	4.31
88	lct010_c17	0.99923	0.00076	0.0028	0.0029	2.938E-07	1.0102E-03	na	105.5	na	4.31
89	lct010_c18	0.99796	0.00082	0.0028	0.0029	2.868E-07	1.0102E-03	na	105.5	na	4.31
90	lct010_c19	0.99726	0.00084	0.0028	0.0029	2.807E-07	1.0102E-03	na	105.5	na	4.31

6.12.9 Sample Input File

A sample input file (NA_MO_P030) is provided for the most reactive case (Case MO13).

```
ATR
999     0      -320:321:-322:323:-324:325                 imp:n=0
900     0      310 -311 312 -313 24 -25     fill=3       imp:n=1
901     2 -1.0 (311:-310:313:-312:-24:25) 320 -321 322 -323 324 -325  imp:n=1
c
c       Universe 1: ATR Fuel Element (infinitely long)
c
2       3 -2.7          -6 8 9 -10                  u=1 imp:n=1 $ left Al piece
4       3 -2.7          -5 7 9 -10                  u=1 imp:n=1 $ right Al piece
6       10 5.5147E-02  52 -53 -14 -13               u=1 imp:n=1 $ plate 1
8       3 -2.7          51 -54   -7 -8        #6   u=1 imp:n=1
10      2 -1.00         54 -55   -7 -8              u=1 imp:n=1
c
12      11 5.5136E-02  56 -57 -16 -15               u=1 imp:n=1 $ plate 2
14      3 -2.7          55 -58   -7 -8        #12  u=1 imp:n=1
16      2 -1.00         58 -59   -7 -8              u=1 imp:n=1
c
18      12 5.4749E-02  60 -61 -16 -15               u=1 imp:n=1 $ plate 3
20      3 -2.7          59 -62   -7 -8        #18  u=1 imp:n=1
22      2 -1.00         62 -63   -7 -8              u=1 imp:n=1
c
24      13 5.4757E-02  64 -65 -16 -15               u=1 imp:n=1 $ plate 4
26      3 -2.7          63 -66   -7 -8        #24  u=1 imp:n=1
28      2 -1.00         66 -67   -7 -8              u=1 imp:n=1
c
30      14 4.6966E-02   68 -69 -16 -15                      u=1 imp:n=1 $ plate 5 U-Mo
31      7 -6.506        400 -68 -16 -15                     u=1 imp:n=1 $ zirc
32      7 -6.506       -401  69 -16 -15                     u=1 imp:n=1 $ zirc
33      3 -2.7          67 -70   -7 -8        #30 #31 #32  u=1 imp:n=1
34      2 -1.00         70 -71   -7 -8                      u=1 imp:n=1
c
35      15 4.7082E-02  72 -73 -16 -15                       u=1 imp:n=1 $ plate 6 U-Mo
36      7 -6.506        402 -72 -16 -15                     u=1 imp:n=1 $ zirc
37      7 -6.506       -403  73 -16 -15                     u=1 imp:n=1 $ zirc
38      3 -2.7          71 -74   -7 -8        #35 #36 #37  u=1 imp:n=1
39      2 -1.00         74 -75   -7 -8                      u=1 imp:n=1
c
40      16 4.7170E-02  76 -77 -16 -15                       u=1 imp:n=1 $ plate 7 U-Mo
41      7 -6.506        404 -76 -16 -15                     u=1 imp:n=1 $ zirc
42      7 -6.506       -405  77 -16 -15                     u=1 imp:n=1 $ zirc
43      3 -2.7          75 -78   -7 -8        #40 #41 #42  u=1 imp:n=1
44      2 -1.00         78 -79   -7 -8                      u=1 imp:n=1
c
45      17 4.7269E-02  80 -81 -16 -15                       u=1 imp:n=1 $ plate 8 U-Mo
46      7 -6.506        406 -80 -16 -15                     u=1 imp:n=1 $ zirc
47      7 -6.506       -407  81 -16 -15                     u=1 imp:n=1 $ zirc
48      3 -2.7          79 -82   -7 -8        #45 #46 #47  u=1 imp:n=1
49      2 -1.00         82 -83   -7 -8                      u=1 imp:n=1
c
50      18 4.7343E-02  84 -85 -16 -15                       u=1 imp:n=1 $ plate 9 U-Mo
51      7 -6.506        408 -84 -16 -15                     u=1 imp:n=1 $ zirc
52      7 -6.506       -409  85 -16 -15                     u=1 imp:n=1 $ zirc
53      3 -2.7          83 -86   -7 -8        #50 #51 #52  u=1 imp:n=1
54      2 -1.00         86 -87   -7 -8                      u=1 imp:n=1
c
55      19 4.7423E-02  88 -89 -16 -15                       u=1 imp:n=1 $ plate 10 U-Mo
56      7 -6.506        410 -88 -16 -15                     u=1 imp:n=1 $ zirc
57      7 -6.506       -411  89 -16 -15                     u=1 imp:n=1 $ zirc
```

```
58      3 -2.7         87 -90   -7 -8       #55 #56 #57  u=1 imp:n=1
59      2 -1.00        90 -91   -7 -8                    u=1 imp:n=1
c
60      20 4.7487E-02  92 -93 -16 -15                    u=1 imp:n=1 $ plate 11 U-Mo
61      7 -6.506       412 -92 -16 -15                   u=1 imp:n=1 $ zirc
62      7 -6.506      -413  93 -16 -15                   u=1 imp:n=1 $ zirc
63      3 -2.7         91 -94   -7 -8       #60 #61 #62  u=1 imp:n=1
64      2 -1.00        94 -95   -7 -8                    u=1 imp:n=1
c
65      21 4.7562E-02  96 -97 -16 -15                    u=1 imp:n=1 $ plate 12 U-Mo
66      7 -6.506       414 -96 -16 -15                   u=1 imp:n=1 $ zirc
67      7 -6.506      -415  97 -16 -15                   u=1 imp:n=1 $ zirc
68      3 -2.7         95 -98   -7 -8       #65 #66 #67  u=1 imp:n=1
69      2 -1.00        98 -99   -7 -8                    u=1 imp:n=1
c
70      22 4.7617E-02  100 -101 -16 -15                  u=1 imp:n=1 $ plate 13 U-Mo
71      7 -6.506       416 -100 -16 -15                  u=1 imp:n=1 $ zirc
72      7 -6.506      -417  101 -16 -15                  u=1 imp:n=1 $ zirc
73      3 -2.7          99 -102   -7 -8     #70 #71 #72  u=1 imp:n=1
74      2 -1.00        102 -103   -7 -8                  u=1 imp:n=1
c
75      23 4.7684E-02  104 -105 -16 -15                  u=1 imp:n=1 $ plate 14 U-Mo
76      7 -6.506       418 -104 -16 -15                  u=1 imp:n=1 $ zirc
77      7 -6.506      -419  105 -16 -15                  u=1 imp:n=1 $ zirc
78      3 -2.7         103 -106   -7 -8     #75 #76 #77  u=1 imp:n=1
79      2 -1.00        106 -107   -7 -8                  u=1 imp:n=1
c
80      24 4.7726E-02  108 -109 -16 -15                  u=1 imp:n=1 $ plate 15 U-Mo
81      7 -6.506       420 -108 -16 -15                  u=1 imp:n=1 $ zirc
82      7 -6.506      -421  109 -16 -15                  u=1 imp:n=1 $ zirc
83      3 -2.7         107 -110   -7 -8     #80 #81 #82  u=1 imp:n=1
84      2 -1.00        110 -111   -7 -8                  u=1 imp:n=1
c
96      25 5.4721E-02  112 -113 -16 -15          u=1 imp:n=1 $ plate 16
98      3 -2.7         111 -114   -7 -8     #96  u=1 imp:n=1
100     2 -1.00        114 -115   -7 -8          u=1 imp:n=1
c
102     26 5.4721E-02  116 -117 -16 -15          u=1 imp:n=1 $ plate 17
104     3 -2.7         115 -118   -7 -8     #102 u=1 imp:n=1
106     2 -1.00        118 -119   -7 -8          u=1 imp:n=1
c
108     27 5.5091E-02  120 -121 -18 -17          u=1 imp:n=1 $ plate 18
110     3 -2.7         119 -122   -7 -8     #108 u=1 imp:n=1
112     2 -1.00        122 -123   -7 -8          u=1 imp:n=1
c
114     3 -2.7         124 -125 -14 -13          u=1 imp:n=1 $ plate 19 (dummy)
116     3 -2.7         123 -126   -7 -8     #114 u=1 imp:n=1
120     2 -1.00        126 -10 -8 -7             u=1 imp:n=1 $ above 19
121     2 -1.00        9 -51 -8 -7               u=1 imp:n=1 $ below 1
122     5 -0.737       5 -11 9 -10               u=1 imp:n=1 $ right neoprene
123     5 -0.737     -12 6 9 -10                 u=1 imp:n=1 $ left neoprene
125     2 -1.0        12:11:-9:10                u=1 imp:n=1
c
c       Universe 20: ATR with pipe (center)
c
200     0  -27 -26 22 -23:26 -20 22 -28:27 -21 22 -28  trcl=1
             fill=1  u=20 imp:n=1
201     2 -0.3      #200 -200                  u=20 imp:n=1 $ between ATR/pipe
202     4 -7.94      200 -201                  u=20 imp:n=1 $ pipe
203     6 -0.096     201 -203 250 -251 252 -253 u=20 imp:n=1 $ insulation
204     0            203 250 -251 252 -253      u=20 imp:n=1 $ insulation to tube
205     4 -7.94      -250:251:-252:253          u=20 imp:n=1 $ tube to inf
c
```

```
c       Universe 21: ATR with pipe (down)
c
210     0  -27 -26 22 -23:26 -20 22 -28:27 -21 22 -28  trcl=2
             fill=1  u=21 imp:n=1
211     2 -0.3     #210 -200                    u=21 imp:n=1 $ between ATR/pipe
212     4 -7.94     200 -201                    u=21 imp:n=1 $ pipe
213     6 -0.096    201 -203 250 -251 252 -253 u=21 imp:n=1 $ insulation
214     0           203 250 -251 252 -253      u=21 imp:n=1 $ insulation to tube
215     4 -7.94     -250:251:-252:253          u=21 imp:n=1 $ tube to inf
c
c       Universe 22: ATR with pipe (up)
c
220     0  -27 -26 22 -23:26 -20 22 -28:27 -21 22 -28  trcl=3
             fill=1  u=22 imp:n=1
221     2 -0.3     #220 -200                    u=22 imp:n=1 $ between ATR/pipe
222     4 -7.94     200 -201                    u=22 imp:n=1 $ pipe
223     6 -0.096    201 -203 250 -251 252 -253 u=22 imp:n=1 $ insulation
224     0           203 250 -251 252 -253      u=22 imp:n=1 $ insulation to tube
225     4 -7.94     -250:251:-252:253          u=22 imp:n=1 $ tube to inf
c
c       Universe 23: ATR with pipe (right)
c
230     0  -27 -26 22 -23:26 -20 22 -28:27 -21 22 -28  trcl=4
             fill=1  u=23 imp:n=1
231     2 -0.3     #230 -200                    u=23 imp:n=1 $ between ATR/pipe
232     4 -7.94     200 -201                    u=23 imp:n=1 $ pipe
233     6 -0.096    201 -203 250 -251 252 -253 u=23 imp:n=1 $ insulation
234     0           203 250 -251 252 -253      u=23 imp:n=1 $ insulation to tube
235     4 -7.94     -250:251:-252:253          u=23 imp:n=1 $ tube to inf
c
c       Universe 24: ATR with pipe (left)
c
240     0  -27 -26 22 -23:26 -20 22 -28:27 -21 22 -28  trcl=5
             fill=1  u=24 imp:n=1
241     2 -0.3     #240 -200                    u=24 imp:n=1 $ between ATR/pipe
242     4 -7.94     200 -201                    u=24 imp:n=1 $ pipe
243     6 -0.096    201 -203 250 -251 252 -253 u=24 imp:n=1 $ insulation
244     0           203 250 -251 252 -253      u=24 imp:n=1 $ insulation to tube
245     4 -7.94     -250:251:-252:253          u=24 imp:n=1 $ tube to inf
c
c       Universe 25: ATR with pipe (up right)
c
250     0  -27 -26 22 -23:26 -20 22 -28:27 -21 22 -28  trcl=6
             fill=1  u=25 imp:n=1
251     2 -0.3     #250 -200                    u=25 imp:n=1 $ between ATR/pipe
252     4 -7.94     200 -201                    u=25 imp:n=1 $ pipe
253     6 -0.096    201 -203 250 -251 252 -253 u=25 imp:n=1 $ insulation
254     0           203 250 -251 252 -253      u=25 imp:n=1 $ insulation to tube
255     4 -7.94     -250:251:-252:253          u=25 imp:n=1 $ tube to inf
c
c       Universe 26: ATR with pipe (up left)
c
260     0  -27 -26 22 -23:26 -20 22 -28:27 -21 22 -28  trcl=7
             fill=1  u=26 imp:n=1
261     2 -0.3     #260 -200                    u=26 imp:n=1 $ between ATR/pipe
262     4 -7.94     200 -201                    u=26 imp:n=1 $ pipe
263     6 -0.096    201 -203 250 -251 252 -253 u=26 imp:n=1 $ insulation
264     0           203 250 -251 252 -253      u=26 imp:n=1 $ insulation to tube
265     4 -7.94     -250:251:-252:253          u=26 imp:n=1 $ tube to inf
c
c       Universe 27: ATR with pipe (down right)
c
270     0  -27 -26 22 -23:26 -20 22 -28:27 -21 22 -28  trcl=8
```

```
            fill=1  u=27 imp:n=1
271     2 -0.3     #270 -200                   u=27 imp:n=1 $ between ATR/pipe
272     4 -7.94     200 -201                   u=27 imp:n=1 $ pipe
273     6 -0.096    201 -203 250 -251 252 -253 u=27 imp:n=1 $ insulation
274     0           203 250 -251 252 -253      u=27 imp:n=1 $ insulation to tube
275     4 -7.94     -250:251:-252:253          u=27 imp:n=1 $ tube to inf
c
c       Universe 28: ATR with pipe (down left)
c
280     0  -27 -26 22 -23:26 -20 22 -28:27 -21 22 -28  trcl=9
            fill=1  u=28 imp:n=1
281     2 -0.3     #280 -200                   u=28 imp:n=1 $ between ATR/pipe
282     4 -7.94     200 -201                   u=28 imp:n=1 $ pipe
283     6 -0.096    201 -203 250 -251 252 -253 u=28 imp:n=1 $ insulation
284     0           203 250 -251 252 -253      u=28 imp:n=1 $ insulation to tube
285     4 -7.94     -250:251:-252:253          u=28 imp:n=1 $ tube to inf
c
c       Universe 3: Array of Packages
c
300   0    -300 301 -302 303 imp:n=1 u=3 lat=1 fill=-4:4 -4:4 0:0
            25 25 25 25 22 26 26 26 26
            25 25 25 25 22 26 26 26 26
            25 25 25 25 22 26 26 26 26
            25 25 25 25 22 26 26 26 26
            23 23 23 23 20 24 24 24 24
            27 27 27 27 21 28 28 28 28
            27 27 27 27 21 28 28 28 28
            27 27 27 27 21 28 28 28 28
            27 27 27 27 21 28 28 28 28

5       p  2.4142136 -1 0 -0.2665911 $ right Al outer
6       p -2.4142136 -1 0 -0.2665911 $ left Al outer
7       p  2.4142136 -1 0 -1.474587  $ right Al inner
8       p -2.4142136 -1 0 -1.474587  $ left Al inner
9       cz 7.52856                   $ Al boundary
10      cz 14.015466                 $ Al boundary
11      p  2.4142136 -1 0  0.563076  $ right neoprene
12      p -2.4142136 -1 0  0.563076  $ left neoprene
c
13      p  2.4142136 -1 0 -2.4370013 $ plate 1 & 19 meat
14      p -2.4142136 -1 0 -2.4370013 $ plate 1 & 19 meat
15      p  2.4142136 -1 0 -1.7732672 $ plate 2-17 meat
16      p -2.4142136 -1 0 -1.7732672 $ plate 2-17 meat
17      p  2.4142136 -1 0 -1.9060140 $ plate 18 meat
18      p -2.4142136 -1 0 -1.9060140 $ plate 18 meat
c
20      p  2.4142136 -1 0   0.6      $ right u0 boundary
21      p -2.4142136 -1 0   0.6      $ left u0 boundary
22      cz 7.51                      $ u0 boundary
23      cz 14.02                     $ u0 boundary
24      pz -60.96                    $ bottom of fuel
25      pz  60.96                    $ top of fuel (48")
26      p  2.4142136 -1 0  0.0       $ neoprene notch
27      p -2.4142136 -1 0  0.0       $ neoprene notch
28      cz 13.9                      $ neoprene notch
c
51      cz 7.67207  $ fuel plate 1 (0.089)
52      cz 7.7343
53      cz 7.7851
54      cz 7.84733
c
55      cz 8.07339  $ fuel plate 2
56      cz 8.09752
```

```
57      cz 8.14832
58      cz 8.17245
c
59      cz 8.39851  $ fuel plate 3
60      cz 8.42264
61      cz 8.47344
62      cz 8.49757
c
63      cz 8.72363  $ fuel plate 4
64      cz 8.74776
65      cz 8.79856
66      cz 8.82269
c
67      cz 9.04875  $ fuel plate 5
400     cz 9.07923
68      cz 9.08177
69      cz 9.11479
401     cz 9.11733
70      cz 9.14781
c
71      cz 9.37387  $ fuel plate 6
402     cz 9.40435
72      cz 9.40689
73      cz 9.43991
403     cz 9.44245
74      cz 9.47293
c
75      cz 9.69899  $ fuel plate 7
404     cz 9.72947
76      cz 9.73201
77      cz 9.76503
405     cz 9.76757
78      cz 9.79805
c
79      cz 10.02411  $ fuel plate 8
406     cz 10.05459
80      cz 10.05713
81      cz 10.09015
407     cz 10.09269
82      cz 10.12317
c
83      cz 10.34923  $ fuel plate 9
408     cz 10.37971
84      cz 10.38225
85      cz 10.41527
409     cz 10.41781
86      cz 10.44829
c
87      cz 10.67435  $ fuel plate 10
410     cz 10.70483
88      cz 10.70737
89      cz 10.74039
411     cz 10.74293
90      cz 10.77341
c
91      cz 10.99947  $ fuel plate 11
412     cz 11.02995
92      cz 11.03249
93      cz 11.06551
413     cz 11.06805
94      cz 11.09853
c
95      cz 11.32459  $ fuel plate 12
```

```
414     cz 11.35507
96      cz 11.35761
97      cz 11.39063
415     cz 11.39317
98      cz 11.42365
c
99       cz 11.64971  $ fuel plate 13
416      cz 11.68019
100      cz 11.68273
101      cz 11.71575
417      cz 11.71829
102      cz 11.74877
c
103      cz 11.97483  $ fuel plate 14
418      cz 12.00531
104      cz 12.00785
105      cz 12.04087
419      cz 12.04341
106      cz 12.07389
c
107      cz 12.29995  $ fuel plate 15
420      cz 12.33043
108      cz 12.33297
109      cz 12.36599
421      cz 12.36853
110      cz 12.39901
c
111      cz 12.62507  $ fuel plate 16
112      cz 12.6492
113      cz 12.7
114      cz 12.72413
c
115      cz 12.95019  $ fuel plate 17
116      cz 12.97432
117      cz 13.02512
118      cz 13.04925
c
119      cz 13.27531  $ fuel plate 18
120      cz 13.29944
121      cz 13.35024
122      cz 13.37437
c
123      cz 13.60043  $ fuel plate 19 (0.089)
124      cz 13.68806
125      cz 13.73886
126      cz 13.82649
c
200      cz 7.3838 $ IR pipe
201      cz 7.6581 $ OR pipe
202      cz 38.1   $ 12" water
203      cz 10.1981 $ 1" insulation
c
250      px  -9.6032 $ square tube
251      px   9.6032
252      py  -9.6032
253      py   9.6032
c
300      px  10.033 $ lattice surfaces/sq. tube
301      px -10.033
302      py  10.033
303      py -10.033
310      px -90.297 $ 9x9 bounds
311      px  90.297
```

```
312      py -90.297
313      py  90.297
320      px -120.777 $ outer bounds
321      px  120.777
322      py -120.777
323      py  120.777
324      pz -91.44
325      pz  91.44

m2      1001.62c  2          $ water
        8016.62c  1
mt2     lwtr.60t
m3      13027.62c 1          $ Al
m4      6000.66c   -0.08     $ SS-304
        14000.60c  -1.0
        15031.66c  -0.045
        24000.50c  -19.0
        25055.62c  -2.0
        26000.55c  -68.375
        28000.50c  -9.5
m5      1001.62c  -0.056920  $ neoprene
        6000.66c  -0.542646
c        17000.66c -0.400434
m6      13027.62c  -26.5     $ insulation material
        14000.60c  -23.4
        8016.62c   -50.2
m7      40000.66c 1          $ zirc
m10     92234.69c 1.5558E-05 $ fuel plate 1
        92235.69c 2.4269E-03
        92236.69c 8.9982E-06
        92238.69c 1.2874E-04
        13027.62c 5.2567E-02
c       total     5.5147E-02
m11     92234.69c 1.5676E-05 $ fuel plate 2
        92235.69c 2.4455E-03
        92236.69c 9.0668E-06
        92238.69c 1.2972E-04
        13027.62c 5.2536E-02
c       total     5.5136E-02
m12     92234.69c 1.9838E-05 $ fuel plate 3
        92235.69c 3.0947E-03
        92236.69c 1.1474E-05
        92238.69c 1.6416E-04
        13027.62c 5.1458E-02
c       total     5.4749E-02
m13     92234.69c 1.9753E-05 $ fuel plate 4
        92235.69c 3.0815E-03
        92236.69c 1.1425E-05
        92238.69c 1.6346E-04
        13027.62c 5.1480E-02
c       total     5.4757E-02
m14     92234.69c 4.8582E-05 $ fuel plate 5
        92235.69c 7.4422E-03
        92236.69c 8.5223E-05
        92238.69c 2.9261E-02
        42000.66c 1.0129E-02
c       total     4.6966E-02
m15     92234.69c 4.8702E-05 $ fuel plate 6
        92235.69c 7.4607E-03
        92236.69c 8.5434E-05
        92238.69c 2.9333E-02
        42000.66c 1.0154E-02
c       total     4.7082E-02
```

```
m16     92234.69c 4.8793E-05 $ fuel plate 7
        92235.69c 7.4745E-03
        92236.69c 8.5592E-05
        92238.69c 2.9388E-02
        42000.66c 1.0173E-02
c       total     4.7170E-02
m17     92234.69c 4.8895E-05 $ fuel plate 8
        92235.69c 7.4903E-03
        92236.69c 8.5773E-05
        92238.69c 2.9450E-02
        42000.66c 1.0195E-02
c       total     4.7269E-02
m18     92234.69c 4.8972E-05 $ fuel plate 9
        92235.69c 7.5020E-03
        92236.69c 8.5907E-05
        92238.69c 2.9496E-02
        42000.66c 1.0211E-02
c       total     4.7343E-02
m19     92234.69c 4.9055E-05 $ fuel plate 10
        92235.69c 7.5147E-03
        92236.69c 8.6052E-05
        92238.69c 2.9546E-02
        42000.66c 1.0228E-02
c       total     4.7423E-02
m20     92234.69c 4.9120E-05 $ fuel plate 11
        92235.69c 7.5248E-03
        92236.69c 8.6167E-05
        92238.69c 2.9585E-02
        42000.66c 1.0242E-02
c       total     4.7487E-02
m21     92234.69c 4.9199E-05 $ fuel plate 12
        92235.69c 7.5367E-03
        92236.69c 8.6304E-05
        92238.69c 2.9632E-02
        42000.66c 1.0258E-02
c       total     4.7562E-02
m22     92234.69c 4.9255E-05 $ fuel plate 13
        92235.69c 7.5454E-03
        92236.69c 8.6404E-05
        92238.69c 2.9666E-02
        42000.66c 1.0270E-02
c       total     4.7617E-02
m23     92234.69c 4.9324E-05 $ fuel plate 14
        92235.69c 7.5559E-03
        92236.69c 8.6525E-05
        92238.69c 2.9708E-02
        42000.66c 1.0284E-02
c       total     4.7684E-02
m24     92234.69c 4.9368E-05 $ fuel plate 15
        92235.69c 7.5627E-03
        92236.69c 8.6602E-05
        92238.69c 2.9734E-02
        42000.66c 1.0293E-02
c       total     4.7726E-02
m25     92234.69c 2.0136E-05 $ fuel plate 16
        92235.69c 3.1412E-03
        92236.69c 1.1646E-05
        92238.69c 1.6663E-04
        13027.62c 5.1381E-02
c       total     5.4721E-02
m26     92234.69c 2.0136E-05 $ fuel plate 17
        92235.69c 3.1412E-03
        92236.69c 1.1646E-05
```

```
        92238.69c 1.6662E-04
        13027.62c 5.1381E-02
c       total     5.4721E-02
m27     92234.69c 1.6158E-05 $ fuel plate 18
        92235.69c 2.5207E-03
        92236.69c 9.3456E-06
        92238.69c 1.3371E-04
        13027.62c 5.2411E-02
c       total     5.5091E-02
c
*tr1     0 -10.8 0                        $ base to center
*tr2     0 7.9 0    180 90 90 90 180 90   $ down
*tr3     0 -7.9 0                         $ up
*tr4    -7.9 0 0    90 180 90 0 90 90     $ right
*tr5     7.9 0 0    90 0 90 180 90 90     $ left
*tr6    -5.6  -5.6 0 45 135 90 45 45 90   $ up/right
*tr7     5.6  -5.6 0 45 45 90 135 45 90   $ up/left
*tr8    -5.6   5.6 0 135 135 90 45 135 90 $ down/right
*tr9     5.6   5.6 0 135 45 90 135 135 90 $ down/left
c
mode   n
kcode  2500 1.0 50 250
sdef    x=d1 y=d2 z=d3
si1     -90 90
sp1     0 1
si2     -90 90
sp2     0 1
si3     -60 60
sp3     0 1
```

6.13 Appendix E: Criticality Analysis for the Cobra Fuel Element

As shown in Section 6.11, Appendix C: *Criticality Analysis for Small Quantity Payloads*, a payload consisting of up to 400 g of HEU has a CSI of 25. There is a need to ship Cobra fuel elements, which have a U-235 content greater than 400 g U-235. The Cobra fuel element is analyzed using the same basic methodology developed for the small quantity payload. To simplify the modeling, the payload is treated as 450 g U-235 homogenized with water, and no credit is taken for fuel element structural materials. This conservatively increases the reactivity compared to modeling an explicit payload. The following analyses demonstrate that the ATR FFSC package with 450 g U-235 complies with the requirements of 10 CFR 71.55 and 71.59. The criticality safety index is 31.3.

6.13.1 Description of Criticality Design

6.13.1.1 Design Features

No special design features are required to maintain criticality safety. No poisons are utilized in the package. The separation provided by the packaging (outer flat-to-flat dimension of 7.9-in), along with the limit on the number of packages per shipment, is sufficient to maintain criticality safety.

6.13.1.2 Summary Table of Criticality Evaluation

The upper subcritical limit (USL) for ensuring that the ATR FFSC (single package or package array) is acceptably subcritical, as determined in Section 6.13.8, *Benchmark Evaluations*, is:

$$USL = 0.9209$$

The package is considered to be acceptably subcritical if the computed k_{safe} (k_s), which is defined as $k_{effective}$ (k_{eff}) plus twice the statistical uncertainty (σ), is less than or equal to the USL, or:

$$k_s = k_{eff} + 2\sigma \leq USL$$

The USL is determined on the basis of a benchmark analysis and incorporates the combined effects of code computational bias, the uncertainty in the bias based on both benchmark-model and computational uncertainties, and an administrative margin. The results of the benchmark analysis indicate that the USL is adequate to ensure subcriticality of the package.

The packaging design is shown to meet the requirements of 10 CFR 71.55(b). Moderation by water in the most reactive credible extent is utilized in both the normal conditions of transport (NCT) and hypothetical accident conditions of transport (HAC) analyses. In the single package NCT models, full-density water fills the accessible cavity, while in the single package HAC models, full-density water fills all cavities. In all single package models, 12-in of water reflection is utilized.

A 3x3x1 array of 8 packages (1 empty location) is utilized for the NCT array, while a 2x2x1 array of 4 packages is utilized in the HAC array. In the HAC array cases, partial moderation is considered to maximize array interaction effects. In all array models, 12-in of water reflection is utilized external to the array.

The maximum results of the criticality calculations are summarized in Table 6.13-1. Analyses are performed for 450 g U-235 in HEU. The maximum calculated k_s is 0.8952, which occurs for the optimally moderated NCT array case. The NCT array is more reactive than the HAC array because the NCT array is larger, and moderation is allowed in both conditions. In this case, the fuel mixture is modeled with a height of 35.0 cm, and void is modeled between the insulation and outer tube.

Table 6.13-1 – Summary of Criticality Evaluation, Cobra Element

Normal Conditions of Transport (NCT)	
Case	k_s
Single Unit Maximum	0.6622
8 Package Array Maximum	0.8952
Hypothetical Accident Conditions (HAC)	
Case	k_s
Single Unit Maximum	0.7409
4 Package Array Maximum	0.8400
USL = 0.9209	

6.13.1.3 Criticality Safety Index

The criticality safety index is defined in 10 CFR 71.59 as 50/N, where 5N packages are used in the NCT array configuration, and 2N packages are used in the HAC array configuration. An array of 4 packages (2N = 4, or N = 2.0) is utilized for the HAC array calculations, while an array of 8 packages (5N = 8, or N = 1.6) is utilized for the NCT array calculations. Therefore, the criticality safety index is 50/N = 50/1.6 = 31.3. With a CSI = 31.3, a maximum of three packages is allowed per exclusive use shipment.

6.13.2 Fissile Material Contents

The fissile material contents are a Cobra fuel element, which contain ≤ 450 g U-235 enriched up to 94% (HEU). Cobra fuel has both HEU and LEU options, and performing the analysis for HEU bounds lower enrichments.

The fuel is modeled as a homogenized mixture of uranium and water. Because the aluminum fuel element and fuel handling enclosure structural materials are conservatively ignored, the homogenized fuel mixture conforms to the cylindrical geometry constraint of the inner circular tube of the packaging. Inert materials in the fuel meat, such as aluminum and silicon, are also conservatively ignored. Modeling the structural and inert fuel meat materials would increase parasitic neutron absorption, as well as enlarge the size of the fissile volume to achieve the same hydrogen/U-235 ratio, and both effects would decrease the reactivity.

In general, for enrichments greater than 5% U-235, a system is more reactive using a homogenized mixture rather than an explicit geometric representation[18]. Therefore, a homogeneous model results in much higher computed reactivities than a heterogeneous model for these fuel types, which are typically enriched to at least ~20%.

[18] JJ Duderstadt and LJ Hamilton, *Nuclear Reactor Analysis*, p. 405, John Wiley & Sons, Inc., 1976.

The contents may contain burnable absorbers, such as gadolinium, samarium, or boron. All burnable absorbers are conservatively neglected in the analysis.

The isotopic distributions of HEU fuel are listed in Table 6.13-2 and are consistent with the isotopic set used in the ATR fuel element analysis. The U-235 enrichment for HEU is set to the maximum value of 94%. The fuel is modeled as homogenized mixture of uranium and water. Optimum reactivity is achieved by varying the height of the fissile mixture. A useful index of moderation for homogeneous systems is the hydrogen to U-235 ratio (hydrogen/U-235). This parameter is adjusted by varying the height of the fissile mixture. Increasing the height of the fissile mixture increases hydrogen/U-235.

The ATR FFSC may contain hydrogenous materials. Fuel elements may be transported in a polyethylene (CH_2) bag. This mass is bounded by considering 100 g of polyethylene. It has been demonstrated in the small quantity analysis (see Section 6.11, *Appendix C: Criticality Analysis for Small Quantity Payloads*) that the system is slightly more reactive when 100 g of polyethylene is included in the fissile mixture. Therefore, 100 g of polyethylene is included in all models.

Neoprene (C_4H_5Cl) is also used as a padding material in the fuel holders. While cellulosic material would not typically be used when transporting a Cobra fuel element, the total mass of neoprene plus cellulosic material is limited to 4000 g. However, it has been established in the small quantity analysis (see Section 6.11) that including neoprene or cellulosic material in the fissile mixture has a large negative effect on reactivity because these materials displace water and are less effective as a moderator than water. Therefore, neoprene and cellulosic material are conservatively neglected.

The atom densities of the homogenized mixture are computed in the following manner. The weight percent of U-235 is 94.0%. Therefore, the total mass of uranium M_U for 450 g U-235 is 450/0.94 = 478.7 g U. The density of uranium is 19.0 g/cm^3, so the solid-volume V_U of 478.7 g U is 478.7/19.0 = 25.2 cm^3. The density of polyethylene is 0.92 g/cm^3, so the solid volume V_P of 100 g polyethylene is 100/0.92 = 108.7 cm^3. The homogenized volume V is $\pi R^2 H$, where R is the inner radius of the ATR FFSC circular tube (7.3838 cm) and H is the height of the fissile mixture. The gram density of uranium in the mixture is then M_U/V, the gram density of polyethylene in the mixture is M_P/V, and if water of density 1.0 g/cm^3 fills the remaining volume, the water density in the mixture is $(V-V_U-V_P)/V$. The atom densities of uranium, polyethylene, and water may then be computed from the mixture gram densities.

Example fuel mixture atom densities are provided in Table 6.13-3 for a height of 35 cm. For this height, the homogenized volume $V = \pi*(7.3838)^2*35 = 5994.8$ cm^3. The gram density of uranium in the mixture is 478.7/5994.8 = 0.080 g/cm^3. The gram density of polyethylene in the mixture is 100/5994.8 = 0.017 g/cm^3. The gram density of water in the mixture is (5994.8 – 25.2 – 108.7)/5994.8 = 0.978 g/cm^3. Based on these gram densities, the atom densities are computed as $\rho A/M$, where

ρ = the gram density of the material (isotope or molecule) (g/cm^3)

A = Avogadro's constant (0.6022 #/b-mole)

M = atomic weight (g/mole)

Atom densities are computed separately for uranium, water, and polyethylene, and then combined to create a total mixture atom density. Cells in Table 6.13-3 marked with "-" are not needed to compute the atom densities.

Table 6.13-2 – Uranium Isotopics

Isotope	HEU (Wt. %)
U-234	0.60
U-235	94.0
U-236	0.35
U-238	5.05

Table 6.13-3 – Example Fissile Mixture Atom Densities (Height = 35 cm)

Material	wt.% in U	Atomic Weight (g/mole)	Density (g/cm^3)	Atom Densities (atom/b-cm)
Uranium (density = 0.080 g/cm^3)				
U-234	0.6	234.040945	0.000479	1.2328E-06
U-235	94	235.043922	0.075065	1.9232E-04
U-236	0.35	236.045561	0.000279	7.1305E-07
U-238	5.05	238.050785	0.004033	1.0202E-05
Water (density = 0.978 g/cm^3)				
H_2O	-	18.01528	0.978	3.2681E-02
H	-	1.00794	-	6.5361E-02
O	-	15.9994	-	3.2681E-02
Polyethylene (density = 0.017 g/cm^3)				
CH_2	-	14.02658	0.017	7.1616E-04
C	-	12.0107	-	7.1616E-04
H	-	1.00794	-	1.4323E-03
Combined Fissile Mixture				
U-234	-	-	-	1.2328E-06
U-235	-	-	-	1.9232E-04
U-236	-	-	-	7.1305E-07
U-238	-	-	-	1.0202E-05
H	-	-	-	6.6794E-02
C	-	-	-	7.1616E-04
O	-	-	-	3.2681E-02
Total	-	-	-	1.0039E-01

6.13.3 General Considerations

6.13.3.1 Model Configuration

The model configuration is relatively simple. Most packaging details are conservatively ignored, particularly at the ends. Because the package is long and narrow, array configurations will stack only in the lateral directions (e.g., 2x2x1). Therefore, the end details, for both the package and the fuel element, are conservatively ignored external to the active fuel region, and these end regions are simply modeled as full-density water.

The package length is modeled as 48-in long to be consistent with the original criticality models using ATR fuel (which has an active length of 48-in), although this length is somewhat arbitrary and is conservatively shorter than the actual inner cavity length of 67.88-in shown on the packaging general arrangement drawing 60501-10. The package is reflected with 12-in of full-density water.

Tolerances on the packaging are selected to result in the most reactive condition, as described in Section 6.3.1, *Model Configuration*. The standard ATR FFSC MCNP models are utilized with no change to the packaging descriptions.

The package consists of two primary structural components, a circular inner tube and a square outer tube. The modeled tube OD is 6.03-in, the modeled wall thickness is 0.108-in, and the modeled tube ID is 5.814-in. The outer tube is modeled with a wall thickness of 0.169-in and outer dimension of 7.9-in.

In the NCT single package models, the inner tube, insulation, and outer tube are modeled explicitly, as shown in Figure 6.13-1 and Figure 6.13-2. Although negligible water ingress is expected during NCT, the inner cavity of the package is assumed to be flooded with water because the package lid does not contain a seal. However, the region between the insulation and the outer tube will remain dry because water cannot enter this region. The fuel is transported in a Fuel Handling Enclosure (FHE), which is conservatively ignored because the fuel is homogenized with water. Modeling the FHE would decrease the reactivity significantly if it is assumed that the fuel is homogenized within the constraint of the FHE. If it is assumed that the homogenized mixture could flow out of the FHE, modeling the FHE would still be less reactive than ignoring it because it would displace fissile material and increase the size of the fissile cylinder.

The dimensions used in the MCNP models as discussed in the preceding paragraphs are summarized in Table 6.13-4.

The fuel elements may be transported in polyethylene bags. A polyethylene mass of 100 g is conservatively homogenized with the fuel/water mixture.

The HAC single package model is essentially the same as the NCT single package model. Damage in the drop tests was shown to be negligible and concentrated at the ends of the package (see Section 2.12.1, *Certification Tests on CTU-1*). As the ends of the package are not modeled, this end damage does not affect the modeling. The various side drops resulted in only minor localized damage to the outer tube, and no observable bulk deformation of the package. Therefore, the minor damage observed will not impact the reactivity. The insulation is replaced with full-density water, and the region between the insulation and outer tube is also filled with full-density water (see Figure 6.13-3). The treatment of the FHE is the same as the NCT single package model.

In the NCT array models, a 3x3x1 array is utilized, although one array position is empty, for a total of 8 packages. The geometry of a package in the NCT array is the same as the NCT single package models. In the HAC array models, a 2x2x1 array is utilized. The HAC array models are essentially the same as the NCT array models, except additional cases are developed to determine the reactivity effect of allowing variable density water in the region between the inner and outer tubes. The FHE is conservatively ignored for the reasons stated in the previous paragraphs. Because the NCT and HAC models are very similar and the NCT models utilize a larger array, the NCT array models are more reactive than the HAC array models.

The detailed moderation assumptions for these cases are discussed more fully in Section 6.13.5, *Evaluation of Package Arrays under Normal Conditions of Transport*, and Section 6.13.6, *Package Arrays under Hypothetical Accident Conditions*.

6.13.3.2 Material Properties

An example fissile material composition is provided in Table 6.13-3. The material properties of the packaging materials are provided in Section 6.3.2, *Material Properties*.

6.13.3.3 Computer Codes and Cross-Section Libraries

The computer codes and cross-section libraries utilized are provided in Section 6.3.3, *Computer Codes and Cross-Section Libraries*.

All cases are run with 5000 neutrons per generation for 850 generations, skipping the first 50. The 1-σ uncertainty is less than 0.001 for all cases.

6.13.3.4 Demonstration of Maximum Reactivity

The fissile material contents are in solid form. The uranium may be bonded to aluminum or silicon. To simplify the modeling and to obtain a conservative result, the fuel element structural materials are ignored, and the uranium is homogenized with water at optimum moderation. The fissile mixture is assumed to fill the inner tube of the ATR FFSC, and moderation is varied by developing cases with different fissile mixture heights. No credit is taken for fuel handling enclosures that would maintain the fuel in a more favorable geometry. Note that the homogenized representation is simply a conservative representation, and it is not implied that the actual fuel would behave in this manner. The fuel, even in accident conditions, would remain largely intact.

In the NCT cases, water fills only the inner tube, because water would not enter the region between the inner circular tube and outer square tube. In the HAC cases, water is allowed in the region between the inner circular tube and outer square tube. Also, insulation is replaced with water in the HAC cases. All single package cases are reflected with 12-in of water.

For the NCT array, 8 packages are modeled in a 3x3x1 array (with 1 empty corner location), while in the HAC array, a smaller 2x2x1 array is utilized. Because negligible damage was observed in the drop tests, the package dimensions are the same between the NCT and HAC models. Dimensions of the packaging are selected to maximize reactivity, and 12-in of close-water reflection is utilized.

The NCT array analysis is rather straightforward, because the only variable is the height of the fissile mixture. In the HAC array analysis, variables include the height of the fissile mixture and the water density of the region between the circular and square tubes. These parameters are varied to find the most reactive HAC condition.

Because fuel elements may be transported in polyethylene bags, 100 g of polyethylene is included in the fissile mixture. Polyethylene has a small, but positive, effect on the reactivity, as indicated in the small quantity payload analysis (See Section 6.11, *Appendix C: Criticality Analysis for Small Quantity Payloads*). The hydrogenous materials neoprene and cellulosic material are shown in the small quantity payload analysis to have a negative effect on reactivity because they are less effective at moderating the fissile mixture than the water that is displaced. Therefore, it is conservative to ignore neoprene and cellulosic material in the water moderated models.

The NCT array is more reactive than the HAC array, primarily because the NCT array is significantly larger, and both cases use a homogenized fuel representation. The most reactive NCT array case (Case CC07) has a fissile mixture height of 35.0 cm and results in $k_s = 0.89519$, which is below the USL of 0.9209. The most reactive HAC array case (Case CD35) has a fissile mixture height of 27.5 cm, 0.6 g/cm^3 water between the inner and outer tubes, and results in $k_s = 0.84001$.

Table 6.13-4 – Key Model Dimensions

Parameter	Drawing Dimension (in)	As-Modeled Dimension (in)	As-Modeled Dimension (cm)
Cavity length	67.88	48.0	121.92
Inner tube outer diameter	6.0	6.03	15.3162
Inner tube thickness	0.12	0.108	0.2743
Outer tube flat-to-flat	8.0	7.9	20.066
Outer tube thickness	0.188	0.169	0.4298
Insulation thickness (if modeled)	1.0	1.0	2.54

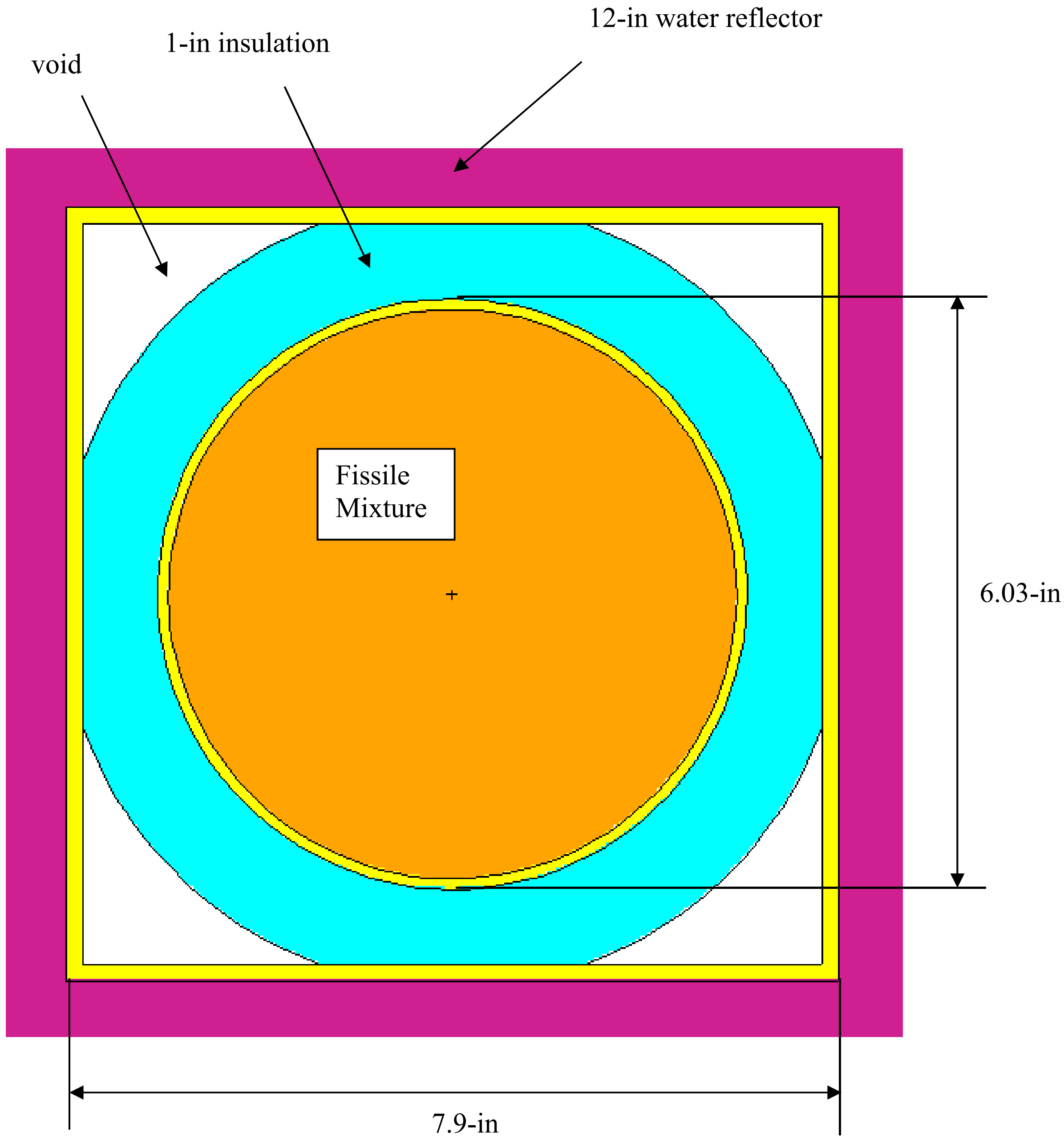

Inner tube thickness = 0.108-in

Outer tube thickness = 0.169-in

Figure 6.13-1 – NCT Single Package Model (planar view)

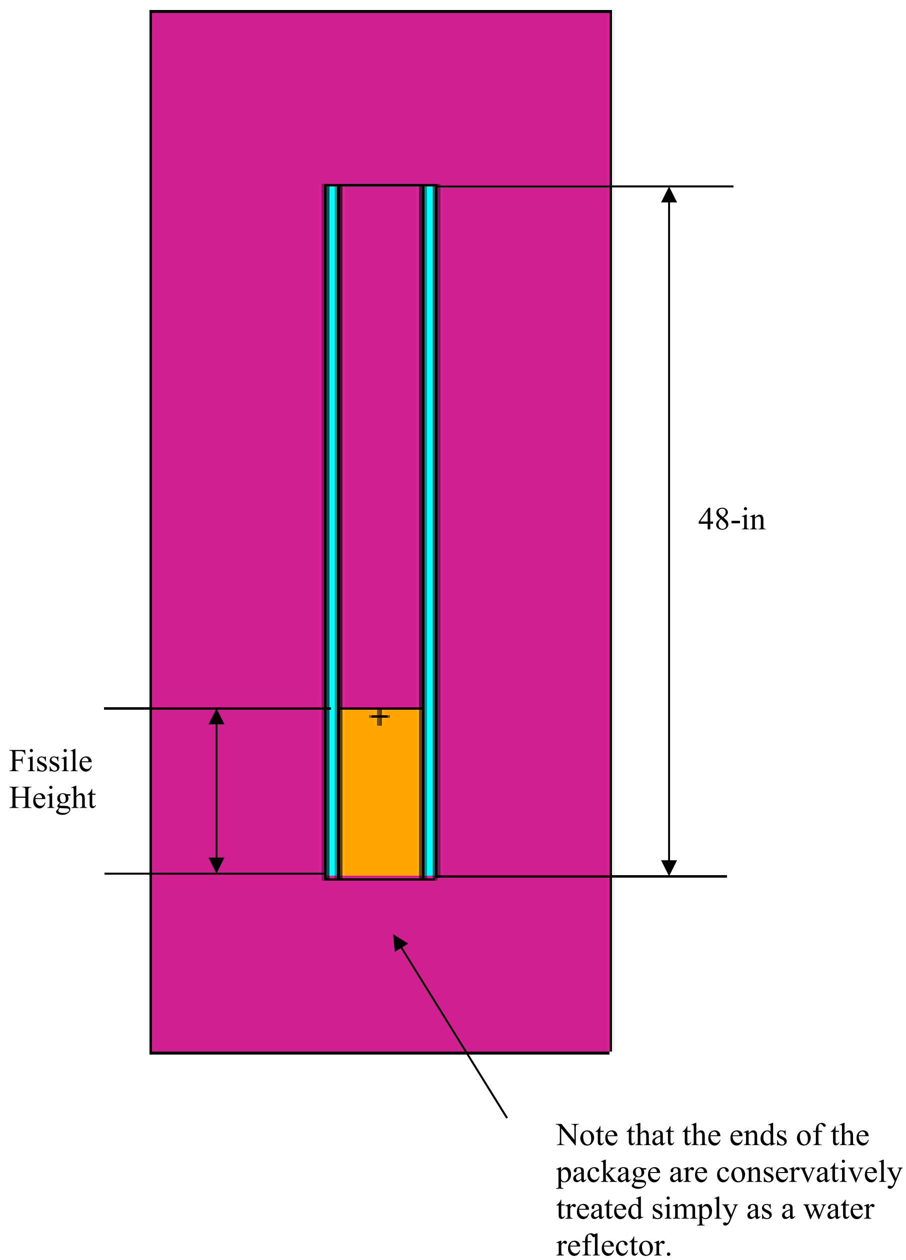

Figure 6.13-2 – NCT Single Package Model (axial view)

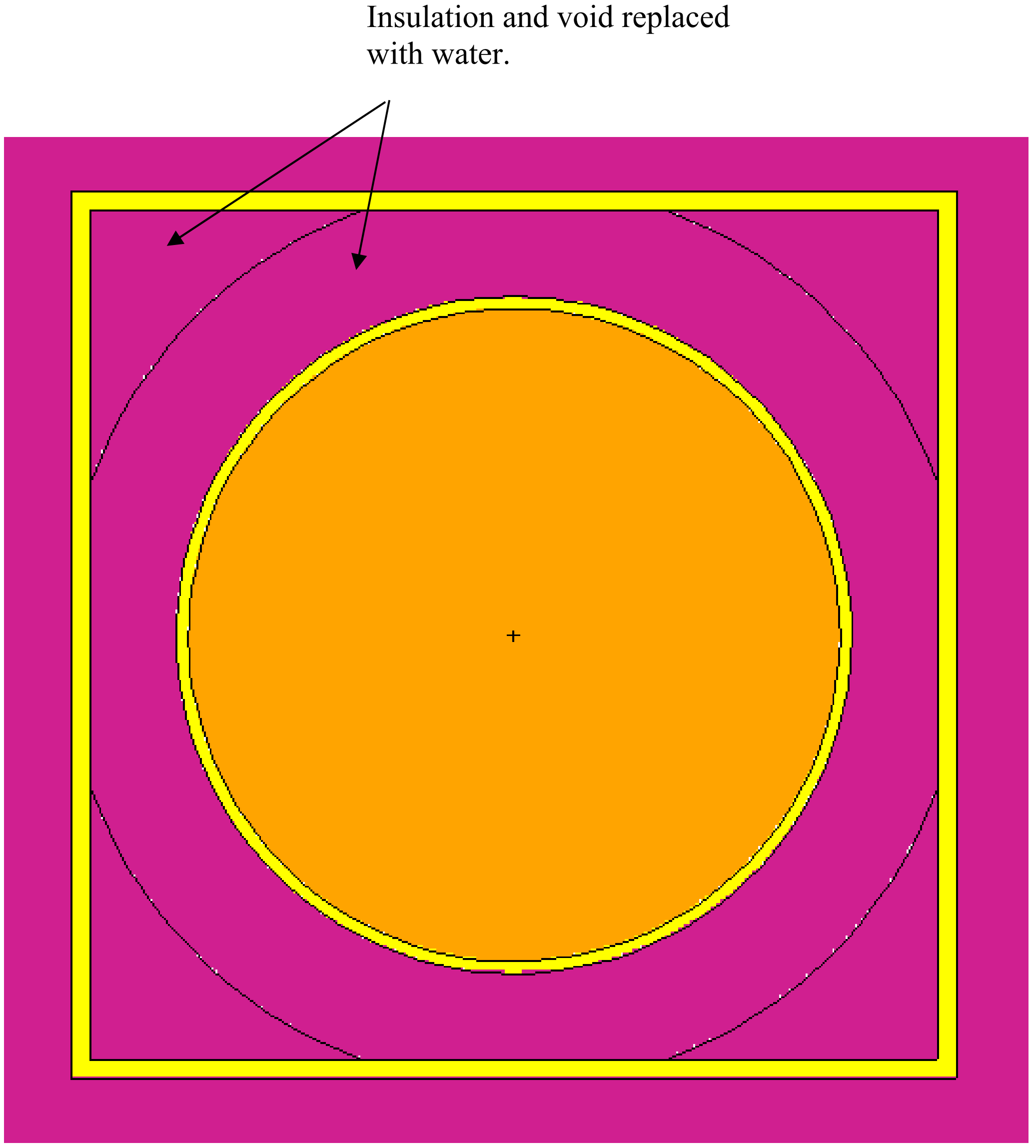

Figure 6.13-3 – HAC Single Package Model (planar view)

6.13.4 Single Package Evaluation

6.13.4.1 Single Package Configuration

6.13.4.1.1 NCT Single Package Configuration

The geometry of the NCT single package configuration is discussed in Section 6.13.3.1, *Model Configuration*. The uranium is homogenized with water for a variety of fissile mixture heights. The fissile mixture height is varied in 5 cm increments, with smaller 2.5 cm increments near the most reactive case. 100 g of polyethylene is included in the fissile mixture for all models. The water above the fissile mixture is modeled at full-density to maximize reflection. The package is reflected with 12-in of water.

Results are provided in Table 6.13-5. Maximum reactivity is achieved for Case CA04, with a fissile mixture height of 25.0 cm. The reactivity of this case is low, with k_s = 0.66215. This result is below the USL of 0.9209.

6.13.4.1.2 HAC Single Package Configuration

The geometry of the HAC single package configuration is discussed in Section 6.13.3.1. The uranium is homogenized with water for a variety of fissile mixture heights. The fissile mixture height is varied in 5 cm increments, with smaller 2.5 cm increments near the most reactive case. The water above the fissile mixture is modeled at full-density to maximize reflection. The insulation is replaced with full-density water, and the full-density water is also modeled between the inner and outer tubes. The package is reflected with 12-in of water.

Results are provided in Table 6.13-6. Maximum reactivity is achieved for Case CB04, with a fissile mixture height of 25.0 cm. The reactivity of this case is low, with k_s = 0.74090. This result is below the USL of 0.9209.

6.13.4.2 Single Package Results

Following are the tabulated results for the single package cases. The most reactive configurations are listed in boldface.

Table 6.13-5 – NCT Single Package Results

Case ID	Filename	Fissile Mixture Height (cm)	k_{eff}	σ	k_s ($k+2\sigma$)
CA01	NS_P100_H15	15.0	0.63301	0.00045	0.63391
CA02	NS_P100_H20	20.0	0.65519	0.00043	0.65605
CA03	NS_P100_H225	22.5	0.65846	0.00044	0.65934
CA04	**NS_P100_H25**	**25.0**	**0.66125**	**0.00045**	**0.66215**
CA05	NS_P100_H275	27.5	0.66043	0.00042	0.66127
CA06	NS_P100_H30	30.0	0.65919	0.00043	0.66005
CA07	NS_P100_H325	32.5	0.65695	0.00043	0.65781
CA08	NS_P100_H35	35.0	0.65196	0.00042	0.65280
CA09	NS_P100_H40	40.0	0.64299	0.00039	0.64377
CA10	NS_P100_H45	45.0	0.63143	0.00041	0.63225

Table 6.13-6 – HAC Single Package Results

Case ID	Filename	Fissile Mixture Height (cm)	k_{eff}	σ	k_s ($k+2\sigma$)
CB01	HS_P100_H15	15.0	0.70875	0.00045	0.70965
CB02	HS_P100_H20	20.0	0.73320	0.00045	0.73410
CB03	HS_P100_H225	22.5	0.73825	0.00044	0.73913
CB04	**HS_P100_H25**	**25.0**	**0.74002**	**0.00044**	**0.74090**
CB05	HS_P100_H275	27.5	0.73922	0.00042	0.74006
CB06	HS_P100_H30	30.0	0.73626	0.00045	0.73716
CB07	HS_P100_H325	32.5	0.73344	0.00044	0.73432
CB08	HS_P100_H35	35.0	0.72887	0.00042	0.72971
CB09	HS_P100_H40	40.0	0.71752	0.00041	0.71834
CB10	HS_P100_H45	45.0	0.70349	0.00043	0.70435

6.13.5 Evaluation of Package Arrays under Normal Conditions of Transport

6.13.5.1 NCT Array Configuration

The NCT array model is a 3x3x1 lattice with one empty corner location for a total of 8 packages, see Figure 6.13-4. Axial stacking configurations, such as 2x2x2, would lower the reactivity because the package is long and narrow, and axial separation would be provided by the ends of the package. The geometry of the individual packages is the same as the NCT single package model. The entire array is reflected with 12-in of full-density water. Moderation is varied by adjusting the height of the fissile mixture. The fissile mixture height is varied in 5 cm increments, with smaller 2.5 cm increments near the most reactive case. The region above the fissile mixture is filled with full density water to maximize reflection. 100 g of polyethylene is conservatively included in all models.

Results are provided in Table 6.13-7. The most reactive condition is Case CC07, which has a fissile height of 35.0 cm. For this case, k_s = 0.89519, which is below the USL of 0.9209.

6.13.5.2 NCT Array Results

Following are the tabulated results for the NCT array cases. The most reactive configuration is listed in boldface.

Table 6.13-7 – NCT Array Results

Case ID	Filename	Fissile Mixture Height (cm)	k_{eff}	σ	k_s ($k+2\sigma$)
CC01	NA_P100_H150	15.0	0.81428	0.00045	0.81518
CC02	NA_P100_H200	20.0	0.85880	0.00044	0.85968
CC03	NA_P100_H250	25.0	0.88397	0.00043	0.88483
CC04	NA_P100_H275	27.5	0.88851	0.00043	0.88937
CC05	NA_P100_H300	30.0	0.89331	0.00045	0.89421
CC06	NA_P100_H325	32.5	0.89382	0.00043	0.89468
CC07	**NA_P100_H350**	**35.0**	**0.89431**	**0.00044**	**0.89519**
CC08	NA_P100_H375	37.5	0.89110	0.00042	0.89194
CC09	NA_P100_H400	40.0	0.88794	0.00042	0.88878
CC10	NA_P100_H450	45.0	0.88014	0.00042	0.88098

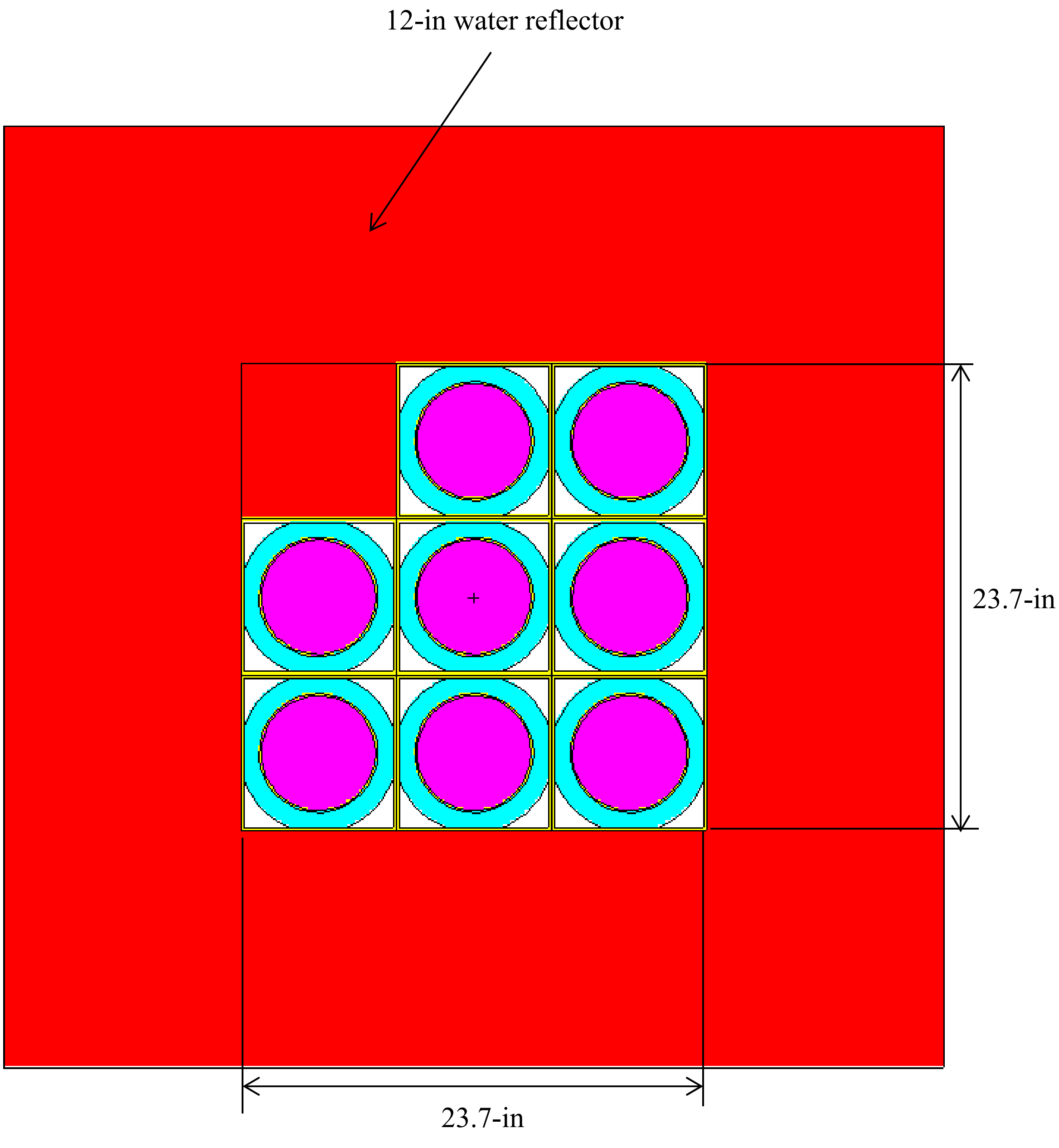

Figure 6.13-4 – NCT Array Geometry

6.13.6 Package Arrays under Hypothetical Accident Conditions

6.13.6.1 HAC Array Configuration

The HAC array model is a 2x2x1 array of the HAC single package model, as shown in Figure 6.13-5. Results are provided in Table 6.13-8. All HAC array cases include 100 g of polyethylene.

It was demonstrated in the small quantity payload analysis that the HAC array is more reactive when the insulation is replaced with water (See Section 6.11, *Appendix C: Criticality Analysis for Small Quantity Payloads*). Therefore, the insulation is replaced with water in all HAC array models. In Series 1, the region between the inner circular tube and outer square tube is filled with full-density water and the fissile mixture height is varied to find the optimum moderation. The fissile mixture height is varied in 5 cm increments, with smaller 2.5 cm increments near the most reactive case. The region above the fissile mixture is filled with full-density water. Case CD04 is the most reactive, with a fissile mixture height of 25.0 cm and $k_s = 0.83324$.

The reactivities of Case CD03 (height = 22.5 cm) through Case CD06 (height = 30.0 cm) are similar to the maximum reactivity Case CD04 (height = 25.0 cm). For each of these fissile mixture heights (i.e., 22.5 cm, 25.0 cm, 27.5 cm, and 30.0 cm), the water density between the tubes is varied between 0.1 g/cm^3 and 0.9 g/cm^3 to determine the most reactive condition. These results are presented in Series 2, 3, 4, and 5 and indicate that using a variable water density between the tubes results in a small increase in reactivity, although the most reactive result from each series is similar. The most reactive case is Case CD35, with a fissile mixture height of 27.5 cm, insulation replaced with water, 0.6 g/cm^3 water between the tubes, with $k_s = 0.84001$. This case is below the USL of 0.9209.

Note that the most reactive HAC array case is less reactive than the most reactive NCT array case (Case CC07, $k_s = 0.89519$) because 8 packages are used in the NCT array, while only 4 packages are used in the HAC array.

6.13.6.2 HAC Array Results

Following are the tabulated results for the HAC array cases. The most reactive configurations are listed in boldface.

Table 6.13-8 – HAC Array Results

Case ID	Filename	Fissile Mixture Height (cm)	Water Density Between Tubes (g/cm^3)	k_{eff}	σ	k_s (k+2σ)
Series 1: Full Density Water Between Tubes						
CD01	HA_H150	15.0	1.0	0.79291	0.00045	0.79381
CD02	HA_H200	20.0	1.0	0.82245	0.00045	0.82335
CD03	HA_H225	22.5	1.0	0.82933	0.00044	0.83021
CD04	**HA_H250**	**25.0**	**1.0**	**0.83236**	**0.00044**	**0.83324**
CD05	HA_H275	27.5	1.0	0.83190	0.00042	0.83274
CD06	HA_H300	30.0	1.0	0.83003	0.00043	0.83089
CD07	HA_H325	32.5	1.0	0.82694	0.00041	0.82776
CD08	HA_H350	35.0	1.0	0.82086	0.00041	0.82168
Series 2: Height = 22.5 cm, Variable Density Water Between Tubes						
CD10	HA_H225_W010	22.5	0.1	0.81167	0.00046	0.81259
CD11	HA_H225_W020	22.5	0.2	0.81917	0.00046	0.82009
CD12	HA_H225_W030	22.5	0.3	0.82534	0.00045	0.82624
CD13	HA_H225_W040	22.5	0.4	0.82944	0.00044	0.83032
CD14	HA_H225_W050	22.5	0.5	0.83126	0.00044	0.83214
CD15	HA_H225_W060	22.5	0.6	0.83218	0.00044	0.83306
CD16	**HA_H225_W070**	**22.5**	**0.7**	**0.83285**	**0.00046**	**0.83377**
CD17	HA_H225_W080	22.5	0.8	0.83150	0.00045	0.83240
CD18	HA_H225_W090	22.5	0.9	0.83103	0.00041	0.83185
Series 3: Height = 25.0 cm, Variable Density Water Between Tubes						
CD20	HA_H250_W010	25.0	0.1	0.81855	0.00043	0.81941
CD21	HA_H250_W020	25.0	0.2	0.82595	0.00045	0.82685
CD22	HA_H250_W030	25.0	0.3	0.83193	0.00045	0.83283
CD23	HA_H250_W040	25.0	0.4	0.83538	0.00043	0.83624
CD24	HA_H250_W050	25.0	0.5	0.83643	0.00045	0.83733
CD25	**HA_H250_W060**	**25.0**	**0.6**	**0.83684**	**0.00042**	**0.83768**
CD26	HA_H250_W070	25.0	0.7	0.83621	0.00042	0.83705
CD27	HA_H250_W080	25.0	0.8	0.83477	0.00044	0.83565
CD28	HA_H250_W090	25.0	0.9	0.83358	0.00043	0.83444

(continued)

Table 6.13-8 – HAC Array Results (concluded)

Case ID	Filename	Fissile Mixture Height (cm)	Water Density Between Tubes (g/cm^3)	k_{eff}	σ	k_s (k+2σ)
Series 4: Height = 27.5 cm, Variable Density Water Between Tubes						
CD30	HA_H275_W010	27.5	0.1	0.82222	0.00043	0.82308
CD31	HA_H275_W020	27.5	0.2	0.82995	0.00046	0.83087
CD32	HA_H275_W030	27.5	0.3	0.83489	0.00043	0.83575
CD33	HA_H275_W040	27.5	0.4	0.83818	0.00044	0.83906
CD34	HA_H275_W050	27.5	0.5	0.83903	0.00043	0.83989
CD35	**HA_H275_W060**	**27.5**	**0.6**	**0.83913**	**0.00044**	**0.84001**
CD36	HA_H275_W070	27.5	0.7	0.83777	0.00044	0.83865
CD37	HA_H275_W080	27.5	0.8	0.83581	0.00045	0.83671
CD38	HA_H275_W090	27.5	0.9	0.83417	0.00044	0.83505
Series 5: Height = 30.0 cm, Variable Density Water Between Tubes						
CD40	HA_H300_W010	30.0	0.1	0.82435	0.00043	0.82521
CD41	HA_H300_W020	30.0	0.2	0.83081	0.00044	0.83169
CD42	HA_H300_W030	30.0	0.3	0.83572	0.00043	0.83658
CD43	HA_H300_W040	30.0	0.4	0.83805	0.00043	0.83891
CD44	**HA_H300_W050**	**30.0**	**0.5**	**0.83823**	**0.00043**	**0.83909**
CD45	HA_H300_W060	30.0	0.6	0.83797	0.00041	0.83879
CD46	HA_H300_W070	30.0	0.7	0.83625	0.00042	0.83709
CD47	HA_H300_W080	30.0	0.8	0.83536	0.00043	0.83622
CD48	HA_H300_W090	30.0	0.9	0.83259	0.00043	0.83345

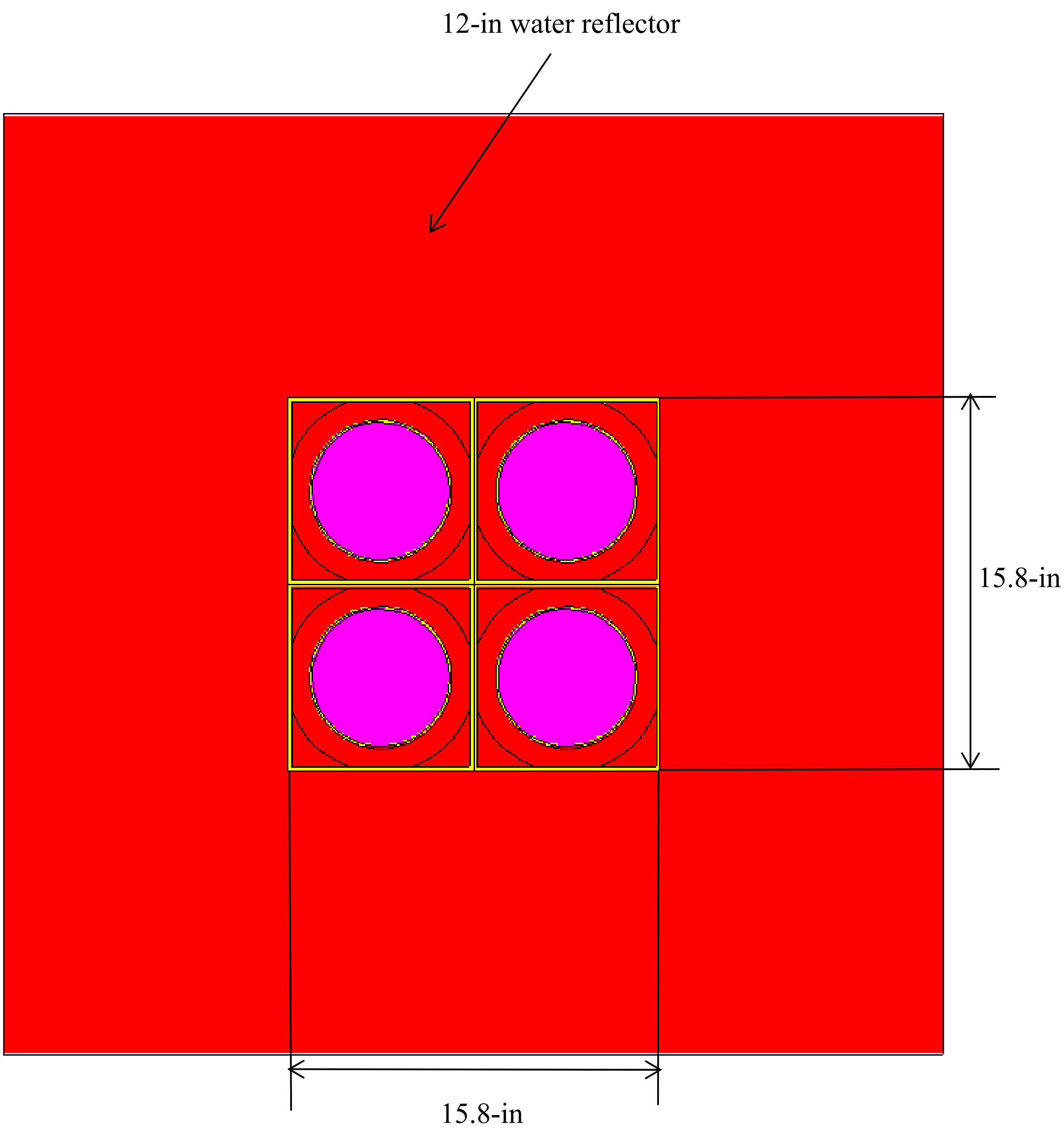

Figure 6.13-5 – HAC Array Geometry

6.13.7 Fissile Material Packages for Air Transport

See Section 6.7, which applies to all contents.

6.13.8 Benchmark Evaluations

The benchmarking analysis performed for the small quantity payload analysis (see Section 6.11.8, *Benchmark Evaluations*) is applicable to the Cobra fuel element analysis. Therefore, a USL of 0.9209 is justified.

For the Cobra fuel element analysis, parameters considered are the Energy of the Average neutron Lethargy causing Fission (EALF) and Hydrogen/U-235 atom ratio (H/U-235). The range of applicability for these parameters are provided in Table 6.11-12, namely, 3.43×10^{-8} MeV $\leq$ EALF $\leq 2.95 \times 10^{-7}$ MeV and $68.2 \leq$ H/U-235 ≤ 1437.5.

For a fissile mixture height of 15 cm, H/U-235 = 149, and for a fissile mixture height of 45 cm, H/U-235 = 447. Therefore, all cases are within the range of applicability of the benchmark experiments for the H/U-235 parameter.

The EALF extracted from the output files are in the range 4.39×10^{-8} MeV $\leq$ EALF $\leq 8.92 \times 10^{-8}$ MeV. Therefore, all cases are within the range of applicability of the benchmark experiments for the EALF parameter.

6.13.9 Sample Input File

A sample input file is provided below for the most reactive case (Case CC07, NCT array, filename NA_P100_H350).

```
ATR Package
999     0      -320:321:-322:323:-324:325                imp:n=0
900     0      310 -311 312 -313 24 -25     fill=3       imp:n=1
901     2 -1.0 (311:-310:313:-312:-24:25) 320 -321 322 -323 324 -325  imp:n=1
c
c       Universe 20: Fuel mixture with pipe
c
200     10 1.0039E-01 -26 -200                   u=20 imp:n=1 $ fuel mix
201     2 -1.0         26 -200                   u=20 imp:n=1 $ water above
fuel
202     4 -7.94     200 -201                     u=20 imp:n=1 $ pipe
203     6 -0.096    201 -203 250 -251 252 -253 u=20 imp:n=1 $ insulation
204     0           203 250 -251 252 -253        u=20 imp:n=1 $ insulation to
tube
205     4 -7.94     -250:251:-252:253            u=20 imp:n=1 $ tube to inf
c
c       Universe 21: Water
c
210     2 -1.0      -204                         u=21 imp:n=1
c
c       Universe 3: Array of Packages
c
300   0    -300 301 -302 303 imp:n=1 u=3 lat=1 fill=-1:1 -1:1 0:0
             20 20 20
             20 20 20
             21 20 20
```

```
24      pz  0             $ bottom of fuel
25      pz  121.92        $ top of cavity (48")
26      pz  35          $ top of fuel mix
c
200      cz 7.3838  $ IR pipe
201      cz 7.6581  $ OR pipe
203      cz 10.1981 $ 1" insulation
204      pz 1000    $ dummy
c
250      px  -9.6032 $ square tube
251      px   9.6032
252      py  -9.6032
253      py   9.6032
c
300      px  10.033 $ lattice surfaces/sq. tube
301      px -10.033
302      py  10.033
303      py -10.033
310      px -30.099 $ 3x3 bounds
311      px  30.099
312      py -30.099
313      py  30.099
320      px -60.579 $ outer bounds
321      px  60.579
322      py -60.579
323      py  60.579
324      pz -30.48
325      pz  152.4

m2      1001.62c  2          $ water
        8016.62c  1
mt2     lwtr.60t
m3      13027.62c 1          $ Al
m4      6000.66c   -0.08     $ SS-304
        14000.60c  -1.0
        15031.66c  -0.045
        24000.50c  -19.0
        25055.62c  -2.0
        26000.55c  -68.375
        28000.50c  -9.5
m5      1001.62c  -0.056920  $ neoprene
        6000.66c  -0.542646
c       17000.66c -0.400434
m6      13027.62c  -26.5     $ insulation material
        14000.60c  -23.4
        8016.62c   -50.2
m10    92234.69c 1.2328E-06 $ HEU fuel H=35 M235=450.0 100g Poly
       92235.69c 1.9232E-04
       92236.69c 7.1305E-07
       92238.69c 1.0202E-05
        1001.62c 6.6794E-02
        6000.66c 7.1616E-04
        8016.62c 3.2681E-02
c          Total 1.0039E-01
mt10    lwtr.60t
c
mode   n
```

```
kcode  5000 1.0 50 850
sdef    x=d1 y=d2 z=d3
si1     -30 30
sp1     0 1
si2     -30 30
sp2     0 1
si3     0 35
sp3     0 1
```

7.0 PACKAGE OPERATIONS

This section provides general instructions for loading and unloading operations of the ATR FFSC. Due to the low specific activity of neutron and gamma emitting radionuclides, dose rates from the contents of the package are minimal. As a result of the low dose rates, there are no special handling requirements for radiation protection.

Package loading and unloading operations shall be performed using detailed written procedures. The operating procedures developed by the user for the loading and unloading activities shall be performed in accordance with the procedural requirements identified in the following sections.

The closure handle must be rendered inoperable for lifting and tiedown during transport per 10 CFR §71.45. To satisfy this requirement either the closure handle may be removed or the cover installed. If the closure handle cover is utilized it may be stored with the closure assembly in the installed position. When stored with the closure assembly the cover must be removed prior to the package loading and unloading operations and may be reinstalled following installation of the closure. The installation of the closure handle cover is presented in Section 7.1.4, *Preparation for Transport*.

7.1 Package Loading

7.1.1 Preparation for Loading

Prior to loading the ATR FFSC, the packaging is inspected to ensure that it is in unimpaired physical condition. The packaging is inspected for:

- Damage to the closure locking mechanism including the spring. Inspect for missing hardware and verify the locking pins freely engage/disengage with the package body mating features.
- Damage to the closure lugs and interfacing body lugs. Inspect lugs for damage that precludes free engagement of the closure with the body.
- Deformation of the inner shell (payload cavity) that precludes free entry/removal of the payload.
- Deformed threads or other damage to the fasteners or body of the loose fuel plate basket.
- Damage to the spring plunger, or ball lock pins and end spacers, as applicable, or body of the fuel handling enclosure.

Acceptance criteria and detailed loading procedures derived from this section are specified in user written procedures. These user procedures are specific to the authorized content of the package and inspections ensure the packaging complies with Appendix 1.3.2, *Packaging General Arrangement Drawings*.

Defects that require repair shall be corrected prior to shipping in accordance with approved procedures consistent with the quality program in effect.

7.1.2 Loading of Contents - ATR Fuel or ATR U-Mo Demonstration Element Fuel Assembly

1. Remove the closure by depressing the spring-loaded pins and rotating the closure 45º to align the closure locking tabs with the mating cut-outs in the body. Remove the closure from the body.
2. Remove the fuel handling enclosure if present in the payload cavity.
3. Prior to loading, visually inspect the ATR fuel handling enclosure for damage, corrosion, and missing hardware to ensure compliance with Appendix 1.3.2, *Packaging General Arrangement Drawings*.
4. Open the ATR fuel handling enclosure lid and place a fuel element into the holder with the narrow end of the fuel element facing the bottom side of the fuel handling enclosure. As a property protection precaution, the fuel element may optionally be inserted into a polyethylene bag prior to placement in the fuel handling enclosure. Verify the total mass of polyethylene per ATR FFSC is ≤ 100 g.
    a. To open the fuel handling enclosure, release the lid by pulling on the spring plunger located at each end and rotate the lid about the hinged side.
    b. To close the fuel handling enclosure, rotate the lid to the closed position, pull the spring plunger located at each end to allow the lid to fully close, align then release the spring plungers with the receiving holes, gently lift the lid to confirm no movement and that the spring plungers are in the locked position.
5. Insert the fuel handling enclosure into the package.
6. Depress the package closure spring-loaded pins, insert closure onto package body by aligning the closure locking tabs with the mating cut-outs in the body, and rotate the closure to the locked position. Release the spring-loaded pins so that they engage with the mating holes in the package body. Observe the pins to ensure they are in the locked position as illustrated in Figure 7.1-1. The closure is fully locked when both locking pins are compressing the sleeve between the locking pin handle and the closure body.

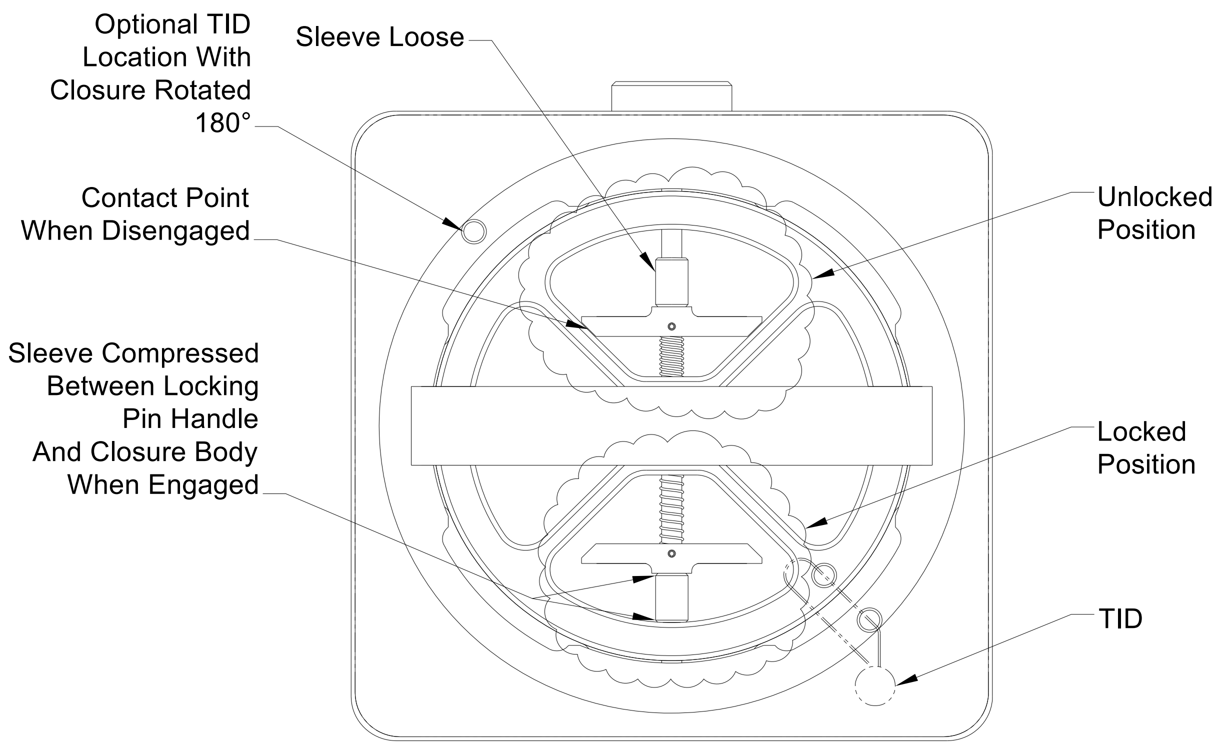

Figure 7.1-1 - Closure Locking Positions

7.1.3 Loading of Contents - Loose ATR Fuel Plates

1. Remove the closure by depressing the spring-loaded pins and rotating the closure 45º to align the closure locking tabs with the mating cut-outs in the body. Remove the closure from the body.
2. Remove the fuel plate basket if present in the payload cavity.
3. Prior to loading, visually inspect the loose fuel plate basket for damage, corrosion, and missing hardware/fastening devices to ensure compliance with Appendix 1.3.2, *Packaging General Arrangement Drawings*.
4. Open the loose fuel plate basket by removing the 8 wing nut fasteners securing each half of the basket.
5. Place the fuel plates into one half of the loose fuel plate basket
    a. Ensure the combined weight of the loose fuel plates and optional dunnage is 20 lbs or less. The loose fuel plates may only be ATR fuel plates.
    b. Ensure the combined fissile mass of the loose fuel plates does not exceed 600 g uranium-235.
    c. Flat and curved fuel plates may not be mixed in the same basket.
    d. As a property protection precaution, the fuel plates may optionally be inserted into polyethylene bag(s) prior to placement in the fuel plate basket. Verify the total mass of polyethylene per ATR FFSC is ≤ 100 g.

    e. Dunnage plates may also be included with the loose fuel plates to reduce any gaps with the basket cavity as a property protection precaution. The dunnage plates may be any aluminum alloy and any size deemed appropriate.

6. Close the fuel plate basket and verify the basket fasteners are installed and finger tight.
    a. With one half of the basket loaded, carefully place the second half over the fuel plates and match the fastener holes.
    b. Insert the 8 spade head screws through the holes and secure with corresponding wing nut (washer optional).
    c. Tighten the 8 wing nut fasteners finger tight.
    d. Visually check the 4 hex head screws located in the center of the basket to verify that they have not loosened. In the event the screws appear to be loose, tighten the fasteners to drawing requirements.
7. Insert the loose fuel plate basket into the package.
8. Depress the package closure spring-loaded pins, insert closure onto package body by aligning the closure locking tabs with the mating cut-outs in the body, and rotate the closure to the locked position. Release the spring-loaded pins so that they engage with the mating holes in the package body. Observe the pins to ensure they are in the locked position as illustrated in Figure 7.1-1. The closure is fully locked when both locking pins are compressing the sleeve between the locking pin handle and the closure body.

7.1.4 Loading of Contents – MIT, MURR, RINSC, or Cobra Fuel Assembly

The loading of MIT, MURR, RINSC, and Cobra fuel elements is procedurally identical, except Cobra fuel has one additional step as shown below.

1. Remove the closure by depressing the spring-loaded pins and rotating the closure 45º to align the closure locking tabs with the mating cut-outs in the body. Remove the closure from the body.
2. Remove the fuel handling enclosure if present in the payload cavity.
3. Prior to loading, visually inspect the fuel handling enclosure for damage, corrosion, and missing hardware to ensure compliance with Appendix 1.3.2, *Packaging General Arrangement Drawings*.
4. Open (disassemble) the fuel handling enclosure and place a fuel element into one enclosure half. Ensure that the MIT, MURR, RINSC, or Cobra fuel element is only used with the corresponding MIT, MURR, RINSC, or Cobra fuel handling enclosure. As a property protection precaution, the fuel element may optionally be inserted into a polyethylene bag prior to placement in the fuel handling enclosure. Verify the total mass of polyethylene per ATR FFSC is $\leq$ 100 g.
    a. To open the fuel handling enclosure, remove the two ball lock pins securing each end spacer. Slide each end spacer from the center enclosure halves allowing the enclosure halves to freely come apart.

   b. To close the fuel handling enclosure, with one enclosure half loaded, carefully place the second enclosure half over the fuel element and align the circular ends. Slide one end spacer over the circular end and insert the ball lock pin through the end spacer and enclosure halve alignment holes. Ensure the ball lock pin is in the locked position by observing the pin and locking mechanism protruding from the back side. Repeat with the second end spacer and ensure it is locked in the same manner.

5. When loading Cobra fuel, verify that the alignment post in the Cobra FHE is inserted into one of the nominally 15-mm diameter holes in the end fittings of the Cobra fuel element.
6. Insert the fuel handling enclosure into the package.
7. Depress the package closure spring-loaded pins, insert closure onto package body by aligning the closure locking tabs with the mating cut-outs in the body, and rotate the closure to the locked position. Release the spring-loaded pins so that they engage with the mating holes in the package body. Observe the pins to ensure they are in the locked position as illustrated in Figure 7.1-1. The closure is fully locked when both locking pins are compressing the sleeve between the locking pin handle and the closure body.

7.1.5 Loading of Contents – Small Quantity Payloads (except RINSC)

The loading of small quantity payloads is procedurally identical.

1. Remove the closure by depressing the spring-loaded pins and rotating the closure 45° to align the closure locking tabs with the mating cut-outs in the body. Remove the closure from the body.
2. Remove the fuel handling enclosure if present in the payload cavity.
3. Prior to loading, visually inspect the fuel handling enclosure for damage, corrosion, and missing hardware to ensure compliance with Appendix 1.3.2, *Packaging General Arrangement Drawings*.
4. Open (disassemble) the small quantity fuel handling enclosure and place the payload into one enclosure half.
   a. To open the fuel handling enclosure, remove the two ball lock pins securing each end spacer. Slide each end spacer from the center enclosure halves allowing the enclosure halves to freely come apart.
   b. To close the fuel handling enclosure, with one enclosure half loaded, carefully place the second enclosure half over the fuel element, loose fuel plates, or foils and align the circular ends. Slide one end spacer over the circular end and insert the ball lock pin through the end spacer and enclosure halve alignment holes. Ensure the ball lock pin is in the locked position by observing the pin and locking mechanism protruding from the back side. Repeat with the second end spacer and ensure it is locked in the same manner.
5. Dunnage shall be used as necessary to reduce the free space between the small quantity payload face and the SQFHE cavity to a maximum of ¼ inches or less. The dunnage shall be made from sheets or shapes of aluminum, including steel or aluminum fasteners if required, or may be made from cellulosic material such as cardboard. Neoprene rub strips, nominally

1/8 inch thick, may also be used as a property protection precaution. Neoprene rub strips may be used between the SQFHE and the small quantity payloads and/or between the dunnage and the small quantity payloads. The 1/8 inch neoprene rub strips shall not be stacked in more than two layers between the small quantity payload and any interior face of the SQFHE. Kraft paper and polyethylene sheeting may also be used as property protection. The sum of the mass of all polyethylene and any other plastic materials such as adhesive tape shall not exceed 100g. The sum of the mass of all cellulosic materials (e.g., paper and cardboard) and neoprene shall not exceed 4 kg.

6. Verify that the total weight of the loaded SQFHE is 50 lb or less.
7. Insert the fuel handling enclosure into the package.
8. Depress the package closure spring-loaded pins, insert closure onto package body by aligning the closure locking tabs with the mating cut-outs in the body, and rotate the closure to the locked position. Release the spring-loaded pins so that they engage with the mating holes in the package body. Observe the pins to ensure they are in the locked position as illustrated in Figure 7.1-1. The closure is fully locked when both locking pins are compressing the sleeve between the locking pin handle and the closure body.

7.1.6 Preparation for Transport

1. Install the closure handle cover by aligning the cover against the handle and insert the fastener through the holes in the cover and behind the handle as illustrated in Figure 7.1-2. Once installed, the cover renders the handle inoperable for lifting or tiedown during transport. Option: In lieu of installing the cover, the closure handle may be removed as a method of rendering the handle inoperable for lifting or tiedown during transport.
2. Install the tamper indicating device between the posts on the package closure and body.
3. Perform a survey of the dose rates and levels of non-fixed (removable) radioactive contamination per 49CFR §173.441 and 49CFR §173.443, respectively. The contamination measurements shall be taken in the most appropriate locations to yield a representative assessment of the non-fixed contamination levels.
4. Complete the necessary shipping papers in accordance with Subpart C of 49 CFR §172.
5. Ensure that the package markings are in accordance with 10 CFR §71.85(c) and Subpart D of 49 CFR §172. Package labeling shall be in accordance with Subpart E of 49CFR §172. Package placarding, for either single package transport or the racked configuration, shall be in accordance with Subpart F of 49 CFR §172.
6. Transfer the package to the conveyance and secure the package(s).

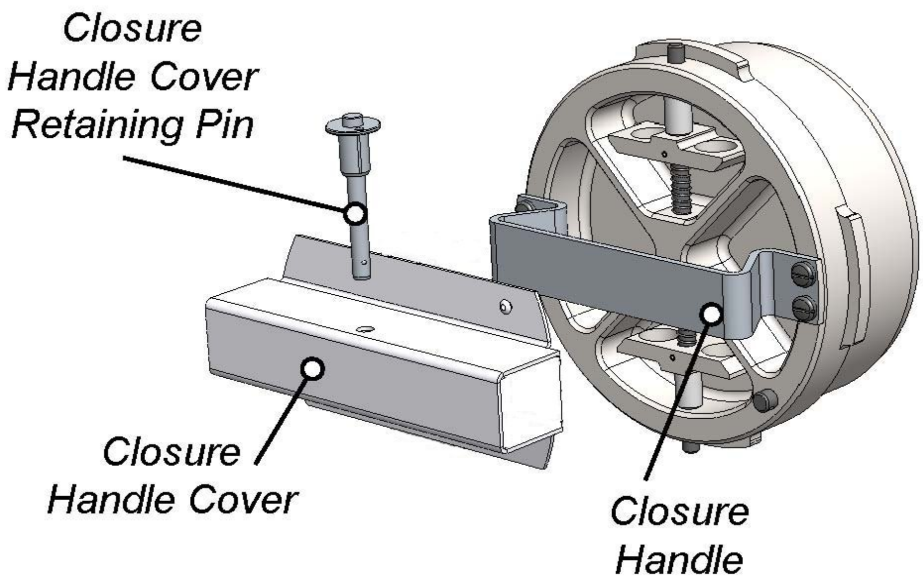

Figure 7.1-2 – Closure Handle Cover Installation

7.2 Package Unloading

7.2.1 Receipt of Package from Conveyance

Radiation and contamination surveys shall be performed upon receipt of the package and the package shall be inspected for damage as required by and in accordance with the user's personnel protection or ALARA program. In addition, the tamper indicating device (TID) shall be inspected. A missing TID or indication of damage to a TID is a Safeguards and Security concern. Disposition of such an incident is beyond the scope of this SAR.

7.2.2 Removal of Contents

1. Remove tamper indicating device.
2. Remove the package closure by depressing the spring-loaded pins and rotating the closure 45º to align the closure locking tabs with the mating cut-outs in the body. Remove the closure from the body.
3. Remove the payload container.
4. Open the payload container (fuel handling enclosure or loose fuel plate basket) and remove the contents.
    a. Open the ATR fuel handling enclosure by releasing the spring plunger located at each end and rotate the lid about the hinged side.
    b. Open the loose fuel plate basket by removing the 8 wing nut fasteners securing each half of the basket.
    c. Open the MIT, MURR, RINSC, Cobra, or small quantity payload fuel handling enclosure by removing the two ball lock pins and sliding the end spacers from each end of the enclosure halves.

5. Close the fuel handling enclosure lid or loose fuel plate basket as appropriate. If required, return the empty payload container to the package.
    a. To close the ATR fuel handling enclosure, rotate the lid to the closed position, pull the spring plunger located at each end to allow the lid to fully close, align then release the spring plungers with the receiving holes, gently lift the lid to confirm no movement and that the spring plungers are in the locked position.
    b. To close the loose fuel plate basket, place each half of the basket together and align the fastener holes. Insert the 8 spade head screws through the holes and secure with corresponding wing nut (washer optional). Tighten each wing nut finger tight.
    c. To close the MIT, MURR, RINSC, Cobra, or small quantity payload fuel handling enclosure, place each enclosure half together and align the circular ends. Slide one end spacer over the circular end and insert the ball lock pin through the end spacer and enclosure halve alignment holes. Ensure the ball lock pin is in the locked position by observing the pin and locking mechanism protruding from the back side. Repeat with the second end spacer and ensure it is locked in the same manner.
6. Depress the package closure spring-loaded pins, insert closure onto package body by aligning the closure locking tabs with the mating cut-outs in the body, and rotate the closure to the locked position. Release the spring-loaded pins so that they engage with the mating holes in the package body. Observe the pins to ensure they are in the locked position as illustrated in Figure 7.1-1. The closure is fully locked when both locking pins are compressing the sleeve between the locking pin handle and the closure body.

7.3 Preparation of Empty Package for Transport

Empty packages are prepared and transported per the guidelines of 49 CFR §173.428. The packaging is inspected to ensure that it is in an unimpaired condition and is securely closed.

Any labels previously applied in conformance with subpart E of 49CFR §172 are removed, obliterated, or covered and the "Empty" label prescribed in 49 CFR §172.450 is affixed to the packaging.

7.4 Other Operations

This section does not apply.

8.0 ACCEPTANCE TESTS AND MAINTENANCE PROGRAM

8.1 Acceptance Tests

Per the requirements of 10 CFR §71.85, the inspections and tests to be performed prior to first use of the package are described in this section.

8.1.1 Visual Inspections and Measurements

All packaging dimensions, tolerances, general notes, materials of construction, and assembly shall be examined in accordance with the requirements delineated on the drawings in Appendix 1.3.2, *Packaging General Arrangement Drawings*. Source inspections and final release of the packaging will be performed, verifying the quality characteristics were inspected and that the packaging is acceptable. Any characteristic that is out of specification shall be reported and dispositioned in accordance with the quality assurance program in effect.

8.1.1.1 Compression Spring

The compression spring is a component of the closure locking system that maintains the locking pin in the closed position. The compression spring shall be procured to Stock Precision Engineered Components (SPEC) catalog number C0360-035-1120 specification, or equivalent, which includes the following:

- Material shall be approximately 0.035 inch diameter stainless steel wire.
- The nominal outside diameter of the spring shall be approximately 0.36 inches.
- The free length of the spring shall be approximately 1.12 inches.
- The solid height of the spring shall be approximately 0.33 inches.
- The spring shall have a 4.77 (-.1, +.5) lb load at a load length of approximately 0.55 inches.
- The spring rate shall be 8.33 (-.1, +.5) lbs/in.

8.1.1.2 Roll Pin

The roll pin is a component of the closure locking system that maintains the locking pin in the closed position. The roll pin shall be procured to Stock Drive Products/Sterling Instrument (SDP/SI) catalog number A9Y35-0324 specification, or equivalent, which includes the following:

- Material shall be stainless steel.
- The free diameter of the roll pin shall be between 0.099 to 0.103 inches.
- The length of the roll pin shall be approximately 0.75 inches

8.1.1.3 Insulating Blanket

The ceramic fiber insulating blanket is a component of the body and closure assemblies used to reduce heat transfer during thermal events. The insulating blanket shall be procured to Unifrax Durablanket S 6 lb/ft^3 specification, or equivalent, which includes the following:

- The material shall be comprised of inorganic ceramic fibers.
- The nominal thickness shall be 0.5 (-0, +.2) inches.
- The nominal density shall be 6 (-15%, +30%) lb/ft^3.
- The specific heat shall be 0.25 Btu/lb$_m$-°F minimum.
- The thermal conductivity shall be 0.145 Btu/hr-ft-°F or less at 1200°F.

8.1.2 Weld Examinations

All welds shall be examined in accordance with the requirements delineated on the drawings in Appendix 1.3.2, *Packaging General Arrangement Drawings*. Visual examinations are performed in accordance with AWS D1.6[1], Section 6 for stainless steel, AWS D1.2[2], for aluminum, and penetrant examinations are performed under procedures written to ASTM E165-02, *Standard Test Method for Liquid Penetrant Examination*.

8.1.3 Structural and Pressure Tests

The packaging does not retain pressure and no pressure testing is required prior to use.

8.1.4 Leakage Tests

The packaging contains no seals or containment boundaries that require leakage rate testing.

8.1.5 Component and Material Tests

No component or material tests are required for this packaging.

8.1.6 Shielding Tests

The packaging does not contain any biological shielding. Shielding tests are not required.

8.1.7 Thermal Tests

The material thermal properties utilized in Chapter 3.0, *Thermal* are nominal. However, the thermal analyses in which these values are used are consistently conservative for the Normal Conditions of Transport (NCT) and Hypothetical Accident Condition (HAC). Therefore, specific acceptance tests for material thermal properties are not required or performed.

---

[1] ANSI/AWS D1.6:1999, *Structural Welding Code – Stainless Steel*, American Welding Society (AWS).

[2] ANSI/AWS D1.2:2003, *Structural Welding Code – Aluminum*, American Welding Society.

8.1.8 Miscellaneous Tests

No other acceptance tests are necessary for the packaging.

8.2 Maintenance Program

This section describes the maintenance program used to ensure continued performance of the packaging. The packaging is maintained consistent with a 10 CFR 71 subpart H QA program. Packagings that do not conform to the license drawings are removed from service until they are brought back into compliance. Repairs are performed in accordance with approved procedures and consistent with the quality assurance program in effect.

8.2.1 Structural and Pressure Tests

There are no structural or pressure tests that are necessary to ensure continued performance of the packaging.

8.2.2 Leakage Rate Tests

No leakage rate tests are necessary to ensure continued performance of the packaging.

8.2.3 Component and Material Tests

There is no predetermined replacement schedule for any packaging components and there are no items that would be expected to wear or become damaged during normal usage. The items identified in this section are routinely used during operations and shall be visually inspected prior to each use. Damaged components shall be repaired or replaced prior to further use.

8.2.3.1 Packaging Body and Closure

The closure assembly locking pin spring shall be visually inspected and replaced if it becomes damaged or otherwise fails to function properly (Drawing 60501-10, Item 20, of Appendix 1.3.2, *Packaging General Arrangement Drawings*).

The index lug screws and corresponding tap, or optional wire insert, shall be visually inspected for deformed or stripped threads prior to installation of the screws (Drawing 60501-10, Items 3 and 16).

8.2.3.2 ATR Fuel Handling Enclosure

The spring plunger shall be visually inspected and replaced if it becomes damaged or otherwise fails to function properly (Drawing 60501-30, Item 6, of Appendix 1.3.2, *Packaging General Arrangement Drawings*).

8.2.3.3 Loose Fuel Plate Basket

All threaded components shall be visually inspected as they are installed for deformed or stripped threads (Drawing 60501-20, Items 2, 3, 4, and 5 of Appendix 1.3.2, *Packaging General Arrangement Drawings*).

8.2.3.4 Fuel Handling Enclosure

The ball lock pin used with the MIT, MURR, RINSC, Small Quantity, and Cobra FHE shall be visually inspected and replaced if it becomes damaged or otherwise fails to function properly, according to the drawings of Appendix 1.3.2, *Packaging General Arrangement Drawings*:

- MIT FHE, Drawing 60501-40, Item 4
- MURR FHE, Drawing 60501-50, Item 4
- RINSC FHE, Drawing 60501-60, Item 5
- Small Quantity FHE, Drawing 60501-70, Item 4
- Cobra FHE, Drawing 60501-90, Item 4

8.2.4 Thermal Tests

No thermal tests are necessary to ensure continued performance of the packaging.

8.2.5 Miscellaneous Tests

No miscellaneous tests are required to ensure continued performance of the packaging.

9.0 QUALITY ASSURANCE

The Advanced Test Reactor Fresh Fuel Shipping Container (ATR FFSC) is anticipated to be used by both U.S. Department of Energy (DOE) and U.S. Nuclear Regulatory Commission (NRC) licensed users. 10 CFR §71.101, *Quality assurance requirements*, requires each licensee's quality assurance program to be approved by the Commission before any use of the package for shipments.

NRC licensed users shall follow their NRC approved quality assurance program and be identified by the Commission as an authorized user. For DOE and its subcontractors, this chapter defines the approved Quality Assurance (QA) requirements and methods of compliance applicable to the ATR FFSC package.

The ATR FFSC package described in this SAR is used to transport unirradiated single fuel elements. The QA requirements for packagings are described in Subpart H of 10 CFR Part 71 (10 CFR 71). Subpart H is an 18-criteria QA program based on ANSI/ASME NQA-1. Guidance for QA programs for packaging is provided by NRC Regulatory Guide 7.10[1]. The DOE QA requirements for the use of 10CFR71 certified packagings are described in DOE Order 460.1B[2].

The ATR FFSC packaging is designed and built for Idaho National Laboratory (INL). Procurement, design, fabrication, assembly, testing, maintenance, repair, modification, and use of the ATR FFSC package are all done under QA programs that meet all applicable NRC and DOE QA requirements.

The DOE Idaho Operations Office approved QA program is implemented for all Nuclear Safety activities. Compliance with NRC and DOT packaging and transportation requirements is mandated by DOE Order 460.1B.

This document establishes the programmatic requirements for site-wide implementation and serves as the basis for INL quality assurance program acceptability. It is designed such that implementation of the full scope of requirements as stated in DOE Orders 414.1C, *Quality Assurance* and 460.1B *Packaging and Transport Safety*, constitutes compliance to nuclear safety quality assurance criteria required by 10 CFR 830, Subpart A, *Nuclear Safety Management Quality Assurance Requirements*.

A detailed discussion of the QA program which governs ATR FFSC packaging operations is presented on the following pages to demonstrate compliance with 10 CFR 71, Subpart H.

9.1 Organization

9.1.1 ATR FFSC Project Organization

This section identifies the organizations involved and describes the responsibilities of and interactions between these organizations.

[1] U.S. Nuclear Regulatory Commission, Regulatory Guide 7.10, *Establishing Quality Assurance Programs for Packaging Used in transport of Radioactive Material, Revision 2*, March 2005.

[2] U.S. Department of Energy Order 460.1B, *Packaging and Transportation Safety,* 4-4-03.

9.1.1.1 Idaho National Laboratory (INL)

INL Contractor Management has overall responsibility for successfully accomplishing activities. Management provides the necessary planning, organization, direction, control, resources, and support to achieve their defined objectives. Management is responsible for planning, performing, assessing, and improving the work.

INL Contractor Management is responsible for establishing and implementing policies, plans, and procedures that control the quality of work, consistent with requirements.

INL Contractor Management responsibilities include:

- Ensuring adequate technical and QA training is provided for personnel performing activities.
- Ensuring compliance with all applicable regulations, DOE orders and requirements, and applicable federal, state, and local laws.
- Ensuring personnel adhere to procedures for the generation, identification, control, and protection of QA records.
- Exercising authority and responsibility to STOP unsatisfactory work such that cost and schedule do not override environmental, safety, or health considerations.
- Developing, implementing, and maintaining plans, policies, and procedures that implement the Quality Assurance Program Description (QAPD).
- Identifying, investigating, reporting, and correcting quality problems.
- Achieving and maintaining quality in their respective areas. (Quality achievement is the responsibility of those performing the work. Quality achievement is verified by persons or organizations not directly responsible for performing the work.)
- Empowering employees by delegating authority and decision making to the lowest appropriate level in the organization.

9.1.1.2 Members of the INL Contractor Workforce (at all levels)

- Implement the organization’s procedures to meet QA requirements.
- Comply with administrative and technical work control requirements.
- Identify and report issues to the responsible manager for resolution and continuous improvement for the work being performed.
- Seek, identify, and recommend work methods or procedural changes that would improve quality and efficiency.

9.1.1.3 INL Contractor Quality Assurance Management

The INL Contractor QA Management provides independent oversight of all quality related activities.

9.2 Quality Assurance Program

9.2.1 General

The INL Contractor's QA Program defines and establishes requirements for programs, projects, and activities.

The INL Contractor QA program is developed and maintained through an ongoing process that selectively applies QA criteria as appropriate to the function or work activity being performed. Applicable QA criteria consist of the following:

- Title 10 CFR Subpart 71, Packaging and Transportation of Radioactive Material
- Title 10 CFR 830.120, Quality Assurance Requirements
- ASME NQA-1-2000, Quality Assurance Requirements for Nuclear Facility Application
- DOE O 414.1C, Quality Assurance
- DOE O 461.1B, Packaging and Transport Safety
- DOE G 414.1-1A, Management Assessment and Independent Assessment

The INL Contractor QA Program is inclusive of applicable requirements from criteria noted above and addresses the following for this SAR:

- Organization
- Quality Assurance Program
- Implementation of the QA Program
- Personnel Qualification and Training
- Quality Improvement
- Documents
- Records
- Work Process
- Procurement
- Inspection and Testing
- Management Assessments
- Independent Assessment

The INL Contractor QA Director is responsible for ensuring implementation of requirements as defined within the QA program and requirements of this SAR, including design, procurement, fabrication, inspection, testing, maintenance, and modifications. Procurement documents are to reflect applicable requirements from 10 CFR 71, Subpart H, ASME NQA-1 and the QA program.

INL Contractor Quality Management assesses the adequacy and effectiveness of the QA program to ensure effective implementation inclusive of objective evidence and independent verification, where appropriate, to demonstrate that specific project and regulatory objectives are achieved.

All INL Contractor personnel and contractors are responsible for effective implementation of the QA program within the scope of their responsibilities. INL Contract packaging and quality engineers are responsible for inspection and testing and are to be qualified, as appropriate, through minimum education and/or experience, formal training, written examination and/or other demonstration of skill and proficiency. Objective evidence of qualifications and capabilities are to be maintained as required. As appropriate, the initial employee training should consist of the following:

- General employee indoctrination
- Program indoctrination
- QA program training
- Applicable NRC and DOT requirements.

Note: Only packaging engineers and Quality Engineers with training and/or experience in applicable NRC and DOT requirements and Safety Analysis Reports (SARs) can plan or determine the application of internal INL processes to ensure compliance with Chapter 9 and this SAR.

9.2.2 ATR FFSC-Specific Program

The ATR FFSC was designed and tested as described in Chapter 2, *Structural Evaluation,* of this SAR. QA requirements are invoked in the design, procurement, fabrication, assembly, testing, maintenance, and use of the packaging to ensure established standards are maintained. Items and activities to be controlled and documented are described in this chapter.

9.2.3 QA Levels

Materials and components of the ATR FFSC are designed, procured, fabricated, assembled, and tested using a graded approach under a 10 CFR 71, Subpart H equivalent QA Program and Regulatory Guide (RG) 7.10. Under that program, the categories critical to safety are established for all ATR FFSC packaging components. These defined quality categories consider the impact to safety if the component were to fail or perform outside design parameters.

9.2.3.1 Graded Quality Category A Items:

These items and services are critical to safe operation and include structures, components, and systems whose failure could directly result in a condition adversely affecting public health and safety. The failure of a single item could cause loss of primary containment leading to a release of radioactive material beyond regulatory requirements, loss of shielding beyond regulatory requirements, or unsafe geometry compromising criticality control.

9.2.3.2 Graded Quality Category B Items:

These items and services have a major impact on safety and include structures, components, and systems whose failure or malfunction could indirectly result in a condition adversely affecting public health and safety. The failure of a Category B item, in conjunction with the failure of an additional item, could result in an unsafe condition.

9.2.3.3 Graded Quality Category C Items:

These items and services have a minor impact on safety and include structures, components, and systems whose failure or malfunction would not significantly reduce the packaging effectiveness and would not be likely to create a situation adversely affecting public health and safety.

9.2.3.4 Application of Quality Categories

The design effort and requirements for a QA program are interrelated and are developed simultaneously. To ensure the development of a QA program in which the application of QA requirements is commensurate with their safety significance, engineering personnel perform a systematic analysis of each component, structure, and system to assess the consequences to the health and safety of the public and the environment that would result from malfunction or failure of such items. This engineering assessment is initiated during the design process and performed in accordance with approved procedures. Establishment of the engineering basis during the design process enables a uniform, consistent application of QA requirements during fabrication, use, and maintenance of packaging.

A logical sequence is established to identifying realistic QA requirements would involve (1) classifying each structure, system, and component (2) grouping items classified as important to safety into quality categories; and (3) specifying the applicable level of QA effort for each category.

The Design Authority (DA) identifies the critical characteristics when they identify design attributes necessary to preserve the safety support function. As necessary, the DA also ensures critical characteristics are included in this SAR by the identification of SSCs and their QA Category designations. Additionally, this SAR includes the safety function, design, and operational attributes necessary for reliable performance. The DA applies design criteria to the design, operation, and maintenance of each critical SSC including recommended codes and standards, as required by RG 7.10. QA requirements shall be applied as necessary to assure the SSCs can perform their function.

The package-specific safety documents identify systems, structures, and components (SSCs) that are important to the safety functions for transportation. As appropriate, the hazard analysis and accident scenarios in the safety basis documents help identify SSCs that must function in order to prevent or mitigate these events. These SSCs are then identified using the classification system found in the NRC QA Category system provided in NRC Regulatory Guide (RG) 7.10. The categories as defined in RG 7.10, and listed below, are analogous to Safety Class, Safety Significant, and General Service that are identified for facility SSCs.

Upon custodianship of the ATR FFSC packages by INL, functional classifications will be used for site operations and activities related to the ATR FFSC. The method of classification is documented as follows.

Quality Category A:

Critical impact on safety and associated functional requirements – items or components whose single failure or malfunction could directly result in an unacceptable condition of containment, shielding, or nuclear criticality control. This is functionally equivalent to “safety class” designation used for nuclear facility safety.

Quality Category B:

Impact on safety and associated functional requirement – components whose failure or malfunction in conjunction with one other independent failure or malfunction could result in an unacceptable condition of containment, shielding, or nuclear criticality control. This is functionally equivalent to “safety significant” designation used for nuclear facility safety.

Quality Category C:

Minor impact on safety and associated functional requirements – components whose failure or malfunction would not result in an unacceptable condition of containment, shielding, or nuclear criticality control regardless of other single failures. This is functionally equivalent to designations given to components that do not meet “safety class or safety significant” criteria used for nuclear facility safety.

The tabulation of this classification process is provided in Tables 9.2-1 and 9.2-2.

Table 9.2-1 - QA Categories for Design and Procurement of ATR FFSC Subcomponents

Component	Subcomponent	Category
Body Assembly	Outer Square Tube	A
	Inner Round Tube	A
	Bottom End Plate	A
	Closure End Plate	A
	Stiffening Ribs	A
	Thermal Shield Sheet	B
	Insulation	B
	Tamper Indicating Device Dowel Pin	C
	Index Lug Screw	B
	Weld Wire	A
Closure Assembly	Outer Plate, Closure	A
	Inner Plate (Insulation Pocket)	B
	Closure Locking Hardware (Pin, Handle, Spring, etc.)	B
	Insulation	B
	Tamper Indicating Device Dowel Pin	C
	Weld Wire	A
Fuel Handling Enclosure	Aluminum Body Sheets	C
	Aluminum End Plates	C
	Fasteners and Hardware	C
Loose Fuel Plate Basket	Machined Aluminum Body	A
	Screws, Wing Nuts, and Hex Nuts	C

Table 9.2-2 - Level of Quality Assurance Effort per QA Element

10CFR71 Subpart H QA Element	Level of QA Effort	QA Category A	QA Category B	QA Category C
1 (71.103)	**QA Organization (¶9.1)**			
	• Organizational structure and authorities defined	X	X	
	• Responsibilities defined	X	X	
	• Reporting levels established	X	X	
	• Management endorsement	X	X	
2 (71.105)	**QA Program (¶9.2)**			
	• Implementing procedures in place	X	X	
	• Trained personnel	X	X	
	• Activities controlled	X	X	
3 (71.107)	**Design (¶9.3)**			
	• Control of design process and inputs	X	X	X
	• Control of design input	X	X	X
	• Software validated and verified	X	X	
	• Design verification controlled	X	X	
	• Quality category assessment performed	X	X	
4 (71.109)	**Procurement Document Control (¶9.4)**			
	• Complete traceability	X	X	
	• Qualified suppliers list	X	X	
	• Commercial grade dedicated items acceptable	X	X	
	• Off-the-shelf item			X
5 (71.111)	**Instructions, Procedures, and Drawings (¶9.5)**			
	• Must be written and controlled	X	X	
	• Qualitative or quantitative acceptance criteria	X	X	
6 (71.113)	**Document Control (¶9.6)**			
	• Controlled issuance	X	X	
	• Controlled changes	X	X	
	• Procurement documents	X	X	X

10CFR71 Subpart H QA Element	Level of QA Effort	QA Category A	QA Category B	QA Category C
7 (71.115)	**Control of Purchased Material, Equipment, and Services (¶9.7)**			
	• Source evaluation and selection plans	X	X	
	• Evidence of QA at supplier	X	X	
	• Inspections at supplier, as applicable	X	X	
	• Receiving inspection	X	X	
	• Objective proof that all specifications are met	X	X	
	• Audits/surveillances at supplier facility, as applicable	X	X	
	• Incoming inspection for damage only			X
8 (71.117)	**Identification and Control of Material, Parts, and Components (¶9.8)**			
	• Positive identification and traceability of each item	X	X	
	• Identification and traceable to heats, lots, or other groupings	X	X	
	• Identification to end use drawings, etc.			X
9 (71.119)	**Control of Special Processes (¶9.9)**			
	• All welding, heat treating, and nondestructive testing done by qualified personnel	X	X	
	• Qualification records and training of personnel	X	X	
	• No special processes			X
10 (71.131)	**Inspection (¶9.10)**			
	• Documented inspection to all specifications required	X	X	
	• Examination, measurement, or test of material or processed product to assure quality	X	X	
	• Process monitoring if quality requires it	X	X	
	• Inspectors must be independent of those performing operations	X	X	X
	• Qualified inspectors only	X	X	X
	• Receiving inspection	X	X	X
11 (71.123)	**Test Control (¶9.11)**			
	• Written test program	X	X	
	• Written test procedures for requirements in the package approval	X	X	
	• Documentation of all testing and evaluation	X	X	
	• Representative of buyer observes all supplier acceptance tests if specified in procurement documents	X		
	• No physical tests required			X

10CFR71 Subpart H QA Element	Level of QA Effort	QA Category A	QA Category B	QA Category C
12 (71.125)	**Control of Measuring and Test Equipment (¶9.12)**			
	• Tools, gauges, and instruments to be in a formal calibration program	X	X	
	• Only qualified inspectors	X	X	
	• No test required			X
13 (71.127)	**Handling, Storage, and Shipping (¶9.13)**			
	• Written plans and procedures required	X	X	
	• Routine handling			X
14 (71.129)	**Inspection, Test, and Operating Status (¶9.14)**			
	• Individual items identified as to status or condition	X	X	
	• Stamps, tags, labels, etc., must clearly show status	X	X	X
	• Visual examination only			X
15 (71.131)	**Nonconforming Materials, Parts, or Components (¶9.15)**			
	• Written program to prevent inadvertent use	X	X	X
	• Nonconformance to be documented and closed	X	X	X
	• Disposal without records			X
16 (71.133)	**Corrective Action (¶9.16)**			
	• Objective evidence of closure for conditions adverse to quality	X	X	X
17 (71.135)	**QA Records (¶9.17)**			
	• Design and use records	X	X	
	• Results of reviews, inspections, test, audits, surveillance, and materials analysis	X	X	
	• Personnel qualifications	X	X	
	• Records of fabrication, acceptance, and maintenance retained throughout the life of package	X	X	X
	• Record of package use kept for three years after shipment	X	X	
	• All records managed by written plans for retention and disposal	X	X	
	• Procurement records	X	X	X
18 (71.137)	**Audits (¶9.18)**			
	• Written plan of periodic audits	X	X	
	• Lead auditor certified	X	X	

9.3 Package Design Control

As required by the INL Contractor's Quality Program, design processes shall be established and implemented to satisfy the requirements of the QAPD. These requirements are to be in accordance with:

- 10 CFR 830.122(f), *Criterion 6 – Performance/Design*[3]
- DOE Order 414C, CRD, Attachment 1, 2.b.(2), *Criterion 6 – Design.*

Requirements are implemented to ensure processes and procedures are in place to ensure design features of packaging systems are appropriately translated into specifications, drawings, procedures, and instructions. Design control measures are established for criticality, shielding, thermal, and structural analyses under both normal and accident condition analyses as defined in NRC regulations.

The INL Contractor is responsible for maintaining the package and this SAR. The design documents (e.g., drawings and specifications) are controlled by incorporation into this SAR, which will be reviewed and approved by the NRC.

The design of the ATR FFSC was performed under an NRC-approved QA Program as required by INL. Design inputs consist of an INL statement of work, applicable DOE orders, national standards, specifications, and drawings.

Procedures control design activities to ensure the following occur:

- Design activities are planned, controlled, and documented.
- Regulatory requirements, design requirements, and appropriate quality standards are correctly translated into specifications, drawings, and procedures.
- Competent engineering personnel, independent of design activities, perform design verification. Verification may include design reviews, alternate calculations, or qualification testing. Qualification tests are conducted in accordance with approved test programs or procedures.
- Design interface controls are established and adequate.
- Design, specification, and procedure changes are reviewed and approved in the same manner as the original issue. In a case where a proposed design change potentially affects licensed conditions, the Quality Assurance Program shall provide for ensuring that licensing considerations have been reviewed and are complied with or otherwise reconciled by amending the license.
- Design errors and deficiencies are documented, corrected and corrective action to prevent recurrence is taken.
- Design organization(s) and their responsibilities and authorities are delineated and controlled through written procedures.

[3] DOE, Code of Federal Regulations, 10 CFR 830.122, *Quality Assurance Criteria*, U.S. Department of Energy, Washington, D.C., 2006.

Materials, parts, equipment, and processes essential to the function of items that are important to safety are selected and reviewed for suitability of application.

Computer programs used for design analysis or verification are controlled in accordance with approved procedures. These procedures provide for verification of the accuracy of computer results and for the assessment and resolution of reported computer program errors.

9.4 Procurement Document Control

As required by the INL Contractor Quality Program, procurement/acquisition processes and related document control activities are established and implemented to satisfy requirements of the QAPD. Requirements are to be in accordance with:

- 10 CFR 830.122(d), *Criterion 4 – Management/Documents and Records*
- 10 CFR 830.122(g), *Criterion 7 – Performance/Procurement*
- DOE Order 414C, CRD, Attachment 1, 2.a.(4), *Criterion 4 – Documents and Records*
- DOE Order 414C, CRD, Attachment 1, 2.b.(3), *Criterion 7 – Procurement*
- DOE Guide 414.1-3, *Suspect/Counterfeit Items.*

Processes and procedures are in place to ensure appropriate levels of quality are achieved in procurement of material, equipment, and services. Quality Level and Quality Category designations assigned by the Design Authority grade the application of QA requirements for procurements based on radiological material at risk, mission importance, safety of workers, public, environment, and equipment, and other differentiating criteria. Implementing procedures provide the logic process for determining Quality Levels used in procurement of equipment and subcontracting of services. Procedures ensure processes address document preparation and document control, and records management to meet regulatory requirements. Procurement records are kept in a manner that satisfies regulatory requirements.

INL Contractor procurement actions for packaging and spare parts shall be controlled. Contracts and Purchase Orders for packaging and spare parts shall require the selected vendor to implement and maintain an NRC approved 10CFR71, Subpart H QA Program.

Implementing procedures ensure procurement documents are prepared to clearly define applicable technical and quality assurance requirements including codes, standards, regulatory requirements and commitments, and contractual requirements. These documents serve as the principal documents for procurement of structures, systems and components, and related services for use in design, fabrication, maintenance and operation, inspection and testing of storage and/or transportation systems. Procedures ensure purchased material, components, equipment, and services adhere to applicable requirements. Furthermore:

- The assignment of quality requirements through procurement documents is administered and controlled.
- Procurement activities are performed in accordance with approved procedures delineating requirements for preparation, review, approval, and control of procurement documents. Revisions to procurement documents are reviewed and approved by the same cognizant groups as the original document.

- Quality requirements are included in quality-related purchase orders as applicable to the scope of the procurement referencing 10 CFR 71, Subpart H or other codes and standards, as appropriate.
- INL Contractor procurement documents will require suppliers to convey appropriate quality assurance program requirements to sub-tier suppliers.
- INL Contractor procurement documents will include provisions that suppliers either maintain or supply those QA records which provide evidence of conformance to the procurement documents. Additionally, procurement documents shall designate the supplier documents required for submittal to INL for review and/or approval.
- INL shall maintain the right of access to supplier facilities and performance of source surveillance and/or audit activities, as applicable. A statement to this effect is to be included in procurement documents.
- INL shall require the Supplier to warrant that all items furnished under the Contract are genuine (i.e., new, not refurbished, not counterfeit) and match the quality, test reports, markings and/or fitness for intended use as required by the Contract. Any materials furnished as part of the Contract which has been previously found to be suspect/counterfeit by the government or other duly recognized agency, shall not be used.

Procurement documents shall also address the applicability of the provisions of 10 CFR 21 for the Reporting of Defects and Noncompliances.

9.5 Instructions, Procedures, and Drawings

As required by the INL Contractor Quality Program*,* instructions, procedures, and drawing work processes and applicable quality improvement activities shall be established and implemented to satisfy the requirements of the QAPD. These requirements are to be in accordance with:

- 10 CFR 830.122(c*), Criterion 3 – Management/Quality Improvement*
- 10 CFR 830.122(e), *Criterion 5 – Performance/Work Processes*
- DOE Order 414C, CRD, Attachment 1, 2.a.(3), *Criterion 3 – Quality Improvement*
- DOE Order 414C, CRD, Attachment 1, 2.b.(1), *Criterion 5 – Work Processes.*

Requirements are implemented to ensure processes and procedures are in place that achieve quality objectives and ensure appropriate levels of quality and safety are applied to critical components of packaging and transportation systems utilizing a graded approach. The program shall ensure processes and procedures in place to identify and correct problems associated with transportation and packaging activities.

Implementing procedures shall be established to ensure that methods for complying with each of the applicable criteria of 10 CFR 71, Subpart H, as applicable, for activities affecting quality during design, fabrication, inspection, testing, use and maintenance are specified in instructions, procedures, and/or drawings. In addition:

- Instructions, procedures, and drawings shall be developed, reviewed, approved, utilized, and controlled in accordance with the requirements of approved procedures. These instructions, procedures, and drawings shall include appropriate quantitative and qualitative acceptance criteria.

- Changes to instructions, procedures and drawings, are developed, reviewed, approved, utilized and controlled using the same requirements and controls as applied to the original documents.
- Compliance with these approved instructions, procedures and drawings is mandatory for INL personnel while performing activities affecting quality.

Specific activities by INL regarding preparation of packaging for use, repair, rework, maintenance, loading contents, unloading contents, and transport, must be accomplished in accordance with written and approved instructions, procedures, specifications, and/or drawings. These documents must identify appropriate inspection and hold points and emphasize those characteristics that are important to safety and quality. Transportation package procedures are to be developed and reviewed by technical and quality staff and shall be approved by appropriate levels of management.

9.5.1 Preparation and Use

Activities concerning loading and shipping are performed in accordance with written operating procedures developed by the user and approved by the package custodian. Packaging first-time usage tests, sequential loading and unloading operations, technical constraints, acceptance limits, and references are specified in the procedures. A pre-planned and documented inspection will be conducted to ensure that each loaded package is ready for delivery to the carrier.

9.5.2 Operating Procedure Changes

Changes in operating procedures that affect the process must be approved at the same supervisory level as the initial issue.

9.5.3 Drawings

Controlled drawings are shown in Appendix 1.3.2, *Packaging General Arrangement Drawings*, of this SAR. Implementation of design revisions is discussed in SAR Section 9.3, *Package Design Control*.

9.6 Document Control

As required by the INL Contractor Quality Program, document control activities shall be established and implemented to satisfy the requirements of the QAPD. These requirements are to be in accordance with:

- 10 CFR 830.122(d), *Criterion 4 – Management/Documents and Records*
- DOE Order 414C, CRD, Attachment 1, 2.a.(4), *Criterion 4 – Documents and Records.*

Requirements are implemented to ensure processes and procedures are in place to address document, document control, and for the management of records. Records (engineering, test reports, user instructions, etc.) must be maintained in a manner that conforms to regulatory requirements.

Document control activities related to the design, procurement, fabrication, and testing of ATR FFSC components; and SAR preparation shall be controlled.

Implementing procedures shall be established to control the issuance of documents that prescribe activities affecting quality and to assure adequate review, approval, release, distribution, use of documents and their revisions. Controlled documents may include, but are not limited to:

- Design specifications
- Design and fabrication drawings
- Special process specifications and procedures
- QA Program Manuals/Plans, etc.
- Implementing procedures
- Test procedures
- Operational test procedures and data.

Requirements shall ensure changes to documents, which prescribe activities affecting quality, are reviewed and approved by the same organization that performed the initial review and approval, or by qualified responsible organizations. Documents that prescribe activities affecting quality are to be reviewed and approved for technical adequacy and inclusion of appropriate quality requirements prior to approval and issuance. Measures are taken to ensure that only current documents are available at the locations where activities affecting quality are performed prior to commencing the work.

Package users are responsible for establishment, development, review, approval, distribution, revision, and retention of their documents. Documents requiring control, the level of control, and the personnel responsibilities and training requirements are to be identified.

Packaging documents to be controlled include as a minimum:

- Operating procedures
- Maintenance procedures
- Inspection and test procedures
- Loading and unloading procedures
- Preparation for transport procedures
- Repair procedures
- Specifications
- Fabrication records
- Drawings of packaging and components
- SAR and occurring supplements.

Revisions are handled in a like manner as the original issue. Only the latest revisions must be available for use.

Documentation received from the supplier for each package must be filed by package serial number. These documents are to be retained in the user's facility.

9.7 Control Of Purchased Material, Equipment And Services

As required by the INL Contractor Quality Program, the control of purchased material, equipment and services and applicable quality improvement activities shall be established and implemented to satisfy the requirements of the QAPD. These requirements are to be in accordance with:

- 10 CFR 830.122(c), *Criterion 3 – Management/Quality Improvement*
- 10 CFR 830.122(g), *Criterion 7 – Performance/Procurement*
- 10 CFR 830.122(h), *Criterion 8 – Performance/Inspection and Acceptance Testing*
- DOE Order 414C, CRD, Attachment 1, 2.b.(3), *Criterion 3 – Quality Improvement*
- DOE Order 414C, CRD, Attachment 1, 2.b.(3), *Criterion 7 – Procurement*
- DOE Order 414C, CRD, Attachment 1, 2.b.(4), *Criterion 8 – Inspection and Acceptance Testing*.

Requirements are implemented to ensure processes and procedures are in place to ensure appropriate inspections and tests are applied prior to acceptance or use of the packaging or component, and to identify the status of packaging items, components, etc. Requirements shall ensure processes and procedures are in place such that appropriate levels of quality are achieved in the procurement of material, equipment, and services. Quality Level and Quality Category designations by the Design Authority are used to grade the application of QA requirements of procurements based on radiological material at risk, mission importance, safety of workers, public, environment, and equipment, and other differentiating criteria. Requirements shall ensure processes and procedures in place to identify and correct problems associated with transportation and packaging activities.

Activities related to the control of purchased material, equipment and services shall be controlled. Control of purchased material, equipment, and services consist of the following elements:

- Implementing procedures shall be established to assure that purchased material, equipment and services conform to procurement documents.
- Procurement documents shall be reviewed and approved by authorized personnel for acceptability of proposed suppliers based on the quality requirements of the item/activity being purchased.
- As required, audits and/or surveys are conducted to determine supplier acceptability. These audits/surveys are based on one or all of the following criteria: the supplier's capability to comply with the requirements of 10 CFR 71, Subpart H that are applicable to the scope of work to be performed; a review of previous records to establish the past performance of the supplier; and/or a survey of the supplier's facilities and review of the

supplier's QA Program to assess adequacy and verify implementation of quality controls consistent with the requirements being invoked.

- Qualified personnel shall conduct audits and surveys. Audit/survey results are to be documented and retained as Quality Assurance Records. Suppliers are re-audited and/or re-evaluated at planned intervals to verify that they continue to comply with quality requirements and to assess the continued effectiveness of their QA Program. Additionally, interim periodic evaluations are to be performed of supplier quality activities to verify implementation of their QA Program.
- Suppliers are required to provide objective evidence that items or services provided meet the requirements specified in procurement documents. Items are properly identified to appropriate records that are available to permit verification of conformance with procurement documents. Any procurement requirements not met by suppliers shall be reported to INL Contractor Quality Management for assessment of the condition. These conditions are reviewed by technical and quality personnel to assure that they have not compromised the quality or service of the item.
- Periodic surveillance of supplier in-process activities is performed as necessary, to verify supplier compliance with the procurement documents. When deemed necessary, the need for surveillance is noted in approved quality or project planning documents. Surveillances are to be performed and documented in accordance with approved procedures. Personnel performing surveillance of supplier activities are to be trained and qualified in accordance with approved procedures.
- Quality planning for the performance of source surveillance, test, shipping and/or receiving inspection activities to verify compliance with approved design and licensing requirements, applicable 10 CFR 71 criteria, procurement document requirements, or contract specifications is to be performed in accordance with approved procedures.
- For commercial "off-the-shelf" items, where specific quality controls appropriate for nuclear applications cannot be imposed in a practical manner, additional quality verification shall be performed to the extent necessary to verify the acceptability and conformance of an item to procurement document requirements. When dedication of a commercial grade item is required for use in a quality-related application, such dedication shall be performed in accordance with approved procedures.

To ensure compliance with procurement requirements, control measures shall include verification of supplier capability and verification of item or service quality. Procurements of ATR FFSC components are required to be placed with pre-qualified and selected vendors. The vendor's QA Plan must address the requirements of 10 CFR 71, Subpart H and defined requirements. A graded approach is used based on the QA Levels established in Table 9.2-2.

The approach used to control the procurement of items and services must include the following:

- Source evaluation and selection
- Evaluation of objective evidence of quality furnished by the supplier
- Source inspection
- Audit
- Examination of items or services upon delivery or completion.

9.8 Identification And Control Of Material, Parts And Components

As required by the INL Contractor Quality Program, activities concerning the identification and control of material, parts, and components shall be established and implemented to satisfy the requirements of QAPD. These requirements are to be in accordance with:

- 10 CFR 830.122(e), *Criterion 5 – Performance/Work Processes*
- 10 CFR 830.122(g), *Criterion 7 – Performance/Procurement*
- 10 CFR 830.122(h), *Criterion 8 – Performance/Inspection and Acceptance Testing*
- DOE Order 414C, CRD, Attachment 1, 2.b.(1), *Criterion 5 – Work Processes*
- DOE Order 414C, CRD, Attachment 1, 2.b.(3), *Criterion 7 – Procurement*
- DOE Order 414C, CRD, Attachment 1, 2.b.(4), *Criterion 8 – Inspection and Acceptance Testing.*

Requirements are implemented to ensure processes and procedures are in place that achieve quality objectives and ensure appropriate levels of quality and safety are applied to critical components of packaging and transportation systems utilizing a graded approach. The program also ensures processes and procedures are in place such that appropriate inspections and tests are applied prior to acceptance or use of the packaging or component, and to identify the status of packaging items, and components. The program shall ensure processes and procedures are in place to ensure appropriate levels of quality are achieved in the procurement of material, equipment, and services.

Activities related to the identification and control of material, parts and components shall be controlled. The requirements for identification and control of material, parts, and components consist of the following elements:

- Implementing procedures are established to identify and control materials, parts, and components. These procedures assure identification of items by appropriate means during fabrication, installation, and use of the items and prevent the inadvertent use of incorrect or defective items.
- Requirements for identification are established during the preparation of procedures and specifications.
- Methods and location of identification are selected to not adversely affect the quality of the item(s) being identified.

- Items having limited shelf or operating life are controlled to prevent their inappropriate use.

Control and identification must be maintained either directly on the item or within documents traceable to the item to ensure that only correct and acceptable items are used. When physical identification is not practical, other appropriate means of control must be established such as bagging, physical separation, or procedural control. Each packaging unit shall be assigned a unique serial number after fabrication or purchase. All documentation associated with subsequent storage, use, maintenance, inspection, acceptance, etc., must refer to the assigned serial number. Verification of acceptance status is required prior to use. Items that are not acceptable must be controlled accordingly. Control of nonconforming items is addressed in Section 9.15, *Nonconforming Parts, Materials, or Components*.

Each ATR FFSC package will be conspicuously and durably marked with information identifying the package owner, model number, unique serial number, and package gross weight, in accordance with 10 CFR 71.85(c).

Replacement parts must be identified to ensure correct application. Minute items must be individually packaged with the package marked with the part identification and traceability information.

9.9 Control Of Special Processes

As required by the INL Contractor Quality Program, activities for the control of special processes shall be established and implemented to satisfy the requirements of the QAPD. These requirements are to be in accordance with:

- 10 CRF 830.122(b), *Criterion 2 – Management/Personnel Training and Qualifications*
- 10 CFR 830.122(e), *Criterion 5 – Performance/Work Processes*
- 10 CFR 830.122(g), *Criterion 7 – Performance/Procurement*
- DOE Order 414C, CRD, Attachment 1, 2.a.(2), *Criterion 2 - Personnel Training and Qualifications*
- DOE Order 414C, CRD, Attachment 1, 2.b.(1), *Criterion 5 – Work Processes*
- DOE Order 414C, CRD, Attachment 1, 2.b.(3), *Criterion 7 – Procurement.*

Requirements will be implemented to ensure only trained and qualified personnel perform transportation and packaging activities. The program shall ensure processes and procedures are in place that achieve quality objectives and ensure appropriate levels of quality and safety are applied to critical components of packaging and transportation systems utilizing a graded approach.

Activities related to the control of special processes shall be controlled. The requirements for control of special processes consist of the following elements:

- Implementing procedures shall be established to control special processes used in the fabrication and inspection of storage/transport systems. These processes may include welding, non-destructive examination, or other special processes as identified in procurement documents.

- Special processes are performed in accordance with approved procedures.
- Personnel who perform special processes shall be trained and qualified in accordance with applicable codes, standards, specifications, and/or other special requirements. Records of qualified procedures and personnel are to be maintained and kept current by the organization that performs the special processes.

Package users are responsible to ensure special processes for welding and nondestructive examination of the ATR FFSC during fabrication, use, and maintenance are controlled. Equipment used in conduct of special processes must be qualified in accordance with applicable codes, standards, and specifications. Special process operations must be performed by qualified personnel and accomplished in accordance with written process sheets or procedures with recorded evidence of verification when applicable. Qualification records of special process procedures, equipment, and personnel must be maintained.

Welders, weld procedures, and examination personnel are to be qualified in accordance with the appropriate articles of ASME BPVC, Section IX, "Welding and Brazing Qualifications";[4] and ASME BPVC, Section V, "Nondestructive Examination."[5]

Special processes for QA Level A and B items must be performed by qualified personnel in accordance with documented and approved procedures. Applicable special processes performed by an outside supplier such as welding, plating, anodizing, and heat treating, which are controlled by the suppliers' quality program, are reviewed and/or witnessed in accordance with procurement requirements.

9.10 Internal Inspection

As required by the INL Contractor Quality Program, internal inspection activities shall be established to satisfy the requirements of the QAPD. These requirements are to be in accordance with:

- 10 CRF 830.122(b), *Criterion 2 – Management/Personnel Training and Qualifications*
- 10 CFR 830.122(h), *Criterion 8 – Performance/Inspection and Acceptance Testing*
- DOE Order 414C, CRD, Attachment 1, 2.a.(2), *Criterion 2 - Personnel Training and Qualifications*
- DOE Order 414C, CRD, Attachment 1, 2.b.(4), *Criterion 8 – Inspection and Acceptance Testing.*

Requirements are implemented to ensure only trained and qualified personnel perform transportation and packaging activities. The program shall ensure processes and procedures are in place to ensure appropriate inspections and tests are applied prior to acceptance or use of the packaging or component, and to identify the status of packaging items, components, etc.

---

[4] ASME, 2004, American Society of Mechanical Engineers Boiler and Pressure Vessel Code, Section IX, *Welding and Brazing Qualifications*, American Society of Mechanical Engineers, New York, NY

[5] ASME, 2004, American Society of Mechanical Engineers Boiler and Pressure Vessel Code, Section V, *Nondestructive Examination*, American Society of Mechanical Engineers, New York, NY

Activities related to internal inspection shall be controlled. The program requirements for control of internal inspection consist of the following elements:

- Implementing procedures shall be established to assure that inspection or surveillance is performed to verify that materials, parts, processes, or other activities affecting quality conform to documented instructions, procedures, specifications, drawings, and/or procurement documents.
- Personnel performing inspection and surveillance activities shall be trained and qualified in accordance with written approved procedures.
- Inspections and surveillances are to be performed by individuals other than those who performed or supervised the subject activities.
- Inspection or surveillance and process monitoring are both required where either one, by itself, will not provide assurance of quality.
- Modifications and/or repairs to and replacements of safety-related and important-to-safety structures, systems, and components are inspected in accordance with the original design and inspection requirements or acceptable alternatives.
- Mandatory hold points, inspection equipment requirements, acceptance criteria, personnel qualification requirements, performance characteristics, variable and/or attribute recording instructions, reference documents, and other requirements are considered and included, as applicable, during inspection and surveillance planning.

9.10.1 Inspections During Fabrication

Specific inspection criteria are incorporated into the drawings for the ATR FFSC packaging. Inspection requirements for fabrication are divided into two responsible areas that document that an accepted ATR FFSC package conforms to tested and certified design criteria. These two areas are:

- In-process inspections performed by the fabricator.
- Independent surveillance of fabrication activities performed by individuals acting on behalf of the purchaser.

The vendor (fabricator) is required to submit Manufacturing/Fabrication Plans prior to the start of fabrication for approval by the customer. These plans shall be used as a tool for establishing witness and hold points. A review for compliance with procurement documents is normally performed as part of the surveillance function at the vendor’s facility. The plans shall define how fabrications and inspections are to be performed, processes to be engaged. Inspections must be documented and records delivered in individual data packages accompanying the package in accordance with the procurement specification.

Independent surveillance activities will be performed by qualified personnel selected with approval of the customer.

9.10.2 Inspections During Initial Acceptance and During Service Life

Independent inspections are performed upon receipt of the ATR FFSC packaging prior to first usage (implemented by package user procedures) and on an annual basis. Post-loading inspections are also performed prior to shipment. Inspection to be implemented by the package user (by qualified independent inspection personnel) must include the following:

- Acceptance – Ensure compliance with procurement documents. Per Chapter 8, *Acceptance Tests and Maintenance Program* of this SAR, perform (as applicable) first-time-usage inspections, and weld examinations.
- Operation – Verify proper assembly and verify that post-load leak testing (if applicable) is carried out as discussed in Chapter 7, *Package Operations*, of this SAR.
- Maintenance – Ensure adequate packaging maintenance to ensure that performance is not impaired as discussed in Chapter 8, *Acceptance Tests and Maintenance Program* of this SAR.
- Final – Verify proper contents, assembly, marking, shipping papers, and implementation of any special instructions.

9.11 Test Control

As required by the INL Contractor Quality Program, test control activities shall be established and implemented to satisfy the requirements of the QAPD. These requirements are to be in accordance with:

- 10 CFR 830.122(e), *Criterion 5 – Performance/Work Processes*
- DOE Order 414C, CRD, Attachment 1, 2.b.(1), *Criterion 5 – Work Processes.*

Requirements are implemented to ensure processes and procedures are in place that achieve quality objectives and ensure appropriate levels of quality and safety are applied to critical components of packaging and transportation systems utilizing a graded approach.

Activities related to test control shall be controlled. The requirements for test control consist of the following elements:

- Implementing procedures shall be established to assure that required proof, acceptance, and operational tests, as identified in design or procurement documents, are performed and appropriately controlled.
- Test personnel shall have appropriate training and shall be qualified for the level of testing which they are performing. Personnel shall be qualified in accordance with approved, written instructions, procedures, and/or checklists.
- Tests are performed by qualified personnel in accordance with approved, written instructions, procedures, and/or checklists. Test procedures are to contain or reference the following information, as applicable:
  - Acceptance criteria contained in the applicable test specifications, or design and procurement documents.
  - Instructions for performance of tests, including environmental conditions.

  - Test prerequisites such as test equipment, instrumentation requirements, personnel qualification requirements, fabrication, or operational status of the items to be tested.
  - Provisions for data recording and records retention.
- Test results are to be documented and evaluated to ensure that acceptance criteria have been satisfied.
- Tests to be conducted after modifications, repairs, or replacements of safety-related and important-to-safety structures, systems, or components are to be performed in accordance with the original design and testing requirements or acceptable alternatives.

Tests are required when it is necessary to demonstrate that an item or process will perform satisfactorily. Test procedures must specify the objectives of the tests, testing methods, required documentation, and acceptance criteria. Tests to be conducted by vendors at vendor facilities must be specified in procurement documents. Personnel conducting tests, test equipment, and procedures must be qualified and records attesting to qualification retained.

9.11.1 Acceptance and Periodic Tests

- The fabricator must supply QA documentation for the fabrication of each ATR FFSC packaging in accordance with applicable drawings, specifications, and/or other written requirements.
- The package user must ensure required ATR FFSC packaging inspections and tests are performed prior to first usage.
- Periodic testing, as applicable, will be performed to ensure the ATR FFSC packaging performance has not deteriorated with time and usage. The requirements for the periodic tests are given in the Chapter 8, *Acceptance Tests and Maintenance Program* of this SAR. The results of these tests are required to be documented and maintained with the specific packaging records by the package user.

9.11.2 Packaging Nonconformance

Packaging that does not meet the inspection criteria shall be marked or tagged as nonconforming, isolated, and documented in accordance with Section 9.15, *Nonconforming Parts, Materials, or Components*. The packaging must not be used for shipment until the nonconformance report has been properly dispositioned in accordance with Section 9.15.

9.12 Control Of Measuring And Test Equipment

As required by the INL Contractor Quality Program, activities pertaining to the control of measuring and test equipment shall be established and implemented to satisfy the requirements of the QAPD. These requirements are to be in accordance with:

- 10 CFR 830.122(h), *Criterion 8 – Performance/Inspection and Acceptance Testing*
- DOE Order 414C, CRD, Attachment 1, 2.b.(4), *Criterion 8 – Inspection and Acceptance Testing.*

Requirements are implemented to ensure processes and procedures are in place to ensure appropriate inspections and tests are applied prior to acceptance or use of the packaging or component, and to identify the status of packaging items, components, etc.

Activities pertaining to the control of measuring and test equipment shall be controlled. The requirements for control of measuring and test equipment shall consist of the following elements:

- Implementing procedures shall be established to assure that tools, gages, instruments and other measuring and testing devices (M&TE) used in activities affecting quality are properly controlled, calibrated and adjusted to maintain accuracy within required limits.
- M&TE are calibrated at scheduled intervals against certified standards having known valid relationships to national standards. If no national standards exist, the basis for calibration shall be documented. Calibration intervals are based on required accuracy, precision, purpose, amount of use, stability characteristics and other conditions that could affect the measurements.
- Calibrations are to be performed in accordance with approved written procedures. Inspection, measuring and test equipment are to be marked to indicate calibration status.
- M&TE are to be identified, labeled or tagged indicating the next required calibration due date, and traceable to calibration records.
- If M&TE is found to be out of calibration, an evaluation shall be performed and documented regarding the validity of inspections or tests performed and the acceptability of items inspected or tested since the previous acceptable calibration. The current status of M&TE is to be recorded and maintained. Any M&TE that is consistently found to be out of calibration shall be repaired or replaced.

Special calibration and control measures on rules, tape measures, levels and other such devices are not required where normal commercial practices provide adequate accuracy.

9.13 Handling, Storage, And Shipping Control

As required by the INL Contractor Quality Program, handling, storage, and shipping control activities shall be established and implemented to satisfy the requirements of the QAPD. These requirements are to be in accordance with:

- 10 CFR 830.122(e), *Criterion 5 – Performance/Work Processes*
- DOE Order 414C, CRD, Attachment 1, 2.b.(1), *Criterion 5 – Work Processes.*

Requirements are implemented to ensure processes and procedures are in place that achieve quality objectives and ensure appropriate levels of quality and safety are applied to critical components of packaging and transportation systems utilizing a graded approach.

Activities pertaining to handling, storage, and shipping shall be controlled. The requirements for handling, storage, and shipping control consist of the following elements:

- Implementing procedures shall be established to assure that materials, parts, assemblies, spare parts, special tools, and equipment are handled, stored, packaged, and shipped in a manner to prevent damage, loss, loss of identity, or deterioration.

- When necessary, storage procedures address special requirements for environmental protection such as inert gas atmospheres, moisture control, temperature levels, etc.

Package users shall ensure that components associated with the ATR FFSC are controlled to prevent damage or loss, protected against damage or deterioration, and provide adequate safety of personnel involved in handling, storage, and shipment (outgoing and incoming) operations. Handling, storage, and shipping must be accomplished in accordance with written and approved instructions, procedures, specifications, and/or drawings. These documents must identify appropriate information regarding shelf life, environment, temperature, cleaning, handling, and preservation, as applicable, to meet design, regulatory, and/or DOE shipping requirements.

Preparation for loading, handling, and shipment will be done accordance with approved procedures to ensure that all requirements have been met prior to delivery to a carrier. A package ready for shipment must conform to its shipping paper.

Empty packages, following usage, must be checked and decontaminated if required. Each package must be inspected, reconditioned, or repaired, as appropriate, in accordance with approved written procedures before storing or loading. Empty ATR FFSC packagings are to be tagged with "EMPTY" labels and stored in designated protected areas in order to minimize environmental effects on the containers.

Routine maintenance on the ATR FFSC packaging may be performed as deemed necessary by package users and is limited to cleaning, rust removal, painting, light metal working to restore the original contours and replacement of damaged, worn, or malfunctioning components. Spare components will be placed in segregated storage to maintain proper identification and to avoid misuse.

9.14 Inspection, Test, And Operating Status

As required by the INL Contractor Quality Program, inspection, test, and operating status activities shall be established and implemented to satisfy the requirements of the QAPD. These requirements are to be in accordance with:

- 10 CFR 830.122(e), *Criterion 5 – Performance/Work Processes*
- 10 CFR 830.122(h), *Criterion 8 – Performance/Inspection and Acceptance Testing*
- DOE Order 414C, CRD, Attachment 1, 2.b.(1), *Criterion 5 – Work Processes*
- DOE Order 414C, CRD, Attachment 1, 2.b.(4), *Criterion 8 – Inspection and Acceptance Testing.*

Requirements are implemented to ensure processes and procedures are in place that achieve quality objectives and ensure appropriate levels of quality and safety are applied to critical components of packaging and transportation systems utilizing a graded approach. In addition, processes and procedures shall be in place to ensure appropriate inspections and tests are applied prior to acceptance or use of the packaging or component, and to identify the status of packaging items, components, etc.

Activities pertaining to inspection, test, and operating status activities shall be controlled. The requirements for inspection, test, and operating status consist of the following elements:

- Implementing procedures shall be established to assure that the inspection and test status of materials, items, structures, systems, and components throughout fabrication, installation, operation, and test are clearly indicated by suitable means, (e.g., tags, labels, cards, form sheets, check lists, etc.).
- Bypassing of required inspections, tests, or other critical operations is prevented through the use of approved instructions or procedures
- As appropriate, the operating status of nonconforming, inoperative or malfunctioning components of a storage/transport system is indicated to prevent inadvertent operation. The application and removal of status indicators is performed in accordance with approved instructions and procedures.
- Any nonconforming items are identified and controlled in accordance with Section 9.15, *Nonconforming Parts, Materials, or Components*, of this SAR.

Package users shall ensure that the status of inspection and test activities are identified on the item or in documents traceable to the item to ensure that proper inspections or tests have been performed and that those items that do not pass inspection are not used. The status of fabrication, inspection, test, assembly, and refurbishment activities must be identified in documents traceable to the package components.

Measures established in specifications, procedures, and other instructions shall ensure that the following objectives are met:

- QA personnel responsible for oversight of packaging inspections can readily ascertain the status of inspections, tests, and/or operating conditions.
- No controlled items are overlooked.
- Inadvertent use or installation of unqualified items is prevented.
- Documentation is complete.

9.15 Nonconforming Materials, Parts, or Components

As required by the INL Contractor Quality Program, control of nonconforming materials, parts, or components shall be established and implemented to satisfy the requirements of the QAPD. These requirements are to be in accordance with:

- 10 CFR 830.122(c), *Criterion 3 – Management/Quality Improvement*
- DOE Order 414C, CRD, Attachment 1, 2.b.(3), *Criterion 3 – Quality Improvement.*

Requirements are implemented to ensure that processes and procedures are in place to identify and correct problems associated with transportation and packaging activities.

Activities pertaining to the control of nonconforming materials, parts, or components shall be controlled. The requirements for nonconforming materials, parts, or components consist of the following elements:

- Implementing procedures shall be established to control materials, parts, and components that do not conform to requirements to prevent their inadvertent use during fabrication or during service.

- Nonconforming items include those items that do not meet specification or drawing requirements. Additionally, nonconforming items include items not fabricated or tested (1) in accordance with approved written procedures, (2) by qualified processes, or (3) by qualified personnel; where use of such procedures, processes, or personnel is required by the fabrication, test, inspection, or quality assurance requirements.
- Nonconforming items are identified and/or segregated to prevent their inadvertent use until properly dispositioned. The identification of nonconforming items is by marking, tagging, or other methods that do not adversely affect the end use of the item. The identification shall be legible and easily recognizable. When identification of each nonconforming item is not practical, the container, package, or segregated storage area, as appropriate, is identified.
- Nonconforming conditions are documented in NCRs and affected organizations are to be notified. The nonconformance report shall include a description of the nonconforming condition. Nonconforming items are dispositioned as use-as-is, reject, repair, or rework.
- Inspection or surveillance requirements for nonconforming items following rework, repair are detailed in the nonconformance reports and approved following completion of the disposition.
- Acceptability of rework or repair of nonconforming materials, parts, and components is verified by re-inspecting and/or re-testing the item to the original requirements or equivalent inspection/testing methods. Inspection, testing, rework, and repair methods are to be documented and controlled.
- The disposition of nonconforming items as use-as-is or repair shall include technical justification and independent verification to assure compliance with design, regulatory, and contractual requirements.
- Items dispositioned as rework or repair are reinspected and retested in accordance with the original inspection and test requirements or acceptable alternatives that comply with the specified acceptance criteria.
- When specified by contract requirements, nonconformances that result in a violation of client contract or specification requirements shall be submitted for client approval.
- Nonconformance reports are made part of the inspection records and are periodically reviewed to identify quality trends. Unsatisfactory quality trends are documented on a Corrective Action Report (CAR) as detailed in Section 9.16, *Corrective Action*, of this SAR. The results of these reviews are to be reported to management.
- Nonconformance reports relating to internal activities are issued to management of the affected organization. The appropriate Quality Assurance Manager shall approve the disposition and performs follow-up activities to assure proper closure.
- Compliance with the evaluation and reporting requirements of 10 CFR 21 related to defects and noncompliances are to be controlled by approved procedures.

9.16 Corrective Action

As required by the INL Contractor Quality Program, requirements for corrective action shall be established and implemented to satisfy the requirements of the QAPD. These requirements are to be in accordance with:

- 10 CFR 830.122(c), *Criterion 3 – Management/Quality Improvement*
- DOE Order 414C, CRD, Attachment 1, 2.b.(3), *Criterion 3 – Quality Improvement.*

Requirements are implemented to ensure that processes and procedures are in place to identify and correct problems associated with transportation and packaging activities.

Activities pertaining to corrective actions shall be controlled. The requirements for corrective action consist of the following elements:

- Implementing procedures shall be established to identify significant conditions adverse to quality. Significant and/or repetitive failures, malfunctions and deficiencies in material, components, equipment, and operations are to be promptly identified and documented on a Corrective Action Reports (CARs) and reported to appropriate management. The cause of the condition and corrective action necessary to prevent recurrence are identified, implemented, and followed up to verify corrective action is complete and effective.
- The INL Contractor Quality Assurance Director (DQA) is responsible for ensuring implementation of the corrective action program, including follow up and closeout actions. The DQA may delegate certain activities in the Corrective Action process to others.

9.17 Quality Assurance Records

As required by the INL Contractor Quality Program, activities associated with QA records shall be established and implemented to satisfy the requirements of the QAPD. These requirements are to be in accordance with:

- 10 CRF 830.122(b), *Criterion 2 – Management/Personnel Training and Qualifications*
- 10 CFR 830.122(d), *Criterion 4 – Management/Documents and Records*
- 10 CFR 830.122(e), *Criterion 5 – Performance/Work Processes*
- 10 CFR 830.122(h), *Criterion 8 – Performance/Inspection and Acceptance Testing*
- DOE Order 414C, CRD, Attachment 1, 2.a.(2), *Criterion 2 - Personnel Training and Qualifications*
- DOE Order 414C, CRD, Attachment 1, 2.a.(4), *Criterion 4 – Documents and Records*
- DOE Order 414C, CRD, Attachment 1, 2.b.(1), *Criterion 5 – Work Processes*
- DOE Order 414C, CRD, Attachment 1, 2.b.(4), *Criterion 8 – Inspection and Acceptance Testing.*

Requirements are implemented to ensure that only trained and qualified personnel perform transportation and packaging activities. The program shall ensure processes and procedures are in place to address document preparation, document control, and management of records. In addition, the program ensures processes and procedures are in place which achieves quality objectives and appropriate levels of quality and safety are applied to critical components of packaging and transportation systems utilizing a graded approach. Finally, the program ensures processes and procedures are in place to identify appropriate inspections and tests are applied prior to acceptance or use of the package or component, and to identify the status of packaging items, components, etc.

Quality assurance records shall be controlled. The requirements for quality assurance records consist of the following elements:

- Implementing procedures shall be established to assure control of quality records. The purpose of the Quality Assurance Records system is to assure that documented evidence relative to quality related activities is maintained and available for use by INL Contractor, its customers, and/or regulatory agencies, as applicable.
- Approved procedures identify the types of documents to be retained as QA records, as well as those to be retained by the originating organization. Lifetime and Non-Permanent records are retained by Records Management (RMA) or its customers, as appropriate. Records are identified, indexed, and stored in accessible locations.
- QA Records are maintained for periods specified to furnish evidence of activities affecting the quality of structures, systems, and components that are safety-related or important-to-safety. These records include records of design, procurement, fabrication, assembly, inspection, and testing.
- Maintenance records shall include the use of operating logs; results of reviews, inspections, tests, and audits; results from monitoring of work performance and material analyses; results of maintenance, modification, and repair activities; qualification of personnel, procedures, and equipment; records of calibration of measuring and test equipment; and related instructions, procedures, and drawings.
- Requirements for indexing, record retention period, storage method(s) and location(s), classification, preservation measures, disposition of nonpermanent records, and responsibility for safekeeping are specified in approved procedures. Record storage facilities are established to prevent destruction of records by fire, flood, theft, and deterioration due to environmental conditions (such as temperature, humidity, or vermin). As an alternative, two identical sets of records (dual storage) may be maintained at separate locations.
- INL shall retain required records for at least three (3) years beyond the date of last engagement of activities.

9.17.1 General

Sufficient records must be maintained by package users to furnish evidence of quality of items and of activities affecting quality. QA records that must be retained for the lifetime of the packaging include:

- Appropriate production-related records that are generated throughout the package manufacturing and fabrication process

- Records demonstrating evidence of operational capability; e.g., completed acceptance tests and inspections
- Records verifying repair, rework, and replacement
- Audit reports, and corrective actions
- Records that are used as a baseline for maintenance
- Records showing evidence of delivery of packages to a carrier and proof that all DOT requirements were satisfied.

9.17.2 Generating Records

Package user documents designated as QA records must be:

- Legible
- Completed to reflect the work accomplished and relevant results or conclusions
- Signed and dated or otherwise authenticated by authorized personnel.

QA records should be placed in a records storage area as soon as is feasible to avoid loss or damage. Individual package QA records must be generated and maintained for each package by the package serial number.

9.17.3 Receipt, Retrieval, and Disposition of Records

The RMA has overall responsibility for records management for the ATR FFSC. Package users are responsible for maintaining records while they are in process and for providing completed records to the RMA. A receipt control system shall be established, and records maintained in-house or at other locations are to be identifiable and retrievable and not disposed of until prescribed conditions are satisfied.

Records are to be available for inspection upon request.

Table 9.17-1 - Quality Assurance Records

Quality Assurance Record	Retention period
Design and Fabrication Drawings	LOP+
Test Reports	LOP+
Independent Design Review Comments	LOP+
Safety Analysis Report for Packaging	LOP+
Vendor Manufacturing and Inspection Plans	LOP+
Material Test Report of Certification of Materials	LOP+
Welding Specifications and Procedures	LOP+
Weld Procedure Qualification Record	LOP+
Welder or Welding Operator Qualification Tests	LOP+
Record of Qualification of Personnel Performing Radiographic and PT Reports	LOP+
Weld Radiographs	LOP+
Liquid Penetrant Reports	LOP+
Dimensional Inspection Report for All Features	LOP+
Visual and Dimensional Inspection upon Receipt of Packaging	LOP+
Package Loading Procedure	S+
Unloading Procedure	S+
Maintenance Procedures	LOP+
Repair Procedures	LOP+
Procurement Specifications	LOP+
Personnel Training and Qualification Documentation	LOP+
Maintenance Log	LOP+
Corrective Action Reports	LOP+
Nonconformance Reports (and resolutions)	LOP+
Incident Reports per 10 CFR 71.95	LOP+
Preliminary Determinations per 10 CFR 71.85	S+
Routine Determinations per 10 CFR 71.87	S+
Shipment Records per 10 CFR 71.91(a), (b), (c), (d)	S+
LOP+ Lifetime of packaging plus 3 years S+ Shipping date plus 3 years	

9.18 Audits

As required by the INL Contractor Quality Program, audit requirements shall be established and implemented to satisfy the requirements of the QAPD. These requirements are to be in accordance with:

- 10 CFR 830.122(i), *Criterion 9 – Assessment/Management Assessment*
- 10 CFR 830.122(j), *Criterion 10 – Assessment/Independent Assessment*
- DOE Order 414C, CRD, Attachment 1, 2.c.(1), *Criterion 9 – Management Assessment*
- DOE Order 414C, CRD, Attachment 1, 2.c.(2), *Criterion 10 – Independent Assessment.*

Requirements are implemented to ensure management assessments are performed on a regular basis. Management assessments are planned and conducted in accordance with written procedures. In addition, the program will be independently assessed periodically in accordance with procedures.

Activities pertaining to audits and assessments shall be controlled. The requirements for audits and assessments consist of the following elements:

- Implementing procedures shall be established to assure that periodic audits verify compliance with all aspects of the Quality Assurance Program and determine its effectiveness. Areas and activities to be audited, such as design, procurement, fabrication, inspection, and testing of storage/transportation systems, are to be identified as part of audit planning.
- INL audits supplier Quality Assurance Programs, procedures, and implementation activities to evaluate and verify that procedures and activities are adequate and comply with applicable requirements.
- Audits are planned and scheduled in a manner to provide coverage and coordination with ongoing Quality Assurance Program activities commensurate with the status and importance of the activities.
- Audits are performed by trained and qualified personnel not having direct responsibilities in the areas being audited and are conducted in accordance with written plans and checklists. Audit results are documented and reviewed by management having responsibility for the area audited. Corrective actions and schedules for implementation are established and recorded. Audit reports include an objective evaluation of the quality-related practices, procedures, and instructions for the areas or activities being audited and the effectiveness of implementation.
- Responsible management shall undertake corrective actions as a follow-up to audit reports when appropriate. The Quality Assurance Management (QAM) shall evaluate audit results for indications of adverse trends that could affect quality. When results of such assessments so indicate, appropriate corrective action will be implemented.

The QAM shall follow up on audit findings to assure that appropriate corrective actions have been implemented and directs the performance of re-audits when deemed necessary.